Dedication

This second edition of my text is dedicated to my family: my wife Peggy and our sons Jamie, Stephen (who died from ALS in 2006), and Ben. They, and their families, have been wonderfully supportive of my efforts in this challenging endeavor. For this, I am truly grateful.

A documentary film, So Much So Fast, *was made about ALS, Stephen, Jamie, and our life together. The Los Angeles film critic's review said of our family: "And what a family; close-knit, loving, and fiercely loyal." I treasure those words.*

Air Esscentials – Exhibit 2007
Aroma 360 v. Air Esscentials
IPR No. 2025-00705

© McGraw-Hill Education. All rights reserved. Any use is subject to the Terms of Use, Privacy Notice and copyright information.

About the Author

John B. Heywood has been a faculty member at the Massachusetts Institute of Technology since 1968, where he was Sun Jae Professor of Mechanical Engineering and Director of the Sloan Automotive Laboratory. His interests are focused on internal combustion engines and their fuels, and on broader studies of future transportation technology and policy, fuel supply options, and vehicular air pollutant and greenhouse gas emissions. He has published over 230 papers in the technical literature, and is the author of five books, including this text. Dr. Heywood is a Fellow of the American Society of Mechanical Engineers, the British Institution of Mechanical Engineers, and the Society of Automotive Engineers. He has received many awards for his work, including the 1996 U.S. Department of Transportation Award for the Advancement of Motor Vehicle Research and Development, the 1999 Soichiro Honda Medal from the American Society of Mechanical Engineers, and the 2008 Society of Automotive Engineers Award for Contributions to Automotive Policy. He is also a Member of the National Academy of Engineering and a Fellow of the American Academy of Arts and Sciences. Dr. Heywood has a Ph.D. in mechanical engineering from MIT (1965), a Sc.D. from Cambridge University for his research contributions (1983), an honorary Doctor of Technology degree from Chalmers University of Technology, Sweden (1999), and an honorary D.Sc. from City University, London (2004).

© McGraw-Hill Education. All rights reserved. Any use is subject to the Terms of Use, Privacy Notice and copyright information.

Preface

There are about two billion internal combustion engines in use in the world today. These engines enable key areas of our daily lives, propelling our many vehicles, generating electricity, and providing mechanical power in a wide range of applications. Their origin dates back to 1876 when Nicolaus Otto first developed the spark-ignition engine, and 1892 when Rudolf Diesel invented the compression-ignition engine. Since then, the utility of spark-ignition and diesel engines has steadily improved as our understanding of engine processes has increased, new technologies have become available, and market and regulatory requirements have become more demanding. A sense of urgency, driven largely by our need to combat global climate change, now requires ever-faster development of better engines and fuels, and exploration of alternative approaches. Increasing engine power density and efficiency and reducing engine emissions are really important objectives. The availability and effective use of our expanding knowledge base on engines and fuels are therefore critical.

The 1988 edition of this book has served as an educational text and professional reference in response to that need for some thirty years. Since 1988, we have steadily improved engine performance, reduced engine fuel consumption, developed air pollutant control technologies that have reduced engine emissions, improved the quality of our mainstream petroleum-based fuels, and made a start on reducing transportation's greenhouse gas emissions. Obviously, over these past thirty years, much new engineering knowledge relevant to engines and fuels has been developed. The purpose of this second edition of my book is to incorporate this new material, update the existing knowledge base, and make available a modern, broader, and thus more useful engine text and reference.

There is a massive amount of material, both analytical and experimentally based, available on internal combustion engines, and no text can include it all. The emphasis here is on the key physical and chemical processes that govern engine operation and design. These include the thermodynamics of energy conversion in engines, the physics and chemistry that govern engine combustion, the engine's fuel requirements, the important fluid flow, heat transfer, friction, and lubrication processes in engines, and the engine's dynamic behavior. These all influence engine performance, efficiency, and emissions.

There are two main types of internal combustion engine: spark-ignition and diesel. The primary organizing approach for the material in this text is how the mixture of fuel and air formed inside the engine cylinder is ignited. From *method of ignition*—spark-ignited or compression-ignited—follows each type of engine's operating cycle, fuel requirements, mixture preparation approach, combustion process, combustion chamber configuration, method used to control load, air pollutant formation mechanisms and control approaches, performance and efficiency characteristics, and greenhouse gas emissions. While many engine processes are similar in both types of engines, the method of ignition is fundamentally different. The consequences of that difference underlie the overall organization of this book.

The book is arranged in four major sections. The first (Chaps. 1 to 5) provides an introduction to, and overview of, the operating characteristics of spark-ignition and compression-ignition (diesel) engines, defines the parameters used to characterize engine operation, and develops the thermodynamics and combustion theory required for a quantitative analysis of engine behavior. It concludes with an integrated treatment of the methods used for analyzing idealized models of internal combustion engine operating cycles.

The second section (Chaps. 6 to 8) focuses on engine flow phenomena. The details of the gas exchange process—intake and exhaust processes in four-stroke and scavenging in two-stroke cycle engines—and the various methods of boosting engines—turbocharging and supercharging—are discussed. The several fuel metering approaches used in spark-ignition engines are reviewed next. Then, the key features of the flows setup inside the engine cylinder are described. These flow processes (along with engine boost levels) control the amount of air the engine will induct, and thus its power, and largely govern the rate at which the fuel-air mixture in the cylinder will burn.

The third section of the book examines engine combustion phenomena. These chapters (9 to 11) are especially important to smooth and robust engine behavior. The combustion process releases the fuel's chemical energy within the engine's cylinders

© McGraw-Hill Education. All rights reserved. Any use is subject to the Terms of Use, Privacy Notice and copyright information.

for eventual conversion to work. The fraction of the fuel's energy that is converted depends strongly on how that combustion process occurs. The spark-ignition and compression-ignition combustion processes (Chaps. 9 and 10, respectively) thus influence essentially all aspects of engine behavior. Air pollutants are undesirable byproducts of combustion. Our extensive knowledge of how air pollutants form inside the engine and how such emissions can be controlled is reviewed in Chap. 11.

The last section of the book focuses on the operating characteristics of these engines. First, the basics of engine heat transfer and friction, both of which degrade engine performance, are developed in Chaps. 12 and 13. Then, Chap. 14 describes the methodologies available for predicting details of key engine processes and overall engine behavior based on realistic models of engine flow and combustion phenomena. The various thermodynamic- and fluid-mechanic-based computer codes that have been developed over the past several decades are widely used in engine research, development, and design, so knowledge of their basic structure and capabilities is important. Chapter 15 then summarizes how the operating characteristics—power, efficiency, and emissions—of spark-ignition and diesel engines depend on the major engine design and operating variables. These final two chapters effectively integrate our analysis-based understanding and practical knowledge of individual engine processes together to describe and explain overall spark-ignition engine, and compression-ignition engine, behavior.

While this book contains much advanced material on engine design and operation intended for the practitioner, each major topic is developed from its beginnings and the more sophisticated chapters have introductory sections to facilitate their use in undergraduate courses. The chapters are extensively cross-referenced and indexed. Each chapter is fully illustrated and referenced, and includes problems for both undergraduate and graduate student courses.

John B. Heywood

© McGraw-Hill Education. All rights reserved. Any use is subject to the Terms of Use, Privacy Notice and copyright information.

Acknowledgments

Many individuals and organizations have assisted me as I have worked on this revision of my engine text over the past ten or so years. I am especially grateful to my colleagues in the Sloan Automotive Laboratory at MIT: Professors Wai Cheng, William Green, and James Keck, and Drs. Leslie Bromberg, Daniel Cohn, Tian Tian, and Victor Wong. They have helped create a stimulating and collegial environment within which we have all expanded our knowledge and understanding of engine and fuels phenomena. Many of the graduate students in our lab have made significant contributions to this text through their research; their names can often be found in the reference list at the end of each chapter.

I am indebted also to many companies in the automotive and energy industries that have supported the research that my colleagues and I have carried out on engine and fuels topics. The fellow professionals in these companies who have helped us in our work (much of it relevant to topics I cover in this book) have provided important practical knowledge and insights that significantly enhanced the value of what we have been able to do. Many engineering advances are a result of team efforts, and as a researcher I really appreciate the contributions of engine practitioners. I also thank those in the engine business who helped me by providing drawings of recent engines that help anchor engine theory in the real world. Their companies are acknowledged in the relevant figure captions.

I want to thank my colleagues and the leadership of our Mechanical Engineering Department at MIT for their encouragement and support in this major endeavor. My department provided administrative support for a part of this effort. My assistant, Karla Stryker-Currier, was responsible for typing and upgrading the many drafts of each chapter and the final versions submitted to the publisher. Her extensive and thorough efforts to help bring this new edition to fruition, over many years, are much appreciated.

I have been fortunate to find focused time for much of the writing, away from the disruptions of regular life, during several long stays at Montestigliano, a farm in Tuscany—the most beautiful place I have ever lived. I am most grateful to the people who manage this Azienda Agricola for their help in making these visits so productive.

Finally, my family has strongly supported me in this time-consuming endeavor. My wife Peggy and sons Jamie, Stephen (now deceased), and Ben continually urged me to "keep going" until the task was completed. As noted in my dedication, I am truly grateful for their encouragement.

© McGraw-Hill Education. All rights reserved. Any use is subject to the Terms of Use, Privacy Notice and copyright information.

Commonly Used Symbols, Subscripts, and Abbreviations

E.1. SYMBOLS

[1]a	Acceleration
	Crank radius
	Sound speed
	Specific availability
A	Area
A_C	Valve curtain area
A_{ch}	Cylinder head area
A_e	Exhaust port area
A_E	Effective area of flow restriction
A_i	Inlet port area
A_p	Piston crown area
A_v	Valve open area
B	Cylinder bore
	Steady-flow availability
c	Distance of piston from TC position
	Specific heat
c_p	Specific heat at constant pressure
c_s	Soot concentration (mass/volume)
c_v	Specific heat at constant volume
C	Absolute gas velocity
C_D	Discharge coefficient
	Vehicle drag coefficient
C_s	Swirl coefficient

© McGraw-Hill Education. All rights reserved. Any use is subject to the Terms of Use, Privacy Notice and copyright information.

D	Diameter
	Diffusion coefficient
D_d	Droplet diameter
D_{SM}	Sauter mean droplet diameter
D_v	Valve diameter
e	Radiative emissive power
	Specific energy
E_A	Activation energy
f	Coefficient of friction
	Fuel mass fraction
F	Force
g	Gravitational acceleration
	Specific Gibbs free energy
G	Gibbs free energy
h	Clearance height
	Oil film thickness
	Specific enthalpy
h_c	Heat-transfer coefficient
h_p	Port open height
h_s	Sensible specific enthalpy
H	Enthalpy
I	Moment of inertia
J	Flux
k	Thermal conductivity
	Turbulent kinetic energy
k_i^+, k_i^-	Forward, backward rate constants for ith reaction
K	Constant

© McGraw-Hill Education. All rights reserved. Any use is subject to the Terms of Use, Privacy Notice and copyright information.

K_c	Equilibrium constant expressed in concentrations
K_p	Equilibrium constant expressed in partial pressures
l	Characteristic length scale
	Connecting rod length
l_T	Characteristic length scale of turbulent flame
L	Piston stroke
L_I	Sound intensity level
$\widetilde{L}_{LO}$	Normalized spray lift-off length
L_n	Fuel-injection-nozzle orifice length
L_v	Valve lift
m	Mass
$\dot{m}$	Mass flow rate
m_r	Mass of residual gas
M	Mach number
	Molecular weight
n	Number of moles
	Polytropic exponent
n_c	Number of cylinders
n_R	Number of crank revolutions per power stroke
N	Crankshaft rotational speed
	Soot particle number density
	Turbocharger shaft speed
p	Cylinder pressure
	Pressure
P	Power
$\dot{q}$	Heat-transfer rate per unit area
	Heat-transfer rate per unit mass of fluid

© McGraw-Hill Education. All rights reserved. Any use is subject to the Terms of Use, Privacy Notice and copyright information.

Q	Heat transfer
$\dot{Q}$	Heat-transfer rate
Q_{ch}	Fuel chemical energy release or gross heat release
Q_{HV}	Fuel heating value
Q_n	Net heat release
r	Radius
r_c	Compression ratio
R	Connecting rod length/crank radius
	Gas constant
	Radius
R^+, R^-	One-way reaction rates
R_s	Swirl ratio
s	Crank axis to piston pin distance
	Specific entropy
S	Entropy
	Spray penetration
S_b	Turbulent burning speed
S_L	Laminar flame speed
S_p	Piston speed
t	Time
T	Temperature
	Torque
u	Specific internal energy
	Velocity
u'	Turbulence intensity
u_s	Sensible specific internal energy
u_T	Characteristic turbulent velocity

© McGraw-Hill Education. All rights reserved. Any use is subject to the Terms of Use, Privacy Notice and copyright information.

U	Compressor/turbine impellor tangential velocity
	Fluid velocity
	Internal energy
v, υ	Specific volume
	Velocity
v_{ps}	Valve pseudo-flow velocity
v_{sq}	Squish velocity
V	Cylinder volume
	Volume
V_c	Clearance volume
V_d	Displaced cylinder volume
w	Relative gas velocity
	Soot surface oxidation rate
W	Work transfer
W_c	Work per cycle
W_p	Pumping work
x, y, z	Spatial coordinates
x	Mass fraction
$\mathfrak{x}$	Mole fraction
x_b	Burned mass fraction
x_r	Residual mass fraction
y	H/C ratio of fuel
	Volume fraction
Y_a	Concentration of species a per unit mass
z	Distance, piston crown to cylinder head
Z	Inlet Mach index
α	Angle
	Thermal diffusivity $k/(\rho c)$

© McGraw-Hill Education. All rights reserved. Any use is subject to the Terms of Use, Privacy Notice and copyright information.

β	Angle
γ	Specific heat ratio c_p/c_v
Γ_c	Angular momentum of charge
δ	Boundary-layer thickness
δ_L	Laminar flame thickness
$\Delta h^{o}_{f,i}$	Molal enthalpy of formation of species i
$\Delta\theta_b$	Rapid burning angle
$\Delta\theta_d$	Flame development angle
ε	$4/(4 + y)$: y = H/C ratio of fuel
	Turbulent kinetic energy dissipation rate
ζ	Percentage of stoichiometric air entrained into fuel spray
η_a	Availability conversion efficiency
η_c	Combustion efficiency
η_{ch}	Charging efficiency
η_f	Fuel conversion efficiency
η_T	Turbine isentropic efficiency
η_{tr}	Trapping efficiency
η_v	Volumetric efficiency
θ	Crank angle
λ	Relative air/fuel ratio
Λ	Delivery ratio
μ	Dynamic viscosity
μ_i	Chemical potential of species i
v	Kinematic viscosity μ/ρ
v_i	Stoichiometric coefficient of species i
ξ	Flow friction coefficient
ρ	Density

© McGraw-Hill Education. All rights reserved. Any use is subject to the Terms of Use, Privacy Notice and copyright information.

$\rho_{a,0}$, $\rho_{a,i}$	Air density at standard, inlet conditions
σ	Normal stress
	Standard deviation
	Stefan-Boltzmann constant
	Surface tension
τ	Characteristic time
	Induction time
	Shear stress
τ_{id}	Ignition delay time
ϕ	Fuel/air equivalence ratio
Φ	Flow compressibility function [Eq. (C.11)]
	Isentropic compression function [Eqs. (4.15*b*), (4.25*b*)]
ψ	Molar N/O ratio
Ψ	Isentropic compression function [Eqs. (4.15*a*), (4.25*a*)]
ω	Angular velocity
	Frequency

[1] Nomenclature specific to a section or chapter is defined in that section or chapter.

E.2. SUBSCRIPTS

a	Air
b	Burned gas
c	Coolant
	Cylinder
C	Compression stroke
	Compressor
cr	Crevice
e	Equilibrium

© McGraw-Hill Education. All rights reserved. Any use is subject to the Terms of Use, Privacy Notice and copyright information.

	Exhaust
E	Expansion stroke
f	Flame
	Friction
	Fuel
g	Gas
i	Indicated
	Intake
	Species *i*
ig	Gross indicated
in	Net indicated
l	Liquid
L	Laminar
p	Piston
	Port
P	Prechamber
r, *θ*, *z*	*r*, *θ*, *z* components
R	Reference value
s	Isentropic
T	Nozzle or orifice throat
	Turbine
	Turbulent
u	Unburned
v	Valve
w	Wall
x, *y*, *z*	*x*, *y*, *z* components
0	Reference value
	Stagnation value

© McGraw-Hill Education. All rights reserved. Any use is subject to the Terms of Use, Privacy Notice and copyright information.

E.3. NOTATION

Δ	Difference
–	Average or mean value
~	Value per mole
[ ]	Concentration, moles/vol
{ }	Mass fraction
·	Rate of change with time
u	Bold type, vector (e.g., velocity)

E.4. ABBREVIATIONS

© McGraw-Hill Education. All rights reserved. Any use is subject to the Terms of Use, Privacy Notice and copyright information.

(*A/F*)	Air/fuel ratio
BC, ABC, BBC	Bottom-center crank position, after BC, before BC
bmep	Brake mean effective pressure
CN	Fuel cetane number
Da	Damköhler number τ_T/τ_L
EGR	Exhaust gas recycle
EI	Emission index
EPC, EPO	Exhaust port closing, opening
EVC, EVO	Exhaust valve closing, opening
(*F/A*)	Fuel/air ratio
(*G/F*)	Gas/fuel ratio
gimep	Gross indicated mean effective pressure
IPC, IPO	Inlet port closing, opening
IVC, IVO	Inlet valve closing, opening
mep	Mean effective pressure
nimep	Net indicated mean effective pressure
Nu	Nusselt number $h_c l/k$
ON	Fuel octane number
Re	Reynolds number $\rho u l/\mu$
sfc	Specific fuel consumption
TC, ATC, BTC	Top-center crank position, after TC, before TC
We	Weber number $\rho_l u^2 D/\sigma$

© McGraw-Hill Education. All rights reserved. Any use is subject to the Terms of Use, Privacy Notice and copyright information.

1.0. CHAPTER PRELIMINARIES

INTRODUCTION AND HISTORICAL PERSPECTIVE

ENGINE CLASSIFICATIONS

ENGINE OPERATING CYCLES

ENGINE COMPONENTS

MULTICYLINDER ENGINES

SPARK-IGNITION ENGINE OPERATION

DIFFERENT TYPES OF FOUR-STROKE SI ENGINES

COMPRESSION-IGNITION ENGINE OPERATION

DIFFERENT TYPES OF DIESEL ENGINES

TWO-STROKE CYCLE ENGINE OPERATION

FUELS

PROBLEMS

REFERENCES

© McGraw-Hill Education. All rights reserved. Any use is subject to the Terms of Use, Privacy Notice and copyright information.

1.1. INTRODUCTION AND HISTORICAL PERSPECTIVE

The purpose of internal combustion engines is to produce mechanical power from the chemical energy contained in the fuel. In *internal* combustion engines, as distinct from *external* combustion engines, this energy is released by burning or oxidizing the fuel *inside* the engine. The fuel-air mixture before combustion and the burned products after combustion are the actual working fluids. The work transfers that provide the desired power output occur directly between these working fluids and the mechanical components of the engine. The internal combustion engines that are the subject of this book are spark-ignition (SI) engines (sometimes called Otto engines, or gasoline or petrol engines, though other fuels can be used) and compression-ignition (CI) or diesel engines.[1] Because of their simplicity, ruggedness, high power to weight ratio, efficiency, and low cost, these two types of engine have found wide application in transportation (land, sea, and air) and power generation. It is the fact that combustion takes place inside the work-producing part of these engines that makes their design and operating characteristics fundamentally different from those of other types of engine.

Power-producing engines have served human beings for over two and a half centuries. For the first 150 years, water, converted to steam, was interposed between the combustion gases produced by burning the fuel and the work-producing piston-in-cylinder expander. It was not until the 1860s that the internal combustion engine became a practical reality.[1,2] The early engines developed for commercial use burned coal-gas air mixtures at atmospheric pressure—there was no compression before combustion. J. J. E. Lenoir (1822–1900) developed the first marketable engine of this type. Gas and air were drawn into the cylinder during the first half of the piston stroke. The charge was then ignited with a spark, the pressure increased, and the burned gases then delivered power to the piston for the second half of the stroke. The cycle was completed with an exhaust stroke. Some 5000 of these engines were built between 1860 and 1865 in sizes up to six horsepower. Efficiency was at best about 5%.

A more successful development—an atmospheric engine introduced in 1867 by Nicolaus A. Otto (1832–1891) and Eugen Langen (1833–1895)—used the pressure rise resulting from combustion of the fuel-air charge early in the outward stroke to accelerate a free piston and rack assembly so its momentum would generate a vacuum in the cylinder. Atmospheric pressure then pushed the piston inward, with the rack engaged through a roller clutch to the output shaft. Production engines, of which about 5000 were built, obtained thermal efficiencies of up to 11%. A slide valve controlled intake, ignition by a gas flame, and exhaust.

To overcome this engine's shortcomings of low thermal efficiency and excessive size and weight, Otto proposed an engine cycle with four piston strokes: an intake stroke, then a compression stroke before ignition, an expansion or power stroke where work was delivered to the crankshaft, and finally an exhaust stroke. He also proposed incorporating a stratified-charge induction system, though this was not achieved in practice. His prototype four-stroke engine first ran in 1876. A comparison between the Otto engine and its atmospheric-type predecessor indicates the reason for its success (Table 1.1): the enormous reduction in engine weight and volume. This was the breakthrough that effectively founded the internal combustion engine industry. By 1890, almost 50,000 of these engines had been sold in Europe and the United States.

© McGraw-Hill Education. All rights reserved. Any use is subject to the Terms of Use, Privacy Notice and copyright information.

Table 1.1 Comparison of Otto's early four-stroke cycle and Otto-Langen's engines[2]

	Otto and Langen	Otto's four-stroke
Brake horsepower	2	2
Weight, lb, approx.	4000	1250
Piston displacement, in^3	4900	310
Power strokes per minute	28	80
Shaft speed, rev/min	90	160
Mechanical efficiency, %	68	84
Overall efficiency, %	11	14
Expansion ratio	10	2.5

In 1884, an unpublished French patent issued in 1862 to Alphonse Beau de Rochas (1815–1893) was found that described the principles of the four-stroke cycle. This chance discovery cast doubt on the validity of Otto's own patent for this concept, and in Germany, it was declared invalid. Beau de Rochas also outlined the conditions under which maximum performance and efficiency in an internal combustion engine could be achieved. These were:

1. The largest possible cylinder volume with the minimum boundary surface
2. The greatest possible working speed
3. The greatest possible expansion ratio
4. The greatest possible pressure at the beginning of expansion

The first condition holds heat losses from the charge to a minimum. The second condition increases the power output from a given size engine. The third condition recognizes that the greater the expansion of the postcombustion gases, the greater the amount of work extracted. The fourth condition recognizes that higher initial pressures make greater expansion possible and give higher pressures throughout the process, both resulting in greater work transfer. Although Beau de Rochas' unpublished writings predate Otto's developments, he never reduced these ideas to practice. Thus Otto, in the broader sense, was the inventor of the modern internal combustion engine as we know it today.

Further developments followed fast once the full impact of what Otto had achieved became apparent. By the 1880s, several engineers (e.g., Dugald Clerk, 1854–1913, James Robson, 1833–1913, in England, and Karl Benz, 1844–1929, in Germany) had successfully developed two-stroke cycle internal combustion engines where the exhaust and intake processes occur during the end of the power stroke and the beginning of the compression stroke. James Atkinson (1846–1914) in England made an engine with a longer expansion than compression stroke, which had a high efficiency for the times but mechanical weaknesses. It was recognized that efficiency was a direct function of expansion ratio, yet compression ratios were limited to less than four if serious knock problems were to be avoided with the available fuels. Substantial carburetor and ignition system developments were required, and occurred, before high-speed gasoline engines suitable for automobiles became available in the late 1880s. Stationary engine progress also continued. By the late 1890s, large single-cylinder engines of 1.3-m bore fueled by low-energy blast furnace gas produced 600 bhp at 90 rev/min. In Britain, legal restrictions on volatile fuels turned their engine builders toward kerosene. Low compression ratio "oil" engines with heated external fuel vaporizers and electric ignition were developed with efficiencies comparable with those of gas engines (14 to 18%). The Hornsby-Ackroyd engine became the most popular oil engine in Britain, and was also built in large numbers in the United States.[2]

© McGraw-Hill Education. All rights reserved. Any use is subject to the Terms of Use, Privacy Notice and copyright information.

In 1892, the German engineer Rudolf Diesel (1858–1913) outlined in his patent a new form of internal combustion engine. His concept of initiating combustion by injecting a liquid fuel into the high-temperature air in the cylinder produced by compression permitted a doubling of efficiency over the other internal combustion engines then available. Much greater compression and expansion ratios, without detonation or knock, were now possible. However, even with the efforts of Diesel and the resources of M.A.N. in Ausburg combined, it took 5 years to develop a practical engine.

Engine developments, perhaps less fundamental but nonetheless important to the steadily widening internal combustion engine markets, have continued ever since.[2-4] There has always been an interest in engine geometries different from the standard reciprocating piston-in-cylinder, connecting rod, and crankshaft arrangement. Especially, there has been an interest in rotary internal combustion engines. Although a wide variety of experimental rotary engines have been proposed over the years,[5] the first practical rotary internal combustion engine, the Wankel, was not successfully tested until 1957. That engine, which evolved through many years of research and development, was based on the designs of the German inventor Felix Wankel.[6,7] While the Wankel engine has been used in niche markets, its advantages of compactness and smoother operation have not been sufficient to overcome its high manufacturing cost.

Fuels have also had a major impact on engine development. The earliest engines used for generating mechanical power burned gaseous fuels. Gasoline, and lighter fractions of crude oil, became available in the late 1800s, and various types of carburetors were developed to vaporize the fuel and mix it with air. Before about 1905, there were few issues with gasoline; though compression ratios had to be low (4 or less) to avoid knock, the highly volatile fuel made starting easy and gave good cold weather performance. However, a serious crude oil shortage developed, and to meet the fivefold increase in gasoline demand between 1907 and 1915, the yield from crude had to be raised. Through the work of William Burton (1865–1954) and his associates of Standard Oil of Indiana, a thermal cracking process was developed whereby heavier oils were heated under pressure and decomposed into less complex, more volatile compounds. These thermally cracked gasolines satisfied demand, but their higher boiling point range created cold weather starting problems. Fortunately, electrically driven starters, introduced in 1912, came along just in time.

On the farm, kerosene was the logical fuel for internal combustion engines since it was used for heat and light. Many early farm engines had heated carburetors or vaporizers to enable them to operate with such a fuel.

The period following World War I saw a tremendous advance in our understanding of how fuels affect combustion, and especially the problem of knock. The antiknock effect of tetraethyl lead was discovered at General Motors,[4] and it became commercially available as a gasoline additive in the United States in 1923. In the late 1930s, Eugene Houdry found that vaporized oils passed over an activated catalyst at 450 to 480°C were converted to high-quality gasoline in much higher yields than was possible with thermal cracking. These advances, and others, permitted fuels with ever better antiknock properties to be produced in large quantities; thus engine compression ratios steadily increased, improving power and efficiency.

During the past several decades, new factors for change have become important and now significantly affect engine design and operation. These factors are, first, the need to control the automotive contribution to urban air pollution and, second, the need to achieve significant improvements in automotive fuel consumption.

The automotive air-pollution problem became apparent in the 1940s in the Los Angeles basin. In 1952, it was demonstrated by Prof. A. J. Haagen-Smit that the smog problem there resulted from reactions between oxides of nitrogen and hydrocarbon compounds in the presence of sunlight.[8] In due course it became clear that the automobile was a major contributor to hydrocarbon and oxides of nitrogen emissions, as well as the prime cause of high carbon monoxide levels in urban areas. Diesel engines are a significant source of small soot or smoke particles, as well as hydrocarbons and oxides of nitrogen. Table 1.2 outlines the dimensions of the problem. As a result of these developments, emission standards for automobiles were introduced first in California, then nationwide in the United States, starting in the 1960s. Emission standards in Japan and Europe, and for other engine applications, have followed. Substantial reductions in emissions from spark-ignition and diesel engines have been achieved. Both the use of catalysts in SI engine exhaust systems for emissions control and concern over the toxicity of lead antiknock additives have resulted in the reappearance of unleaded gasoline as the dominant part of the automotive fuels market. These emission-control requirements and fuel developments have produced significant changes in the way internal combustion engines are now designed and operated.

© McGraw-Hill Education. All rights reserved. Any use is subject to the Terms of Use, Privacy Notice and copyright information.

Table 1.2 The automotive urban air-pollution problem: typical vehicle emissions*

Pollutant	Impact	Mobil source emissions as % of total†	Automobile emissions, SI engines		Truck emissions, diesel engines,	
			Precontrol vehicles, g/km‡	Current vehicles, g/km	Precontrol engines, g/kWh	Current engines, g/kWh
Oxides of nitrogen (NO and NO_2)	Reactant in photochemical smog; NO_2 is toxic	50–60	2.0	0.03	21	0.25
Carbon monoxide (CO)	Toxic	60	60	2	~ 20	low
Unburned hydrocarbons (HC, many hydrocarbon compounds)	Reactant in photochemical smog	25	10	0.05	~ 1	low
Particulates (soot, hydrocarbons, sulfates)	Some of HC compounds mutagenic; reduces visibility	5–10	0.5§	0.007§	1	0.02

*Varies from country to country. The United States, Canada, Western Europe, and Japan have standards with different degrees of severity. The United States, Europe, and Japan have different test procedures. Standards are strictest in the United States and Japan.

†Depends on type of urban area and source mix. Approximate percentages.

‡Average values for pre-1968 automobiles that had no emission controls, determined by U.S. test procedure that simulates typical urban and highway driving. Exhaust emissions, except for HC where 55% are exhaust emissions, 20% are evaporative emissions from fuel tank and carburetor, and 25% are crankcase blowby gases.

§Diesel engine automobiles only. Particulate emissions from spark-ignition engines are relatively low.

Internal combustion engines are also an important source of noise. There are several sources of engine noise: the exhaust system, the intake system, the fan used for cooling, and the engine block surface. The noise may be generated by aerodynamic effects, may be due to forces that result from the combustion process, or may result from mechanical excitation by rotating or reciprocating engine components. Vehicle noise legislation to reduce this impact on the ambient environment (and thus on people) was first introduced in the early 1970s.

During the 1970s, the price of crude petroleum rose rapidly to several times its cost (in real terms) in 1970. In the 1980s, the price of crude oil fell, and then fluctuated at relatively low levels until the early 2000s when it rose to close to its late 1970s values. The price then fell rapidly, and then rose again. Currently, the growth in oil demand in the developing world, the uncertainty in future extraction from established fields and discovery of new sources of oil, and the nonuniform concentration of petroleum reserves in a few nations, suggest that the balance between global oil production and transportation fuel demand will be tight over the next few decades. This uncertainty regarding the longer-term availability of adequate supplies of petroleum-based fuels is creating substantial pressures for significant improvements in internal combustion engine efficiency (in all the engine's many applications). Much work is being done to develop the supply and use of alternative fuels to gasoline and diesel. Of the nonpetroleum-based fuels, natural gas, methanol (methyl alcohol), and biomass-derived fuels such as ethanol (ethyl alcohol) and biodiesel are receiving significant attention. Synthetic gasoline and diesel are being made from tar (oil) sands, and could be produced from shale oil or coal. Hydrogen is being considered as a longer-term zero carbon containing possibility.

The growing consumption of fossil fuels has raised the concern that the greenhouse gas (GHG) emissions from our energy supply and use are causing global warming that could lead to changes in our climate. Emissions of carbon dioxide, along with other GHGs—methane, nitrous oxide, three groups of fluorinated gases (sulfur hexafluoride, hydrofluorocarbons, and perfluorocarbons), ozone—will need to be significantly reduced over the next several decades. Thus, internal combustion engines will need to become more efficient, and low GHG emitting sources of energy will need to be developed so that

© McGraw-Hill Education. All rights reserved. Any use is subject to the Terms of Use, Privacy Notice and copyright information.

consumption of petroleum-based fuels—gasoline and diesel—can be significantly reduced. Transportation is estimated to be the source of about one-quarter of the world's GHG emissions.

Table 1.3 lists the CO_2 emissions of various fuels and other sources of energy that might be used in transportation. Emissions from the various fossil fuels listed vary by about a factor of two. Emissions from biofuel production are generally lower (and could be significantly lower), depending on the biomass feedstock, the choice of fuel produced, and the process used to produce that fuel.[2]

Table 1.3 CO_2 emissions per unit chemical energy from various fuels or energy sources[9]

	gCO_2/MJ
Gasoline	93
Diesel (fuel oil)	99
Natural gas	74
Liquid petroleum gas	86
Ethanol*	34–73
Biodiesel	45–73
Hydrogen†	100–200
Electricity‡	90–160

*Varies with biomass feedstock and process used.

†From steam reforming of natural gas (low end) or from electrolysis (high end).

‡Depends on electricity generating system source mix (especially the fraction from coal).

The lower value given for hydrogen (which contains no carbon) is based on the current industrial hydrogen production process—steam reforming of natural gas. The electricity carbon dioxide-emissions intensity value depends on the mix of coal, natural gas, nuclear, hydro, wind (and solar) used to generate the electricity. While this electricity generating mix varies country to country, the major roles of coal and natural gas are common to most regions.

What would such fuel changes mean for internal combustion engines? With appropriate changes in engine design and operation, natural gas and the liquid fuels listed in Table 1.3 can be effectively utilized; indeed engines using these fuels are in use today. While the potential for hydrogen as a major transportation energy source (actually an *energy storage* medium) is partly based on large-scale use of highly efficient fuel cell technology, it can be used effectively in suitably designed SI engines. Vehicle propulsion system electrification is already occurring through the use of hybrid electric vehicle (HEV) technology—a combination of a battery, electric motor, internal combustion engine, and generator. The next step in vehicle electrification is to expand the battery's energy storage capacity and recharge (in part) from the electricity supply grid: deployment of this plug-in hybrid (PHEV) technology is occurring. HEV and PHEV propulsion systems require an internal combustion engine, albeit with specific characteristics that improve its efficiency (see Sec. 1.7.2). Some view the pure battery electric vehicle is the final step in this electrification process. Whether, and how far into the future complete electrification might occur is currently unclear.

This brings us back to internal combustion engines. It might be thought that after over a century of development, the internal combustion engine has reached its peak and little potential for further improvement remains. Such is not the case. As spark-

© McGraw-Hill Education. All rights reserved. Any use is subject to the Terms of Use, Privacy Notice and copyright information.

ignition and diesel engine technology evolves, these engines continue to show substantial improvements in efficiency, power density, degree of emission control, and operational capacity. Changes in engine operation and design are steadily improving engine performance in its broadest sense. New materials becoming available and more knowledge-based design offer the potential for continuing to reduce engine weight, size, and cost, for a given power output, and for different and more efficient internal combustion engine concepts. Emissions control technologies, in both the engine and the exhaust system, are becoming more effective and robust. Variable valve control is replacing fixed valve control approaches, with performance and efficiency benefits. Direct-injection gasoline engines, which offer improved dynamic engine control relative to port fuel injection, are now in large-scale production. These technologies are enabling increasing deployment of more highly boosted turbocharged gasoline and diesel engines.[10] Looking ahead, the engine development opportunities of the future are many and substantial. While they present a formidable challenge to automotive engineers, they will be made possible in large part by the enormous expansion of our knowledge of engine processes that the last several decades have witnessed.

[1] The gas turbine is also, by this definition, an "internal combustion engine." Conventionally, however, the term is used for spark-ignition and compression-ignition engines. The operating principles of gas turbines are fundamentally different, and they are not discussed in this book.

[2] The conversion of the carbon in the biomass source to CO_2 is often regarded as "carbon neutral" since that carbon came from CO_2 in the atmosphere. This topic is the subject of ongoing research.

© McGraw-Hill Education. All rights reserved. Any use is subject to the Terms of Use, Privacy Notice and copyright information.

1.2. ENGINE CLASSIFICATIONS

There are many different types of internal combustion engines. They can be classified by:[11]

1. *Application.* Automobile, truck, bus, locomotive, light aircraft, marine, portable power system, power generation
2. *Basic engine configuration.* Reciprocating engines (in turn subdivided by arrangement of cylinders: e.g., in-line, V, radial, opposed), rotary engines (Wankel and other geometries)
3. *Working cycle.* Four-stroke cycle: naturally-aspirated (admitting atmospheric air), supercharged (admitting precompressed air), and turbocharged (admitting air compressed in a compressor driven by an exhaust turbine). Two-stroke cycle: crankcase scavenged, supercharged, and turbocharged
4. *Valve or port design and location.* Four-stroke cycle: Overhead (or I-head) valves, underhead (or L-head) valves, with two, three, or four valves per cylinder, and fixed or variable valve control (timing, opening and closing points, and lift), rotary valves. Two-stroke cycle: cross-scavenged porting (inlet and exhaust ports on opposite sides of cylinder at one end), loop-scavenged porting (inlet and exhaust ports on same side of cylinder at one end), through- or uniflow-scavenged (inlet and exhaust ports or valves at different ends of cylinder)
5. *Fuel.* Gasoline (or petrol), fuel oil (or diesel fuel), natural gas, liquid petroleum gas (LPG), alcohols (methanol, ethanol), hydrogen, dual fuel
6. *Method of mixture preparation.* Carburetion or single-point fuel injection upstream of the throttle, fuel injection into the intake ports, fuel injection directly into the engine cylinder
7. *Method of ignition.* Spark ignition in engines where the in-cylinder fuel-air mixture is uniform and in stratified-charge engines where the mixture is nonuniform; compression ignition locally of the evolving in-cylinder fuel-air mixture in diesel engines, as well as ignition in natural gas engines by pilot injection of fuel oil)
8. *Combustion chamber design.* Open chamber (many designs: e.g., disc, wedge, hemisphere, pent-roof, bowl-in-piston), divided chamber (small and large auxiliary chambers; many designs: e.g., swirl chambers, prechambers)
9. *Method of load control.* Varying fuel and air flow together so mixture composition is essentially unchanged, control of fuel flow alone, a combination of these
10. *Method of cooling.* Water cooled, air cooled, uncooled (other than by natural convection and radiation)

All these distinctions are important and they illustrate the breadth of engine designs available. Because this book approaches the operating and emissions characteristics of internal combustion engines from a fundamental point of view, method of ignition has been selected as the primary classifying feature. From the method of ignition—SI or CI[1]—follow the important characteristics of the fuel used, method of mixture preparation, method of load control, combustion chamber design, details of the combustion process, engine emissions, and operating characteristics. Some of the other classifications are used as subcategories within this basic classification. The engine operating cycle—four-stroke or two-stroke is next in importance; the principles of these two cycles are described in the following section.

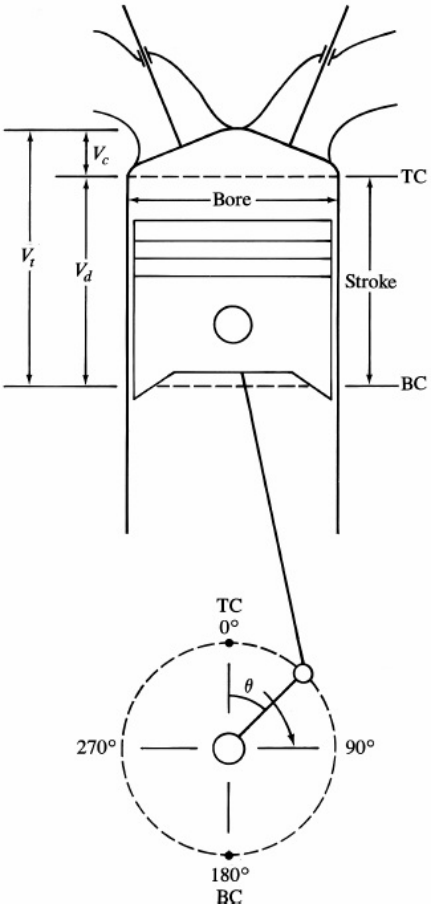
[1] In the remainder of the book, these terms will often be abbreviated by SI and CI, respectively.

© McGraw-Hill Education. All rights reserved. Any use is subject to the Terms of Use, Privacy Notice and copyright information.

1.3. ENGINE OPERATING CYCLES

Most of this book is about *reciprocating engines*, where each piston moves back and forth in a cylinder and transmits power from the high-pressure and temperature burned gases inside the cylinder through the piston and the connecting rod and crank mechanism to the drive shaft as shown in Fig. 1.1. The rotation of the crank produces a cyclical piston motion. The piston comes to rest at the top-center (TC) crank position and bottom-center (BC) crank position when the cylinder volume is a minimum or maximum, respectively.[1] The minimum cylinder volume is called the clearance volume V_c. The volume swept out by the piston, the difference between the maximum or total volume V_t and the clearance volume, is called the displaced or swept volume V_d. The ratio of maximum volume to minimum volume is the compression ratio r_c. Values of r_c are 8 to 12 for SI engines and typically in the ranges of 14 to 22 for CI engines.

Figure 1.1 Basic geometry of the reciprocating internal combustion engine. V_c, V_d, and V_t indicate clearance, displaced, and total cylinder volumes.



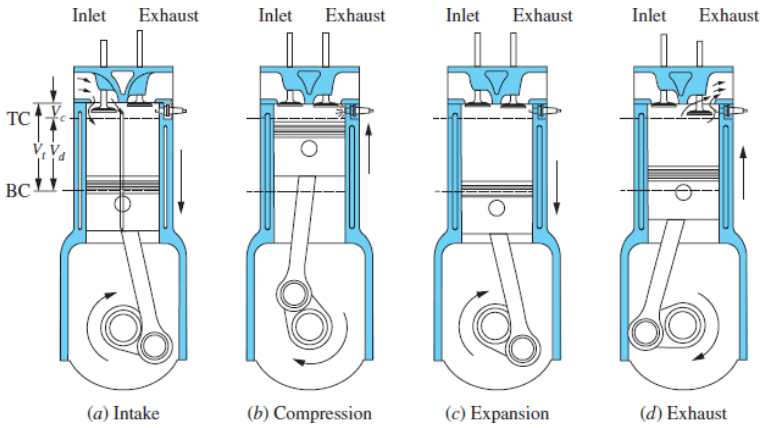
The majority of reciprocating engines operate on what is known as the *four-stroke cycle*. Each cylinder requires four strokes of its piston—two revolutions of the crankshaft—to complete the sequence of events that produces one power stroke. Both SI and CI engines use this cycle that comprises (Fig. 1.2):

1. *An intake stroke*, which starts with the piston at TC and ends with the piston at BC, which draws fresh air or fuel-air mixture into the cylinder. To increase the mass inducted, the inlet valve opens shortly before the stroke starts and closes after it ends.

© McGraw-Hill Education. All rights reserved. Any use is subject to the Terms of Use, Privacy Notice and copyright information.

2. *A compression stroke*, which starts with the piston at BC and ends at TC, when the mixture inside the cylinder is compressed to a small fraction of its initial volume. Toward the end of the compression stroke, combustion is initiated and the cylinder pressure rises more rapidly.
3. *A power stroke*, or expansion stroke, which starts with the piston at TC and ends at BC as the high-temperature, high-pressure gases push the piston down and force the crank to rotate. About five times as much work is done on the piston during the power stroke as the piston had to do during compression. As the piston approaches BC, the exhaust valve opens to initiate the exhaust process and drop the cylinder pressure to close to the exhaust system pressure.
4. *An exhaust stroke*, where, as the piston moves from BC to TC, the remaining burned gases exit the cylinder: first, because the cylinder pressure may be significantly higher than the exhaust pressure; then as these gases are swept out by the piston as it moves toward TC. As the piston approaches TC the inlet valve opens and just after TC the exhaust valve closes. The cycle then starts again.

Figure 1.2 The four-stroke operating cycle.[12]



Though often called the Otto cycle after its inventor, Nicolaus Otto, who built the first engine operating on these principles in 1876, the more descriptive four-stroke nomenclature is preferred.

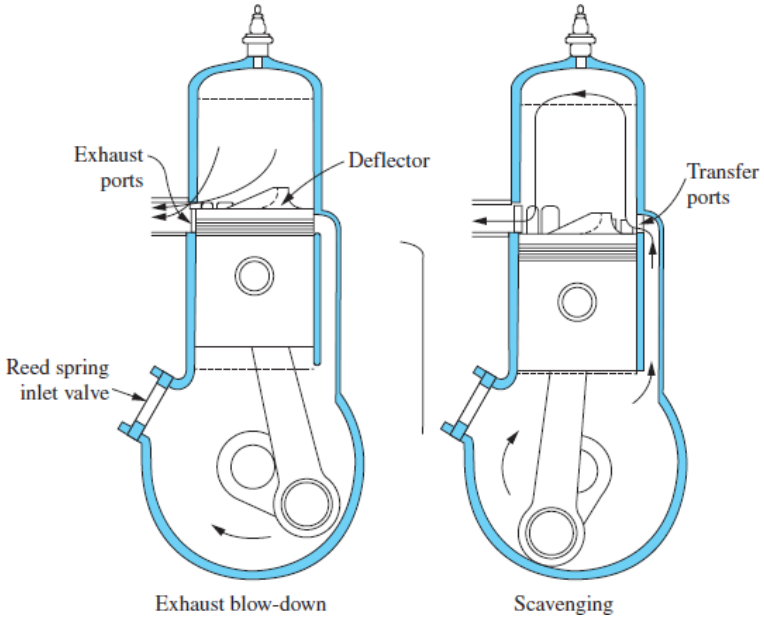
The four-stroke cycle requires, for each engine cylinder, two crankshaft revolutions for each power stroke. To obtain a higher power output from a given engine size, and a simpler valve design, the *two-stroke* cycle was developed. The two-stroke cycle is applicable to both SI and CI engines.

Figure 1.3 shows one of the simplest types of two-stroke engine designs. Ports in the cylinder liner, opened and closed by the piston motion, control the exhaust flow out of the cylinder and the fresh charge flow into the cylinder, while the piston is close to BC. The two strokes are:

1. *A compression stroke*, which starts with the closing of the fresh charge transfer ports and then the exhaust ports, and compresses the cylinder contents as the piston moves up the cylinder, and also draws fresh charge into the crankcase through the inlet Reed valve. As the piston approaches TC, combustion is initiated.
2. *A power or expansion stroke*, similar to that in the four-stroke cycle until the piston approaches BC, when first the exhaust ports and then the transfer ports are uncovered (Fig. 1.3). Most of the burnt gases exit the cylinder in an exhaust blowdown process. When the transfer ports are uncovered, the fresh charge that has been compressed in the crankcase flows into the cylinder. The piston and the ports are generally shaped to deflect the incoming charge from flowing directly into the exhaust ports, and to achieve effective scavenging of the residual in-cylinder burned gases by this fresh charge.

© McGraw-Hill Education. All rights reserved. Any use is subject to the Terms of Use, Privacy Notice and copyright information.

Figure 1.3 The two-stroke operating cycle. A crankcase-scavenged engine is shown.[12]



Each engine cycle with one power stroke is completed in one crankshaft revolution. However, it is difficult to fill completely the displaced volume with fresh charge, and some of the fresh mixture flows directly out of the cylinder during the scavenging process.[2] The example shown is a *cross-scavenged* design; other approaches use *loop-scavenging* or *uniflow* gas exchange processes (see Sec. 6.6).

[1] These crank positions are also referred to as top-dead-center (TDC) and bottom-dead-center (BDC).

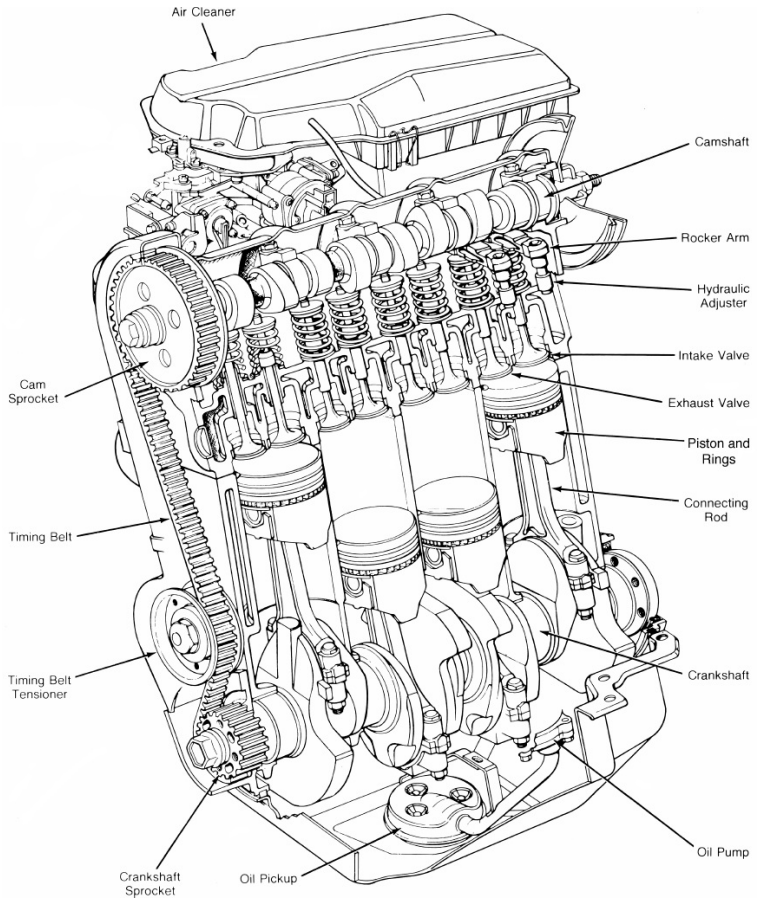
[2] It is primarily for this reason that two-stroke SI engines are at a disadvantage because the lost fresh charge contains fuel and air.

© McGraw-Hill Education. All rights reserved. Any use is subject to the Terms of Use, Privacy Notice and copyright information.

1.4. ENGINE COMPONENTS

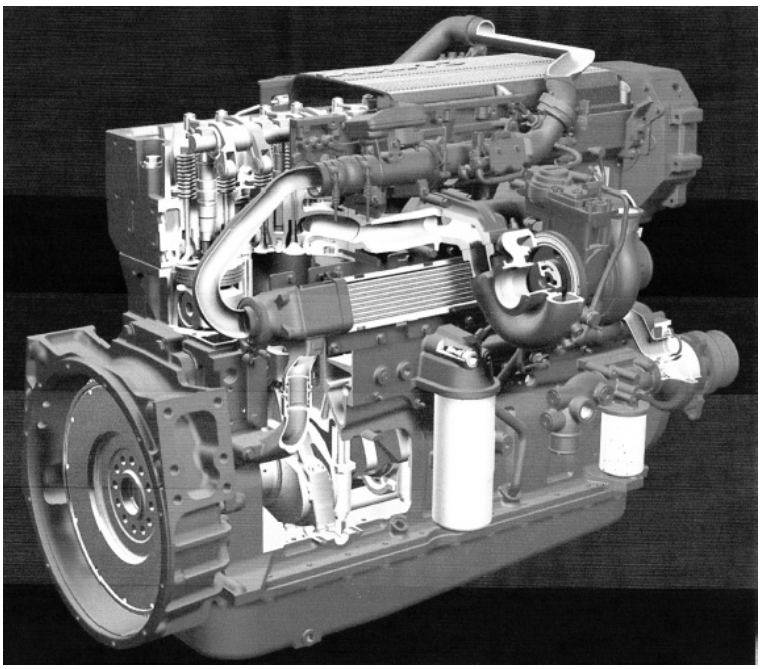
Cutaway drawings of a four-stroke spark-ignition (SI) engine and a diesel (CI) engine are shown in Figs. 1.4 and 1.5, respectively. The SI engine is a four-cylinder in-line automobile engine. The major components are labeled. The diesel is a six-cylinder in-line heavy-duty truck engine. The function of the major components of these engines and their construction materials will now be reviewed.

Figure 1.4 Cutaway drawing of 2.2-liter displacement four-cylinder spark-ignition engine. Bore 87.5 mm, stroke 92 mm, compression ratio 8.9.



© McGraw-Hill Education. All rights reserved. Any use is subject to the Terms of Use, Privacy Notice and copyright information.

Figure 1.5 Cross-section drawing of a four-stroke cycle 6.7-liter in-line six-cylinder turbocharged diesel engine. Bore 107 mm, stroke 124 mm, compression ratio 17.3, maximum torque 1200 N · m at 1600 rev/min, maximum power 285 kW at 2800 rev/min. (Courtesy Cummins Engines.)



The engine cylinders are contained in the engine block. The block has traditionally been made of gray cast iron because of its good wear resistance and low cost, but is often now made of aluminum. Passages for the cooling water are cast into the block. Heavy-duty and truck engines often use removable cylinder sleeves pressed into the block that can be replaced when worn. These are called *wet liners* or *dry liners* depending on whether the sleeve is in direct contact with the cooling water. Aluminum is used in automotive SI engine blocks to reduce engine weight. Iron cylinder liners may be inserted at the casting stage, or later on in the machining and assembly process. The crankcase is often integral with the cylinder block.

The crankshaft has traditionally been a steel forging; nodular cast iron crankshafts are also accepted practice in automotive engines. The crankshaft is supported in main bearings. The number of crankshaft bearings depends largely on the engine's loading and maximum speed. The maximum number of main bearings is one more than the number of cylinders; there may be less. The crank has eccentric portions (crank throws); the connecting rod big-end bearings attach to the crank pin on each throw. Both main and connecting rod bearings use steel-backed precision inserts with bronze, babbit, or aluminum as the bearing materials. The crankcase is sealed at the bottom with a pressed-steel or cast aluminum oil pan, which acts as an oil reservoir for the lubricating system.

Pistons are made of aluminum in smaller engines or cast iron in larger slower-speed engines. The piston both seals the cylinder and transmits the combustion-generated gas pressure to the crank pin via the connecting rod. The connecting rod, usually a steel or alloy forging (though sometimes aluminum), is fastened to the piston by means of a steel piston pin through the rod upper end. The piston pin is usually hollow to reduce its weight.

The oscillating motion of the connecting rod exerts an oscillating force on the cylinder walls via the piston skirt (the region below the piston rings). The piston skirt is usually shaped to provide appropriate thrust surfaces. The piston is fitted with rings that ride in grooves cut in the piston head to seal against gas leakage and control oil flow. The upper ring is the compression ring that is forced outward against the cylinder wall and downward onto the groove face. The lower rings scrape the surplus oil from the cylinder wall to reduce exposure to the hot burned gases, and return it to the crankcase. The crankcase must be ventilated to remove gases that blow by the piston rings, to prevent pressure buildup. The crankcase gases are recycled to the engine intake.

© McGraw-Hill Education. All rights reserved. Any use is subject to the Terms of Use, Privacy Notice and copyright information.

The cylinder head (or heads in V engines) seals off the cylinders and is made of aluminum or cast iron. It must be strong and rigid to distribute the gas forces acting on the head as uniformly as possible through the engine block. The cylinder head contains the spark plug (for an SI engine) or fuel injector (for a CI or direct-injection engine), and, in overhead valve engines, parts of the valve mechanism.

The valves shown in Fig. 1.4 are poppet valves, the valve type normally used in four-stroke engines. The engine shown has one intake and one exhaust valve: most modern engines have four valves per cylinder (two intake and two exhaust valves), or three valves (two intake and one exhaust). Valves are made from forged alloy steel; the cooling of the exhaust valve, which operates at up to about 700°C, may be enhanced by using a hollow stem partially filled with sodium, which through evaporation and condensation carries heat from the hot valve head to the cooler stem. Most modern SI engines have overhead valve locations (sometimes called valve-in-head or I-head configurations) as shown in Fig. 1.4. This geometry leads to a compact combustion chamber with minimum heat losses and flame travel time, and improves the breathing capacity. Older geometries such as the L head where valves are to one side of the cylinder are now only used in small low-cost engines.

The valve stem moves in a valve guide, which can be an integral part of the cylinder head (or engine block for L-head engines), or may be a separate unit pressed into the head (or block). The valve seats may be cut in the head or block metal (if cast iron) or hard steel inserts may be pressed into the head or block. A valve spring, attached to the valve stem with a spring washer and split keeper, holds the valve closed. A valve rotator turns the valves a few degrees on opening to wipe the valve seat, avoid local hot spots, and prevent deposits building up in the valve guide.

A camshaft made of cast iron or forged steel with one cam per valve (or pair of valves in four valves per cylinder engines) is used to open and close the valves. The cam surfaces are hardened to obtain adequate life. In four-stroke cycle engines, camshafts turn at one-half the crankshaft speed. Mechanical or hydraulic lifters or tappets slide in the block and ride or roll on the cam. Depending on valve and camshaft location, additional members are required to transmit the tappet motion to the valve stem; for example, in in-head valve engines with the camshaft at the side, a push rod and rocker arm are used. A trend in high-speed automotive engines is to mount the camshaft over the head with the cams acting either directly or through a pivoted follower on the valve. Also, variable control of valve opening and closing as a function of engine operating conditions, in its simplest form using a camshaft phasing device, is replacing fixed valve timing engine designs. Camshafts are gear, belt, or chain driven from the crankshaft.

An intake manifold (aluminum, cast iron, or plastic) and an exhaust manifold (generally of cast iron) complete the SI engine assembly. Other engine components specific to SI engines—fuel injectors, ignition systems—are described in more detail in the remaining sections in this chapter.

The four-stroke cycle diesel engine shown in Fig. 1.5 is an in-line six-cylinder design commonly used for large trucks. The engine is turbocharged to increase the amount of air that enters the cylinder each cycle. The turbocharger consists of a centrifugal compressor (which compresses the air prior to entry into the cylinder on the same shaft as the exhaust-gas-driven turbine that powers the compressor). In diesel engines, the fuel injectors are mounted in the cylinder head. Diesel fuel-injection systems are discussed in more detail in Sec. 1.8.

© McGraw-Hill Education. All rights reserved. Any use is subject to the Terms of Use, Privacy Notice and copyright information.

1.5. MULTICYLINDER ENGINES

Small engines are used in many applications: for example, lawn mowers, chain saws, in portable power generation, as outboard motorboat engines, and in motorcycles. These are often single-cylinder engines. In the above applications, simplicity and low cost in relation to the power generated are the most important characteristics; fuel consumption, engine vibration, high power to weight or volume ratio, and engine durability are usually less important. A single-cylinder engine gives only one power stroke per revolution (two-stroke cycle) or two revolutions (four-stroke cycle). Hence, the individual cycle torque pulses are widely spaced, and engine vibration and smoothness are significant issues.

Multicylinder configurations are invariably used in practice in all but the smallest engines. As rated power increases, the advantages of smaller cylinders in regard to bulk size, weight, improved engine performance, and engine balance and smoothness all point toward increasing the number of cylinders so the engine's total displaced volume is spread out amongst several smaller cylinders. The increased frequency of power strokes with smaller and increasing number of cylinders produces more frequent and smaller torque pulses, and thus smoother output. The forces in each component are smaller, so structural design requirements are reduced. Multicylinder engines can also achieve a much better state of balance than single-cylinder engines. A force must be applied to each piston to accelerate it during the first half of its travel from BC or TC. The piston then exerts a force on the crankshaft as it decelerates during the second part of the stroke. It is desirable to cancel these inertia forces through the choice of number and arrangement of cylinders to achieve a *primary* balance. Note, however, that the motion of the piston is more rapid during the upper half of its stroke than during the lower half (a consequence of the connecting rod and crank mechanism evident from Fig. 1.1; see also Sec. 2.2). The resulting inequality in acceleration and deceleration of pairs of pistons (one moving up and one moving down) produces corresponding differences in inertia forces generated. Certain combinations of cylinder number and arrangement balance out these *secondary* inertia force effects.

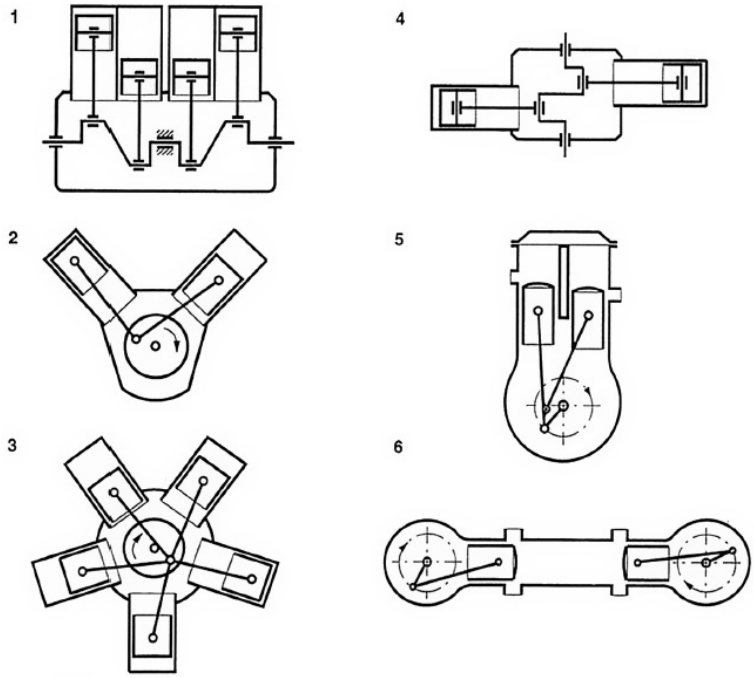
For a given engine displaced volume, the larger the number of cylinders, the higher the engine's maximum power. The reciprocating speed of an engine's pistons is limited by the airflow into each cylinder. Once the flow through the intake valve becomes sonic—reaches the speed of sound—higher piston speeds do not increase airflow. For a given engine displacement, increasing the number of cylinders, and thus reducing their size, raises the crankshaft rotational speed at which this sonic airflow limit is reached. Since engine power is proportional to the engine's rotational (crankshaft) speed, maximum performance is improved.

Other operational issues are affected by cylinder size. The relative importance of heat losses from the in-cylinder gases depends on the relative importance of the combustion chamber surface area to its volume. The SI engine compression-ratio limiting phenomenon called knock is adversely affected by the flame travel distance (spark plug gap to farthest combustion chamber wall).

Common four-stroke multicylinder configurations are shown in Fig. 1.6.[13] These multicylinder configurations normally use equal crankshaft rotation firing intervals between cylinders. In *in-line engines*, the cylinders are arranged in a single plane. Three-, four-, five-, and six-cylinder in-line configurations are used. Four-cylinder in-line engines are the most common arrangement for automobile engines from 1.2 to about 2.5-liter displacement. An example of this in-line arrangement is shown in Fig. 1.4. It is compact—an important consideration for small passenger cars. It provides two torque pulses per revolution of the crankshaft, and primary inertia forces (though not secondary forces) are balanced. Six-cylinder in-line diesel engines are commonly used in the truck market with up to 12-liter displacement.

© McGraw-Hill Education. All rights reserved. Any use is subject to the Terms of Use, Privacy Notice and copyright information.

Figure 1.6 Multicylinder engine configurations: (1) In-line engine; (2) V-engine; (3) Radial engine; (4) Opposed-cylinder engine; (5) U-engine; (6) Opposed-piston engine.[13] (Courtesy Robert Bosch GmbH and SAE.)



The vee (V) arrangement, with two banks of cylinders set at an angle to each other, provides a compact engine block and is used extensively for larger displacement automotive engines. Vee six, eight, ten, and twelve configurations are used. In a V-6 engine, the six cylinders are arranged in two banks of three, usually with a 60° angle between their axis. Six cylinders are normally used in gasoline SI engines in the 2.4- to 3.6-liter displacement range. Six-cylinder engines provide smoother operation with three torque pulses per revolution. The in-line arrangement is fully balanced. However, it gives rise to crankshaft torsional vibration, and also makes even distribution of air to each cylinder more difficult. The V-6 arrangement is more compact than an in-line 6, and provides primary balance of the reciprocating components. With the V-engine, however, a rocking moment is imposed on the crankshaft due to the secondary inertia forces, which results in the engine being less well balanced than the in-line version. The V-8 arrangement, in sizes between 3.2 and 6 or more liters, is commonly used to provide compact, smooth, low-vibration, larger—displacement, SI engines, as are V-10 and V-12 designs.

The radial engine configuration, with cylinders arranged in one or more radial planes, as shown, was common in larger piston-driven aircraft engines. Opposed cylinder engine designs are occasionally used. As Fig. 1.6 indicates, the motion of pairs of pistons with this design is fully balanced. The U-cylinder configuration, where the pistons move in the same direction, and the opposed-piston configuration have been used in special purpose two-stroke engine concepts.

© McGraw-Hill Education. All rights reserved. Any use is subject to the Terms of Use, Privacy Notice and copyright information.

1.6. SPARK-IGNITION ENGINE OPERATION

In SI engines, the fuel must be vaporized and well mixed with the air inducted into the cylinder, prior to combustion. Historically, the fuel flow was metered with a carburetor or single-point fuel-injection system (Fig. 1.7*a*) upstream of the throttle, which controls the airflow. This approach has been superceded by intake-port fuel injection (Fig. 1.7*b*) where a pulsed liquid fuel spray is directed toward the intake valve. Injection of gasoline directly into each cylinder (Fig. 1.7*c*) is now in large-scale production. Moving the point of fuel injection closer to the cylinder enables better dynamic response during engine transients.

Figure 1.7 Different fuel-injection approaches for gasoline spark-ignition engines. (a) Single-point injection; (b) Multipoint port injection; (c) Direct in-cylinder injection. (1) Fuel supply; (2) Air supply; (3) Throttle valve; (4) Intake manifold; (5) Injectors; (6) Engine.[13] (Courtesy Robert Bosch GmbH and SAE.)

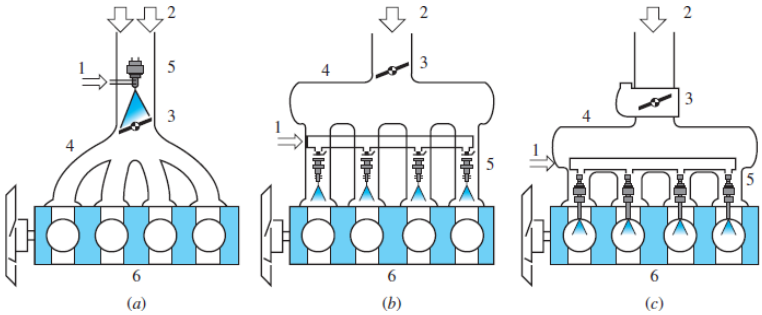
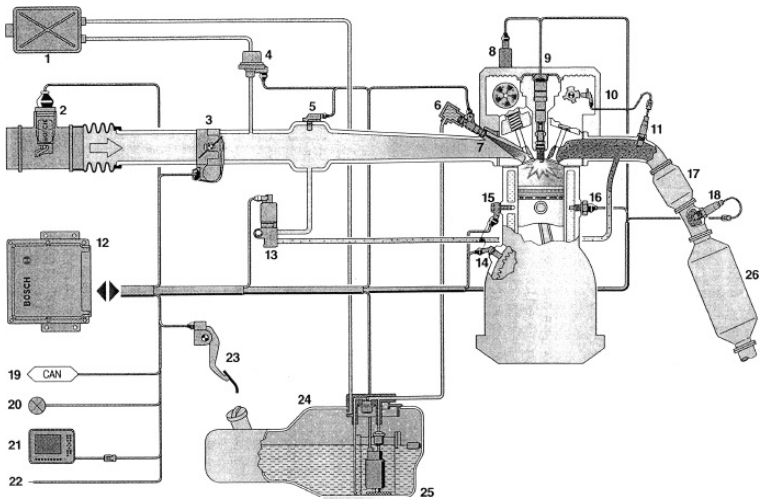


Figure 1.8 shows the layout of a modern SI engine management system. The airflow, fuel flow, exhaust gas characteristics, and engine operating state are all monitored and controlled as shown to provide the desired engine performance with good combustion characteristics, high efficiency, and low exhaust air pollutant emissions. The ratio of mass flow of air to mass flow of fuel must be held approximately constant at about 15 to ensure reliable combustion and facilitate exhaust emissions control. The appropriate fuel flow is determined for the engine airflow in the following manner. The airflow into the intake system is measured with an air mass-flow meter. A throttle valve or plate, which can be opened or closed, controls the airflow. The appropriate amount of fuel required per cylinder per cycle to generate the desired engine output is then determined by the engine control unit. In naturally-aspirated engines, the intake airflow is reduced by throttling to below atmospheric pressure by reducing the flow area when the power required (at any engine speed) is below the maximum, which is obtained when the throttle is wide open.

© McGraw-Hill Education. All rights reserved. Any use is subject to the Terms of Use, Privacy Notice and copyright information.

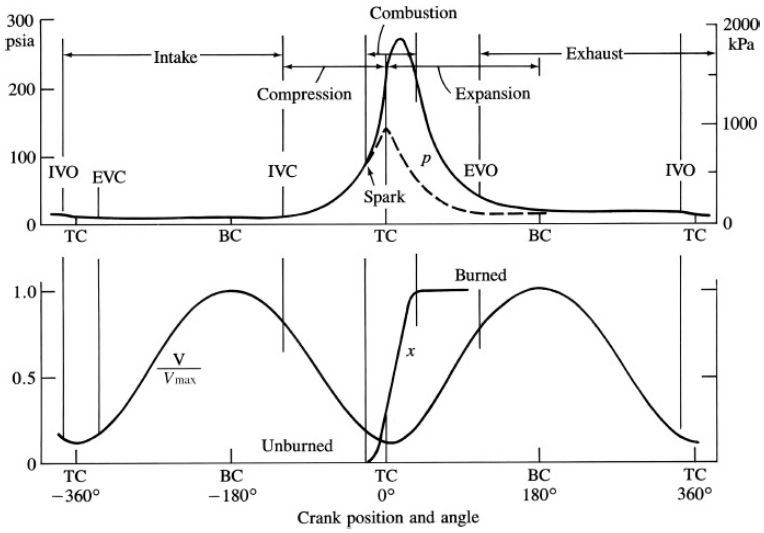
Figure 1.8 Schematic of modern port-injected engine management system (Bosch ME-Motronic system). (1) Carbon fuel-vapor absorbing canister; (2) Hot-film air-mass meter with integrated temperature sensor; (3) Throttle device; (4) Canister-purge valve; (5) Intake-manifold pressure sensor; (6) Fuel-distribution pipe; (7) Injector; (8) Actuators and sensors for variable valve timing; (9) Ignition coil with attached spark plug; (10) Camshaft phase sensor; (11) Lambda oxygen sensor upstream of primary catalytic converter; (12) Engine control unit; (13) Exhaust-gas recirculation valve; (14) Speed sensor; (15) Knock sensor; (16) Engine-temperature sensor; (17) Primary three-way catalytic converter; (18) Lambda oxygen sensor downstream of primary catalytic converter: (19) CAN interface; (20) Fault lamp; (21) Diagnosis interface; (22) Interface to immobilizer control unit; (23) Accelerator-pedal module with pedal-travel sensor; (24) Fuel tank; (25) In-tank unit with electric fuel pump, fuel filter, and fuel-pressure regulator; (26) Main three-way catalytic converter.[13] *(Courtesy Robert Bosch GmbH and SAE.)*



The sequence of events that take place inside the engine cylinder is illustrated in Fig. 1.9. Several variables are plotted against crank angle through the entire four-stroke SI engine cycle. Crank angle is a useful independent variable because the various engine processes occupy almost constant crank angle intervals over a wide range of engine-operating conditions. The figure shows the valve opening and closing angles, and volume relationship, for a typical fixed valve-timing automotive SI engine. To maintain high mixture flows at high engine speeds (and thus high power outputs) the inlet valve, which opens before TC, closes substantially after BC. During intake, the inducted fuel and air mix in the cylinder with the *residual* burned gases remaining from the previous cycle. After the intake valve closes, the cylinder contents are compressed to above atmospheric pressure and temperature as the cylinder volume is reduced. Some heat transfer between the in-cylinder gases and the piston, cylinder head, and cylinder walls occur—first a heating of the gases, then a cooling, but the effect on unburned gas properties is modest.

© McGraw-Hill Education. All rights reserved. Any use is subject to the Terms of Use, Privacy Notice and copyright information.

Figure 1.9 Sequence of events in four-stroke spark-ignition engine-operating cycle. Cylinder pressure p (solid line, firing cycle; dashed line, motored cycle), cylinder volumeV/V_{max}, and mass fraction burned x_b are plotted against crank angle.



Between about 10 and 40 crank angle degrees before TC, an electrical discharge across the spark plug starts the combustion process. Before the desired ignition point, the ignition driver switches a current to the primary circuit of the ignition coil. At the ignition point, the primary winding is interrupted, generating in the secondary ignition coil winding that is connected to the spark plug, a high voltage across the plug electrodes as the magnetic field collapses. This switching is done electronically. A flame develops from the spark discharge, propagates through the mixture of air, fuel, and residual gas in the cylinder, and extinguishes at the combustion chamber walls. The duration of this burning process varies with engine design and operation, but is typically 40 to 60 crank angle degrees, as shown in Fig. 1.9. As fuel-air mixture burns in the flame, the cylinder pressure (solid line in Fig. 1.9) rises above the level due to compression alone (dashed line). This latter curve—called the *motored* cylinder pressure—is the pressure trace obtained from a motored or nonfiring engine.[1] Note that due to differences in the flow pattern and mixture composition between cylinders and within each cylinder, cycle-by-cycle, the development of each combustion process differs somewhat. As a result, the shape of the pressure versus crank angle curve in each cylinder, and cycle-by-cycle, is not exactly the same.

There is an optimum spark timing which, for a given mass of fuel, air, and residual inside the cylinder, gives maximum torque. More advanced (earlier) timing or retarded (later) timing than this optimum gives lower output. Called *maximum brake-torque* (MBT) timing,[2] this optimum timing is an empirical compromise between starting combustion too early in the compression stroke (when the work transfer is *to* the cylinder gases) and completing combustion too late in the expansion stroke (and so lowering peak expansion stroke pressures).

About two-thirds of the way through the expansion stroke, the exhaust valve starts to open. The cylinder pressure is significantly higher than the exhaust manifold pressure and a *blowdown* process occurs. The burned gases flow through the valve into the exhaust port and manifold until the cylinder pressure and exhaust pressure equilibrate. The duration of this process depends on the pressure level in the cylinder. The piston then *displaces* most of the remaining burned gases from the cylinder into the manifold during the exhaust stroke. The exhaust valve opens before the end of the expansion stroke to ensure that the blowdown process does not last too far into the exhaust stroke when the piston travels upwards. The actual timing is a compromise that balances reduced work transfer *to the piston* before BC against reduced work transfer *to the cylinder contents* after BC.

The exhaust valve remains open until just after TC; the intake opens just before TC. The valves are opened and closed slowly to avoid noise and excessive cam wear. To ensure the valves are fully open when piston velocities are at their highest, the valve open periods usually overlap somewhat. If the intake flow is throttled to below exhaust manifold pressure, then backflow

© McGraw-Hill Education. All rights reserved. Any use is subject to the Terms of Use, Privacy Notice and copyright information.

of burned gases from the cylinder into the intake manifold occurs when the intake valve is first opened. During the valve overlap period, backflow of burned gas from the exhaust port into the cylinder occurs.

With variable valve control, the trade-offs that fixed valve timing requires can be relaxed. The simplest approach varies intake and exhaust valve timing by rotating the camshafts to change their phasing relative to the crankshaft. More complex systems vary valve lift as well as varying the valve opening and closing angles. Variable valve control is attractive because it improves maximum engine power (at high speed) and maximum torque at lower speeds, and can improve part-load engine efficiency. It can also be used to control the mass of burned residual gas, and fresh air, trapped in the engine cylinder.

[1] In practice, the intake and compression processes of a firing engine and a motored engine are not the same due to the presence of burned gases from the previous cycle under firing conditions.

[2] MBT timing was traditionally defined as the minimum spark advance for best torque. Since the torque first increases and then decreases as spark timing is advanced, the definition used here is more precise.

© McGraw-Hill Education. All rights reserved. Any use is subject to the Terms of Use, Privacy Notice and copyright information.

1.7. DIFFERENT TYPES OF FOUR-STROKE SI ENGINES

A variety of SI engines are used in practice, depending on the application. Small SI engines are used in many applications: in the home (e.g., lawn mowers, chain saws), in portable power generation, as outboard motorboat engines, and in motorcycles. These are often single—cylinder engines producing a few kW of power. In the above applications, light weight, small bulk, and low cost in relation to the power generated are the most important characteristics; fuel consumption, engine vibration, and engine durability are less important. A single-cylinder engine gives only one power stroke per crank revolution (two-stroke cycle) or two revolutions (four-stroke cycle). Hence, the torque pulses are widely spaced, and engine vibration and smoothness are significant problems.

Multicylinder engines are invariably used in automotive practice. As rated power increases, the advantages of smaller cylinders in regard to size, weight, power density, improved engine balance, and smoothness point toward increasing the number of cylinders per engine: see Sec. 1.5. Multicylinder SI engines (in the power range 25 to 400 kW) are used in cars, light trucks, vans, light-duty commercial vehicles, and in stationary applications to produce mechanical and electrical power. Many of these markets are shared with diesel (CI) engines. Low engine emissions and high operating efficiency are important, especially in these transportation applications. Precise control of fuel and airflow is critical to achieving these objectives. What used to be the dominant fuel metering device—the carburetor—has been superceded by electrically controlled fuel injection into each intake port. Now, injection of the gasoline directly into each engine cylinder is coming into production (Fig. 1.7). Each of these technology steps improves control of the amount of fuel entering each cylinder per cycle, and thus the dynamic response of the engine to changes in load (engine output) and speed.

The work transfer per cycle to each piston depends on the amount of fuel burned per cylinder per cycle, which depends on the amount of fresh air inducted each cycle. Variable valve control over the engine's speed range can be used to increase the mass of air inducted into each cylinder in four-stroke SI engines (especially at low and high speed), and thus increase the wide-open-throttle torque and power. Engine output from a given displacement engine can be increased by boosting—increasing the density of the air supplied to the engine intake by compressing atmospheric air. Thus, compressing the air prior to entry into the cylinder with a supercharger or a turbocharger increases the output from a given displacement engine.

Examples of various types of SI engines in practical use follow to provide the context for reviewing critical engine processes, a primary objective of this text.

1.7.1. Spark-Ignition Engines with Port Fuel Injection

Spark-ignition (SI) engines have traditionally been operated with a premixed fuel vapor/air mixture inside the cylinder, prepared by feeding liquid gasoline into the engine intake. Carburetors were used to meter the fuel flow in proportion to the airflow. This technology has largely been replaced by port fuel injection (see Fig. 1.8) where an injector in each cylinder's intake port or manifold injects a pulsed fuel spray toward the intake valve, once per cycle. The hot valve surface and warm intake port (once the engine has warmed-up) promote rapid evaporation of the liquid fuel, and the airflow through the port(s) past the intake valve(s) and into the cylinder, coupled with the in-cylinder flow and mixing with the hot residual gas, produces a nearly homogeneous mixture by the time combustion starts. Here, we show some examples of SI engines with this method of mixture preparation.

Figure 1.10 shows a small single-cylinder air-cooled SI engine with a displaced volume of 149 cm^3 and power output of 2.8 kW (3.9 hp). The objective of such simple construction SI engines is to produce modest power levels at low cost. A primary benefit of air-cooled, as compared to the water-cooled, engines is lower engine weight. The fins on the cylinder block and head are necessary to increase the external heat-transfer surface area to achieve the required heat rejection. In small engines, such as in Fig. 1.10, natural convection promotes adequate airflow around the outside of the engine. In larger engines, an air blower provides forced air convection over the block. The blower is driven off the driveshaft.

© McGraw-Hill Education. All rights reserved. Any use is subject to the Terms of Use, Privacy Notice and copyright information.

Figure 1.10 Cutaway drawing of single-cylinder air-cooled spark-ignition engine. Displacement 149 cm^3, bore 65 mm, stroke 45 mm, compression ratio 9.2, maximum power 2.8 kW at 3000 rev/min. (Courtesy Kohler Co.)

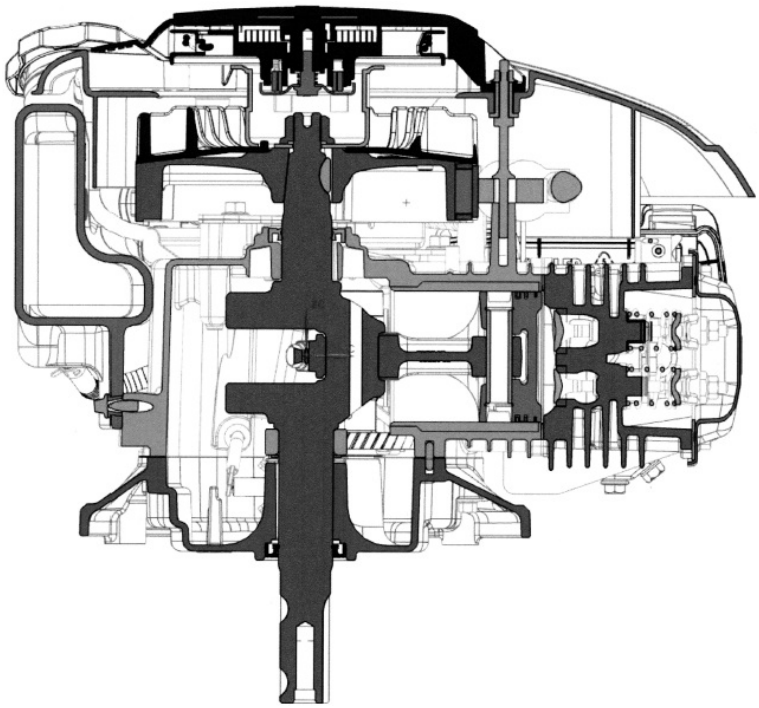
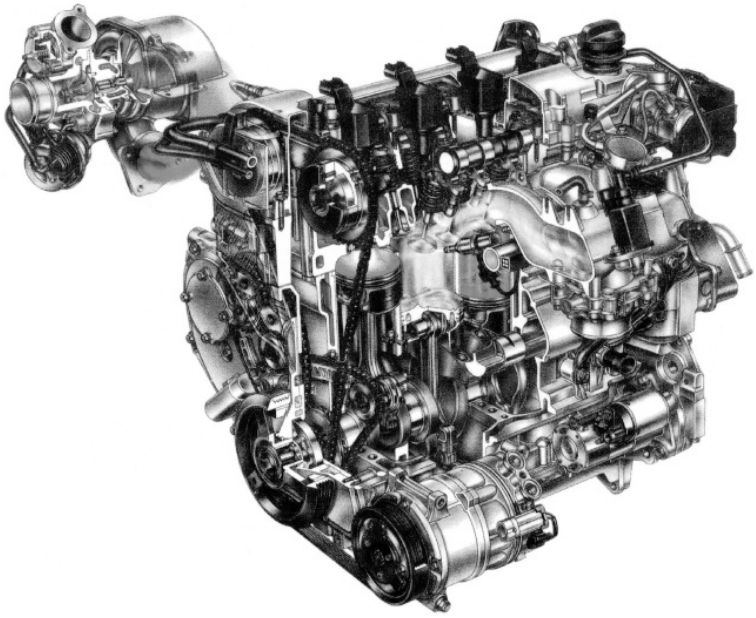


Figure 1.11 shows a turbocharged automobile engine that incorporates many of the features now used to improve engine performance and efficiency. The in-line arrangement with four cylinders provides a compact block, and when turbocharged, increases the power per unit engine displaced volume significantly. This engine features all-aluminum construction, four valves per cylinder, dual overhead camshafts, friction reducing roller finger followers in the valve train, variable phasing on each cam to control the relative phasing of intake and exhaust valves, and piston-cooling oil jets to control piston temperatures in this high-performance engine. Other performance enhancing features now being designed into such automobile engines are cylinder cut out (or displacement on demand) where, for example, in a V-8 engine, at the lighter loads, the valves in half the cylinders are deactivated so only four cylinders provide torque. This reduces the pumping work over the exhaust and intake strokes and thereby improves engine fuel consumption.

© McGraw-Hill Education. All rights reserved. Any use is subject to the Terms of Use, Privacy Notice and copyright information.

Figure 1.11 Cutaway drawing of General Motors four-cylinder turbocharged DI Ecotec gasoline spark-ignition engine. Displacement 2.0 liters, bore 86 mm, stroke 86 mm, compression ratio 9.2, maximum power 187 kW (250 hp) at 5300 rev/min, maximum torque 353 N · m (260 lb · ft) at 2000 rev/min.[14] (Courtesy General Motors Corporation.)



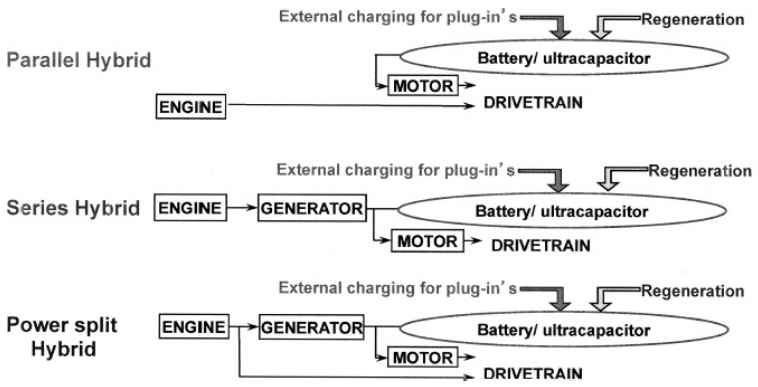
Variable valve control improves engine performance, efficiency, and emissions (see Sec. 6.3.3). The simpler systems used vary the relative phasing of the intake and exhaust valve opening and closing by rotating the camshafts relative to the crankshaft. Valve lift profiles and open duration remain fixed. This is the approach used in the engine shown in Fig. 1.11. (The cam-phasing system is apparent upper center of the engine drawing.) More sophisticated approaches vary valve timing, lift profile, and open duration (e.g., BMW's Valvetronic system[15]). This technology can eliminate the need for throttle valves by accurately controlling the cylinder charging process by intake valve control.

1.7.2. SI Engines for Hybrid Electric Vehicles

The use of internal combustion engines in automotive hybrid propulsion systems is prompting additional SI engine developments. In such a hybrid system, an internal combustion engine, a generator, battery, and electric motor are combined. Figure 1.12 shows three categories of hybrid systems: a*parallel* hybrid, a *series* hybrid, and a *power split* hybrid. In the parallel approach, the engine can drive the wheels directly, the battery can drive via the electric motor, or both can be combined to drive the wheels to obtain a high overall propulsion system efficiency at all loads and speeds.

© McGraw-Hill Education. All rights reserved. Any use is subject to the Terms of Use, Privacy Notice and copyright information.

Figure 1.12 Diagrams of parallel, series, and power split hybrid electric vehicle propulsion systems.



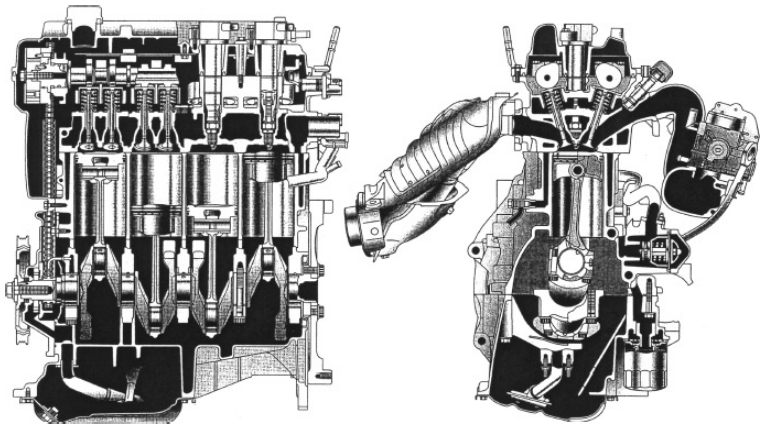
In the series approach, the electric motor drives the vehicle's wheels. The engine can drive through the generator and motor, or recharge the battery via the generator. Since the vehicle is propelled solely by electrical energy, the engine is not coupled to the wheels. Thus its operating conditions are not dependent on the vehicle's operation so it can be operated in its higher efficiency modes. In the power-split system, a planetary gear set is used to transmit power from the engine. This arrangement allows both parallel and series-type operation to be combined. Power from the engine can flow directly to the wheels via the ring of the planetary gear system. Engine power can also flow through the generator, producing electrical power that can drive the wheels through the electric motor.

These hybrid propulsion systems provide increased vehicle drive efficiency relative to direct internal combustion engine drive for three basic reasons. First, *regenerative braking*—applying a braking torque by connecting the generator to the vehicle's wheels is then used to recharge the battery—converts a substantial fraction of the vehicle's kinetic energy as the vehicle slows down to store electrical energy. Second, when the engine is being used, it can operate much of the time at a higher efficiency than would be the case with a stand-alone engine vehicle propulsion system. Third, the battery electric drive mode allows the engine to be shut down when the vehicle is decelerating or idling.

Figure 1.13 shows an SI engine designed specifically for this application. The engine employs a modified version of the four-stroke cycle called the *Atkinson cycle*, where the volume ratio used for expansion is higher than the volume ratio for compression. The engine shown has a displaced volume of 1.5 liters, a geometric (TC to BC) compression/expansion ratio of 13:1, and uses variable valve timing with late intake valve closing during compression and late exhaust valve opening during expansion to achieve a higher effective expansion than compression. This increases engine efficiency. Maximum engine speed is held to 5000 rev/min to minimize the pumping penalties of this Atkinson cycle approach.

© McGraw-Hill Education. All rights reserved. Any use is subject to the Terms of Use, Privacy Notice and copyright information.

Figure 1.13 Four-cylinder Toyota spark-ignition engine designed for a hybrid electric automobile propulsion system.[16] This 1.5-liter (bore = 75 mm, stroke = 84.7 mm), four valves per cylinder, variable valve timing engine uses the Atkinson cycle with a geometric compression/expansion ratio of 13:1. Maximum power is 57 kW (76 hp) at 5000 rev/min. Valve timings are: intake opening 18 to −15° BTC, closing 72 to 105° ABC; exhaust opening 34° BBC, closing 2° ATC.



An alternative to this hybrid electric vehicle (HEV) system, which overall is powered solely by a fuel such as gasoline, is the plug-in hybrid (PHEV) system. Here a larger battery, with some 10 to 30 mile (15 to 50 km) all electric driving range rather than the electric range of a few miles of the HEV system, is used that can be recharged from the electrical grid. Thus the PHEV can be driven with electricity or with a hydrocarbon fuel similarly to an HEV. There is an important but different role for SI engines (and potentially diesels) to play as a key component of these more efficient hybrid systems: the engine preserves the driving flexibility that vehicles require, as the electrification of propulsion systems continues to evolve.

1.7.3. Boosted SI Engines

The work transfer to each piston per cycle that can be obtained from a given displacement engine determines the amount of torque the engine can deliver. This work transfer depends on the amount of fuel that can be burned in each cylinder each cycle. This depends on the amount of fresh air that is inducted into each cylinder each cycle. Increasing the air density prior to its entry into each cylinder thus increases the maximum torque that an engine of a given displacement can deliver. This can be done with a supercharger, a compressor mechanically driven by the engine. More often it is done with a turbocharger, a compressor-turbine combination, which uses the energy available in the engine exhaust stream to provide via the turbine the power required to compress the intake air.

Figure 1.14 shows a cutaway drawing of a turbocharged automobile SI engine, which illustrates how the turbocharger connects with the engine's cylinders. The airflow passes through an air filter (1) into a centrifugal compressor (2) where the radially outward flowing air is compressed by the rotating varies. Next the air flows through an intercooler (3) to reduce the compressed air temperature (further increasing its density), through the intake manifold (4) into the intake port where the fuel is injected, past the intake valve (5), and into the cylinder (6). When the exhaust valve (7) opens, the hot and higher-than-atmospheric pressure exhaust gas flows through the valve and exhaust manifold (8) into the turbine (9). The exhaust gas is directed radially inward and circumferentially at high velocity by vanes (nozzles) onto the turbine wheel's blades where some of the exhaust gas energy is extracted as work or power. The turbine drives the compressor. A wastegate (valve) just upstream of the turbine bypasses some of the exhaust gas flow when necessary to prevent the boost pressure becoming too high. The wastegate linkage (11) is controlled by a boost pressure regulator (12). Figure 1.15 shows a cutaway drawing of a small automotive turbocharger. The arrangement of the compressor and turbine rotors connected via the central shaft and of the turbine and compressor flow passages are evident.

© McGraw-Hill Education. All rights reserved. Any use is subject to the Terms of Use, Privacy Notice and copyright information.

Figure 1.14 Drawing of turbocharger system connected to four-cylinder automobile spark-ignition engine. See text for details. (Courtesy Regie Nationale des Usines.)

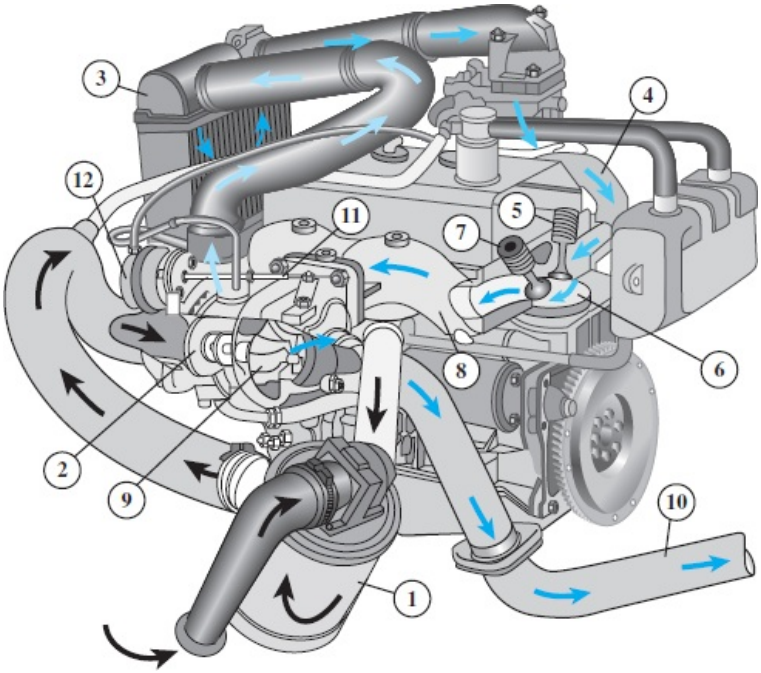
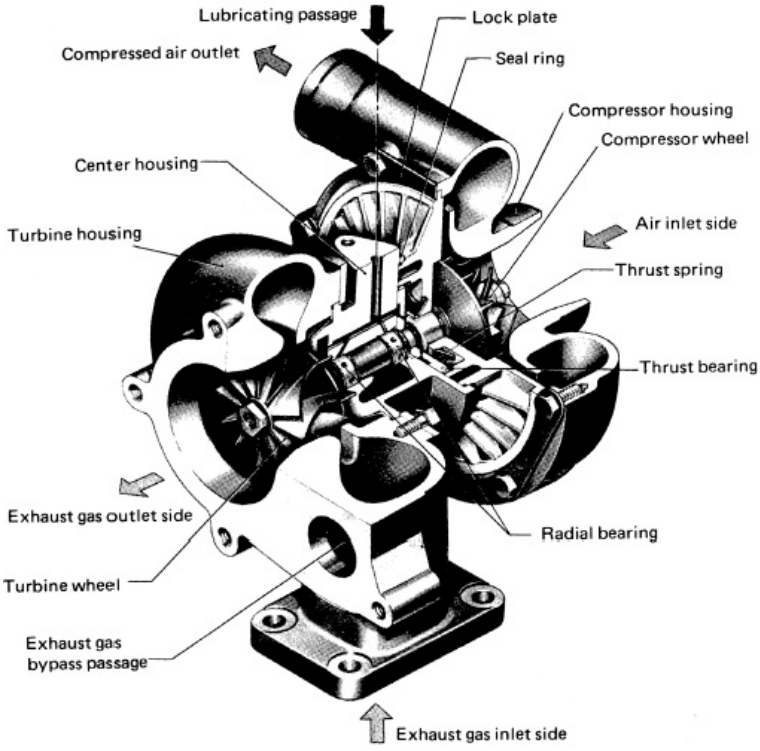


Figure 1.15 Cutaway view of small automotive SI engine turbocharger. (Courtesy Nissan Motor Co. Ltd.)



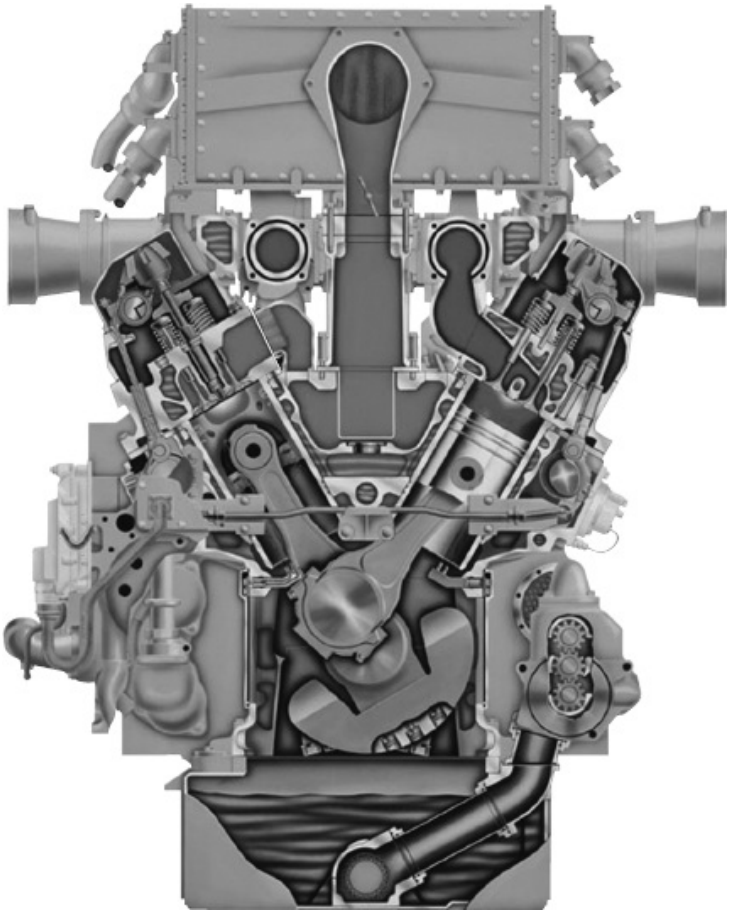
Increasing the intake air density, through boosting, increases the mass of air trapped within the cylinder, the mass of fuel burned, and thus the torque a given size engine can protrude. Torque increases of more than a factor of two can be realized. Turbocharging of SI engines is made difficult by the SI engine's knock constraint. The onset of knock (the rapid spontaneous ignition of a fraction of the in-cylinder fuel-air mixture) during the latter part of combustion) depends on the maximum mixture

© McGraw-Hill Education. All rights reserved. Any use is subject to the Terms of Use, Privacy Notice and copyright information.

temperature and pressure reached inside the engine cylinder, and boosting raises both these variables. Special measures such as reducing the compression ratio, higher octane—better knock resisting—fuels have to be used to control knock. Direct fuel injection into the cylinder (see following section), with its charge-cooling effect, eases this problem.

A different type of boosted SI engine is large natural-gas fueled engines. These are used in electric power generation, propulsion, and marine applications. An example is shown in Fig. 1.16. It uses an encapsulated spark plug with orifices to improve ignition.

Figure 1.16 Large natural-gas-fueled boosted SI engine used in electric power generation. Bore 170 mm, stroke 190 mm, displaced volume per cylinder 4.3 liters, compression ratio 12:1, power (eight cylinders) 965 kW at 1500 rev/min. (Courtesy Caterpillar, Inc.)



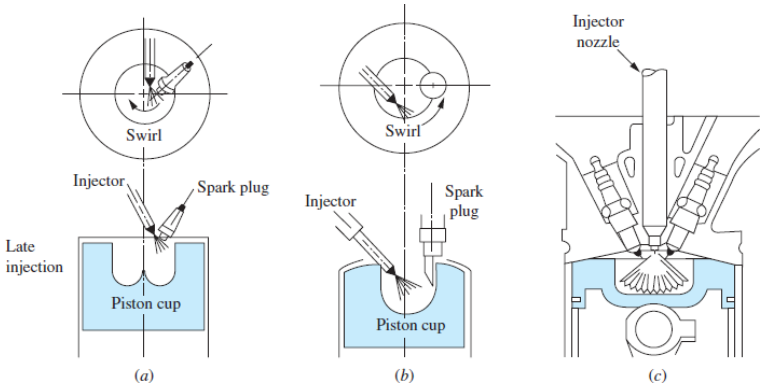
1.7.4. Direct-Injection SI Engines

Since the 1920s, attempts have been made to develop internal combustion engines that combine the best features of the SI engine and the diesel. By injecting the gasoline fuel directly into each cylinder of the engine, better control of the fuel's behavior can be achieved, improving the engine's dynamic performance, permitting use of higher compression ratios, and reducing the losses resulting from throttling the airflow in the standard port-injected SI engine. Diesels are more efficient because they operate close to the optimum compression ratio (14 to 18), operate fuel lean (with excess air), and control engine output by varying the fuel flow rate while leaving the airflow unthrottled. Historically, direct-injection SI engines have often been called *stratified-charge engines* since to realize all these benefits, the mixing process between the evaporating fuel jet and the air in the cylinder must produce a "stratified" or nonuniform fuel-air mixture, with an easily ignitable composition at the spark plug at the time of ignition, and with excess air surrounding the fuel-containing spray.

© McGraw-Hill Education. All rights reserved. Any use is subject to the Terms of Use, Privacy Notice and copyright information.

Over the years, many different types of stratified-charge engine have been proposed; some are now being used in practice.[17] The operating principles of three of these early designs are shown in Fig. 1.17. The combustion chambers are bowl-in-piston designs, and a high degree of air swirl (rotation about the cylinder axis) is created during intake and enhanced in the piston bowl during compression to achieve rapid fuel-air mixing. With the Texaco[18] and MAN[19] systems (Figs. 1.17*a* and *b*), fuel is injected into the cylinder in tangentially into the bowl during the latter stages of compression. A long-duration spark discharge ignites the fuel-air jet as it passes the spark plug; the flame spreads downstream, and consumes the fuel-air mixture. Figure 1.17*c* shows the Ford PROCO system[20] with its centrally located injector and hollow cone spray injected earlier in the compression stroke to get more complete fuel vapor/air mixing, so that high air utilization could be achieved to obtain high outputs.

Figure 1.17 Three historical stratified-charge engines that were developed for production: (a) Texaco Controlled Combustion System (TCCS);[18] (b) M.A.N.-FM Combustion System;[19] (c) Ford PROCO Combustion System.[20]



Modern direct-injection SI engines are often divided in so-called spray-guided, wall-guided, and air-guided categories: see Fig. 1.18. This classification is based on the primary mechanism used to control the development of the fuel spray. In practice, mixture stratification is achieved through a combination of these mechanisms. The Texaco TCCS system in Fig. 1.17*a* and the PROCO system in Fig. 1.17*c* are examples of the former. The MAN system, Fig. 1.17*b*, is primarily wall guided (with air swirl also playing an important role). The Texaco system, Fig. 1.17*a*, is also air guided, with high air swirl generated during intake and augmented by the bowl-in-piston combustion chamber during compression. Many systems with significantly different geometric details are now being developed and employed in production:[17] see Sec. 7.7.2. Generally, spray-guided approaches require a closer spacing between the injector and spark plug electrode location, as shown in Fig. 1.18, to limit the dispersion of the fuel spray and provide substantial mixture stratification. Wider spacing allows more time for fuel-air mixing, produces a more uniform composition spray, but then requires a specific combination of charge motion and wall guiding to achieve the desired spray behavior, and combustion, and emissions characteristics.

Figure 1.18 Illustrations of spray-guided, wall-guided, and air-guided direct-injection SI combustion systems.[17]

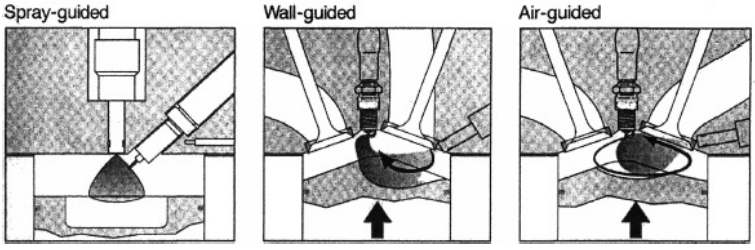
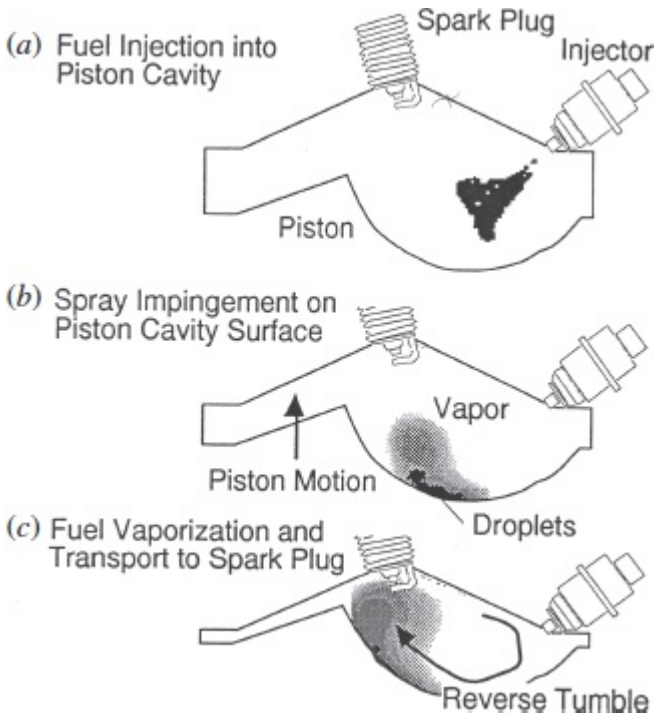


Figure 1.19 shows a production example of a direct-injected (DI) wall-guided system. This Mitsubishi gasoline DI engine used a spherically shaped cavity in the piston crown and an upright intake port to generate a reverse tumbling airflow in the cylinder

© McGraw-Hill Education. All rights reserved. Any use is subject to the Terms of Use, Privacy Notice and copyright information.

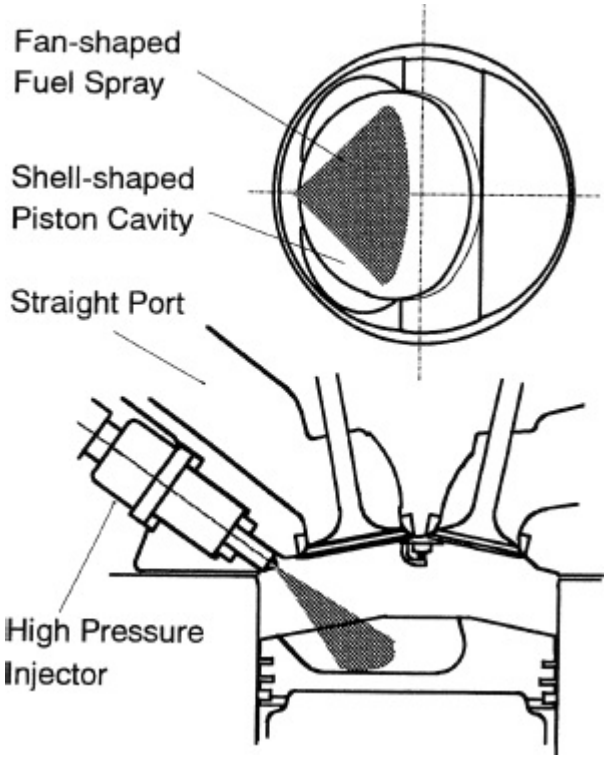
during intake, to "guide" the developing spray toward the spark plug in the center of the cylinder head. Figure 1.20 shows a Toyota direct-injection engine design that uses a fan-shaped fuel spray directed into a shell-shaped bowl in the piston crown to provide rapid air-fuel mixing and fuel vaporization, and by the in-cylinder flow set-up by the straight intake port, to guide the spray so it reaches the spark plug location at the appropriate point in the cycle. To achieve high engine outputs, both these concepts transition from *late injection* (i.e., injection during the latter half of the compression stroke) when stratified operation is desired, to *early injection* (injection during the intake stroke) when essentially complete mixing of the injected fuel with*all* the air in the cylinder is required. This latter mode is called *homogeneous-charge* operation, as distinct from stratified operation.

Figure 1.19 Mitsubishi gasoline direct-injection SI engine design. It uses a wide spacing between injector and spark plug; the spray is guided by the hemispherical piston cavity, and the reverse tumble produced by the upright intake port. In this 1.83-liter, four-cylinder, 12:1 compression ratio engine, the bore is 81 mm and the stroke is 89 mm. The fuel system uses an electromagnetic-controlled high pressure (5 MPa) swirl injector.[21]



© McGraw-Hill Education. All rights reserved. Any use is subject to the Terms of Use, Privacy Notice and copyright information.

Figure 1.20 Toyota gasoline direct-injection SI engine design uses a wide-angle fan-shaped fine-atomization fuel spray injected into a shell-shaped piston cavity to achieve a stratified mixture with late injection, and homogeneous mixture with early (during intake stroke) injection.[22] This concept is also used in Toyota's homogeneous-charge direct-injection engines.



Homogeneous-charge operation at all engine loads and speeds is a viable direct—injection SI engine approach, and is used in production engines. While the efficiency benefit of stratified operation with excess air (which the diesel enjoys) is lost, the in-cylinder charge cooling due to liquid fuel vaporization that increases the amount of air inducted and reduces the propensity of the engine to knock, and the more accurate control of fuel flow during engine transients, are retained. Homogeneous direct-injection engine concepts thus can increase compression ratio and efficiency, increase maximum power, and benefit from the effective emission-control technology that has been developed for port-injected SI engines.

Most production designs of direct-injection engines have used the four-stroke cycle. Direct-injection is, however, especially helpful in controlling fuel carry through in two-stroke cycle engines (see Sec. 1.10). Direct fuel is especially attractive with turbocharged engines to increase their power density. The charge cooling, which evaporation of the in-cylinder fuel spray produces, reduces the engine's propensity to knock.

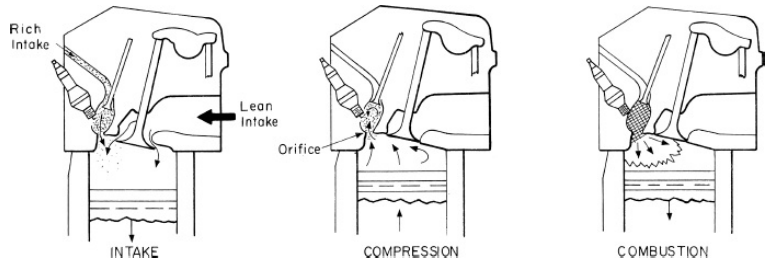
1.7.5. Prechamber SI Engines

An alternative to these open-chamber SI engines described above is a prechamber engine concept, which has been mass produced. It uses a small *prechamber* fed during intake with an auxiliary fuel system to obtain an easily ignitable mixture around the spark plug. This concept, first proposed by Ricardo in the 1920s and extensively developed in the Soviet Union and Japan, is often called a *jet-ignition* or *torch-ignition* stratified-charge engine. Its operating principles are illustrated in Fig. 1.21, which shows a three-valve carbureted version of the concept.[23] A separate carburetor and intake manifold feed a fuel-rich mixture (which contains fuel beyond the amount that can be burned with the available air) through a separate small intake valve into the prechamber that contains the spark plug. At the same time, a lean mixture (which contains excess air beyond that required to burn the fuel completely) is fed to the main combustion chamber through the normal intake manifold. During intake, the rich prechamber flow fully purges the prechamber volume. After intake valve closing, lean mixture from the main

© McGraw-Hill Education. All rights reserved. Any use is subject to the Terms of Use, Privacy Notice and copyright information.

chamber is compressed into the prechamber bringing the mixture at the spark plug to an easily ignitable, slightly rich composition. After combustion starts in the prechamber, rich burning mixture issues as a jet (or series of jets) through one or more orifices into the main chamber, entraining and igniting the lean main chamber charge. This engine is really a jet-ignition concept whose primary function is to extend the operating limit of conventionally ignited SI engines to mixtures leaner than could normally be burned. This approach has been used in large natural gas engines to provide rapid initiation of the combustion process.

Figure 1.21 Schematic of three-valve torch-ignition stratified-charge spark-ignition engine.[23]



1.7.6. Rotary Engines

The reciprocating engine geometry discussed so far dominates the practical world of internal combustion engines. However, motivated by the fact that engine power is delivered through a rotating drive shaft, over the years many rotary engine designs have been proposed.[5] One of these, the Wankel rotary engine[6,7] has and continues to be used in limited production. Its attractive features are its compactness and higher engine speed (which result in high power/weight and power/volume ratios), and its inherent balance and smoothness. These benefits are, however, offset by its higher heat transfer, and the engine's gas sealing and leakage problems.

Figure 1.22 shows the major mechanical parts of a simple single-rotor Wankel engine and illustrates its geometry and operation. There are two rotating parts: the triangular-shaped rotor and the output shaft with its integral eccentric. The rotor revolves directly on the eccentric. The rotor has an internal timing gear, which meshes with the fixed timing gear on one side housing to maintain the correct phase relationship between the rotor and eccentric shaft rotations. Thus the rotor rotates and orbits around the shaft axis. Breathing is through ports in the center housing (and sometimes the side housings). The combustion chamber lies between the center housing and rotor surface and is sealed by seals at each apex of the rotor and around the perimeters of the rotor sides. Figure 1.22 also shows how the Wankel rotary geometry operates with the four-stroke cycle. The figure shows the induction, compression, power, and exhaust processes of the four-stroke cycle for the chamber defined by rotor surface AB. The remaining two chambers defined by the other rotor surfaces undergo exactly the same sequence. As the rotor makes one complete rotation, during which the eccentric shaft rotates through three revolutions, each chamber produces one power "stroke." Three power pulses occur, therefore, for each rotor revolution; thus for each eccentric (output) shaft revolution, there is one torque pulse. Figure 1.23 shows a cutaway drawing of an intake-port injected two-rotor automobile Wankel engine. The two rotors are out of phase to provide a greater number of torque pulses per shaft revolution. Note the combustion chamber cut out in each rotor face, and the rotor apex and side seals. Two spark plugs per firing chamber are often used to obtain a faster combustion process. Large area side intake and exhaust ports are used to increase airflow, and improve burned gas outflow.

© McGraw-Hill Education. All rights reserved. Any use is subject to the Terms of Use, Privacy Notice and copyright information.

Figure 1.22 *(a) Major components of the Wankel rotary engine. (b) Induction, compression, power, and exhaust processes of the four-stroke cycle for the chamber defined by rotor surface AB. (From Mobil Technical Bulletin, Rotary Engines, © Mobil Oil Corporation, 1971)*

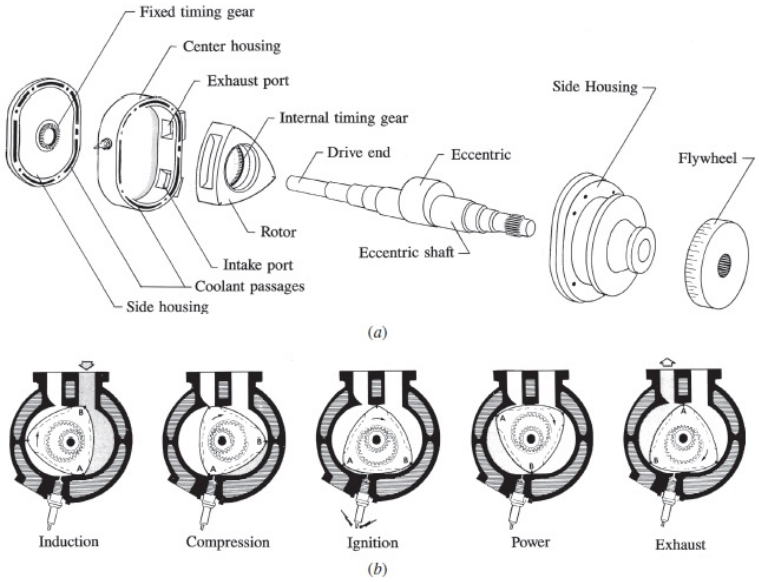
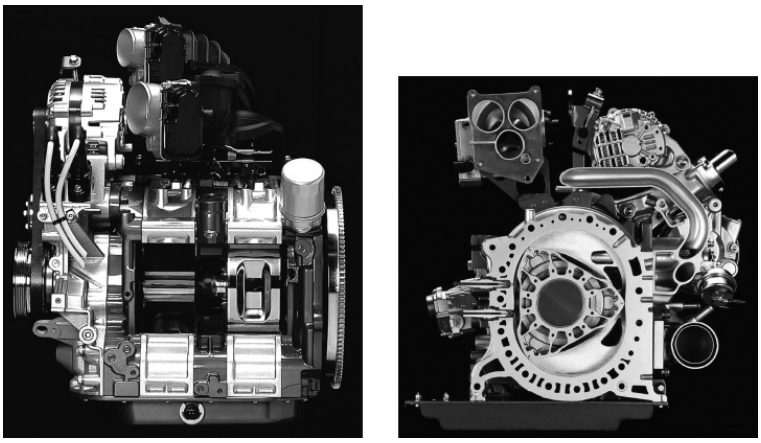


Figure 1.23 *Mazda 1.3-liter RENESIS two-rotor Wankel rotary engine. Compression ratio 10:1, 15-mm eccentricity (offset between eccentric shaft axis and rotor centerlines), 105-mm generating radius (distance between rotor centerline and apex), trochaic (rotor) chamber width is 80 mm, giving 654 cm^3 displaced volume for each rotor chamber (1308 cm^3 total). Produces 184 kW at 8200 rev/min and 216 N · m of torque at 5500 rev/min.[24] (Courtesy Mazda Motor Co.)*



© McGraw-Hill Education. All rights reserved. Any use is subject to the Terms of Use, Privacy Notice and copyright information.

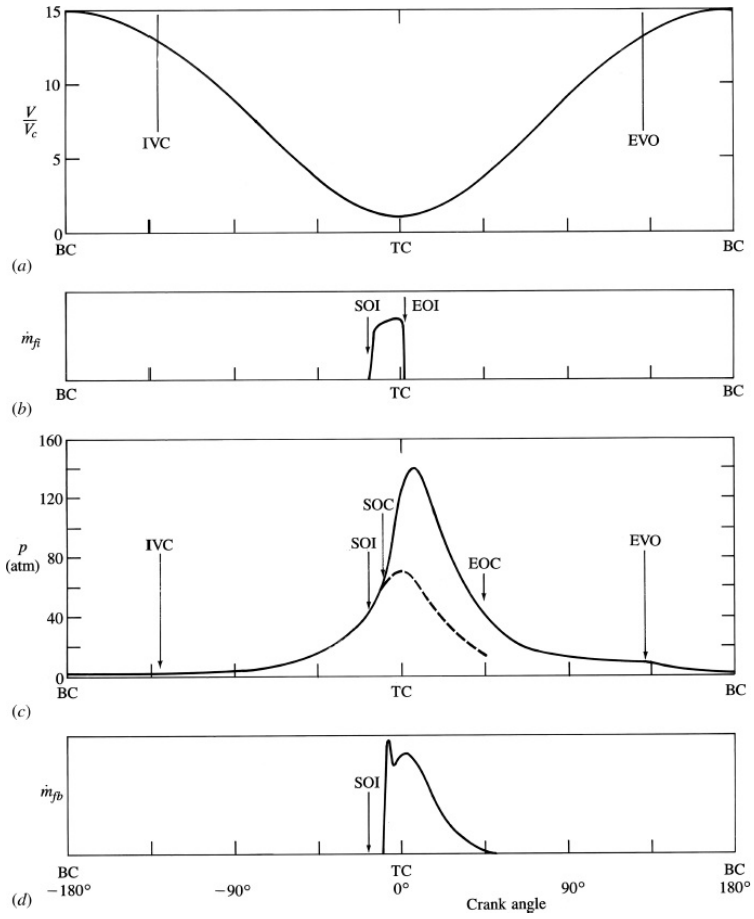
1.8. COMPRESSION-IGNITION ENGINE OPERATION

In compression-ignition or diesel engines, air alone is drawn into the cylinder during intake. The fuel (in most applications a light fuel oil, though heated residual fuel is used in large marine and power-generating diesels) is injected directly into each cylinder just before the combustion process is required to start. Load control is achieved by varying the amount of fuel injected each cycle; the airflow at a given engine speed is not directly controlled, and in naturally-aspirated engines is essentially unchanged. There are a great variety of CI engine designs in use in a wide range of applications—automobile, truck, locomotive, marine, power generation. Both naturally-aspirated engines where atmospheric air is inducted, and boosted engines where the inlet air is compressed by a turbocharger—an exhaust-driven turbine-compressor combination—are common. Turbocharging increases engine output by increasing the air mass flow per unit displaced volume, thereby allowing an increase in fuel flow. These devices are used to reduce engine size and weight for a given power output. In large engine sizes, the two-stroke cycle is competitive with the four-stroke cycle because in these large low-speed engines, the cylinder can be scavenged more effectively and, with the diesel's direct fuel injection, only air is lost in the scavenging process.

The operation of a typical four-stroke naturally-aspirated CI engine is illustrated in Fig. 1.24. The compression ratio of diesels is much higher than typical SI engine values, and is in the range 14 to 22, depending on the type of diesel engine and whether the engine is naturally aspirated or turbocharged. The valve timings used are similar to those of SI engines. In a naturally-aspirated engine, air at close-to-atmospheric pressure is inducted during the intake stroke and then compressed to a pressure of about 5 MPa (50 atm) and temperature of about 900 K (600°C) during the compression stroke. At about 20 crank angle degrees before TC, fuel injection into the engine cylinder commences; a typical rate of injection profile is shown in Fig. 1.24*b*. Usually there are four to eight or more liquid fuel jets; each jet exiting the injector nozzle atomizes into drops and entrains air to form a set of sprays that penetrate into the bowl-in-piston combustion chamber, as shown in Fig. 1.25. In each spray, the liquid fuel drops evaporate, and the fuel vapor then mixes with the entrained air. The fuel-vapor air mixture temperature and pressure are above the ignition point where fuel oxidation chemistry can occur. Thus, after a short *delay period*, spontaneous ignition (autoignition) of parts of the nonuniform fuel-air mixture within these sprays initiates the combustion process, and the cylinder pressure (solid line in Fig. 1.24*c*) rises above the nonfiring engine level as fuel chemical energy is released. A diffusion flame then spreads rapidly to surround each fuel spray, with partly reacted fuel-air mixture in the spray on the inside of the flame, and the additional air in the cylinder on the outside. As the expansion process proceeds, mixing between fuel vapor, air, and burning gases continues, accompanied by further combustion (Fig. 1.24*d*). At full load, the mass of fuel injected is about 5% of the mass of air in the cylinder. At higher fueling levels, increasing amounts of black smoke in the exhaust limit the quantity of fuel that can be burned efficiently. The exhaust process is similar to that of the four-stroke SI engine: a rapid outflow or blowdown of burned gases as soon as the exhaust valves start opening, followed by displacement of the remaining burned gases from the cylinder during the exhaust stroke. At the end of the exhaust stroke, the cycle starts again.

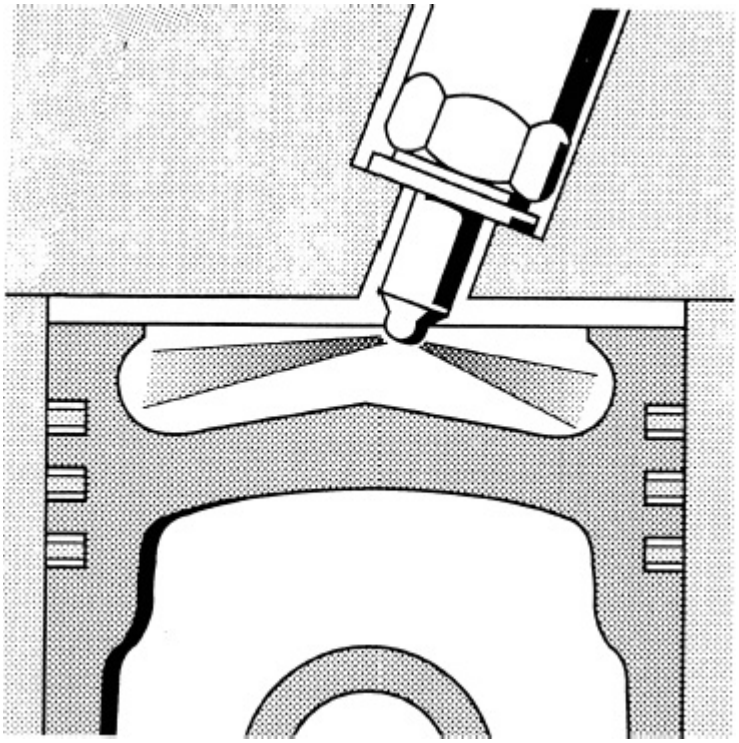
© McGraw-Hill Education. All rights reserved. Any use is subject to the Terms of Use, Privacy Notice and copyright information.

Figure 1.24 Sequence of events during compression, combustion, and expansion processes of a naturally-aspirated compression-ignition engine operating cycle. (a) Cylinder volume/clearance volume V/V_c, (b) rate of fuel injection $\dot{m}_{fi}$, (c) cylinder pressure p (solid line, firing cycle; dashed line, motored cycle), and (d) rate of fuel burning (or fuel chemical energy release rate) $\dot{m}_{fb}$ are plotted against crank angle.



© McGraw-Hill Education. All rights reserved. Any use is subject to the Terms of Use, Privacy Notice and copyright information.

Figure 1.25 *Schematic of diesel engine fuel sprays, formed from liquid fuel jets injected at high pressure through individual injection nozzle holes, penetrating the diesel bowl-in-piston combustion chamber.*



In this diesel combustion process, the fuel is injected directly into the engine cylinder at a pressure of between several hundred and more than 2000 bar.[25] The diesel fuel-injection system consists of a low-pressure pump, and a high-pressure injection pump, delivery pipes, and fuel injector nozzles. Several different types of injection pumps and nozzles are used. In one common system shown in Fig. 1.26, an in-line pump containing a set of cam-driven plungers (one for each cylinder) operate in closely fitting barrels. Early in the stroke of the plunger, the inlet port is closed and the fuel trapped above the plunger is forced through a check valve into the injection line. The injection nozzle (Fig. 1.27) has one or more holes through which the fuel sprays into the cylinder. A spring-loaded valve closes these holes until the pressure in the injection line, acting on part of the valve surface, overcomes the spring force and opens the valve. Injection starts shortly after the line pressure begins to rise. Thus, the phasing of the pump camshaft relative to the engine crankshaft controls the start of injection. Injection is stopped when the inlet port of the pump is uncovered by a helical groove in the pump plunger, because the high pressure above the plunger is then released (Fig. 1.27, bottom). The amount of fuel injected (which controls the load) is determined by the injection pump cam design and the position of the helical groove. Thus for a given cam design, rotating the plunger and its helical groove varies the load.

© McGraw-Hill Education. All rights reserved. Any use is subject to the Terms of Use, Privacy Notice and copyright information.

Figure 1.26 Diesel fuel system with in-line fuel-injection pump.[25] (Courtesy Robert Bosch GmbH and SAE.)

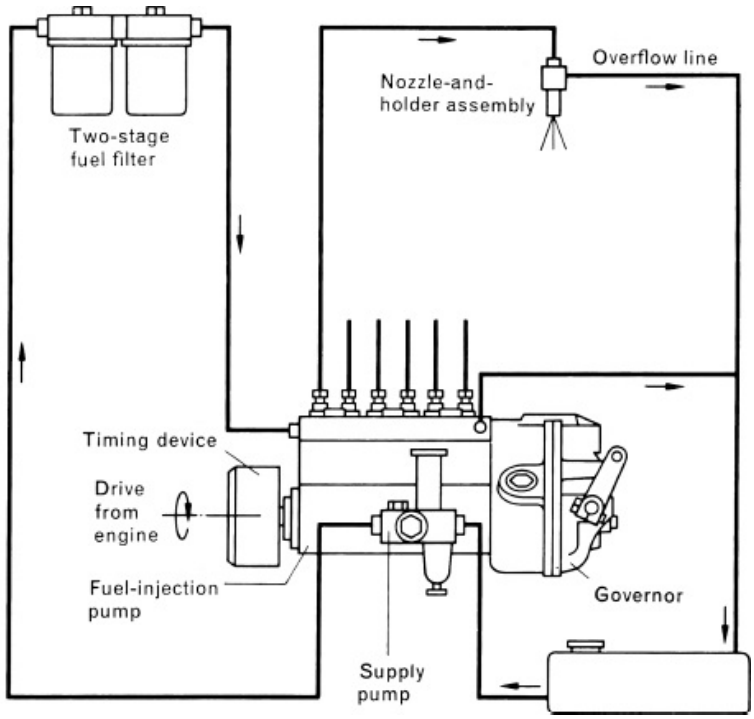
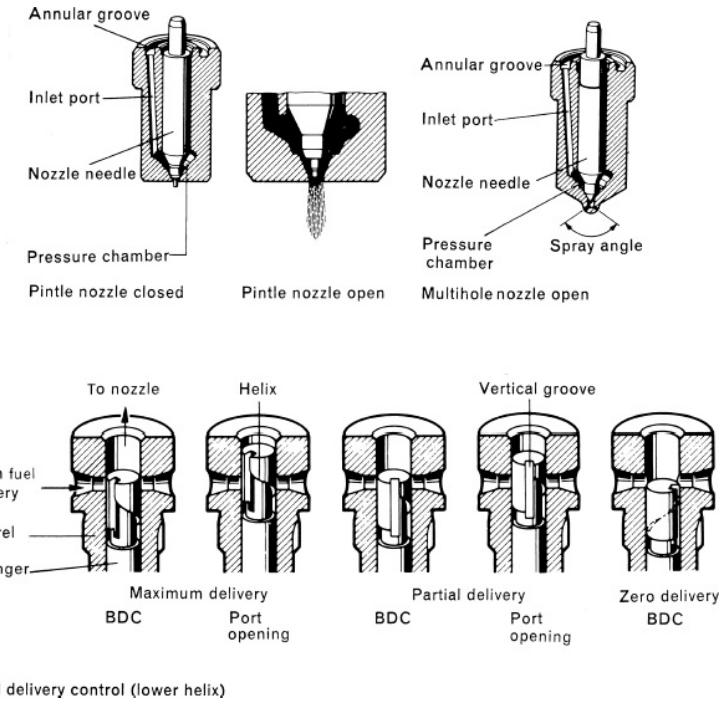


Figure 1.27 Details of fuel-injection nozzles and fuel-delivery control.[26] (Courtesy Robert Bosch GmbH and SAE.)



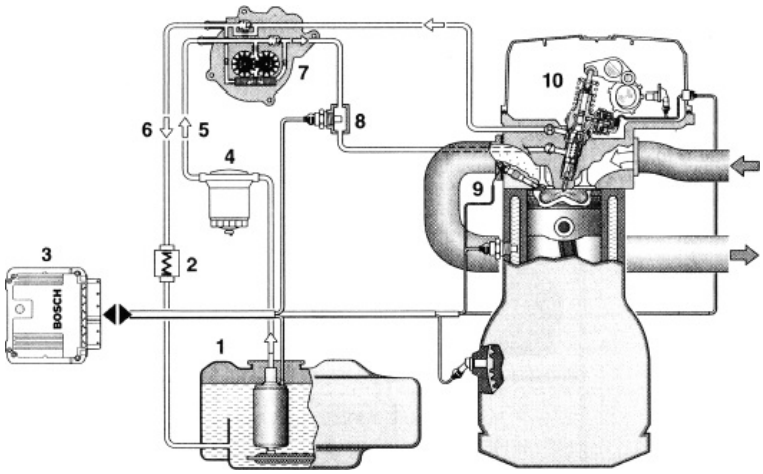
In smaller diesel engines, distributor-type fuel pumps are often used. These have one pump plunger and barrel, which meters and distributes the fuel to all the injection nozzles. The unit contains a high-pressure injection pump, an overspeed governor, and an injection timer. High pressure is generated by the plunger, which is made to describe a combined rotary and stroke movement. This rotary motion distributes the fuel to the individual injection nozzles. Distributor pumps can operate at higher

© McGraw-Hill Education. All rights reserved. Any use is subject to the Terms of Use, Privacy Notice and copyright information.

speed and take up less space than in-line pumps. They are normally used on smaller three- to six-cylinder diesel engines. In-line pumps are used in larger, midsize engines.

An alternative fuel-injection approach uses individual single-barrel injection pumps, close mounted to each cylinder with an external drive. These unit injector systems (UIS) combine the pump and injector into a single unit. Figure 1.28 illustrates how this system operates. The unit is driven by the engine camshaft, and the start of injection and injected fuel quantity are controlled by a solenoid valve in the injector. With this type of system, very high injection pressures (some 2000 bar) are achieved along with precise control of the amount and timing of injection.

Figure 1.28 Diesel fuel-injection system with unit injector (for passenger cars). (1) Fuel tank with fuel supply pump; (2) Fuel cooler; (3) Electronic control unit; (4) Fuel filter; (5) Fuel feed line; (6) Fuel return line; (7) Tandem pump; (8) Fuel-temperature sensors; (9) Glow plug; (10) Injector.[26] (Courtesy Robert Bosch GmbH and SAE.)



Common rail (or fuel accumulation) injection systems allow greater freedom to control the fuel-injection process, and thus combustion. The functions of fuel pressure generation and fuel injection are separated by an accumulator or common rail. Figure 1.29 shows the system layout. The high-pressure pump feeds the common rail, which feeds each of the injectors. Control of this system can readily be integrated with other engine parameters as indicated. Injection pressures of 1400 to 1800 bar can be achieved. By repeated activation of the fast-acting solenoid valve within the injector, multiple injection pulses in each injection cycle can be realized. It is often advantageous to use a short *pilot injection* before the main injection, to initiate combustion with a small amount of fuel, and reduce engine noise. Multiple pulse main injections can help control emissions. Both solenoid-controlled injectors and piezo-actuated injectors are used. Figure 1.30 shows a piezoelectric injector that provides more precise control of injection pulses and improves fuel atomization within the cylinder.

© McGraw-Hill Education. All rights reserved. Any use is subject to the Terms of Use, Privacy Notice and copyright information.

Figure 1.29 *Common rail accumulator fuel-injection system on a four-cylinder automobile diesel.[25] (1) Air-mass flow meter; (2) Electronic control unit; (3) High-pressure pump; (4) High-pressure accumulator (rail); (5) Injectors; (6) Crankshaft speed sensor; (7) Coolant temperature sensor; (8) Fuel filter; (9) Accelerator-pedal sensor. (Courtesy Robert Bosch GmbH and SAE.)*

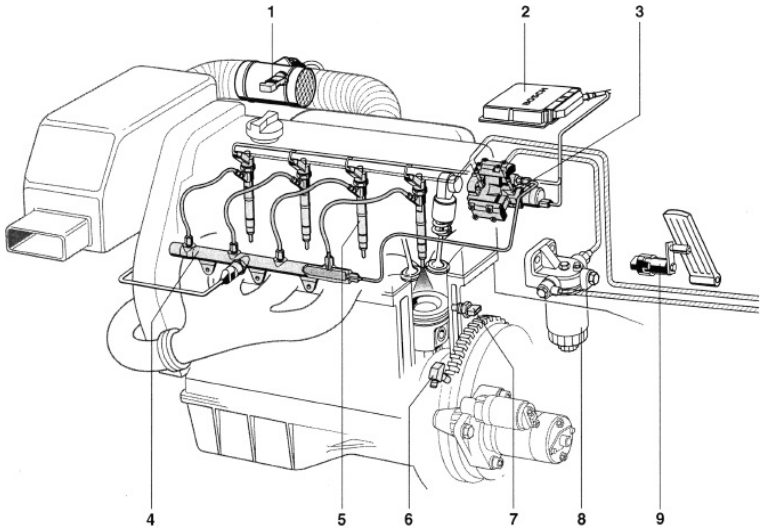
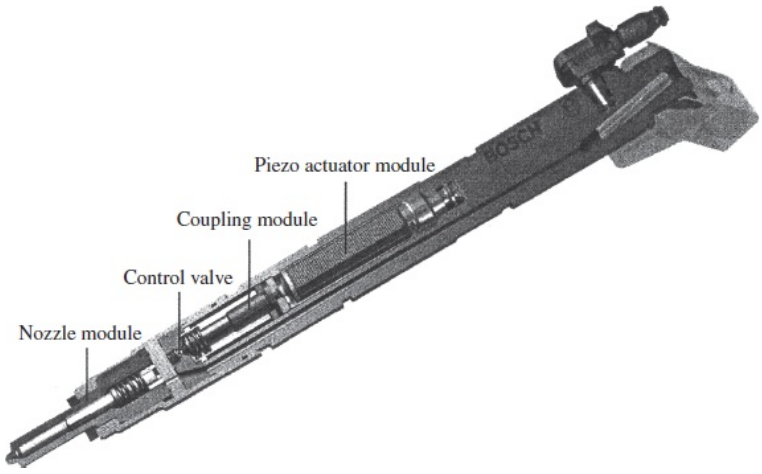


Figure 1.30 *Bosch piezoelectric fuel injector that provides more precise fuel injection control on opening and closing, and finer atomization.[27] (Courtesy Robert Bosch GmbH and SAE.)*



© McGraw-Hill Education. All rights reserved. Any use is subject to the Terms of Use, Privacy Notice and copyright information.

1.9. DIFFERENT TYPES OF DIESEL ENGINES

A large number of diesel engine configurations and designs are in common use. The largest marine and stationary power-generating diesels are two-stroke cycle engines and are discussed in the next section, 1.10. Small- and medium-size diesel engines use the four-stroke cycle. Because air capacity is an important constraint on the amount of fuel that can be burned in the diesel engine, and therefore on power, turbocharging is used extensively. Larger engines are almost always turbocharged. Small low-cost diesels are not usually turbocharged. The details of the engine design also vary significantly over the diesel size range. In particular, different combustion chamber geometries and fuel-injection characteristics are required to deal effectively with a major diesel engine design problem: achieving sufficiently rapid fuel-air mixing rates to complete the fuel-burning process in the short time available. Smaller engines run at higher maximum speeds. Thus, a wide variety of inlet port geometries, cylinder head and piston cavity or bowl shapes, and fuel-injection patterns are used to achieve the airflows and fuel flows needed to accomplish fast enough combustion over the diesel size range.

Figure 1.31 shows a diesel engine typical of the heavy-duty truck application. The design shown is a six-cylinder in-line engine. The drawing indicates that diesel engines are generally substantially more rugged and heavier than SI engines because stress levels are higher due to the significantly higher pressure levels of the diesel cycle. The engine shown has a displacement of 12.9 liters, a compression ratio of 16.5, and is turbocharged. This type of diesel is called a *direct-injection* diesel since the fuel is injected directly into a combustion chamber above the piston crown. The combustion chamber shown is a "bowl-in-piston" design, which puts most of the clearance volume into a compact cavity in the piston crown. With this type of diesel engine, it is often necessary to use a swirling airflow rotating about the cylinder axis, which is created by suitable design of the inlet port and valve, to achieve fast enough fuel-air mixing and fuel-burning rates. The fuel injector, shown on the cylinder axis in the drawing, has a multihole nozzle. It typically has four to six holes in this application. The fuel jets move out radially from the nozzle holes close to the center of the piston bowl into the (swirling) airflow.

Figure 1.31 Six-cylinder 12.9-liter turbocharged direct-injection truck diesel engine: transverse and longitudinal sections. Bore 135 mm, stroke 150 mm, compression ratio 16:1, governed speed 2100 rev/min, maximum output 294 kW, maximum torque 1667 N · m at 1300 rev/min.[28]

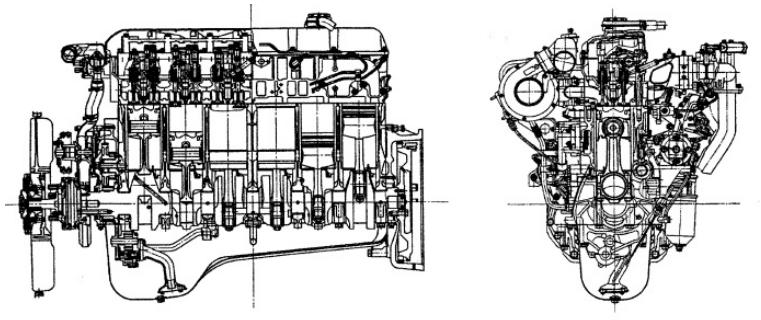
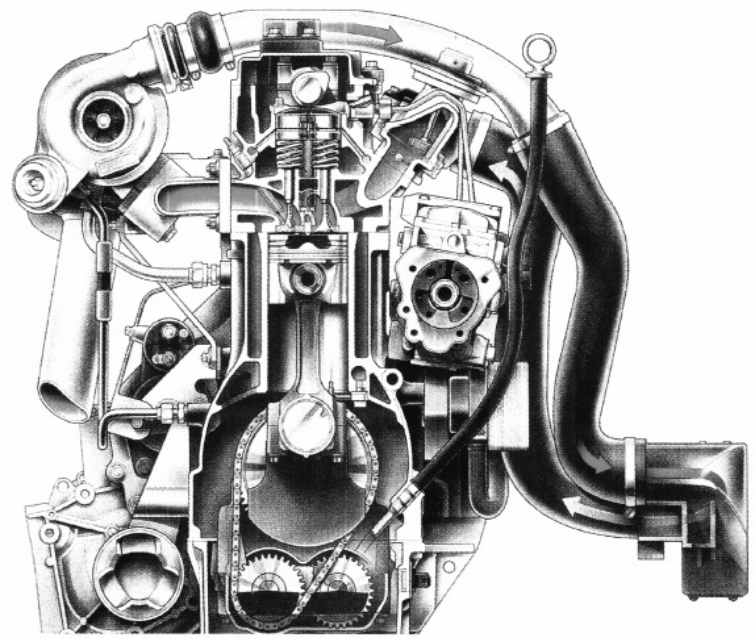


Figure 1.32 shows a 2.2-liter four-cylinder high-speed direct-injection (HSDI) diesel typical of those used in automobiles. It has four valves per cylinder, with the fuel injector and bowl-in-piston combustion chamber centered on each cylinder axis. These types of engines are highly boosted to give high torque at low- to mid-engine speeds per unit displaced cylinder volume. The compressor exit air, cooled in a heat exchanger, enters the cylinder via intake ports that generate swirl about the cylinder axis. During the compression stroke, the flow of this swirling air into the reentrant bowl-in-piston significantly enhances the swirl, thereby achieving high rates of mixing of air with the injected fuel sprays close to top center. Maximum rated speeds (4500 to 5000 rev/min) are lower than maximum speeds of gasoline SI engines due to fuel-air mixing rate limitations. The compression ratio of these HSDI engines is 18 to 20:1, somewhat above the value that gives maximum engine efficiency. This is done to obtain higher air compression temperatures to enable cold engine starting at low cranking speeds. An electrically heated ceramic *glow plug* is usually inserted through the cylinder head in these size engines to assist the cold starting process.

© McGraw-Hill Education. All rights reserved. Any use is subject to the Terms of Use, Privacy Notice and copyright information.

Figure 1.32 Small 2.2-liter four-cylinder high-speed direct-injection automobile diesel engine: maximum power 93 kW; maximum torque 285 N · m at 1750 rev/min; maximum boost 0.9 bar (gauge); compression ratio 18.5. (Courtesy SAE and Saab.)



The smallest diesels operate at higher engine speeds than do larger engines: hence the time available for burning the fuel is less and the fuel-injection and combustion systems must achieve faster fuel-air mixing rates. Figure 1.32 shows how this rapid combustion is realized in HSDI diesels. Historically, in the smallest sizes diesel engines, this can be accomplished by using an *indirect-injection* or prechamber type of diesel. Fuel is injected into an auxiliary combustion chamber that is separated from the main combustion chamber above the piston by a passageway or nozzle. During the latter stages of the compression process, air is forced through this nozzle from the cylinder into the prechamber at high velocity. Fuel is injected into the highly turbulent and often rapidly swirling flow in this prechamber, and very high fuel-air mixing rates are achieved. Combustion starts in the prechamber, and the resulting pressure rise in the prechamber forces burning gases, fuel, and air into the main chamber. Since this outflow is also extremely vigorous, rapid mixing then occurs in the main chamber as the burning jet exiting the prechamber mixes with the remaining air and combustion is completed. A glow plug is also shown in the auxiliary chamber; this plug is electrically heated during cold engine start-up to raise the temperature of the air charge and the fuel sufficiently to achieve autoignition. The compression ratio of this engine is high—around 20. Indirect-injection diesel engines require higher compression ratios than direct-injection engines to start adequately when cold.

© McGraw-Hill Education. All rights reserved. Any use is subject to the Terms of Use, Privacy Notice and copyright information.

1.10. TWO-STROKE CYCLE ENGINE OPERATION

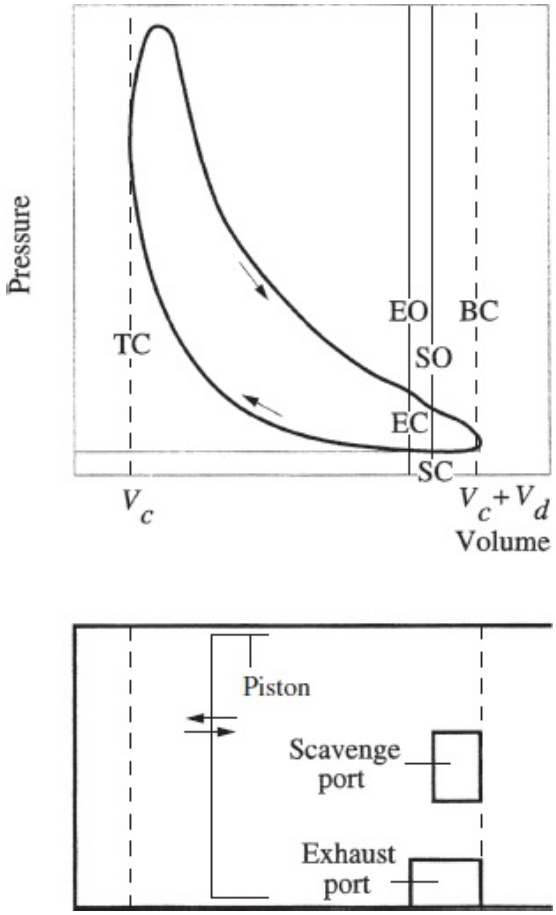
The two-stroke engine is used at the small-size and very large-size ends of the engine market. In small sizes, the two-stroke cycle SI engine is cheap, compact and light, simple, and robust. This is the basis of its market appeal in mopeds, scooters, motorcycles, and snowmobiles, in portable devices such as chain-saws and bush cutters, in agricultural and construction devices such as lawn mowers, disc saws, and snow blowers, in the outboard marine engine arena, and in light and in remotely piloted aircraft. The very large diesel engines used in marine and power-generation applications are also two-stroke cycle engines. These large internal combustion engines are the most efficient and cost effective prime movers currently available. The two-stroke diesel has also been used in the locomotive and in parts of the truck market.[29,30] The passenger-car and truck engine markets are now, however, dominated by four-stroke cycle engines.

Key operating features of the two-stroke cycle are its power stroke every crankshaft revolution and its scavenging of the burned gases from the engine cylinder with fresh charge. Doubling the number of power strokes per unit time relative to the four-stroke cycle increases the power output per unit displaced volume. It does not, however, increase by a factor of two. The outputs of two-stroke engines range from only 20% to 60% above those of equivalent-size four-stroke units. This lower increase in practice is a result of the poorer than ideal charging efficiency, that is, incomplete filling of the cylinder volume with fresh air due to incomplete scavenging of the residual burned gases. Doubling the number of power strokes per unit time also halves the intervals between combustion-generated pressure impulses. This results in a smoother crankshaft torque versus time profile.

The two-stroke cycle's process of scavenging the burned gases from the engine cylinder with fresh charge—its gas exchange process—has several consequences. First, charging losses are inevitable. Under higher load conditions, in a typical small two-stroke engine, some 20% or more of the fresh charge that enters the cylinder is lost due to short-circuiting to the exhaust. When the fuel is mixed with air prior to cylinder entry, this process results in very high hydrocarbon emissions and poor fuel consumption compared with the four-stroke cycle engine. However, as both exhaust and charging occur around BC, the exhaust and intake ports can be situated near the bottom end of the cylinder and can be covered and uncovered by a long-skirt piston (see Fig. 1.33). This simple geometric two-stroke cycle configuration obviates the need for valves and their actuating gear. It also substantially simplifies the engine structure and the production process, and significantly reduces engine cost.

© McGraw-Hill Education. All rights reserved. Any use is subject to the Terms of Use, Privacy Notice and copyright information.

Figure 1.33 *Cylinder-pressure versus cylinder-volume trace for a two-stroke cycle engine cylinder. Exhaust and transfer or scavenge ports are uncovered by the piston as shown.*



In the two-stroke engine cycle, the compression, combustion, and expansion processes are similar to the equivalent four-stroke cycle processes; it is the intake and exhaust processes that are different (Fig. 1.33). The sequence of events in a port-scavenged two-stroke engine is illustrated in Fig. 1.34. In such engines, both exhaust and the scavenging (or transfer) ports are at the same end of the cylinder and are uncovered as the piston approaches BC (Fig. 1.34). After the exhaust ports open, the cylinder pressure falls rapidly as burned gases flow out of the cylinder into the exhaust system, in a blowdown process as shown. The scavenging or transfer ports then open, and once the cylinder pressure p falls below the scavenging pressure p_i, fresh charge flows into the cylinder. Burned gases, displaced by this fresh charge, continue to flow out of the exhaust port (along with some of the fresh charge). Once the ports close as the piston starts the compression stroke, compression, fuel—injection and fuel-air mixing in direct-injection engines, combustion, and expansion processes proceed as in the equivalent four-stroke engine cycle.[29, 30] (Fresh charge is fuel vapor and air in engines where fuel and air are "premixed" before entry into the cylinder: the fresh charge is air if direct fuel injection is used.)

© McGraw-Hill Education. All rights reserved. Any use is subject to the Terms of Use, Privacy Notice and copyright information.

Figure 1.34 Sequence of events during expansion, gas exchange, and compression processes in a loop-scavenged two-stroke cycle compression-ignition engine. Cylinder volume/clearance volume V/V_c, cylinder pressure p, exhaust port open area A_e, and intake port open area A_i are plotted against crank angle.

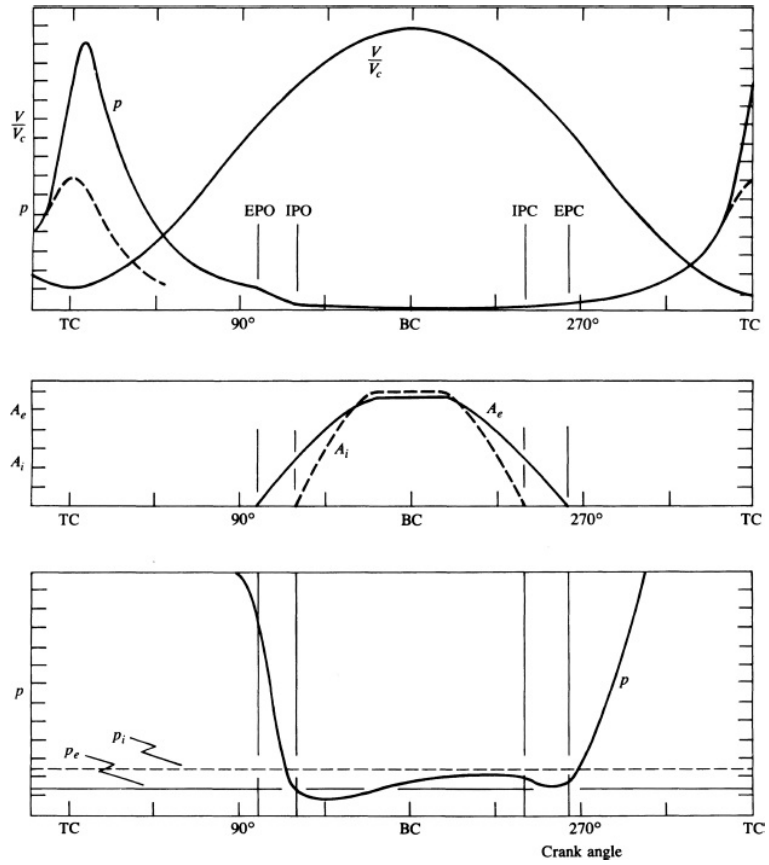
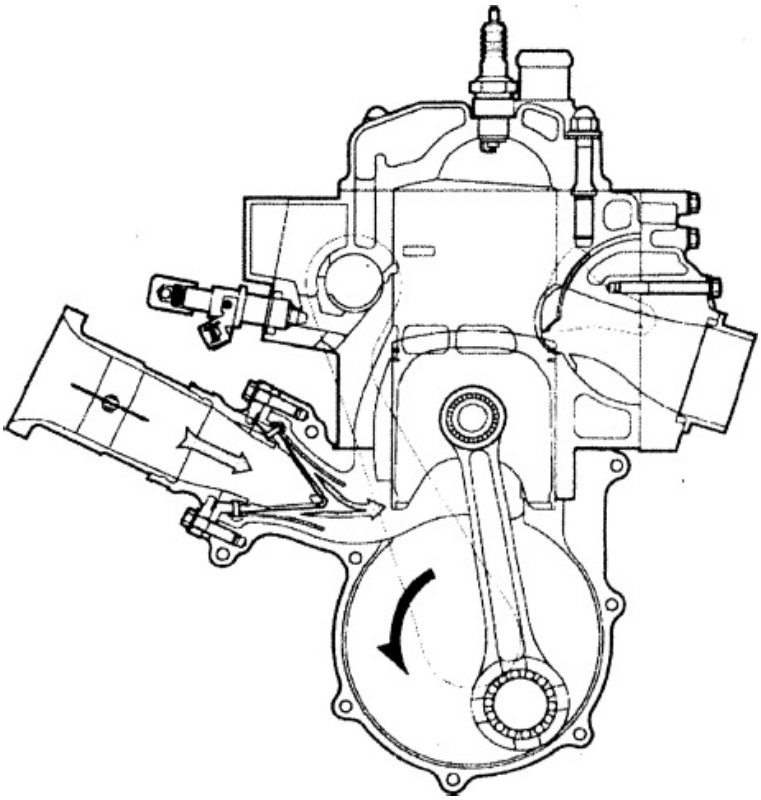


Figure 1.35 shows how this two-stroke cycle is realized in a small gasoline engine.[31] This is an experimental single-cylinder crankcase-scavenged engine, with a pneumatic direct fuel injection system to avoid high hydrocarbon emissions and achieve good fuel consumption. Air flows into the crankcase, through Reed valves, as the piston travels up the cylinder. This air is compressed as the piston travels down. Air flows into the cylinder once the transfer or scavenging ports, which connect the crankcase to the cylinder, are uncovered. Fuel is injected after the transfer ports have been closed off. This engine employs a novel combustion approach—often called *activated radical combustion*. By retaining the appropriate amount of burned residual gas within the cylinder by restricting the flow out of the exhaust ports with a throttle valve, the in-cylinder unburned gas temperature at the end of compression can be raised and controlled. This in-cylinder mixture can then be made to autoignite at the appropriate point in the cycle—at the end of compression, just before TC. This spontaneous autoignition of the complete well-mixed fuel vapor, air, and burned residual in-cylinder charge is an alternative combustion process to the standard spark-ignited or diesel combustion processes. It is often called *homogeneous charge compression ignition* (HCCI) or *controlled autoignition* (CAI). This HCCI combustion concept is also being developed for four-stroke cycle engines. At high outputs, when effective scavenging of the burned gases becomes important, this two-stroke cycle engine reverts to the normal spark-ignition engine flame propagation process.

© McGraw-Hill Education. All rights reserved. Any use is subject to the Terms of Use, Privacy Notice and copyright information.

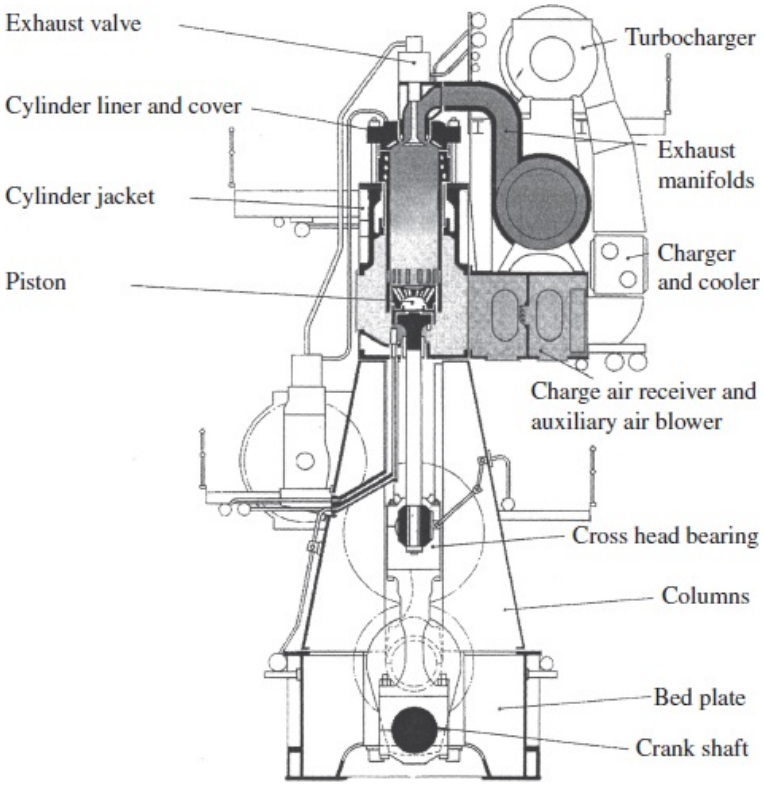
Figure 1.35 Honda experimental two-stroke cycle loop-scavenged engine with pneumatic direct in-cylinder fuel injection, employing an activated radical combustion process—controlled autoignition of the in-cylinder fuel-vapor, air, burned residual mixture just before top center. 402 cm^3 displacement, bore and stroke 80 mm, trapped compression ratio 6:1. Generates 33 kW at 6900 rev/min.[31]



Diesels, in the very large size engines, used for marine propulsion and electrical power generation, also operate using the two-stroke cycle. Figure 1.36 shows such a two-stroke cycle marine engine, available with 4 to 12 cylinders, with a maximum bore of 0.6 to 0.9 m and stroke of 2 to 3 m, which operates at speeds of about 100 rev/min. These engines are normally of the crosshead type shown to reduce piston side forces on the cylinder. The gas exchange process is initiated by opening the exhaust valve in the cylinder head, followed by the piston uncovering the transfer ports at the lower end of the cylinder liner. The expanding exhaust gases leave the cylinder via the exhaust valve and manifold, and pass through the turbocharger turbine. Compressed air enters the cylinder via the transfer ports, continuing the scavenging process; the air is supplied from the turbocharger compressor and intercooler. At part load, electrically driven blowers cut in to compress the scavenge air. Because these large engines operate at low speed, the motion induced by the injected fuel jets is sufficient to mix the fuel with air and burn it in the time available. Thus, a simple open combustion chamber shape can be used, which achieves efficient combustion even with the low-quality heavy fuels used with these types of engines. The pistons are water cooled in these very large engines. The splash or jetted oil piston cooling used in small- and medium-size diesels is not adequate.

© McGraw-Hill Education. All rights reserved. Any use is subject to the Terms of Use, Privacy Notice and copyright information.

Figure 1.36 *Cross-section of an IHI-Sulzer uniflow-scavenged large two-stroke cycle turbocharged diesel engine, developing 1590 kW per cylinder at 127 rev/min. Stroke to bore ratio about 2:5.*[30]



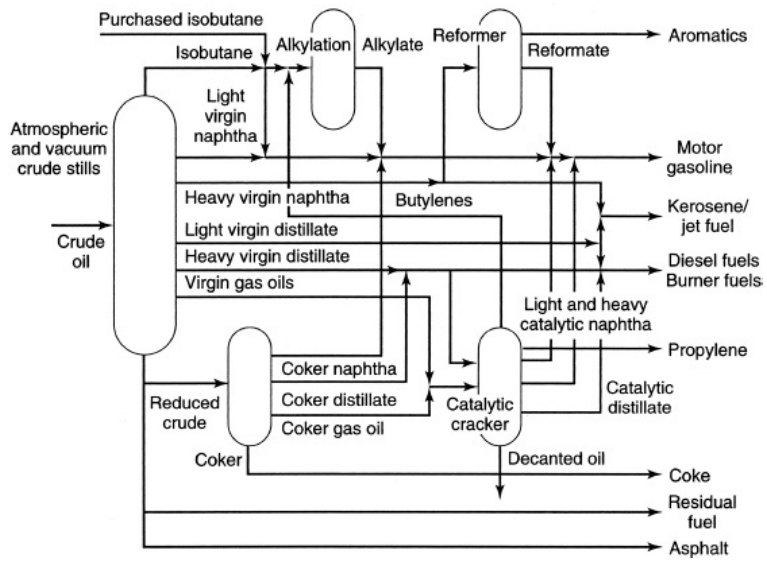
© McGraw-Hill Education. All rights reserved. Any use is subject to the Terms of Use, Privacy Notice and copyright information.

1.11. FUELS

1.11.1. Gasoline and Diesel

Crude oil is the primary source or *feedstock* used today to produce transportation fuels, accounting for more than 95% of transport energy. The gasoline (or petrol) and diesel fuel produced from crude oil are the overwhelmingly dominant *energy carriers* used in SI and CI (or diesel) engines, respectively. Crude oil contains a large number of different hydrocarbons, and these compounds range from gases to liquids to waxes. In a refinery, the crude oil is physically separated by distillation into various fractions. Portions of these fractions are then chemically processed into fuels and other products.[32] Figure 1.37 shows the layout of a typical refinery.[33] The crude oil is first separated into various fractions (each with a higher boiling point range) referred to as *naphtha, distillate, gas oil*, and *residual oil*. The terms *light*, *middle*, or *heavy* break these out further by volatility. The terms *virgin* or *straight run* indicate that no chemical processing has been done to the fraction. As shown, virgin naphtha can be used directly as gasoline. Figure 1.37 also shows the different chemical processes typically used: alkylation, reforming, coking, and catalytic cracking. The refinery products are gasoline, kerosene and jet fuel, diesel, heating oil, burner fuel, residual fuel oil, coke, chemical feedstocks, and asphalt. On average, a refinery will refine 25 to 45% of the input crude oil into gasoline, 25 to 40% into diesel, jet fuel, and heating oil, 5 to 20% into heavy fuel oils, and the remaining 20% into other products.

Figure 1.37 Schematic layout (simplified) of crude oil refinery process.[33]



Gasoline is a blend of hydrocarbons with boiling points ranging from about 25 to 200°C; diesel fuel is a blend of hydrocarbons with boiling points ranging from about 160 to 350°C. Chemical processing is used to convert one fraction into another to upgrade a given fraction so the refinery output meets each fuels' specifications. Alkylation is used to increase the fuel's molecular weight and knock resistance or octane number,[1] by adding alkyl radicals to gaseous hydrocarbon molecules to create branched paraffinic compounds (alkanes). Light olefin gases are reacted with isobutene in the presence of a catalyst. This process consumes relatively little energy. Catalytic cracking breaks up heavy oil molecules to produce a range of lighter products including aromatics and olefins for use in gasoline. The products of catalytic cracking go into high octane gasolines. The catalytic cracking reactions occur at high temperatures so considerable energy is consumed in this process. The reformer changes the molecular structure of specific streams such as naphtha to yield higher octane gasoline (e.g., conversion of paraffins into aromatic hydrocarbons, and straight chain hydrocarbons into branched hydrocarbons) in the presence of a catalyst. Considerable hydrogen is produced that is used elsewhere in the refinery. The coker converts the heavy reduced

© McGraw-Hill Education. All rights reserved. Any use is subject to the Terms of Use, Privacy Notice and copyright information.

crude fraction to naphtha and distillate fractions. The reduced crude is heated in an oven where the molecules undergo pyrolytic decomposition and recombination. While the average molecular weight of the fraction remains the same, a greater spectrum of components is produced. The heaviest component is coke, a solid largely carbonaceous material.[34]

Gasoline, or petrol, is the dominant SI engine fuel. It is a blend of light distillate hydrocarbons (paraffins, naphthenes, olefins, aromatics). Like all liquid hydrocarbons, it has a very high chemical energy density—energy per unit mass or volume. This chemical energy is stored in the carbon-hydrogen and carbon-carbon bonds and is released as thermal energy when these elements are oxidized by burning the fuel with air. In the United States, fuel requirements for SI engines are defined by the American Society for Testing and Materials in ASTM 4814.[35] The equivalent European Standard is EN 228.[36] The average molecular composition of a typical gasoline is close to C_7H_{13}; it includes hydrocarbon molecules containing between four and ten carbon atoms. The C:H atom ratio in commercial gasolines varies from about 1.6 to 2.2.

In terms of SI engine operation, the most critical gasoline properties are its volatility and its resistance to autoignition (or knock) during the latter part of the combustion process. A gasoline's volatility is characterized by its distillation curve, the volume fraction evaporated at atmospheric pressure as a function of temperature. Typically 10% of gasoline vaporizes below about 50°C (T_{10}), 50% vaporizes below 100°C (T_{50}), and 90% below 170°C (T_{90}). Winter gasolines are more volatile than summer gasolines. The fuel must contain enough highly volatile components to ensure rapid and low-emission cold starts. The lower temperature end of the distillation curve affects the fraction of the fuel injected into the port that vaporizes under these conditions. It also affects evaporative hydrocarbon emissions from the vehicle's fuel system. The upper end of the distillation curve is controlled to reduce hydrocarbon emissions and lubricating oil dilution with fuel.

A fuel's resistance to knock is defined by its octane rating. Two standard tests (see Sec. 9.6.3) define the *research octane number* and *motor octane number* of a fuel. The number displayed on gasoline pumps in the United States, the antiknock index, is the average of these. A typical regular (standard) gasoline would have a research octane number of 92, a motor octane number of 82, with an antiknock index of 87. Historically, this antiknock index correlated the knock resistance behavior of fuels in engines in vehicles on the road. Modern engine antiknock requirements are better correlated by the research octane number, which is the fuel's octane number used in Europe. At least two quality gasolines are usually marketed: regular and one or more higher octane grades. Premium gasolines have higher antiknock ratings (up to 98 RON) and often higher levels of additives that are used to control deposit build-up tendencies in various parts of the engine and fuel system. Lead alkyl additives were once widely used to improve the antiknock resistance of gasolines. Since lead is highly toxic, and the catalytic converters used in engines' exhaust systems to reduce emissions (and the oxygen exhaust sensors used for modern engine control) are poisoned by lead, unleaded gasolines are now required in the developed world. While leaded gasoline is still available in some countries, their number is steadily decreasing.

Environmental authorities are imposing increasingly stringent regulations for fuels (gasoline and diesel) to ensure low hydrocarbon evaporative emissions and exhaust pollutant emissions. Thus *reformulated fuels* are now widely used. The main characteristics of reformulated gasolines are reduced vapor pressure (i.e., reduced low-end volatility), lower concentrations of aromatic compounds and benzene, and a lower final boiling point (T_{90}—temperature at which 90% of fuel is evaporated). In the United States, additives that inhibit deposit formation in the engine intake are also required. These reformulated gasolines usually contain oxygenated organic compounds [historically, methyl tertiary-butyl ether (MBTE), now–ethyl alcohol]. In some parts of the United States, these oxygenates are required in winter gasolines (at least 2.7% oxygen) to reduce engine carbon monoxide emissions. Year round, to encourage the use of biofuels, gasolines with up to 5, 10, or 15% ethanol can be marketed (amount depending on country or region). Both MBTE and ethanol have higher octane numbers than the base gasoline so they improve the fuels knock resistance. However, since MTBE can contaminate drinking water supplies, its use in gasolines has been discontinued. The sulfur levels in these clean unleaded gasolines are being reduced from historical levels [some 300 parts per million (ppm) by mass] to levels approaching 10 ppm. Sulfur is a catalyst poison that degrades the effectiveness of exhaust emission-control catalyst systems.

Diesel fuels contain many individual hydrocarbon compounds with boiling points ranging from about 180 to 370°C. As shown in Fig. 1.37, they are a primary product of the crude oil distillation process. To meet the growing demand for diesel fuel, refineries are adding increasing amounts of conversion products through cracking and coking of heavy oil. Diesel fuel is a

© McGraw-Hill Education. All rights reserved. Any use is subject to the Terms of Use, Privacy Notice and copyright information.

mixture of paraffins, napthas, olefins, and aromatics; these have higher molecular weights (and different proportions) than these types of hydrocarbons in gasolines. The average molecular composition is $(CH_{1.8})_n$, and average molecular size is $C_{13}H_{24}$. The molecular weight range of the diesel hydrocarbons is about 170 to 200. The density of diesel fuel is important because fuel-injection systems are designed to deliver a specified *volume* of fuel whereas the combustion characteristics depend on the fuel/air *mass* ratio. The average diesel fuel density in Europe and the United States is about 0.84 kg/liter; the density, in other major geographic regions, varies between 0.81 and 0.86 kg/liter. Because the density of diesel fuel is higher than gasoline, the chemical energy content (heating value) *per unit volume* of fuel is about 10% higher. Other properties related to density are volatility and viscosity. Fuel volatility is defined by the distillation curve and the flash point. The distillation curve effectively defines the vaporization of the fuel inside the engine cylinder. The flash point is the minimum temperature to which the fuel must be heated to produce vapor that ignites in the presence of a flame. The viscosity of diesel fuel affects the fuel's performance in the fuel-injection system; it affects both the fuel pump and injector behavior, and the atomization process in the fuel injector nozzle holes. The low temperature flow characteristics of the fuel in the fuel system (especially the fuel filter) are a critical issue in regions with low winter temperatures where waxes can precipitate out.

Diesel fuel must have appropriate autoignition characteristics—that is, spontaneously ignite fast enough within the developing fuel sprays (see Sec. 1.8) to initiate combustion at the desired point in the engine cycle. This characteristic of diesel fuels is defined by the *cetane number*, which compares the autoignition characteristics of a diesel fuel with those of defined reference fuels (see Sec. 10.5.2). Typical cetane numbers are in the 40 to 55 range; the higher the cetane number, the easier (more rapid) is autoignition in the engine at around top center, just after injection starts. Fuel composition is adjusted to provide the appropriate cetane number; it can be enhanced by ignition improving additives—active oxidizers such as alkyl nitrates. Diesel fuel property requirements are defined in ASTM D975.[37]

1.11.2. Alternative Fuels

Alternative fuels to the gasolines and diesel fuels produced from petroleum are in limited use in IC engines, and are being explored for expanded use in the future. Important driving forces are the need to reduce transportation's dependence on petroleum, and to reduce emissions of GHGs—especially CO_2. LPG and natural gas are in limited use as SI engine fuels in specific applications. Ethanol, produced from biomass, to date is used primarily as a gasoline blending agent. Alternative diesel fuels—for example, biodiesel (methyl esters made from rape seed or soybeans); also dimethyl ether (DME), Fischer-Tropsch gas-to—liquids fuels made from natural gas (or from coal)—are being produced and explored. Hydrogen is being examined as a possible longer-term SI engine fuel largely for its potential, once on the vehicles, to be a noncarbon-emitting energy carrier.

The more important properties of these alternative fuels, along with those of gasoline and diesel, are tabulated inApp. D. An important property of these fuels relevant to their use in engines is their chemical energy content or heating value per unit volume of fuel-vapor/air mixture, which has just enough air for complete combustion (i.e., just enough for full oxidation of the fuel's carbon and hydrogen to CO_2 and H_2O—the stoichiometric mixture ratio). The basic objective of the SI engine's intake process is to fill each cylinder with such a mixture. In the diesel, this objective is met locally as the fuel is combusted. While the heating value of these different fuels *per unit mass of fuel* varies substantially, the differences in the composition of these fuels (and thus the amount of air each fuel requires for complete combustion) bring their heating values *per unit volume* of stoichiometric (chemically correct) mixture to surprisingly similar values. Thus SI engine outputs (i.e., maximum power per unit displaced volume with other parameters held fixed) over a wide range of fuels are closely comparable.

Note also that the combustion characteristics of these fuels when mixed with air in engines are similar (with some important differences in details—especially their anti-knock ratings). The exception is hydrogen which has a much higher flame speed than the hydrocarbon fuels.

Liquid petroleum gas, which consists of C_3 and C_4 hydrocarbons, is produced either by its removal from natural gas during the gas extraction process, or from the refining of crude oil. The fraction of LPG used in transportation varies widely (from a percent or so in the United States to significantly higher levels in some other countries), as does the composition of LPG. The

© McGraw-Hill Education. All rights reserved. Any use is subject to the Terms of Use, Privacy Notice and copyright information.

dominant component is propane (C_3H_8): this can range from 30 to over 90%. Propylene, butanes, and ethane make up the remainder. In vehicles, LPG is stored as a compressed liquid at pressures between about 10 and 15 bar, in cylindrical on-board tanks, at ambient temperature. In most LPG fueling systems, the fuel is injected into the intake manifold in similar manner to multipoint injection gasoline systems. A common fuel rail and one injector valve for each cylinder inject the LPG (in liquid or gaseous form) into each intake manifold, continuously or intermittently.[13]

The components of LPG have higher octane ratings or knock resistance than gasoline, so higher engine compression ratios can be used. However, since the fuel is a gas with a lower molecular weight than gasoline, when mixed with air, the volume occupied by the fuel becomes more significant. LPG fuel therefore displaces more air than does gasoline vapor, and results in a modest loss in power. Air pollutant emissions from a LPG-fueled SI engine (prior to any catalyst in the exhaust) are usually lower than from gasoline-fueled engines.

Natural gas is a primary energy source and carrier. It is largely (80 to 98%) methane, CH_4. The remainder is ethane (1 to 8%), propane (up to 2%), with varying amounts of nitrogen (from a few to 10%). Thus it has a higher molar hydrogen:carbon ratio, so its CO_2 emissions on complete combustion are lower than those of gasoline and diesel by about 25%. However, methane itself is a GHG with a global warming potential about 20 times (per molecule) higher than CO_2. Natural gas leakage and unburned methane emissions would need to be carefully controlled if natural gas is used in transportation on a much larger scale.

Methane has a high octane number, or antiknock rating, though the other hydrocarbon species in natural gas reduce this somewhat depending on their relative amounts. Its combustion characteristics are comparable to those of gasoline.

Natural gas is, of course, a gas and thus storing adequate quantities storage on board the vehicle is a challenging problem. Storage as high-pressure compressed gas (35 MPa) is expensive and requires a substantial volume even for limited vehicle range. At these conditions, the volumetric energy density (MJ/m^3) of compressed natural gas is about one—quarter that of gasoline. Also, because it is a gas with low molecular weight (methane's is 16), when natural gas is mixed with air to combustible proportions, it displaces about 10% of the air (at fixed pressure and temperature) thus reducing the torque that can be produced per unit displaced cylinder volume. Similarly to LPG, natural gas is delivered to the engine intake manifold or intake port via a pressure regulator low pressure common rail, and injectors that inject natural gas intermittently into the intake. Because the fuel is a gas, mixture formation is easier to control since there are no liquid fuel drops and films to vaporize.

Alcohols, such as **ethanol** C_2H_6O and **methanol** CH_4O, can be used as SI engine fuels. Ethanol can be produced from biomass; methanol can be produced form natural gas. These alcohols contain oxygen, so their chemical energy content or heating value per unit mass is less than that of hydrocarbons (0.45 for methanol and 0.61 for ethanol). Heating values per unit mass of stoichiometric mixture are 5% less than gasoline.

These alcohols can be used as stand-alone fuels, or blended with gasoline at high or low fractions. These are designated E100 or M100 for ethanol or methanol alone. Blends with about 15% gasoline (e.g., E85 or M85) are used to broaden the volatility or vaporization characteristics of the single compound alcohol. Ethanol is the more practical of these two fuels. A disadvantage of methanol is its toxicity. Ethanol is used extensively as a transportation fuel in Brazil, where it is made from sugar cane. It is also made from corn (and can be more efficiently made from cellulosic biomass sources such as switchgrass and fast growing bushes and trees). Gasolines blended with up to 10% ethanol are used in the United States and elsewhere to both meet government requirements for oxygen content in "clean" lower-emission reformulated gasolines, and as an outlet for ethanol fuel.

Both ethanol and methanol have significantly higher antiknock or octane ratings than gasoline; the value depends on whether the fuels are tested or used as stand-alone fuels or in gasoline blends (see Table D4, App. D).

Hydrogen can be produced from natural gas, coal, biomass, and by electrolyzing water. Hydrogen for industrial use is currently largely made from steam reforming of natural gas. Storage of hydrogen on board vehicles is a major challenge. As compressed gas, at 70 MPa (10,000 psi), about the maximum practical storage pressure, hydrogen has about one-third the energy density per unit volume of natural gas. Liquid hydrogen, at 20 K, has about one-fourth the energy density per unit

© McGraw-Hill Education. All rights reserved. Any use is subject to the Terms of Use, Privacy Notice and copyright information.

volume of a hydrocarbon fuel. When mixed with air to stoichiometric proportions, the hydrogen in the fuel-air mixture occupies about 30% of the mixture volume, compared with less than 2% for gasoline vapor-air mixtures, reducing the power per unit displaced cylinder volume at constant conditions.

The combustion characteristics of hydrogen are substantially different to those of hydrocarbons, and thus gasoline. The laminar flame speed (a fundamental combustion characteristics of fuel-air mixtures) in hydrogen-air mixtures is several times higher than that of equivalent hydrocarbon-air mixtures due to the much faster diffusion of hydrogen species within the flame. Its flammability limits are broad (4 to 75% by volume at standard atmospheric conditions) and its self-ignition temperature is lower than that of gasoline. However, it has a higher knock resistance and octane number than do gasolines.

Several other fuel's pathways are potential alternatives to petroleum-based diesel fuel. Fuels made via the Fischer-Tropsch process from natural gas are being produced from natural gas reserves that are difficult to transport to the major natural gas markets. Fischer-Tropsch F-T fuels can also be made from coal. The F-T process catalytically combines CO and hydrogen, usually produced by reforming natural gas, to form CH_2 radicals that are combined to form larger hydrocarbon chains. These fuels are completely paraffinic, have very low levels of sulfur, and excellent autoignition characteristics (a high cetane number). They would thus be excellent diesel engine fuels.

Other potential diesel fuels are DME C_2H_6O, and biodiesel. DME is a gas at ambient pressure and temperature; it can be liquefied at about 5 bar pressure. It burns easily in a diesel engine, and its oxygen component helps inhibit the formation of soot and diesel smoke. Vegetable oils, such as rapeseed methyl ester and soybean methyl ester, can be processed to produce biodiesel fuels. Their potential attractiveness is that they are produced from biomass and thus are a possible low GHG emitting source of diesel fuel.

[1] See Sec. 9.6.3.

© McGraw-Hill Education. All rights reserved. Any use is subject to the Terms of Use, Privacy Notice and copyright information.

1.12. PROBLEMS

1.1. Describe the major functions of the following reciprocating engine components: piston, connecting rod, crankshaft, cams and camshaft, valves, intake, and exhaust manifolds.

1.2. Indicate on an appropriate sketch the different forces that act on the piston, and the direction of these forces, during the engine's expansion stroke with the piston, connecting rod, and crank in the positions shown in Fig. 1.1. Explain how the reciprocating engine geometry generates torque. Illustrate on a sketch.

1.3. List six important differences between the design and operating characteristics of spark-ignition and compression-ignition (diesel) engines. Start with the more fundamental of these.

1.4. Indicate the approximate crank angle at which the following events in the four-stroke and two-stroke internal combustion engine cycles occur on a line representing the full cycle (720° for the four-stroke cycle; 360° for the two-stroke cycle): bottom- and top-center crank positions, inlet and exhaust valve or port opening and closing, start of combustion process, end of combustion process, maximum cylinder pressure.

1.5. Explain briefly the following differences between a standard automobile spark-ignition engine and a truck diesel engine:

a. Where the fuel is injected and why

b. How the load is varied at fixed speed

c. How the combustion process starts, develops, and ends

d. How the fuels are different and why

e. How the in-cylinder pressure varies as a function of crank angle (draw qualitatively the pressure traces for both engines in the same graph showing their relative magnitudes and when approximately the combustion starts and ends in each case).

1.6. The two-stroke cycle has twice as many power strokes per crank revolution as the four-stroke cycle. However, two-stroke cycle engine power outputs per unit displaced volume are less than twice the power output of an equivalent four-stroke cycle engine at the same engine speed. Suggest reasons why this potential advantage of the two-stroke cycle is offset in practice.

1.7. Suggest reasons why multicylinder engines prove more attractive than single-cylinder engines once the total engine displaced volume exceeds a few hundred cubic centimeters.

1.8. The gasoline spark-ignition engine dominates the light-duty vehicle market in the United States. Briefly discuss the following:

a. For light-duty vehicles, what other competing "prime mover" technologies might be attractive? Think both in terms of fuel used and the means by which the fuel's energy is converted to useful work.

b. In what ways is each of these fuels or technologies better (or worse) than a gasoline spark-ignition engine? Think both in terms of a single vehicle's performance and the "big picture" resulting from having many such vehicles. You do not need to be quantitative.

c. Now imagine that you are ready to buy your first car. Which of the factors you listed above are most important to you? Which "engine" and energy source would you choose?

© McGraw-Hill Education. All rights reserved. Any use is subject to the Terms of Use, Privacy Notice and copyright information.

1.13. REFERENCES

1. Cummins, Jr., C. L.: *Internal Fire: The Internal Combustion Engine 1673-1900,* 3rd ed., Society of Automotive Engineers, Warrendale, PA, 2000.
2. Cummins, Jr., C. L.: "Early IC and Automotive Engines," SAE paper 760604 in*A History of the Automotive Internal Combustion Engine*, SP-409, *SAE Trans.*, vol. 85, 1976.
3. Hempson, J. G. G.: "The Automobile Engine 1920–1950," SAE paper 760605 in*A History of the Automotive Internal Combustion Engine*, SP-409, SAE, 1976.
4. Agnew, W. G.: "Fifty Years of Combustion Research at General Motors,"*Prog. Energy Combust. Sci.*, vol. 4, pp. 115–156, 1978.
5. Wankel, F.: *Rotary Piston Machines*, Iliffe Books, London, 1965.
6. Ansdale, R. F.: *The Wankel RC Engine Design and Performance*, Iliffe Books, London, 1968.
7. Yamamoto, K.: *Rotary Engine*, Toyo Kogyo Co. Ltd., Hiroshima, 1969.
8. Haagen-Smit, A. J.: "Chemistry and Physiology of Los Angeles Smog,"*Ind. Eng. Chem.*, vol. 44, p. 1342, 1952.
9. Heywood, J. B., and MacKenzie, D. (eds): *On the Road Toward 2050*, MIT Energy Initiative Report, 2015.
10. Heywood, J. B., and Welling, O. Z.: "Trends in Performance Characteristics of Modern Automobile SI and Diesel Engines," SAE paper 2009-01-1892, *SAE Int. J. Engines*, vol. 2, no. 1, pp. 1650–1662, 2009.
11. Taylor, C. F.: *The Internal Combustion Engine in Theory and Practice*, vol. 2, Table 10-1, MIT Press, Cambridge, MA, 1968.
12. Rogowski, A. R.: *Elements of Internal Combustion Engines*, McGraw-Hill, New York, 1953.
13. Bosch, R.: *Automotive Handbook*, 6th ed., Robert Bosch GmbH, SAE, 2004.
14. SAE: *Automotive Engineering International*, February 2011 issue, SAE, 2011.
15. SAE: *Automotive Engineering International,* March 2004 issue, SAE, 2004.
16. Inoue, T., Kusada, M., Kanai, H., and Hino, S.: "Improvement of a Highly Efficient Hybrid Vehicle and Integrating Super Low Emissions," SAE paper 2000-01-2930, SAE, 2000.
17. Zhao, F., Harrington, D.L., and Lai, M-C.: *Automotive Gasoline Direct-Injection Engines,* SAE, Warrendale, PA, 2002.
18. Alperstein, M., Schafer, G. H., and Villforth, F. J.: "Texaco's Stratified Charge Engine—Multifuel, Efficient, Clean, and Practical," SAE paper 740563, SAE, 1974.
19. Urlaub, A. G., and Chmela, F. G.: "High-Speed, Multifuel Engine: L9204 FMV," SAE paper 740122, SAE, 1974.
20. Scussel, A., Simko, A., and Wade, W.: "The Ford PROCO Engine Update," SAE paper 780699, SAE, 1978.
21. Iwamoto, Y., Noma, K., Nakayama, O., Yamauchi, T., and Ando, H.: "Development of Gasoline Direct Injection Engine," SAE paper 970541, SAE, 1997.
22. Kanda, M., Barka, T., Kato, S., Iwamuro, M., Koike, M., and Saito, A.: "Application of a New Combustion Concept to Direct Injection Gasoline Engine," SAE paper 2000-01-0531, SAE, 2000.
23. Date, T., and Yagi, S.: "Research and Development of the Honda CVCC Engine," SAE paper 740605, SAE, 1974.
24. Yamaguchi, Y.: "Mazda RX-8," *Automotive Engineering International*, July 2003 issue, SAE, 2003.

© McGraw-Hill Education. All rights reserved. Any use is subject to the Terms of Use, Privacy Notice and copyright information.

25. Bosch, R.: *Diesel-Engine Management*, 2nd ed., Robert Bosch GmbH, Stuttgart, 1999.
26. Bosch, R.: *Automotive Handbook,* 8th ed., Robert Bosch GmbH, Plochingen, Germany, Au and SAE, Warrendale, PA, 2011.
27. Broge, J. L.: "The Diesel is Coming," *Automotive Engineering International* (aei), January 2004 issue, p. 35, SAE, 2004.
28. Kakinai, A., Yamamoto, A., Sugihara, H., Nakagawa, H., Shoyama, K., and Uchino, N.: "Development of the New K13C Engine with Common-Rail Fuel Injection System," SAE paper 1996-01-0833, SAE, 1996.
29. Blair, G. P.: *Design and Simulation of Two-Stroke Engines,* Society of Automotive Engineers, 1996.
30. Heywood, J. B., and Sher, E.: *The Two-Stroke Cycle Engine, Its Development, Operation and Design,* Taylor and Francis, Philadelphia, 1999.
31. Ishibashi, Y., and Asai, M.: "A Low Pressure Pneumatic Direct Injection Two-Stroke Engine by Activated Radical Combustion Concept," SAE paper 980757, SAE, 1998.
32. Guibet, J. C.: *Engines and Fuels: Technology, Energy, Environment,* vols. 1 and 2, Editions TECHNIP, Paris, 1999.
33. Lawrence, D. K., Plautz, D. A., Keller, B. D., and Wagner, T. O.: "Automotive Fuels—Refinery Energy and Economics," SAE paper 800225, SAE, 1980.
34. Ferguson, C. R., and Kirkpatrick, A. T., *Internal Combustion Engines, Applied Thermosciences,* 2nd ed., John Wiley & Sons, Inc., New York, 2001.
35. ASTM 4814, *Standard Specification for Automotive Spark-Ignition Engine Fuel*, American Society of Testing and Materials, ASTM International, West Conshohocken, PA, 2016.
36. DIN EN 228, *European Standard for Automotive Fuels-Unleaded Petrol-Requirements and Test Methods*, SAI Global, Ltd., Sydney, 2015.
37. ASTM D975, *Standard Specification for Diesel Fuel Oils*, American Society of Testing and Materials, ASDTM International, West Conshohocken, PA, 2015.

© McGraw-Hill Education. All rights reserved. Any use is subject to the Terms of Use, Privacy Notice and copyright information.

2.0. CHAPTER PRELIMINARIES

IMPORTANT ENGINE CHARACTERISTICS

GEOMETRICAL RELATIONSHIPS FOR RECIPROCATING ENGINES

FORCES IN RECIPROCATING MECHANISM

BRAKE TORQUE AND POWER

INDICATED WORK PER CYCLE

MECHANICAL EFFICIENCY

MEAN EFFECTIVE PRESSURE

SPECIFIC FUEL CONSUMPTION AND EFFICIENCY

AIR/FUEL AND FUEL/AIR RATIOS

VOLUMETRIC EFFICIENCY

SPECIFIC POWER, SPECIFC WEIGHT, AND SPECIFIC VOLUME

CORRECTION FACTORS FOR POWER AND VOLUMETRIC EFFICIENCY

SPECIFIC EMISSIONS AND EMISSIONS INDEX

RELATIONSHIPS BETWEEN PERFORMANCE PARAMETERS

ENGINE DESIGN AND PERFORMANCE DATA

VEHICLE POWER REQUIREMENTS

PROBLEMS

REFERENCES

© McGraw-Hill Education. All rights reserved. Any use is subject to the Terms of Use, Privacy Notice and copyright information.

2.1. IMPORTANT ENGINE CHARACTERISTICS

In this chapter, the basic geometrical relationships and the parameters commonly used to quantify engine operation are developed. The characteristics important to an engine user are:

1. The engine's maximum performance over its full operating speed range
2. The engine's fuel consumption within this operating range and the cost of the required fuel
3. The engine's noise and air pollutant emissions within this operating range
4. The initial cost of the engine and its installation
5. The reliability and durability of the engine, its maintenance requirements, and how these affect engine availability and operating costs

These factors control total engine operating costs—usually the primary consideration of the user—and whether the engine in operation can satisfy environmental regulations. This book is concerned primarily with the performance, efficiency, and emissions -characteristics of engines; the omission of the other factors listed above does not, in any way, reduce their importance.

Engine performance is more precisely defined by:

1. The maximum torque available at each speed over the useful engine operating range
2. The maximum engine speed, and thus the maximum power
3. The range of speed and torque (or power) over which engine operation is satisfactory

The following definitions are commonly used to define maximum performance of the engine:

Maximum rated power. The highest power an engine is allowed to develop for short periods of operation.

Normal rated power. The highest power an engine is allowed to develop in continuous operation.

Rated speed. The crankshaft rotational speed at which rated power is developed.

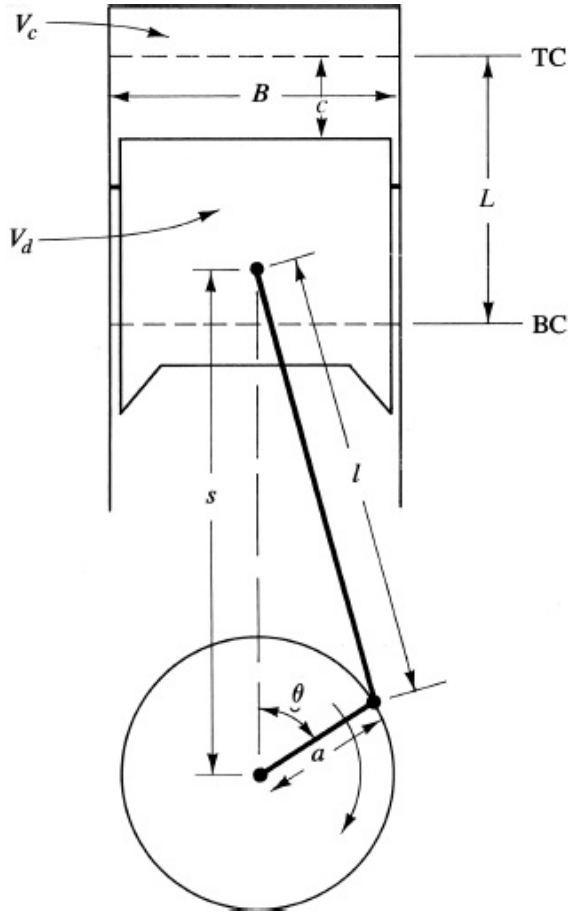
© McGraw-Hill Education. All rights reserved. Any use is subject to the Terms of Use, Privacy Notice and copyright information.

2.2. GEOMETRICAL RELATIONSHIPS FOR RECIPROCATING ENGINES

Useful insights can be obtained from analyzing the geometry of the piston-in-cylinder, connecting rod, and crank mechanism. For example, the cylinder volume as a function of time effectively defines the in-cylinder gas density and amount of gas compression or expansion. The cylinder head, liner, and piston surface areas enter linearly into wall heat transfer calculations. Piston motion drives most engine gas flows, and piston acceleration at higher engine speeds plays a significant role in the periodic inertia forces that this reciprocating engine mechanism produces.

The following parameters define the basic geometry of a reciprocating engine (Fig. 2.1):

Figure 2.1 Geometry of cylinder, piston, connecting rod, and crankshaft whereB = bore, L = stroke, l = connecting rod length, a = crank radius, θ = crank angle.



Compression ratio r_c:

$$r_c = \frac{\text{maximum cylinder volume}}{\text{minimum cylinder volume}} = \frac{V_d + V_c}{V_c}$$

(2.1)

© McGraw-Hill Education. All rights reserved. Any use is subject to the Terms of Use, Privacy Notice and copyright information.

where
V_d is the displaced or swept volume and
V_c is the clearance volume.

Ratio of cylinder bore to piston stroke:

$$R_{\text{bs}} = \frac{B}{L}$$

(2.2)

Ratio of connecting rod length to crank radius:

$$R = \frac{l}{a}$$

(2.3)

In addition, the stroke and crank radius are related by

$$L = 2a$$

Typical values of these parameters are:
r_c = 9 to 12 for spark-ignition (SI) engines and
r_c = 14 to 22 for compression-ignition (CI) engines; *B/L* = 0.8 to 1.2 for small- and medium-size engines, decreasing to about 0.5 for large slow-speed CI engines; *R* = 3 to 3.5 for small- and medium-size engines, increasing to 5 to 9 for large slow-speed CI engines.

The cylinder volume *V* at any crank position θ is the clearance volume plus the swept volume:

$$V = V_c + \frac{\pi B^2}{4} c$$

(2.4)

where *c* is the piston clearance from its top center position. It can be found from *s*, the distance between the crank axis and the piston pin axis (Fig. 2.1), which is given by

$$s = a\,cos\,\theta + (l^2 - a^2 \sin^2\theta)^{1/2}$$

(2.5)

The piston clearance height *c*, which is
$(\ell + a) - s$, is given by

$$c = \frac{L}{2}\left[R + 1 - \cos\theta - (R^2 - \sin^2\theta)^{1/2}\right]$$

© McGraw-Hill Education. All rights reserved. Any use is subject to the Terms of Use, Privacy Notice and copyright information.

(2.6)

The angle θ, defined as shown in Fig. 2.1, is called the *crank angle*. Equation (2.4) with the above definitions can be rearranged:

$$\frac{V}{V_c} = 1 + \frac{1}{2}(r_c - 1)[R + 1 - \cos\theta - (R^2 - \sin^2\theta)^{1/2}]$$

(2.7)

The combustion chamber surface area
A_s at any crank position θ is given by

$$A_s = A_{\text{ch}} + A_p + \pi Bc$$

(2.8)

where
A_{ch} is the cylinder head surface area and
A_p is the piston crown surface area. For flat-topped pistons,
$A_p = \pi B^2/4$. Using Eq. (2.6), Eq. (2.8) can be rearranged:

$$A_s = A_{\text{ch}} + A_p + \frac{\pi BL}{2}\left[R + 1 - \cos\theta - (R^2 - \sin^2\theta)^{1/2}\right]$$

(2.9)

An important characteristic engine speed is the *mean piston speed*
$\overline{S}_p$:

$$\overline{S}_p = 2LN$$

(2.10)

where *N* is the rotational speed of the crankshaft. Mean piston speed is often a more appropriate parameter than crank rotational speed for correlating engine behavior as a function of speed. For example, gas-flow velocities in the intake and the cylinder all scale with
$\overline{S}_p$. The *instantaneous piston velocity*
S_p is obtained from

$$S_p = \frac{ds}{dt}$$

(2.11)

The piston velocity is zero at the beginning of the stroke, reaches a maximum near the middle of the stroke, and decreases to zero at the end of the stroke. Differentiation of Eq. (2.5) and substitution gives

© McGraw-Hill Education. All rights reserved. Any use is subject to the Terms of Use, Privacy Notice and copyright information.

$$\frac{S_p}{\overline{S}_p} = \frac{\pi}{2}\sin\theta\left[1 + \frac{\cos\theta}{(R^2 - \sin^2\theta)^{1/2}}\right]$$

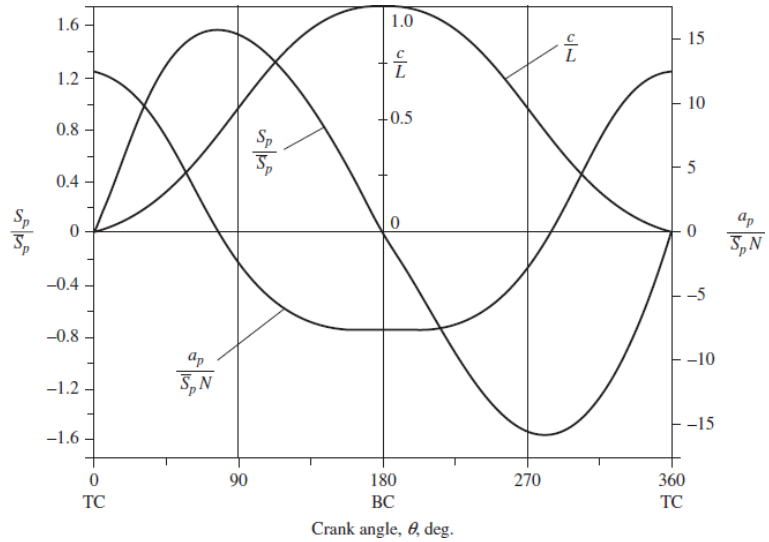
(2.12)

Figure 2.2 shows how S_p, and the piston displacement, vary over each stroke for R = 3.5. Equation (2.12) can be approximated (with error less than 5%) by the equation

$$\frac{S_p}{\overline{S}_p} = \frac{\pi}{2}\sin\theta\left(1 + \frac{1}{R}\cos\theta\right)$$

(2.13)

Figure 2.2 Piston displacement from top center TC, c/L (where L is the stroke), instantaneous piston speed/mean piston speed $S_p/\overline{S}_p$, *and piston acceleration* $a_p/(\overline{S}_p N)$ *as a function of crank angle for R = 3.5.*



Resistance to gas flow into the engine cylinder limits the maximum mean piston speed to about 15 m/s, independent of engine size (the flow becomes choked). Automobile SI engines typically operate with maximum mean piston speeds in the range 14 to 20 m/s. Values between 10 and 14 are typical of diesel engines, where maximum speed is limited by the fuel-air mixing process.

The piston's acceleration is obtained by differentiating Eq. (2.12) or (2.13). The latter leads to this expression for a_p:

$$a_p = \pi^2 \overline{S}_p N\left(\cos\theta + \frac{1}{R}\cos 2\theta\right)$$

(2.14)

© McGraw-Hill Education. All rights reserved. Any use is subject to the Terms of Use, Privacy Notice and copyright information.

Figure 2.2 shows how $a_p/(\overline{S}_p N)$ varies with crank angle for one crankshaft revolution.

Note that the piston motion during each stroke in Fig. 2.2 is not as straightforward as it may appear. From TC to 90° after TC, the piston does not quite get to half stroke (*c*/*L* = 0.5), and the piston velocity S_p reaches a maximum at about 74° ATC (not 90° ATC). Only as ℓ/a becomes large (typically, for small- and mid-size engines, it is 3 to 3.5) does the piston motion during the second half of the downward (or upward) stroke become "symmetric" with the first half of the stroke.

In practical reciprocating engines, two modifications to this axisymmetric geometry are sometimes used: (1) piston pin offset and (2) crankshaft axis offset. The piston pin is frequently offset by about 1.5% of the bore toward the major thrust side of the liner. (The major thrust side is the left-hand side for the arrangement shown in Fig. 2.1 with clockwise crank rotation: it is the side of the liner against which the piston is pushed by the compression force in the connecting rod during the power or expansion stroke.) Piston pin offset reduces the piston impact with the liner close to top center as the piston transitions from the minor thrust side, (right-hand side in Fig. 2.1) to the major thrust side between the compression and expansion strokes. This piston transition with pin offset occurs earlier, before TC, when the forces acting on the piston are lower. Piston pin offset can be incorporated into engine geometry analysis. Its effect on cylinder volume is small (maximum error at mid-stroke is about 0.4%).

The crankshaft axis may be offset about 15% of the bore toward the major thrust side of the cylinder (to the left of the symmetric on-cylinder-axis position shown in Fig. 2.1). This reduces the sideways force the piston exerts on the cylinder liner during the expansion stroke and thus reduces engine friction. It also reduces the piston speed during the earlier part of the expansion stroke, effectively completing combustion sooner and improving engine efficiency. This change in the crankshaft axis location can also be incorporated into engine geometry analysis. Note that offsetting the crank axis changes the compression ratio slightly.

© McGraw-Hill Education. All rights reserved. Any use is subject to the Terms of Use, Privacy Notice and copyright information.

2.3. FORCES IN RECIPROCATING MECHANISM

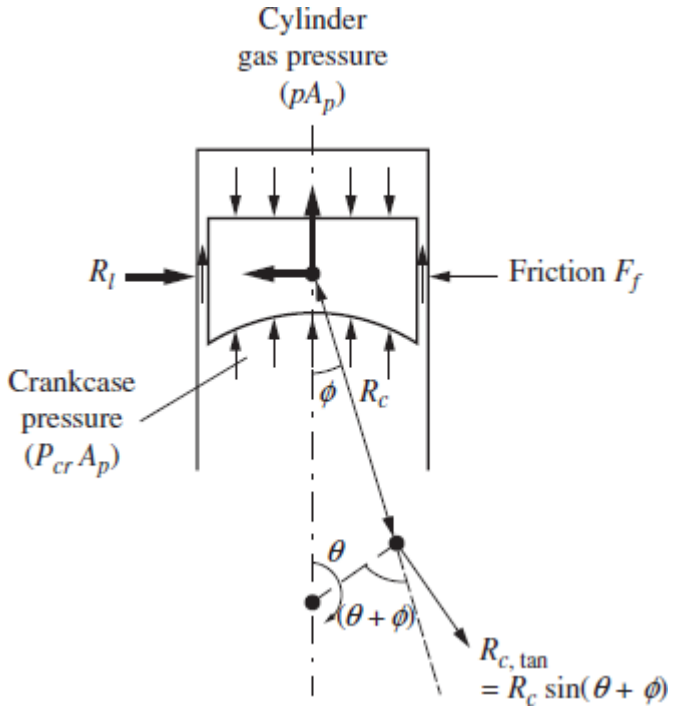
The engine's reciprocating mechanism generates torque about the crankshaft axis through the force generated in the connecting rod. Figure 2.3 shows the forces acting on the piston, and in the connecting rod. Cylinder gas pressure pushes down on the piston crown; crankcase gas pressure acts on the piston underside. Friction acts to retard the piston motion via the friction force *F* on the piston ring and skirt surfaces. During the expansion stroke, the cylinder gas pressure force dominates, creating a compressive reaction force
R_c in the connecting rod. An axial force balance, downward, on the piston yields

$$m_p a_p = \Sigma F_{\text{axial}} = (p - p_{cr}) A_p - F - R_c \cos\phi$$

(2.15)

where
m_p is the mass of the piston, rings, piston pin, and upper part of the connecting rod.[1] Note that
$\ell \sin\phi = \text{a} \sin\phi$ from Fig. 2.1. If the cylinder gas pressure and crankcase pressure are known, and the friction force can be estimated, with
a_p obtained from Eq. (2.14), the connecting rod force
R_c can be calculated.

Figure 2.3 The forces acting on the piston and connecting rod, and the resultant crankshaft torque, during expansion stroke.



A transverse force balance relates the reaction force the liner exerts on the piston,
R_l, to
R_c:

© McGraw-Hill Education. All rights reserved. Any use is subject to the Terms of Use, Privacy Notice and copyright information.

$$R_l = R_c \sin\phi$$

(2.16)

This liner reaction force has an important effect on engine friction.

The component of the connecting rod force perpendicular to the crank radius generates torque about the crank axis. This torque, *T*, is therefore given by

$$T = aR_c \sin(\theta + \phi)$$

(2.17)

Using the fact that
$a\sin\theta = \ell\sin\phi$, and expanding
$\sin(\theta + \phi)$, yields

$$\sin(\theta + \phi) = \sin\theta\left(1 - \frac{a^2}{l^2}\sin^2\theta\right)^{1/2} + \frac{a}{\ell}\sin\theta\cos\theta$$

Equation (2.15), with Eq. (2.14), allows the connecting rod force
R_c as a function of crank angle to be calculated for a given engine geometry and speed, from known cylinder pressure, crankcase pressure, and friction force profiles. The torque each piston and connecting rod exert on the crankshaft, as a function of crank angle, can then be obtained from Eq. (2.17) and is given by

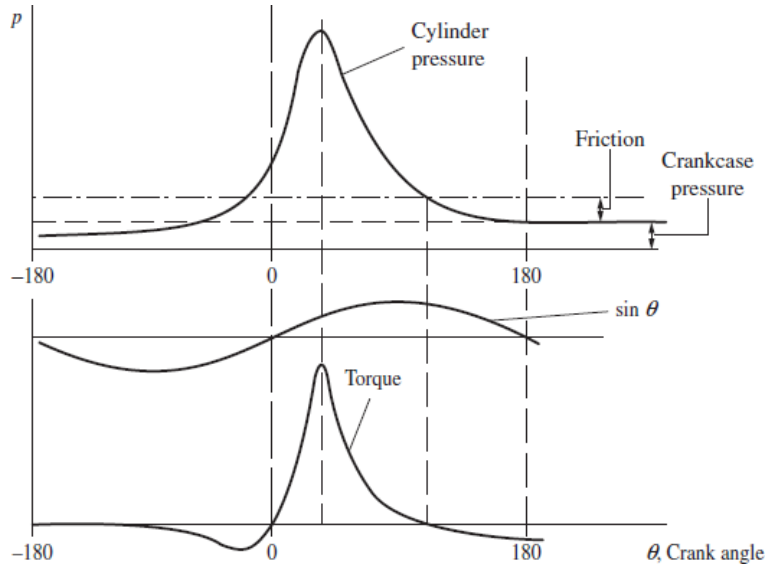
$$T = a\sin\theta\left[(p - p_{cc})A_p - F - m_p a_p\right]\left[1 + \frac{a}{\ell}\cos\theta\frac{1}{\left(1 - \frac{a^2}{\ell^2}\sin^2\theta\right)^{1/2}}\right]$$

(2.18)

Figure 2.4 illustrates how the different time-varying forces on the piston, and piston motion, combine to produce an oscillating torque at the crankshaft through the four-stroke cycle of a given cylinder in an SI engine. Note that
a/ℓ is about 0.3, so the effect of the
a^2/ℓ^2 term is small. At low engine speeds, the piston inertia force
$m_p a_p$ is small relative to gas pressure forces. At high engine speeds, the inertia forces are much more important (see Sec. 15.7.2). The relative importance of the piston friction forces depends on engine load—that is, the magnitude of the cylinder pressure force—and speed. Note that the torque pulse each cycle rises from zero at TC to a maximum slightly after the crank angle of peak pressure, and decays to close to zero by mid-expansion stroke. For a multicylinder engine, the time—varying crankshaft torque is obtained by superposing curves like those for a single cylinder in Fig. 2.4, with an appropriate phase difference (720°/, where
n_c is the number of cylinders).

© McGraw-Hill Education. All rights reserved. Any use is subject to the Terms of Use, Privacy Notice and copyright information.

Figure 2.4 Forces acting on the piston (cylinder pressure, crankcase pressure, friction), and the crankshaft torque, as a function of crank angle for an SI engine at low engine speed. At high engine speed, the piston inertia force $m_p a_p$ *is significant.*



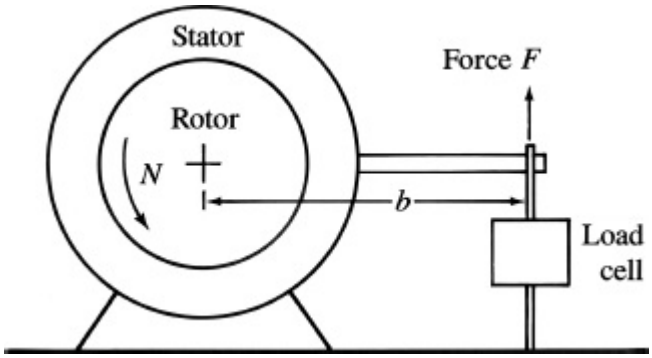
[1] The mass of the upper part of the connecting rod is often taken as the mass above the center of gravity of the connecting rod.

© McGraw-Hill Education. All rights reserved. Any use is subject to the Terms of Use, Privacy Notice and copyright information.

2.4. BRAKE TORQUE AND POWER

The torque an engine delivers through its driveshaft is normally measured with a dynamometer. The engine is mounted on a test bed and the shaft is connected to the dynamometer rotor. Figure 2.5 illustrates the operating principle of a dynamometer. The rotor is coupled electromagnetically, hydraulically, or by mechanical friction to a stator, which is supported in low friction bearings. The stator is balanced with the rotor stationary. The torque exerted on the stator with the rotor turning is measured by balancing the stator with weights, springs, or pneumatic means. The dynamometer usually has sufficient inertia that this procedure with a multicylinder engine sums the torque contributions from each cylinder, and measures the time-averaged torque.

Figure 2.5 Schematic of principle of operation of dynamometer.



Using the notation in Fig. 2.5, if the average torque exerted by the engine is T

$$T = Fb$$

(2.19)

The power P delivered by the engine and absorbed by the dynamometer is the product of torque and angular speed:

$$P = 2\pi NT$$

(2.20*a*)

where N is the crankshaft rotational speed. In SI units

$$P(\mathrm{kW}) = 2\pi N(\mathrm{rev/s})\, T(\mathrm{N \cdot m}) \times 10^{-3}$$

(2.20*b*)

or in U.S. units

$$P(\mathrm{hp}) = \frac{N(\mathrm{rev/min})\, T(\mathrm{lbf \cdot ft})}{5252}$$

(2.20*c*)

© McGraw-Hill Education. All rights reserved. Any use is subject to the Terms of Use, Privacy Notice and copyright information.

The value of engine power measured as described above is called the *brake power* P_b. This power is the usable power delivered by the engine to the load—in this case, a "brake."

Torque is a measure of an engine's ability to do work; power is the rate at which work is done. These are important practical parameters, and their maximum values define an engine's performance. *Load* (e.g., mid load) is often used to denote where in an engine's torque range, zero to maximum, the engine is operating.

© McGraw-Hill Education. All rights reserved. Any use is subject to the Terms of Use, Privacy Notice and copyright information.

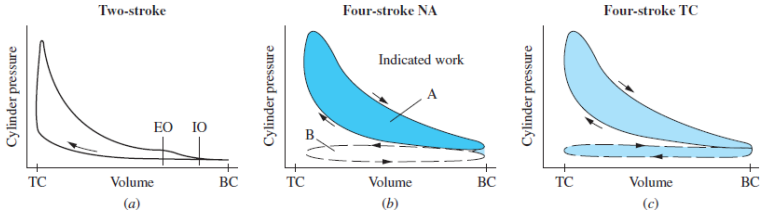
2.5. INDICATED WORK PER CYCLE

Work is produced inside each engine cylinder as gas pressure pushes the piston downward during the expansion stroke. Pressure data for the gas in the cylinder over the operating cycle of the engine can be used to calculate this work transfer from the gas to the piston. The cylinder pressure and corresponding cylinder volume throughout the engine cycle can be plotted on a *p-V* diagram as shown in Fig. 2.6. The *indicated work per cycle* $W_{c,i}$[1] (per cylinder) is obtained by integrating around the curve to obtain the area enclosed on the diagram:

$$W_{c,i} = \oint p\, dV \tag{2.21}$$

With two-stroke cycles (Fig. 2.6*a*), the application of Eq. (2.21) is straightforward.[1]

Figure 2.6 Examples of p-V diagrams illustrating the indicated work per cycle, for (a) a two-stroke cycle engine; (b) a naturally-aspirated four-stroke cycle engine at part load; (c) a turbocharged four-stroke cycle engine at high load.



With the addition of inlet and exhaust strokes for the four-stroke cycle, two definitions of indicated output are in common use. These are:

1. *Gross indicated work per cycle*
   $W_{c,\mathrm{ig}}$: Work delivered to the piston over the compression and expansion strokes only.
2. *Net indicated work per cycle*
   $W_{c,\mathrm{in}}$: Work delivered to the piston over the entire four-stroke cycle.

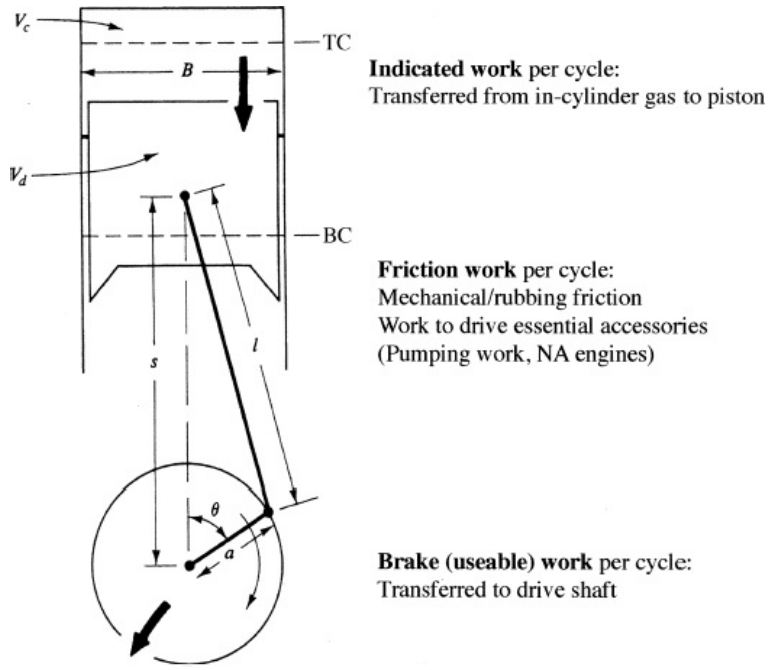
Figures 2.6*b* and *c* show *p-V* diagrams for a naturally-aspirated and a turbocharged four-stroke cycle engine. The blue-colored areas in each figure show the commonly used definition of indicated work per cycle for these two types of engines. The work transfer between the piston and the cylinder gases during the inlet and exhaust strokes is called the *pumping work* W_p (see Chaps. 5 and 13). This pumping work transfer will be *to* the in-cylinder gases when the cylinder pressure during the intake stroke is less than the cylinder pressure during the exhaust stroke (area B in Fig. 2.6*b*). This is the situation with naturally-aspirated engines. The pumping work transfer will be *from* the in-cylinder gases to the piston if the exhaust stroke pressure is lower than the intake pressure, which is normally the case with highly loaded turbocharged engines (Fig. 2.6*c*). Pumping work transfer to the in-cylinder gases reduces the work transferred to the crankshaft, and constitutes one component of engine friction (this work is dissipated pumping the exhaust gas out and pulling fresh charge into the cylinder).[2] Thus the gross indicated work per cycle (i.e., $\int pdV$ over the compression and expansion strokes, area A in Fig. 2.6*b*) is often used with naturally—aspirated engines since it represents the maximum amount of work produced inside the engine. With -turbocharged engines where the pumping work

© McGraw-Hill Education. All rights reserved. Any use is subject to the Terms of Use, Privacy Notice and copyright information.

can be positive (i.e., to the piston) and therefore adds to the positive work transfer produced during the compression and expansion strokes, the net indicated work per cycle definition—$\int pdV$over the full four-stroke cycle—is usually used. Note that with turbocharged engine operation there are still frictional gas-flow losses during the exhaust and intake strokes. However, at higher engine loads, with turbocharged engines, the difference between the compressor outlet pressure and turbine inlet pressure is often sufficiently large to more than offset these losses.

Increasingly, the net definition of imep is being used to quantify the work transferred to the piston because the integral of Eq. (2.21) over the full two revolutions—four strokes—better represents the impacts of the in-cylinder processes per cycle. The increasing use of variable valve control in engines makes the separation between energy conversion and transfer processes during the compression and expansion strokes, and the gas exchange processes, more complex. Then the friction work [and friction mean effective pressure (fmep)] is the sum of the mechanical "rubbing" friction and the work required to drive the essential engine accessories. Figure 2.7 shows how these indicated and brake definitions of work per cycle (and mep) fit with the reciprocating piston-in-cylinder engine geometry and work transfers.

Figure 2.7 Schematic of how indicated work, friction work, and brake work transfers relate to the reciprocating engine geometry.



The power per cylinder is related to the indicated work per cycle by

$$P_i = \frac{W_{c,i} N}{n_R}$$

(2.22)

where
n_R is the number of crank revolutions for each power stroke. For four-stroke cycles,
n_R equals 2; for two-stroke cycles,
n_R equals 1. This power is the indicated power; that is, the rate of work transfer from the gas within the cylinder to the piston. It differs from the brake power by the power absorbed (dissipated) in overcoming engine friction, driving engine accessories,

© McGraw-Hill Education. All rights reserved. Any use is subject to the Terms of Use, Privacy Notice and copyright information.

and (in the case of naturally-aspirated engines) the pumping power. In discussing indicated quantities of the four-stroke cycle engine, such as work per cycle or power, the definition used for "indicated" (i.e., gross or net) *should always be explicitly stated*.

The indicated work per cycle (or power) represents the sum of the useful work (or power) available at the drive shaft plus the work (or power) required to overcome all the engine's frictional losses. The standard engine test codes define procedures for measuring brake power and friction power (the friction power test provides a close approximation to the total lost power in the engine).[2] Thus the sum of brake power and friction power provides an alternative way of estimating indicated power or work per cycle. The terms *brake* and *indicated* are used to describe other parameters such as mep, specific fuel consumption, and specific emissions (see the following sections) in a manner similar to that used for work per cycle and power.

[1] The term indicated is used because such p-V diagrams used to be generated directly with a device called an engine indicator.

[2] With many two-stroke engine concepts, there is a piston pumping work term associated with compressing the scavenging air in the crankcase.[1]

© McGraw-Hill Education. All rights reserved. Any use is subject to the Terms of Use, Privacy Notice and copyright information.

2.6. MECHANICAL EFFICIENCY

In naturally-aspirated engines, a part of the (gross) indicated work per cycle or power is used to expel exhaust gases and induct fresh charge. In all engines, a portion of the work per cycle is used to overcome the friction of the bearings, pistons, and other mechanical components of the engine, and to drive the essential engine accessories. All of these power requirements are grouped together and called *friction power* P_f.[1] Thus,

$$P_i = P_b + P_f$$

(2.23)

Friction power is difficult to determine accurately. One common approach is to drive or motor the engine with a dynamometer (i.e., operate the engine without firing it) and measure the power that has to be supplied by the dynamometer to overcome *all* the frictional losses. The engine speed, throttle setting, oil and water temperatures, and ambient conditions are kept the same in the motored test as under firing conditions. The major sources of inaccuracy with this method are that gas pressure forces on the piston and rings are lower in the motored test than when the engine is firing, the oil temperatures on the cylinder wall are also lower under motoring conditions, and the motored exhaust gas (air) is more dense than the burned exhaust gas when firing. These differences between firing engine friction and this measured motoring friction both add and subtract: it turns out that the difference between motored and fired engine friction is modest.

The ratio of the brake (or useful) power delivered by the engine to the indicated power is called the *mechanical efficiency* η_m. It is a measure of the relative importance of engine friction.

$$\eta_m = \frac{P_b}{P_{ig}} = 1 - \frac{P_f}{P_{ig}}$$

(2.24)

Since in naturally-aspirated engines, the friction power includes the power required to pump gas into and out of the engine, mechanical efficiency in such SI engines depends on throttle position as well as engine design details and engine speed. Typical values of mechanical efficiency for a modern automotive engine at wide-open or full throttle are close to 90% at speeds below about 1800 to 2400 rev/min (30 to 40 rev/s), decreasing to 75% at the engine's maximum rated speed. As the engine is throttled, mechanical efficiency decreases, eventually to zero at idle operation where the brake output is negligible.

[1] The various components of friction are examined in detail in Chap. 13.

© McGraw-Hill Education. All rights reserved. Any use is subject to the Terms of Use, Privacy Notice and copyright information.

2.7. MEAN EFFECTIVE PRESSURE

While torque is an important measure of a particular engine's ability to do work, it depends on engine size. A more useful relative engine performance measure is obtained by dividing the work per cycle by the cylinder volume displaced per cycle. The parameter so obtained has units of force per unit area and is called the *mean effective pressure*. Since, from Eq. (2.22),

$$\text{Work per cycle} = \frac{Pn_R}{N}$$

where
n_R is the number of crank revolutions for each power stroke per cylinder (two for four-stroke cycles; one for two-stroke cycles), then

$$\text{mep} = \frac{Pn_R}{V_d N}$$

(2.25*a*)

In SI and U.S. units, respectively,

$$\text{mep}(\text{kPa}) = \frac{P(\text{kW})n_R \times 10^3}{V_d(\text{dm}^3)N(\text{rev/s})}$$

(2.25*b*)

$$\text{mep}(\text{lb/in}^2) = \frac{P(hp)n_R \times 396{,}000}{V_d(\text{in}^3)N(\text{rev/min})}$$

(2.25*c*)

Both indicated, brake, and friction mep can be calculated from the indicated, brake, and friction work per cycle or power. Brake mep can also be expressed in terms of torque using Eq. (2.20): effectively it is the volume normalized torque, multiplied by
4π for four-stroke cycle engines.

$$\text{bmep}(\text{kPa}) = \frac{6.28n_R T(\text{N}\cdot\text{m})}{V_d(\text{dm}^3)}$$

(2.26*a*)

or

© McGraw-Hill Education. All rights reserved. Any use is subject to the Terms of Use, Privacy Notice and copyright information.

$$\text{bmep}(\text{lb/in}^2) = \frac{75.4 n_R T(\text{lb}_\text{f} \cdot \text{ft})}{V_d(\text{in}^3)}$$

(2.26*b*)

Best brake mep values of good engine designs of a given type of engine, at maximum torque and maximum power, are well established, and are essentially the same over a wide range of engine sizes. Thus, the actual bmep that a particular engine develops can be compared with this norm, and the effectiveness with which the engine designer has used the engine's displaced volume can be assessed. Also, for design calculations, the engine displacement required to provide a given torque or power, at a specified speed, can be estimated by assuming appropriate values for bmep for that particular type of engine.

Typical best values for bmep are as follows: For naturally-aspirated four-stroke SI engines, maximum values are in the range of 1050 to 1250 kPa at the engine speed where maximum torque is obtained (at a mean piston speed of about 11 m/s). Two-valve-per-cylinder engines are at the low end of this range, four-valve-per-cylinder engines with variable valve timing at the high end. At the maximum rated power, bmep values are some 10% lower than these bmep values corresponding to maximum torque. For turbocharged automotive SI engines, the maximum bmep is in the 1800 to 2400 kPa range. For naturally-aspirated four-stroke diesels, the maximum bmep is in the 800 to 900 kPa range, with bmep at the maximum rated power of about 750 kPa. Turbocharged four-stroke diesel maximum bmep values are typically in the range of 1600 to 2400 kPa with the higher values for turbocharged after-cooled engines. At maximum rated power, bmep is between about 1400 and 2200 kPa. Two-stroke cycle SI engines have maximum bmep values of 400 to 750 kPa (small single-cylinder engines at the low end, larger multicylinder engines at the high end). Larger two-stroke cycle diesels have comparable performance to four-stroke cycle engines. Large low-speed marine and power-generating two-stroke cycle engines can achieve bmep values of about 1750 kPa.[1]

An example of how the above engine performance parameters can be used to initiate an engine design is given below.

Example

EXAMPLE 2.1

A four-cylinder four-valve-per-cylinder naturally-aspirated automotive SI engine is being designed to provide a maximum torque of 195 N·m in the mid-speed range (~4000 rev/min). Estimate the required engine displacement, bore, and stroke, and the maximum brake power the engine will deliver.

Equation (2.26*a*) relates torque and mep. Assume that 1200 kPa is an appropriate value for bmep at the maximum engine torque point for this type of engine. Equation (2.26*a*) gives

$$V(\text{dm}^3) = \frac{6.28 n_R T_{\max}(\text{N} \cdot \text{m})}{\text{bmep}_{\max}(\text{kPa})} = \frac{6.28 \times 2 \times 195}{1200} = 2\text{dm}^3$$

For a four-cylinder engine, the displaced volume, bore, and stroke are related by

$$V_d = 4 \times \frac{\pi}{4} B^2 L$$

Assume $B = L$; this gives $B = L = 86$ mm.

The maximum rated engine speed can be estimated from an appropriate value for the maximum mean piston speed, 17 m/s (see Sec. 2.2):

© McGraw-Hill Education. All rights reserved. Any use is subject to the Terms of Use, Privacy Notice and copyright information.

$$\overline{S}_{p\max} = 2LN_{\max} \rightarrow N_{\max} = 17/(2 \times 0.086) = 99\,\text{rev/s}\,(5900\,\text{rev/min})$$

The maximum brake power can be estimated from the typical bmep value at maximum power, 1080 kPa (about 10% less than 1200 kPa), using Eq. (2.25b):

$$P_{\max}(\text{kW}) = \frac{\text{bmep(kPa)}V(\text{dm}^3)N_{\max}(\text{rev/s})}{N_R \times 10^3} = \frac{1080 \times 2 \times 99}{2 \times 10^3} = 107\,\text{kW}$$

[1] Note that these typical best values of bmep for different types of engines increase over time as engines are improved. The average improvement is on the order of 1% per year.[3]

© McGraw-Hill Education. All rights reserved. Any use is subject to the Terms of Use, Privacy Notice and copyright information.

2.8. SPECIFIC FUEL CONSUMPTION AND EFFICIENCY

In engine tests, the fuel consumption is measured as a flow rate—mass flow per unit time $\dot{m}_f$. A more useful parameter is the *specific fuel consumption* (sfc)—the fuel flow rate per unit power output. It is a normalized parameter (i.e., independent of engine size), and measures how efficiently an engine is using the fuel supplied to produce work at a specific operating condition:

$$\text{sfc} = \frac{\dot{m}_f}{P}$$

(2.27)

With units,

$$\text{sfc}(\text{mg/J}) = \frac{\dot{m}_f(\text{g/s})}{P(\text{kW})}$$

(2.28*a*)

or

$$\text{sfc}(\text{g/kW}\cdot\text{h}) = \frac{\dot{m}_f(\text{g/h})}{P(\text{kW})} = 608.3\ \text{sfc}(\text{lb}_\text{m}/\text{hp}\cdot\text{h})$$

(2.28*b*)

or

$$\text{sfc}(\text{lb}_\text{m}/\text{hp}\cdot\text{h}) = \frac{\dot{m}_f(\text{lb}_m/\text{h})}{P(\text{hp})} = 1.644\times 10^3 \text{sfc}(\text{g/kW}\cdot\text{h})$$

(2.28c)

Low values of sfc are obviously desirable. For SI engines, typical best values of brake—specific fuel consumption are about 65 μg/J = 235 g/kW·h = 0.41 lb_m/hp·h. For CI engines, best values are lower, and in larger engines can go below 50 μg/J = 180 g/kW·h = 0.29 lb_m/hp·h.

The specific fuel consumption has units. A dimensionless parameter that relates the desired engine output (work per cycle or power) to the necessary input (fuel flow) has more fundamental value. The ratio of the work produced per cycle to the amount of fuel chemical energy supplied per cycle that can be released in the combustion process is commonly used for this purpose. It is a measure of the engine's efficiency. The fuel energy supplied that can be released by combustion is given by the mass of fuel supplied to the engine per cycle times the heating value of the fuel. The heating value of a fuel, Q_{HV}, defines its chemical energy content. It is determined in a standardized test procedure in which a known mass of fuel is fully burned with air, and the chemical energy released by the combustion process is absorbed as thermal energy in a calorimeter as the combustion products cool down to their original temperature.

© McGraw-Hill Education. All rights reserved. Any use is subject to the Terms of Use, Privacy Notice and copyright information.

This measure of an engine's "efficiency," called the *fuel conversion efficiency*[1] η_f, is given by

$$\eta_f = \frac{W_c}{m_f Q_{\mathrm{HV}}} = \frac{(P n_R/N)}{(\dot{m}_f n_R/N) Q_{\mathrm{HV}}} = \frac{P}{\dot{m}_f Q_{\mathrm{HV}}}$$

(2.29)

where
m_f is the mass of fuel inducted per cycle. Substitution for
$P/\dot{m}_f$ from Eq. (2.27) gives

$$\eta_f = \frac{1}{\mathrm{sfc}\, Q_{\mathrm{HV}}}$$

(2.30*a*)

or with units

$$\eta_f = \frac{1}{\mathrm{sfc}(\mathrm{mg/J}) Q_{\mathrm{HV}}(\mathrm{MJ/kg})}$$

(2.30*b*)

$$\eta_f = \frac{3600}{\mathrm{sfc}(\mathrm{g/kW \cdot h}) Q_{\mathrm{HV}}(\mathrm{MJ/kg})}$$

(2.30*c*)

$$\eta_f = \frac{2545}{\mathrm{sfc}(\mathrm{lb_m/hp \cdot h}) Q_{\mathrm{HV}}(\mathrm{Btu/lb_m})}$$

(2.30*d*)

Typical heating values for the commercial hydrocarbon fuels used in engines are in the range of 42 to 44 MJ/kg (18,000 to 19,000 Btu/l
$\mathrm{b_m}$). Thus, specific fuel consumption is inversely proportional to fuel conversion efficiency for normal hydrocarbon fuels.

Note that the fuel energy supplied to the engine per cycle is not fully released as sensible or thermal energy in the combustion process because the actual combustion process is incomplete. When enough air is present in the cylinder to oxidize the fuel completely, almost all (about 95% or more) of this fuel energy supplied is transferred as thermal energy to the working fluid. When insufficient air is present to oxidize the fuel completely, lack of oxygen prevents this supplied fuel energy from being fully released. This topic is discussed in more detail in Secs. 3.5 and 4.9.4.

© McGraw-Hill Education. All rights reserved. Any use is subject to the Terms of Use, Privacy Notice and copyright information.

[1] This empirically defined engine efficiency has previously been called thermal efficiency or enthalpy efficiency. The term fuel conversion efficiency is preferred because it describes this quantity more precisely, and distinguishes it clearly from other definitions of engine efficiency, which will be developed in Sec. 3.6. Note that there are several different definitions of heating value (see Sec. 3.5). The numerical values do not normally differ by more than a few percent, however. In this text, the lower heating value at constant pressure is used in evaluating the fuel conversion efficiency.

© McGraw-Hill Education. All rights reserved. Any use is subject to the Terms of Use, Privacy Notice and copyright information.

2.9. AIR/FUEL AND FUEL/AIR RATIOS

In engine testing, both the air mass flow rate $\dot{m}_a$ and the fuel mass flow rate $\dot{m}_f$ are normally measured. The ratio of these flow rates is useful when defining engine operating conditions:

$$\text{Air/fuel ratio } (A/F) = \frac{\dot{m}_a}{\dot{m}_f}$$

(2.31)

$$\text{Fuel/air ratio } (F/A) = \frac{\dot{m}_f}{\dot{m}_a}$$

(2.32)

The normal operating range for a conventional SI engine using gasoline fuel is 12 ≤*A/F* ≤ 15 (0.067 ≤ *F/A* ≤ 0.083); for CI engines with diesel fuel, it is 20 ≤ *A/F* ≤ 80 (0.013 ≤ *F/A* ≤ 0.05).

© McGraw-Hill Education. All rights reserved. Any use is subject to the Terms of Use, Privacy Notice and copyright information.

2.10. VOLUMETRIC EFFICIENCY

The intake system—the air filter, intake duct, throttle plate (in an SI engine), intake manifold, intake port, intake valve—restricts the amount of air that an engine of given displacement can induct. The parameter used to measure the effectiveness of an engine's induction process is the *volumetric efficiency*
η_v. Volumetric efficiency is only used with four-stroke cycle engines that have a distinct induction process. It is defined as the volume flow rate of air into the intake system (at defined air conditions) divided by the rate at which volume is displaced by the piston:

$$\eta_v = \frac{2\dot{m}_a}{\rho_{a,i} V_d N}$$

(2.33a)

where
$\rho_{a,i}$ is the inlet air density. An alternative equivalent definition for volumetric efficiency is

$$\eta_v = \frac{m_a}{\rho_{a,i} V_d}$$

(2.33b)

where
m_a is the mass of air inducted into the cylinder per cycle.

With naturally-aspirated engines, the inlet density is usually taken to be atmosphere air density (in which case
η_v measures the air-flow performance of the entire intake system), or may be taken as the air density in the inlet manifold (in which case
η_v measures the air-flow performance of the inlet port and valve only). Typical maximum values of
η_v for naturally-aspirated engines are about 90%. Volumetric efficiency is discussed more fully in Sec. 6.2. It is not normally used with turbocharged engines.

Two-stroke cycle engines, where intake and exhaust processes overlap during scavenging, use different parameters to quantify the cylinder charging process (see Sec. 6.6.2).[1]

© McGraw-Hill Education. All rights reserved. Any use is subject to the Terms of Use, Privacy Notice and copyright information.

2.11. SPECIFIC POWER, SPECIFC WEIGHT, AND SPECIFIC VOLUME

The *specific power*

$$\text{Specific power} = P_{b,\max}/V_d$$

(2.34)

is often used as a normalized measure of an engine's maximum power. Here V_d is the total engine displaced volume. Typical best values for SI engines are 40 to 65 kW/liter (lower end, two valves per cylinder; higher end, four valve with variable valve control), about 80 kW/liter for turbocharged SI engines, about 30 kW/liter for naturally-aspirated truck diesels, and about 40 to 50 kW/liter for turbocharged diesels (higher values for passenger car diesels).

Engine weight and bulk volume for a given maximum power are important in many applications. Two parameters useful for comparing these attributes from one engine to another are:

$$\text{Specific weight} = \frac{\text{engine weight}}{\text{maximum power}}$$

(2.35)

$$\text{Specific volume} = \frac{\text{engine volume}}{\text{maximum power}}$$

(2.36)

For these parameters to be useful in engine comparisons, a consistent definition of what components and auxiliaries are included in the term *engine* must be adhered to. These parameters indicate the effectiveness with which the engine designer has used the engine materials and packaged the engine components.

© McGraw-Hill Education. All rights reserved. Any use is subject to the Terms of Use, Privacy Notice and copyright information.

2.12. CORRECTION FACTORS FOR POWER AND VOLUMETRIC EFFICIENCY

The pressure, humidity, and temperature of the ambient air inducted into an engine, at a given engine speed, affect the air mass flow rate and the power output. Correction factors are used to adjust measured wide-open-throttle power and volumetric efficiency values to standard atmospheric conditions to provide a more accurate basis for comparisons between engines. Typical standard ambient conditions used are:

Dry air pressure	Water vapor pressure	Temperature
736.6 mmHg	9.65 mmHg	29.4°C
29.00 inHg	0.38 inHg	85°F

The basis for the correction factor for maximum power and torque is the equation for one-dimensional steady compressible air flow through an orifice or flow restriction of effective area
A_E (see App. C). The flow resistances in the intake system, port, and valve effectively act as such a flow restriction. Thus

$$\dot{m} = \frac{A_E p_0}{\sqrt{RT_0}} \left\{ \frac{2\gamma}{\gamma - 1} \left[\left(\frac{p}{p_0} \right)^{2/\gamma} - \left(\frac{p}{p_0} \right)^{(\gamma+1)/\gamma} \right] \right\}^{1/2}$$

(2.37)

In deriving this equation, it has been assumed that air is an ideal gas with gas constant*R* and that the ratio of specific heats
$(c_p/c_v = \gamma)$ is a constant;
p_0 and
T_0 are the total pressure and temperature upstream of the restriction and*p* is the pressure at the throat of the restriction.

If, in the engine,
p/p_0 is assumed constant at wide-open throttle, then for a given intake system and engine, the mass flow rate of dry air
$\dot{m}_a$ at higher engine speeds varies as

$$\dot{m}_a \propto \frac{p_0}{\sqrt{T_0}}$$

(2.38)

For mixtures containing the proper amount of fuel to use all the air available (and thus provide maximum power), the indicated power at full throttle
P_i will be proportional to
$\dot{m}_a$, the *dry* air-flow rate. Thus if

$$P_{i,s} = C_F P_{i,m}$$

© McGraw-Hill Education. All rights reserved. Any use is subject to the Terms of Use, Privacy Notice and copyright information.

(2.39)

where the subscripts *s* and *m* denote values at the standard and measured conditions, respectively, the correction factor C_F is given by

$$C_F = \frac{p_{s,d}}{p_m - p_{v,m}} \left(\frac{T_m}{T_s} \right)^{1/2}$$

(2.40)

where

$p_{s,d}$ = standard dry-air absolute pressure

p_m = measured ambient-air absolute pressure

$p_{v,m}$ = measured ambient-water vapor partial pressure

T_m = measured ambient temperature, K

T_s = standard ambient temperature, K

The maximum *brake* power is corrected by using Eq. (2.40) to correct the *indicated* power, and making the assumption that friction power is unchanged. Thus

$$P_{b,s} = C_F P_{i,m} - P_{f,m}$$

(2.41)

Volumetric efficiency is proportional to $\dot{m}_a / \rho_a$ [see Eq. (2.33)]. Since ρ_a is proportional to *p/T*, the correction factor for volumetric efficiency, C'_F, is

$$C'_F = \frac{\eta_{v,s}}{\eta_{v,m}} = \left(\frac{T_s}{T_m} \right)^{1/2}$$

(2.42)

© McGraw-Hill Education. All rights reserved. Any use is subject to the Terms of Use, Privacy Notice and copyright information.

2.13. SPECIFIC EMISSIONS AND EMISSIONS INDEX

Levels of emissions of oxides of nitrogen (nitric oxide, NO, and nitrogen dioxide, NO_2, usually grouped together as NO_x), carbon monoxide (CO), unburned hydrocarbons (HC), and particulates are important engine operating characteristics.

The concentrations of gaseous emissions in the engine exhaust gases are usually measured in parts per million or percent by volume (which corresponds to the mole fraction multiplied by 10^6 or by 10^2, respectively). Normalized indicators of emissions levels are also useful, however, and two of these are in common use. *Specific emissions* are the mass flow rates of pollutant per unit power output:

$$\mathrm{sNO}_x = \frac{\dot{m}_{\mathrm{NO}_x}}{P}$$

(2.43*a*)

$$\mathrm{sCO} = \frac{\dot{m}_{\mathrm{CO}}}{P}$$

(2.43*b*)

$$\mathrm{sHC} = \frac{\dot{m}_{\mathrm{HC}}}{P}$$

(2.43*c*)

$$\mathrm{sPart} = \frac{\dot{m}_{\mathrm{part}}}{P}$$

(2.43*d*)

Indicated and brake-specific emissions can be defined. Units in common use are μg/J, g/kW·h, and g/hp·h.

Alternatively, emission rates can be normalized by the fuel flow rate. An *emission index* (EI) is commonly used, for example,

$$\mathrm{EI}_{\mathrm{NO}_x} = \frac{\dot{m}_{\mathrm{NO}_x}(\mathrm{g/s})}{\dot{m}_f(\mathrm{kg/s})}$$

(2.44)

with similar expressions for CO, HC, and particulates.

© McGraw-Hill Education. All rights reserved. Any use is subject to the Terms of Use, Privacy Notice and copyright information.

2.14. RELATIONSHIPS BETWEEN PERFORMANCE PARAMETERS

The importance of the parameters defined in Secs. 2.4 to 2.10 to engine performance becomes evident when power, torque, and mep are expressed in terms of these parameters. From the definitions of engine brake power [Eq. (2.20)], mep [Eq. (2.25)], fuel conversion efficiency [Eq. (2.29)], mechanical efficiency [Eq. (2.24)], fuel/air ratio [Eq. (2.32)], and volumetric efficiency [Eq. (2.33)], the following relationships between engine performance parameters can be developed. For brake power P_b,

$$P_b = \frac{\eta_{f,b} m_a N Q_{\text{HV}} (F/A)}{n_R}$$

(2.45)

For four-stroke cycle engines, volumetric efficiency can be introduced:

$$P_b = \frac{\eta_v \eta_{f,b} N V_d Q_{\text{HV}} \rho_{a,i} (F/A)}{2}$$

(2.46)

Note that since $\eta_{f,b} = \eta_m \eta_{f,i}$, the indicated power P_i is given by equations identical to Eqs. (2.45) and (2.46) with $\eta_{f,b}$ replaced by $\eta_{f,i}$.

For torque *T*,

$$T = \frac{\eta_v \eta_{f,b} V_d Q_{\text{HV}} \rho_{a,i} (F/A)}{4\pi}$$

(2.47)

For brake or indicated mep,

$$\text{mep} = \eta_v n_f Q_{\text{HV}} \rho_{a,i} (F/A)$$

(2.48)

with the fuel conversion efficiency $\eta_{f,b}$ or $\eta_{f,i}$, respectively.

The power per unit piston area, often called the *specific power*, is a measure of the engine designer's success in using the available piston area regardless of cylinder size. From Eq. (2.46), the specific power is

© McGraw-Hill Education. All rights reserved. Any use is subject to the Terms of Use, Privacy Notice and copyright information.

$$\frac{P}{A_p} = \frac{\eta_v \eta_f N L \rho_{a,i} (F/A) Q_{\mathrm{HV}}}{2}$$

(2.49)

with
η_f being
$\eta_{f,b}$ or $\eta_{f,i}$ for brake or indicated specific power. The mean piston speed can be introduced with Eq. (2.10) to give

$$\frac{P}{A_p} = \frac{\eta_v \eta_f \rho_{a,i} Q_{\mathrm{HV}} \overline{S}_p}{4}$$

(2.50)

Combining Eqs. (2.48) and (2.50), we see that specific power is proportional to the product of mep and mean piston speed.

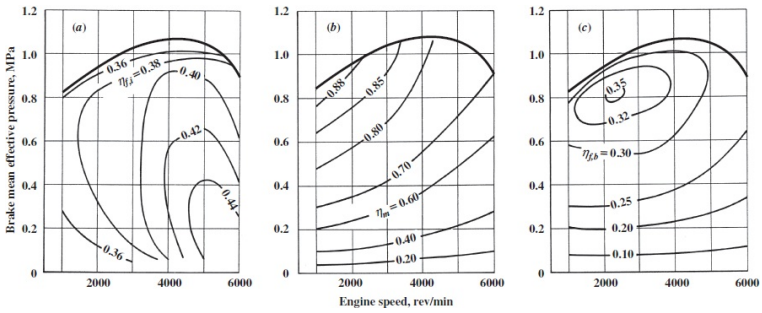
These relationships illustrate the direct importance to (brake) engine performance of:

1. High volumetric efficiency and intake air density to maximize amount of air inducted into each cylinder
2. Maximum fuel/air ratio that can be burned in each cylinder to fully utilize that air
3. High indicated fuel conversion efficiency to use the fuel's chemical energy effectively
4. Low engine friction to minimize losses and achieve a high mechanical efficiency
5. For power, high mean piston speed consistent with high volumetric efficiency

The brake fuel conversion efficiency
$\eta_{f,b}$ of an engine is the product of the indicated fuel conversion efficiency
$\eta_{f,i}$ and the mechanical efficiency
η_m. The indicated fuel conversion efficiency defines the fraction of the fuel's chemical energy that is transferred to the piston as work. The mechanical efficiency defines that fraction of this work transferred to the piston (the indicated work) that is used to overcome the friction in the engine. Both efficient energy conversion and low friction are important to achieving a high brake fuel-conversion efficiency (low brake-specific fuel consumption). Figure 2.8 shows how these parameters $\eta_{f,i}$, η_m, and $\eta_{f,b}$ vary over the operating regime or map for a naturally—aspirated SI engine. The top line in each figure is the wide-open-throttle brake mean effective pressure. The engine's operating regime beneath the WOT line shows contours of constant indicated fuel conversion efficiency (Fig. 2.8*a*), mechanical engineering (Fig. 2.8*b*), and brake fuel conversion efficiency (Fig. 2.8c). The indicated efficiency is essentially constant at about 40% over most of the map. The mechanical efficiency, however, varies from about 0.9 at high load and low speed, to zero at engine idle. The brake fuel conversion efficiency decreases steadily, as load or output is reduced, from a maximum of 35% at 2000 to 2500 rev/min, to zero at idle. It scales, essentially, with the mechanical efficiency underlining the importance of low engine friction.

© McGraw-Hill Education. All rights reserved. Any use is subject to the Terms of Use, Privacy Notice and copyright information.

Figure 2.8 Performance map for a modern spark-ignition engine. Top line in each figure shows wide-open-throttle brake mean effective pressure as a function of engine speed. Figures show: (a) lines of constant (gross) indicated fuel-conversion efficiency; (b) lines of constant mechanical efficiency; (c) lines of constant brake fuel conversion efficiency. Data from Ref. 4. Note $\eta_{f,b} = \eta_m \eta_{f,i}$.

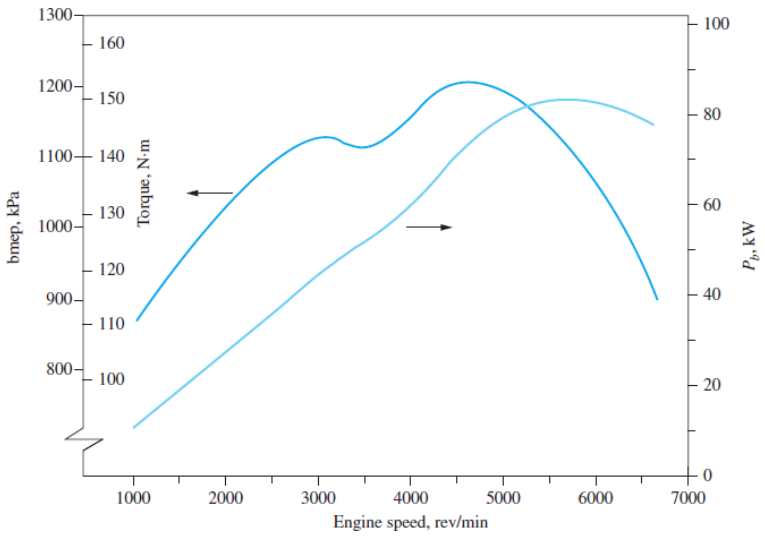


© McGraw-Hill Education. All rights reserved. Any use is subject to the Terms of Use, Privacy Notice and copyright information.

2.15. ENGINE DESIGN AND PERFORMANCE DATA

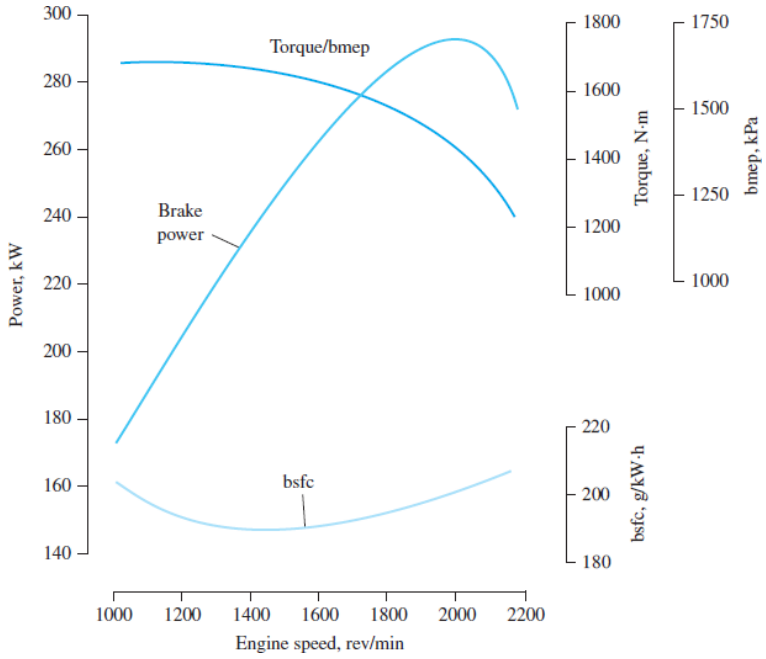
Figures 2.9 and 2.10 show the maximum torque and bmep, and the maximum brake power, as a function of speed for a typical naturally-aspirated light-duty-vehicle SI engine and a turbocharged truck diesel engine. Engines can, of course, operate at any point below these maximum output curves. Engine ratings usually indicate the maximum power and speed at which manufacturers expect their products to give satisfactory economy, reliability, and durability under service conditions. Maximum torque, and the speed at which it is achieved, is also usually given.[1] For the naturally-aspirated gasoline engine, the torque (and bmep) at maximum power is lower than the maximum torque by about 10%, since at higher speed, the volumetric efficiency is lower (due to increased flow resistances) and friction is higher. For the turbocharged diesel engine, the shape of the maximum torque/bmep versus speed curve depends on the relative sizing of the engine and the turbocharger. Usually, as shown in Fig. 2.10, a relatively smaller turbocharger is used to provide high torque at low to mid engine speeds. A relatively larger turbocharger would raise the high speed end of the torque curve, and lower the low speed end.

Figure 2.9 Wide-open-throttle torque, bmep, and power versus speed for a typical automobile SI engine. DaimlerChrysler four-cylinder in-line 1.6-liter engine: four valves per cylinder, bore = 77 mm, stroke = 85.8 mm, compression ratio = 10.5, fixed valve timing.[5]



© McGraw-Hill Education. All rights reserved. Any use is subject to the Terms of Use, Privacy Notice and copyright information.

Figure 2.10 Full-load torque, bmep, and power versus speed for a typical turbocharged and intercooled direct-injection truck diesel engine. Hino K13C in-line six-cylinder engine; 12.9-liter displacement, bore = 135 mm, stroke = 150 mm, compression ratio = 16.5.6



Since both power and torque depend on displaced volume, for comparative analyses between engines of different displacements in a given engine category, normalized performance parameters are more useful. The following measures, at the operating points indicated, have most significance:[7]

1. At maximum rated power:

   Mean piston speed. Measures comparative success in reducing resistance to air flow, handling loads due to inertia of the reciprocating parts, and engine friction.

   Brake mean effective pressure. In naturally-aspirated engines, bmep is not stress limited. It reflects the product of volumetric efficiency (ability to induct air), fuel/air ratio (effectiveness of air utilization in combustion), indicated fuel conversion efficiency, and reducing engine friction. In boosted (supercharged or turbocharged) engines, bmep indicates, also, the degree of success in handling higher gas pressures and thermal loading.

   Power per unit piston area. Measures the effectiveness with which the piston area is used, regardless of cylinder size.

   Specific weight. Indicates relative economy with which materials are used.

   Specific volume. Indicates relative effectiveness with which the space occupied by the engine has been utilized.

2. At all speeds at which the engine will be used with full throttle or with maximum fuel-pump setting:

   Brake mean effective pressure. Measures ability to obtain/provide high air flow and use that air effectively to generate torque.

3. In all useful regimes of operation, and especially in those regimes where the engine is run for long periods of time:

   Brake specific fuel consumption or fuel conversion efficiency.

   Brake specific emissions.

Typical performance data for SI and diesel engines over the normal production size range are summarized in Table 2.1. The four-stroke cycle dominates except in the smallest and largest engine sizes. The larger engines are turbocharged and/or

© McGraw-Hill Education. All rights reserved. Any use is subject to the Terms of Use, Privacy Notice and copyright information.

supercharged. The maximum rated engine speed decreases as engine size increases, maintaining the maximum mean piston speed in the range of about 10 to 20 m/s. The maximum brake mep for turbocharged engines is significantly higher than for naturally-aspirated engines. Because the maximum fuel/air ratio for SI engines is higher than for diesels, their naturally-aspirated maximum bmep levels (at equal boost pressures) are higher. As engine size increases, brake specific fuel consumption decreases and fuel conversion efficiency increases, due to reduced importance of friction and heat losses. For the largest diesel engines, brake fuel conversion efficiencies of up to 55% (and indicated fuel conversion efficiencies approaching 60%) can be obtained.

Table 2.1 Typical design and operating data for internal combustion engines[1, 4, 8]

					Rated maximum				
	Operating cycle	Compression ratio	Bore, m	Stroke/bore	Speed, rev/min	bmep, bar	Power per unit volume kW/dm^3	Weight/power, kg/kW	Best bsfc, g/kW·h
Spark-ignition engines:									
Small (e.g., motorcycles)	2S	7–11	0.05–0.08	1.2–0.9	4500–14,000	5–12	40–160	2–0.4	380
	4S	9–12			5000–13,000	9–13	50–150	2.5–0.5	320
Passenger cars (NA)	4S	10–12	0.07–0.1	1.1–0.9	5000–8000	11–13	40–80	2–0.8	240
(TC,CAC)	4S	9–11			5000–7500	16–24	60–110	1.5–0.5	230
Trucks (NA)	4S	9–11	0.09–0.13	1.2–0.7	2000–3500	8–10	20–35	5.0–3.0	240
Large gas engines	4S	9–12	0.22–0.45	1.1–1.4	300–1000	7–14	30–40	7–3	200
Wankel engine	4S	10	0.65 dm^3 per chamber		8500	10.5	140	~ 1	280
Diesel engines:									
Passenger cars (NA)	4S	19–24	0.075–0.1	1.2–0.9	3500–5000	7–9	20–35	4–2	240
(TC)	4S	18–22			3500–4500	12–20	35–55	3–1.3	220
Trucks (NA)	4S	16–18	0.1–0.15	1.3–0.8	2000–4000	7–10	15–25	6–3	210

© McGraw-Hill Education. All rights reserved. Any use is subject to the Terms of Use, Privacy Notice and copyright information.

	Operating cycle	Compression ratio	Bore, m	Stroke/bore	Rated maximum Speed, rev/min	Rated maximum bmep, bar	Rated maximum Power per unit volume kW/dm	Weight/power, kg/kW	Best bsfc, g/kW·h
(TC,CAC)	4S	15–18	0.1–0.15	1.3–0.8	1800–3200	18–24	30–45	4–3	200
Locomotive, industrial	4S, 2S	12–18	0.15–0.4	1.1–1.3	425–1800	7–23	5–20	6–18	180
Large engines, marine, power generation	2S	10–12	0.4–1	1.2–3	110–400	10–20	2–8	20–50	160

Abbreviations: 2S, two stroke; 4S, four stroke; NA, naturally-aspirated; TC, turbocharged; CAC, charge-air cooling.

[1] The dip in the WOT torque curve at 3500 rev/min is due to intake tuning effects (see Sec. 6.2.6).

© McGraw-Hill Education. All rights reserved. Any use is subject to the Terms of Use, Privacy Notice and copyright information.

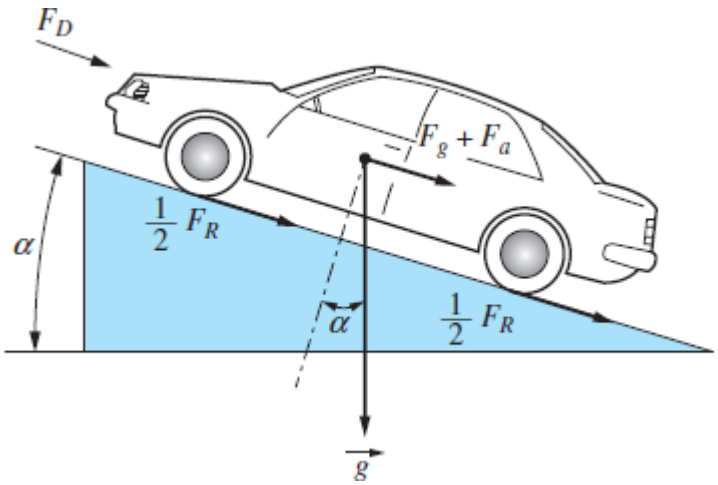
2.16. VEHICLE POWER REQUIREMENTS

When an engine is driving a vehicle, it must provide enough power to overcome the resistances to vehicle motion and accelerate the vehicle, as well as overcome the losses in the transmission and driveline. The vehicle resistances and the inertia force, illustrated in Fig. 2.11, are: tire rolling resistance
F_R, vehicle aerodynamic drag
F_D, vehicle acceleration
F_a (negative when decelerating), gravity when climbing a grade
F_g (negative when descending a grade), and any braking force
F_b. The power required at the wheels to drive the vehicle (
P_v) is, therefore,

$$P_v = (F_R + F_D + F_a + F_g + F_b)\, S_v$$

(2.51)

Figure 2.11 Forces resisting the motion of a vehicle climbing a grade.



This vehicle power is the engine power multiplied by the combined transmission and driveline efficiency. These individual resistances (forces) are given by:

$$F_R = C_R m_v g \cos\alpha$$

(2.52*a*)

$$F_D = \frac{1}{2}\rho_a C_D A_v S_v^2$$

(2.52*b*)

$$F_a = m_v a_v$$

© McGraw-Hill Education. All rights reserved. Any use is subject to the Terms of Use, Privacy Notice and copyright information.

(2.52c)

$$F_g = m_v g \sin \alpha$$

(2.52*d*)

where

C_R = coefficient of rolling resistance ($0.01 < C_R < 0.02$)[8]

m_v = mass of vehicle (curb mass plus payload; in U.S. units W_v = vehicle weight in $\mathrm{lb_f}$)

g = acceleration due to gravity

α = grade angle

ρ_a = ambient air density

C_D = drag coefficient (for cars: $0.2 < C_D \leq 0.5$); average about 0.33[8]

A_v = frontal area of vehicle (≈ 0.9 × vehicle height × width)[8]

S_v = vehicle speed

a_v = vehicle acceleration

A part-load power level useful as a reference point for testing automobile engines is the power required to drive the vehicle on a level road at a steady speed. Called *road-load power*, this power overcomes the tire rolling resistance and the aerodynamic drag of the vehicle. Rolling resistance and drag coefficients, C_R and C_D, respectively, are determined empirically. Equations (2.51) and (2.52) give the formula for road-load power P_r as

$$P_r = (C_R m_v g + \frac{1}{2}\rho_a C_D A_v S_v^2) S_v$$

(2.53)

With the quantities in the units indicated:

$$P_r(\mathrm{kW}) = \left[2.73 C_R m_v(\mathrm{kg}) + 0.0126 C_D A_v(m^2) S^2{}_v(\mathrm{km/h})^2\right] S_v(\mathrm{km/h}) \times 10^{-3}$$

(2.54*a*)

or

© McGraw-Hill Education. All rights reserved. Any use is subject to the Terms of Use, Privacy Notice and copyright information.

$$P_r(\text{hp}) = \frac{\left[C_r W_v(\text{lb}_\text{f}) + 0.0025 C_D A_v(\text{ft}^2) S^2{}_v(\text{mi/h})^2\right] S_v(\text{mi/h})}{375}$$

(2.54*b*)

© McGraw-Hill Education. All rights reserved. Any use is subject to the Terms of Use, Privacy Notice and copyright information.

2.17. PROBLEMS

2.1. Explain why the brake mean effective pressure of a naturally-aspirated diesel engine is lower than that of a naturally-aspirated spark-ignition engine. Explain why the bmep is lower at the maximum rated power for a given engine than the bmep at the maximum torque.

2.2. Calculate the mean piston speed, bmep, and specific power of: **(a)** the spark-ignition engines in Figs. 1.11 and 1.13 at their maximum rated power and torque; and **(b)** the mean piston speed, bmep, and specific power of the diesel engines in Figs. 1.31 and 1.32 at their maximum rated power and torque. Briefly explain any significant differences between these two types of engine.

2.3. Develop an equation for the power required to drive a vehicle at constant speed up a hill of angle α, in terms of vehicle speed, mass, frontal area, drag coefficient, coefficient of rolling resistance, α, and acceleration due to gravity. Calculate this power when the car mass is 1500 kg, the hill angle is 15 degrees, and the vehicle speed is 50 mi/h (80 km/h).

2.4. The spark-ignition engine in Fig. 1.4 is operating at a mean piston speed of 10 m/s. The measured air flow is 60 g/s. Calculate the volumetric efficiency (based on atmospheric conditions).

2.5. The diesel engine of Fig. 1.31 is operating with a mean piston speed of 8 m/s. Calculate the air flow if the volumetric efficiency is 0.92. If (*F/A*) is 0.05, what is the fuel flow rate and the mass of fuel injected per cylinder per cycle?

2.6. The brake fuel conversion efficiency of a spark-ignition engine is 0.3, and varies little with fuel type. Calculate the brake specific fuel consumption for isooctane, gasoline, ethanol, methanol, and hydrogen (relevant data are in App. D).

2.7. You are doing a preliminary design study of a turbocharged four-stroke diesel engine. The maximum rated power is limited by stress considerations to a brake mean effective pressure of 1200 kPa and maximum value of the mean piston speed of 12 m/s.

a. Derive an equation relating the engine inlet pressure (pressure in the intake manifold at the turbocharger compressor exit) to the fuel/air ratio at this maximum rated power operating point. Other reciprocating engine parameters (e.g., volumetric efficiency, fuel conversion efficiency, bmep, etc.) appear in this equation also.

b. The maximum rated brake power requirement for this engine is 400 kW. Estimate appropriate values for number of cylinders, cylinder bore, and stroke, and determine the maximum rated speed of this preliminary engine design.

c. If the pressure ratio across the compressor is 2, estimate the overall fuel/air and air/fuel ratios at the maximum rated power. Assume appropriate values for any other parameters you may need.

2.8. The brake fuel conversion efficiency of an engine is 0.3. The mechanical efficiency is 0.8. The combustion efficiency is 0.94. The heat losses to the coolant and oil are 60 kW. The fuel chemical energy entering the engine per unit time, $\dot{m}_f Q_{\mathrm{HV}}$, is 190 kW. What percentage of this energy becomes **(a)** brake work; **(b)** friction work; **(c)** heat losses; **(d)** exhaust chemical energy; and **(e)** exhaust sensible energy?

2.9. A modern naturally-aspirated spark-ignition engine has an indicated fuel conversion efficiency $\eta_{f,i}$ of 38% over its operating range. At 2000 rev/min, the mechanical friction mean effective pressure (mfmep) is 90 kPa and the accessory (water, oil, and fuel pump) friction (afmep) is 20 kPa; both are independent of load. The engine operates at stoichiometric and MBT spark timing at all intake manifold pressures. The exhaust pressure is p_e, fuel heating value Q_{HV}, fuel/air ratio, intake system air density $\rho_{a,i}$ just downstream of the throttle, and the volumetric efficiency η_v is based on

© McGraw-Hill Education. All rights reserved. Any use is subject to the Terms of Use, Privacy Notice and copyright information.

$\rho_{a,i}$.

a. Develop an expression for the brake fuel conversion efficiency as a function of
   $\eta_{f,i}$ mfmep, afmep, intake manifold pressure
   p_i, exhaust manifold pressure
   p_e, fuel heating value
   Q_{HV}, fuel/air ratio, intake system air density
   $\rho_{a,i}$ just downstream of the throttle, and volumetric efficiency
   η_v is based on
   $\rho_{a,i}$.

b. Evaluate the engine's mechanical efficiency and brake fuel conversion efficiency, at an intake manifold pressure of 0.4, 0.7, and 1.0 bar.

c. Assuming that the mechanical and accessory friction values remain the same at idle, determine the intake manifold pressure at idle.

2.10. In the reciprocating engine, during the power or expansion stroke, the gas pressure force acting on the piston is transmitted to the crankshaft via the connecting rod. List the forces acting on the piston during this part of the operating cycle. Show the direction of the forces acting on the piston on a sketch of the piston, cylinder, connecting rod, crank arrangement. Write out the force balance for the piston **(a)** along the cylinder axis and **(b)** transverse to the cylinder axis in the plane containing the connecting rod. (You are not asked to manipulate or solve these equations.)

2.11. Several velocities, time, and length scales are useful in understanding what goes on inside engines. Make estimates of the following quantities for a 1.6-liter displacement four-cylinder spark—ignition engine, operating at wide-open throttle at 2500 rev/min.

a. The mean piston speed and the maximum piston speed.

b. The maximum charge velocity in the intake port (the port area is about 20% of the piston area).

c. The time occupied by one engine operating cycle, the intake process, the compression process, the combustion process, the expansion process, and the exhaust process. (*Note*: The word *process* is used here, not the word *stroke*.)

d. The average velocity with which the flame travels across the combustion chamber.

e. The length of the intake system (the intake port, the manifold runner, etc.) that is filled by one cylinder charge just before the intake valve opens and this charge enters the cylinder (i.e., how far back from the intake valve, in centimeters, does one cylinder volume of gas extend into the intake system).

f. The length of exhaust system filled by one cylinder charge after it exits the cylinder (assume an average exhaust gas temperature of 425°C).

You will have to make several appropriate geometric assumptions. The calculations are straight-forward, and only approximate answers are required.

2.12. A four-cylinder, four-stroke diesel engine is being designed. A bore of 100 mm and a stroke of 120 mm have been selected and the operating speed of interest is 1500 rev/min. A turbocharging system is envisioned that will supply inlet manifold air at 2.0 bar and 380 K. The volumetric efficiency is expected to be 90%. The indicated fuel conversion efficiency has been estimated at 55%, and an air/fuel ratio of 28:1 is to be used. The friction mean effective pressure is expected to be 2.2 bar. The heating value of the fuel is 42.5 MJ/kg.

Estimate:

a. Mass flow rate of air into the engine (kg/s)

© McGraw-Hill Education. All rights reserved. Any use is subject to the Terms of Use, Privacy Notice and copyright information.

b. Mass of fuel burned per cylinder per cycle (mg)

c. The indicated work done per cylinder per cycle (kJ)

d. The brake mean effective pressure (kPa)

e. The engine shaft power output (kW)

f. The brake specific fuel consumption (g/kW·h)

g. The brake fuel conversion efficiency

2.13. An automobile engine must provide enough power to overcome the vehicle's resistances. These resistances include the rolling resistance due to friction between the tires and the road, aerodynamic drag, gravity (when traveling up a hill), as well as the inertia of the vehicle while accelerating.

For a Ford Taurus vehicle that weighs 1515 kg and has a relatively flat maximum engine torque versus speed curve of 247 N·m for medium engine speeds, estimate the following:

a. The road load power (power required to drive the vehicle on a level road at steady speed) when the vehicle speed is 50 km/h and 100 km/h. How does the relative importance of each resistance change as vehicle speed increases?

b. The power required to drive the vehicle up a 20% gradient hill at a steady speed of 50 km/h.

c. The minimum time required to accelerate the vehicle from 40 to 80 km/h on a level road with the vehicle in third gear. (In third gear for this vehicle, the ratio of engine to wheel speed is 3.27:1.)

Make appropriate estimates for tire rolling resistance and car drag coefficient and geometry (frontal area, wheel radius).

2.14. At 45° after top center on the expansion stroke, the pressure in the engine's cylinder is 1000 kPa. The bore and stroke are 80 mm, the compression ratio is 10, the con rod length: crank radius is 3.5, the crankcase pressure is 100 kPa, the axial friction force on the piston is 65 N. The mass of the piston (and piston pin and half the con rod) is 0.57 kg. The engine speed is 2500 rev/min.

a. Calculate the forces acting on the piston, the compression force in the connecting rod, and the torque delivered to the crankshaft.

b. At this same crank position during the intake stroke, the pressure in the cylinder is 0.5. The friction force is about the same. Estimate the force in the connecting rod under these conditions.

2.15. Laboratory project: Disassembly of a multi-cylinder production gasoline.

During the lab session you will disassemble an engine, and make and record the following measurements:

a. Cylinder bore (at top center and bottom center)

Connecting rod length (pin center to pin center)

Stroke

Piston top land diameter

Piston top land height

Piston top ring groove dimensions

Piston top ring thickness, height, and circumference

Piston diameter, skirt center to skirt center

© McGraw-Hill Education. All rights reserved. Any use is subject to the Terms of Use, Privacy Notice and copyright information.

Overall piston height

b. Intake and exhaust valve head diameter

   Intake and exhaust valve seat diameter (mean value)

   Intake and exhaust valve stem diameter

   Angle between the valve stems

   Maximum intake and exhaust valve lift

   Minimum intake port cross-sectional area

   Mean intake port length

   Mean intake manifold "diameter"

   Mean intake manifold runner length

c. Do some hand-drawn, carefully proportioned sketches to illustrate the geometry of the piston, con rod, etc., in the cylinder, and a cross-section through the cylinder head and ports.

d. Calculate these geometric ratios:

   Bore/stroke

   Mean clearance height/bore

   Connecting rod length/crank radius

   Intake valve seat diameter/bore

   Maximum intake valve lift/valve diameter

   Intake valve head diameter/mean seat diameter

   Exhaust valve seat diameter/bore

   Maximum exhaust valve lift/valve diameter

   Exhaust valve head diameter/mean seat diameter

   Volume of one intake port plus one intake manifold runner/displaced volume of one cylinder

e. What in addition to the components that were part of the engine you disassembled is needed for that engine to operate continuously? Write out a list.

© McGraw-Hill Education. All rights reserved. Any use is subject to the Terms of Use, Privacy Notice and copyright information.

2.18. REFERENCES

1. Heywood, J. B., and Sher, E.: *The Two-Stroke Cycle Engine; Its Development, Operation, and Design,* SAE and Taylor & Francis, Philadelphia, 1999.
2. SAE International: "Engine Power Test Code—Spark Ignition and Compression Ignition—As Installed Net Power Rating," J1349, *SAE Handbook*. 2005.
3. Chon, D., and Heywood, J. B.: "Performance Scaling of Spark-Ignition Engines: Correlation and Historical Analysis of Production Engine Data," SAE paper 2000-01-0565, SAE, 2000.
4. Gruden, D., Kuper, P. F., and Porsche, F.: "Heat Balance of Modern Passenger Car SI Engines," in *Heat and Mass Transfer in Gasoline and Diesel Engines,* D. B. Spalding and N. H. Afgan (eds), Hemisphere Publishing Corporation, New York, 1989.
5. Regueiro, A.: "DaimlerChrysler's New 1.6L, Multi-Valve 4-Cylinder Engine Series," SAE paper 2001-01-0330 in *Advanced Engine, Powerplant, and Component Design*, SP-1620, SAE, 2001.
6. Kakinai, A., Yamamoto, A., and Sugihara, H.: "Development of the New K13C Engine with Common-Rail Fuel Injection System," SAE paper 1999-01-0833, 1999.
7. Taylor, C. F.: *The Internal Combustion Engine in Theory and Practice*, vol. II, MIT Press, Cambridge, MA, 1968.
8. Bosch, R.: *Automotive Handbook*, 6th English edition, Robert Bosch GmbH, Stuttgart, SAE, 2004.

© McGraw-Hill Education. All rights reserved. Any use is subject to the Terms of Use, Privacy Notice and copyright information.

3.0. CHAPTER PRELIMINARIES

CHARACTERIZATION OF FLAMES

IDEAL GAS MODEL

COMPOSITION OF AIR AND FUELS

COMBUSTION STOICHIOMETRY

THE FIRST LAW OF THERMODYNAMICS AND COMBUSTION

THE SECOND LAW OF THERMODYNAMICS APPLIED TO COMBUSTION

CHEMICALLY REACTING GAS MIXTURES

PROBLEMS

REFERENCES

© McGraw-Hill Education. All rights reserved. Any use is subject to the Terms of Use, Privacy Notice and copyright information.

3.1. CHARACTERIZATION OF FLAMES

Combustion of the fuel-air mixture inside the engine cylinder is one of the key processes that controls engine power, efficiency, and emissions. Some background in relevant combustion phenomena is therefore a necessary preliminary to understanding engine operation. These combustion phenomena are different for the two main types of engines—spark-ignition and diesel—which are the subject of this book. In spark-ignition (SI) engines, the fuel is normally well mixed with air, either in the engine's intake ports or within the engine's cylinders. Following the compression of this fuel-air mixture, an electrical discharge initiates the combustion process; a flame develops from the "kernel" created by the spark discharge, and propagates across the cylinder to the combustion chamber walls. At the walls, the flame is "quenched" or extinguished as heat transfer and destruction of active species at the wall become the dominant processes. An undesirable combustion phenomenon—the "spontaneous" ignition of a substantial mass of fuel-air mixture ahead of the flame, before the flame can propagate through this mixture (which is called the end gas)—can also occur. This autoignition or self-explosion combustion phenomenon is the cause of spark—ignition engine knock which due to the high pressures generated, can lead to engine damage.

In the diesel engine, the fuel is injected into the cylinder into air already at high pressure and temperature, near the end of the compression stroke. The autoignition, or self-ignition, of portions of the developing mixture of already injected and vaporized fuel with this hot air starts the combustion process, which spreads rapidly. Burning then proceeds as fuel and air mix to the appropriate composition for combustion to take place. Thus, fuel-air mixing plays a controlling role in the diesel combustion process.

Chapters 3 and 4 focus on the thermochemistry of combustion, that is, the composition and thermodynamic properties of the pre- and postcombustion working fluids in engines and the energy changes associated with the combustion processes that take place inside the engine cylinder. Later chapters (9 and 10) deal with the phenomenological aspects of engine combustion, that is, the details of the physical and chemical processes by which the fuel-air mixture is converted to burned products. At this point it is useful to review the key combustion phenomena that occur in engines to provide an appropriate background for the material that follows. More detailed information on these combustion phenomena can be found in texts on combustion such as those of Borman and Ragland[1] and Glassman.[2]

The combustion process is a fast exothermic gas-phase reaction where oxygen is a critical reactant. A flame is the region within which the combustion reaction takes place, which can propagate subsonically through space; motion of the flame relative into the unburned gas is the important feature. The existence of a propagating flame implies that the reaction is confined to a zone that is small in thickness compared to the dimensions of the apparatus—in our case, the engine combustion chamber. This flame characteristic of spatial propagation is the result of the strong coupling between chemical reaction, the transport processes of mass diffusion and heat conduction, and fluid flow. The generation of heat and active species accelerate the chemical reaction; the supply of fresh reactants, governed by the convection velocity, limits the reaction. When these processes are in balance, a steady-state flame results.

Flames are usually classified according to the following overall characteristics. The first of these has to do with the composition of the reactants as they enter the reaction zone. If the fuel (in vapor form) and oxidizer are essentially uniformly mixed together, the flame is designated as *premixed*. If the reactants are not premixed and must mix together in the region where reaction takes place, the flame is called a *diffusion* flame because the mixing is accomplished by the diffusion of fuel and air into the reaction zone. The second means of classification relates to the basic character of the gas flow through the reaction zone: whether it is *laminar* or *turbulent*. In laminar flow, mixing and transport occur through molecular processes. Laminar flows occur only at low Reynolds number. The Reynolds number (fluid density × velocity × length scale/viscosity) is the ratio of inertial to viscous forces. In turbulent flows, mixing and transport are enhanced (usually by a substantial factor) by the macroscopic relative motion of eddies or lumps of fluid, which are the characteristic feature of turbulent (high Reynolds number) flows. A third area of classification is whether the flame is *steady* or *unsteady*. The distinguishing feature here is

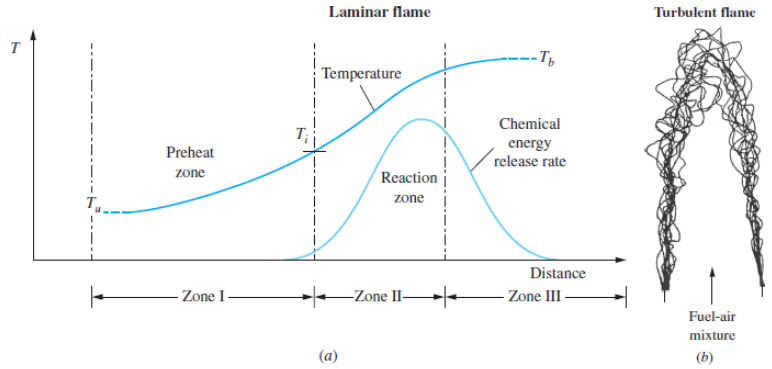
© McGraw-Hill Education. All rights reserved. Any use is subject to the Terms of Use, Privacy Notice and copyright information.

whether the flame structure and motion change with time. The final characterizing feature is the *initial phase* of the reactants—gas, liquid, or solid.

Flames in engines are unsteady, an obvious consequence of the internal combustion engine's operating cycle. Engine flames are turbulent. Only with substantial augmentation of laminar transport processes by turbulent convection can mixing and burning rates and flame-propagation rates be made fast enough to complete the engine combustion process within the time available.

The conventional spark-ignition flame is thus a premixed unsteady turbulent flame, and the fuel-air mixture through which the flame propagates is in the gaseous state. The structure of this premixed flame is illustrated in Fig. 3.1. Within the thin flame sheet (about 0.2 mm thick), the processes that dominate are laminar, that is, governed by molecular diffusion, as illustrated in Fig. 3.1*a*. The combustion reactions that release the fuel's chemical energy occur in the downstream part of the flame (zone II). The thermal energy released there is both conducted upstream into zone I, the preheating zone, where the temperature of the as yet unreacted fuel-air mixture flowing through the zone steadily rises, and is also carried away downstream in the high temperature burned gases flowing out of the flame into zone III. Effectively, the temperature of the unburned mixture must be raised above an *ignition temperature*, T_i, before significant chemical reaction and energy release can occur. Note that the flame structure illustrated shows unburned fuel-air mixture flowing into the flame from the left; the observer is thus moving with the flame. Within the spark-ignition engine, the flame propagates across the combustion chamber moving into the unburned mixture ahead of it. This spark-ignition engine flame is a turbulent premixed flame. Figure 3.1*b* shows several short time scale realizations of a turbulent premixed flame: the fuel-air mixture flows out of the tube as shown, and through the "wrinkled" thin flame sheet. The turbulent fluid motion convects, distorts, and stretches this flame sheet producing a "laminar-like wrinkled flame." Locally, at each point of this turbulent flame sheet, the laminar flame structure shown in Fig. 3.1*a* pertains.

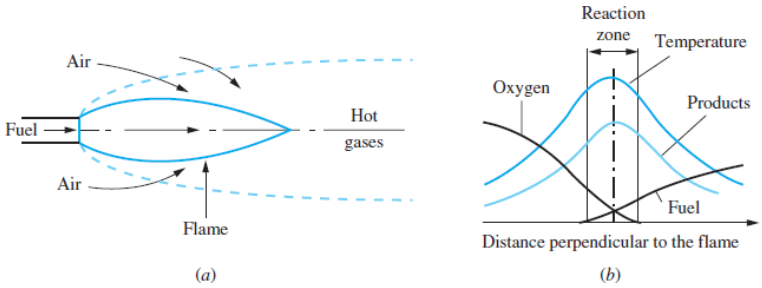
Figure 3.1 Premixed flame structure: (a) Temperature and chemical energy release-rate profiles through a premixed laminar flame; (b) multiple short time-exposure realizations of a turbulent premixed flame.



The diesel engine combustion process is predominantly an unsteady turbulent diffusion flame, and the fuel is initially in the liquid phase. Figure 3.2 illustrates the structure of this diffusion flame. In diffusion flames, the fuel and air are initially separate, as shown in Fig. 3.2*a*. Fuel vapor [produced within each diesel engine fuel spray (see Fig. 1.25) by evaporation of the liquid fuel drops] flows into the inside of the flame; air flows into the flame from the outside (Fig. 3.2*b*). Chemical reaction occurs where the temperatures are highest; that is, where there is just enough air to fully release the fuel's chemical energy—the stoichiometric mixture composition. As shown, the combustion products diffuse away from the diffusion flame on the outside into the surrounding air, and on the inside where the downstream flow within the spray/flame boundary also moves these products away from the flame. In the diesel combustion process, the diffusion flame which surrounds each fuel spray, is also turbulent; the thin flame is made irregular in shape (i.e., wrinkled) by the turbulent flow. Locally it retains the structure shown in Fig. 3.2*b*.

© McGraw-Hill Education. All rights reserved. Any use is subject to the Terms of Use, Privacy Notice and copyright information.

Figure 3.2 Diffusion flame structure: (a) Fuel, air, and flame location in a jet diffusion flame; (b) concentration profiles of fuel, oxidizer, products, and temperature, through the flame.



Both these engine flames are extremely complicated because they involve the coupling of the multispecies chemical mechanism by which fuel and oxidizer react to form products, with the turbulent convective transport process. The diesel combustion process is even more complicated than the spark-ignition engine combustion process because vaporization of liquid fuel and the fuel-air mixing process are involved too. Chapters 9 and 10 contain a more detailed discussion of the SI engine and diesel combustion processes, respectively. This chapter reviews the basic thermodynamic and chemical composition aspects of engine combustion.

© McGraw-Hill Education. All rights reserved. Any use is subject to the Terms of Use, Privacy Notice and copyright information.

3.2. IDEAL GAS MODEL

The gas species that make up the working fluids in internal combustion engines (e.g., oxygen, nitrogen, fuel vapor, carbon dioxide, water vapor, etc.) can usually be treated as ideal gases. The relationships between the thermodynamic properties of an ideal gas and of ideal gas mixtures are reviewed in App. B. There can be found the various forms of the ideal gas law:

$$pV = mRT = m\frac{\widetilde{R}}{M}T = n\widetilde{R}T$$

(3.1)

where *p* is the pressure, *V* the volume, *m* the mass of gas, *R* the gas constant for the gas, *T* the temperature, $\widetilde{R}$ the universal gas constant, *M* the molecular weight, and *n* the number of moles. Relations for evaluating the specific internal energy *u*, enthalpy *h*, and entropy *s*, specific heats at constant volume c_v and constant pressure $c_p (c_p = c_v + R)$ on a per unit mass basis and on a per mole basis (where the notation $\tilde{u}, \tilde{h}, \tilde{s}, \tilde{c}_v$, and $\tilde{c}_p$ is used) of an ideal gas, are developed there. Also given are equations for calculating the thermodynamic properties of mixtures of ideal gases.

© McGraw-Hill Education. All rights reserved. Any use is subject to the Terms of Use, Privacy Notice and copyright information.

3.3. COMPOSITION OF AIR AND FUELS

Normally in engines, fuels are burned with air. Dry air is a mixture of gases that has a representative composition by volume of 20.95% oxygen, 78.09% nitrogen, 0.93% argon, and trace amounts of carbon dioxide, neon, helium, methane, and other gases. Table 3.1 shows the relative proportions of the major constituents of dry air.[3]

Table 3.1 Principle constituents of dry air

Gas	ppm by volume	Molecular weight	Mole fraction	Molar ratio
O_2	209,480	31.998	0.2095	1
N_2	780,840	28.012	0.7905	3.773
Ar	9300	39.948		
CO_2	404	44.009		
Air	1,000,000	28.962	1.0000	4.773

In combustion, oxygen is the reactive component of air. It is usually sufficiently accurate to regard air as consisting of 21% oxygen and 79% inert gases taken as nitrogen (often called atmospheric or apparent nitrogen). For each mole of oxygen in air, there are

$$\frac{1-0.2095}{0.2095}=3.773$$

moles of atmospheric nitrogen. The molecular weight of air is obtained from Table 3.1 with Eq. (B.17) as 28.962, usually approximated by 29. Because atmospheric nitrogen contains traces of other species, its molecular weight is slightly different from that of pure molecular nitrogen, that is,

$$M_{a\mathrm{N}_2}=\frac{28.962-0.2095\times 31.998}{1-0.2095}=28.16$$

In the following sections, *nitrogen* will refer to atmospheric nitrogen and a molecular weight of 28.16 will be used. An air composition of 3.773 moles of nitrogen per mole of oxygen will be assumed.

The density of dry air can be obtained from Eq. (3.1) with R = 8314.3 J/kmol·K and M = 28.962:

$$\rho(\mathrm{kg/m^3})=\frac{3.483\times 10^{-3}p(\mathrm{Pa})}{T(K)}$$

(3.2*a*)

or

© McGraw-Hill Education. All rights reserved. Any use is subject to the Terms of Use, Privacy Notice and copyright information.

$$\rho(\mathrm{lb}_m/\mathrm{ft}^3) = \frac{2.699p(\mathrm{lb}_f/\mathrm{in}^2)}{T(^\circ R)}$$

(3.2*b*)

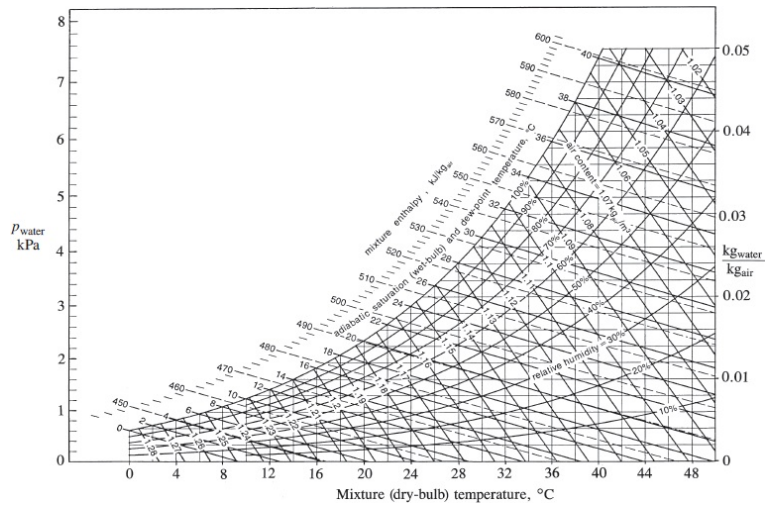
Thus, the value for the density of dry air at 1 atmosphere (1.0133×10^5 Pa, 14.696 lb_f/in^2) and 25°C (77°F) is 1.184 kg/m^3 (0.0739 lb_m/ft^3).

Actual air contains water vapor, the amount depending on temperature, and degree of saturation. Typically the proportion by mass is about 1%, though it can rise to about 4% under extreme conditions. The *relative humidity* compares the water vapor content of air with that required to saturate. It is defined as:

> The ratio of the partial pressure of the water vapor actually present to the saturation pressure at the same temperature.

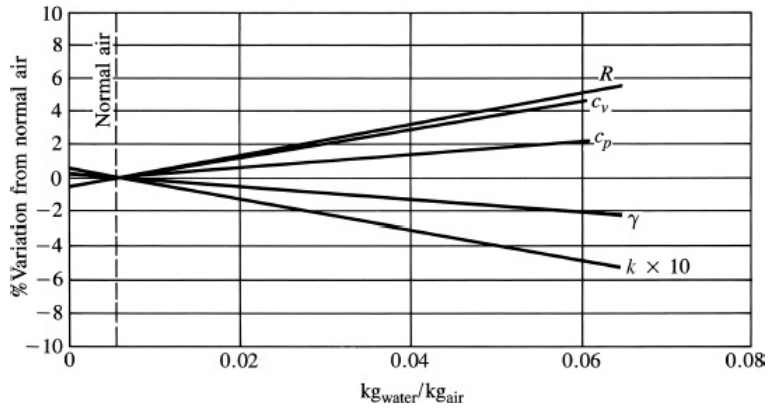
Water vapor content is measured with a wet- and dry-bulb psychrometer. This consists of two thermometers exposed to a stream of moist air. The dry-bulb temperature is the temperature of the air. The bulb of the other thermometer is wetted by a wick in contact with a water reservoir. The wet-bulb temperature is lower than the dry-bulb temperature due to evaporation of water from the wick. It is a good approximation to assume that the wet-bulb temperature is the adiabatic saturation temperature. Water vapor pressure can be obtained from observed wet- and dry-bulb temperatures and a psychrometric chart such as Fig. 3.3.[4] The effect of humidity on the properties of air is given inFig. 3.4.[5]

Figure 3.3 Psychrometric chart for air-water mixtures at 1 atmosphere. (From Reynolds.[4])



© McGraw-Hill Education. All rights reserved. Any use is subject to the Terms of Use, Privacy Notice and copyright information.

Figure 3.4 Effect of humidity on properties of air: R is the gas constant; c_v *and* c_p *are specific heats at constant volume and pressure, respectively;* $\gamma = c_p/c_v$; k *is the thermal conductivity. (From Taylor.*[5]*)*



The fuels most commonly used in internal combustion engines (gasoline or petrol, and diesel) are blends of many different hydrocarbon compounds obtained by refining petroleum or crude oil. These fuels are predominantly carbon and hydrogen (typically about 86% carbon and 14% hydrogen by weight). In some regions of the world, diesel fuels can contain up to about 1% sulfur. Other fuels of interest are alcohols (which contain oxygen),[1] gaseous fuels (natural gas and liquid petroleum gas), and single hydrocarbon compounds (e.g., methane, propane, isooctane) that are often used in engine research. Properties of the more common internal combustion engine fuels are summarized in App. D.

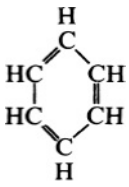
Some knowledge of the different classes of organic compounds and their molecular structure is necessary in order to understand combustion mechanisms.[6] The different classes are as follows:

3.3.1. Alkyl Compounds

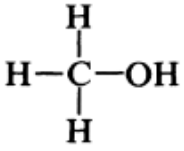
Paraffins (alkanes) C_nH_{2n+2}	Single-bonded open-chain saturated hydrocarbon molecules, that is, no more hydrogen can be added. For the larger molecules, different isomers—straight-chain and branched-chain configurations—exist. These are called normal (*n*-) and iso compounds, respectively. Examples: CH_4, methane; C_2H_6, ethane; C_3H_8, propane; C_8H_{18}, *n*-octane and isooctane. There are several "isooctanes," depending on the relative position of the branches. By isooctane is usually meant the molecule 2,2,4-trimethylpentane, indicating five carbon atoms in the straight chain (pentane) with three methyl (CH_3) branches located, respectively, at C-atoms 2, 2, and 4. Radical molecules deficient in one hydrogen atom take the name methyl, ethyl, propyl, etc.
Cycloparaffins or naphthenes (cyclanes) C_nH_{2n}	Single-bond (no double-bond) ring hydrocarbons: Unsaturated, since ring can be broken and additional hydrogen added. Examples: C_3H_6, cyclopropane (three C-atom ring); C_4H_8, cyclobutane (four C-atom ring); C_5H_{10}, cyclopentane (five C-atom ring).
Olefins (alkenes) C_nH_{2n}	Open-chain hydrocarbons containing a double bond; hence they are unsaturated. Examples: C_2H_4, ethene (or ethylene); C_3H_6, propene (or propylene); C_4H_8, butene (or butylene). From butene upward, several structural isomers are possible depending on the location of the double bond in the basic carbon chain. Straight- and branched-chain structures exist. Diolefins contain two double bonds.
Acetylenes (alkynes) C_nH_{2n-2}	Open-chain unsaturated hydrocarbons containing one carbon-carbon triple bond. First member is acetylene, H−C≡C−H. Additional members of the alkyne series comprise open-chain molecules, similar to higher alkenes but with each double bond replaced by a triple bond.

© McGraw-Hill Education. All rights reserved. Any use is subject to the Terms of Use, Privacy Notice and copyright information.

3.3.2. Aromatics

 C_nH_{2n-6}	Building block for aromatic hydrocarbons is the benzene (C_6H_6) ring structure shown. This ring structure is very stable and accommodates additional $-CH_2$ and $-CH_3$ groups in side chains and not by ring expansion. Examples: C_7H_8, toluene; C_8H_{10}, xylene (several structural arrangements). More complex aromatic hydrocarbons incorporate ethyl, propyl, and heavier alkyl side chains in a variety of structural arrangements.

3.3.3. Alcohols

Monohydric alcohols  $C_nH_{2n+1}OH$	In these organic compounds, one hydroxyl (–OH) group is substituted for one hydrogen atom. Thus methane becomes methyl alcohol, CH_3OH (also called methanol); ethane becomes ethyl alcohol, C_2H_5OH (ethanol); etc.

[1] Blends of alcohols with gasoline are now being used, for example, an E10 blend combines 10% ethanol (by volume) with 90% gasoline.

© McGraw-Hill Education. All rights reserved. Any use is subject to the Terms of Use, Privacy Notice and copyright information.

3.4. COMBUSTION STOICHIOMETRY

This section develops relations between the composition of the reactants (fuel and air) in a combustible mixture and the composition of the products. Since these relations depend only on the conservation of mass of each chemical element in the reactants, only the relative elemental composition of the fuel and the relative proportions of fuel and air are needed.

If sufficient oxygen is available, a hydrocarbon fuel can be completely oxidized. The carbon in the fuel is then converted to carbon dioxide, CO_2, and the hydrogen to water, H_2O. For example, consider the overall chemical equation for the complete combustion of one mole of propane C_3H_8:

$$C_3H_8 + aO_2 = bCO_2 + cH_2O$$

(3.3)

A carbon balance between the reactants and products gives $b = 3$. A hydrogen balance gives $2c = 8$, or $c = 4$. An oxygen balance gives $2b + c = 10 = 2a$, or $a = 5$. Thus Eq. (3.3) becomes

$$C_3H_8 + 5O_2 = 3CO_2 + 4H_2O$$

(3.4)

Note that Eq. (3.4) only relates the elemental composition of the reactant and product species; it does not indicate the chemical mechanism by which combustion proceeds, which is much more complex.

Air contains nitrogen, but when the products are at relatively low temperatures, the nitrogen is not significantly affected by the reaction. Consider the complete combustion of a general hydrocarbon fuel of average molecular composition C_aH_b with air. The overall complete combustion equation is

$$C_aH_b + \left(a + \frac{b}{4}\right)(O_2 + 3.773N_2) = aCO_2 + \frac{b}{2}H_2O + 377.3\left(a + \frac{b}{4}\right)N_2$$

(3.5)

Note that only the *ratios* of the numbers in front of the symbol for each chemical species are defined by Eq. (3.5) that is, only the relative proportions on a molar basis are obtained. Thus the fuel composition could have been written as CH_y where $y = b/a$.

Equation (3.5) defines the *stoichiometric* (or chemically correct or theoretical) proportions of fuel and air: that is, there is just enough oxygen for conversion of all the fuel into completely oxidized products. The stoichiometric air/fuel or fuel/air ratios (see Sec. 2.9) depend on fuel composition. From Eq. (3.5):

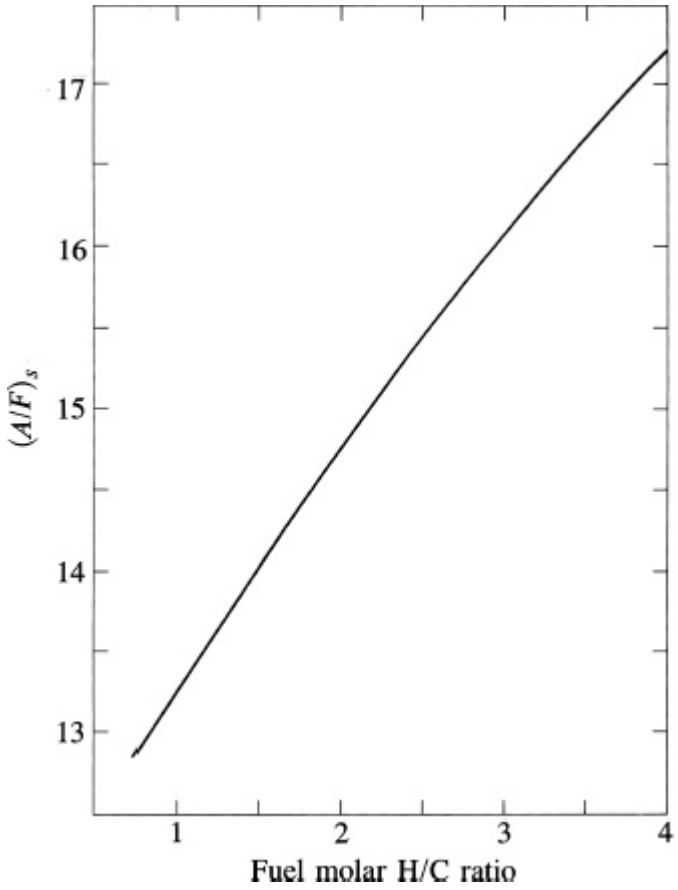
$$\left(\frac{A}{F}\right)_s = \left(\frac{F}{A}\right)_s^{-1} = \frac{(1 + y/4)(32 + 3.773 \times 28.16)}{12.011 + 1.008y} = \frac{34.56(4 + y)}{12.011 + 1.008y}$$

© McGraw-Hill Education. All rights reserved. Any use is subject to the Terms of Use, Privacy Notice and copyright information.

(3.6)

The molecular weights of oxygen, atmospheric nitrogen, atomic carbon, and atomic hydrogen are, respectively, 32, 28.16, 12.011, and 1.008.
$(A/F)_s$ depends only on *y*; Fig. 3.5 shows the variation in
$(A/F)_s$ as *y* varies from 1 (e.g., benzene) to 4 (methane).

Figure 3.5 Stoichiometric air/fuel ratio for air-hydrocarbon fuel mixtures as a function of fuel molar H/C ratio.



Example

EXAMPLE 3.1

A hydrocarbon fuel of composition 84.1% by mass C and 15.9% by mass H has a molecular weight of 114.15. Determine the number of moles of air required for stoichiometric combustion and the number of moles of products produced per mole of fuel. Calculate
$(A/F)_s$,
$(F/A)_s$, and the molecular weights of the reactants and the products.

Assume a fuel composition
C_aH_b. The molecular weight relation gives

$$114.15 = 12.011a + 1.008b$$

© McGraw-Hill Education. All rights reserved. Any use is subject to the Terms of Use, Privacy Notice and copyright information.

The gravimetric analysis of the fuel gives

$$\frac{b}{a} = \frac{15.9/1.008}{84.1/12.011} = 2.25$$

Thus,[1]

$$a = 8 \quad b = 18^{b}$$

The fuel is octane
C_8H_{18}. Equation (3.5) then becomes

$$\overset{\text{Fuel}}{C_8H_{18}} + 12.5(O_2 + \overset{\text{Air}}{3.773N_2}) = 8CO_2 + 9\overset{\text{Products}}{H_2O} + 47.16N_2$$

In moles:

$$\begin{aligned} 1 + 12.5(1 + 3.773) &= 8 + 9 + 47.16 \\ 1 + 59.66 &= 64.16 \end{aligned}$$

Relative mass:

$$\begin{aligned} 114.15 + 59.66 \times 28.96 &= 8 \times 44.01 + 9 \times 18.02 + 47.16 \times 28.16 \\ 114.5 + 1727.8 &= 1842.3 \end{aligned}$$

Per unit mass fuel:

$$1 + 15.14 = 16.4$$

Thus for stoichiometric combustion, 1 mole of fuel requires 59.66 moles of air and produces 64.16 moles of products. The stoichiometric
$(A/F)_s$ is 15.14 and
$(F/A)_s$ is 0.0661.

The molecular weights of the reactants
M_R and products
M_P are

$$M_R = \frac{1}{n}\sum n_i M_i = \frac{1}{60.66}(1 \times 114.15 + 59.66 \times 28.96)$$
$$M_p = \frac{1}{n}\sum n_i M_i = \frac{1}{64.16}(8 \times 44.01 + 9 \times 18.02 + 47.16 \times 28.16)$$

Thus,

© McGraw-Hill Education. All rights reserved. Any use is subject to the Terms of Use, Privacy Notice and copyright information.

$$M_R = 30.36 \quad M_p = 28.71$$

Fuel-air mixtures with more than or less than the stoichiometric air requirement can be burned. With excess air or fuel-lean combustion, the extra air appears in the products in essentially unchanged form. For example, the combustion of isooctane with 25% excess air, or 1.25 times the stoichiometric air requirement, gives

$$\mathrm{C_8H_{18}} + 1.25 \times 12.5(\mathrm{O_2} + 3.773\mathrm{N_2}) = 8\mathrm{CO_2} + 9\mathrm{H_2O} + 3.13\mathrm{O_2} + 58.95\mathrm{N_2}$$

(3.7)

With less than the stoichiometric air requirement, that is, with fuel-rich combustion, there is insufficient oxygen to oxidize fully the fuel C and H to
$\mathrm{CO_2}$ and
$\mathrm{H_2O}$. The products are a mixture of
$\mathrm{CO_2}$ and
$\mathrm{H_2O}$, with carbon monoxide CO and hydrogen $\mathrm{H_2}$ (as well as $\mathrm{N_2}$). The product composition cannot be determined from an element balance alone, and an additional assumption about the chemical composition of the product species must be made (see Secs. 4.2 and 4.9.2).

Because the composition of the combustion products is significantly different for fuel-lean and fuel-rich mixtures, and because the stoichiometric fuel/air ratio depends on fuel composition, the ratio of the actual fuel/air ratio to the stoichiometric ratio (or the inverse of this ratio) is a more informative parameter for defining mixture composition. The *fuel/air equivalence ratio* ϕ,

$$\phi = \frac{(F/A)_{\text{actual}}}{(F/A)_s}$$

(3.8)

will be used throughout this text for this purpose: The inverse of ϕ, the *relative air/fuel ratio* λ,

$$\lambda = \phi^{-1} = \frac{(A/F)_{\text{actual}}}{(A/F)_s}$$

(3.9)

is also used extensively. These parameters define the following fuel-air mixture stoichiometry regimes:

$$\begin{aligned}&\text{For fuel-lean mixtures: } \phi < 1, \lambda > 1\\ &\text{For stoichiometric mixtures: } \phi = \lambda = 1\\ &\text{For fuel-rich mixtures: } \phi > 1, \lambda < 1\end{aligned}$$

When the fuel contains oxygen (e.g., with alcohols), the procedure for determining the overall combustion equation is the same except that fuel oxygen is included in the oxygen balance between reactants and products. For methyl alcohol (methanol), $\mathrm{CH_3OH}$, the stoichiometric combustion equation is

© McGraw-Hill Education. All rights reserved. Any use is subject to the Terms of Use, Privacy Notice and copyright information.

$$CH_3OH + 1.5(O_2 + 3.773N_2) = CO_2 + 2H_2O + 5.66N_2$$

(3.10)

and
$(A/F)_s$ = 6.47. For ethyl alcohol (ethanol),
C_2H_5OH, the stoichiometric combustion equation is

$$C_2H_5OH + 3(O_2 + 3.773N_2) = 2CO_2 + 3H_2O + 11.32N_2$$

(3.11)

and
$(A/F)_s$ = 9.00.

If there are significant amounts of sulfur in the fuel, the appropriate oxidation product for determining the stoichiometric air and fuel proportions is sulfur dioxide,
SO_2.

For hydrogen fuel, the stoichiometric equation is

$$H_2 + \frac{1}{2}(O_2 + 3.773N_2) = H_2O + 1.887N_2$$

(3.12)

and the stoichiometric (*A/F*) ratio is 34.3.

Note that the actual composition of the products of combustion in Eqs. (3.7) and (3.10) to (3.12) may not occur in practice. At normal combustion temperatures, significant dissociation of
CO_2 and of
H_2O occurs (see Sec. 3.7.1). At lower temperatures, how close recombination brings the product composition to that indicated by these overall chemical equations depends on the rate of cooling of the product gases. More general relationships for the composition of unburned and burned gas mixtures are developed in Chap. 4.

The stoichiometric (*A/F*) and (*F/A*) ratios of common fuels and representative single hydrocarbon and other compounds are given in App. D along with other fuel data. Figure 3.5 shows how this stoichiometric
$(A/F)_s$ varies with fuel H:C ratio.

[1] Note that for fuels, which are mixtures of hydrocarbons, *a* and *b* need not be integers.

© McGraw-Hill Education. All rights reserved. Any use is subject to the Terms of Use, Privacy Notice and copyright information.

3.5. THE FIRST LAW OF THERMODYNAMICS AND COMBUSTION

3.5.1. Energy and Enthalpy Balances

[1]In a combustion process, fuel and oxidizer react to produce products of different composition. The actual path by which this transformation takes place is understood only for relatively simple fuels such as hydrogen, methane, *n*-heptane, isooctane, toluene, methanol, and ethanol. For fuel mixtures such as gasoline, or with more complicated molecular structure, the details are not well defined. Nonetheless, the first law of thermodynamics can be used to relate the end states of mixtures undergoing a combustion process; its application does not require that the details of the process be known.

The first law of thermodynamics relates changes in internal energy (or enthalpy) to heat and work transfer interactions. In applying the first law to a system whose chemical composition changes, care must be exercised in relating the reference states at which zero internal energy or enthalpy for each species or groups of species are assigned. We are not free, when chemical reactions occur, to choose independently the zero internal energy or enthalpy reference states of chemical substances transformed into each other by reaction.

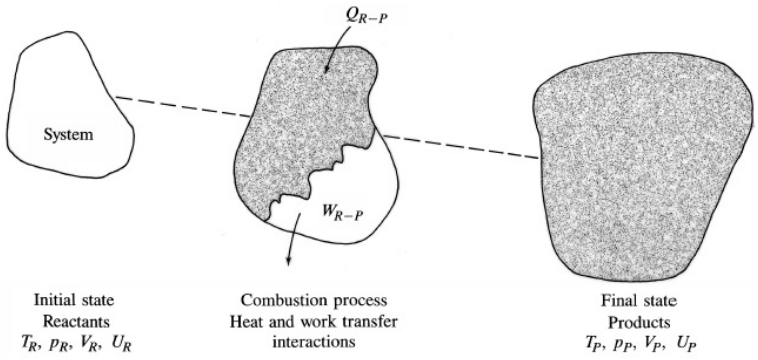
Consider a system of mass *m* that changes its composition from reactants to products by chemical reaction as indicated in Fig. 3.6. Applying the first law to the system between its initial and final states gives

$$Q_{R-P} - W_{R-P} = U_P - U_R$$

(3.13)

Heat transfer
Q_{R-P}, and work transfer
W_{R-P} due to normal force displacements, may occur across the system boundary. The standard thermodynamic sign convention for each energy transfer interaction—positive for heat transfer *to* the system and positive for work transfer *from* the system—is used.

Figure 3.6 System changing from reactants to products for first law analysis.



We will consider a series of special processes: first, a *constant volume* process where the initial and final temperatures are the same,
T'. Then Eq. (3.13) becomes

© McGraw-Hill Education. All rights reserved. Any use is subject to the Terms of Use, Privacy Notice and copyright information.

$$Q_{R-P} = U'_P - U'_R = (\Delta U)_{V,T'}$$

(3.14)

The internal energy of the system has changed by an amount $(\Delta U)_{V,T'}$, which can be measured or calculated. Since combustion processes are exothermic, Q_{R-P} and $(\Delta U)_{V,T'}$ are negative; therefore, the system's internal energy decreases. If Eq. (3.14) is expressed per mole of fuel, then $(\Delta U)_{V,T'}$ is known as the increase in internal energy at constant volume, and $(\Delta U)_{V,T'}$ is known as the *heat of reaction at constant volume* at temperature T'.

Next, consider a *constant pressure* process where the initial and final temperatures are the same, T'. For a constant pressure process

$$W_{R-P} = \int_R^P p dV = p(V_P - V_R)$$

(3.15)

so Eq. (3.13) becomes

$$Q_{R-P} - p(V'_P - V'_R) = U'_P - U'_R$$

or

$$\begin{aligned} Q_{R-P} &= p(U'_P - pV'_P) - U'_R + pV'_R) \\ &= H'_P - H'_R = (\Delta H)_{p,T'} \end{aligned}$$

(3.16)

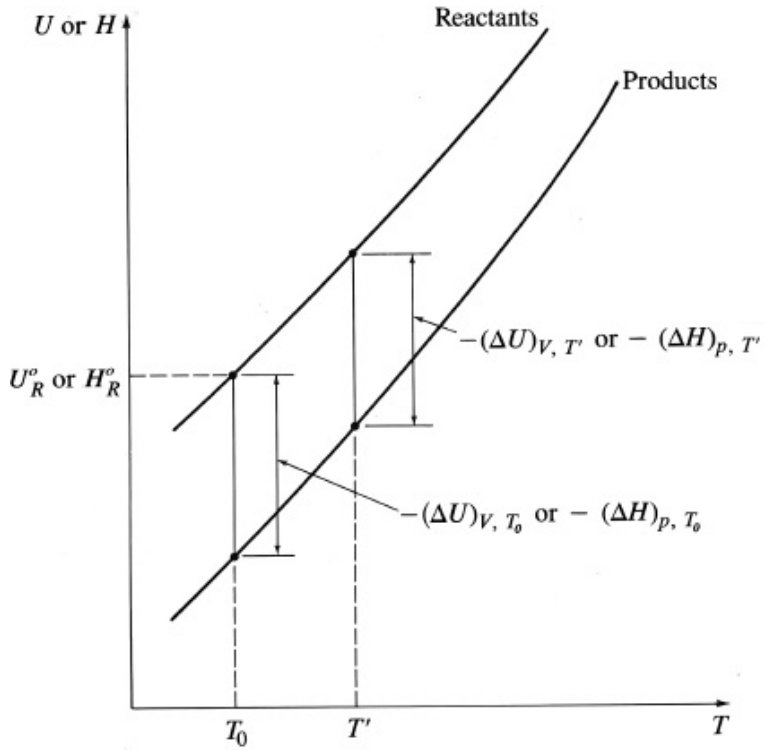
The enthalpy of the system has changed by an amount $(\Delta H)_{p,T'}$, which can be measured or calculated. Again, for combustion reactions, $(\Delta H)_{p,T'}$ is a negative quantity. If Eq. (3.16) is written per mole of fuel, $(\Delta H)_{p,T'}$ is called the increase in enthalpy at constant pressure and $-(\Delta H)_{p,T'}$ is called the *heat of reaction at constant pressure* at T'.

These processes can be displayed, respectively, on the internal energy or enthalpy versus temperature plot shown schematically in Fig. 3.7. If *U* (or *H*) for the reactants is arbitrarily assigned a value U°_R (or H°_R) at some reference temperature T_0, then the value of $(\Delta U)_{V,T_0}$ or $(\Delta H)_{p,T_0}$ fixes the relationship between *U*(*T*) or *H*(*T*), respectively, for the products and the reactants. Note that the slope of these lines (the specific heat at constant volume or pressure, if the vertical axis is expressed per unit mass or per mole)

© McGraw-Hill Education. All rights reserved. Any use is subject to the Terms of Use, Privacy Notice and copyright information.

increases with increasing temperature; also, the magnitude of $(\Delta U)_{V,T'}$ or $(\Delta H)_{p,T'}$ decreases with increasing temperature because c_v (or c_p) for the products is greater than that for the reactants.

Figure 3.7 Schematic plot of internal energy (U) or enthalpy (H) of reactants and products as a function of temperature.



The difference between $(\Delta H)_{p,T'}$ and $(\Delta U)_{V,T'}$ is

$$(\Delta H)_{p,T'} - (\Delta U)_{V,T'} = p(V_P - V_R)$$

(3.17)

Only if the volumes of the products and reactants in the constant pressure process are the same, are $(\Delta H)_{p,T'}$ and $(\Delta U)_{V,T'}$ equal. If all the reactant and product species are ideal gases, then the ideal gas law Eq. (3.1) gives

$$(\Delta H)_{p,T'} - (\Delta U)_{V,T'} = \tilde{R}(n'_P - n'_R)T'$$

(3.18)

Note that any inert gases do not contribute to $(n'_P - n'_R)$.

© McGraw-Hill Education. All rights reserved. Any use is subject to the Terms of Use, Privacy Notice and copyright information.

With a hydrocarbon fuel, one of the products, H_2O, can be in the gaseous or liquid phase. The internal energy (or enthalpy) of the products in the constant volume or constant pressure processes described above in Fig. 3.7 will depend on the relative proportions of the water in the gaseous and liquid phases. The limiting cases of all vapor and all liquid are shown in Fig. 3.8*a* for a *U-T* plot. The internal energy differences between the curves is

$$\left|(\Delta U)_{V,T',\,\mathrm{H_2O\,liq}}\right| - \left|(\Delta U)_{V,T',\,\mathrm{H_2O\,vap}}\right| = m_{\mathrm{H_2O}} u'_{fg\mathrm{H_2O}}$$

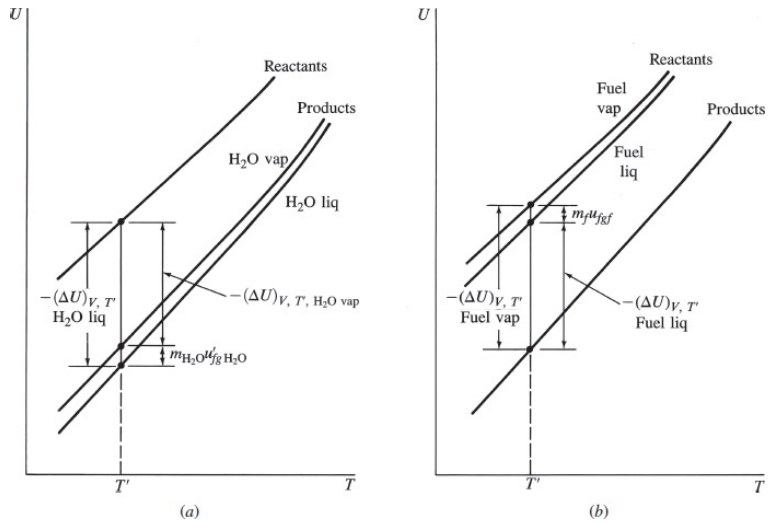
(3.19)

where
$m_{\mathrm{H_2O}}$ is the mass of water in the products and
$u'_{fg\mathrm{H_2O}}$ is the internal energy of vaporization of water at the temperature and pressure of the products. Similar curves and relationships apply for enthalpy:

$$\left|(\Delta H)_{p,T',\,\mathrm{H_2O\,liq}}\right| - \left|(\Delta H)_{p,T',\,\mathrm{H_2O\,vap}}\right| = m_{\mathrm{H_2O}} h'_{fg\mathrm{H_2O}}$$

(3.20)

Figure 3.8 Schematic plots of internal energy of reactants and products as a function of temperature: (a) Effect of water in products as either vapor or liquid; (b) effect of fuel in reactants as either vapor or liquid.



For some fuels, the reactants may contain the fuel as either liquid or vapor. The *U—T* (or *H—T*) line for the reactants with the fuel as liquid or as vapor will be different, as indicated in Fig. 3.8*b*. The vertical distance between the two reactant curves is $m_f u_{fgf}$ (or $m_f h_{fgf}$) where the subscript *f* denotes fuel.

3.5.2. Enthalpies of Formation

For fuels that are single hydrocarbon compounds, or where the precise fuel composition is known, the internal energies or enthalpies of the reactants and the products can be related through the enthalpies of formation of the reactants and products.

© McGraw-Hill Education. All rights reserved. Any use is subject to the Terms of Use, Privacy Notice and copyright information.

The *enthalpy of formation* $\Delta\tilde{h}_f^\circ$ of a chemical compound is the enthalpy increase associated with the reaction of forming one mole of the given compound from its elements, with each substance in its thermodynamic standard state at the given temperature.

The *standard state* is the state at one atmosphere pressure and the temperature under consideration. We will denote the standard state by the superscript °.

Since thermodynamic calculations are made as a difference between an initial and a final state, it is necessary to select a *datum state* to which all other thermodynamic states can be referred. While a number of datum states have been used in the literature, the most common datum is 298.15 K (25°C) and 1 atmosphere. We will use this datum throughout this text. Elements at their *reference state* are arbitrarily assigned zero enthalpy at the datum temperature. The reference state of each element is its stable standard state: for example, for oxygen at 298.15 K, the reference state is O_2 gas.

Enthalpies of formation are tabulated as a function of temperature for all commonly occurring species. For inorganic compounds, the *JANAF Thermochemical Tables* are the primary reference source.[8] These tables include values of the molar specific heat at constant pressure, standard entropy, standard Gibbs free energy (called free energy in the tables), standard enthalpy, enthalpy of formation and Gibbs free energy of formation, and $\log_{10}$ equilibrium constant for the formation of each species from its elements. Some primary references for thermodynamic data on fuel compounds are Maxwell,[9] Rossini et al.,[10] and Stull et al.[11] Enthalpies of formation of species relevant to hydrocarbon fuel combustion are tabulated in Table 3.2. Selected values of thermodynamic properties of relevant species are tabulated in App. D.

© McGraw-Hill Education. All rights reserved. Any use is subject to the Terms of Use, Privacy Notice and copyright information.

Table 3.2 Standard enthalpies of formation

Species	State*	$\Delta\tilde{h}_f^\circ$, MJ/kmol
O_2	Gas	0
N_2	Gas	0
H_2	Gas	0
C	Gas	0
CO_2	Gas	−393.52
H_2O	Gas	−241.83
H_2O	Liquid	−285.84
CO	Gas	−110.54
CH_4	Gas	−74.87
C_3H_8	Gas	−103.85
CH_3OH	Gas	−201.17
CH_3OH	Liquid	−238.58
C_8H_{18}†	Gas	−224.1
C_8H_{18}†	Liquid	−259.3

*At 298.15 K (25°C) and 1 atm.

†Isooctane.

For a given combustion reaction, the enthalpy of the products at the standard state relative to the enthalpy datum is then given by

$$H_P^\circ = \sum_{\text{products}} n_i \Delta\tilde{h}_{f,i}^\circ$$

(3.21*a*)

and the enthalpy of the reactants is given by

$$H_R^\circ = \sum_{\text{products}} n_i \Delta\tilde{h}_{f,i}^\circ$$

(3.21*b*)

The enthalpy increase,

© McGraw-Hill Education. All rights reserved. Any use is subject to the Terms of Use, Privacy Notice and copyright information.

$(\Delta H)_{p,T_0}$, is then obtained from the difference $(H_P^\circ - H_R^\circ)$. The internal energy increase can be obtained with Eq. (3.17).

Example

EXAMPLE 3.2

Calculate the enthalpy of the products and reactants, and the enthalpy increase and internal energy increase of the reaction, of a stoichiometric mixture of methane and oxygen at 298.15 K.

The stoichiometric reaction is

$$\mathrm{CH_4} + 2\mathrm{O_2} = \mathrm{CO_2} + 2\mathrm{H_2O}$$

For $\mathrm{H_2O}$ gas, from Table 3.2 and Eqs. (3.21*a* and *b*):

$$H_P^\circ = -393.52 + 2(-241.83) = -877.18\ \mathrm{MJ/kmol\ CH_4}$$

For $\mathrm{H_2O}$ liquid:

$$\begin{aligned} H_P^\circ &= -393.52 + 2(-285.84) = -965.20\,\mathrm{MJ/kmol\ CH_4} \\ H_R^\circ &= -74.87\,\mathrm{MJ/kmol\,CH_4} \end{aligned}$$

Hence for $\mathrm{H_2O}$ gas:

$$(\Delta H)_P^\circ = -877.18 + 74.87 = -802.31\,\mathrm{MJ/kmol\,CH_4}$$

and for $\mathrm{H_2O}$ liquid:

$$(\Delta H)_P^\circ = -965.20 + 74.87 = -890.33\,\mathrm{MJ/kmol\,CH_4}$$

Use Eq. (3.18) to find $(\Delta U)_V^\circ$. With $\mathrm{H_2O}$ gas, the number of moles of reactants and products are equal, so

$$(\Delta U)_V^\circ = (\Delta H)_P^\circ = -802.3\,\mathrm{MJ/kmol\,CH_4}$$

For $\mathrm{H_2O}$ liquid:

© McGraw-Hill Education. All rights reserved. Any use is subject to the Terms of Use, Privacy Notice and copyright information.

$$(\Delta U)_V^\circ = -890.33 - 8.3143 \times 10^{-3}(1-3)298.15\,\mathrm{MJ/kmol\,CH_4}$$
$$(\Delta U)_V^\circ = -885.4\,\mathrm{MJ/kmol\,CH_4}$$

Note that the presence of nitrogen in the mixture or oxygen in excess of the stoichiometric amount would not change any of these calculations.

3.5.3. Heating Values

For fuels where the precise fuel composition is not known, the enthalpy of the reactants cannot be determined from the enthalpies of formation of the reactant species. The *heating value* of the fuel is then measured directly.

The heating value
Q_{HV} or calorific value of a fuel is the magnitude of the heat of reaction at constant pressure or at constant volume at a standard temperature [usually 25°C (77°F)] for the complete combustion of unit mass of fuel. Thus

$$\mathrm{Q_{HV}}_p = -(\Delta H)_{p,T_0}$$

(3.22*a*)

and

$$\mathrm{Q_{HV}}_v = -(\Delta U)_{v,T_0}$$

(3.22*b*)

Complete combustion means that all carbon is converted to
$\mathrm{CO_2}$, all hydrogen is converted to
$\mathrm{H_2O}$, and any sulfur present is converted to
$\mathrm{SO_2}$. The heating value is usually expressed in joules per kilogram or joules per kilomole of fuel (British thermal units per pound-mass or British thermal units per pound-mole). It is therefore unnecessary to specify how much oxidant was mixed with the fuel, though this must exceed the stoichiometric requirement. It is immaterial whether the oxidant is air or oxygen.

For fuels containing hydrogen, we have shown that whether the
$\mathrm{H_2O}$ in the products is in the liquid or gaseous phase affects the value of the heat of reaction. The term *higher heating value*
$\mathrm{Q_{HMV}}$ (or gross heating value) is used when the
$\mathrm{H_2O}$ formed is all condensed to the liquid phase; the term *lower heating value*
$\mathrm{Q_{LHV}}$ (or net heating value) is used when the
$\mathrm{H_2O}$ formed is all in the vapor phase. The two heating values at constant pressure are related by

$$Q_{\mathrm{HMV}_p} = Q_{\mathrm{LHV}_p} + \left(\frac{m_{\mathrm{H_2O}}}{m_f}\right) h_{fg\mathrm{H_2O}}$$

(3.23)

where
$(m_{\mathrm{H_2O}}/m_f)$ is the ratio of mass of

© McGraw-Hill Education. All rights reserved. Any use is subject to the Terms of Use, Privacy Notice and copyright information.

H_2O produced to mass of fuel burned. A similar expression with u_{fgH_2O} replacing h_{fgH_2O} applies for the higher and lower heating value at constant volume. The difference between these two heating values for hydrocarbon-based fuels is in the 4 to 11% range, depending on C:H ratio.

The heating value at constant pressure is the more commonly used one; often the qualification "at constant pressure" is omitted. The difference between the heating values at constant pressure and constant volume is small.

Heating values[2] of fuels are measured in calorimeters. For gaseous fuels, it is most convenient and accurate to use a continuous-flow atmosphere pressure calorimeter. The entering gaseous fuel is saturated with water vapor and mixed with sufficient saturated air for complete combustion at the reference temperature. The mixture is burned in a burner and the combustion products cooled with water-cooled metal tube coils to close to the inlet temperature. The heat transferred to the cooling water is calculated from the measured water flow rate and water temperature rise. The heating value determined by this process is the higher heating value at constant pressure.

For liquid and solid fuels, it is more satisfactory to burn the fuel with oxygen under pressure at constant volume in a calorimeter. A sample of the fuel is placed in the calorimeter, which is a stainless-steel container immersed in cooling water at the standard temperature. Sufficient water is placed in the calorimeter to ensure that the water produced in the combustion process will condense. Oxygen at 30 atmospheres is admitted into the calorimeter. A length of firing cotton is suspended into the sample from an electrically heated wire filament to act as a source of ignition. When combustion is complete, and the combustion products and calorimeter have thermally equilibrated, the temperature rise of the calorimeter and its cooling water is measured. The heating value determined by this process is the higher heating value at constant volume.

The heating values of common fuels are tabulated with other fuel data in App. D. The following example illustrates how the enthalpy of a reactant mixture relative to the enthalpy datum we have defined can be determined from the measured heating value of the fuel.

Example

EXAMPLE 3.3

Liquid kerosene fuel with a lower heating value (determined in a calorimeter) of 43.2 MJ/kg and average molar H/C ratio of 2 is mixed with the stoichiometric air requirement at 298.15 K. Calculate the enthalpy of the reactant mixture relative to the datum of zero enthalpy for C, O_2, N_2, and H_2 at 298.15 K.

The combustion equation per mole of fuel can be written as

$$CH_2 + \tfrac{3}{2}(O_2 + 3.773N_2) = CO_2 + H_2O + 5.660N_2$$

or

$$14\ \text{kg fuel} + \left.\begin{matrix}7.160\,\text{kmol}\\ 207.4\ \text{kg}\end{matrix}\right\}\text{air} \rightarrow \left.\begin{matrix}7.66\,\text{kmol}\\ 221.4\ \text{kg}\end{matrix}\right\}\text{products}$$

where M = 28.962 for atmospheric air.

© McGraw-Hill Education. All rights reserved. Any use is subject to the Terms of Use, Privacy Notice and copyright information.

The heating value given is at constant volume, $-(\Delta U)^\circ_V$. $-(\Delta H)^\circ_p$ is obtained from Eq. (3.18), noting that the fuel is in the liquid phase:

$$\begin{aligned}(\Delta H)^\circ_P &= -43.2 + 8.3143 \times 10^{-3}(7.66 - 7.160) \times \frac{298.15}{14} \\ &= -43.2 + 0.09 = -43.1\,\text{MJ/kg fuel}\end{aligned}$$

The enthalpy of the products per kilogram of mixture is found from the enthalpies of formation of CO_2 and H_2O vapor given in Table 3.2:

$$\begin{aligned}h_P &= \frac{1 \times (-393.52) + 1 \times (-241.83)}{221.4} \\ &= -2.87\,\text{MJ/kg}\end{aligned}$$

The enthalpy of the reactants per kilogram of mixture is then

$$h_R = h_P - (\Delta h)^\circ_p = -2.87 + \frac{43.1 \times 14}{221.4} = -0.145\,\text{MJ/kg}$$

3.5.4. Adiabatic Combustion Processes

We now use the relationships developed above to examine two other special processes important in engine analysis: constant-volume and constant-pressure adiabatic combustion. For an adiabatic constant-volume process, Eq. (3.13) becomes

$$U_P - U_R = 0$$

(3.24)

when U_P and U_R are evaluated relative to the same datum (e.g., the enthalpies of C, O_2, N_2, and H_2 are zero at 298.15 K, the datum used throughout this text).

Frequently, however, the data on internal energy or enthalpy for species and reactant or product mixtures that are available give internal energies or enthalpies relative to the species or mixture value at some reference temperature T_0: e.g., $U(T)$ – $U(T_0)$ or $H(T)$ – $H(T_0)$ are tabulated or graphed. Since

$$U_P(T_0) - U_R(T_0) = (\Delta U)_{V,T_0}$$

© McGraw-Hill Education. All rights reserved. Any use is subject to the Terms of Use, Privacy Notice and copyright information.

it follows from Eq. (3.24) that

$$[U_P(T) - U_P(T_0)] - [U_R(T) - U_R(T_0)] = -(\Delta U)_{V,T_0}$$

(3.25)

relates the product and reactant states. Figure 3.9 illustrates the adiabatic constant-volume combustion process on a *U-T* diagram. Given the initial state of the reactants (T_R, V), we can determine the final state of the products (T_P, p).

For an adiabatic constant-pressure combustion process, Eq. (3.13) gives

$$H_P - H_R = 0$$

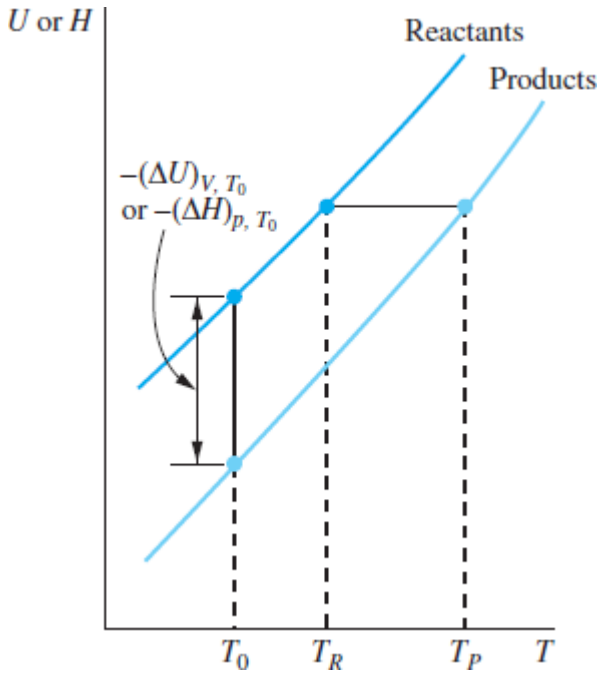
which combines with Eq. (3.16) to give

$$[H_P(T) - H_p(T_0)] - [H_R(T) - H_R(T_0)] = -(\Delta H)_{p,T_0}$$

(3.26)

Figure 3.9 illustrates this process also. Given the initial reactant state (T_R, p), we can determine the final product state (T_P, p).

Figure 3.9 Adiabatic constant-volume combustion process on U-T diagram or adiabatic constant-pressure combustion process on H-T diagram.



Note that while in Figs. 3.7, 3.8, and 3.9 we have shown *U* and *H* for the reactants and products to be functions of *T* only, in practice for the products at high temperature, *U* and *H* will be functions of *p* and *T*. The analysis presented here is general;

© McGraw-Hill Education. All rights reserved. Any use is subject to the Terms of Use, Privacy Notice and copyright information.

however, to determine the final state of the products in an adiabatic combustion process, the constant-volume or constant-pressure constraint must also be used explicitly.

The final temperature of the products in an adiabatic combustion process is called the *adiabatic flame temperature*. Examples of typical adiabatic flame temperatures are shown later in Fig. 3.13.

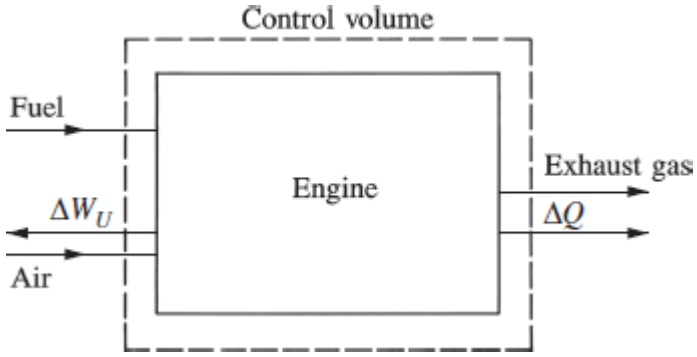
3.5.5. Combustion Efficiency of an Internal Combustion Engine

In practice, the exhaust gas of an internal combustion engine contains incomplete combustion products (e.g., CO, H_2, unburned hydrocarbons, soot) as well as complete combustion products (CO_2 and H_2O); see Sec. 4.9. Under lean operating conditions, the amounts of incomplete combustion products are small. Under fuel-rich operating conditions, these amounts become more substantial since there is insufficient oxygen to complete combustion. Because a fraction of the fuel's chemical energy is not fully released inside the engine during the combustion process, it is useful to define a *combustion efficiency*. The engine can be analyzed as an open system that exchanges heat and work with its surrounding environment (the atmosphere). Reactants (fuel and air) flow into the system; products (exhaust gases) flow out. Consider a mass *m* that passes through the control volume surrounding the engine shown in Fig. 3.10; the *net chemical energy release* due to combustion within the engine is given by

$$[H_R(T_A) - H_p(T_A)] = m\left(\sum_{i,\text{reactants}} n_i \Delta\tilde{h}^\circ_{f,i} - \sum_{i,\text{products}} n_i \Delta\tilde{h}^\circ_{f,i}\right)$$

Enthalpy is the appropriate property since $p_R = p_P = p_{\text{atm}}$: n_i is the number of moles of species *i* in the reactants or products per unit mass of working fluid, and $\Delta\tilde{h}^\circ_{f,i}$ is the standard enthalpy of formation of species *i* at ambient temperature T_A.

Figure 3.10 Control volume surrounding engine. ΔW_U is the useful work produced by the engine; ΔQ is the heat lost from the cylinder charge to the walls.



The maximum amount of fuel energy *supplied* to the control volume around the engine that can be released by combustion is $m_f Q_{\text{HV}}$. Hence, the *combustion efficiency*—the fraction of the fuel energy supplied that is released in the combustion process—is given by[12]

© McGraw-Hill Education. All rights reserved. Any use is subject to the Terms of Use, Privacy Notice and copyright information.

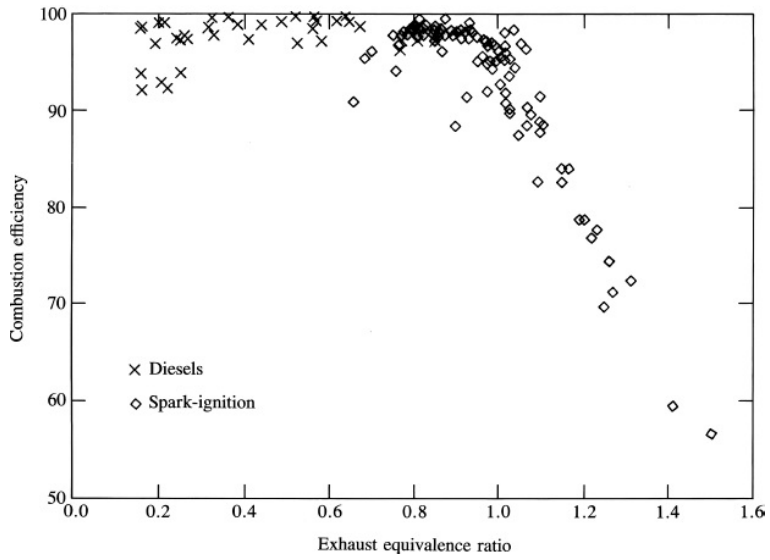
$$\eta_c = \frac{H_R(T_A) - H_P(T_A)}{m_f Q_{\text{HV}}}$$

(3.27)

Note that *m* and
m_f can be replaced by the average mass flow rates
$\dot{m}$ and
$\dot{m}_f$.

Figure 3.11 shows how combustion efficiency varies with the fuel/air equivalence ratio for internal combustion engines. For spark-ignition engines, for lean equivalence ratios, the combustion efficiency is usually in the range of 95 to 98%. For mixtures richer than stoichiometric, lack of oxygen prevents complete combustion of the fuel carbon and hydrogen, and the combustion efficiency steadily decreases as the mixture becomes richer. Combustion efficiency is little affected by other engine operating and design variables, provided the engine combustion process remains stable. For diesel engines, which always operate lean, the combustion efficiency is slightly higher—about 98%. Details of exhaust gas composition, on which these combustion efficiencies are based, can be found in Sec. 4.9. There, in Eq. (4.67), Eq. (3.27) is expressed in terms of the concentrations of the incomplete combustion species (e.g., CO,
H_2, and HC) and their heating values.

Figure 3.11 Variation of engine combustion efficiency with fuel/air equivalence ratio.



[1] The approach used here follows that developed by Spalding and Cole.[7]

[2] Standard methods for measuring heating values are defined by the American Society for Testing Materials.

© McGraw-Hill Education. All rights reserved. Any use is subject to the Terms of Use, Privacy Notice and copyright information.

3.6. THE SECOND LAW OF THERMODYNAMICS APPLIED TO COMBUSTION

3.6.1. Entropy

In App. B, it is shown how the entropy of a mixture of ideal gases of known composition can be calculated. The discussion earlier relating the enthalpies (or internal energies) of the reactant and the product mixtures applies to entropy also. For example, the standard-state entropies of chemical species are tabulated in the JANAF[8] tables relative to zero entropy at 0 K. If the entropies of the elements at a datum-state temperature and pressure are (arbitrarily) set equal to zero, then the values of the entropy of a reactant mixture of given composition, temperature and pressure, and of the product mixture of given composition, temperature and pressure, can both be determined.

3.6.2. Maximum Work from an Internal Combustion Engine and Efficiency

An internal combustion engine can be analyzed as an open system that exchanges heat and work with its surrounding environment (the atmosphere). Reactants (fuel and air) flow into the system; products (exhaust gases) flow out. By applying the second law of thermodynamics to a control volume surrounding the engine, as illustrated in Fig. 3.10, we can derive an expression for the maximum useful work that the engine can deliver.

Consider a mass *m* of fluid as it passes through the control volume surrounding the engine. The first law gives

$$\Delta Q - \Delta W_U = \Delta H$$

where
ΔW_U is the useful work transfer (i.e., non-*pdV* work) to the environment and
$\Delta H = H_P - H_R$. Since the heat transfer
ΔQ occurs only with the atmosphere at temperature
T_A, from the second law

$$\frac{\Delta Q}{T_A} \leq \Delta S$$

These equations combine to give

$$\Delta W_U \leq -(\Delta H - T_A \Delta S) = -\Delta B$$

where *B* is the steady-flow availability function,
$H - T_A S$.[13] Usually, for the entering gases,
$p_R = p_A$ and
$T_R = T_A$, and the maximum work will be obtained when
$p_P = p_A$ and

© McGraw-Hill Education. All rights reserved. Any use is subject to the Terms of Use, Privacy Notice and copyright information.

$T_P = T_A$.

Under these conditions,

$$\Delta W_U \leq -\left[(H - TS)_{P_{T_A,p_A}} - (H - TS)_{R_{T_A,p_A}}\right] = -(\Delta G)_{T_A,p_A}$$

(3.28)

or

$$\Delta W_{\max} = -(\Delta G)_{T_A,p_A}$$

G is the Gibbs free energy, *H* – *TS*, and
$(\Delta G)_{T_A,p_A}$ is the Gibbs free energy increase in the reaction of the fuel-air mixture to products at atmospheric temperature and pressure.
$-(\Delta G)_{T_A,p_A}$ will be a maximum when combustion is complete.

A fundamental measure of the effectiveness of any practical internal combustion engine is the ratio of the actual work delivered compared with this maximum work. This ratio is called the *availability conversion efficiency*
η_a:

$$\eta_a = \frac{\Delta W}{\Delta W_{U\max}} = -\frac{\Delta W}{(\Delta G)T_{A,pA}}$$

(3.29)

The property *availability* is the maximum useful work transfer that can be obtained from a system atmosphere or control-volume atmosphere combination. This efficiency therefore defines the fraction of the availability of the unburned fuel-air mixture which, passing through the engine and interacting only with the atmosphere, is actually converted to useful work. Availability analysis of engine operation is proving valuable in identifying where the significant irreversibilities or losses in availability occur. This topic is discussed more fully in Sec. 5.7.

$(\Delta G)_{T_A,p_A}$, or
$(\Delta g)_{T_A,p_A}$, is not an easy quantity to evaluate for practical fuels; it is the heating value,
$-(\Delta h)_{T_A}$, which is usually measured. Values of
$(\Delta g)^\circ_{298}$ and
(Δh°_{298}) for selected fuel combustion reactions are given in Table 3.3. For the pure hydrocarbons, they are closely comparable because at 298 K,
$\Delta \tilde{s}^\circ << \Delta \tilde{h}^\circ / T$. For alcohols the difference is larger, 7% rather than about 1.5%. Because for practical fuels
$-(\Delta h)^\circ_{298}$ is measured directly as the heating value of the fuel, it is standard practice to use the following definition of efficiency:

$$\eta_f = \frac{W_c}{m_f Q_{\text{HV}}}$$

(3.30)

© McGraw-Hill Education. All rights reserved. Any use is subject to the Terms of Use, Privacy Notice and copyright information.

which was defined as the *fuel conversion efficiency* in Sec. 2.8. Note that sometimes the higher heating value is used in Eq. (3.30) and sometimes the lower heating value. Whichever value is used should be explicitly stated. The normal practice in internal combustion engine analysis is to use the lower heating value at constant pressure, since the engine overall is a steady flow device and the water in the exhaust is normally in vapor form. We will use $Q_{\mathrm{LHV},p}$ in Eq. (3.30) throughout this text. The fuel conversion efficiency is the most commonly used definition of engine efficiency because it uses an easily measured quantity, the heating value, to define the usable fuel energy supplied to the engine. For hydrocarbon fuels, since $\Delta\tilde{h}^\circ \approx \Delta\tilde{g}^\circ$ the fuel conversion efficiency and the availability conversion efficiency are closely comparable in value.

Table 3.3 Enthalpies and free energies of combustion reactions

Reaction*	$\Delta\tilde{h}^\circ_{298}$, MJ/kmol	$\Delta\tilde{g}^\circ_{298}$, MJ/kmol
$C + O_2 \rightarrow H_2O$	−393.52	−394.40
$H_2 + \frac{1}{2}O_2 \rightarrow H_2O$	−240.91	−232.78
$CH_4 + 2O_2 \rightarrow CO_2 + 2H_2O$	−802.30	−800.76
$CH_4O(l) + \frac{3}{2}O_2 \rightarrow CO_2 + 2H_2O$	−638.59	−685.35
$C_3H_8(g) + 5O_2 \rightarrow 3CO_2 + 4H_2O$	−2044.0	−2074.1
$C_6H_6(l) + \frac{15}{2}O_2 \rightarrow 6CO_2 + 3H_2O$	−3135.2	−3175.1
$C_8H_{18}(l) + \frac{25}{2}O_2 \rightarrow 8CO_2 + 9H_2O$	−5074.6	−5219.9
*In the products, H_2O is a gas.		

In practice, not all the fuel energy supplied to the engine is released by the combustion process since combustion is incomplete: the combustion efficiency [Eq. (3.27)] is less than unity. It is sometimes useful to separate out the effects of incomplete combustion by defining an efficiency that relates the actual work per cycle to the amount of fuel chemical energy released in the combustion process. We will call this the *thermal conversion efficiency* η_t:

$$\eta_t = \frac{W_c}{H_R(T_A) - H_p(T_A)} = -\frac{W_c}{(\Delta H)_{TA}} = \frac{W_c}{\eta_c m_f Q_{HV}}$$

(3.31)

Obviously the fuel conversion, thermal conversion, and combustion efficiencies are related by

$$\eta_f = \eta_c \eta_t$$

(3.32)

It is important to understand that there is a fundamental difference between the availability conversion efficiency of an internal combustion engine as defined by Eq. (3.29) [and the fuel conversion efficiency, Eq. (3.30), which closely approximates it], and the efficiency of a thermodynamic heat engine. The second law limit to the availability conversion efficiency is unity. For a

© McGraw-Hill Education. All rights reserved. Any use is subject to the Terms of Use, Privacy Notice and copyright information.

thermodynamic heat engine (defined as a system executing cycles experiencing heat-transfer interactions with two heat reservoirs, one at a higher and one at a lower temperature), the efficiency is limited to a value substantially less than unity by the temperatures of the heat reservoirs.[13] The maximum value of the efficiency of such engines is the Carnot cycle efficiency, $1 - (T_{\text{low}}/T_{\text{high}})$. However, internal combustion engines are steady-flow devices, interacting with the atmosphere, which produce work, where fuel and air flow in and burned gases flow out. They are *not heat engines*—systems (working fluids) executing cycles, interacting with heat reservoirs. So the Carnot cycle efficiency limit has no direct relevance to the efficiency of internal combustion engines.

© McGraw-Hill Education. All rights reserved. Any use is subject to the Terms of Use, Privacy Notice and copyright information.

3.7. CHEMICALLY REACTING GAS MIXTURES

The working fluids in engines are mixtures of gases. Depending on the process under consideration and the portion of the engine cycle in which it occurs, chemical reactions may: (1) be so slow that they have a negligible effect on mixture composition (the mixture composition is essentially "frozen"); (2) be so rapid that as the mixture state changes, the composition remains in chemical equilibrium; (3) be one of the rate-controlling processes that determine how the composition of the mixture changes with time.

3.7.1. Chemical Equilibrium

It is a good approximation for performance estimates in engines to regard the burned gases produced by the combustion of fuel and air as in chemical equilibrium.[1] By this we mean that the chemical reactions by which individual species in the burned gases react together, produce and remove each species at equal rates. No net change in species composition results.

For example, if the temperature of a mass of carbon dioxide gas in a vessel is increased sufficiently, some of the CO_2 molecules *dissociate* into CO and O_2 molecules. If the mixture of CO_2, CO, and O_2 is in equilibrium, then CO_2 molecules are dissociating into CO and O_2 at the same rate as CO and O_2 molecules are *recombining* in the proportions required to satisfy the equation

$$CO + \frac{1}{2}O_2 = CO_2$$

In combustion products of hydrocarbon fuels, the major species present at low temperatures are N_2, H_2O, CO_2, and O_2 or CO and H_2. At higher temperatures (greater than about 2200 K), these major species dissociate and react to form additional species in significant amounts. For example, the adiabatic combustion of a stoichiometric mixture of a typical hydrocarbon fuel with air produces products with species mole fractions of: $N_2 \sim 0.8$; H_2O, $CO_2 \sim 0.1$; CO, OH, O_2, NO, $H_2 \sim 0.01$; H, O ~ 0.001; and other species in lesser amounts.

The second law of thermodynamics defines the criterion for chemical equilibrium as follows. Consider a system of chemically reacting substances undergoing a constant-pressure, constant-temperature process. In the absence of shear work (and electrical work, gravity, motion, capillarity), the first law gives

© McGraw-Hill Education. All rights reserved. Any use is subject to the Terms of Use, Privacy Notice and copyright information.

$$\delta Q = dH$$

The second law gives

$$\delta Q \leq T\,dS$$

Combining these gives

$$dH - T\,dS \leq 0$$

Since we are considering constant-temperature processes, this equation holds for finite changes:

$$\Delta H - T\Delta S = \Delta G \leq 0$$

Thus, reactions can only occur (at constant pressure and temperature) if *G* (= *H* − *TS*) for the products is less than *G* for the reactants. Hence at equilibrium

$$(\Delta G)_{p,T} = 0$$

(3.33)

Consider a reactive mixture of ideal gases. The reactant species
M_a,
M_b, etc., and product species
M_l,
M_m, etc., are related by the general reaction whose stoichiometry is given by

$$\nu_a M_a + \nu_b M_b + \cdots = \nu_l M_l + \nu_m M_m + \cdots$$

(3.34*a*)

This can be written as

$$\sum_i \nu_i M_i = 0$$

(3.34*b*)

where the
ν_i are the stoichiometric coefficients and by convention are positive for the product species and negative for the reactant species.

Let an amount
δn_a of
M_a react with
δn_b of

© McGraw-Hill Education. All rights reserved. Any use is subject to the Terms of Use, Privacy Notice and copyright information.

M_b, etc., and produce
δn_l of
M_l,
δn_m of
M_m, etc. These amounts are in proportion:

$$\delta n_i = \nu_i \delta n$$

(3.35)

The change in Gibbs free energy of a mixture of ideal gases, at constant pressure and temperature, as the composition changes is given by

$$(\Delta G)_{p,T} = \sum_i \tilde{\mu}_i \delta n_i$$

(3.36)

where
Δn_i is the change in number of moles of species *i*, and
$\tilde{\mu}$ is the *chemical potential*. The chemical potential, an intensive property, is defined as

$$\tilde{\mu}_i = \left(\frac{\partial G}{\partial n_i} \right)_{p,T,n_j(j \neq i)}$$

(3.37)

It is equal in magnitude to the specific Gibbs free energy at a given temperature and pressure. For an ideal gas, it follows from Eqs. (B.13), (B.15), and (3.37) that

$$\tilde{\mu}_i = \tilde{\mu}_i^\circ(T) + \tilde{R}T \ln \frac{p_i}{p_0}$$

(3.38)

where
$\tilde{\mu}_i^\circ$ equals
$\tilde{g}_i^\circ$, the standard specific Gibbs free energy of formation. The standard state pressure
p_0 is usually 1 atmosphere.

Substitution in Eq. (3.36) gives, at equilibrium,

$$\sum \left(\tilde{\mu}_i^\circ + \tilde{R}T \ln \frac{p_i}{p_0} \right) \delta n_i = 0$$

or

© McGraw-Hill Education. All rights reserved. Any use is subject to the Terms of Use, Privacy Notice and copyright information.

$$\sum \left(\tilde{\mu}_i^{\circ} + \tilde{R}T \ln \frac{p_i}{p_0} \right) v_i \delta n = 0$$

We can divide by Δn and rearrange, to obtain

$$\sum \ln \left(\frac{p_i}{p_0} \right)^{v_i} = -\frac{\left(\sum \tilde{\mu}_i^{\circ} v_i \right)}{RT} = -\frac{\Delta G^{\circ}}{RT} = \ln K_p$$

(3.39)

K_p is the equilibrium constant at constant pressure:

$$k_p = \prod_i \left(\frac{p_i}{p_0} \right)^{v_i}$$

(3.40)

It is obtained from the Gibbs free energy of the reaction that can be calculated from the Gibbs free energy of formation of each species in the reaction, as indicated in Eq. (3.39) above. It is a function of temperature only.

In many chemical reaction data bases (e.g., the JANAF tables[8]), to simplify the calculation of equilibrium constants, values of $\log_{10}(k_p)_i$, the equilibrium constants of formation of one mole of each species from their elements in their standard states, are tabulated against temperature. The equilibrium constant for a specific reaction is then obtained via the relation

$$\log_{10}(K_p)_{\text{reaction}} = \sum_i v_i \log_{10}(k_p)_i$$

(3.41)

With the JANAF table values of $(k_p)_i$, the pressures in Eqs. (3.40) and (3.41) must be in atmospheres.

The effect of pressure on the equilibrium composition can be deduced from Eq. (3.40). Substitution of the mole fractions $\tilde{x}_i$ and mixture pressure *p* gives

$$\prod_i \left(\frac{p_i}{p_0} \right)^{v_i} = \prod_i \left(\tilde{x}_i \frac{p}{p_0} \right)^{v_i} = \left(\frac{p}{p_0} \right)^{\sum_i v_i} \prod_i \tilde{x}_i^{v_i} = K_p$$

If $\sum_i v_i = 0$ changes in pressure have no effect on the composition. If $\sum_i v_i > 0$ (dissociation reactions), then the mole fractions of the dissociation products decrease as pressure increases. If $\sum_i v_i < 0$ (recombination reactions), the converse is true.

An equilibrium constant,

© McGraw-Hill Education. All rights reserved. Any use is subject to the Terms of Use, Privacy Notice and copyright information.

K_c, based on concentrations (usually expressed in gram moles per cubic centimeter) is also used:

$$K_c = \prod_i [M_i]^{v_i}$$

(3.42)

Equation (3.40) can be used to relate K_p and K_c:

$$K_p = K_c(\tilde{R}T)^{\sum_i v_i}$$

(3.43)

for $p_0 = 1$ atmosphere. For $\sum_i v_i = 0$, K_p and K_c are equal.

Example

EXAMPLE 3.4

A stoichiometric mixture of CO and O_2 in a closed vessel, initially at 1 atm and 300 K, is exploded. Calculate the composition of the products of combustion at 2500 K and the gas pressure.

The combustion equation is

$$CO + \frac{1}{2}O_2 = CO_2$$

The JANAF tables give $\log_{10}K_p$ (equilibrium constants of formation from the elements in their standard state) at 2500 K of CO_2, CO, and O_2 as 8.280, 6.840, and 0, respectively. Thus, the equilibrium constant for the CO combustion reaction above is, from Eq. (3.41),

$$\log_{10}K_p = 8.280 - 6.840 = 1.440$$

which gives $K_p = 27.5$ = 27.5.

If the degree of dissociation in the products is *α* (i.e., a fraction *α* of the

© McGraw-Hill Education. All rights reserved. Any use is subject to the Terms of Use, Privacy Notice and copyright information.

CO_2 formed by complete combustion is dissociated), the product composition is

$$CO_2(1-\alpha); CO, \alpha; O_2, \frac{\alpha}{2}$$

For this mixture, the number of moles of reactants
n_R is
$\frac{3}{2}$ the number of moles of products
n_P is
$(1+\alpha/2)$.

The ideal gas law gives

$$p_R V = n_R \tilde{R} T_R, p_P V = n_P \tilde{R} T_P$$

Thus

$$\frac{p_p}{n_p} = \frac{1}{1.5} \times \frac{2500}{300} = 5.555 \text{ atm/mol}$$

The equilibrium relation [Eq. (3.40)] gives

$$\frac{1-\alpha}{\alpha(\alpha/2)^{1/2}} \left(\frac{n_p}{p_p}\right)^{1/2} = 27.5$$

which can be solved to give α = 0.074.

The composition of the products in mole fractions is, therefore,

$$\begin{aligned} \tilde{x}_{CO_2} &= \frac{1-\alpha}{n_P} = 0.893 \\ \tilde{x}_{CO} &= \frac{\alpha}{n_P} = 0.071 \\ \tilde{x}_{O_2} &= \frac{\alpha/2}{n_P} = 0.037 \end{aligned}$$

The pressure of the product mixture is

$$p = 5.555 n_P = 5.76 \text{ atm}$$

Example

EXAMPLE 3.5

In fuel-rich combustion product mixtures, equilibrium between the species

© McGraw-Hill Education. All rights reserved. Any use is subject to the Terms of Use, Privacy Notice and copyright information.

CO_2,
H_2O, CO, and
H_2 is often assumed to determine the burned gas composition. For ϕ = 1.2, for -air combustion products, determine the mole fractions of the product species at 1700 K.

The reaction relating these species (often called the water-gas reaction) is

$$CO_2 + H_2 = CO + H_2O$$

From the JANAF tables, values of the
$\log_{10} K_p$ of formation for these species at 1700 K are:
CO_2, 12.180; H_2, 0; CO, 8.011; $H_2O(g)$, 4.699. The equilibrium constant for the above reaction is, from Eq. (3.41),

$$\log_{10} K_p = 8.011 + 4.699 - 12.180 = 0.530$$

from which
$K_p = 3.388$.

The combustion reaction for
C_8H_{18}–air with ϕ = 1.2 can be written

$$C_8H_{18} + \frac{12.5}{1.2}(O_2 + 3.773N_2) \rightarrow aCO_2 + bH_2O + cCO + dH_2 + 39.30N_2$$

A carbon balance gives:
$a + c = 8$

A hydrogen balance gives:
$2b + 2d = 18$

An oxygen balance gives:
$2a + b + c = 20.83$

The equilibrium relation gives
$(bc)/(ad) = 3.388$ (since the equilibrated reaction has the same number of moles as there are reactants or products, the moles of each species can be substituted for the partial pressures).

These four equations can be solved to obtain

$$c^2 - 19.3c + 47.3 = 0$$

which gives c = 2.89, a = 5.12, b = 7.72, and d = 1.29. The total number of moles of products is

$$a + b + c + d + 39.3 = 56.3$$

and the mole fractions of the species in the burned gas mixture are

© McGraw-Hill Education. All rights reserved. Any use is subject to the Terms of Use, Privacy Notice and copyright information.

$$CO_2, 0.0908; \quad H_2O, 0.137; \quad CO, 0.051; \quad H_2, 0.023; \quad N_2, 0.698$$

Our development of the equilibrium relationship for one reaction has placed no restrictions on the occurrence of simultaneous equilibria. Consider a mixture of *N* reacting gases in equilibrium. If there are *C* chemical elements, conservation of elements will provide *C* equations that relate the concentrations of these *N* species. Any set of (*N* - *C*) chemical reactions, each in equilibrium, which includes each species at least once, will then provide the additional equations required to determine the concentration of each species in the mixture. Unfortunately, this complete set of equations is a coupled set of *C* linear and (*N* - *C*) nonlinear equations that is difficult to solve for cases where (*N* - *C*) > 2. For complex systems such as this standardized computer methods for the calculation of complex chemical equilibrium compositions are now used, for example, Chemkin.[14] The approach taken is to minimize explicitly the Gibbs free energy of the reacting mixture (at constant temperature and pressure) subject to the constraints of element mass conservation.

A thermodynamic state of a gas mixture is commonly specified by a temperature *T* and pressure *p*. Other pairs of state variables: enthalpy and pressure (useful for constant-pressure combustion processes); temperature and volume; internal energy and volume (useful for constant-volume combustion processes); entropy and pressure, and entropy and volume (useful for isentropic compressions and expansions) can be used.

For each reactant composition and pair of thermodynamic state variables, such chemical-equilibrium computer programs calculate and print out the following:

1. *Thermodynamic mixture properties* (obtained from the equilibrium composition and the appropriate gas mixture rule; see App. B). *p, T, ρ, h, s, M,* $(\partial \ln V/\partial \ln p)_T, (\partial \ln V/\partial \ln T)_p; c_p, \gamma,$ and *a* (sound speed)
2. *Equilibrium composition*. Mole fractions of each species (which are present in significant amounts), $\tilde{x}_i$

Figure 3.12 shows how the equilibrium composition of the products of combustion of isooctane-air mixtures at selected temperatures and 30 atm pressure varies with the fuel-air equivalence ratio. At low temperatures, the products are $N_2, CO_2 H_2O$ and O_2 for lean mixtures and N_2, CO_2, H_2O, CO, and H_2 for rich mixtures. As temperature increases, the burned-gas mixture composition becomes much more complex with dissociation products such as OH, O, and H becoming significant. Figure 3.13 shows adiabatic flame temperatures for typical engine conditions as a function of the fuel-air equivalence ratio, obtained using the methodology reviewed in this section. The isooctane-air unburned mixture state was 700 K and 10 atm (values typical for the end of compression in a gasoline SI engine). Flame temperatures for adiabatic combustion at constant pressure (where p_R and H_R are specified) and at constant volume (where V_R and U_R are specified) are shown. Flame temperatures at constant volume are higher because the final pressure is higher and less dissociation occurs. Maximum flame temperatures occur slightly rich of stoichiometric.

© McGraw-Hill Education. All rights reserved. Any use is subject to the Terms of Use, Privacy Notice and copyright information.

Figure 3.12 *Mole fractions of equilibrium combustion products of isooctane-air mixtures as a function of fuel/air equivalence ratio at 30 atmospheres and (a) 1750 K; (b) 2250 K; (c) 2750 K.*

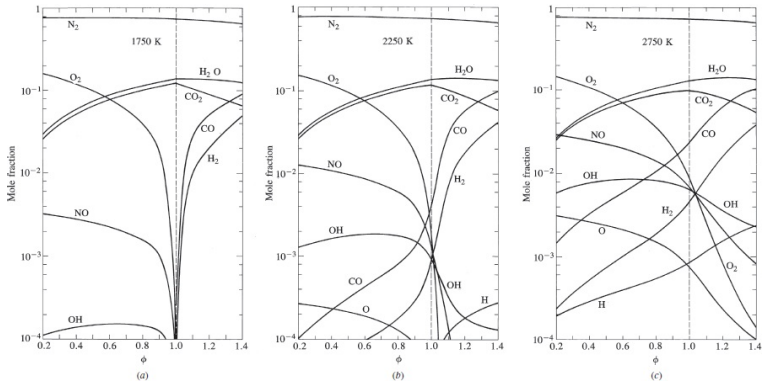
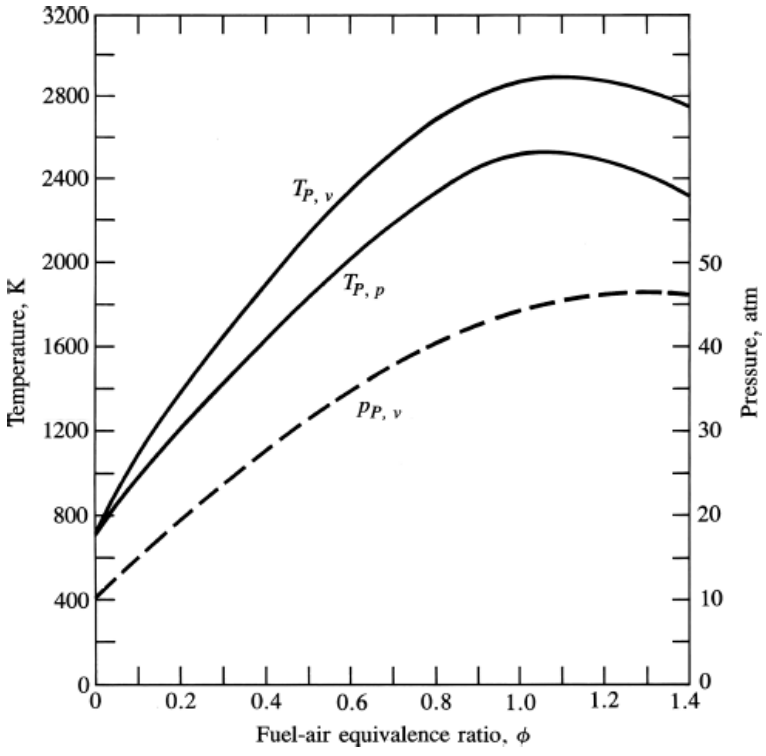


Figure 3.13 *Equilibrium combustion product gas temperatures for constant-volume* (T_{pv}) *and constant-pressure* (T_{pp}) *adiabatic combustion of isooctane-air mixture initially at 700 K and 10 atm (typical end-of-compression mixture conditions in a gasoline SI engine), as a function of fuel/air equivalence ratio. Pressure* $(p_{p,v})$ *is equilibrium pressure for adiabatic constant-volume combustion.*



3.7.2. Chemical Reaction Rates

Whether a system is in chemical equilibrium depends on whether the time constants of the controlling chemical reactions are short compared with time scales over which the system conditions (temperature and pressure) change. Chemical processes in engines are often not in equilibrium. Important examples of nonequilibrium phenomena are the flame reaction zone where the fuel is oxidized, and the air pollutant formation mechanisms. Such nonequilibrium processes are controlled by the rates at which the actual chemical reactions that convert reactants to products occur. The rates at which chemical reactions proceed

© McGraw-Hill Education. All rights reserved. Any use is subject to the Terms of Use, Privacy Notice and copyright information.

depend on the concentration of the reactants, temperature, and whether any catalyst is present. This field is called chemical kinetics and some of its basic relations will now be reviewed.[2]

Most of the chemical reactions of interest in combustion are binary reactions, where two reactant molecules, M_a and M_b, with the capability of reacting together collide and form two product molecules, M_c and M_d, that is,

$$\mathrm{M}_a + \mathrm{M}_b = \mathrm{M}_c + \mathrm{M}_d$$

(3.44)

An important example of such a reaction is the rate-controlling step in the process by which the pollutant nitric oxide, NO, forms:

$$\mathrm{O} + \mathrm{N}_2 = \mathrm{NO} + \mathrm{N}$$

This is a second-order reaction since the stoichiometric coefficients of the reactants v_a and are each unity and sum to 2. (The only relevant first-order reactions are decomposition processes.) Third-order reactions are important in combustion, also. Examples are the recombination reactions by which radical species such as H, O, and OH combine during the final stage of the fuel oxidation process, for example,

$$\mathrm{H} + \mathrm{H} + \mathrm{M} = \mathrm{H}_2 + \mathrm{M}^*$$

(3.45)

M is any molecule (such as N_2) which takes part in the collision, which then carries away the excess energy (as M*).

The *law of mass action* states that the rate at which product species are produced, also the rate at which reactant species are removed, is proportional to the product of the concentrations of reacting species, with the concentration of each species raised to the power of its stoichiometric coefficient ν_i. Thus, for reaction (3.44) above, the reaction rate R^+ in the forward (+) direction, reactants to products, is given by

$$R^+ = \frac{d[M_a]^+}{dt} = \frac{d[M_c]^+}{dt} = k^+[M_a][M_b]$$

(3.46)

If the reaction can also proceed in the reverse (−) direction, then the backward rate R^- is given by

$$R^- = -\frac{d[M_c]^-}{dt} = \frac{d[M_a]^-}{dt} = k^-[M_c][M_d]$$

© McGraw-Hill Education. All rights reserved. Any use is subject to the Terms of Use, Privacy Notice and copyright information.

(3.47)

k^+ and
k^- are the rate constants in the forward and reverse directions for this reaction. The *net rate* of production of products or removal of reactants is, therefore,

$$\begin{aligned} R^+ - R^- &= \frac{d[\mathrm{M}_c]^+}{dt} + \frac{d[\mathrm{M}_c]^-}{dt} = -\frac{d[\mathrm{M}_a]^+}{dt} + \frac{d[\mathrm{M}_a]^-}{dt} \\ &= k^+[\mathrm{M}_a][\mathrm{M}_b] - k^-[\mathrm{M}_c][\mathrm{M}_d] \end{aligned}$$

(3.48)

These results can be stated more generally as follows. Any reaction can be written as

$$\sum_{i=1}^{n} v_{R_i} M_{R_i} = \sum_{i=1}^{m} v_{P_i} M_{P_i}$$

(3.49)

where
ν_i is the stoichiometric coefficient of species
M_i, subscripts *R* and *P* denote reactants and products, respectively, and there are *n* reactant species and *m* product species. The forward reaction rate
R^+ and the reverse reaction rate
R^- are given by

$$R^+ = k^+ \prod_{i=1}^{n} [M_{R_i}]^{v_{R_i}}$$

$$R^- = k^- \prod_{i=1}^{m} [M_{P_i}]^{v_{P_i}}$$

(3.50)

The net rate of removal of reactant species
M_{R_i} is

$$-\frac{d[\mathrm{M}_{R_i}]}{dt} = v_{R_i}(R^+ - R^-)$$

(3.51a)

and the net rate of production of product species
M_{P_i} is

$$\frac{d[\mathrm{M}_{P_i}]}{dt} = v_{P_i}(R^+ - R^-)$$

© McGraw-Hill Education. All rights reserved. Any use is subject to the Terms of Use, Privacy Notice and copyright information.

(3.51b)

The rate constants, *k*, usually follow the Arrhenius form:

$$k = A \exp\left(-\frac{E_A}{RT}\right)$$

(3.52)

where *A* is called the frequency or pre-exponential factor and may be a (moderate) function of temperature; E_A is the activation energy. The Boltzmann factor exp ($-E_A/RT$) defines the fraction of all collisions that have an energy greater than E_A, that is, sufficient energy to break the molecular bonds and cause the reaction to take place. The functional dependence of *k* on *T* and the constants in the Arrhenius form, Eq. (3.52) (if that equation is appropriate), are determined experimentally.

At equilibrium, the forward and reverse reaction rates are equal. Then, from Eq. (3.48), with $R^+ - R^- = 0$:

$$\frac{k^+}{k^-} = \frac{[M_c][M_d]}{[M_a][M_b]} = K_c$$

where K_c is the equilibrium constant based on concentrations defined by Eq. (3.42). It can be related to K_p, the equilibrium constant based on partial pressures, by Eq. (3.43).

The chemical reaction mechanisms of importance in combustion are much more complex than the above illustrations of rate-controlled processes. Such mechanisms usually involve both parallel and sequential interdependent reactions. The methodology reviewed above still holds; however, one must sum algebraically the forward and reverse rates of all the reactions that produce (or remove) a species of interest. In such complex mechanisms, it is often useful to assume that (some of) the reactive intermediate species or radicals are in *steady state*. That is, these radicals react so quickly once they are formed that their concentrations are maintained in steady state—effectively, in equilibrium—with the species with which they react. The net rate at which their concentration changes with time is set equal to zero.

[1] This assumption is not valid late in the expansion stroke and during the exhaust process (see Sec. 4.9). Nor does it take account of pollutant formation processes (see Chap. 11).

© McGraw-Hill Education. All rights reserved. Any use is subject to the Terms of Use, Privacy Notice and copyright information.

3.8. PROBLEMS

3.1. Gasoline is supplied to a four-cylinder spark-ignition engine at 2 g/s. Calculate the air-flow rate for stoichiometric combustion. If the engine is operating at 1500 rev/min, estimate the mass of fuel and air entering each cylinder per cycle. The engine displaced volume is 2.4 liters. What is the volumetric efficiency?

3.2. Calculate the exhaust gas composition of a butane-fueled spark-ignition engine operating with a fuel/air equivalence ratio of 0.9. Assume the fuel is fully burned within the cylinder. Butane is C_4H_{10}.

3.3. The molar composition of dry exhaust gas of a propane-fueled SI engine is given below (water was removed before the measurement). Calculate the relative air/fuel ratio.

$$CO_2 = 10.8\%, \quad O_2 = 4.5\%, \quad CO = 0\%, \quad H_2 = 0\%$$

3.4. Evaluate and compare the lower heating values per unit mass of stoichiometric mixture and per unit volume of stoichiometric mixture (at standard atmospheric conditions) for methane, isooctane, gasoline, ethanol, methanol, and hydrogen. Assume the fuel is fully vaporized. Heating values for these fuels are given in App. D.

3.5. The measured engine fuel flow rate is 0.4 g/s, the air flow rate is 5.6 g/s, and the exhaust gas composition (measured dry) is $CO_2 = 13.0\%$, CO = 2.8% with O_2 essentially zero. Unburned hydrocarbon emissions can be neglected. Compare the equivalence ratio calculated from the fuel and air flow with the equivalence ratio calculated from the exhaust gas composition. The fuel is gasoline with a H/C ratio of 1.87. Assume a H_2 concentration equal to one-third the CO concentration.

3.6. This problem assesses several fuels for use in an internal combustion engine. The fuels of interest are gasoline, diesel fuel, methane, ethanol, and hydrogen. Properties of these fuels can be found in Table D.4 of App. D.

a. For each of these fuels, determine the lower heating value per unit volume of stoichiometric mixture at standard temperature and pressure. Normalize your results by the gasoline value.

b. Also calculate the lower heating value per unit volume of each fuel at standard temperature and pressure. Again normalize your results by the gasoline value.

c. What do these results tell you about how the engine's output (maximum torque and power) change (for a fixed engine size) when using each of these fuels? How does the amount of energy able to be stored onboard (in a nonpressurized tank of fixed size) change when using each of these fuels?

3.7. Here, we examine the effects of using reformulated gasoline in a spark-ignition engine. Reformulated gasoline (to lower the engine's emissions) contains 2% by weight of oxygen. One approach is to blend ethanol (C_2H_6O) with the gasoline (approximate as C_7H_{13}) in the appropriate ratio to provide this 2% oxygen. The heating value of gasoline is 44 MJ/kg; the heating value of ethanol is 26.9 MJ/kg. The density of the two fuels is essentially the same, $0.76\,\mathrm{Mg/m^3}$.

a. Calculate the required mass fraction of ethanol in the ethanol-gasoline mixture.

b. The stoichiometric air/fuel ratios for ethanol and gasoline are 9.0 and 14.6, respectively. Determine the stoichiometric A/F ratio for the mixture.

© McGraw-Hill Education. All rights reserved. Any use is subject to the Terms of Use, Privacy Notice and copyright information.

c. The fuel system injects a given volume of fuel based on the measured mass flow rate of air. So in a spark-ignition engine designed for stoichiometric operation with gasoline, the engine will run lean with the ethanol-gasoline mixture. At what lean relative air/fuel ratio will it operate?

3.8. An internal combustion engine is being operated with a pure alcohol as fuel. The fuel molecule has 7 carbon atoms. A detailed analysis of the exhaust gas constituents on a wet molar basis (i.e., with the H_2O present) in the exhaust manifold yielded the following:

$$CO_2 : 13\%,\ CO: 5.2\%, H_2O{:}9.1\%, H_2 : 1.3\%, \text{and } N_2 : 71.3\%$$

a. Determine the elemental composition of the fuel molecule.

b. Determine the relative air-fuel ratio. Is this lean, stoichiometric, or rich?

c. The engine is a four-valve per cylinder naturally-aspirated spark-ignition engine. It has a displaced volume of 3 liters, the air flow is 0.06 kg/s, and the engine speed is 3000 rev/min. Estimate the engine load (i.e., the approximate ratio of the actual brake torque to the maximum brake torque) at these conditions. The friction mean effective pressure is 200 kPa at this speed and is essentially independent of load at the loads considered here. The gross indicated fuel conversion efficiency is also independent of load.

Hints: You may need to make appropriate assumptions concerning the engine's breathing characteristics and normalized torque, according to the given engine technology.

3.9. An upper estimate can be made of the amount of NO formed in an engine from considering the equilibrium of the reaction $N_2 + O_2 = 2NO$. Calculate the NO concentration at equilibrium at 2500 K and 30 atm. $\text{Log}_{10}K_p = -1.2$ for this reaction at 2500 K. Assume N/O ratio in the combustion products is 15. N_2, O_2, and NO are the only reacting species present.

3.10. Carbon monoxide reacts with air at 1 atm and 1000 K in an exhaust gas reactor. The mole fractions of the exhaust gas-air mixture flowing into the reactor are CO, 3%; O_2, 7%; N_2, 74%; CO_2, 6%; H_2O, 10%.

a. Calculate the concentration of CO and O_2 in gram moles per cm^3 in the entering mixture.

b. The rate of reaction is given by

$$d[\text{CO}]/dt = -4.3 \times 10^{11} \times [\text{CO}][\text{O}_2]^{0.25} \exp[-E/(RT)]$$

[ ] denotes concentration in gram moles per cm^3, *E/R* = 20,000 K. Calculate the initial reaction rate of CO, *d*[CO]/*dt*: time is in seconds.

c. The equilibrium constant K_p for the reaction $CO + \frac{1}{2}O_2 = CO_2$ at 1000 K is 10^{10}. Find the equilibrium CO concentration.

© McGraw-Hill Education. All rights reserved. Any use is subject to the Terms of Use, Privacy Notice and copyright information.

d. Determine the time to reach this equilibrium concentration of CO using the initial reaction rate. (The actual time will be longer but this calculation indicates approximately the time required.)

3.11. The exhaust gases of a hydrogen-fueled engine contain 22.3% H_2O, 7.44% O_2, and 70.2% N_2. At what fuel/air equivalence ratio and relative air/fuel ratio is it operating?

3.12. Gas is sampled at 1 bar pressure from the exhaust manifold of an internal combustion engine and analyzed. The mole fractions of species in the exhaust are:

$$H_2O\,0.0468; \quad CO_2\,0.0585; \quad O_2 0.123; \quad N_2 0.772$$

Other species such as CO and unburned hydrocarbons can be neglected.

a. The fuel is a synthetic fuel derived from coal and biomass containing only carbon and hydrogen. What is the ratio of hydrogen atoms to carbon atoms in the fuel?

b. Calculate the fuel/air equivalence ratio at which this engine is operating.

c. Is the internal combustion engine a conventional spark-ignition or a diesel engine? Explain your logic.

d. The engine has a displaced volume of 2 liters. Estimate approximately the percentage by which the fuel flow rate would be increased if this engine were operated at its maximum load at this same speed (2000 rev/min). Explain briefly what limits the equivalence ratio at maximum load.

3.13. Liquid petroleum gas (LPG) is used to fuel spark-ignition engines. A typical sample of the fuel consists of

70% by volume propane

5% by volume butane

25% by volume propene

The *higher heating values* of the fuels are: propane, 50.38 MJ/kg; butane, 49.56 MJ/kg; propylene (propene), 48.95 MJ/kg.

a. Work out the overall combustion reaction for stoichiometric combustion of 1 mole of LPG with air, and the stoichiometric *F/A* and *A/F*.

b. What are the higher and lower heating values for combustion of this fuel with excess air, per unit mass of LPG?

3.14. A spark-ignition engine is operated on isooctane fuel (C_8H_{18}). The exhaust gases are cooled, dried to remove water, and then analyzed for CO_2, CO, H_2, O_2. Using the overall combustion reaction for a range of equivalence ratios from 0.5 to 1.5, calculate the mole fractions of CO_2, CO, H_2, and O_2 in the dry exhaust gas, and plot the results as a function of equivalence ratio. Assume:

a. that all the fuel is burnt inside the engine (almost true) and that the ratio of moles CO to moles H_2 in the exhaust is 3:1, and

b. that there is no hydrogen in the exhaust for lean mixtures.

© McGraw-Hill Education. All rights reserved. Any use is subject to the Terms of Use, Privacy Notice and copyright information.

For high power engine operation, the air/fuel ratio is 14:1. What is the exhaust gas composition, in mole fractions,*before* the water is removed?

© McGraw-Hill Education. All rights reserved. Any use is subject to the Terms of Use, Privacy Notice and copyright information.

3.9. REFERENCES

1. Borman, G. L., and Ragland, K. W.: *Combustion Engineering,* McGraw-Hill, New York, 1998.
2. Glassman, I.: *Combustion*, 3rd ed., Academic Press, Orlando, London,1996.
3. Kaye, G. W. C., and Laby, T. H.: *Tables of Physical and Chemical Constants*, 16th ed., Longmans, London, 1995.
4. Reynolds, W. C.: *Thermodynamic Properties in SI*, Department of Mechanical Engineering, Stanford University, Palo Alto, 1979.
5. Taylor, C. F.: *The Internal Combustion Engine in Theory and Practice*, vol. 1, MIT Press, Cambridge, 1960.
6. Goodger, E. M.: *Hydrocarbon Fuels*, Macmillan, London, 1975.
7. Spalding, D. B., and Cole, E. H.: *Engineering Thermodynamics*, 3rd ed., Edward Arnold, London, 1973.
8. *JANAF Thermochemical Tables*, National Bureau of Standards Publication NSRDS-NBS 37, U. S. Department of Commerce, U. S. Printing Office, Washington D.C., 1971.
9. Maxwell, J. B.: *Data Book on Hydrocarbons*, Van Nostrand, New York, 1950.
10. Rossini, F. D., Pitzer, K. S., Arnelt, R. L., Braun, R. M., and Primentel, G. C.: *Selected Values of Physical and Thermodynamic Properties of Hydrocarbons and Related Compounds*, Carnegie Press, Pittsburgh, 1953.
11. Stull, D. R., Westrum, E. F., and Sinke, G. C.: *The Chemical Thermodynamics of Organic Compounds*, John Wiley, New York, 1969.
12. Matthews, R. D.: "Relationship of Brake Power to Various Energy Efficiencies and Other Engine Parameters: The Efficiency Rule," *Int. J. of Vehicle Design*, vol. 4, no. 5, pp. 491–500, 1983.
13. Keenan, J. H.: *Thermodynamics*, John Wiley, New York, 1941; MIT Press, Cambridge, 1970.
14. CHEMKIN (or CHEMKIN-PRO); URL: www.reactiondesign.com; Reaction Design, Inc., San Diego, 2016.

© McGraw-Hill Education. All rights reserved. Any use is subject to the Terms of Use, Privacy Notice and copyright information.

4.0. CHAPTER PRELIMINARIES

INTRODUCTION

UNBURNED MIXTURE COMPOSITION

GAS PROPERTY RELATIONSHIPS

A SIMPLE ANALYTIC IDEAL GAS MODEL

THERMODYNAMIC PROPERTY CHARTS

TABLES OF PROPERTIES AND COMPOSITION

COMPUTER ROUTINES FOR PROPERTY AND COMPOSITION CALCULATIONS

TRANSPORT PROPERTIES

EXHAUST GAS COMPOSITION

PROBLEMS

REFERENCES

© McGraw-Hill Education. All rights reserved. Any use is subject to the Terms of Use, Privacy Notice and copyright information.

4.1. INTRODUCTION

The study of engine operation through an analysis of the processes that occur inside the engine has a long and productive history. The earliest attempts at this analysis used the constant-volume and constant-pressure ideal cycles as approximations to real engine processes (see Chap. 5). With the development of high-speed digital computers, the simulation of engine processes has become much more sophisticated and accurate (see Chap. 14). All these engine simulations (from the simplest to the most complex) require models for the composition and properties of the working fluids inside the engine, as well as models for the individual processes—induction, compression, combustion, expansion, and exhaust—that make up the engine operating cycle. This chapter deals with models for the working fluid composition, and thermodynamic and transport properties.

The composition of the working fluid, which changes during the engine operating cycle, is summarized inTable 4.1. The unburned mixture for a spark-ignition engine during intake and compression consists of air, fuel, and previously burned gases. It is, therefore, a mixture of
N_2,
O_2,
CO_2,
H_2O, with CO, and
H_2 for fuel-rich mixtures, and fuel (usually vapor). The composition of the unburned mixture does not change significantly during intake and compression. It is sufficiently accurate to assume the composition is *frozen*. For the compression-ignition engine, the unburned mixture prior to injection contains no fuel; it consists of air and previously burned gas.

© McGraw-Hill Education. All rights reserved. Any use is subject to the Terms of Use, Privacy Notice and copyright information.

Table 4.1 Working fluid constituents

Process	Spark-ignition engine	Compression-ignition engine
Intake	Air	Air
	Fuel*	Recycled exhaust†
	Recycled exhaust†	Residual gas‡
	Residual gas‡	
Compression	Air	Air
	Fuel vapor	Recycled exhaust
	Recycled exhaust	Residual gas
	Residual gas	
Expansion	Combustion products (mixture of N_2, H_2O, CO_2, CO, H_2, O_2, NO, OH, O, H, ...)	Combustion products (mixture of N_2, H_2O, CO_2, CO, H_2, O_2, NO, OH, O, H, ...)
Exhaust	Combustion products [mainly N_2, CO_2, H_2O, and either O_2 ($\phi < 1$) or CO and H_2 ($\phi > 1$)]	Combustion products (mainly N_2, CO_2, H_2O, and O_2)

*With port fuel injection, mainly vapor within the cylinder: with direct injection, liquid and vapor.

†Often used to control NO_x emissions (see Secs. 11.2, 15.3.2, and 15.5.1).

‡Within the cylinder.

The combustion products or burned mixture gases, during the combustion process and much of the expansion process, are close to *thermodynamic equilibrium*. The composition of such mixtures has already been discussed (Sec. 3.7.1). As these combustion products cool, recombination occurs as indicated in Fig. 3.12. Toward the end of the expansion process, the gas composition departs from the equilibrium composition; recombination can no longer occur fast enough to maintain the reacting mixture in equilibrium. During the exhaust process, reactions in the burned gases are sufficiently slow so that for calculating thermodynamic properties the composition can be regarded as *frozen*.

The models used for predicting the thermodynamic properties of unburned and burned mixtures can be grouped into the five categories listed in Table 4.2. The first category is only useful for illustrative purposes since the specific heats of unburned and burned mixtures are significantly different. While the specific heats of the working fluids do increase with increasing temperature in the range of interest, a constant—specific—heat model can be matched to the thermodynamic data over a limited temperature range. This approach provides a simple *analytic* model that can be useful when moderate accuracy of prediction will suffice. The appropriateness of frozen and equilibrium assumptions has already been discussed above. Approximations to thermodynamic equilibrium calculations have been useful in the past because of the savings in computational time, relative to full equilibrium calculations, which can result.

© McGraw-Hill Education. All rights reserved. Any use is subject to the Terms of Use, Privacy Notice and copyright information.

Table 4.2 Categories of models for thermodynamic properties

Unburned mixture	Burned mixture
1. Single ideal gas throughout operating cycle with c_v (and hence c_p) constant	
2. Ideal gas; $c_{v,u}$ constant	Ideal gas; $c_{v,b}$ constant
3. Frozen mixture of ideal gases; $c_{v,i}(T)$	Frozen mixture of ideal gases; $c_{v,i}(T)$
4. Frozen mixture of ideal gases; $c_{v,i}(T)$	Approximations fitted to equilibrium thermodynamic properties
5. Frozen mixture of ideal gases; $c_{v,i}(T)$	Mixture of reacting ideal gases in thermodynamic equilibrium
Note: Subscripts *i, u*, and *b* denote species *i* in the gas mixture, the unburned mixture, and burned mixture properties, respectively.	

Values of thermodynamic properties of unburned and burned mixtures relevant to engine calculations are available from charts, tables, algebraic relationships developed to match tabulated data, and computer programs. A selection of this material is included in this chapter and App. D. The references indicate additional sources.

© McGraw-Hill Education. All rights reserved. Any use is subject to the Terms of Use, Privacy Notice and copyright information.

4.2. UNBURNED MIXTURE COMPOSITION

The mass of charge trapped in the cylinder (m_c) is the inducted mass per cycle (m_i), plus the residual mass (m_r) left over from the previous cycle. The residual fraction (x_r) is

$$x_r = \frac{m_r}{m_c}$$

(4.1)

Typical residual fractions in spark-ignition engines range from some 30% at idle to about 5% at full load. In diesels, the residual fraction is smaller (a few percent) due to the higher compression ratio, and in naturally-aspirated engines is approximately constant since the intake is unthrottled. If the inducted mixture is fuel and air (or air only), then the *burned gas fraction* (x_b) in the unburned mixture during compression equals the residual fraction.

In some engines, a fraction of the engine exhaust gases is recycled to the intake to dilute the fresh mixture for control of NO_x emissions (see Sec. 11.2). The percent of exhaust gas recycled (%EGR) is usually defined as the percent of the total intake mixture which is recycled exhaust,[1]

$$\mathrm{EGR}(\%) = \left(\frac{m_{\mathrm{EGR}}}{m_i}\right) \times 100$$

(4.2)

where m_{EGR} is the mass of exhaust gas recycled, then the burned gas fraction in the fresh mixture is

$$x_b = \frac{m_{\mathrm{EGR}} + m_r}{m_c} = \left(\frac{\mathrm{EGR}}{100}\right)(1 - x_r) + x_r$$

(4.3)

Depending on operating conditions, in SI engines up to about 30% of the exhaust can be recycled; in diesel engines, much higher levels may be used.

The composition of the burned gas fraction in the unburned mixture can be calculated as follows. The combustion equation for a hydrocarbon fuel of average molar H/C ratio *y* [e.g., Eq. (3.5)] can be written per mole O_2 as

$$\varepsilon\phi\mathrm{C} + 2(1-\varepsilon)\phi\mathrm{H}_2 + \mathrm{O}_2 + \psi\mathrm{N}_2 \rightarrow n_{\mathrm{CO}_2}\mathrm{CO}_2 + n_{\mathrm{H}_2\mathrm{O}}\mathrm{H}_2\mathrm{O} + n_{\mathrm{CO}}\mathrm{CO} + n_{\mathrm{H}_2}\mathrm{H}_2 + n_{\mathrm{O}_2}\mathrm{O}_2 + n_{\mathrm{N}_2}\mathrm{N}_2$$

© McGraw-Hill Education. All rights reserved. Any use is subject to the Terms of Use, Privacy Notice and copyright information.

(4.4)

where

$\psi =$ the molar N/O ratio (3.773 for air)

$\varepsilon = \dfrac{4}{4+y}$

$y =$ the molar H/C ratio of the fuel

$\phi =$ fuel/air equivalence ratio

$n_i =$ moles of species i per mole O_2 reactant

The n_i are determined using the following assumptions:

1. For lean and stoichiometric mixtures ($\phi \le 1$) CO and H_2 can be neglected.
2. For rich and stoichiometric mixtures ($\phi \ge 1$) O_2 can be neglected.
3. For rich mixtures, either (*a*) the water–gas reaction

$$CO_2 + H_2 = CO + H_2O$$

can be assumed to be in equilibrium with the equilibrium constant $K(T)$:

$$K(T) = \frac{n_{H_2O} n_{CO}}{n_{CO_2} n_{H_2}}$$

where $K(T)$ can be determined from a curve fit to JANAF Tables data:[1]

$$\ln K(T) = 2.743 - \frac{1.761 \times 10^3}{T} - \frac{1.611 \times 10^6}{T^2} + \frac{0.2803 \times 10^9}{T^3}$$

(4.5)

where *T* is in *K*, or (*b*) *K* can be assumed constant over the normal engine operating range. A value of 3.5 is often assumed (see Sec. 4.9), which corresponds to evaluating the equilibrium constant at 1740 K.

The n_i obtained from an element balance and the above assumptions are shown in Table 4.3. The value of *c* is obtained by solving the quadratic:

$$(K-1)c^2 - c\{K[2(\phi-1)+\varepsilon\phi] + 2(1-\varepsilon\phi)\} + 2K\varepsilon\phi(\phi-1) = 0$$

(4.6)

© McGraw-Hill Education. All rights reserved. Any use is subject to the Terms of Use, Privacy Notice and copyright information.

Table 4.3 Burned gas composition under 1700 K

Species	n_i, moles/mole O_2 reactant	
	$\phi \le 1$	$\phi > 1$*
CO_2	$\varepsilon\phi$	$\varepsilon\phi - c$
H_2O	$2(1-\varepsilon)\phi$	$2(1-\varepsilon\phi) + c$
CO	0	c
H_2	0	$2(\phi - 1) - c$
O_2	$1 - \phi$	0
N_2	ψ	ψ
Sum: n_b	$(1-\varepsilon)\phi + 1 + \psi$	$(2-\varepsilon)\phi + \psi$

*c defined by Eq. (4.6).

The mole fractions are given by

$$\tilde{x}_i = \frac{n_i}{n_b}$$

where
$n_b = \sum_i n_i$ is given in the bottom line of Table 4.3.

While Eq. (4.4) is for a fuel containing C and H only, it can readily be modified for alcohols or alcohol—hydrocarbon blends. For a fuel of molar composition
CH_yO_z, the reactant mixture

$$CH_yO_z + \frac{1}{\phi}\left(1 + \frac{y}{4} - \frac{z}{2}\right)(O_2 + \psi N_2)$$

can be rearranged per mole of
O_2 reactant as

$$\zeta\phi\varepsilon C + 2\zeta\phi(1-\varepsilon)H_2 + O_2 + \left(1 - \frac{\varepsilon z}{2}\right)\zeta\psi N_2$$

(4.7*a*)

where

$$\zeta = \frac{2}{2 - \varepsilon z(1-\phi)}$$

© McGraw-Hill Education. All rights reserved. Any use is subject to the Terms of Use, Privacy Notice and copyright information.

(4.7*b*)

If we write

$$\phi^* = \zeta\phi \quad \text{and} \quad \psi^* = \left(1 - \frac{\varepsilon z}{2}\right)\zeta\psi$$

(4.7*c*)

the reactant expression (4.7*a*) becomes

$$\varepsilon\phi^*\mathrm{C} + 2(1-\varepsilon)\phi^*\mathrm{H_2} + \mathrm{O_2} + \psi^*\mathrm{N_2}$$

which is identical in form to the reactant expression for a hydrocarbon fuel, Eq. (4.4). Thus, Table 4.3 can still be used to give the composition of the burned gas residual fraction in the unburned mixture, except that ϕ^* replaces ϕ and ψ^* replaces ψ in the expressions for
n_i.

Now consider the unburned mixture. The number of moles of fuel per mole
$\mathrm{O_2}$ in the mixture depends on the molecular weight of the fuel,
M_f. If the average molecular formula of the fuel is
$(\mathrm{CH}_y)_\alpha$ then

$$M_f = \alpha(12 + y)$$

The fresh fuel-air mixture (not yet diluted with EGR or residual),

$$\varepsilon\phi\mathrm{C} + 2(1-\varepsilon)\phi\mathrm{H_2} + \mathrm{O_2} + \psi\mathrm{N_2}$$

then becomes

$$\frac{4}{M_f}(1+2\varepsilon)\phi(\mathrm{CH}_y)_\alpha + \mathrm{O_2} + \psi\mathrm{N_2}$$

The unburned mixture (fuel, air, and a burned gas fraction), per mole
$\mathrm{O_2}$ in the mixture, can be written:

$$(1-x_b)\left[\frac{4}{M_f}(1+2\varepsilon)\phi(\mathrm{CH}_y)_\alpha + \mathrm{O_2} + \psi\mathrm{N_2}\right] + x_b(n_{\mathrm{CO_2}} + n_{\mathrm{H_2O}} + n_{\mathrm{CO}} + n_{\mathrm{H_2}} + n_{\mathrm{O_2}} + n_{\mathrm{N_2}})$$

The number of moles of each species in the unburned mixture, per mole
$\mathrm{O_2}$, is summarized in Table 4.4. The mole fractions of each species are then obtained by dividing by the total number of moles of unburned mixture
n_u,

© McGraw-Hill Education. All rights reserved. Any use is subject to the Terms of Use, Privacy Notice and copyright information.

$$n_u = (1 - x_b)\left[\frac{4(1+2\varepsilon)\phi}{M_f} + 1 + \psi\right] + x_b n_b$$

(4.8)

where
n_b is given in Table 4.3.

Table 4.4 Unburned mixture composition

Species	n_i, moles/mole O_2 reactant	
	$\phi \le 1$	$\phi > 1$
Fuel	$4(1 - x_b)(1 + 2\varepsilon)\phi/M_f$	
O_2	$1 - x_b\,\phi$	$1 - x_b$
N_2	ψ	ψ
CO_2	$x_b\varepsilon\phi$	$x_b(\varepsilon\phi - c)$
H_2O	$2x_b(1 - \varepsilon)\phi$	$x_b[2(1 - \varepsilon\phi) + c]$
CO	0	$x_b c$
H_2	0	$x_b[2(\phi - 1) - c]$
Sum*	n_u	n_u

*Given by Eq. (4.8).

The molecular weights of the (low-temperature) burned and unburned mixture can now be determined. The mass of mixture (burned or unburned) per mole
O_2 in the mixture,
m_{RP}, is given by

$$m_{\mathrm{RP}} = 32 + 4\phi(1 + 2\varepsilon) + 28.16\psi$$

(4.9)

The molecular weight of the burned mixture,
M_b, is therefore

$$M_b = \frac{m_{\mathrm{RP}}}{n_b}$$

(4.10)

The molecular weight of the unburned mixture,
M_u, is

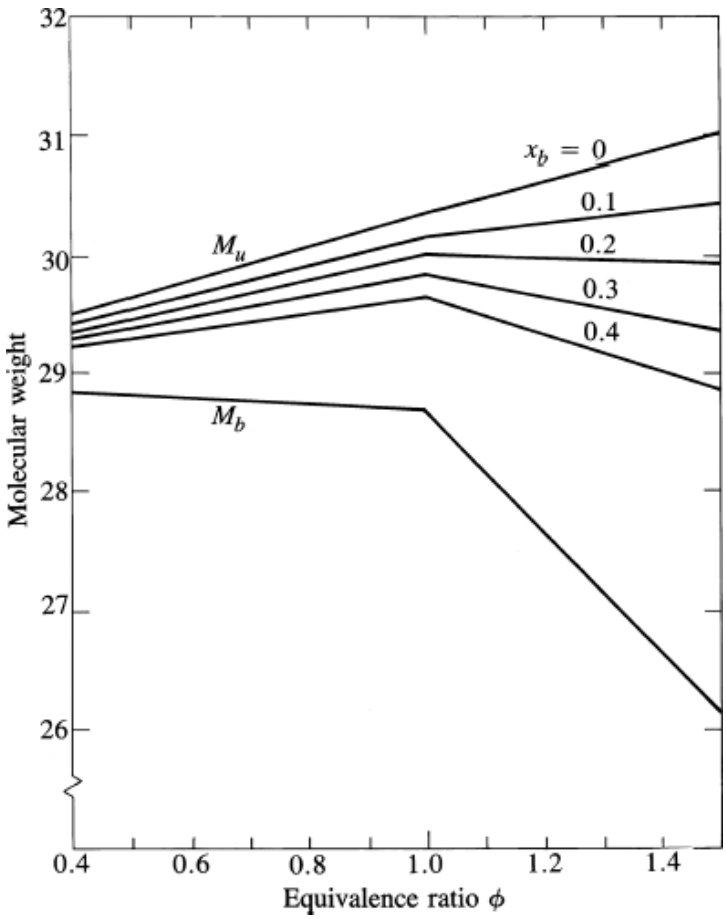
© McGraw-Hill Education. All rights reserved. Any use is subject to the Terms of Use, Privacy Notice and copyright information.

$$M_u = \frac{m_{\mathrm{RP}}}{n_u}$$

(4.11)

Figure 4.1 gives
M_u and
M_b for a range of ϕ and
x_b for air, isooctane, burned gas mixtures.

Figure 4.1 Molecular weight of unburned and low-temperature burned isooctane-air mixtures as a function of fuel/air equivalence ratio and burned gas fraction.



Frequently, thermodynamic properties of unburned and burned mixtures are expressed per unit mass of *air* in the *original* mixture (for burned mixture this is the mixture before combustion). To obtain properties in these units, we need the mass of original air, per mole
O_2 in the mixture, which is

$$(32 + 28.16\psi)$$

with units of kilograms per kilomole or pound-mass per pound-mole.

Table 4.5 summarizes the factors needed to relate properties expressed on a molar and a mass basis.

© McGraw-Hill Education. All rights reserved. Any use is subject to the Terms of Use, Privacy Notice and copyright information.

Table 4.5 Factors for relating properties on molar and mass basis

Quantity, per mole O_2 in the mixture	General equation*		Equation for C_8H_{18}-air mixtures
Moles of burned mixture n_b	$n_b = (1 - \varepsilon)\phi + 1 + \psi$,	$\phi \le 1$	$n_b = 0.36\phi + 4.773$
	$n_b = (2 - \varepsilon)\phi + \psi$,	$\phi > 1$	$n_b = 1.36\phi + 3.773$
Moles of unburned mixture n_u	$(1 - x_b)\left[\frac{4(1+2\varepsilon)\phi}{M_f} + 1 + \psi\right] + x_b n_b$	$\begin{cases}\phi \le 1\\ \phi > 1\end{cases}$	$n_u = 0.08\phi + 4.773 + 0.28x_b\phi$ $n_u = 0.08\phi + 4.773 + x_b(1.28\phi - 1)$
Mass of mixture† (burned or unburned)	$m_{RP} = 32 + 4\phi(1 + 2\varepsilon) + 28.16\psi$		$138.2 + 9.12\phi$
Mass of air†	$32 + 28.16\ \psi$		138.2

*For hydrocarbon fuels, ψ for air = 3.773; for fuels containing oxygen, ϕ^* and ψ^* given by Eq. (4.7c) are substituted for ϕ and ψ, respectively.

†Units: kg/kmol or lb_m/lb·mol.

[1] An alternative definition of percent EGR (EGR*) is also used based on the ratio of EGR to fresh mixture (fuel and air): $\mathrm{EGR}^*(\%) = \left(\frac{m_{\mathrm{EGR}}}{m_a + m_f}\right) \times 100$ The two definitions are related by $\frac{\mathrm{EGR}^*}{100} = \frac{\mathrm{EGR}}{100 - \mathrm{EGR}}$ and $\frac{\mathrm{EGR}}{100} = \frac{\mathrm{EGR}}{100 + \mathrm{EGR}^*}$

© McGraw-Hill Education. All rights reserved. Any use is subject to the Terms of Use, Privacy Notice and copyright information.

4.3. GAS PROPERTY RELATIONSHIPS

The individual species in the unburned and burned gas mixtures can with sufficient accuracy be modeled as ideal gases. Ideal gas relationships are reviewed in App. B. The most important relationships for property determination for engine calculations are summarized below.

Since internal energy and enthalpy are functions of temperature only, the specific heats at constant volume and constant pressure are given by

$$c_v = \left(\frac{\partial u}{\partial T}\right)_v = \frac{du}{dT} = c_v(T)$$

(4.12*a*)

$$c_p = \left(\frac{\partial h}{\partial T}\right)_p = \frac{dh}{dT} = c_p(T)$$

(4.12*b*)

and

$$u - u_0 = \int_{T_0}^{T} c_v dT$$

(4.13*a*)

$$h - h_0 = \int_{T_0}^{T} c_p dT$$

(4.13*b*)

The entropy, *s(T, v)* or *s(T, p)*, is given by

$$s - s_0 = \int_{T_0}^{T} c_v \frac{dT}{T} + R\ln\frac{v}{v_0}$$

(4.14*a*)

$$s - s_0 = \int_{T_0}^{T} c_p \frac{dT}{T} + R\ln\frac{p}{p_0}$$

(4.14*b*)

© McGraw-Hill Education. All rights reserved. Any use is subject to the Terms of Use, Privacy Notice and copyright information.

The integrals in Eqs. (4.14*a*, *b*) are functions of temperature only, and are useful in evaluating entropy changes and in following isentropic processes. If we define

$$\Psi(T) = \int_{T_0}^{T} c_v(T) \frac{dT}{T}$$

(4.15*a*)

and

$$\Phi(T) = \int_{T_0}^{T} c_p(T) \frac{dT}{T}$$

(4.15*b*)

then

$$s - s_0 = \Psi + R \ln\left(\frac{v}{v_0}\right)$$

(4.16*a*)

$$s - s_0 = \Phi + R \ln\left(\frac{p}{p_0}\right)$$

(4.16*b*)

Thus, for example, the entropy change between states
(T_1, p_1) and
(T_2, p_2) is

$$s_2 - s_1 = \Phi_2 - \Phi_1 - R \ln\left(\frac{p_2}{p_1}\right)$$

(4.17)

For an isentropic process,

$$\ln\left(\frac{p_2}{p_1}\right) = \frac{\Phi_2 - \Phi_1}{R}$$

(4.18)

In these equations, the units of *u* and *h* can be on a per unit mass or molar basis (i.e., joules per kilogram or joules per kilomole); similarly, *s*,
c_v,

© McGraw-Hill Education. All rights reserved. Any use is subject to the Terms of Use, Privacy Notice and copyright information.

c_p, R, ψ, and Φ can be in joules per kilogram-kelvin.

For gas mixtures, once the composition is known, mixture properties are determined either on a mass or molar basis from

$$u = \sum x_i u_i \qquad \tilde{u} = \sum \tilde{x}_i \tilde{u}_i$$

(4.19*a*)

$$h = \sum x_i h_i \qquad \tilde{h} = \sum \tilde{x}_i \tilde{h}_i$$

(4.19*b*)

$$s = \sum x_i s_i \qquad \tilde{s} = \sum \tilde{x}_i \tilde{s}_i$$

(4.19*c*)

and

$$c_v = \sum x_i c_{v,i} \qquad \tilde{c}_v = \sum \tilde{x}_i \tilde{c}_{v,i}$$

(4.20*a*)

$$c_p = \sum x_i c_{p,i} \qquad \tilde{c}_p = \sum \tilde{x}_i \tilde{c}_{p,i}$$

(4.20*b*)

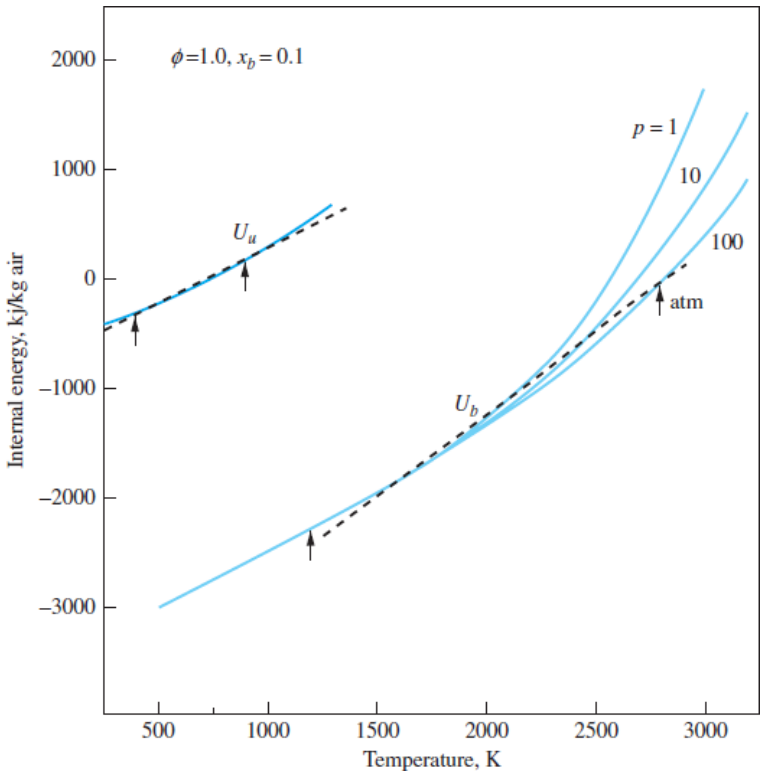
© McGraw-Hill Education. All rights reserved. Any use is subject to the Terms of Use, Privacy Notice and copyright information.

4.4. A SIMPLE ANALYTIC IDEAL GAS MODEL

While the first category of model listed in Table 4.2 is too inaccurate for other than illustrative purposes, the second category —constant but different specific heats for the unburned and burned gas mixtures—can with careful choice of specific heat values be made much more precise. The advantages of a simple analytic model may be important for certain problems.

Figure 4.2 shows an internal energy versus temperature plot for a stoichiometric mixture. It is a quantitative version of Fig. 3.5. The unburned mixture line is for a burned gas fraction of 0.1. The fuel is isooctane. Data to construct such graphs can be obtained from charts or tables or computer programs (see Secs. 4.5 to 4.7). The units for u are kilojoules per kilogram of air in the original mixture (the units of the charts in Sec. 4.5). The datum is zero enthalpy for
O_2,
N_2,
H_2, and C (solid) at 298 K. Note that the specific heats of the unburned and burned mixtures (the slopes of the lines in Fig. 4.2) are a function of temperature; at high temperatures, the internal energy of the burned mixture is a function of temperature and pressure.

Figure 4.2 Internal energy versus temperature plot for stoichiometric unburned and burned gas mixtures: isooctane fuel; unburned residual fraction 0.1.



However, the temperature range of interest for the unburned mixture in an SI engine is 400 to 1000 K; for the burned gas mixture, the extreme end states are approximately 2800 K, 35 atm and 1200 K, 2 atm. Linear approximations to the unburned and burned mixture curves, which minimize the error in u over the temperature (and pressure) ranges of interest, are shown as dashed lines. The error in T for a given u is less than 50 K.

The basis for this ideal gas model is

© McGraw-Hill Education. All rights reserved. Any use is subject to the Terms of Use, Privacy Notice and copyright information.

$$u_u = c_{v,u}T_u + h_{f,u} \qquad h_u = c_{p,u}T_u + h_{f,u}$$

(4.21*a*, *b*)

$$u_b = c_{v,b}T_b + h_{f,b} \qquad h_b = c_{p,b}T_b + h_{f,b}$$

(4.22*a*, *b*)

where
$h_{f,u}$ and
$h_{f,b}$ are the enthalpies of formation of unburned and burned gas mixture, respectively, at 0 K.

Then, for a constant-volume adiabatic combustion process,

$$u_u = u_b$$

or

$$c_{v,u}T_u + h_{f,u} = c_{v,b}T_b + h_{f,b}$$

If we solve for
T_b and use the relations
$(R_b/R_u) = (M_u/M_b)$ and
$c_v/R = 1/(\gamma - 1)$, we obtain

$$T_b = (\gamma_b - 1)\left(\frac{M_b}{M_u}\right)\left(\frac{T_u}{\gamma_u - 1} + \frac{\Delta h_f}{R_u}\right)$$

(4.23)

where
$\Delta h_f = h_{f,u} - h_{f,b}$.

For a constant-pressure adiabatic combustion process,

$$h_u = h_b$$

and it can similarly be shown that

$$T_b = \frac{\gamma_b - 1}{\gamma_b}\left(\frac{M_b}{M_u}\right)\left(\frac{\gamma_u}{\gamma_u - 1}T_u + \frac{\Delta h_f}{R_u}\right)$$

(4.24)

To use the model, suitable values of
γ_u, γ_b, M_u, (M_b/M_u), and

© McGraw-Hill Education. All rights reserved. Any use is subject to the Terms of Use, Privacy Notice and copyright information.

$\Delta h_f/R_u$ must be determined. Values for M_u and M_b can be obtained from Eqs. (4.10) and (4.11).[1] Values of γ_u, γ_b, and $\Delta h_f/R_u$ can be obtained from graphs such as Fig. 4.2 (see Example 4.1 below). Values for γ_u, γ_b, and $\Delta h_f/R_u$ are available in the literature (e.g. Ref. 1) and this chapter, for a range of ϕ and x_b. Values used for computations should be checked over the temperature range of interest, to ensure that the particular linear fit to $u(T)$ used is appropriate.

Example

EXAMPLE 4.1

Determine the values of γ_u, γ_b, and $\Delta h_f/R_u$ which correspond to the straight-line fits for $u_u(T)$ and $u_b(T)$ in Fig. 4.2.

Equations for the straight lines in Fig. 4.2 are

$$u_u(\text{kJ/kg air}) = 0.96T(\text{K}) - 700$$

and

$$u_b(\text{kJ/kg air}) = 1.5T(\text{K}) - 4250$$

From Table 4.5, for isooctane fuel with ϕ = 1.0 and x_b = 0.1, the number of moles of unburned mixture per mole O_2 in the mixture is

$$n_u = 0.08 \times 1 + 4.773 + 0.28 \times 0.1 \times 1 = 4.881$$

The mass of air per mole O_2 in the mixture is 138.2. Thus, the number of moles of unburned mixture per unit mass of air in the original mixture is

$$\frac{4.881}{138.2} = 0.0353$$

The molar specific heat of the unburned mixture $\tilde{c}_{v,u}$ is therefore

$$\tilde{c}_{v,u} = \frac{0.96}{0.0353} = 27.2\ \text{kJ/kmol} \cdot \text{K}$$

© McGraw-Hill Education. All rights reserved. Any use is subject to the Terms of Use, Privacy Notice and copyright information.

Since
$\tilde{R} = 8.314\ \mathrm{kJ/kmol \cdot K}$,

$$\gamma_u = \frac{27.2 + 8.314}{27.2} = 1.31$$

The number of moles of burned mixture per mole
O_2 is (from Table 4.5)

$$n_b = 0.36 \times 1 + 4.773 = 5.133$$

The number of moles of burned mixture per unit mass of air in the original mixture is

$$\frac{5.133}{138.2} = 0.0371$$

The molar specific heat
$\tilde{c}_{v,b}$ is therefore

$$\tilde{c}_{v,b} = \frac{1.5}{0.0371} = 40.4\ \mathrm{kJ/kmol \cdot K}$$

and
γ_b is

$$\gamma_b = \frac{40.4 + 8.314}{40.4} = 1.21$$

To find
$\Delta h_f / R_u$, R_u is given by

$$R_u = 8.314 \times 0.0353 = 0.293\ \mathrm{kJ/kg\,air \cdot K}$$

and so

$$\frac{\Delta h_f}{R_u} = \frac{(-700) - (-4250)}{0.293} = 1.2 \times 10^4 \mathrm{K}$$

[1] The error in ignoring the effect of dissociation on M_b is small.

© McGraw-Hill Education. All rights reserved. Any use is subject to the Terms of Use, Privacy Notice and copyright information.

4.5. THERMODYNAMIC PROPERTY CHARTS

One method of presenting thermodynamic properties of unburned and burned gas mixtures for internal combustion engine calculations is on charts. Such charts in US units were developed by Hottel et al.[2] and Newhall and Starkman.[3,4] We developed a new set of charts in SI units, following the approach of Newhall and Starkman. While charts are no longer used extensively for engine cycle calculations—computer models for the thermodynamic properties of working fluids have replaced them—these charts are useful for illustrative purposes, and afford an easy and accurate approach where the number of calculations is limited. The charts presented below are for isooctane fuel, and the following equivalence ratios: ϕ = 0.4, 0.6, 0.8, 1.0, 1.2.

4.5.1. Unburned Mixture Charts

The thermodynamic properties of each unburned fuel-air mixture are represented by two charts. The first chart is designed to relate the mixture temperature, pressure, and volume at the beginning and at the end of the compression process; the second gives the mixture internal energy and enthalpy as functions of temperature.

The following assumptions are made:

1. The compression process is reversible and adiabatic.
2. The fuel is in the vapor phase.
3. The mixture composition is homogeneous and frozen (no reactions between the fuel and air).
4. Each species in the mixture can be modeled as an ideal gas.
5. The burned gas fraction is zero.[1]

It proves convenient to assign zero internal energy or enthalpy to the unburned mixture at 298.15 K. Internal energy and enthalpies relative to this datum are called *sensible internal energy* u_s *or sensible enthalpy* h_s. By sensible we mean changes in *u* or *h* which result from changes in temperature alone, and we exclude changes due to chemical reaction or phase change.

Table 4.6 provides the basic composition data for the unburned mixture charts. Equations (4.13*a*, *b*) provide the basis for obtaining the $u_{s,u}(T)$ and $h_{s,u}(T)$ curves shown in Fig. 4.3.

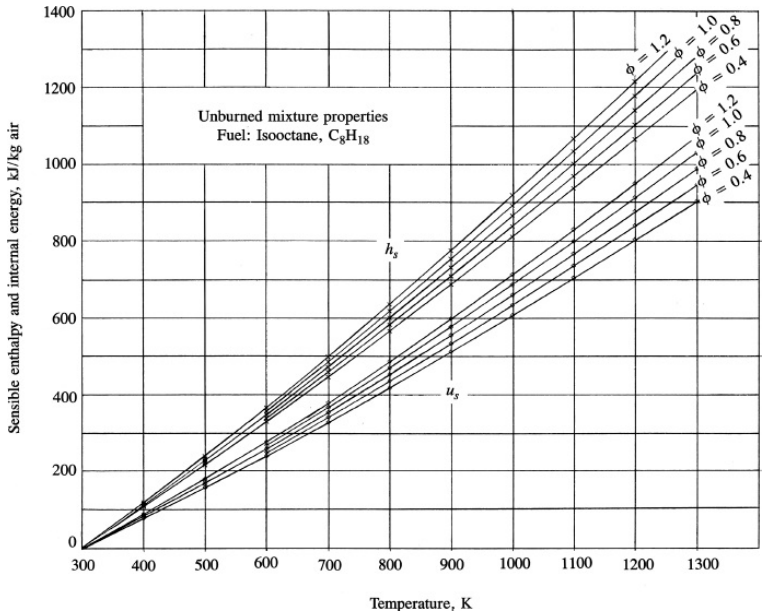
© McGraw-Hill Education. All rights reserved. Any use is subject to the Terms of Use, Privacy Notice and copyright information.

Table 4.6 Unburned mixture composition for charts

Equivalence ratio ϕ	(F/A)	Kilograms of mixture per kilogram of air	Moles of mixture per mole of O_2	Kilomole of mixture per kilogram of air	$n_u\widetilde{R}$, * $\mathrm{J/kg\,air\cdot K}$
0.4	0.0264	1.0264	$4.805 + 0.112x_b$	$0.0348 + 0.00081x_b$	289
0.6	0.0396	1.0396	$4.821 + 0.168x_b$	$0.0349 + 0.00122x_b$	290
0.8	0.0528	1.0528	$4.837 + 0.224x_b$	$0.0350 + 0.00162x_b$	291
1.0	0.0661	1.0661	$4.853 + 0.280x_b$	$0.0351 + 0.00203x_b$	292
1.2	0.0792	1.0792	$4.869 + 0.536x_b$	$0.0352 + 0.00388x_b$	292

*For $x_b = 0$. Error in neglecting x_b is usually small.

Figure 4.3 Sensible enthalpy and internal energy of unburned isooctane-air mixtures as function of temperature. Units: kJ/kg air in mixture.



Equations (4.15) and (4.16) provide the basis for following a reversible adiabatic (i.e., isentropic) compression process. Between end states 1 and 2, we obtain, per kilogram of air in the mixture,

$$\Psi(T_2) = \Psi(T_1) - n_u\widetilde{R}\ln\left(\frac{v_2}{v_1}\right)$$

(4.25*a*)

$$\Phi(T_2) = \Phi(T_1) + n_u\widetilde{R}\ln\left(\frac{p_2}{p_1}\right)$$

(4.25*b*)

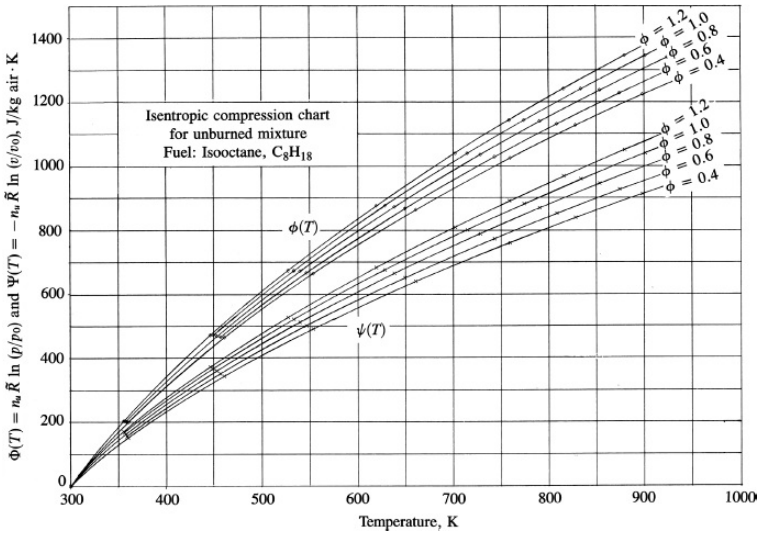
© McGraw-Hill Education. All rights reserved. Any use is subject to the Terms of Use, Privacy Notice and copyright information.

where
n_u is the number of moles of unburned mixture per kilogram of air. Values of
n_u and
$n_u\widetilde{R}$ are given in Table 4.6.
$\Psi(T)$ and
$\Phi(T)$ are given in Fig. 4.4. Note that *v*, *p*, and *T* are related by

$$p(\mathrm{Pa})v(\mathrm{m}^3/\mathrm{kg\,air}) = n_u\widetilde{R}(\mathrm{J/kg\,air\cdot K})\,T(\mathrm{K})$$

(4.26)

Figure 4.4 Isentropic compression functions, Φ and ψ as function of temperature for unburned isooctane-air mixtures. Units: J/kg air · K.



Example

EXAMPLE 4.2

The compression process in an internal combustion engine can be modeled approximately as adiabatic and reversible (i.e., as an isentropic process). A spark-ignition engine with a compression ratio of 8 operates with a stoichiometric fuel vapor—air mixture, which is at 350 K and 1 atm at the start of the compression stroke. Find the temperature, pressure, and volume per unit mass of air at the end of the compression stroke. Calculate the compression stroke work.

Given
T_1 = 350 K at the start of compression, find
T_2 at the end of compression using the isentropic compression chart, Fig. 4.4, and Eq. (4.25*a*). For
$T_1 = 350\,\mathrm{K}$, $\Psi_1 = 150\,\mathrm{J/kg\,air\cdot K}$. From Eq. (4.25*a*),

$$\Psi_2(T_2) = \Psi_1(T_1) - n_u\widetilde{R}\ln\left(\frac{v_2}{v_1}\right) = 150 - 292\ln\left(\frac{1}{8}\right) = 757\,\mathrm{J/kg\,air\cdot K}$$

Figure 4.4 then gives

© McGraw-Hill Education. All rights reserved. Any use is subject to the Terms of Use, Privacy Notice and copyright information.

$$T_2 = 682\,\mathrm{K}$$

The ideal gas law [Eq. (4.26)] gives

$$v_1 = \frac{292 \times 350}{1 \times 1.013 \times 10^5} = 1.0\,\mathrm{m^3/kg\,air}$$

and

$$\begin{aligned} p_2 &= p_1\left(\frac{T_2}{T_1}\right)\left(\frac{v_1}{v_2}\right) = \frac{682}{350} \times 8 = 15.5\,\mathrm{atm} \\ v_2 &= \frac{1.0}{8} = 0.125\,\mathrm{m^3/kg\,air} \end{aligned}$$

Note that
p_2 can also be obtained from Fig. 4.4 and Eq. (4.25*b*):

$$\begin{aligned} \ln\left(\frac{p_2}{p_1}\right) &= \frac{\Phi_2 - \Phi_1}{n_u \tilde{R}} = \frac{980 - 180}{292} = 2.74 \\ p_2 &= 15.5\,\mathrm{atm} = 1.57\,\mathrm{MPa} \end{aligned}$$

The compression stroke work, assuming the process is adiabatic and using the data in Fig. 4.3, is

$$-W_{1-2} = u_s(T_2) - u_s(T_1) = 350 - 40 = 310\,\mathrm{kJ/kg\,air}$$

4.5.2. Burned Mixture Charts

The primary burned mixture charts are for the products of combustion at high temperatures, that is, for the working fluid during the expansion process. The following assumptions are made:

1. Each species in the mixture can be modeled as an ideal gas.
2. The mixture is in thermodynamic and chemical equilibrium at temperatures above 1700 K; the mixture composition is frozen below 1700 K.
3. *Datum*. At the datum state of 298.15 K (25°C or 77°F) and 1 atm, the chemical elements in their naturally occurring form (N_2, O_2, H_2 as diatomic gases and C as solid graphite) are assigned zero enthalpy and entropy.

The charts were prepared with the NASA equilibrium program described in Sec. 3.7.[5,6] The C/H/O/N ratio of the mixture is specified for each chart. The intensive properties (internal energy, enthalpy, entropy, and specific volume) are all expressed per unit mass of air in the original mixture; that is, they correspond to the combustion of 1 kg of air with the appropriate mass of fuel. The mass basis for the unburned and burned mixture charts are the same.

Figures 4.5 to 4.9 are property charts for the high-temperature burned gas; each is a plot of internal energy versus entropy for

© McGraw-Hill Education. All rights reserved. Any use is subject to the Terms of Use, Privacy Notice and copyright information.

a particular fuel and equivalence ratio. Lines of constant temperature, pressure, and specific volume are drawn on each chart. An illustration of the use of these charts follows.

Figure 4.5 Internal energy versus entropy chart for equilibrium burned gas mixture, isooctane fuel; equivalence ratio 0.4.

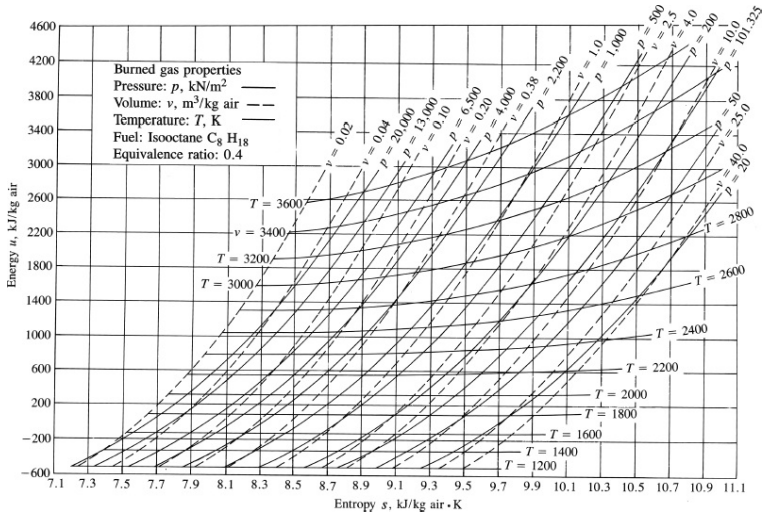
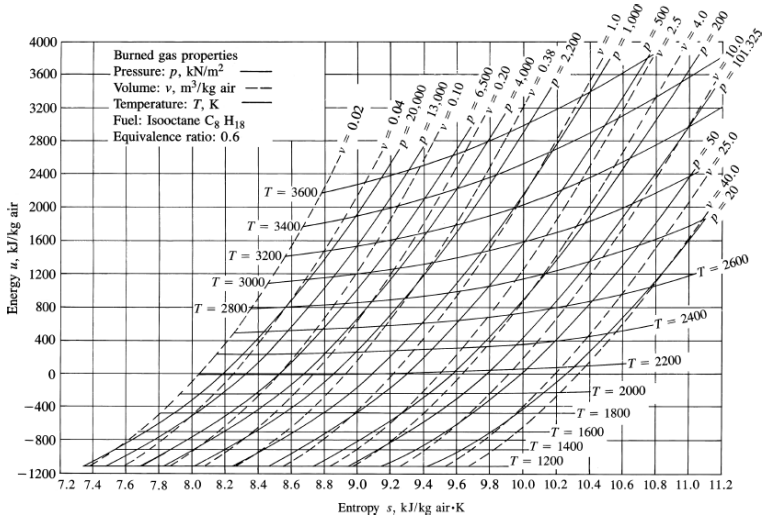


Figure 4.6 Internal energy versus entropy chart for equilibrium burned gas mixture, isooctane fuel; equivalence ratio 0.6.



© McGraw-Hill Education. All rights reserved. Any use is subject to the Terms of Use, Privacy Notice and copyright information.

Figure 4.7 Internal energy versus entropy chart for equilibrium burned gas mixture, isooctane fuel; equivalence ratio 0.8.

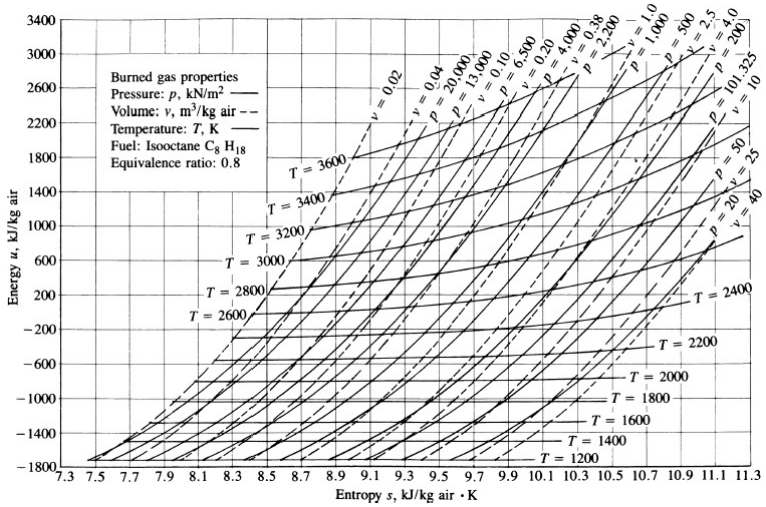
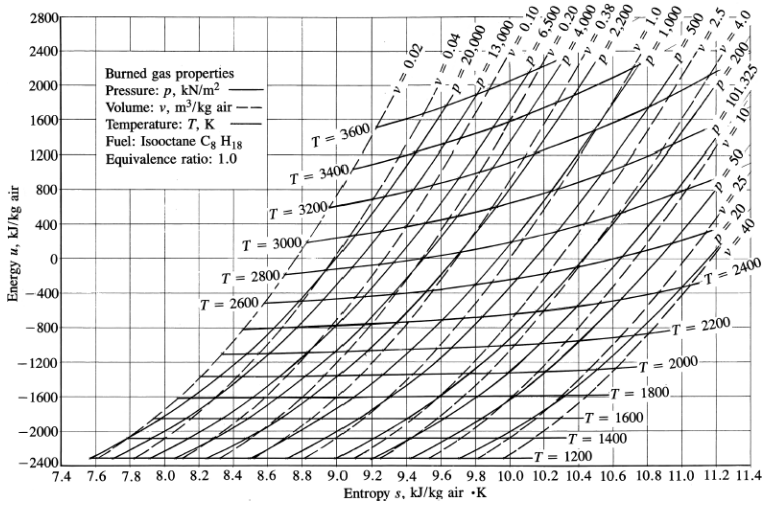
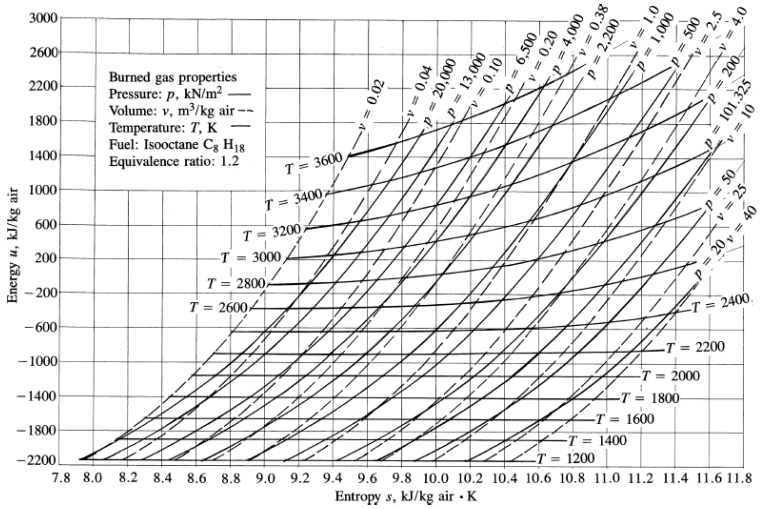


Figure 4.8 Internal energy versus entropy chart for equilibrium burned gas mixture, isooctane fuel; equivalence ratio 1.0.



© McGraw-Hill Education. All rights reserved. Any use is subject to the Terms of Use, Privacy Notice and copyright information.

Figure 4.9 Internal energy versus entropy chart for equilibrium burned gas mixture, isooctane fuel; equivalence ratio 1.2.



Example

EXAMPLE 4.3

The expansion process in an internal combustion engine, following completion of combustion, can be modeled approximately as an adiabatic and reversible process (i.e., isentropic). Under full-load operation, the pressure in the cylinder of a spark-ignition engine at top-center immediately following combustion is 7100 kPa. Find the gas state at the end of the expansion stroke and the expansion stroke work. The compression ratio is 8, the mixture is stoichiometric, and the volume per unit mass of air at the start of expansion is 0.125 m^3/kg air.

Locate
p_1 = 7100 kPa and
v_1 = 0.125 m_3/kg air on the ϕ = 1.0 burned gas chart (Fig. 4.8). This gives
T_1 = 2825 K,
u_1 = −5 kJ/kg air, and
s_1 = 9.33 kJ/kg air·K. The gas expands at constant entropy to
v_2 = 8 ×
v_1 = 1 m^3/kg air. Following a constant entropy process from state 1 onFig. 4.8 gives

$$T_2 = 1840\,\mathrm{K}, \qquad p_2 = 570\,\mathrm{kPa}, \qquad \text{and} \qquad u_2 = -1540\,\mathrm{kJ/kg\,air}$$

The expansion stroke work, assuming the process is adiabatic, is

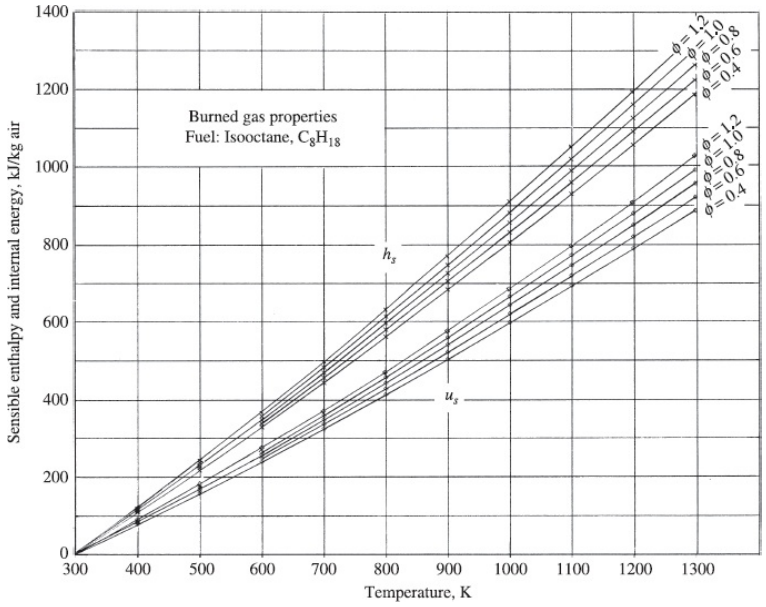
$$W_{1-2} = -(u_2 - u_1) = 1540 - 5 = 1535\,\mathrm{kJ/kg\ air}$$

As the burned gases in an engine cylinder cool during the expansion process, the composition eventually "freezes"—becomes fixed in composition—because the chemical reactions become extremely slow. This is usually assumed to occur at about 1700 K (see Sec. 4.9). The equilibrium composition assumption is then no longer valid. For lean and stoichiometric mixtures this distinction is not important because the mole fractions of dissociated species below this temperature are small. For rich mixtures, a frozen composition must be selected and used because the mole fractions of

© McGraw-Hill Education. All rights reserved. Any use is subject to the Terms of Use, Privacy Notice and copyright information.

CO_2, CO,
H_2O, and
H_2 would continue to change if equilibrium is assumed as the temperature decreases. Internal energy and enthalpy, per kilogram of air in the original mixture, of the frozen burned mixture are plotted against temperature in Fig. 4.10. The assumed frozen burned mixture compositions are listed in Table 4.7. These are sensible internal energies and enthalpies, given relative to their values at 298.15 K.

Figure 4.10 Sensible enthalpy and internal energy of low-temperature burned gases as function of temperature, isooctane fuel. Units: kJ/kg air in original mixture.



© McGraw-Hill Education. All rights reserved. Any use is subject to the Terms of Use, Privacy Notice and copyright information.

Table 4.7 Frozen burned gas composition: C_8H_{18}-air combustion

ϕ	CO_2	H_2O	CO	H_2	O_2	N_2	Sum	Units
0.4	0.0521	0.0586	—	—	0.122	0.767	1.000	mole fractions
	1.85	2.08	—	—	4.34	27.3	35.6	mol/kg air*
0.6	0.0770	0.0866	—	—	0.0802	0.756	1.000	mole fractions
	2.78	3.13	—	—	2.89	27.3	36.1	mol/kg air*
0.8	0.101	0.113	—	—	0.0395	0.746	1.000	mole fractions
	3.70	4.14	—	—	1.45	27.3	36.6	mol/kg air*
1.0	0.125	0.140	—	—	—	0.735	1.000	mole fractions
	4.64	5.2	—	—	—	27.3	37.1	mol/kg air*
1.2†	0.0905	0.138	0.0516	0.0224	—	0.698	1.000	mole fractions
	3.54	5.38	2.02	0.876	—	27.3	39.1	mol/kg air*

*Note mol/kg air; multiply by 10^{-3} for kmol/kg air.

Note, to obtain these burned-gas mole fractions, $K(T)$ in Eq. (4.6) was evaluated at 1740 K; $K = 3.5$.

4.5.3. Relation between Unburned and Burned Mixture Charts

We now address the questions: Given unburned mixture at
T_1,
p_1,
v_1, what is the state of the burned mixture following (1) constant-volume adiabatic combustion or (2) constant-pressure adiabatic combustion?

The datum for internal energy and enthalpy for the unburned mixture in Fig. 4.3 is different from the datum for internal energy and enthalpy for the burned mixture. For the unburned mixture, zero internal energy and enthalpy for the *mixture* at 298.15 K was assumed. For the burned mixture, zero enthalpy for the gaseous species
O_2,
N_2, and
H_2, and C (solid graphite) at 298.15 K was assumed. These data can be related through the enthalpies of formation, from
O_2,
N_2,
H_2, and C, of each species in the unburned mixture.

If
$\Delta\tilde{h}^{\circ}_{f,i}$ is the enthalpy of formation of species *i* at 298.15 K, per kilomole, and
$\Delta h^{\circ}_{f,u}$ is the enthalpy of formation of the unburned mixture at 298.15 K, per kilogram of air in the original mixture, then

© McGraw-Hill Education. All rights reserved. Any use is subject to the Terms of Use, Privacy Notice and copyright information.

$$\Delta h^\circ_{f,u} = \sum_i n_i \Delta \tilde{h}^\circ_{f,i}$$

(4.27)

where
n_i is the number of kilomoles of species *i* per kilogram of air. The unburned mixture enthalpy
h_u, with the same datum as the burned mixture enthalpy, is therefore given by the sum of the sensible enthalpy
$h_{s,u}$ and
$\Delta h^\circ_{f,u}$:

$$h_u = h_{s,u} + \Delta h^\circ_{f,u}$$

(4.28)

Similarly, the internal energy
u_u is given by

$$u_u = u_{s,u} + \Delta u^\circ_{f,u}$$

(4.29)

$\Delta u^\circ_{f,u}$ can be obtained from

$$\Delta u^\circ_{f,u} = \sum_i n_i \, \Delta \tilde{u}^\circ_{f,i}$$

(4.30)

Alternately, Eq. (3.18) can be used to obtain
$\Delta u^\circ_{f,u}$ from
$\Delta h^\circ_{f,u}$:

$$\Delta u^\circ_{f,u} = \Delta h^\circ_{f,u} - (n_p - n_R)\tilde{R}T$$

(4.31)

Enthalpies and internal energies of formation of the relevant burned gas species and individual fuel compounds are given in Table 4.8 and App. D. Values of
n_i are obtained from Tables 4.4 and 4.7. Following the procedure used in Example 4.4 below, expressions for
$\Delta h^\circ_{f,u}$ and
$\Delta u^\circ_{f,u}$ in kilojoules per kilogram of air can be obtained. For the charts of Figs. 4.3 and 4.5 to 4.9, these expressions are:

© McGraw-Hill Education. All rights reserved. Any use is subject to the Terms of Use, Privacy Notice and copyright information.

$$\phi = 0.4: \quad \Delta h^\circ_{f,u} = -51.9 - 1181x_b \quad \Delta u^\circ_{f,u} = -47.3 - 1183x_b$$

$$\phi = 0.6: \quad \Delta h^\circ_{f,u} = -77.8 - 1771x_b \quad \Delta u^\circ_{f,u} = -70.9 - 1774x_b$$

$$\phi = 0.8: \quad \Delta h^\circ_{f,u} = -103.8 - 2361x_b \quad \Delta u^\circ_{f,u} = -94.6 - 2365x_b$$

$$\phi = 1.0: \quad \Delta h^\circ_{f,u} = -129.7 - 2951x_b \quad \Delta u^\circ_{f,u} = -118.2 - 2956x_b$$

$$\phi = 1.2: \quad \Delta h^\circ_{f,u} = -155.6 - 2759x_b \quad \Delta u^\circ_{f,u} = -141.9 - 2769x_b$$

(4.32)

Table 4.8 Standard enthalpies and internal energies of formation*

	$\Delta h^\circ_{f,i}$, MJ/kmol	$\Delta u^\circ_{f,i}$, MJ/kmol
CO_2	−393.5	−393.5
H_2O (gas)	−241.8	−240.6
CO	−110.5	−111.7
C_8H_{18} (gas)	−224.1	−204.3

*At 298.15 K.
$\Delta h^\circ_{f,i}$ for O_2, N_2, and H_2 is zero by definition.

Sources: JANAF tables;[1] Rossini et al.[7]

Example

EXAMPLE 4.4

Calculate
$\Delta h^\circ_{f,u}$, the enthalpy of formation of the unburned mixture, and
$\Delta u^\circ_{f,u}$ the internal energy of formation of the unburned mixture, for a
C_8H_{18}-air mixture with ϕ = 1.0 and burned gas fraction
x_b.

Table 4.4 gives the moles of each species in the unburned mixture, per mole O_2 with ϕ = 1.0, as

$C_8H_{18}, 0.08(1 - x_b)$	$CO_2, 0.64x_b$
$O_2, 1 - x_b$	$H_2O, 0.72x_b$
$N_2, 3.773$	CO and H_2, 0

© McGraw-Hill Education. All rights reserved. Any use is subject to the Terms of Use, Privacy Notice and copyright information.

Table 4.5 gives the mass of air per mole O_2 as 138.2 kg/kmol. Thus the number of kilomoles of each species per kilogram of air is

$$\begin{aligned} &C_8H_{18},\ 5.787\times10^{-4}(1-x_b) \qquad CO_2,\ 4.629\times10^{-3}x_b \\ &O_2,\ 7.233\times10^{-3}(1-x_b) \qquad H_2O,\ 5.208\times10^{-3}x_b \\ &N_2,\ 2.729\times10^{-2} \qquad CO \text{ and } H_2,\ 0 \end{aligned}$$

With $\Delta\tilde{h}^\circ_{f,i}$ from Table 4.8, Eq. (4.27) gives

$$\begin{aligned} \Delta h^\circ_{f,u} &= 5.787\times10^{-4}\times(-224.1\times10^6)(1-x_b) \\ &\quad + x_b\left[4.629\times10^{-3}\times(-393.5\times10^6)+5.208\times10^{-3}\times(-241.8\times10^6)\right] \\ \Delta h^\circ_{f,u} &= (-129.7-2951x_b)\times10^3\,\text{kJ/kg air} \end{aligned}$$

With $\Delta\tilde{u}^\circ_{f,i}$ from Table 4.8, Eq. (4.30) gives

$$\begin{aligned} \Delta u^\circ_{f,u} &= 5.787\times10^{-4}\times(-204.3\times10^6)(1-x_b) \\ &\quad + x_b\left[4.629\times10^{-3}\times(-393.5\times10^6)+5.208\times10^{-3}\times(-240.6\times10^6)\right] \\ \Delta u^\circ_{f,u} &= (-118.2-2956x_b)\times10^3\,\text{J/kg air} \end{aligned}$$

Alternatively, we can determine $\Delta u^\circ_{f,u}$ from $\Delta h^\circ_{f,u}$ using Eq. (4.31). For this calculation, the "product" gas is the unburned mixture and the "reactant" gas is the mixture of elements from which the unburned mixture is formed. The number of gaseous moles in the unburned mixture n_p, per mole O_2 in the original mixture, is (from Table 4.5 for $\phi \le 1$)

$$n_P = (1-x_b)\left[4(1+2\varepsilon)\frac{\phi}{M_f}+1+\psi\right]+x_b\left[(1-\varepsilon)\phi+1+\psi\right]$$

The elemental reactant mixture from which the unburned mixture is formed is, from Eq. (4.4),

$$\varepsilon\phi C + 2(1-\varepsilon)\phi H_2 + O_2 + \psi N_2$$

Thus, n_R, the moles of *gaseous* elements, is

$$n_R = 2(1-\varepsilon)\phi + 1 + \psi$$

© McGraw-Hill Education. All rights reserved. Any use is subject to the Terms of Use, Privacy Notice and copyright information.

For air, $\psi = 3.773$; for C_8H_{18} fuel, $\varepsilon = 0.64$ and $M_f = 114$. For $\phi = 1$,

$$n_P - n_R = -0.64 + 0.28x_b \quad \text{moles/mole } O_2$$

and

$$(n_P - n_R)\tilde{R}T = (-0.64 + 0.28x_b) \times 8.3143 \times 10^3 \times \frac{298.15}{138.2}$$

or

$$(n_P - n_R)\tilde{R}T = (-11.5 + 5.0x_b) \times 10^3 \,\text{J/kg air}$$

Since

$$\Delta u^\circ_{f,u} = \Delta h^\circ_{f,u} - (n_P - n_R)\tilde{R}T$$
$$\Delta u^\circ_{f,u} = (-129.7 - 2951x_b) \times 10^3 - (-11.5 + 5.0x_b) \times 10^3$$
$$\Delta u^\circ_{f,u} = (-118.2 - 2956x_b) \times 10^3 \,\text{J/kg air}$$

The combustion process links the unburned and burned mixture properties as follows: For an adiabatic constant-volume combustion process,

$$u_b = u_u = u_{s,u} + \Delta u^\circ_{f,u}$$

(4.33)

and

$$v_b = v_u$$

Thus, given $u_{s,u}$ and v_u, the state of the burned mixture can be determined from the appropriate burned mixture chart.

For an adiabatic constant-pressure combustion process,

$$h_b = h_u = h_{s,u} + \Delta h^\circ_{f,u}$$

(4.34)

Since

© McGraw-Hill Education. All rights reserved. Any use is subject to the Terms of Use, Privacy Notice and copyright information.

$$u_b = h_b - pv_b$$

given
$h_{s,u}$ and p,
u_b and
v_b must be found by trial and error along the specified constant-pressure line on the appropriate burned mixture chart.

Example

EXAMPLE 4.5

Calculate the temperature and pressure after constant-volume adiabatic combustion and constant-pressure adiabatic combustion of the unburned mixture (with ϕ = 1.0 and
x_b = 0.08) at the state corresponding to the end of the compression process examined in Example 4.2.

The state of the unburned mixture at the end of the compression process in Example 4.2 was

$$T_u = 682\,\mathrm{K}, \quad u_{s,u} = 350\,\mathrm{kJ/kg\ air}, \quad p_u = 1.57\,\mathrm{MPa}, \quad v_u = 0.125\,\mathrm{m^3/kg\,air}$$

For an adiabatic *constant-volume* combustion process [Eq. (4.33)],

$$u_b = u_u = u_{s,u} + \Delta u^\circ_{f,u}$$

For ϕ = 1.0,
$\Delta u^\circ_{f,u}$ is given by Eq. (4.32) as

$$\Delta u^\circ_{f,u} = -118.2 - 2956x_b = -118.2 - 236.5 = -355\,\mathrm{kJ/kg\,air}$$

Hence

$$u_b = 350 - 355 = -5\,\mathrm{kJ/kg\,air}$$

Also

$$v_b = v_u = 0.125\,\mathrm{m^3/kg\,air}$$

Locating (
u_b,
v_b) on the burned gas chart (Fig. 4.8) gives

$$T_b = 2825\,\mathrm{K}, \quad p_b = 7100\,\mathrm{kPa}$$

For a *constant-pressure* combustion process [Eq. (4.34)],

© McGraw-Hill Education. All rights reserved. Any use is subject to the Terms of Use, Privacy Notice and copyright information.

$$h_b = h_u = h_{s,u} + \Delta h^\circ_{f,u}$$

For ϕ = 1.0,
$\Delta h^\circ_{f,u}$ is given by Eq. (4.32) as

$$\Delta h^\circ_{f,u} = -129.7 - 2951 x_b = -129.7 - 236 = -366\,\mathrm{kJ/kg\,air}$$

At
T_u = 682 K,
$h_{s,u}$ = 465 kJ/kg air, so

$$h_b = 465 - 366 = 99\,\mathrm{kJ/kg\,air}$$

Since
p_b =
p_u = 1.57 MPa, the internal energy
u_b is given by

$$u_b = h_b - p_b v_b = 99 - 1.57 \times 10^3 v_b\,\mathrm{kJ/kg\,air}$$

A trial—and—error solution for
v_b and
u_b along the *p* = 1570 kPa line on Fig. 4.8 gives

$$u_b = -655\,\mathrm{kJ/kg\ air}, \quad T_b = 2440\,\mathrm{K}, \quad v_b = 0.485\,\mathrm{m^3/kg\,air}$$

(Use the ideal gas law to estimate *p*, *T*, or *v* more accurately.)

[1] This assumption introduces negligible error into calculations of the compression process for mixtures with normal burned gas fractions, since the major constituent of the residual is N_2. The burned gas fraction must, however, be included when the unburned mixture properties are related to burned mixture properties in a combustion process.

© McGraw-Hill Education. All rights reserved. Any use is subject to the Terms of Use, Privacy Notice and copyright information.

4.6. TABLES OF PROPERTIES AND COMPOSITION

Tables of thermodynamic properties of air are useful for analysis of motored engine operation, diesels, and compressors. Keenan, Chao, and Kaye's *Gas Tables*[8] are the standard reference for the thermodynamic properties of air at low pressures (i.e., at pressures substantially below the critical pressure when the ideal gas law is accurate). These gas tables are in U.S. and SI units. A set of tables for air in SI units has been prepared by Reynolds[9] following the format of the Keenan et al. tables. A condensed table of thermodynamic properties of air, derived from Reynolds, is given in App. D. It contains:

h = enthalpy, kJ/kg

u = internal energy, kJ/kg

$$\Psi = \int_0^T \left(\frac{c_v}{T}\right) dT,\ \mathrm{kJ/kg \cdot K}$$

$$\Phi = \int_0^T \left(\frac{c_p}{T}\right) dT,\ \mathrm{kJ/kg \cdot K}$$

p_r = relative pressure

v_r = relative volume

c_p = specific heat at constant pressure, kJ/kg·K

c_v = specific heat at constant volume, kJ/kg·K

γ = ratio of specific heats

all as a function of *T*(K).

ψ and Φ are the standard state entropy at temperature *T* and 1 atm pressure relative to the entropy at 0 K and 1 atm pressure. [See Eqs. (4.14) to (4.17).] The entropy at pressures other that 1 atm is obtained using Eq. (4.14).

The relative pressure
p_r is defined by

$$\ln p_r = \frac{\Phi}{R}$$

(4.35)

and is a function of *T* only. Along a given isentropic, it follows from Eq. (4.18) that the ratio of actual pressures
p_2 and
p_1 corresponding to temperatures
T_2 and
T_1 is equal to the ratio of relative pressures, that is,

$$\left(\frac{p_2}{p_1}\right)_{s=\mathrm{const}} = \left(\frac{p_{r_2}}{p_{r_1}}\right)$$

© McGraw-Hill Education. All rights reserved. Any use is subject to the Terms of Use, Privacy Notice and copyright information.

(4.36)

This affords a means of determining
T_2, for an isentropic process, given
T_1 and
p_2/p_1 (see Example 4.6).

The relative volume v_r is defined by

$$v_r = \frac{RT}{p_r}$$

(4.37)

The units are selected so that v_r is in cubic meters per kilogram when T is in kelvins and p_r is in pascals. Along a given isentropic, the ratio of actual volumes
V_2 and
V_1 (for a fixed mass) at temperatures
T_2 and
T_1, from Eq. (4.37), is equal to the ratio of relative volumes

$$\left(\frac{V_2}{V_1}\right)_{s=\text{const}} = \left(\frac{v_{r_2}}{v_{r_1}}\right)$$

(4.38)

This affords a means of determining
T_2 for an isentropic process, given
T_1 and
V_2/V_1 (see Example 4.6).

Tables giving the composition and thermodynamic properties of combustion products have been compiled. They are useful sources of property and species concentrations data in burned gas mixtures for a range of equivalence ratios, temperatures, and pressures. Summary information on four generally available sets of tables is given in Table 4.9. The most extensive set of tables of combustion product composition and thermodynamic properties is the AGARD set, *Properties of Air and Combustion Products with Kerosene and Hydrogen Fuels*, by Banes et al.[10] Note, however, that their enthalpy datum differs from the usual datum (enthalpy for
O_2,
N_2,
H_2, and C is zero at 298.15 K). The elements in their reference state at 298.15 K were assigned arbitrary positive values for enthalpy to avoid negative enthalpies for the equilibrium burned gas mixture.

© McGraw-Hill Education. All rights reserved. Any use is subject to the Terms of Use, Privacy Notice and copyright information.

Table 4.9 Tables of properties of air and combustion products

Source	Properties P, composition C	Mixture	Units	ϕ range	T range	p range	Enthalpy datum
Keenan et al.[8]	P	Air	U.S., SI		100–3600 K	Low	h = 0 at 0 K
		$(CH_2)_n$-air		0.25, 0.5, 1.0	100–2000 K	Low	$\tilde{h}_b = 0$ at 0 K
Reynolds[9]	P	Air	SI		200–1500 K	Low	
General Electric[11]	P and C	Air-$(CH_2)_n$	U.S.	0.25–4	600–5000°R	0.01–30 atm	h of C, H_2, N_2, O_2 zero at 0°R
AGARD[10]	P and C	Air	SI		100–6000 K	1–800 atm	Arbitrary, to keep $h_b > 0$
		$(CH_2)_n$-air		0.2–2			
		H_2-air		0.2–2			

Example

EXAMPLE 4.6

In a diesel engine, the air conditions at the start of compression are p_1 = 1 atm and T_1 = 325 K. At the end of compression p_2 = 60 atm. Find the temperature T_2 and the compression ratio V_1/V_2.

Air tables (see App. D), at T_1 = 325 K, give

$$p_{r_1} = 97.13 \quad \text{and} \quad v_{r_1} = 960.6$$

Use Eq. (4.36),

$$\frac{p_{r_2}}{p_{r_1}} = \frac{p_2}{p_1} = 60$$

to give

$$p_{r_2} = 5828$$

© McGraw-Hill Education. All rights reserved. Any use is subject to the Terms of Use, Privacy Notice and copyright information.

Tables then give

$$T_2 = 992\,\mathrm{K} \quad \text{and} \quad v_{r_2} = 48.92$$

The compression ratio is given by

$$\frac{V_1}{V_2} = \frac{v_{r_1}}{v_{r_2}} = \frac{960.6}{48.92} = 19.6$$

© McGraw-Hill Education. All rights reserved. Any use is subject to the Terms of Use, Privacy Notice and copyright information.

4.7. COMPUTER ROUTINES FOR PROPERTY AND COMPOSITION CALCULATIONS

When large numbers of computations are being made and high accuracy is required, engine process calculations are carried out on a computer. Relationships which model the composition and/or thermodynamic properties of unburned and burned gas mixtures have been developed for computer use.

The most complete models are based on polynomial curve fits to the thermodynamic data for each species in the mixture and the assumptions that (1) the unburned mixture is frozen in composition and (2) the burned mixture is in equilibrium. The approach used as the basis for representing JANAF table thermodynamic data[1] in the NASA equilibrium program[5,6] (see Sec. 3.7) will be summarized here because it is consistent with the approach used throughout to calculate unburned and burned mixture properties.

For each species *i* in its standard state at temperature *T*(K), the specific heat $\tilde{c}_{p,i}$ is approximated by

$$\frac{\tilde{c}_{p,i}}{R} = a_{i1} + a_{i2}T + a_{i3}T^2 + a_{i4} + a_{i5}T^4$$

(4.39)

The standard state enthalpy of species *i* is then given by

$$\frac{\tilde{h}_i}{\tilde{R}T} = a_{i1} + \frac{a_{i2}}{2}T + \frac{a_{i3}}{3}T^2 + \frac{a_{i4}}{4}T^3 + \frac{a_{i5}}{5}T^4 + \frac{a_{i6}}{T}$$

(4.40)

The standard state entropy of species *i* at temperature T(K) and pressure 1 atm, from Eq. (4.14), is then

$$\frac{\tilde{s}_i}{\tilde{R}} = a_{i1}\ln T + a_{i2}T + \frac{a_{i3}}{2}T^2 + \frac{a_{i4}}{3}T^3 + \frac{a_{i5}}{4}T^4 + a_{i7}$$

(4.41)

Values of the coefficients a_{ij} for
CO_2,
H_2O, CO,
H_2,
O_2,
N_2, OH, NO, O, and H from the NASA program are given in Table 4.10. Two temperature ranges are given. The 300 to 1000 K range is appropriate for unburned mixture property calculations. The 1000 to 5000 K range is appropriate for burned mixture property calculations. Figure 4.11 gives values of
c_p/R for the major species,
CO_2,

© McGraw-Hill Education. All rights reserved. Any use is subject to the Terms of Use, Privacy Notice and copyright information.

H_2O,
O_2,
N_2,
H_2, and CO, as a function of temperature.

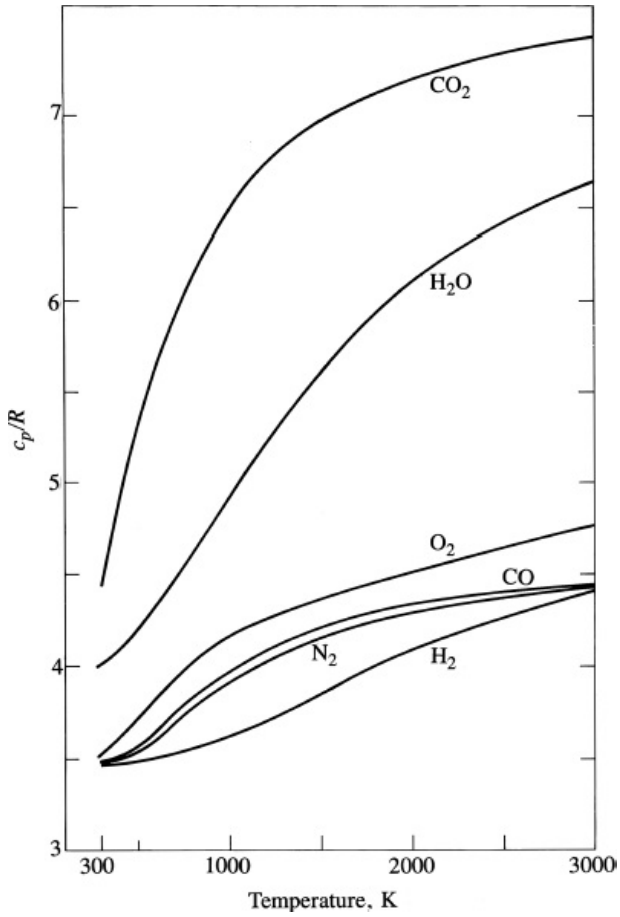
Table 4.10 Coefficients for species thermodynamic properties

Species	*T* range, *K*	a_{i1}	a_{i2}	a_{i3}	a_{i4}	a_{i5}	a_{i6}	a_{i7}
CO_2	1000–5000	0.44608(+1)	0.30982(−2)	−0.12393(−5)	0.22741(−9)	−0.15526(−13)	−0.48961(+5)	−0.98636(0)
	300–1000	0.24008(+1)	0.87351(−2)	−0.66071(−5)	0.20022(−8)	0.63274(−15)	−0.48378(+5)	0.96951(+1)
H_2O	1000–5000	0.27168(+1)	0.29451(−2)	−0.80224(−6)	0.10227(−9)	−0.48472(−14)	−0.29906(+5)	0.66306(+1)
	300–1000	0.40701(+1)	−0.11084(−2)	0.41521(−5)	−0.29637(−8)	0.80702(−12)	−0.30280(+5)	−0.32270(0)
CO	1000–5000	0.29841(+1)	0.14891(−2)	−0.57900(−6)	0.10365(−9)	−0.69354(−14)	−0.14245(+5)	0.63479(+1)
	300–1000	0.37101(+1)	−0.16191(−2)	0.36924(−5)	−0.20320(−8)	0.23953(−12)	−0.14356(+5)	0.29555(+1)
H_2	1000–5000	0.31002(+1)	0.51119(−3)	0.52644(−7)	−0.34910(−10)	0.36945(−14)	−0.87738(+3)	−0.19629(+1)
	300–1000	0.30574(+1)	0.26765(−2)	−0.58099(−5)	0.55210(−8)	−0.18123(−11)	−0.98890(+3)	−0.22997(+1)
O_2	1000–5000	0.36220(+1)	0.73618(−3)	−0.19652(−6)	0.36202(−10)	−0.28946(−14)	−0.12020(+4)	0.36151(+1)
	300–1000	0.36256(+1)	−0.18782(−2)	0.70555(−5)	−0.67635(−8)	0.21556(−11)	−0.10475(+4)	0.43053(+1)
N_2	1000–5000	0.28963(+1)	0.15155(−2)	−0.57235(−6)	0.99807(−10)	−0.65224(−14)	−0.90586(+3)	0.61615(+1)
	300–1000	0.36748(+1)	−0.12082(−2)	0.23240(−5)	−0.63218(−9)	−0.22577(−12)	−0.10612(+4)	0.23580(+1)
OH	1000–5000	0.29106(+1)	0.95932(−3)	−0.19442(−6)	0.13757(−10)	0.14225(−15)	0.39354(+4)	0.54423(+1)
NO	1000–5000	0.31890(+1)	0.13382(−2)	−0.52899(−6)	0.95919(−10)	−0.64848(−14)	0.98283(+4)	0.67458(+1)
O	1000–5000	0.25421(+1)	−0.27551(−4)	−0.31028(−8)	0.45511(−11)	−0.43681(−15)	0.29231(+5)	0.49203(+1)
H	1000–5000	0.25(+1)	0.0	0.0	0.0	0.0	0.25472(+5)	−0.46012(0)

Source: NASA Equilibrium Code.[5]

© McGraw-Hill Education. All rights reserved. Any use is subject to the Terms of Use, Privacy Notice and copyright information.

Figure 4.11 Specific heat at constant pressure, c_p/R, as function of temperature for species CO_2, H_2O, O_2, N_2, H_2, and CO. (From JANAF tables.[1])



4.7.1. Unburned Mixtures

Polynomial functions for various fuels (in the vapor phase) have been fitted to the functional form:[12–14]

$$\tilde{c}_{p,f} = A_{f1} + A_{f2}t + A_{f3}t^2 + A_{f4}t^3 + \frac{A_{f5}}{t^2}$$

(4.42)

$$\tilde{h}_f = A_{f1}t + A_{f2}\frac{t^2}{2} + A_{f3}\frac{t^3}{3} + A_{f4}\frac{t^4}{4} - \frac{A_{f5}}{t} + A_{f6} + A_{f8}$$

(4.43)

where $t = T(\text{K})/1000$.
A_{f6} is the constant for the datum of zero enthalpy for C,
H_2,
O_2, and

© McGraw-Hill Education. All rights reserved. Any use is subject to the Terms of Use, Privacy Notice and copyright information.

N_2 at 298.15 K. For a 0-K datum,
A_{f8} is added to
A_{f6}. For pure hydrocarbon compounds, the coefficients
A_{fi} were found by fitting Eqs. (4.42) and (4.43) to data from Rossini et al.[7] Values for relevant pure fuels are given in Table 4.11. The units for
$\tilde{c}_{p,f}$ are cal/gmol·K, and for
$\tilde{h}_f$ are kcal/gmol.

Table 4.11 Coefficients for polynomials [Eqs. (4.42) and (4.43)] for fuel enthalpy and specific heat

Fuel	Formula	Molecular weight	$(A/F)_s$	$(F/A)_s$	A_{f1}	A_{f2}	A_{f3}	A_{f4}	A_{f5}	A_{f6}	A_{f8}
Methane	CH_4	16.04	17.23	0.0580	−0.29149	26.327	−10.610	1.5656	0.16573	−18.331	4.3000
Propane	C_3H_8	44.10	15.67	0.0638	−1.4867	74.339	−39.065	8.0543	0.01219	−27.313	8.852
Hexane	C_6H_{14}	86.18	15.24	0.0656	−20.777	210.48	−164.125	52.832	0.56635	−39.836	15.611
Isooctane	C_8H_{18}	114.2	15.14	0.0661	−0.55313	181.62	−97.787	20.402	−0.03095	−60.751	20.232
Methanol	CH_3OH	32.04	6.47	0.1546	−2.7059	44.168	−27.501	7.2193	0.20299	−48.288	5.3375
Ethanol	C_2H_5OH	46.07	9.00	0.1111	6.990	39.741	−11.926	0	0	−60.214	7.6135
Gasoline	$C_{8.26}H_{15.5}$	114.8	14.64	0.0683	−24.078	256.63	−201.68	64.750	0.5808	−27.562	17.792
	$C_{7.76}H_{13.1}$	106.4	14.37	0.0696	−22.501	227.99	−177.26	56.048	0.4845	−17.578	15.235
Diesel	$C_{10.8}H_{18.7}$	148.6	14.4	0.0694	−9.1063	246.97	−143.74	32.329	0.0518	−50.128	23.514

Units of A_{fi} such that
$\tilde{h}_f$ is in kcal/gmol and
$\tilde{c}_{p,f}$ is in cal/gmol·K with $t = T(K)/1000$.

A_{f6} gives enthalpy datum at 298.15 K; (A_{f6} + A_{f8}) gives enthalpy datum at 0 K.

Multicomponent fuel coefficients were determined as follows.[13] Chemical analysis of the fuel was performed to obtain the H/C ratio, average molecular weight, heating value, and the weight percent of aromatics, olefins, and total paraffins (including cycloparaffins). The fuel was then modeled as composed of a representative aromatic, olefin, and paraffin hydrocarbon. From atomic conservation of hydrogen and carbon and the chemical analysis results, component molar fractions and average carbon numbers can be determined. Table 4.11 gives values for the coefficients
A_{f1} to
A_{f8} for typical petroleum-based fuels. The units of the coefficients give

© McGraw-Hill Education. All rights reserved. Any use is subject to the Terms of Use, Privacy Notice and copyright information.

$\tilde{c}_{p,f}$ and
$\tilde{h}_f$ in cal/gmol·K and kcal/gmol, respectively, with $t = T(\text{K})/1000$.

The thermodynamic properties of the unburned mixture can now be obtained. With the moles of each species per mole O_2,
n_i, determined from Table 4.4, and the mass of mixture per mole
O_2, m_{RP}, determined from Table 4.5, the unburned mixture properties are given by

$$c_{p,u} = \frac{1}{m_{\text{RP}}} \sum_i n_i \tilde{c}_{p,i}$$

(4.44*a*)

$$h_u = \frac{1}{m_{\text{RP}}} \sum_i n_i \tilde{h}_i$$

(4.44*b*)

$$s_u = \frac{1}{m_{\text{RP}}} \left\{ \sum n_i \left[\tilde{s}_i^\circ - \tilde{R} \ln \left(\frac{n_i}{n_u} \right) \right] - n_{nu} \tilde{R} \ln p \right\}$$

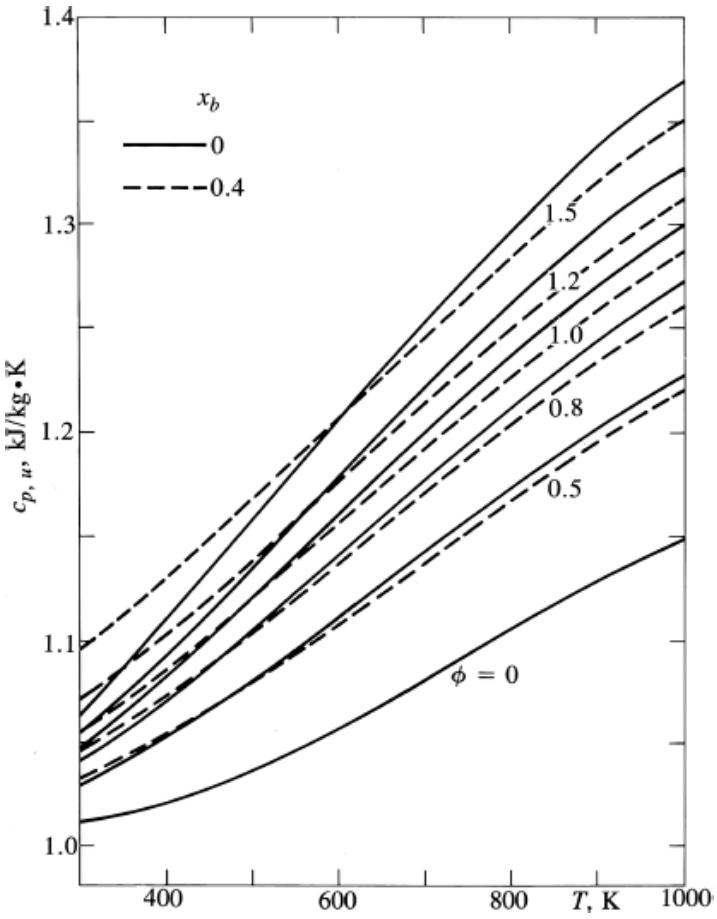
(4.44*c*)

where p is in atmospheres.

Figures 4.12 and 4.13, obtained with the above relations, show how $c_{p,u}$ and
$\gamma_u (= c_{p,u}/c_{v,u})$ vary with temperature, equivalence ratio, and burned gas fraction, for a gasoline-air mixture.

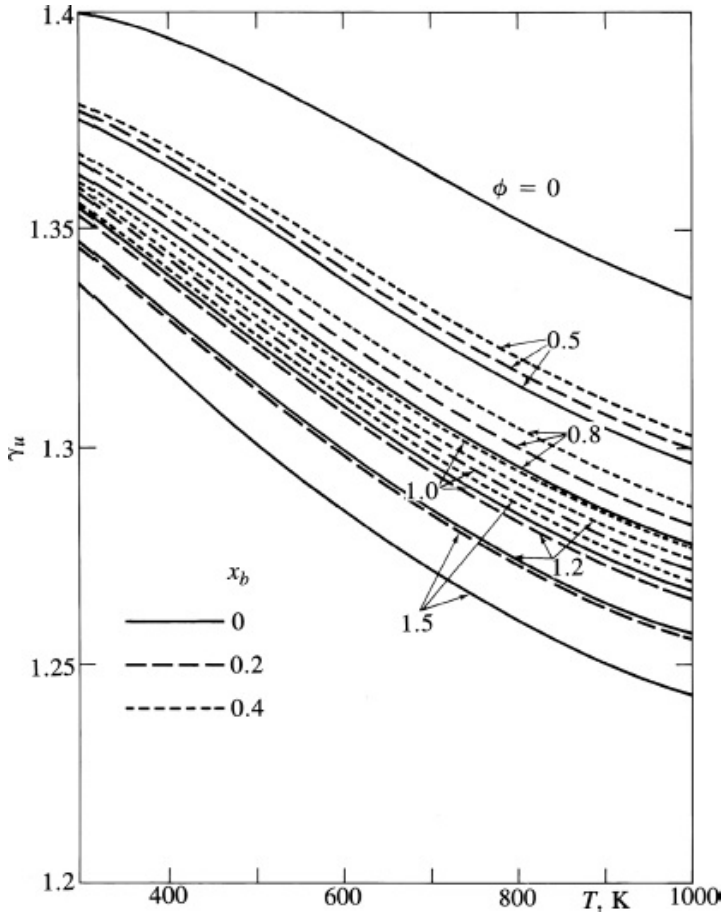
© McGraw-Hill Education. All rights reserved. Any use is subject to the Terms of Use, Privacy Notice and copyright information.

Figure 4.12 *Specific heat at constant pressure of unburned gasoline, air, burned gas mixtures as function of temperature, equivalence ratio, and burned gas fraction. Units: kJ/kg mixture·K.*



© McGraw-Hill Education. All rights reserved. Any use is subject to the Terms of Use, Privacy Notice and copyright information.

Figure 4.13 *Ratio of specific heats, $\gamma_u = c_{p,u}/c_{v,u}$, of unburned gasoline, air, burned gas mixtures as function of temperature, equivalence ratio, and burned gas fraction.*



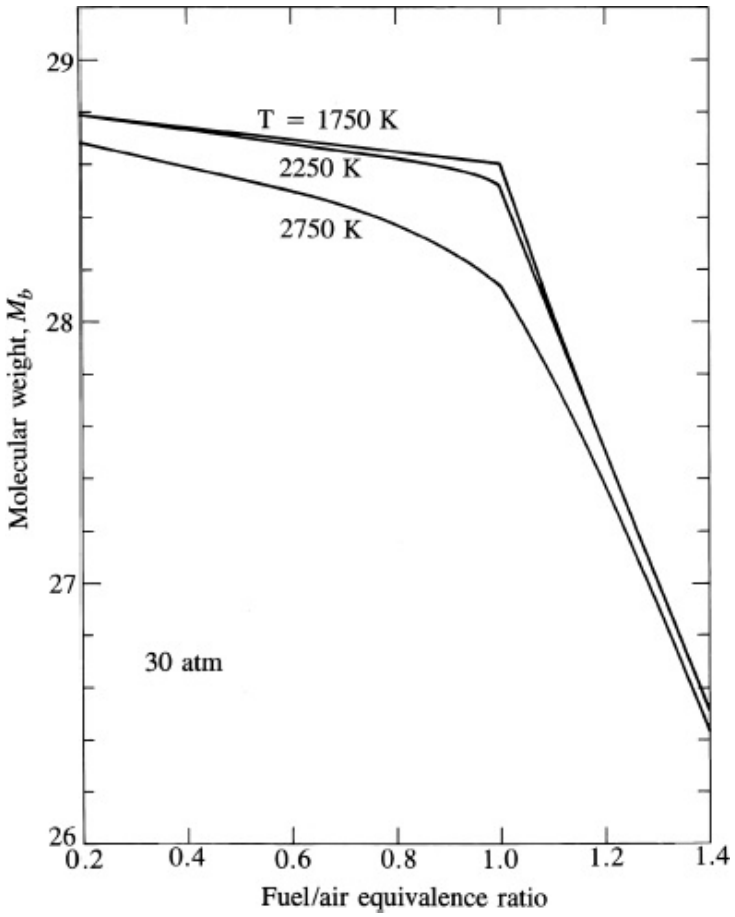
4.7.2. Burned Mixtures

The most accurate approach for burned mixture property and composition calculations is to use a thermodynamic equilibrium program at temperatures above about 1700 K and a frozen composition below 1700 K. The properties of each species at high and low temperatures are given by polynomial functions such as Eqs. (4.39) to (4.41) and their coefficients in Table 4.10. The NASA equilibrium program (see Sec. 3.7) is readily available for this purpose and is well documented.[5, 6] The following are examples of its output.

Figure 3.10 showed species concentration data for burned gases as a function of equivalence ratio at 1750, 2250, and 2750 K, at 30 atm. Figure 4.14 shows the burned gas molecular weight M_b, and Figs. 4.15 and 4.16 give $c_{p,b}$ and γ_b as functions of equivalence ratio at 1750, 2250, and 2750 K at 30 atm.Figures 4.17 and 4.18 show $c_{p,b}$ and γ_b as a function of temperature and pressure for selected equivalence ratios for mixtures lean and rich of stoichiometric.[15] For rich mixtures ($\phi > 1$), for $T > 2000$ K, $c_{p,b}$ and γ_b are equilibrium values. For 1200 K ≤ T ≤ 2000 K, "frozen" composition data are shown where the gas composition is in equilibrium at the given T and p but is frozen as c_p and c_v are computed. Below about 1500 K, fixed composition data are shown corresponding to a value of 3.5 for the water—gas equilibrium constant which adequately describes exhaust gases [see Eq. (4.60), Sec. 4.9].

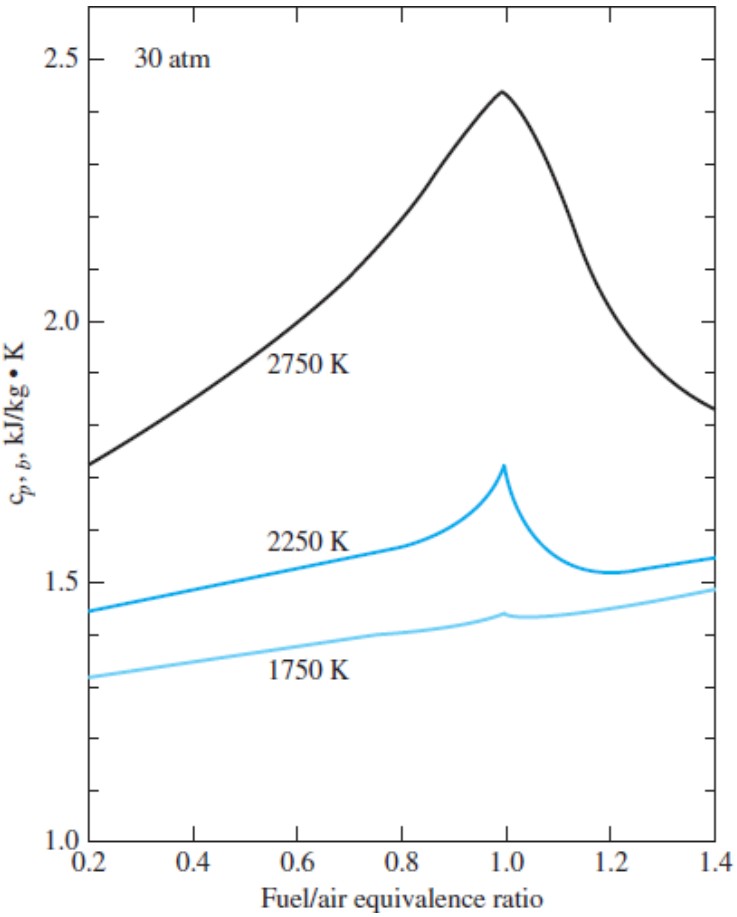
© McGraw-Hill Education. All rights reserved. Any use is subject to the Terms of Use, Privacy Notice and copyright information.

Figure 4.14 *Molecular weight of equilibrium burned gases as a function of equivalence ratio at T = 1750, 2250, and 2750 K, and 30 atm. Fuel: isooctane.*



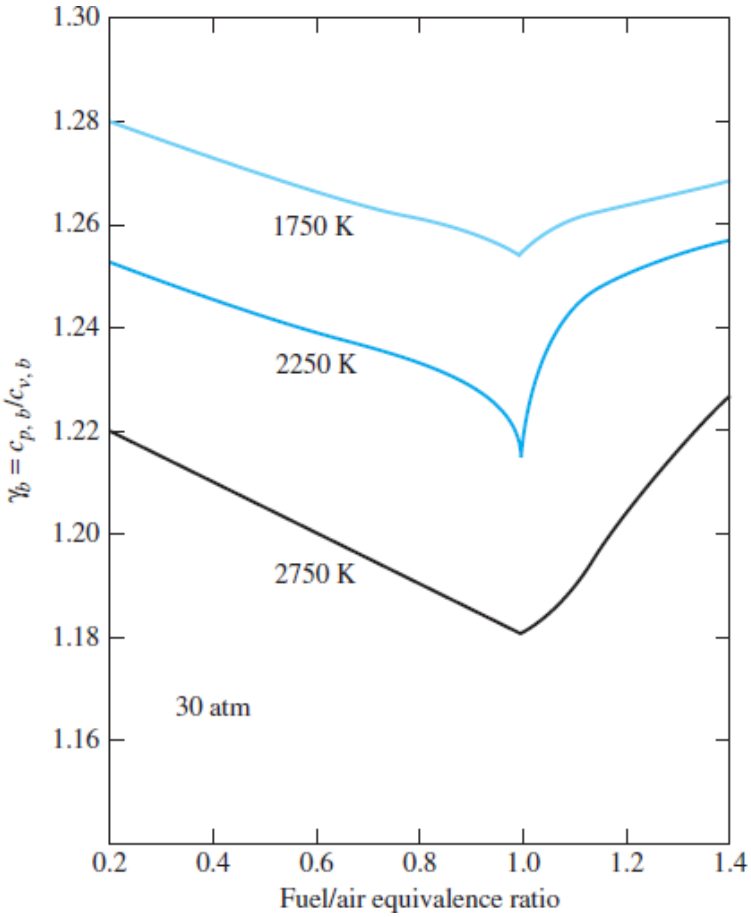
© McGraw-Hill Education. All rights reserved. Any use is subject to the Terms of Use, Privacy Notice and copyright information.

Figure 4.15 *Specific heat at constant pressure of equilibrium burned gases as a function of equivalence ratio at T = 1750, 2250, and 2750 K, and 30 atm. Fuel: isooctane. Units: kJ/kg mixture·K.*



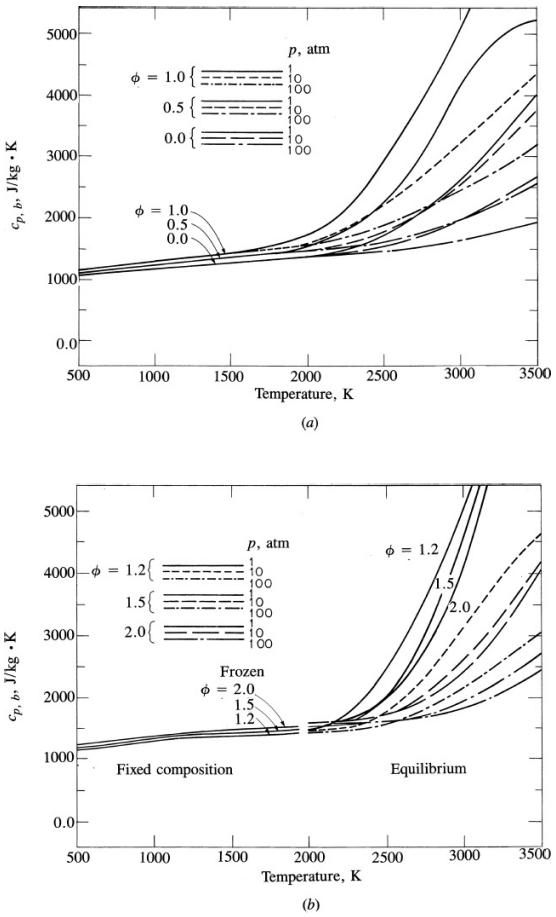
© McGraw-Hill Education. All rights reserved. Any use is subject to the Terms of Use, Privacy Notice and copyright information.

Figure 4.16 *Ratio of specific heats, $\gamma_b = c_{p,b}/c_{v,b}$, for equilibrium burned gases as a function of equivalence ratio at T = 1750, 2250, and 2750 K, and 30 atm. Fuel: isooctane.*



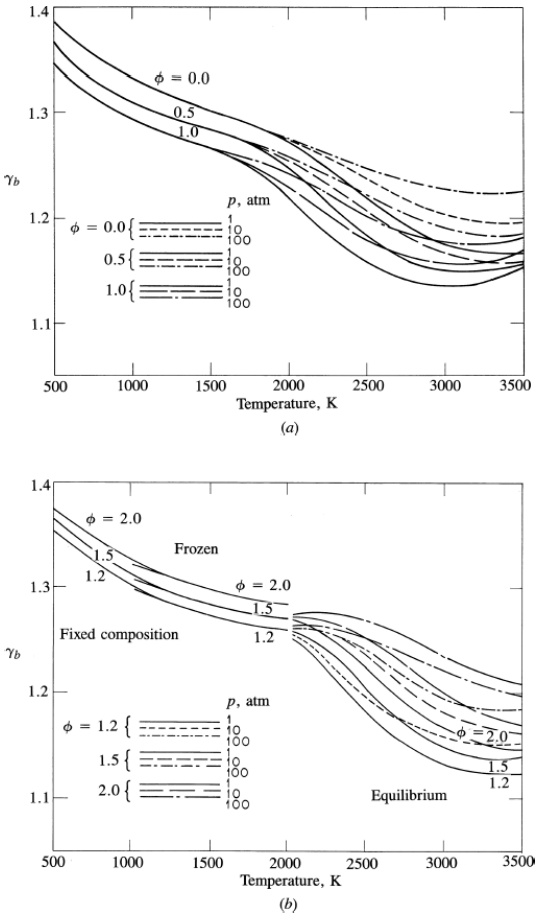
© McGraw-Hill Education. All rights reserved. Any use is subject to the Terms of Use, Privacy Notice and copyright information.

Figure 4.17 Specific heat at constant pressure for equilibrium, frozen, and fixed composition burned gases as a function of temperature and pressure: (a) equivalence ratio $\phi \leq 1.0$; (b) equivalence ratio $\phi > 1$. Units: J/kg mixture·K. Fuel: C_nH_{2n}.



© McGraw-Hill Education. All rights reserved. Any use is subject to the Terms of Use, Privacy Notice and copyright information.

Figure 4.18 *Ratio of specific heats, $\gamma_b = c_{p,b}/c_{v,b}$, for equilibrium, frozen, and fixed composition burned gases as a function of temperature.*



© McGraw-Hill Education. All rights reserved. Any use is subject to the Terms of Use, Privacy Notice and copyright information.

4.8. TRANSPORT PROPERTIES

The processes by which mass, momentum, and energy are transferred from one point in a system to another are called rate processes. In internal combustion engines, examples of such processes are evaporation of liquid fuel, fuel-air mixing, friction at a gas/solid interface, and heat transfer between gas and the walls of the engine combustion chamber. In engines, most of these processes are turbulent and are therefore strongly influenced by the properties of the fluid flow. However, turbulent rate processes are usually characterized by correlations between dimensionless numbers (e.g., Reynolds, Prandtl, Nusselt numbers, etc.), which contain the fluid's transport properties of viscosity, thermal conductivity, and diffusion coefficient as well as the flow properties.

The simplest approach for computing the transport properties is based on the application of kinetic theory to a gas composed of hard-sphere molecules. By analyzing the momentum flux in a plane Couette flow,[1] it can be shown (Chapman and Cowling,[16] p. 218) that the viscosity μ of a monatomic hard-sphere gas [where $\mu = \tau/(du/dx)$, τ being the shear stress and (du/dx) the velocity gradient] is given by

$$\mu = \frac{\left[5/(16\sqrt{\pi})\right](m\tilde{k}T)^{1/2}}{d^2}$$

(4.45)

where m is the mass of the gas molecule, d is the molecular diameter, and $\tilde{k}$ is Boltzmann's constant, 1.381×10^{-23} J/K.

For such a gas, the viscosity varies as $T^{1/2}$, but will not vary with gas pressure or density. Measurements of viscosity show it does only vary with temperature, but generally not proportionally to $T^{1/2}$. The measured temperature dependence can only be explained with more sophisticated models for the intermolecular potential energy than that of a hard sphere. Effectively, at higher temperatures, the higher average kinetic energy of a pair of colliding molecules requires that they approach closer to each other and experience a greater repulsive force to be deflected in the collision. As a result, the molecules appear to be smaller spheres as the temperature increases.

An expression for the thermal conductivity k of a monatomic hard-sphere gas [$k = \dot{q}/(dT/dx)$, where $\dot{q}$ is the heat flux per unit area and dT/dx is the temperature gradient] can be derived from an analysis of the thermal equivalent of plane Couette flow (Ref. 16, p. 235):

$$k = \frac{\left[75/(64\sqrt{\pi})\right](\tilde{k}^3 T/m)^{1/2}}{d^2}$$

(4.46)

which has the same temperature dependence as μ. Equations (4.45) and (4.46) can be combined to give

$$k = \frac{5}{2}\mu c_v$$

since, for a monatomic gas, the specific heat at constant volume is 3

© McGraw-Hill Education. All rights reserved. Any use is subject to the Terms of Use, Privacy Notice and copyright information.

$\tilde{k}/(2m)$. This simple equality is in good agreement with measurements of μ and k for monatomic gases.

The above model does not take into account the vibrational and rotational energy exchange in collisions between polyatomic molecules which contribute to energy transport in gases of interest in engines. Experimental measurements of k and μ show that k is less than $(5/2)\mu c_v$ for such polyatomic gases, where c_v is the sum of the translational specific heat and the specific heat due to internal degrees of freedom. It was suggested by Eucken that transport of vibrational and rotational energy was slower than that of translational energy. He proposed an empirical expression

$$k = \frac{9\gamma - 5}{4}\mu c_v$$

or

$$\mathrm{Pr} = \frac{\mu c_p}{k} = \frac{4\gamma}{9\gamma - 5}$$

(4.47)

where Pr is the Prandtl number, which is in good agreement with experimental data.

A similar analysis of a binary diffusion process, where one gas diffuses through another, leads to an expression for the binary diffusion coefficient D_{ij}. D_{ij} is a transport property of the gas mixture composed of species i and j, defined by Fick's law of molecular diffusion which relates the fluxes of species i and j, Γ_{xi} and Γ_{xj}, in the x direction to the concentration gradients, dn_i/dx and dn_j/dx (n is the molecular number density):

$$\Gamma_{xi} = -D_{ij}\left(\frac{dn_i}{dx}\right) \qquad \Gamma_{xj} = -D_{ij}\left(\frac{dn_j}{dx}\right)$$

The binary diffusion coefficient for a mixture of hard-sphere molecules is (Ref. 16, p. 245)

$$D_{ij} = \frac{3}{16nd^2}\left(\frac{2\tilde{k}T}{\pi m_{ij}}\right)^{1/2}$$

(4.48)

where m_{ij} is the reduced mass $m_i m_j/(m_i + m_j)$.

A more rigorous treatment of gas transport properties, based on more realistic intermolecular potential energy models, can be found in Hirschfelder et al.,[17] who also present methods for computing the transport properties of mixtures of gases. The NASA computer program "Thermodynamic and Transport Properties of Complex Chemical Systems"[6] computes the viscosity, thermal conductivity, and Prandtl number in addition to the thermodynamic calculations described in Secs. 3.7 and 4.7 for high-temperature equilibrium and frozen gas composition mixtures. The procedures used in the NASA program to compute these transport properties are based on the techniques described in Hirschfelder et al.[17] The NASA program has been used to compute the transport properties of hydrocarbon—air combustion products.[15] These quantities are functions of temperature T, equivalence ratio ϕ, and (except for viscosity) pressure p. Approximate correlations were then fitted to the calculated data of viscosity and Prandtl number. The principal advantage of these correlations is computational speed. For Prandtl number

© McGraw-Hill Education. All rights reserved. Any use is subject to the Terms of Use, Privacy Notice and copyright information.

($\mu c_p/k$), it was found convenient to use γ, the specific heat ratio (c_p/c_v), as an independent variable. Values of γ and c_p then permit determination of the thermal conductivity.

The viscosity of hydrocarbon–air combustion products over the temperature range 500 up to 4000 K, for pressures from 1 up to 100 atm, for ϕ = 0 up to ϕ = 4 is shown in Fig. 4.19. The viscosity as a function of temperature of hydrocarbon—air combustion products differs little from that of air. Therefore, a power law based on air viscosity data was used to fit the data:

$$\mu_{\text{air}}(\text{kg/m} \cdot \text{s}) = 3.3 \times 10^{-7} \times T^{0.7}$$

(4.49)

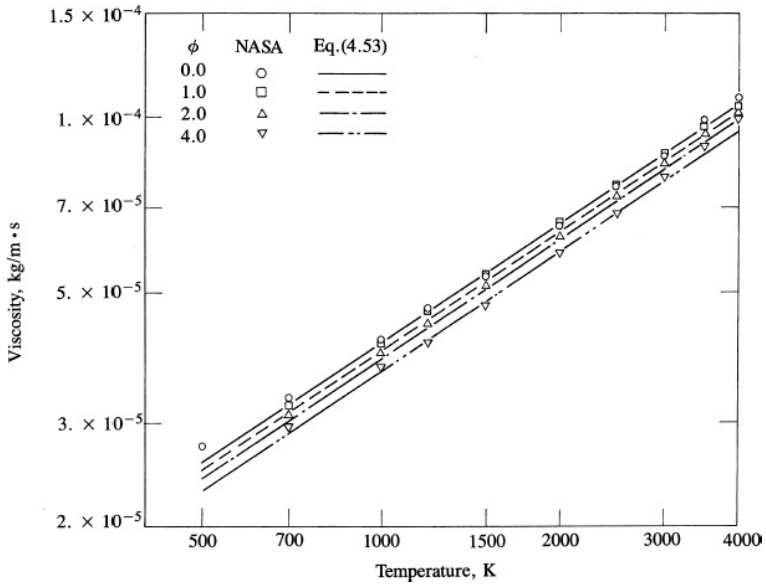
where T is in kelvins. The viscosity of combustion products is almost independent of pressure. This correlation was corrected to include the effect of the equivalence ratio ϕ on the viscosity of hydrocarbon—air combustion products:

$$\mu_{\text{prod}} = \frac{\mu_{\text{air}}}{1 + 0.027\phi}$$

(4.50)

Figure 4.19 shows that the viscosity predicted using Eqs. (4.49) and (4.50) is very close to the viscosity values calculated with the NASA program. There is less than 4% error.

Figure 4.19 Viscosity, kg/m·s, of combustion products as a function of temperature and equivalence ratio. Equations shown are (4.49) and (4.50).



The Prandtl number of hydrocarbon—air combustion products has also been correlated over the above ranges of temperatures, pressures, and equivalence ratios. Since the expression for Prandtl number of a monatomic hard-sphere molecule gas is a function of γ, a second-order polynomial of γ was used to curve-fit the calculated Prandtl number data. A good fit to the data for lean combustion product mixtures was the following:

$$\text{Pr} = 0.05 + 4.2(\gamma - 1) - 6.7(\gamma - 1)^2 \quad \phi \leq 1$$

© McGraw-Hill Education. All rights reserved. Any use is subject to the Terms of Use, Privacy Notice and copyright information.

(4.51)

The values of Pr predicted with Eq. (4.51) are within 5% of the equilibrium Pr values calculated with the NASA program. For rich mixtures the following equation is a good fit to the equilibrium values of Pr using equilibrium values of γ, for temperatures greater than 2000 K:

$$\mathrm{Pr} = \frac{0.05 + 4.2(\gamma - 1) - 6.7(\gamma - 1)^2}{1 + 0.015 \times 10^{-6}(\phi T)^2} \qquad 1 < \phi \leq 4$$

(4.52)

The predicted values of Pr in this case are also close to the calculated values of Pr, with less than 10% error. Equation (4.52) is also a reasonable fit to the frozen values[2] of Pr for rich mixtures, using frozen values of γ, for the temperature range 1200 to 2000 K. As there are no data for Pr of rich mixtures at low temperatures, we suggest that where a fixed composition for the mixture is appropriate (e.g., during the exhaust process in an internal combustion engine), Eq. (4.52) can also be used with fixed composition values of γ.

The Prandtl number can be obtained from the above relations if γ is known. The thermal conductivity can be obtained from the Prandtl number if values of μ and c_p are known. Values of γ_b and $c_{p,b}$ as functions of temperature, pressure, and equivalence ratio are given in Figs. 4.15 to 4.18.

Since the fundamental relations for viscosity and thermal conductivity are complicated, various approximate methods have been proposed for evaluating these transport properties for gas mixtures. A good approximation for the viscosity of a multicomponent gas mixture is

$$\mu_{\mathrm{mixt}} = \sum_{i=1}^{v} \frac{\tilde{x}_i^2}{\tilde{x}_i^2/\mu_i + 1.385 \sum_{j=1, j\neq 1}^{v} \tilde{x}_i \tilde{x}_j (\tilde{R}T/pM_i D_{ij})}$$

(4.53)

where
$\tilde{x}_i$ and M_i are the mole fraction and molecular weight of the ith species, μ_i is the viscosity of the ith species, v is the number of species in the mixture, and D_{ij} is the binary diffusion coefficient for species i and j.[17]

[1] In Couette flow, the fluid is contained between two infinite plane parallel surfaces, one at rest and one moving with constant velocity. In the absence of pressure gradients, the fluid velocity varies linearly across the distance between the surfaces.

[2] In the NASA program, "frozen" means the gas composition is in equilibrium at the given T and p, but is frozen as c_p, c_v, and k are computed.

© McGraw-Hill Education. All rights reserved. Any use is subject to the Terms of Use, Privacy Notice and copyright information.

4.9. EXHAUST GAS COMPOSITION

While the formulas for the products of combustion used in Sec. 3.4 are useful for determining unburned mixture stoichiometry, they do not correspond closely to the actual burned gas composition. At high temperatures (e.g., during combustion and the early part of the expansion stroke) the burned gas composition is close to the equilibrium composition at the local temperature, pressure, and equivalence ratio. During the expansion process, recombination reactions simplify the burned gas composition. However, late in the expansion stroke and during exhaust blowdown, the recombination reactions are unable to maintain the gases in chemical equilibrium and, in the exhaust process, the composition becomes frozen. In addition, not all the fuel which enters the engine is fully burned inside the cylinder; the combustion inefficiency even when excess air is present is a few percent (see Fig. 3.11). Also, the contents of each cylinder are not necessarily uniform in composition, and the amounts of fuel and air fed to each cylinder of a multicylinder engine are not exactly the same. For all these reasons, the composition of the engine exhaust gases cannot easily be calculated.

The composition of engine exhaust gases can readily be measured. This is done to determine engine emissions (e.g., CO, NO_x, unburned hydrocarbons, and particulates). It is also done to determine the relative proportions of fuel and air which enter the engine so that its operating equivalence ratio can be computed. In this section, typical engine exhaust gas composition will be reviewed, and techniques for calculating the fuel/air equivalence ratio from exhaust gas composition will be given.

4.9.1. Species Concentration Data

Standard instrumentation for measuring the concentrations of the major exhaust gas species has been developed.[18] Normally a small fraction of the engine exhaust gas stream is drawn off into a sample line. Part of this sample is fed directly to the instrument used for unburned hydrocarbon analysis, a flame ionization detector (FID). The hydrocarbons present in the exhaust gas sample are burned in a small hydrogen—air flame, producing ions in an amount proportional to the number of carbon atoms burned. The FID is effectively a carbon atom counter. It is calibrated with sample gases containing known amounts of hydrocarbons. Unburned hydrocarbon concentrations are normally expressed as a mole fraction or volume fraction in parts per million (ppm) as C_1. Sometimes results are expressed as ppm propane (C_3H_8) or ppm hexane (C_6H_{14}); to convert these to ppm C_1 multiply by 3 or 6, respectively. Measurements of unburned hydrocarbons are sometimes made with a nondispersive infrared (NDIR) analyzer, where the infrared absorption by the hydrocarbons in a sample cell was used to determine their concentration. Values of HC concentrations in engine exhaust gases measured by an FID are about two times the equivalent values measured by an NDIR analyzer (on the same carbon number basis, e.g., C_1). NDIR-obtained concentrations are usually multiplied by 2 to obtain an estimate of actual HC concentrations. Substantial concentrations of oxygen in the exhaust gas can affect the FID measurements. Analysis of *unburned* fuel-air mixtures should be done with special care. To prevent condensation of hydrocarbons in the sample line (especially important in diesel exhaust gas), the sample line is often heated.

NDIR analyzers are used for CO_2 and CO concentration measurements. Infrared absorption in a sample cell containing exhaust gas is compared to absorption in a reference cell. The detector contains the gas being measured in two compartments separated by a diaphragm. Radiation not absorbed in the sample cell is absorbed by the gas in the detector on one side of the diaphragm. Radiation not absorbed in the reference cell is absorbed by the gas in the other half of the detector. Different amounts of absorption in the two halves of the detector result in a pressure difference being built up which is measured in terms of diaphragm distention. NDIR detectors are calibrated with sample gases of known composition. Since water vapor IR absorption overlaps CO_2 and CO absorption bands, the exhaust gas sample is dried with an ice bath and chemical dryer before it enters the NDIR instrument.

Oxygen concentrations are usually measured with paramagnetic analyzers. Oxides of nitrogen, either the amount of nitric

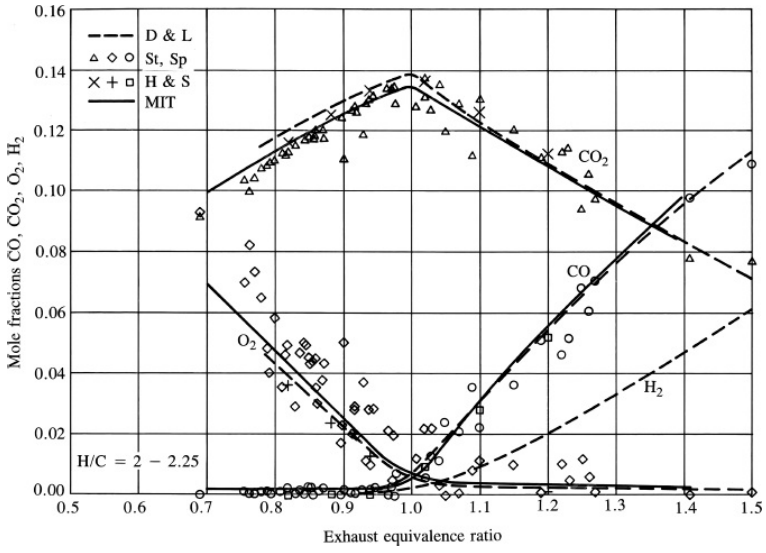
© McGraw-Hill Education. All rights reserved. Any use is subject to the Terms of Use, Privacy Notice and copyright information.

oxide (NO) or total oxides of nitrogen (NO + NO_2, NO_x), are measured with a chemiluminescent analyzer. The NO in the exhaust gas sample stream is reacted with ozone in a flow reactor. The reaction produces electronically excited NO_2 molecules which emit radiation as they decay to the ground state. The amount of radiation is measured with a photomultiplier and is proportional to the amount of NO. The instrument can also convert any NO_2 in the sample stream to NO by decomposition in a heated stainless steel tube so that the total NO_x (NO + NO_2) concentration can be determined. Gas chromatography can be used to determine all the inorganic species (N_2, CO_2, O_2, CO, H_2) or can be used to measure the individual hydrocarbon compounds in the total unburned hydrocarbon mixture. Particulate emissions are measured by filtering the particles from the exhaust gas stream onto a previously weighed filter, drying the filter plus particulate, and reweighing.

4.9.1.1. Spark-Ignition Engine Data

Dry exhaust gas composition data, as a function of the fuel/air equivalence ratio, for several different multi- and single-cylinder automotive spark-ignition engines over a range of engine speeds and loads are shown in Fig. 4.20. The fuel compositions (gasolines and isooctane) had H/C ratios ranging from 2.0 to 2.25. Exhaust gas composition is substantially different on the lean and the rich side of the stoichiometric air/fuel or fuel/air ratios; thus, the fuel/air equivalence ratio ϕ (or its inverse, the relative air/fuel ratio λ) is the appropriate correlating parameter. On the lean side of stoichiometric, as ϕ decreases, CO_2 concentrations fall, oxygen concentrations increase, and CO levels are low but not zero (~ 0.2%). On the rich side of stoichiometric, CO and H_2 concentrations rise steadily as ϕ increases and CO_2 concentrations fall. O_2 levels are low (~ 0.2 to 0.3%) but are not zero. At stoichiometric operation, there is typically half a percent O_2 and three-quarters of a percent CO.

Figure 4.20 Spark-ignition engine exhaust gas composition data in mole fractions as a function of fuel/air equivalence ratio. Fuels: gasoline and isooctane, H/C 2 to 2.25. (From D'Alleva and Lovell,[19] Stivender,[20] Harrington and Shishu,[21] Spindt,[22] and data from the author's laboratory at MIT.)



The carbon:hydrogen ratio of the fuel has only a modest effect on the magnitude of the species concentrations shown.

© McGraw-Hill Education. All rights reserved. Any use is subject to the Terms of Use, Privacy Notice and copyright information.

Measurements with a wide range of liquid fuels show that CO concentrations depend only on the equivalence ratio or relative fuel/air ratio (see Fig. 11.20).[21] A comparison of exhaust CO concentrations with gasoline, propane (C_3H_8), and natural gas (predominantly methane, CH_4) shows that only with the high H/C ratio of methane, and then only for CO ≥ 4%, is fuel composition significant.[23] The values of CO_2 concentration at a given ϕ are slightly affected by the fuel H/C ratio. For example, for stoichiometric mixtures with 0.5% O_2 and 0.75% CO, as the H/C ratio decreases CO_2 concentrations increase from 13.7% for isooctane (H/C = 2.25) to 14.2 to 14.5% for typical gasolines (H/C in range 2 to 1.8), to 16 for toluene (H/C = 1.14).[24]

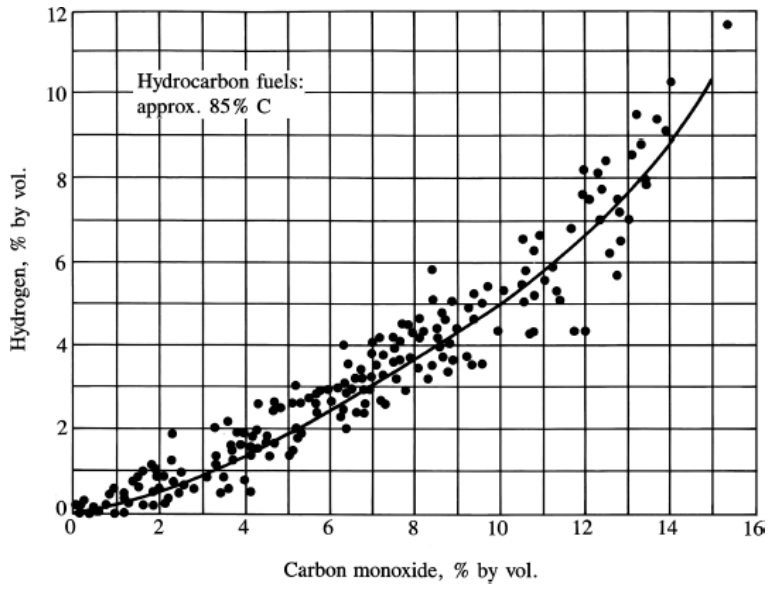
Unburned hydrocarbon exhaust concentrations vary significantly with engine design and operating conditions. Spark-ignition engine exhaust levels in a modern low-emission engine are typically of the order of 2000 ppm C_1 with liquid hydrocarbon fuels, and about half that level with natural gas and propane fuels.

Hydrogen concentrations in engine exhaust are not routinely measured. However, when the mixture is oxygen deficient (i.e., fuel rich), hydrogen is present with CO as an incomplete combustion product. Figure 4.21 summarizes much of the available data on H_2 concentrations plotted as a function of CO.[25] Approximations for estimating hydrogen concentrations in spark-ignition engine exhaust gases have been proposed: for example, the molar concentration of H_2 is half the molar concentration of CO. This is a reasonable approximation to the data in Fig. 4.21 for $4\% \lesssim \tilde{x}_{CO} \lesssim 10\%$. The curve shown in the figure corresponds to

$$\tilde{x}_{H_2} = 0.3\,\tilde{x}_{CO} + 0.02\,\tilde{x}_{CO}^2 + 3 \times 10^{-5}\tilde{x}_{CO}^3$$

(4.54)

Figure 4.21 Hydrogen concentration in spark-ignition engine exhaust as a function of carbon monoxide concentration. Units: percent by volume.[25]



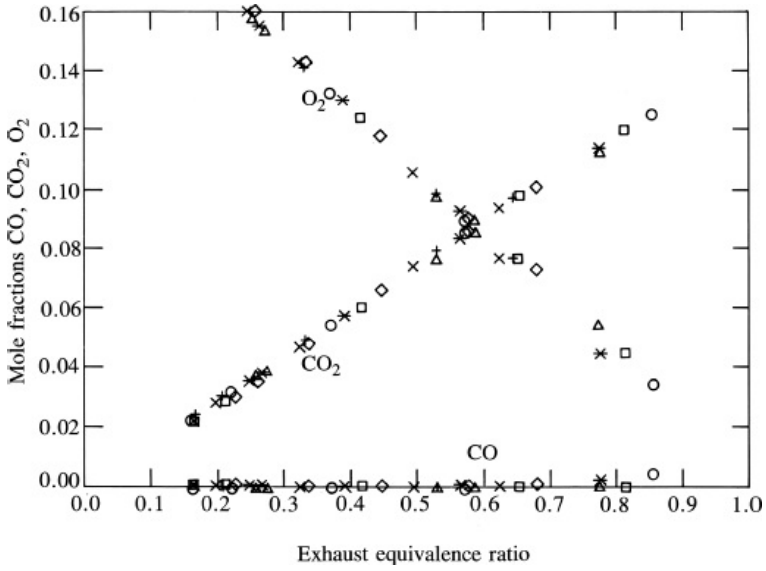
4.9.1.2. Diesel Exhaust Data

Since diesels normally operate significantly lean of stoichiometric ($\phi \lesssim 0.8$) and the diesel combustion process is essentially complete (combustion inefficiency is less than 2%), their exhaust gas composition is straight forward. Figure 4.22 shows that

© McGraw-Hill Education. All rights reserved. Any use is subject to the Terms of Use, Privacy Notice and copyright information.

O_2 and
CO_2 concentrations vary linearly with the fuel/air equivalence ratio over the normal operating range. Diesel emissions of CO and unburned HC are low.

Figure 4.22 Exhaust gas composition from several diesel engines in mole fractions on a dry basis as a function of fuel/air equivalence ratio.[26]



4.9.2. Equivalence Ratio Determination from Exhaust Gas Constituents

Exhaust gas composition depends on the relative proportions of fuel and air fed to the engine, fuel composition, and completeness of combustion. These relationships can be used to determine the operating fuel/air equivalence ratio of an engine from a knowledge of its exhaust gas composition. A general formula for the composition of fuel can be represented as $C_nH_mO_r$. For conventional petroleum-based fuels, oxygen will be absent; for fuels containing alcohols, oxygen will be present. The overall combustion reaction can be written as

$$\text{Fuel} + \text{oxidizer} \rightarrow \text{products}$$

The fuel is $C_nH_mO_r$; the oxidizer is air (
O_2 + 3.773
N_2). The products are
CO_2,
H_2O, CO,
H_2,
O_2, NO_x,
N_2, unburned hydrocarbons (unburned fuel and products of partial fuel reaction), and soot particles (which are mainly solid carbon). The amount of solid carbon present is usually sufficiently small (≤ 0.5% of the fuel mass) for it to be omitted from the analysis. The overall combustion reaction can be written explicitly as

© McGraw-Hill Education. All rights reserved. Any use is subject to the Terms of Use, Privacy Notice and copyright information.

$$\mathrm{C}_n\mathrm{H}_m\mathrm{O}_r + \frac{n_{\mathrm{O}_2}}{\phi}(\mathrm{O}_2 + 3.773\mathrm{N}_2) = n_P(\tilde{x}_{\mathrm{C}_a\mathrm{H}_b}\mathrm{C}_a\mathrm{H}_b + \tilde{x}_{\mathrm{CO}}\mathrm{CO} + \tilde{x}_{\mathrm{CO}_2}\mathrm{CO}_2 + \tilde{x}_{\mathrm{O}_2}\mathrm{O}_2 + \tilde{x}_{\mathrm{N}_2}\mathrm{N}_2 + \tilde{x}_{\mathrm{NO}}\mathrm{NO} + \tilde{x}_{\mathrm{NO}_2}\mathrm{NO}_2 + \tilde{x}_{\mathrm{H}_2\mathrm{O}}\mathrm{H}_2\mathrm{O} + \tilde{x}_{\mathrm{H}_2}\mathrm{H}_2)$$

(4.55)

where ϕ is the measured fuel/air equivalence ratio $[(F/A)_{\text{actual}}/(F/A)_{\text{stoichiometric}}]$, n_{O_2} is the number of O_2 molecules required for complete combustion ($n + m/4 - r/2$), n_P is the total number of moles of exhaust products, and $\tilde{x}_i$ is the mole fraction of the ith component.

There are several methods for using Eq. (4.55) to determine ϕ, the equivalence ratio, depending on the amount of information available. Normally CO_2, CO, O_2, NO_x concentrations as mole fractions and unburned hydrocarbon (as mole fraction or ppm C_1, i.e., $\tilde{x}_{\mathrm{CH}_{b/a}}$) are measured. The concentrations of the inorganic gases are usually measured *dry* (i.e., with $\mathrm{H}_2\mathrm{O}$ removed) or *partially dry*. Unburned hydrocarbons may be measured *wet* or *dry* or *partially dry*. NO_x is mainly nitric oxide (NO); its concentration is usually sufficiently low (<0.5%) for its effect on equivalence ratio determination to be negligibly small. Thus, in Eq. (4.55) there are seven unknowns, which are: ϕ, $\tilde{x}_{\mathrm{H}_2}$, $\tilde{x}_{\mathrm{H}_2\mathrm{O}}$, $\tilde{x}_{\mathrm{N}_2}$, n_P, a, b. (There will be additional unknowns if the measurements listed above are incomplete.)

To solve for these unknowns we need seven additional equations. We can obtain five equations using an atomic balance for each element and the definition of mole fraction, as follows:

Carbon balance:

$$n = n_P(a\tilde{x}_{\mathrm{C}_a\mathrm{H}_b} + \tilde{x}_{\mathrm{CO}} + \tilde{x}_{\mathrm{CO}_2})$$

(4.56)

Hydrogen balance:

$$m = n_P(b\tilde{x}_{\mathrm{C}_a\mathrm{H}_b} + 2\tilde{x}_{\mathrm{H}_2\mathrm{O}} + 2\tilde{x}_{\mathrm{H}_2})$$

(4.57)

Oxygen balance:

$$r + \frac{2n_{\mathrm{O}_2}}{\phi} = n_P(\tilde{x}_{\mathrm{CO}} + 2\tilde{x}_{\mathrm{CO}_2} + \tilde{x}_{\mathrm{NO}} + 2\tilde{x}_{\mathrm{O}_2} + \tilde{x}_{\mathrm{H}_2\mathrm{O}})$$

(4.58)

Nitrogen balance:

$$\frac{7.546n_{\mathrm{O}_2}}{\phi} = n_P(2\tilde{x}_{\mathrm{N}_2} + \tilde{x}_{\mathrm{NO}})$$

© McGraw-Hill Education. All rights reserved. Any use is subject to the Terms of Use, Privacy Notice and copyright information.

(4.59)

The mole fractions add up to 1:

$$\tilde{x}_{C_aH_b} + \tilde{x}_{CO} + \tilde{x}_{H_2} + \tilde{x}_{H_2O} + \tilde{x}_{N_2} + \tilde{x}_{NO} + \tilde{x}_{CO_2} + \tilde{x}_{O_2} = 1$$

(4.60)

An additional assumption is made, based on available exhaust gas composition data, that
CO_2, CO,
H_2O, and
H_2 concentrations are related by

$$\frac{\tilde{x}_{CO}\tilde{x}_{H_2O}}{\tilde{x}_{CO_2}\tilde{x}_{H_2}} = K$$

(4.61)

where *K* is a constant.[1] Values of 3.8[22, 23] and 3.5[25] are commonly used for *K*. The difference between these values has little effect on the computed magnitude of ϕ. To complete the analysis, various assumptions are made concerning the composition and relative importance of the unburned hydrocarbons. The most common approaches are summarized below.

4.9.2.1. Oxygen Balance Air/Fuel and Equivalence Ratios

For fuels composed of carbon and hydrogen only, when all species are measured with the *same background moisture* (wet, dry, or partially dry), the following expression based on the ratio of measured and computed oxygen-containing species to measured carbon-containing species gives the air/fuel ratio. It has been assumed that the unburned hydrocarbons have the same C/H ratio as the fuel:[27]

$$\left(\frac{A}{F}\right) = 4.773\left(\frac{M_{air}}{M_f}\right)\frac{(CO_2) + (CO)/2 + (H_2O)/2 + (NO)/2 + (NO_2) + (O_2)}{(HC) + (CO) + (CO_2)}$$

(4.62)

where ( ) denotes molar concentration (all with the same background moisture) in percent; M_{air} = 28.96, M_f = 12.01 + 1.008*y* where *y* is the H/C ratio of the fuel, (HC) is molar percent unburned hydrocarbons as C_1, and

$$(H_2O) = 0.5y\frac{(CO_2) + (CO)}{(CO)/[K(CO_2)] + 1}$$

(4.63)

Since nitrogen oxides collectively comprise less than 0.5% of the exhaust mixture, their concentrations can be omitted with negligible error.

The fuel/air equivalence ratio ϕ is obtained from the ratio of the stoichiometric air/fuel ratio [Eq. (3.6)] and Eq. (4.62) above.

© McGraw-Hill Education. All rights reserved. Any use is subject to the Terms of Use, Privacy Notice and copyright information.

4.9.2.2. Carbon Balance Air/Fuel and Equivalence Ratios

When oxygen analysis is not available, for fuels composed of carbon and hydrogen only, a carbon balance air/fuel ratio may be employed:[20, 27]

$$\frac{A}{F} = \frac{M_{\text{air}}}{M_f}\left[\frac{100 + (\text{HC}) - (\text{CO})/2 + 3(\text{H}_2\text{O})/2 - (\text{H}_2\text{O})_a}{(\text{HC}) + (\text{CO}) + (\text{CO}_2)} - \frac{y}{2}\right]$$

(4.64)

The symbols are as defined above.
(H_2O) is the molar percent water in the combustion products defined by Eq. (4.63) and
$(\text{H}_2\text{O})_a$ is the molar percent water vapor at the analyzers.

This carbon balance (*A/F*) is sensitive to moisture concentration at the analyzers. The use of ice bath exhaust sample chillers generally reduces the
$(\text{H}_2\text{O})_a$ term to less than 1% and little accuracy is then lost by neglecting it. For completely "wet" analysis (uncondensed), $(\text{H}_2\text{O})_a = (\text{H}_2\text{O})$, and Eq. (4.64) is accurate. For partially dry exhaust gas analysis, knowledge of the dew point of the mixture will provide the
$(\text{H}_2\text{O})_a$ term by reference to steam tables.

The fuel/air equivalence ratio ϕ is obtained from the ratio of the stoichiometric air/fuel ratio [Eq. (3.6)] and Eq. (4.64) above.

4.9.2.3. Equivalence Ratio Based on Wet HC and Dry Inorganic Gas Analysis

Engine exhaust gas composition is often determined by analyzing a fully dried sample stream for
CO_2, CO,
O_2, and NO_x, and a fully wet (uncondensed) stream with an FID for unburned hydrocarbons. Equations (4.62) and (4.64) are not applicable under these circumstances. The following equations define the exhaust gas composition and equivalence ratio under these conditions. The notation
$\tilde{x}_i$ denotes the wet mole fraction of species *i* and
$\tilde{x}_i^*$ denotes the dry mole fraction of species *i*. Equations (4.55) to (4.60), with Eq. (4.61) to relate
CO_2, CO,
H_2O, and
H_2 concentrations and the assumption that *b/a* = *m/n*, were used to derive these results. The equations apply for a fuel of composition $\text{C}_m\text{H}_n\text{O}_r$.

The fuel/air equivalence ratio is given by

$$\phi = \frac{2n_{\text{O}_2}}{n_P\tilde{x}_{\text{H}_2\text{O}} + n_P(1 - \tilde{x}_{\text{H}_2\text{O}})\left(\tilde{x}^*_{\text{CO}} + 2\tilde{x}^*_{\text{CO}_2} + 2\tilde{x}^*_{\text{O}_2} + \tilde{x}^*_{\text{NO}} + 2\tilde{x}^*_{\text{NO}_2}\right) - r}$$

(4.65)

where the wet and dry mole fractions are related by

© McGraw-Hill Education. All rights reserved. Any use is subject to the Terms of Use, Privacy Notice and copyright information.

$$\tilde{x}_i = (1 - \tilde{x}_{H_2O})\,\tilde{x}_i^*$$

and

$$n_P = \frac{n}{\tilde{x}_{CH_{b/a}} + (1 - \tilde{x}_{H_2O})\left(\tilde{x}^*_{CO} + \tilde{x}^*_{CO_2}\right)}$$

$$n_P = \frac{n}{\tilde{x}_{CH_{b/a}} + (1 - \tilde{x}_{H_2O})\left(\tilde{x}^*_{CO} + \tilde{x}^*_{CO_2}\right)}$$

$$\tilde{x}_{H_2O} = \frac{m}{2n}\,\frac{\tilde{x}^*_{CO} + \tilde{x}^*_{CO_2}}{\left[1 + \tilde{x}^*_{CO}/\left(K\tilde{x}^*_{CO_2}\right) + (m/2n)\left(\tilde{x}^*_{CO} + \tilde{x}^*_{CO_2}\right)\right]}$$

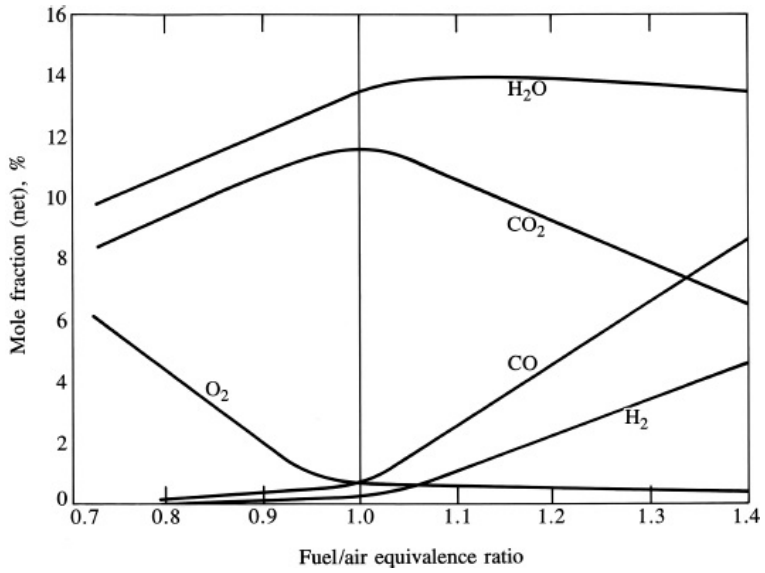
$$\tilde{x}_{H_2} = \frac{\tilde{x}_{H_2O}\tilde{x}^*_{CO}}{K\tilde{x}^*_{CO_2}}$$

$$\tilde{x}_{N_2} = \frac{3.773\,n_{O_2}}{\phi n_P} - (1 - \tilde{x}_{H_2O})\,\frac{\left(\tilde{x}^*_{NO} + \tilde{x}^*_{NO_2}\right)}{2}$$

(4.66)

Note that
$\tilde{x}_{CH_{b/a}}$ is the measured (wet) HC concentration as a mole fraction C_1 (ppm $C_1 \times 10^{-6}$):
$\tilde{x}_{CH_{b/a}} = a\tilde{x}_{C_aH_b}$. Figure 4.23 shows wet exhaust gas concentrations, based on the MIT measured dry concentrations of CO_2, CO,
O_2 shown in Fig. 4.20, and wet HC concentration, as well as Eqs. (4.66).

Figure 4.23 Wet exhaust gas species concentrations as a function of fuel/air equivalence ratio based on the dry exhaust gas composition data in Fig. 4.20 and Eqs. (4.66).



© McGraw-Hill Education. All rights reserved. Any use is subject to the Terms of Use, Privacy Notice and copyright information.

For lean mixtures, varying the value of K between 1.5 and 5.5 has a negligible effect on the value of ϕ computed from Eq. (4.65). For stoichiometric mixtures, varying K from 2.5 to 4.5 varied the computed ϕ by 2 to 3%. For $\phi \approx 1.2$, varying K from 2.5 to 4.5 varied the computed ϕ by 3 to 4%. The error in ϕ involved in omitting NO_x is 0.2% for an NO_x level of 1000 ppm, increasing to 1% for an NO_x level of 5000 ppm. The sensitivity of the computed ϕ to errors in the measurements of CO_2, CO, and O_2 is modest within the normal range of ϕ used. A 2% error in CO_2 or CO or O_2 at $\phi \approx 1$ gives about a 0.1% error in computed ϕ. For leaner and richer mixtures, the error in ϕ increases for errors in measured CO_2 concentration, and CO ($\phi > 1$) and O_2 ($\phi < 1$) concentrations, but is still significantly less than the measurement error in fuel and air flow.

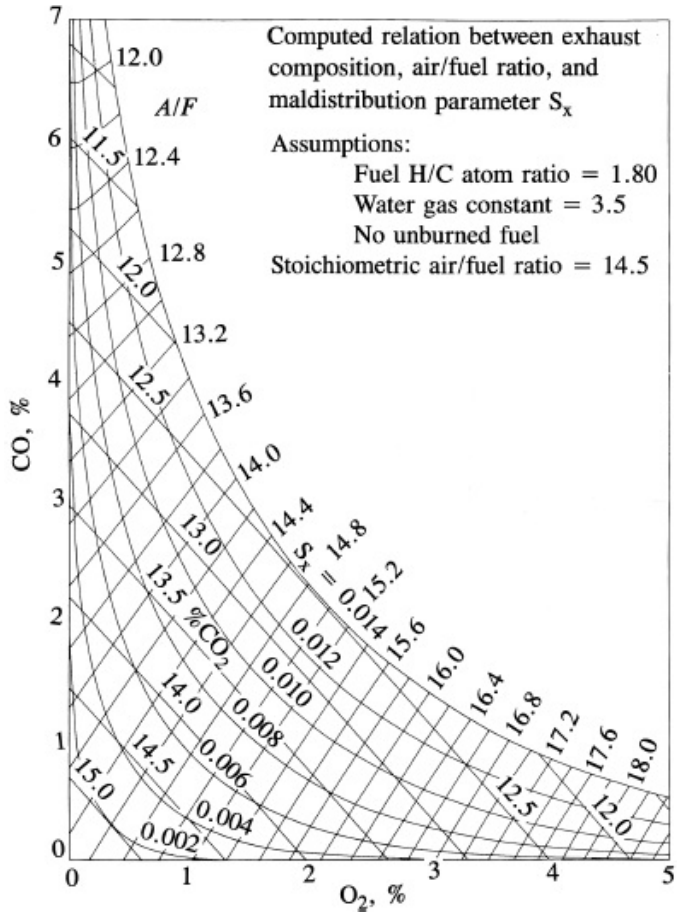
4.9.3. Effects of Fuel/Air Ratio Nonuniformity

Neither the masses of air inducted into the different cylinders of a multicylinder engine per cycle nor the masses of fuel which enter the different cylinders per cycle are exactly equal. In addition, mixing of fuel and air within each cylinder is not necessarily completely uniform. Thus the exhaust gas composition may correspond to a distribution in the fuel/air ratio in the unburned mixture about the mean value. For example, if the mean fuel/air ratio is stoichiometric, extra oxygen will be contributed by any cylinders operating lean of the average and extra carbon monoxide by any cylinders rich of the average, so that the exhaust gas will have higher levels of O_2 and CO (and a lower level of CO_2) relative to an engine operating with identical fuel/air ratios in each cylinder.

Eltinge has developed a method for defining this nonuniformity in the fuel/air ratio distribution for spark-ignition engines which operate close to stoichiometric.[24] A function $f(x)$ for the fuel/air ratio distribution ($x = F/A$) was assumed, with standard deviation S_x. For each value of x (i.e., F/A) complete utilization of the available oxygen was assumed (i.e., no exhaust HC) and the CO_2, H_2O, CO, H_2 concentrations were related by Eq. (4.61) (with $K = 3.5$). The concentrations of each species for each (F/A) were weighted by the distribution function $f(x)$ and summed to produce the average exhaust concentration. (A correction to allow for the presence of unburned HC in the exhaust was also developed.) Figure 4.24 shows one set of results, for a fuel H/C ratio of 1.8 (typical of gasoline), for a normal distribution in the fuel/air ratio. For each mean (F/A) and maldistribution parameter S_x (the standard deviation of the F/A distribution) the corresponding dry concentrations of CO_2, CO, and O_2 are shown. This type of information can be used to define the fuel-air mixture nonuniformities in spark-ignition engines operating relatively close to stoichiometric. For diesel engines the variations of major exhaust gas species concentrations with fuel/air equivalence ratio are linear, so the effects of any nonuniformities are not apparent in this manner (see Fig. 4.22).

© McGraw-Hill Education. All rights reserved. Any use is subject to the Terms of Use, Privacy Notice and copyright information.

Figure 4.24 Computed relationship between dry exhaust gas composition (CO_2, CO, and O_2), air/fuel ratio, and maldistribution parameter S_x. Fuel: $(CH_{1.8})_n$. The correction to be added to the burned gas (F/A) which allows for the measured unburned hydrocarbon concentration is $4.7 \times 10^7 \times$ HC (ppm C_1). (From Eltinge.[24])



4.9.4. Combustion Inefficiency

Internal combustion engine exhaust contains combustible species: CO, H_2, unburned hydrocarbons, and particulates. When their concentrations are known, the combustion efficiency η_c given by Eq. (3.27) can be calculated. The chemical energy carried out of the engine in these combustibles represents the combustion inefficiency, $1 - \eta_c$:

$$1 - \eta_c = \frac{\sum_i x_i Q_{\mathrm{HV}}}{\left[\dot{m}_f / \left(\dot{m}_a + \dot{m}_f\right)\right] Q_{\mathrm{HV}_f}}$$

(4.67)

where the x_i are the mass fractions of CO, H_2, HC, and particulates, respectively; the Q_{HV_i} are the lower heating values of these species; and the subscripts *f* and *a* denote fuel and air. The heating values for CO (10.1 MJ/kg) and H_2 (120 MJ/kg) are well defined. The composition of the unburned HC is not usually known. However, the heating values of

© McGraw-Hill Education. All rights reserved. Any use is subject to the Terms of Use, Privacy Notice and copyright information.

hydrocarbons are closely comparable, so the fuel heating value (typically 42 to 44 MJ/kg) is used. The particulates (only present in diesels) are soot with some adsorbed hydrocarbons; usually the mass fraction is low enough for their contribution to be small, and a heating value for solid carbon (32.8 MJ/kg) can be used. Combustion efficiency data as a function of equivalence ratio have already been presented in Fig. 3.9.

[1] Equation (4.61) is often described as assuming a specific value for the water-gas reaction equilibrium constant. In fact, K is an empirical constant determined from exhaust gas composition data.

© McGraw-Hill Education. All rights reserved. Any use is subject to the Terms of Use, Privacy Notice and copyright information.

4.10. PROBLEMS

4.1.

a. Calculate the low-temperature burned gas composition resulting from the combustion of 7 g/s air with 0.48 g/s ethane (C_2H_6). Assume K = 3.5 in Eq. (4.6).

b. Calculate the low-temperature burned gas composition for the combustion of 7 g/s air with 0.48 g/s ethanol (C_2H_6O). Assume K = 3.5 in Eq. (4.6). (Note the difference in relative air/fuel ratio and burned gas composition due to this difference in fuel.)

4.2. To evaluate the accuracy of the simple analytic ideal gas model, use the results of Example 4.1 and Eqs. (4.23) (constant-volume adiabatic combustion) and (4.24) (constant-pressure adiabatic combustion) to calculate T_b for a stoichiometric isooctane-air mixture. Compare this result with that obtained using Figs. 4.3 and 4.8. Assume the following unburned mixture conditions: T = 700 K, v = 0.125 m_3/kg air, p = 15 bar, and x_b = 0.1.

4.3. Show how, for an ideal gas with fixed composition, the molecular weight M is related to the specific heats c_p and c_v, and $\tilde{R}$. Use Figs. 4.15 and 4.16 to calculate M_b for T_b = 1750, 2250, and 2750 K, and λ = 1.0. Compare these results with values of M_b obtained from Fig. 4.14 and explain any differences.

4.4. EGR, exhaust gas recirculation, is often used to reduce NO_x by acting as a diluent in the intake mixture.

a. For low-temperature isooctane—air combustion products at ϕ = 1.0, determine the percentage of the burned gases average specific heat at constant pressure which comes from each component in the burned gas mixture.

b. Compare the specific heat at constant pressure of isooctane—air combustion products at ϕ = 1.0 to that of air, both at 1750 K. This difference is one reason why EGR instead of leaner fuel-air mixture is used to control NO_x emissions.

4.5. Explain qualitatively the causes of the trends in the curves in Fig. 4.23 as ϕ is increased from 1.0, and decreased from 1.0.

4.6. Compare the O_2, CO_2, and CO data in Fig. 4.22 with the predictions of the elemental balance summarized in Table 4.3. Explain any differences. Assume the fuel is a hydrocarbon with H/C ratio of 2.

4.7. The following exhaust data were obtained from a four-stroke cycle spark-ignition engine. CO, CO_2, and NO_x molar concentrations are all measured fully dry; HC is measured fully wet as ppm C_1. Determine the fuel/air equivalence ratio ϕ for the following three sets of data. Make the following assumptions: (1) the constant K in Eq. (4.61) equals 3.5; (2) the fuel composition is C_8H_{15}; (3) the unburned hydrocarbon H/C ratio is the same as that of the fuel; and (4) NO_x is entirely NO.

a. CO_2 14.0%, CO 0.64%, O_2 0.7%, NO_x 3600 ppm, HC 3200 ppm C_1.

b. CO_2 13.8%, CO 3.05%, O_2 0%, NO_x 1600 ppm, HC 3450 ppm C_1.

c. CO_2 12.5%, CO 0.16%, O_2 4.0%, NO_x 4600 ppm, HC 2100 ppm C_1.

4.8. The exhaust from a spark-ignition engine has the following composition (in mole fractions):

$$\mathrm{CO_2} = 0.12; \quad \mathrm{H_2O} = 0.14; \quad \mathrm{CO} = 0.01; \quad \mathrm{H_2} = 0.005;$$
$$\mathrm{N_2} = 0.7247; \quad \mathrm{C_8H_{18}} = 0.0003$$

© McGraw-Hill Education. All rights reserved. Any use is subject to the Terms of Use, Privacy Notice and copyright information.

The fuel is isooctane, C_8H_{18}; as shown above, a small fraction of the fuel escapes from the cylinder unburned. The lower heating value of isooctane is 44.4 MJ/kg, of carbon monoxide is 10.1 MJ/kg, and of hydrogen is 120 MJ/kg. The atomic weights of the elements are: C = 12, O = 16, H = 1, N = 14.

a. Calculate the combustion *in*efficiency of the engine; that is, the percentage of the entering fuel enthalpy which is not fully released in the combustion process and leaves the engine in the exhaust gases (for this problem, the exhaust can be assumed to be at room temperature).

b. What fraction of this inefficiency is due to the unburned fuel (HC) emissions?

4.9. A 2-liter displacement four-cylinder engine, operating at 2000 rev/min and 30% of its maximum power at that speed, has the following exhaust composition (in percent by volume or mole percent):

CO_2, 11%; H_2O, 11.5%; CO, 0.5%; H_2, 0%; O_2, 2%; unburned hydrocarbons (expressed as CH_2, i.e., with a molecular weight of 14), 0.5%; N_2, 74.5%.

The fuel is $(CH_2)_n$ with a heating value of 44 MJ/kg. The atomic weights of the elements are C = 12, H = 1, O = 16, N = 14. The heating values of CO and HC are 10 and 44 MJ/kg, respectively.

a. Is the engine a diesel or spark-ignition engine? Is there enough oxygen in the exhaust to burn the fuel completely? Briefly explain.

b. Calculate the fraction of the input fuel energy ($m_f Q_{HV}$) which exits the engine unburned as (1) CO and (2) unburned HC.

c. An inventor claims a combustion efficiency of 100% can be achieved. What percentage improvement in engine specific fuel consumption would result?

4.10. A gasoline engine operates steadily on a mixture of isooctane and air. The air and fuel enter the engine at 25°C. The fuel consumption is 3.0 g/s. The output of the engine is 50 kW. The temperature of the combustion products in the exhaust manifold is 660 K. At this temperature, an analysis of the combustion products yields the following values (on a dry volumetric basis): CO_2, 11.4%; O_2, 1.6%; CO, 2.9%; N_2, 84.1%.

a. Find the composition in moles (number of moles per mole of isooctane) of the reactants and the reaction products.

b. Determine the heat-transfer rate from the working fluid as the working fluid passes through the engine.

Constants for the calculations:

	Enthalpy of formation, kJ/kmol	Sensible enthalpy at 660 K, kJ/kmol
C_8H_{18}	−259,280	—
CO_2	−393,522	15,823
CO	−110,529	10,789
H_2O	−241,827	12,710
O_2	—	11,200
N_2	—	10,749

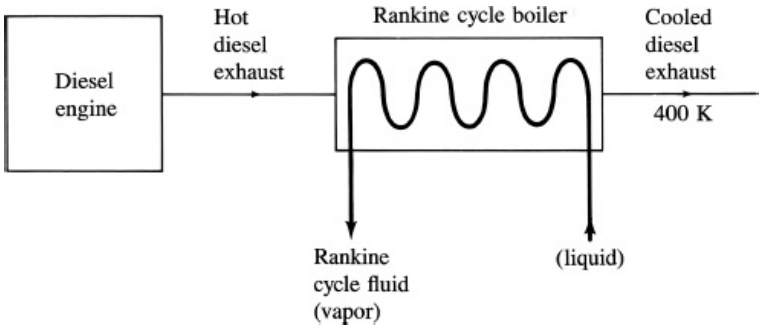
4.11. A direct-injection four-stroke cycle diesel engine is used to provide power for pumping water. The engine operates at its maximum rated power at 2000 rev/min, with an equivalence ratio of 0.8 and an air flow of 0.5 kg/s. The gross indicated fuel conversion efficiency is 45%, and the heat losses from the working fluid to the engine coolant and elsewhere

© McGraw-Hill Education. All rights reserved. Any use is subject to the Terms of Use, Privacy Notice and copyright information.

within the engine are 280 kW. Diesel fuel has a heating value of 42 MJ/kg and stoichiometric fuel/air ratio of 0.067. Fuel and air enter the engine at ambient conditions. The mechanical efficiency of the diesel engine is 85%.

a. Calculate the rated brake power of the engine, the average sensible enthalpy of the exhaust gases as they leave the engine, and the average exhaust gas temperature.

b. Since the exhaust gas temperature is significantly above ambient, the advantages of using the diesel exhaust gas stream to heat the boiler of a Rankine cycle (see sketch) and generate additional power are to be explored. If the exhaust gases *leave* the Rankine-cycle system boiler at 400 K and 30% of the heat transferred from the exhaust gas stream in the boiler is converted to power at the Rankine-cycle power plant drive shaft, calculate the additional power obtained and the brake fuel conversion efficiency of the combined cycle system (diesel plus Rankine cycle).



4.12. A diesel engine has a compression ratio of 22:1. The conditions in the cylinder at the start of compression are p = 101.3 kPa and T = 325 K. Calculate the pressure and temperature at the end of compression, assuming the compression process is isentropic:

a. Assume the cylinder contains an ideal gas with γ = 1.4 and R = 287 J/kg·K.

b. Assume the cylinder contains air which may be regarded as a semiperfect gas (use the gas tables).

c. Compare the work of compression in (*a*) and (*b*) above.

In practice, heat losses reduce the final compression temperature by 100 K. For a diesel engine operating at an equivalence ratio of 0.75 (full load).

d. Calculate the ratio of heat loss during compression to the fuel energy added per cycle.

4.13. While the geometric compression ratio of an engine is V_{max}/V_{min}, the actual compression process starts somewhere between bottom-center and when the intake valve closes, and it is conditions at time of spark (for an SI engine) or fuel injection (for a CI engine) that determine ignition. At low engine speed, compression starts about the time when the intake valve closes. With this assumption, for the diesel engine of Prob. 4.12, calculate the air pressure and temperature at the start of injection. The intake valve closes at 30° after BC; injection commences 15° before TC. Use the gas tables. Compare your answers with those of Prob. 4.12(*b*).

4.14. Use an equilibrium computer code (which calculates the composition and properties of chemically reacting gas mixtures in equilibrium) to calculate the data you need for the following graphs:

a. Values of c_p, γ, molecular weight, and gas composition (mole fractions of N_2, CO_2, H_2O, CO, H_2, O_2, OH, O, H, and NO) as a function of the equivalence ratio (ϕ = 0.2 to 1.4) for products of combustion of isooctane (C_8H_{18}) with air at p = 40 atm and T = 2500 K. Put all species concentrations on the same graph. Use a log scale for the composition axis.

b. Unburned mixture consisting of isooctane vapor and air at 700 K and 20 atm is burned first at constant pressure and then at constant volume.

1. Calculate the enthalpy and internal energy of isooctane vapor at 700 K in cal/gmol; also calculate the volume per unit mass of mixture (cm_3/g) for ϕ = 0.2, 0.4, 0.6, 0.8, 1.0, 1.2, 1.4.

© McGraw-Hill Education. All rights reserved. Any use is subject to the Terms of Use, Privacy Notice and copyright information.

2. Use these data and the equilibrium program to calculate the temperature attained after combustion at constant pressure, and temperature and pressure attained after combustion at constant volume. Plot these temperatures and pressures against the equivalence ratio ϕ.

Thermodynamic data for isooctane vapor

T, K	$\bar{c}_p$, cal/mol·K	$\bar{h} - \bar{h}_{298}$, kcal/mol	$\Delta \bar{h}_f^\circ$, kcal/mol
298	45.14	0.00	−53.57
700	85.66	27.02	−62.79

4.15. A strong walled vessel with a volume of 1000 cm_3 contains a mixture of isooctane with the stoichiometric air requirement at p = 101.3 kPa and T = 25°C. The mixture is then ignited with a spark. Find the pressure and temperature of the equilibrium combustion products just after combustion is complete (i.e., before heat losses to the wall are significant). Assume the burned gases are uniform.

© McGraw-Hill Education. All rights reserved. Any use is subject to the Terms of Use, Privacy Notice and copyright information.

4.11. REFERENCES

1. *JANAF Thermochemical Tables*, 2nd ed., NSRDS–NB537, U.S. National Bureau of Standards, June 1971.
2. Hottel, H. C., Williams, G. C., and Satterfield, C. N.: *Thermodynamic Charts for Combustion Processes*, John Wiley, New York, 1949. See also charts in C. F. Taylor, *The Internal Combustion Engine in Theory and Practice*, vol. 1, MIT Press, Cambridge, MA, 1960.
3. Newhall, H. K., and Starkman, E. S.: "Thermodynamic Properties of Octane and Air for Engine Performance Calculations," in *Digital Calculations of Engine Cycles, Progress in Technology*, vol. TP-7, pp. 38–48, SAE, 1964.
4. Starkman, E. S., and Newhall, H. K.: "Thermodynamic Properties of Methane and Air, and Propane and Air for Engine Performance Calculations," SAE paper 670466, *SAE Trans.*, vol. 76, 1967.
5. Gordon, S., and McBride, B. J.: "Computer Program for the Calculation of Complex Chemical Equilibrium Composition, Rocket Performance, Incident and Reflected Shocks, and Chapman-Jouguet Detonations," NASA publication SP-273, 1971 (NTIS number N71-37775).
6. Svehla, R. A., and McBride, B. J.: "Fortran IV Computer Program for Calculation of Thermodynamic and Transport Properties of Complex Chemical Systems," NASA technical note TND-7056, 1973 (NTIS number N73-15954).
7. Rossini, F. D., Pitzer, K. S., Arnett, R. L., Braun, R. M., and Primentel, G. C.: *Selected Values of Physical and Thermodynamic Properties of Hydrocarbons and Related Compounds*, Carnegie Press, Pittsburgh, PA, 1953.
8. Keenan, J. H., Chao, J., and Kaye, J.: *Gas Tables*, 2nd ed., John Wiley, New York, 1983.
9. Reynolds, W. C.: *Thermodynamic Properties in SI; Graphs, Tables, and Computational Equations for Forty Substances*, Department of Mechanical Engineering, Stanford University, Palo Alto, CA, 1979.
10. Banes, B., McIntyre, R. W., and Sims, J. A.: *Properties of Air and Combustion Products with Kerosene and Hydrogen Fuels*, vols. I-XIII, Propulsion and Energetics Panel, Advisory Group for Aerospace Research and Development (AGARD), NATO, published by Bristol Siddeley Engines Ltd., Filton, Bristol, England, 1967.
11. Fremont, H. A., et al.: *Properties of Combustion Gases*, General Electric Company, Cincinnati, OH, 1955.
12. Hires, S. D., Ekchian, A., Heywood, J. B., Tabaczynski, R. J., and Wall, J. C.: "Performance and NO_x Emissions Modelling of a Jet Ignition Prechamber Stratified Charge Engine," SAE paper 760161, *SAE Trans.*, vol. 85, 1976.
13. LoRusso, J. A.: "Combustion and Emissions Characteristics of Methanol, Methanol-Water, and Gasoline-Methanol Blends in a Spark Ignition Engine," S.M. Thesis, Department of Mechanical Engineering, MIT, May 1976.
14. By, A., Kempinski, B., and Rife, J. M.: "Knock in Spark-Ignition Engines," SAE paper 810147, 1981.
15. Mansouri, S. H., and Heywood, J. B.: "Correlation for the Viscosity and Prandtl Number of Hydrocarbon-Air Combustion Products," *Combust. Sci. Technology*, vol. 23, pp. 251–256, 1980.
16. Chapman, S., and Cowling, T. G.: *The Mathematical Theory of Non-Uniform Gases*, Cambridge University Press, Cambridge, 1955.
17. Hirschfelder, J. O., Curtiss, C. F., and Bird, R. B.: *Molecular Theory of Gases and Liquids*, John Wiley, New York, 1954.
18. Bosch, R.: *Automotive Handbook*, 6th edition, Robert Bosch GmbH and SAE, 2004.
19. D'Alleva, B. A., and Lovell, W. G.: "Relation of Exhaust Gas Composition to Air-Fuel Ratio," *SAE J.*, vol. 38, no. 3, pp. 90–96, March 1936.
20. Stivender, D. L.: "Development of a Fuel-Based Mass Emission Measurement Procedure," SAE paper 710604, 1971.

© McGraw-Hill Education. All rights reserved. Any use is subject to the Terms of Use, Privacy Notice and copyright information.

21. Harrington, J. A., and Shishu, R. C.: "A Single-Cylinder Engine Study of the Effects of Fuel Type, Fuel Stoichiometry and Hydrogen-to-Carbon Ratio on CO, NO, and HC Exhaust Emissions," SAE paper 730476, 1973.
22. Spindt, R. S., "Air-Fuel Ratios from Exhaust Gas Analysis," SAE paper 650507,*SAE Trans.*, vol. 74, 1965.
23. Fleming, R. D., and Eccleston, D. B.: "The Effect of Fuel Composition, Equivalence Ratio, and Mixture Temperature on Exhaust Emissions," SAE paper 710012, 1971.
24. Eltinge, L.: "Fuel-Air Ratio and Distribution from Exhaust Gas Composition," SAE paper 680114,*SAE Trans.*, vol. 77, 1968.
25. Leonard, L. S.: "Fuel Distribution by Exhaust Gas Analysis," SAE paper 379A, 1961.
26. Bishop, R. P.: "Combustion Efficiency in Internal Combustion Engines," B.S. Thesis, Department of Mechanical Engineering, MIT, February 1985.
27. The Engine Test Code Subcommittee of the General Technical Committee,*General Motors Automotive Engine Test Code for Four Cycle Spark Ignition Engines*, 6th ed., 1975.

© McGraw-Hill Education. All rights reserved. Any use is subject to the Terms of Use, Privacy Notice and copyright information.

5.0. CHAPTER PRELIMINARIES

INTRODUCTION

IDEAL MODELS OF ENGINE PROCESSES

THERMODYNAMIC RELATIONS FOR ENGINE PROCESSES

CYCLE ANALYSIS WITH IDEAL GAS WORKING FLUID WITH c_v AND c_p CONSTANT

FUEL-AIR CYCLE ANALYSIS

OVEREXPANDED ENGINE CYCLES

AVAILABILITY ANALYSIS OF ENGINE PROCESSES

COMPARISON WITH REAL ENGINE CYCLES

PROBLEMS

REFERENCES

© McGraw-Hill Education. All rights reserved. Any use is subject to the Terms of Use, Privacy Notice and copyright information.

5.1. INTRODUCTION

The operating cycle of an internal combustion engine can be broken down into a sequence of separate processes: intake, compression, combustion, expansion, and exhaust. With models for each of these processes, a simulation of a complete engine cycle can be built up which can be analyzed to provide information on engine performance. Models of individual engine processes at various levels of approximation have been developed. In this chapter we consider the simplest set of models which provide useful insights into the performance and efficiency of engines. The cycles analyzed are commonly called the constant-volume, constant-pressure, and limited-pressure cycles; each title describes the approximation made for the engine combustion process.[1] The description of more accurate simulations of engine processes is deferred untilChap. 14.

For each engine cycle, a choice of models for working fluid thermodynamic properties must be made. These models have been reviewed in Chap. 4. Ideal engine cycle models combined with a simple ideal gas model (specific heats constant throughout the engine cycle, model 1 in Table 4.2) provide analytic results and are useful for illustrative purposes; we will call these cycles *ideal gas standard cycles.* Ideal engine cycles combined with more realistic models of working fluid properties (a frozen mixture of ideal gases for the unburned mixture and an equilibrium mixture for the burned mixture, model 5 in Table 4.2) are called *fuel-air cycles* and provide more quantitative information on engine operation.

An internal combustion engine is not a heat engine in the thermodynamic definition of the term. The engine's boundaries do not define a closed system. The working fluid does not execute a thermodynamic cycle. The temperature changes which occur around minimum and maximum cylinder volumes are not primarily a result of heat-transfer interactions. An internal combustion engine can best be analyzed as an open system which exchanges heat and work with its surrounding environment (the atmosphere). Reactants (fuel and air) flow into the engine; products (exhaust gases) flow out. (An overall second law analysis of the engine from this point of view has already been presented in Sec. 3.6.) Thus, the cycles discussed in this chapter are not thermodynamic cycles. Rather, each is a sequence of processes through which we can follow the state of the working fluid as the engine executes a complete *operating* cycle.

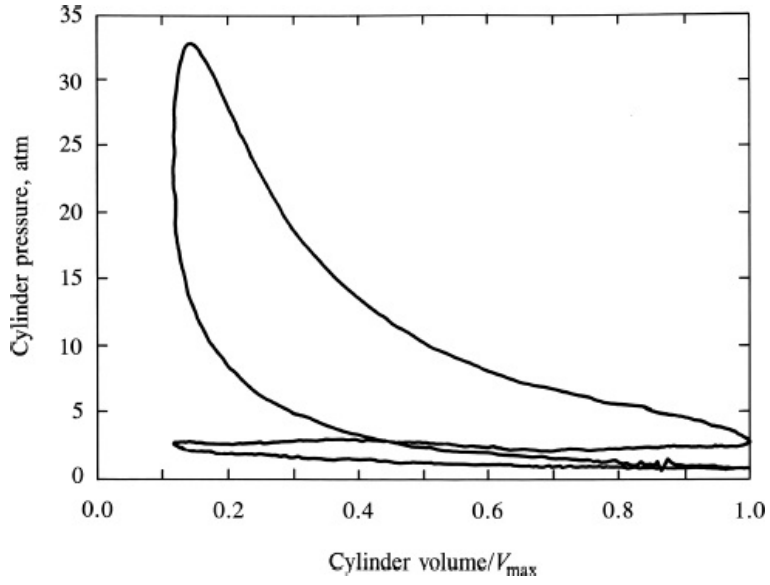
[1] These cycles are also referred to by the titles Otto cycle, Diesel cycle, and dual cycle, respectively, for historical reasons. The more descriptive titles used above are preferred because they avoid the often-made assumption that the spark-ignition or Otto engine is best approximated by the constant-volume cycle, and the compression-ignition or diesel engine is best approximated by the constant-pressure cycle. These assumptions are not necessarily correct.

© McGraw-Hill Education. All rights reserved. Any use is subject to the Terms of Use, Privacy Notice and copyright information.

5.2. IDEAL MODELS OF ENGINE PROCESSES

The sequence of processes which make up a typical SI and CI engine operating cycle has been described in Sec. 1.3. To illustrate these processes, cylinder pressure (p) and volume (V) data from a throttled four-stroke cycle SI engine are plotted as a p-V diagram in Fig. 5.1. The cycle can be divided into compression, combustion, expansion, exhaust, and intake processes. Sets of assumptions which simplify each of these processes to a form convenient for analysis are given in Table 5.1.

Figure 5.1 Pressure-volume diagram of firing spark-ignition engine. r_c = 8.4, 3500 rev/min, p_i = 0.4 atm, p_e = 1 atm, $imep_n$ = 2.9 atm.



© McGraw-Hill Education. All rights reserved. Any use is subject to the Terms of Use, Privacy Notice and copyright information.

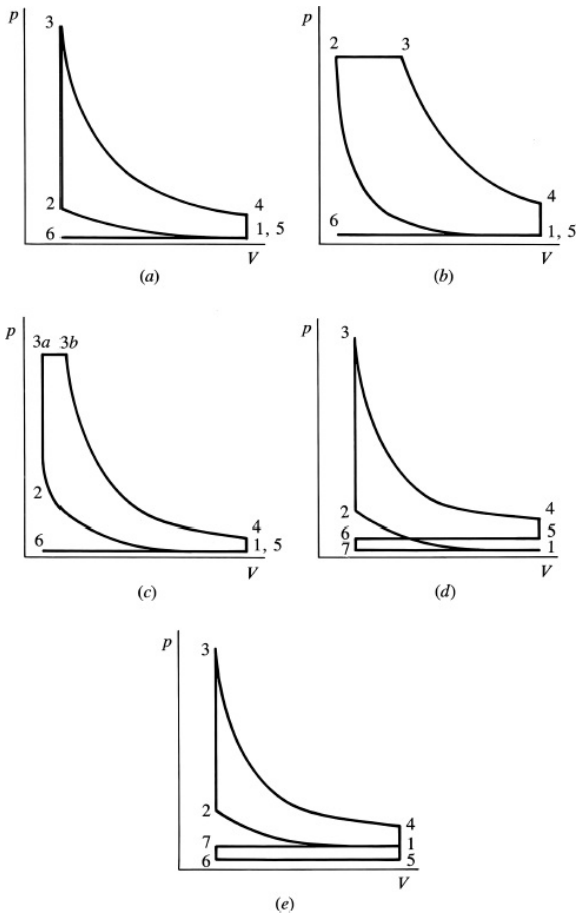
Table 5.1 Ideal models of engine processes

Process	Assumptions
Compression (1-2)	1. Adiabatic and reversible (hence isentropic)
Combustion (2-3)	1. Adiabatic 2. Combustion occurs at a. Constant volume b. Constant pressure c. Part at constant volume and part at constant pressure (called limited pressure) 3. Combustion is complete ($\eta_c = 1$)
Expansion (3-4)	1. Adiabatic and reversible (hence isentropic)
Exhaust (4-5-6) and intake (6-7-1)	1. Adiabatic 2. Valve events occur at top- and bottom-center 3. No change in cylinder volume as pressure differences across open valves drop to zero 4. Inlet and exhaust pressures constant 5. Velocity effects negligible

Pressure-volume diagrams for the constant-volume, constant-pressure, and limited-pressure cycles for unthrottled engine operation are illustrated in Figs. 5.2*a* to *c*. Throttled engine operation ($p_i < p_e$) and supercharged engine operation ($p_i > p_e$) are shown in Figs. 5.2*d* and *e*. In each cycle, 1-2 is the compression process, 2-3 is the combustion process, 3-4 (or 2-4 in the constant-pressure cycle) is the expansion process, 4-5-6 is the exhaust process, and 6-7-1 is the intake process.

© McGraw-Hill Education. All rights reserved. Any use is subject to the Terms of Use, Privacy Notice and copyright information.

Figure 5.2 *Pressure-volume diagrams of ideal cycles. Unthrottled operation: (a) constant-volume combustion; (b) constant-pressure combustion; (c) limited-pressure combustion. (d) Throttled constant-volume cycle; (e) supercharged constant-volume cycle.*



The most critical assumption in determining how useful these ideal cycles are as indicators of engine performance is the form assumed for the combustion process. The real engine combustion process occupies a finite crank angle period (between about 20 and 60 crank angle degrees), and the spark or fuel-injection timing may be retarded from its optimum advance to closer to top center, TC. The constant-volume cycle is the limiting case of infinitely fast combustion at TC; the constant-pressure cycle would correspond to slow and late combustion; the limited-pressure cycle lies in between.

© McGraw-Hill Education. All rights reserved. Any use is subject to the Terms of Use, Privacy Notice and copyright information.

5.3. THERMODYNAMIC RELATIONS FOR ENGINE PROCESSES

The overall engine operating parameters of greatest interest which can be determined from a thermodynamic analysis of the engine operating cycle are:

The indicated fuel conversion efficiency
$\eta_{f,i}$:

$$\eta_{f,i} = \frac{W_{c,i}}{m_f Q_{\text{LHV}}}$$

(5.1)

(which, since the combustion efficiency is unity, is equal to the indicated thermal conversion efficiency
$\eta_{t,i}$; see Sec. 3.6.2.)

The indicated mean effective pressure (imep):

$$\text{imep} = \frac{W_{c,i}}{V_d} = \frac{m_f Q_{\text{LHV}} \eta_{f,i}}{V_d}$$

(5.2)

$W_{c,i}$, the indicated work per cycle, is the algebraic sum of the expansion stroke work and the compression stroke work (a negative quantity):

$$W_{c,i} = W_E + W_C$$

(5.3)

Using the notation of Fig. 5.2 to define the endpoints of each engine process, the following relationships are obtained by applying the first and second laws of thermodynamics to the cylinder contents:

Compression stroke:

$$\frac{v_1}{v_2} = r_c$$

(5.4)

Since the process is adiabatic and reversible,

$$s_2 = s_1$$

(5.5)

© McGraw-Hill Education. All rights reserved. Any use is subject to the Terms of Use, Privacy Notice and copyright information.

The compression work is

$$W_C = U_1 - U_2 = m(u_1 - u_2)$$

(5.6)

Combustion process:

For the constant-volume cycle,

$$v_3 = v_2 \qquad u_3 - u_2 = 0$$

(5.7*a*, *b*)

For the constant-pressure cycle,

$$p_3 = p_2 \qquad h_3 - h_2 = 0$$

(5.7*c*, *d*)

For the limited-pressure cycle,

$$v_{3a} = v_2 \qquad p_{3b} = p_{3a}$$

(5.7*e*, *f*)

and

$$u_{3a} - u_2 = 0 \qquad h_{3b} - h_{3a} = 0$$

(5.7*g*, *h*)

Expansion stroke:

For the constant-volume cycle,

$$\frac{v_4}{v_3} = r_c \qquad s_4 = s_3$$

(5.8*a*, *b*)

and the expansion work is

$$W_E = U_3 - U_4 = m(u_3 - u_4)$$

(5.9)

For the constant-pressure cycle,

© McGraw-Hill Education. All rights reserved. Any use is subject to the Terms of Use, Privacy Notice and copyright information.

$$p_3 = p_2 \qquad \frac{v_4}{v_2} = r_c \qquad s_4 = s_3$$

(5.10*a*, *b*, *c*)

and the expansion work is

$$\begin{aligned} W_E &= U_3 - U_4 + p_2(V_3 - V_2) \\ &= m\left[(u_3 - u_4) + p_2(v_3 - v_2)\right] \\ &= m\left[(h_3 - h_4) + p_4 v_4 - p_2 v_2\right] \end{aligned}$$

(5.11)

For the limited-pressure cycle,

$$v_4/v_{3a} = r_c \qquad p_{3b} = p_{3a} \qquad s_4 = s_{3b}$$

(5.12*a*, *b*, *c*)

and the expansion work is

$$\begin{aligned} W_E &= U_{3b} - U_4 + p_3(V_{3b} - V_{3a}) \\ &= m\left[(u_{3b} - u_4) + p_3(v_{3b} - v_{3a})\right] \\ &= m\left[(h_{3b} - h_4) + p_4 v_4 - p_3 v_{3a}\right] \end{aligned}$$

(5.13)

The indicated fuel conversion efficiency is found by substitution into Eqs. (5.3) and (5.1):

For the constant-volume cycle:

$$\eta_{f,i} = \frac{m\left[(u_3 - u_4) - (u_2 - u_1)\right]}{m_f Q_{\mathrm{LHV}}}$$

(5.14)

For the constant-pressure cycle:

$$\eta_{f,i} = \frac{m\left[(h_3 - h_4) - (u_2 - u_1) + p_4 v_4 - p_2 v_2\right]}{m_f Q_{\mathrm{LHV}}}$$

(5.15)

For the limited-pressure cycle:

© McGraw-Hill Education. All rights reserved. Any use is subject to the Terms of Use, Privacy Notice and copyright information.

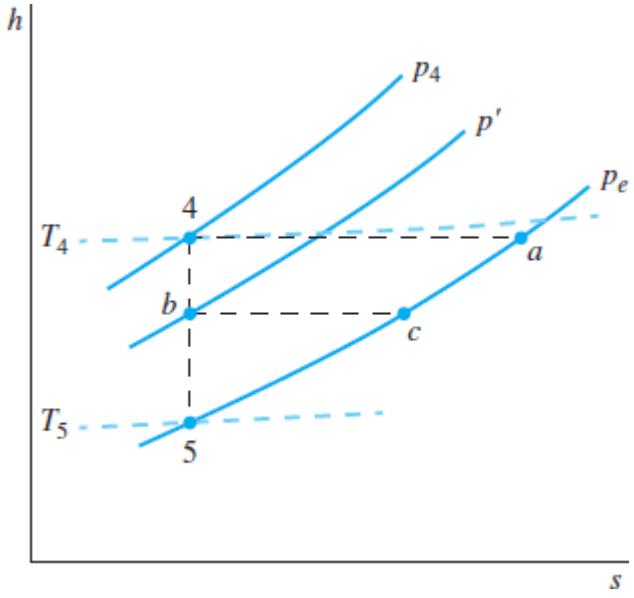
$$\eta_{f,i} = \frac{m\left[(h_{3b} - h_4) - (u_2 - u_1) + p_4 v_4 - p_3 v_{3a}\right]}{m_f Q_{\mathrm{LHV}}}$$

(5.16)

The state of the mixture at point 1 in the cycle depends on the intake mixture properties and the residual gas properties at the end of the exhaust stroke. When the exhaust valve opens at point 4, the cylinder pressure is above the exhaust manifold pressure and a *blowdown* process occurs. In the ideal exhaust process model, this blowdown occurs with the piston stationary at BC. During this blowdown process, the gas which remains inside the cylinder expands isentropically. The gases escaping from the cylinder undergo an unrestrained expansion or throttling process which is irreversible. It is assumed that the kinetic energy acquired by each gas element as it is accelerated through the exhaust valve is dissipated in a turbulent mixing process in the exhaust port into internal energy and flow work. Since it is also assumed that no heat transfer occurs, the enthalpy of each element of gas after it leaves the cylinder remains constant.

These processes are illustrated on an *h-s* diagram in Fig. 5.3. The gas remaining in the cylinder expands isentropically along the line 4-5. The first element of gas which leaves the cylinder at point 4 enters the exhaust manifold at state *a* on the pressure = p_e line. An element that leaves the cylinder at an intermediate state*b* on the expansion line 4-5 would enter the exhaust manifold at state *c*. At the end of the blowdown process the gas in the cylinder and the last gas to leave have the same state, 5. There is, therefore, a gradient in temperature within the exhausted gas. The temperature of the first element exhausted, T_a, is slightly less than T_4; the temperature of the last element exhausted is T_5.

Figure 5.3 Enthalpy-entropy diagram of gas state during exhaust process. See text for explanation.



A displacement of gas out of the cylinder follows the blowdown process as the piston moves from BC to TC. If heat-transfer and kinetic energy dissipation effects are neglected, no change in thermodynamic state of the gas occurs. In this *displacement* process, the mass of gas within the cylinder at the end of the blowdown process is further decreased by the ratio V_5/V_6.

The mass of residual gas m_r in the cylinder at point 6 in the cycle is obtained by first determining the state of the gas (T_5, v_5) at the end of the blowdown process following an isentropic expansion from p_4 to p_e and then by reducing the cylinder volume to the clearance volume V_6. The residual mass fraction is thus given by

$$\frac{m_r}{m} = x_r = \frac{v_4/v_5}{r_c} = \frac{v_2}{v_5}$$

© McGraw-Hill Education. All rights reserved. Any use is subject to the Terms of Use, Privacy Notice and copyright information.

(5.17)

The average state of the exhausted gas can be determined by considering the open system defined by the piston face, cylinder walls, and cylinder head, shown in Fig. 5.4. Applying the first law of thermodynamics for an open system gives

$$U_6 - U_4 = p_e(V_4 - V_6) - H_e$$

(5.18*a*)

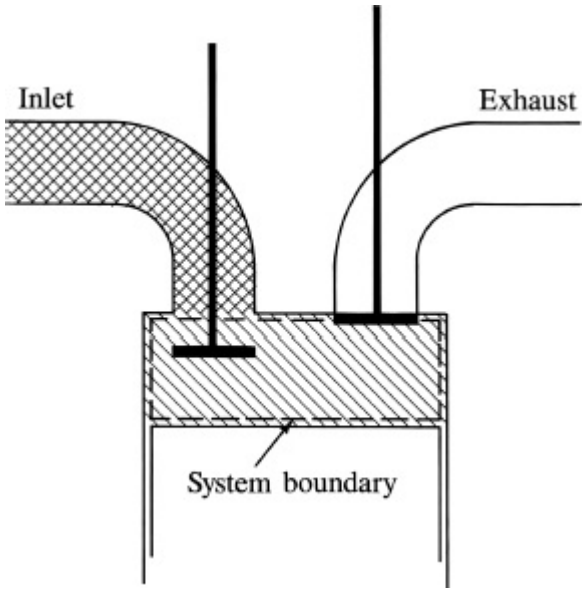
where H_e is the enthalpy of the mass of gas exhausted from the cylinder. The average specific exhaust enthalpy is, therefore,

$$h_e = \frac{m_4 u_4 - m_6 u_6 + p_e V_d}{m_4 - m_6}$$

(5.18*b*)

which, with $p = p_e$, defines the average exhausted-gas state.

Figure 5.4 Definition of system boundary for thermodynamic analysis of ideal cycle processes.



The mixture temperature at the end of the intake stroke and at the start of the compression stroke (point 1 in Fig. 5.2) can now be determined, again using the open system in Fig. 5.4. Application of the first law between points 6 and 1 gives

$$U_1 - U_6 = -p_i(V_1 - V_6) + (m_1 - m_6)h_i$$

(5.19*a*)

or

$$m_1 u_1 - m_6 u_6 = -p_i(V_1 - V_6) + (m_1 - m_6)h_i$$

(5.19*b*)

© McGraw-Hill Education. All rights reserved. Any use is subject to the Terms of Use, Privacy Notice and copyright information.

or

$$m_1 h_1 = m_6 h_6 + (m_1 - m_6) h_i + V_2 (p_i - p_e)$$

(5.19c)

where h_i is the specific enthalpy of the inlet mixture and $p_1 = p_i$.

Note that when $p_i < p_e$, part of the residual gas in the cylinder at the end of the exhaust stroke will flow into the intake system when the intake valve opens. This flow will cease when the cylinder pressure equals p_i. However, provided no heat transfer occurs, this backflow will not affect Eqs. (5.19) above, since the flow of residual through the intake valve is then a constant enthalpy process.

In many engines, the closing of the exhaust valve and the opening of the intake valve overlap. Flow of exhausted gases from the exhaust system through the cylinder into the intake system can then occur. Equations (5.18) and (5.19) would have to be modified to account for valve overlap.

In the four-stroke engine cycle, work is done on the piston during the intake and the exhaust processes. The work done by the cylinder gases on the piston during exhaust is

$$W_e = p_e (V_2 - V_1)$$

(5.20)

The work done by the cylinder gases on the piston during intake is

$$W_i = p_i (V_1 - V_2)$$

(5.21)

The net work to the piston over the exhaust and intake strokes, the *pumping work*, is

$$W_p = (p_i - p_e)(V_1 - V_2)$$

(5.22)

which, for the cylinder gas system, is negative for $p_i < p_e$ and positive for $p_i > p_e$.[1] The pumping mean effective pressure (pmep) is usually defined as a positive quantity. Thus:

For

$$p_i < p_e : \quad \text{pmep} = p_e - p_i$$

(5.23a)

For

$$p_i > p_e : \quad \text{pmep} = p_i - p_e$$

© McGraw-Hill Education. All rights reserved. Any use is subject to the Terms of Use, Privacy Notice and copyright information.

(5.23*b*)

The net and gross indicated mean effective pressures are related by

$$\text{imep}_n = \text{imep}_g - (p_e - p_i)$$

(5.24)

The net indicated fuel conversion efficiency is related to the gross indicated fuel conversion efficiency by

$$\eta_{f,\text{in}} = \eta_{f,\text{ig}} \left(1 - \frac{p_e - p_i}{\text{imep}_g} \right)$$

(5.25)

[1] Note that the underside of the piston, as it moves up and down the cylinder, does work on the gas in the crankcase. If the crankcase gas pressure is constant (a good assumption, especially in multicylinder four-stroke engines), then the intake and exhaust stroke crankcase gas work transfer are opposite in sign and cancel out.

© McGraw-Hill Education. All rights reserved. Any use is subject to the Terms of Use, Privacy Notice and copyright information.

5.4. CYCLE ANALYSIS WITH IDEAL GAS WORKING FLUID WITH c_v AND c_p CONSTANT

If the working fluid in these ideal cycles is assumed to be an ideal gas, withc_v and c_p constant throughout the engine operating cycle, the equations developed in the previous section which describe engine performance and efficiency can be further simplified. We will use the notation of Fig. 5.2.

5.4.1. Constant-Volume Cycle

The compression work [Eq. (5.6)] becomes

$$W_C = mc_v(T_1 - T_2)$$

(5.26)

The expansion work [Eq. (5.9)] becomes

$$W_E = mc_v(T_3 - T_4)$$

(5.27)

The denominator in Eq. (5.14), $m_f Q_{\text{LHV}}$, can be related to the temperature rise during combustion. For the working fluid model under consideration, the *U(T)* lines for the reactants and products on a *U-T* diagram such as Fig. 3.5 are parallel and have equal slopes, of magnitude c_v. Hence, for a constant-volume adiabatic combustion process

$$mc_v(T_3 - T_2) = m_f Q_{\text{LHV}}$$

(5.28)[1]

Note that the heating values at constant volume and constant pressure are the same for this working fluid. For convenience we will define

$$Q^* = \frac{m_f Q_{\text{LHV}}}{m}$$

(5.29)

*Q** is the specific internal energy (and enthalpy) decrease during isothermal combustion, per unit mass of working fluid.

The relation for indicated fuel conversion efficiency [Eq. (5.14)] becomes

$$\eta_{f,i} = \frac{(T_3 - T_4) - (T_2 - T_1)}{T_3 - T_2} = 1 - \frac{T_4 - T_1}{T_3 - T_2}$$

© McGraw-Hill Education. All rights reserved. Any use is subject to the Terms of Use, Privacy Notice and copyright information.

(5.30)

Since 1-2 and 3-4 are isentropic processes between the same volumes, V_1 and V_2,

$$\frac{T_2}{T_1} = \left(\frac{V_1}{V_2}\right)^{\gamma-1} = r_c^{\gamma-1} = \left(\frac{V_4}{V_3}\right)^{\gamma-1} = \frac{T_3}{T_4}$$

where $\gamma = c_p/c_v$ Hence:

$$\frac{T_4}{T_1} = \frac{T_3}{T_2}$$

and Eq. (5.30) can be rearranged as

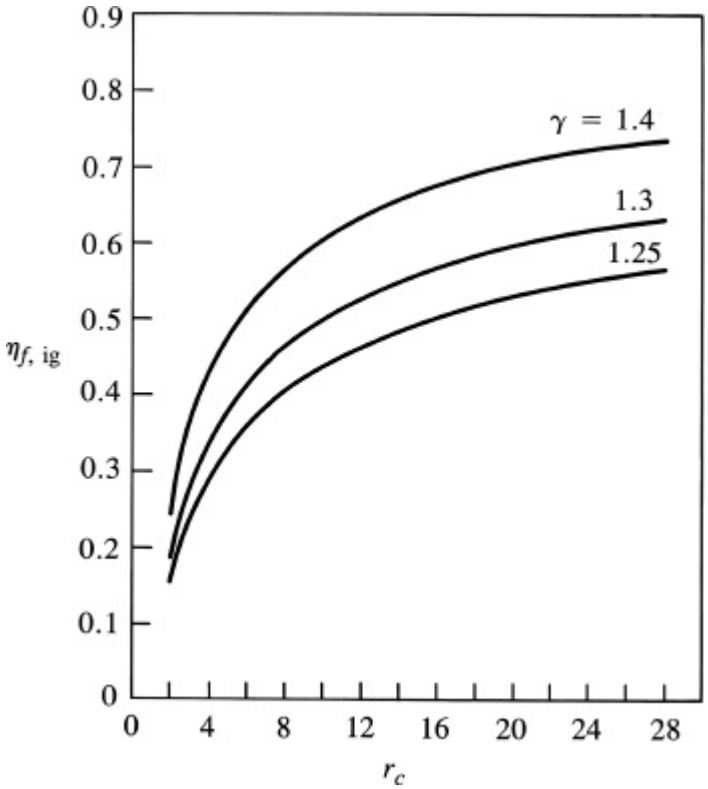
$$\eta_{f,i} = 1 - \frac{1}{r_c^{\gamma-1}}$$

(5.31)

Values of
$\eta_{f,i}$ for different values of
γ (a variable that depends on mixture composition) are shown in Fig. 5.5. The indicated fuel conversion efficiency increases with increasing compression ratio, and as
γ increases.

© McGraw-Hill Education. All rights reserved. Any use is subject to the Terms of Use, Privacy Notice and copyright information.

Figure 5.5 Ideal gas constant-volume cycle fuel conversion efficiency as a function of compression ratio; $\gamma = c_p/c_v$



These trends can be explained by examining how the *p-V* diagrams for the constant-volume cycle change as r_c and γ are increased, at constant cylinder displaced volume V_d. Increasing r_c at fixed γ increases the pressure at the start of expansion, and the volume ratio through which the charge expands during the expansion stroke. Both of these effects add to the indicated work per cycle. They add positive area to the *p-V* diagram which more than offsets a slight increase in the (negative) work required during compression. The effect of increasing γ at constant r_c has an analogous impact. The peak pressure (and temperature and energy) at the start of expansion is increased and the charge expands through a larger temperature ratio during expansion due to its higher γ, thus transferring a larger fraction of its energy at start of expansion to the piston as work.

The indicated mean effective pressure, using Eqs. (5.2) and (5.31), becomes

$$\frac{\text{imep}}{p_1} = \left(\frac{Q^*}{c_v T_1}\right)\left(\frac{1}{\gamma - 1}\right)\left(\frac{r_c}{r_c - 1}\right)\left(1 - \frac{1}{r_c^{\gamma-1}}\right)$$

(5.32)

The dimensionless numbers r_c, γ, and $Q^*/(c_v\, T_1)$ are sufficient to describe the characteristics of the constant-volume ideal gas standard cycle, relative to its initial conditions p_1, T_1.

It is useful to compare the imep—a measure of the effectiveness with which the displaced volume of the engine is used to produce work—and the maximum pressure in the cycle, p_3. The ratio p_3/p_1 can be determined from the ideal gas law applied at points 2 and 3, and the relation

© McGraw-Hill Education. All rights reserved. Any use is subject to the Terms of Use, Privacy Notice and copyright information.

$$\frac{T_3}{T_2} = 1 + \frac{Q^*}{c_v T_1 r_c^{\gamma-1}}$$

(5.33)

obtained from Eq. (5.28). Equations (5.32) and (5.33) then give

$$\frac{\text{imep}}{p_3} = \frac{1}{(\gamma-1)r_c^{\gamma}}\left(\frac{r_c}{r_c-1}\right)\frac{1-1/r_c^{\gamma-1}}{c_v T_1/Q^* + 1/r_c^{\gamma-1}}$$

(5.34)

A high value of imep/p_3 is desirable. Engine weight will increase with increasing p_3 to withstand the increasing stresses in components.

The indicated fuel conversion efficiency and the ratios imep/p_1 and imep/p_3 for this ideal cycle model do not depend on whether the cycle is throttled or supercharged. However, the relationships between the working fluid properties at points 1 and 6 do depend on the degree of throttling or supercharging. For throttled engine operation, the residual gas mass fraction x_r can be determined as follows. From Eq. (5.17), since state 5 corresponds to an isentropic expansion from state 4 to$p = p_e$, x_r is given by

$$x_r = \frac{(p_e/p_4)^{1/\gamma}}{r_c} = \frac{(p_e/p_i)^{1/\gamma}(p_1/p_4)^{1/\gamma}}{r_c}$$

Since

$$\frac{p_1}{p_4} = \frac{p_1}{p_2}\frac{p_2}{p_3}\frac{p_3}{p_4} = \frac{1}{r_c^{\gamma}}\frac{T_2}{T_3}r_c^{\gamma} = \left(1 + \frac{Q^*}{c_v T_1 r_c^{\gamma-1}}\right)^{-1}$$

it follows that

$$x_r = \frac{1}{r_c}\frac{(p_e/p_i)^{1/\gamma}}{\left[1 + Q^*/(c_v T_1 r_c^{\gamma-1})\right]^{1/\gamma}}$$

(5.35)

The residual mass fraction increases as p_i decreases below p_e, decreases as r_c increases, and decreases as $Q^*/(c_v\, T_1)$ increases.

Through a similar analysis, the temperature of the residual gas T_6 can be determined:

$$\frac{T_6}{T_1} = \left(\frac{p_e}{p_i}\right)^{(\gamma-1)/\gamma}\left(1 + \frac{Q^*}{c_v T_1 r_c^{\gamma-1}}\right)^{1/\gamma}$$

© McGraw-Hill Education. All rights reserved. Any use is subject to the Terms of Use, Privacy Notice and copyright information.

(5.36)

The mixture temperature at point 1 in the cycle can be related to the inlet mixture temperature, T_i, with Eq. (5.19). For a working fluid with c_v and c_p constant, this equation becomes

$$c_p T_1 = x_r c_p T_6 + (1 - x_r) c_p T_i - \frac{R T_1}{r_c}\left(\frac{p_e}{p_i} - 1\right)$$

(5.37)

Use of Eqs. (5.36) and (5.37) leads to the relation

$$\frac{T_1}{T_i} = \frac{1 - x_r}{1 - 1/(\gamma r_c)\left[p_e/p_i + (\gamma - 1)\right]}$$

(5.38)

Extensive results for the constant-volume cycle with $\gamma = 1.4$ can be found in Taylor.[1]

5.4.2. Limited- and Constant-Pressure Cycles

The constant-pressure cycle is a limited-pressure cycle with $p_3 = p_2$. For the limited-pressure cycle, the compression work remains

$$W_C = m c_v (T_1 + T_2)$$

(5.39)

The expansion work, from Eq. (5.13), becomes

$$W_E = m\left[c_v (T_{3b} - T_4) + p_3 (v_{3b} - v_{3a})\right]$$

(5.40)

For the combustion process, Eqs. (5.7*g, h*) give

$$m_{f2-3a} Q_{\mathrm{LHV}} = m c_v (T_{3a} - T_2)$$

(5.41*a*)

$$m_{f3a-3b} Q_{\mathrm{LHV}} = m c_p (T_{3b} - T_{3a})$$

(5.41*b*)

or

© McGraw-Hill Education. All rights reserved. Any use is subject to the Terms of Use, Privacy Notice and copyright information.

$$m_f Q_{\text{LHV}} = m\left[c_v(T_{3a} - T_2) + c_p(T_{3b} - T_{3a})\right]$$

(5.41*c*)

for a working fluid with c_v and c_p constant throughout the cycle.

Combining Eqs. (5.1), (5.3), and (5.39) to (5.41) and simplifying gives

$$\eta_{f,i} = 1 - \frac{T_4 - T_1}{(T_{3a} - T_2) + \gamma(T_{3b} - T_{3a})}$$

Use of the isentropic relationships for the working fluid along 1-2 and 3*b*-4, with the substitutions

$$\alpha = \frac{p_3}{p_2} \qquad \beta = \frac{V_{3b}}{V_{3a}}$$

(5.42*a*, *b*)

leads to the result

$$\eta_{f,i} = 1 - \frac{1}{r_c^{\gamma-1}}\left[\frac{\alpha\beta^\gamma - 1}{\alpha\gamma(\beta - 1) + \alpha - 1}\right]$$

(5.43)

For $\beta = 1$ this result becomes the constant-volume cycle efficiency [Eq. (5.31)]. For $\alpha = 1$, this result gives the constant-pressure cycle efficiency as a special case.

The mean effective pressure is related to p_1 and p_3 via

$$\frac{\text{imep}}{p_1} = \frac{Q^*}{c_v T_1(\gamma - 1)}\left(\frac{r_c}{r_c - 1}\right)\eta_{f,i}$$

(5.44)

$$\frac{\text{imep}}{p_3} = \frac{1}{\alpha r_c^\gamma}\left(\frac{Q^*}{c_v T_1}\right)\left(\frac{1}{\gamma - 1}\right)\left(\frac{r_c}{r_c - 1}\right)\eta_{f,i}$$

(5.45)

5.4.3. Cycle Comparison

The above expressions are most useful if values for γ and $Q^*/(c_v T_1)$ are chosen to match real working fluid properties. Figure 5.5 has already shown the sensitivity of $\eta_{f,i}$ for the constant-volume cycle to the value of γ chosen. In Sec. 4.4, average values of γ_u and γ_b were determined which match real working fluid properties over the compression and expansion strokes,

© McGraw-Hill Education. All rights reserved. Any use is subject to the Terms of Use, Privacy Notice and copyright information.

respectively. Values for a stoichiometric mixture appropriate to an SI engine are $\gamma_u \approx 1.3$, $\gamma_b \approx 1.2$. However, analysis of pressure-volume data for real engine cycles indicates that pV^n, where $n \approx 1.3$, is also a good fit to the expansion stroke p-V data.[2] Heat transfer from the burned gases increases the exponent above the value corresponding to γ_b. A value of $\gamma = 1.3$ for the entire cycle is thus a reasonable compromise.

Q^*, defined by Eq. (5.29), is the enthalpy decrease during isothermal combustion per unit mass of working fluid. Hence

$$Q^* = \left(\frac{m_f}{m_a}\right) Q_{\mathrm{LHV}} \left(\frac{m_a}{m}\right)$$

(5.46)

A simple approximation for (m_a/m) is $(r_c - 1)/r_c$; that is, fresh air fills the displaced volume and the residual gas fills the clearance volume at the same density. Then, for isooctane fuel, for a stoichiometric mixture, Q^* is given by 2.92×10^6 $(r_c - 1)/r_c$ J/kg air. For $\gamma = 1.3$ and an average molecular weight $M = 29.3$, $c_v = 946$ J/kg · K. For $T_1 = 333$ K, $Q^*/(c_v T_1)$ becomes 9.3 $(r_c - 1)/r_c$. For this value of $Q^*/(c_v T_1)$ all cycles would be burning a stoichiometric mixture with an appropriate residual gas fraction.

Pressure-volume diagrams for the three ideal cycles for the same compression ratio and unburned mixture composition are shown in Fig. 5.6. For each cycle, $\gamma = 1.3$, $r_c = 12$, $Q^*/(c_v T_1) = 9.3(r_c - 1)/r_c = 8.525$. Overall performance characteristics for each of these cycles are summarized in Table 5.2. The constant-volume cycle has the highest efficiency, the constant-pressure cycle the lowest efficiency. This can be seen from Eq. (5.43) where the term in square brackets is equal to unity for the constant-volume cycle and greater than unity for the limited- and constant-pressure cycles. The imep values are proportional to $\eta_{f,i}$ since the mass of fuel burned per cycle is the same in all three cases.

© McGraw-Hill Education. All rights reserved. Any use is subject to the Terms of Use, Privacy Notice and copyright information.

Figure 5.6 Pressure-volume diagrams for constant-volume, limited-pressure, and constant-pressure ideal gas standard cycles. $r_c = 12$, $\gamma = 1.3$, $Q^*/(c_v T_1) = 9.3(r_c - 1)/r_c = 8.525$, $p_{3a}/p_1 = 67$.

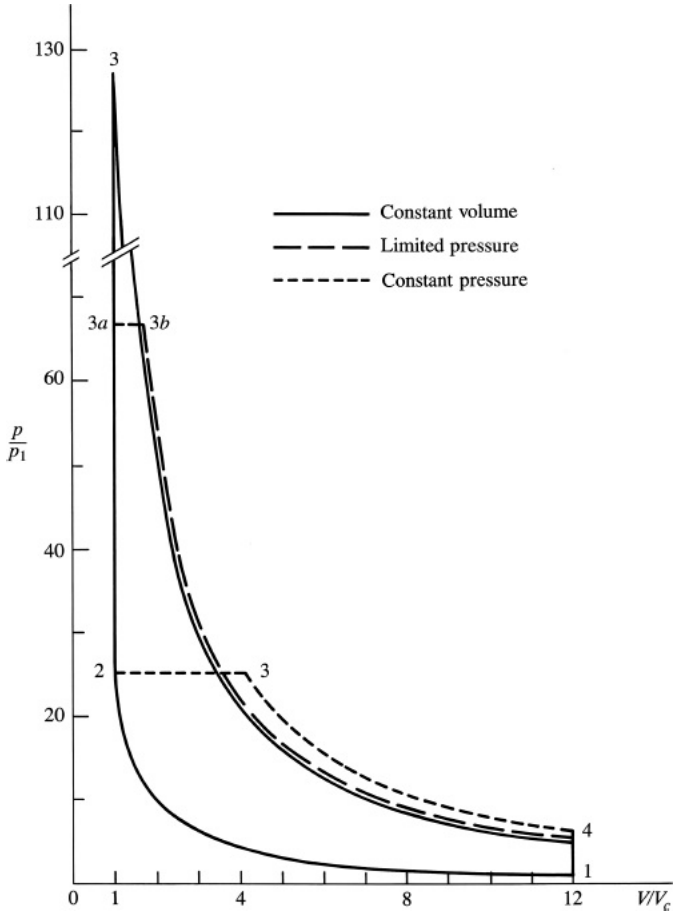


Table 5.2 Comparison of ideal cycle results

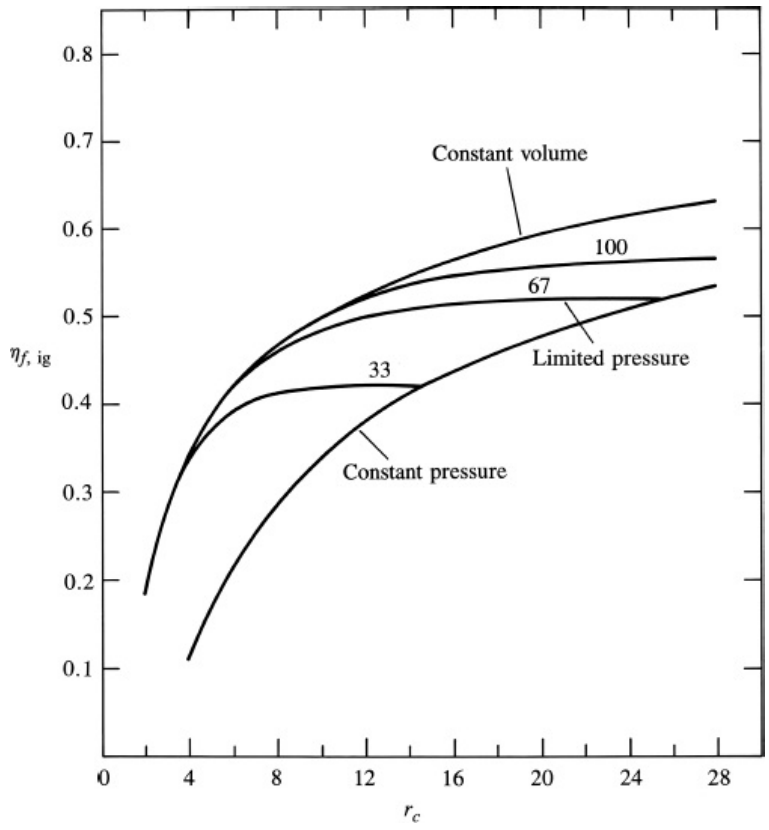
	$\eta_{f,i}$	$\frac{\text{imep}}{p_1}$	$\frac{\text{imep}}{p_3}$	$\frac{p_{\max}}{p_1}$
Constant volume	0.525	16.3	0.128	128
Limited pressure	0.500	15.5	0.231	67
Constant pressure	0.380	11.8	0.466	25.3
$\gamma = 1.3$; $r_c = 12$; $Q^*/(c_v T_1) = 8.525$.				

As the peak pressure p_3 is decreased, the ratio of imep to p_3 increases. This ratio is important because imep is a measure of the useful pressure on the piston, and the maximum pressure chiefly affects the strength required of the engine structure.

A more extensive comparison of the three cycles is given in Figs. 5.7 and 5.8, over a range of compression ratios. For all cases $\gamma = 1.3$ and $Q^*/(c_v T_1) = 9.3(r_c - 1)/r_c$. At any given r_c, the constant-volume cycle has the highest efficiency and lowest imep/p_3. For a given maximum pressure p_3, the constant-pressure cycle has the highest efficiency (and the highest compression ratio). For the limited-pressure cycle, at constant p_3/p_1, there is little improvement in efficiency and imep above a compression ratio of about 10 as r_c is increased.

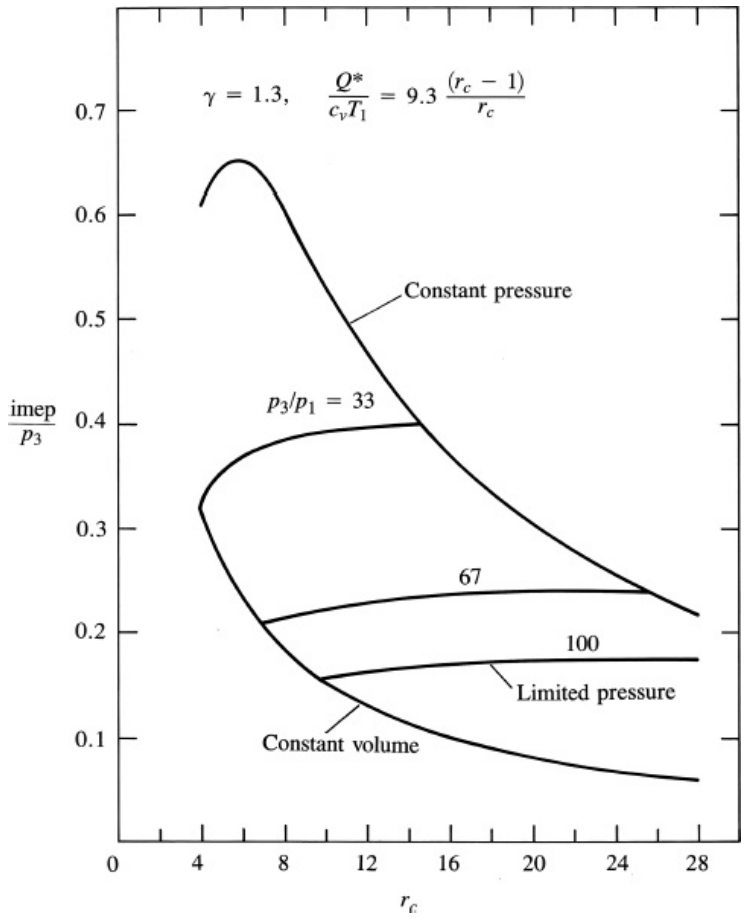
© McGraw-Hill Education. All rights reserved. Any use is subject to the Terms of Use, Privacy Notice and copyright information.

Figure 5.7 Fuel conversion efficiency as a function of compression ratio, for constant-volume, constant-pressure, and limited-pressure ideal gas cycles. $\gamma = 1.3$, $Q^*/(c_v T_1) = 9.3(r_c - 1)/r_c$. For limited-pressure cycle, $p_3/p_1 = 33, 67, 100$.



© McGraw-Hill Education. All rights reserved. Any use is subject to the Terms of Use, Privacy Notice and copyright information.

Figure 5.8 Indicated mean effective pressure (imep) divided by maximum cycle pressure (p_3) as a function of compression ratio for constant-volume, constant-pressure, and limited-pressure cycles. Details same as Fig. 5.7.



Example 5.1 shows how ideal cycle equations relate residual and intake conditions with the gas state at point 1 in the cycle. An iterative procedure is required if intake conditions are specified.

Example

EXAMPLE 5.1

For $\gamma = 1.3$, compression ratio $r_c = 6$, and a stoichiometric mixture with intake temperature 300 K, find the residual gas fraction, residual gas temperature, and mixture temperature at point 1 in the constant-volume cycle for $p_e/p_i = 1$ (unthrottled operation) and 2 (throttled operation).

For a stoichiometric mixture, for isooctane,

$$Q^* = \frac{m_f}{m} Q_{\text{LHV}} = \left(\frac{m_f}{m_i}\right)\left(\frac{m_i}{m}\right) Q_{\text{LHV}} = \frac{44.38}{16.14}(1 - x_r) = 2.75(1 - x_r) \qquad \text{MJ/kg}$$

For $\gamma = 1.3$, $c_v = 946$ J/kg · K,

© McGraw-Hill Education. All rights reserved. Any use is subject to the Terms of Use, Privacy Notice and copyright information.

$$\frac{Q^*}{c_v T_1} = \frac{2.75 \times 10^6}{946 T_1}(1 - x_r) = \frac{2910}{T_1}(1 - x_r)$$

(*a*)

and Eqs. (5.35), (5.36), and (5.38), for $r_c = 6$ and $\gamma = 1.3$, become

$$x_r = \frac{1}{6} \frac{(p_e/p_i)^{0.769}}{6\left[1 + Q^*/(c_v T_1 \times 6^{0.3})\right]^{0.769}}$$

(*b*)

$$\frac{T_r}{T_1} = \left(\frac{p_e}{p_i}\right)^{0.23} \left(1 + \frac{Q^*}{c_v T_1 \times 6^{0.3}}\right)^{0.769}$$

(*c*)

$$\frac{T_1}{300} = \frac{1 - x_r}{1 - [1/(1.3 \times 6)]\,(p_e/p_i + 0.3)}$$

(*d*)

A trial-and-error solution of Eqs. (*a*) to (*d*) is required. It is easiest to estimate x_r, solve for T_1 from (*d*), evaluate $Q^*/(c_v T_1)$ from (*a*), and check the value of x_r assumed with that given by (*b*).

For $(p_e/p_i) = 1$ (unthrottled operation) the following solution is obtained:

$$x_r = 0.044, \qquad T_1 = 344\,\mathrm{K}, \qquad \frac{Q^*}{c_v T_1} = 8.1, \qquad T_r = 1316\,\mathrm{K}$$

For $(p_e/p_i) = 2$ the following solution is obtained:

$$x_r = 0.082, \qquad T_1 = 391\,\mathrm{K}, \qquad \frac{Q^*}{c_v T_1} = 6.8, \qquad T_r = 1580\,\mathrm{K}$$

[1] Note that if insufficient air is available for complete combustion of the fuel, Eq. (5.28) must be modified. The right-hand side of the equation should then be $\eta_c m_f Q_{\mathrm{LHV}}$, where η_c is the combustion efficiency given by Eq. (3.27).

© McGraw-Hill Education. All rights reserved. Any use is subject to the Terms of Use, Privacy Notice and copyright information.

5.5. FUEL-AIR CYCLE ANALYSIS

A more accurate representation of the properties of the working fluid inside the engine cylinder is to treat the unburned mixture as frozen in composition and the burned gas mixture as in equilibrium. Values for thermodynamic properties for these working fluid models can be obtained with the charts for unburned and burned gas mixtures described in Sec. 4.5, or computer codes such as those summarized in Sec. 4.7. When these working fluid models are combined with the ideal engine process models in Table 5.1, the resulting cycles are called fuel-air cycles.[1] The sequence of processes and assumptions are (with the notation of Fig. 5.2):

1-2 Reversible adiabatic compression of a mixture of air, fuel vapor, and residual gas without change in chemical composition.

2-3 Complete combustion (at constant volume or limited pressure or constant pressure), without heat loss, to burned gases in chemical equilibrium.

3-4 Reversible adiabatic expansion of the burned gases which remain in chemical equilibrium.

4-5-6 Ideal adiabatic exhaust blowdown and displacement processes with the burned gases fixed in chemical composition.

6-7-1 Ideal intake process with adiabatic mixing between residual gas and fresh mixture, both of which are fixed in chemical composition.

The basic equations for each of these processes have already been presented in Sec. 5.3. The use of the charts for a complete engine cycle calculation will now be illustrated.

5.5.1. SI Engine Cycle Simulation

The mixture conditions at point 1 must be known or must be estimated. The following approximate relationships can be used for this purpose:[3]

$$x_r = \left\{ 1 + \frac{T_r}{T_i} \left[r_c \left(\frac{p_i}{p_e} \right) - \left(\frac{p_i}{p_e} \right)^{(\gamma-1)/\gamma} \right] \right\}^{-1}$$

(5.47)

$$T_1 = T_r r_c x_r \left(\frac{p_i}{p_e} \right)$$

(5.48)

where T_r = 1400 K and $(\gamma - 1)/\gamma$ = 0.24 are appropriate average values to use for initial estimates.

Given the equivalence ratio ϕ and initial conditions T_1(K), $p_1 = p_i$ (Pa), and v_1(m^3/kg air), the state at point 2 at the end of compression through a volume ratio $v_1/v_2 = r_c$ is obtained from Eq. (4.25*a*) and the isentropic compression chart (Fig. 4.4). The compression work W_c(J/kg air) is found from Eq. (5.6) with the internal energy change determined from the unburned mixture chart (Fig. 4.3).

© McGraw-Hill Education. All rights reserved. Any use is subject to the Terms of Use, Privacy Notice and copyright information.

The use of charts to relate the state of the burned mixture to the state of the unburned mixture prior to combustion, for adiabatic constant-volume and constant-pressure combustion, has already been illustrated in Sec. 4.5.3.

For the *constant-volume cycle*,

$$u_3 = u_{s2} + \Delta u^\circ_{f,u} \quad \mathrm{J/kg\,air}$$

(5.49)

where
u_{s2} is the sensible internal energy of the unburned mixture at T_2 from Fig. 4.3 and
$\Delta u^\circ_{f,u}$ is the internal energy of formation of the unburned mixture [given by Eq. (4.32)]. Since $v_3 = v_2$, the burned gas state at point 3 can be located on the appropriate burned gas chart (Figs. 4.5 to 4.9).

For the *constant-pressure cycle*,

$$h_3 = h_{s2} + \Delta h^\circ_{f,u} \quad \mathrm{J/kg\,air}$$

(5.50)

Since $p_3 = p_2$, the burned gas state at point 3 can be located (by iteration) on the high-temperature burned gas charts, as illustrated by Example 4.5.

For the *limited-pressure cycle*, application of the first law to the mixture between states 2 and 3*b* gives

$$h_{3b} = u_{3b} + p_3 v_{3b} = u_2 + p_3 v_2 = u_{s2} + \Delta u^\circ_{f,u} + p_3 v_2 \quad \mathrm{J/kg\,air}$$

(5.51)

Since p_3 for a limited-pressure cycle is given, point 3*b* can be located on the appropriate burned gas chart.

The expansion process 3-4 follows an isentropic line from v_3 to v_4 ($v_4 = v_1$) on the burned mixture charts. Equation (5.9) [or (5.11) or (5.13)] now gives the expansion work W_E. The state of the residual gas at points 5 and 6 in the cycle is obtained by continuing this isentropic expansion from state 4 to $p = p_e$. The residual gas temperature can be read from the equilibrium burned gas chart; the residual gas fraction is obtained from Eq. (5.17). If values of T_r and x_r were assumed at the start of the cycle calculation to determine T_1, the assumed values can be checked against the calculated values and an additional cycle computation carried out with the new calculated values if required. The convergence is rapid.

The indicated fuel conversion efficiency is obtained from Eq. (5.1). The indicated mean effective pressure is obtained from Eq. (5.2). The volumetric efficiency (see Sec. 2.10) for a four-stroke cycle engine is given by

$$\eta_v = \frac{r_c(1 - x_r)}{v_1 \rho_{a,i}(r_c - 1)}$$

(5.52)

where $\rho_{a,i}$ is the inlet air density (in kilograms per cubic meter) and v_1 is the chart mixture specific volume (in cubic meters per kilogram of air in the original mixture).

© McGraw-Hill Education. All rights reserved. Any use is subject to the Terms of Use, Privacy Notice and copyright information.

Example

EXAMPLE 5.2

Calculate the performance characteristics of the constant-volume fuel-air cycle defined by the initial conditions of Examples 4.2, 4.3, and 4.5. The compression ratio is 8; the fuel is isooctane and the mixture is stoichiometric; the pressure and temperature inside the cylinder at the start of compression are 1 atm and 350 K, respectively. The notation of Fig. 5.2*a* is used to define the states at the beginning and end of each process.

Example 4.2 analyzed the compression process:

$$T_1 = 350\,\mathrm{K}, \quad p_1 = 101.3\,\mathrm{kPa}, \quad v_1 = 1\,\mathrm{m^3/kg\ air}, \qquad u_{s1} = 40\,\mathrm{kJ/kg\,air}$$
$$T_2 = 682\,\mathrm{K}, \quad p_2 = 1.57\,\mathrm{MPa}, \quad v_2 = 0.125\,\mathrm{m^3/kg\ air}, \quad u_{s2} = 350\,\mathrm{kJ/kg\,air}$$
$$W_{1\text{-}2} = W_C = -310\,\mathrm{kJ/kg\,air}$$

Example 4.5 analyzed the constant-volume adiabatic combustion process (it was assumed that the residual gas fraction was 0.08):

$$u_{b3} = u_{u2} = u_{s,u2} + \Delta u^{\circ}_{f,u} = -5\,\mathrm{kJ/kg\,air}, \quad s_3 = 9.33\,\mathrm{kJ/kg\,air \cdot K}$$
$$v_3 = v_2 = 0.125\,\mathrm{m^3/kg\,air}, \qquad T_3 = 2825\,\mathrm{K}, \qquad p_3 = 7100\,\mathrm{kPa}$$

Example 4.3 analyzed the expansion process, from these conditions after combustion at TC, to the volume v_4 at BC of 1 m^3/kg air:

$$T_4 = 1840\,\mathrm{K}, \qquad p_4 = 570\,\mathrm{kPa}, \qquad u_4 = -1540\,\mathrm{kJ/kg\,air}$$
$$W_{3\text{-}4} = W_E = 1535\,\mathrm{kJ/kg\,air}$$

To check the assumed residual gas fraction, the constant entropy expansion process on the chart in Fig. 4.8 is continued from state 4 to the exhaust pressure p_5 of 1 atm = 101.3 kPa. This gives v_5 = 4.0 m^3/kg air and T_5 = 1320 K. The residual fraction from Eq. (5.17) is

$$x_r = \frac{v_2}{v_5} = \frac{0.125}{4.0} = 0.031$$

which is significantly different from the assumed value of 0.08. The combustion and expansion calculations are now repeated with the new residual fraction of 0.031 (the compression process will not be changed significantly and the initial temperature is assumed fixed):

$$u_{b3} = 350 - 118.2 - 2956 \times 0.031 = 140\,\mathrm{kJ/kg\,air}$$

With
$v_3 = 0.125\,\mathrm{m^3/kg\,air}$, Fig. 4.8 gives

$$p_3 = 7270\,\mathrm{kPa}, \quad T_3 = 2890\,\mathrm{K}$$

© McGraw-Hill Education. All rights reserved. Any use is subject to the Terms of Use, Privacy Notice and copyright information.

Expand at constant entropy to
$v_4 = 1\,\mathrm{m^3/kg\,air}$:

$$p_4 = 595\,\mathrm{kPa}, \qquad T_4 = 1920\,\mathrm{K}, \quad u_4 = -1457\,\mathrm{kJ/kg\,air}$$
$$W_{3\text{-}4} = W_E = 1597\,\mathrm{kJ/kg\,air}$$

Continue expansion at constant entropy to the exhaust pressure, p_5 = 1 atm:

$$v_5 = 4\,\mathrm{m^3/kg\,air}, \quad T_5 = 1360\,\mathrm{K}$$

Equation (5.17) now gives the residual fraction

$$x_r = \frac{v_2}{v_5} = \frac{0.125}{4} = 0.031$$

which agrees with the value assumed for the second iteration.

The fuel conversion efficiency can now be calculated:

$$\eta_{f,i} = \frac{W_E + W_C}{m_f Q_{\mathrm{LHV}}}$$

where

$$m_f = \text{kg fuel/kg air at state 1} = \left(\frac{F}{A}\right)(1 - x_r)$$

Thus

$$\eta_{f,i} = \frac{1597 - 310}{0.0661 \times (1 - 0.031) \times 44.4 \times 10^3} = 0.45$$

The indicated mean effective pressure is

$$\mathrm{imep} = \frac{W_E + W_C}{V_d} = \frac{1597 - 310}{1 - 0.125} = 1470\,\mathrm{kPa}$$

or

$$\frac{\mathrm{imep}}{p_1} = 14.6$$

© McGraw-Hill Education. All rights reserved. Any use is subject to the Terms of Use, Privacy Notice and copyright information.

5.5.2. CI Engine Cycle Simulation

With a diesel engine fuel-air cycle calculation, additional factors must be taken into account. The mixture during compression is air plus a small amount of residual gas. At point 2 liquid fuel is injected into the hot compressed air at temperature $T_{2'}$; as the fuel vaporizes and heats up, the air is cooled. For a constant-volume mixing process which is adiabatic overall, the mixture internal energy is unchanged, that is:

$$m_f\left[u_{fg}+c_{v,f}(T_{2'}-T_0)\right]+m_a c_{v,a}(T_{2'}-T_2)=0$$

(5.53)

where
m_f is the mass of fuel injected,
u_{fg} is the latent heat of vaporization of the fuel,
$c_{v,f}$ $c_{v,f}$ is the specific heat at constant volume of the fuel vapor,
$T_{2'}$ is the mixture temperature (assumed uniform) after vaporization and mixing is complete,
m_a is the mass of air used, and
$c_{v,a}$ is the specific heat at constant volume of air. Substitution of typical values for fuel and air properties gives $(T_{2'}-T_2)\approx 70\,\mathrm{K}$ at full load. Localized cooling in a real engine will be greater.

The limited-pressure cycle is a better approximation to the diesel engine than the constant-pressure or constant-volume cycles. Note that because nonuniformities in the fuel/air ratio exist during and after combustion in the CI engine, the burned gas charts, which assume uniform composition, will not be as accurate an approximation to working fluid properties as they are for SI engines.

5.5.3. Results of Cycle Calculations

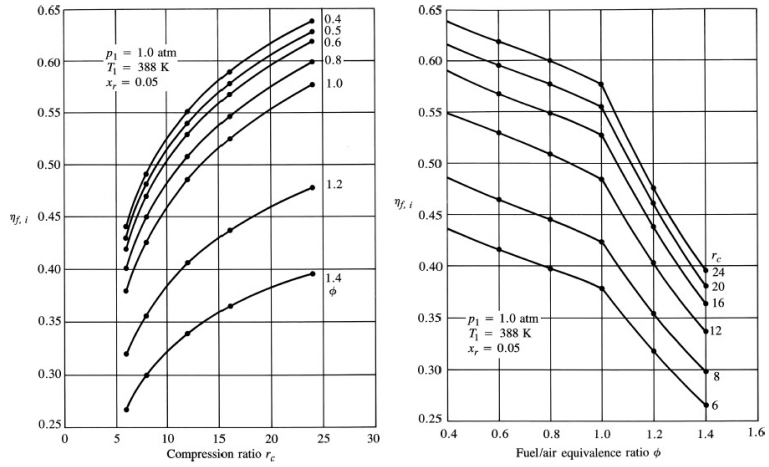
Extensive results of constant-volume fuel-air cycle calculations are available.[1,3,4] Efficiency is little affected by variables other than the compression ratio r_c and equivalence ratio ϕ. Figures 5.9 and 5.10 show the effect of variations in these two parameters on indicated fuel conversion efficiency and mean effective pressure. From the available results, the following conclusions can be drawn:

1. The effect of increasing the compression ratio on efficiency at a constant equivalence ratio is similar to that demonstrated by the constant γ constant-volume cycle analysis provided the appropriate value of γ is used. For a stoichiometric mixture, $\gamma=1.27$ in Eq. (5.31) matches the fuel-air cycle $\phi=1$ data well.
2. As the equivalence ratio is decreased below unity (i.e., the fuel-air mixture is made progressively leaner than stoichiometric), the efficiency increases. This occurs because the burned gas temperatures after combustion decrease, decreasing the burned gas specific heats and thereby increasing the effective value of γ over the expansion stroke. The efficiency increases because, for a given volume-expansion ratio, the burned gases expand through a larger temperature ratio prior to exhaust; therefore, per unit mass of fuel, the expansion stroke work is increased.
3. As the equivalence ratio increases above unity (i.e., the mixture is made progressively richer than stoichiometric), the efficiency decreases because lack of sufficient air for complete oxidation of the fuel more than offsets the effect of decreasing burned gas temperatures which decrease the mixture's specific heats.

© McGraw-Hill Education. All rights reserved. Any use is subject to the Terms of Use, Privacy Notice and copyright information.

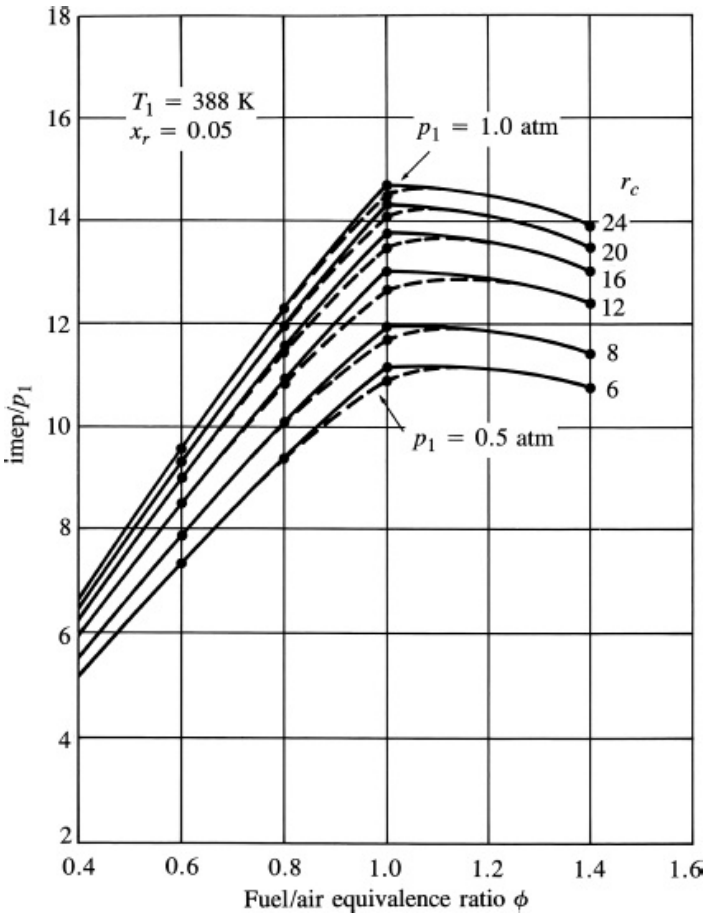
4. The mean effective pressure, from Eq. (5.2), is proportional to the product $\phi\eta_{f,i}$. This product is essentially constant between $\phi \approx 1.0$ and $\phi \approx 1.2$ (i.e., slightly rich of stoichiometric). For ϕ less than the value corresponding to this maximum, the decreasing fuel mass per unit displaced volume more than offsets the increasing fuel conversion efficiency. For ϕ greater than about 1.2, the decreasing fuel conversion efficiency (due to decreasing combustion efficiency) more than offsets the increasing fuel mass.
5. Variations in initial pressure, inlet temperature, residual gas fraction, and atmospheric moisture fraction have only a modest effect on the fuel conversion efficiency. The effects of variations in these variables on imep are more substantial, however, because imep depends directly on the initial charge density.[1]
6. Comparison of results from limited-pressure and constant-volume fuel-air cycles[1] shows that placing a realistic limit on the maximum pressure reduces the advantages of increased compression ratio on both efficiency and imep.

Figure 5.9 Fuel-air cycle results for indicated fuel conversion efficiency as a function of compression ratio and equivalence ratio. Fuel: octene. p_1 = 1 atm, T_1 = 388 K, x_r = 0.05. (From Edson and Taylor.[4])



© McGraw-Hill Education. All rights reserved. Any use is subject to the Terms of Use, Privacy Notice and copyright information.

Figure 5.10 *Fuel-air cycle results for indicated mean effective pressure as a function of equivalence ratio and compression ratio. Fuel: octene. p_1 = 1 atm, T_1 = 388 K, x_r = 0.05. (From Edson and Taylor.[4])*

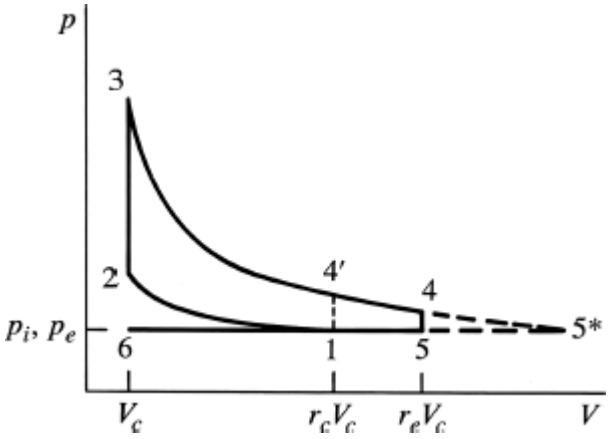


© McGraw-Hill Education. All rights reserved. Any use is subject to the Terms of Use, Privacy Notice and copyright information.

5.6. OVEREXPANDED ENGINE CYCLES

The gas pressure within the cylinder of a conventional four-stroke engine at exhaust valve opening is greater than the exhaust pressure. The available energy of the cylinder gases at this point in the cycle is then dissipated in the exhaust blowdown process. Additional expansion within the engine cylinder would increase the indicated work per cycle, as shown in Fig. 5.11, where expansion continues beyond point 4' (the conventional ideal cycle exhaust valve opening point) at $V_{4'} = r_c V_c$ to point 4 at $V_4 = r_e V_c$, where r_e is the volume expansion ratio. The exhaust stroke in this overexpanded cycle is 4-5-6. The intake stroke is 6-1. The area 14'451 has been added to the conventional cycle *p-V* diagram area, for the same fuel input, thereby increasing the engine's efficiency.

*Figure 5.11 Pressure-volume diagram for overexpanded engine cycle (1234561) and Atkinson cycle (1235*61). r_c and r_e are volumetric compression and expansion ratios, respectively.*



Complete expansion within the cylinder to exhaust pressure p_e (point 5*) is called the *Atkinson cycle*. Unthrottled operation is shown in Fig. 5.11; throttled operating cycles can also be generated. Many crank and valve mechanisms have been proposed to achieve this additional expansion. For example, it can be achieved in a conventional four-stroke cycle engine by suitable choice of exhaust valve opening and intake valve closing positions relative to BC. If the crank angle between exhaust valve opening and BC on the expansion stroke is less than the crank angle between BC and intake valve closing on the compression stroke, then the actual volumetric expansion ratio is greater than the actual volumetric compression ratio (these *actual* ratios are both less than the *nominal* compression ratio with normal valve timing).

The effect of overexpansion on efficiency can be estimated from an analysis of the ideal cycle shown inFig. 5.11. An ideal gas working fluid with specific heats constant throughout the cycle will be assumed. The indicated work per cycle for the overexpanded cycle is

$$W_{c,i} = m\left[(u_3 - u_4) - (u_2 - u_1) - p_1(v_4 - v_1)\right]$$

(5.54)

The isentropic relations for 1-2 and 3-4 are

$$\frac{T_2}{T_1} = r_c^{\gamma-1} \qquad \frac{T_3}{T_4} = r_e^{\gamma-1}$$

© McGraw-Hill Education. All rights reserved. Any use is subject to the Terms of Use, Privacy Notice and copyright information.

With Eq. (5.33) to relate T_3 and T_2, the following expression for indicated fuel conversion efficiency can be derived from Eqs. (5.1), (5.29), and (5.54):

$$\eta_{f,i} = 1 - \frac{1}{(rr_c)^{\gamma-1}}\left\{1 + \frac{c_v T_1}{Q^*} r_c^{\gamma-1}\left[1 - \gamma r^{\gamma-1} + (\gamma - 1)r^{\gamma}\right]\right\}$$

(5.55)

where

$$r = \frac{r_e}{r_c}$$

Note that the efficiency given by Eq. (5.55) is a function of load (via Q^*), and is a maximum at maximum load. This contrasts with the ideal constant-volume cycle efficiency [Eq. (5.31)], which is independent of load. The ratio r_e/r_c for complete expansion is given by

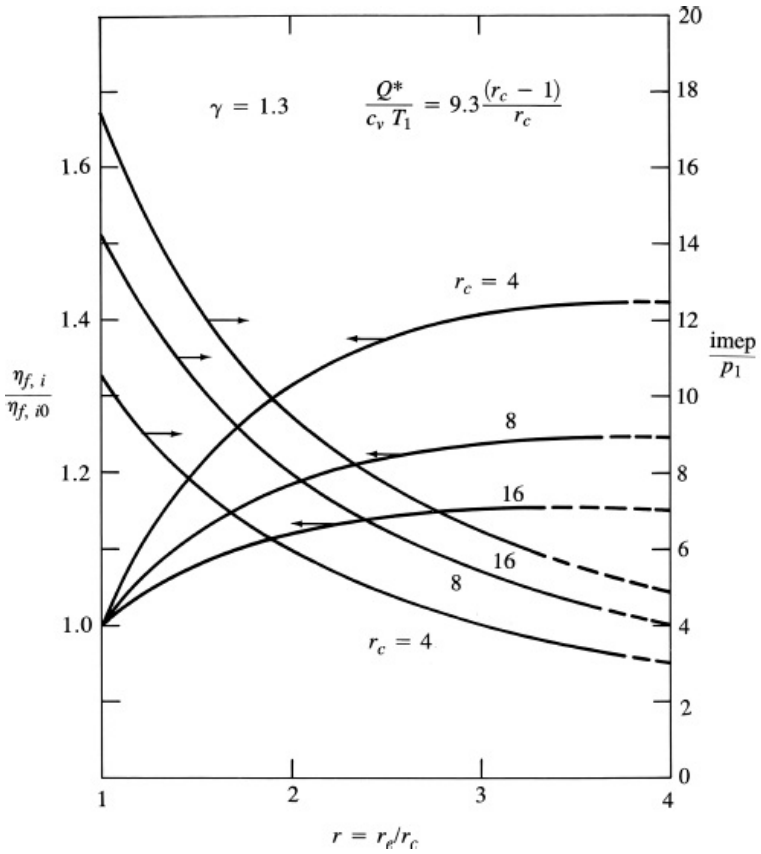
$$r^{\gamma} = 1 + \frac{Q^*}{c_v T_1 r_c^{\gamma-1}}$$

(5.56)

The effect of overexpansion on fuel conversion efficiency is shown in Fig. 5.12 for r_c = 4, 8, and 16 with γ = 1.3. The ratio of overexpanded cycle efficiency to the standard cycle efficiency is plotted against r. The Atkinson cycle (complete expansion) values are indicated by the transition from a continuous line to a dashed line. Significant increases in efficiency can be achieved, especially at low compression ratios.

© McGraw-Hill Education. All rights reserved. Any use is subject to the Terms of Use, Privacy Notice and copyright information.

Figure 5.12 Indicated fuel conversion efficiency and mean effective pressure for overexpanded engine cycle as a function of r_e/r_c. Efficiencies given relative to $r_e = r_c$ value, $\eta_{f,i0}$, $\gamma = 1.3$, $Q^*/(c_v T_1) = 9.3(r_c - 1)/r_c$. Solid to dashed line transition marks the complete expansion point (Atkinson cycle).



One major disadvantage of this cycle is that imep and power density decrease significantly because only part of the total displaced volume is filled with fresh charge. From Eqs. (5.2), (5.29), and the relations $V_d = V_1(r_e - 1)/r_c$ and $p_1 V_1 = mRT_1$, it follows that imep for the overexpanded cycle is given by

$$\frac{\text{imep}}{p_1} = \left(\frac{Q^*}{c_v T_1}\right)\left(\frac{1}{\gamma - 1}\right)\left(\frac{r_c}{r_e - 1}\right)\eta_{f,i} \tag{5.57}$$

Values of imep/p_1 are plotted in Fig. 5.12 as a function of $r(= r_e/r_c)$. The substantial decrease from the standard constant-volume cycle values at $r = 1$ is clear.

© McGraw-Hill Education. All rights reserved. Any use is subject to the Terms of Use, Privacy Notice and copyright information.

5.7. AVAILABILITY ANALYSIS OF ENGINE PROCESSES

5.7.1. Availability Relationships

Of interest in engine performance analysis is the amount of *useful work* that can be extracted from the gases within the cylinder at each point in the operating cycle. The problem is that of determining the maximum possible work output (or minimum work input) when a system (the charge within the cylinder) is taken from one specified state to another in the presence of a specified environment (the atmosphere). The first and second laws of thermodynamics together define this maximum or minimum work, which is best expressed in terms of the property of such a system-environment combination called *availability*[5] or sometimes *exergy*.[6,7]

Consider the system-atmosphere combination shown in Fig. 5.13. In the absence of mass flow across the system boundary, as the system changes from state 1 to state 2, the first and second laws give

$$\begin{aligned} W_{1\text{-}2} &= -(U_2 - U_1) + Q_{1\text{-}2} \\ Q_{1\text{-}2} &\leq T_0(S_2 - S_1) \end{aligned}$$

Combining these two equations gives the *total work* transfer:

$$W_{t,1\text{-}2} \leq -[(U_2 - U_1) - T_0(S_2 - S_1)]$$

(5.58)

The work done by the system against the atmosphere is not available for productive use. It must, therefore, be subtracted from the total work to obtain the *useful work transfer*:

$$W_{U,1\text{-}2} \leq -[(U_2 - U_1) + p_0(V_2 - V) - T_0(S_2 - S_1)]$$

(5.59)

The *maximum* useful work will be obtained when the final state of the system is in thermal and mechanical equilibrium with the atmosphere.[1] The *availability* of this system which is in communication with the atmosphere

$$A = U + p_0V - T_0S$$

(5.60)

is thus the property of the system-atmosphere combination which defines its capacity for useful work. The useful work such a system-atmosphere combination can provide, as the system changes from state 1 to state 2, is less than or equal to the change in availability:

$$W_{U,1\text{-}2} \leq -(A_2 - A_1)$$

(5.61)

© McGraw-Hill Education. All rights reserved. Any use is subject to the Terms of Use, Privacy Notice and copyright information.

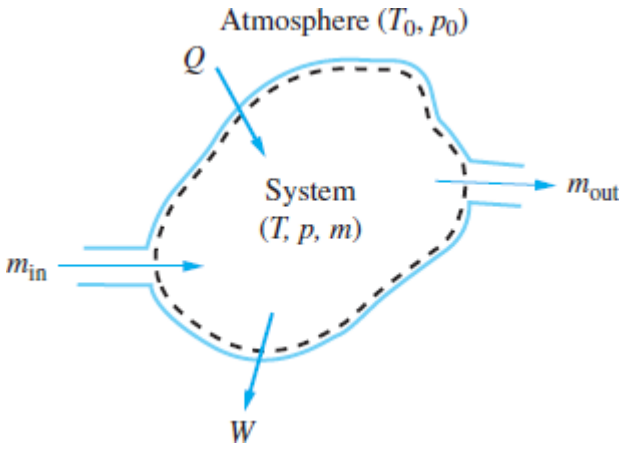
When mass flow across the system boundary occurs, the availability associated with this mass flow is

$$B = H - T_0 S$$

(5.62)

B is usually called the *steady-flow availability function*.

Figure 5.13 *System-atmosphere configuration for availability analysis.*



With these relations, an availability balance for the gas working-fluid system around the engine cycle can be carried out. For any process between specified end states which this system undergoes (interacting only with the atmosphere), the change in availability D*A* is given by

$$\Delta A = A_{in} - A_{out} - A_{destroyed}$$

(5.63)

The availability transfers in and out occur as a result of work transfers, heat transfers, and mass transfers across the system boundary. The availability transfer associated with a work transfer is equal to the work transfer. The availability transfer dA_Q associated with a heat transfer δQ occurring when the system temperature is T is given by

$$dA_Q = \delta Q \left(1 - \frac{T_0}{T}\right)$$

(5.64)

since both an energy and entropy transfer occurs across the system boundary. The availability transfer associated with a mass transfer is given by Eq. (5.62). Availability is destroyed by the irreversibilities that occur in any real process. The availability destroyed is given by

$$A_{destroyed} = T_0 \Delta S_{irrev}$$

(5.65)

where ΔS_{irrev} is the entropy increase associated with the irreversibilities occurring within the system boundary.[7,8]

© McGraw-Hill Education. All rights reserved. Any use is subject to the Terms of Use, Privacy Notice and copyright information.

5.7.2. Entropy Changes in Ideal Cycles

The ideal models of engine processes examined earlier in this chapter provide useful illustrative examples for availability analysis. First, however, we will consider the variation in the entropy of the cylinder gases as they proceed through these ideal operating cycles.

For an adiabatic reversible compression process, the entropy is constant. For the combustion process in each of the ideal gas standard cycles, the entropy increase can be calculated from the relations of Eq. (4.14) (with constant specific heats):

$$s - s_0 = c_v \ln\left(\frac{T}{T_0}\right) + R \ln\left(\frac{v}{v_0}\right) = c_p \ln\left(\frac{T}{T_0}\right) - R \ln\left(\frac{p}{p_0}\right)$$

For the constant-volume cycle:

$$S_3 - S_2 = m(s_3 - s_2) = mc_v \ln\left(\frac{T_3}{T_2}\right)$$

(5.66*a*)

For the constant-pressure cycle:

$$S_3 - S_2 = m(s_3 - s_2) = mc_p \ln\left(\frac{T_3}{T_2}\right)$$

(5.66*b*)

For the limited-pressure cycle:

$$S_{3b} - S_2 = mc_v \ln\left(\frac{T_{3a}}{T_2}\right) + mc_p \ln\left(\frac{T_{3b}}{T_{3a}}\right) = mc_v \ln \alpha + mc_p \ln \beta$$

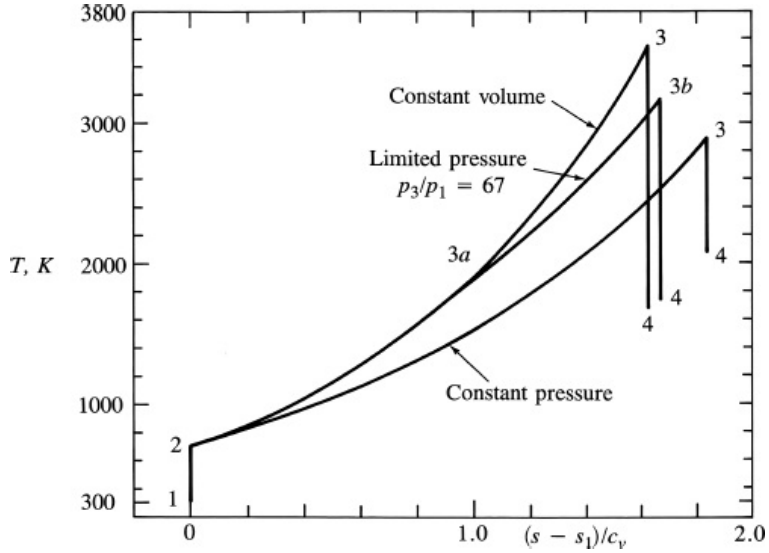
(5.66*c*)

with α and β defined by Eq. (5.42).

Since the expansion process, after combustion is complete, is adiabatic and reversible, there is no further change in entropy, 3 to 4 (or 3*b* to 4). Figure 5.14 shows the entropy changes that occur during each process of these three ideal engine operating cycles, calculated from the above equations, on a *T*-*s* diagram. The three cycles shown correspond to those of the *p*-*V* diagrams of Fig. 5.6 with $r_c = 12$, $\gamma = 1.3$, and $Q^*/(c_v T_1) = 8.525$. Since the combustion process was assumed to be adiabatic, the increase in entropy during combustion clearly demonstrates the irreversible nature of this process.

© McGraw-Hill Education. All rights reserved. Any use is subject to the Terms of Use, Privacy Notice and copyright information.

Figure 5.14 Temperature-entropy diagram for ideal gas constant-volume, constant-pressure, and limited-pressure cycles. Assumptions same as in Fig. 5.6.



5.7.3. Availability Analysis of Ideal Cycles

An availability analysis for each process in the ideal cycle illustrates the magnitude of the availability transfers and where the losses in availability occur.[9] In general, for the system of Fig. 5.4 in communication with an atmosphere at p_0, T_0 as indicated in Fig. 5.13, the change in availability between states *i* and *j* during the portion of the cycle when the valves are closed is given by

$$A_j - A_i = m(a_j - a_i) = m\left[(u_j - u_i) + p_0(v_j - v_i) - T_0(s_j - s_i)\right]$$

(5.67)

The appropriate normalizing quantity for these changes in availability is the availability of the fuel supplied to the engine cylinder each cycle, $m_f(-\Delta\gamma_{298})$[2] (see Sec. 3.6.2). However, it is more convenient to use $m_f(-\Delta h_{298})$[3]> = $m_f Q_{LHV}$ as the normalizing quantity since it can be related to the temperature rise during combustion via Eq. (5.28). As shown in Table 3.3, these two quantities differ by only a few percent for common hydrocarbon fuels. Equation (5.67), with Eq. (5.29), then becomes

$$\frac{A_j - A_i}{m_f Q_{\mathrm{LHV}}} = \frac{m(a_j - a_i)}{m_f Q_{\mathrm{LHV}}} = \frac{a_j - a_i}{Q^*}$$

(5.68)

The compression process is isentropic, so:

© McGraw-Hill Education. All rights reserved. Any use is subject to the Terms of Use, Privacy Notice and copyright information.

$$\begin{aligned}\frac{A_2 - A_1}{m_f Q_{\text{LHV}}} &= \frac{a_2 - a_1}{Q^*} = \frac{(u_2 - u_1) + p_0(v_2 - v_1)}{Q^*} \\ &= \frac{c_v T_1}{Q^*}\left[\left(\frac{T_2}{T_1} - 1\right) - (\gamma - 1)\left(1 - \frac{V_2}{V_1}\right)\right] \\ &= \frac{c_v T_1}{Q^*}\left[(r_c^{\gamma} - 1) - (\gamma - 1)\left(1 - \frac{1}{r_c}\right)\right]\end{aligned}$$

(5.69)

where we have assumed $p_0 = p_1$. The first term in the square brackets is the compression stroke work transfer. The second term is the work done by the atmosphere on the system, which is subtracted because it does not increase the *useful work* which the system-atmosphere combination can perform.

During combustion, for the constant-volume cycle, the volume and internal energy remain unchanged [Eqs. (5.7*a, b*)]. Thus

$$\begin{aligned}\frac{A_3 - A_2}{m_f Q_{\text{LHV}}} &= \frac{a_3 - a_2}{Q^*} = -\frac{T_0(s_3 - s_2)}{Q^*} \\ &= -\frac{c_v T_0}{Q^*}\ln\left(\frac{T_3}{T_2}\right) = -\frac{c_v T_0}{Q^*}\ln\left(1 + \frac{Q^*}{c_v T_1 r_c^{\gamma - 1}}\right)\end{aligned}$$

(5.70)

This loss in availability results from the increase in entropy associated with the irreversibilities of the combustion process. This lost or destroyed availability, as a fraction of the initial availability of the fuel-air mixture, decreases as the compression ratio increases (since T_2 increases as the compression ratio increases, T_3/T_2 decreases for fixed heat addition) and increases as Q^* decreases [e.g., when the mixture is made leaner; see Eq. (5.46)]. The changes in availability during combustion for the constant-pressure and limited-pressure cycles are more complex because there is a transfer of availability out of the system equal to the expansion work transfer which occurs.

For the constant-volume cycle expansion stroke:

$$\begin{aligned}\frac{A_4 - A_3}{m_f Q_{\text{LHV}}} &= \frac{a_4 - a_3}{Q^*} = \frac{(u_4 - u_3) + p_0(v_4 - v_3)}{Q^*} \\ &= \frac{c_v T_3}{Q^*}\left[\left(\frac{T_4}{T_3} - 1\right) + (\gamma - 1)\left(\frac{p_0}{p_3}\right)\left(\frac{V_4}{V_3} - 1\right)\right] \\ &= \left[\left(1 + \frac{c_v T_1 r_c^{\gamma - 1}}{Q^*}\right)\left(1 - \frac{1}{r_c^{\gamma - 1}}\right) - (\gamma - 1)\frac{c_v T_1}{Q^*}\left(\frac{r_c - 1}{r_c}\right)\right]\end{aligned}$$

(5.71)

The availability of the exhaust gas at state 4 relative to its availability at (T_1, p_1) is given by

$$\frac{A_4 - A_1}{m_f Q_{\text{LHV}}} = \frac{c_v T_1}{Q^*}\left[\left(\frac{T_4}{T_1} - 1\right) - \frac{T_0}{T_1}\ln\left(\frac{T_4}{T_1}\right)\right]$$

© McGraw-Hill Education. All rights reserved. Any use is subject to the Terms of Use, Privacy Notice and copyright information.

(5.72)

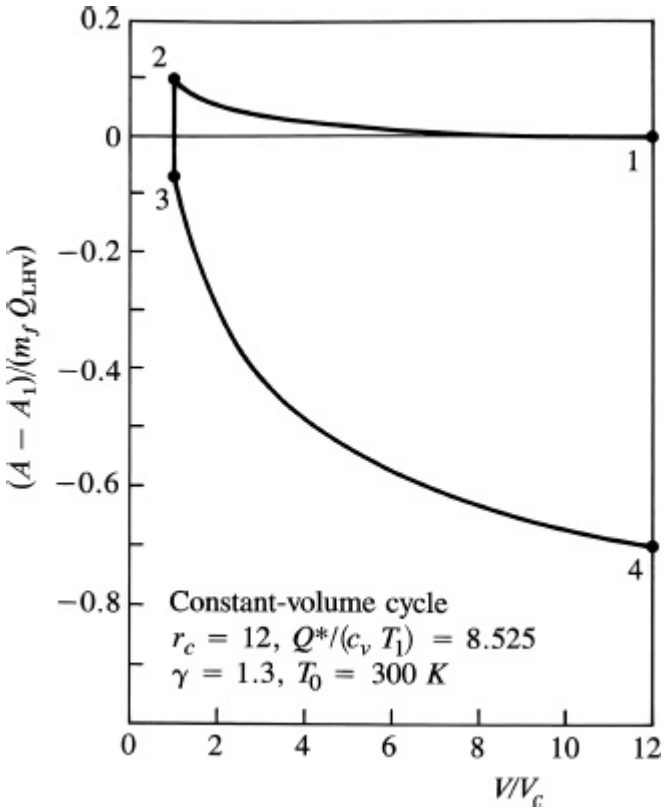
The availability of the gases inside the cylinder relative to their availability at (T_1, p_1) over the compression and expansion strokes of the constant-volume operating cycle example used in Figs. 5.6 and 5.14 is shown in Fig. 5.15. Equations (5.69) and (5.71), with T_2 and T_4 replaced by the appropriate temperatures intermediate between T_1 and T_2 and T_3 and T_4, respectively, were used to compute the variations during compression and expansion. Table 5.3 summarizes the changes in availability during each process and the availability of the cylinder gases, at the beginning and end of each process, relative to the datum for the atmosphere (1 atm, 300 K). The availability at state 1 of the fuel, air, residual-gas mixture is $(1.0286 + 0.0008)m_f Q_{\mathrm{LHV}}$. 1.0286 is the ratio $(-\Delta g^\circ_{298})/(-\Delta h^\circ_{298})$ for isooctane (see Table 3.3). The second number, 0.0008, allows for the difference between T_1 and T_0. Because both work-transfer processes in this ideal cycle case are reversible, the fuel conversion efficiency $\eta_{f,i}$ is given by $(A_3 - A_4)/(m_f Q_{\mathrm{LHV}}) - (A_2 - A_1)/(m_f Q_{\mathrm{LHV}})$. It is, of course, equal to the value obtained for r_c = 12 and γ = 1.3 from the formula for efficiency Eq. (5.31), obtained previously. The availability conversion efficiency is $\eta_{f,i}/1.0286$. Note that it is the availability destroyed during combustion, plus the inability of this ideal constant-volume cycle to use the availability remaining in the gas at state 4, that decrease the availability conversion efficiency below unity. Both these loss mechanisms decrease in magnitude, relative to the fuel availability, as the compression ratio increases. This is the fundamental reason why engine indicated efficiency increases with an increasing compression ratio.

Table 5.3 Availability changes in constant-volume cycle

Process or state	$\frac{A_j - A_i}{m_f Q_{\mathrm{LHV}}}$	$\frac{A_i}{m_f Q_{\mathrm{LHV}}}$
1		1.0294
1-2	0.0976	
2		1.1270
2-3	−0.1710	
3		0.9560
3-4	−0.6237	
4		0.3323
Fuel conversion efficiency $\eta_{f,i}$	0.526	
Availability conversion efficiency $\eta_{a,i}$	0.511	
$r_c = 12,\ \gamma = 1.3,\ Q^*/(c_v T_1) = 8.525,\ T_0 = 300\,\mathrm{K},\ T_1 = 333\,\mathrm{K}.$		

© McGraw-Hill Education. All rights reserved. Any use is subject to the Terms of Use, Privacy Notice and copyright information.

Figure 5.15 Availability of cylinder charge relative to availability at state 1 for constant-volume ideal gas cycle as a function of cylinder volume. Availability made dimensionless by $m_f Q_{LHV}$. Assumptions as in Fig. 5.6.



5.7.4. Effect of Equivalence Ratio

The fuel-air cycle with its more accurate models for working fluid properties can be used to examine the effect of variations in the fuel/air equivalence ratio on the availability conversion efficiency. Figure 5.16 shows the temperature attained and the entropy rise that occurs in constant-volume combustion of a fuel-air mixture of different equivalence ratios, following isentropic compression from ambient temperature and pressure through different volumetric compression ratios.[8] The entropy increase is the result of irreversibilities in the combustion process and mixing of complete combustion products with excess air. The significance of these combustion-related losses the destruction of availability that occurs in this process is shown in Fig. 5.17 where the availability after constant-volume combustion divided by the availability of the initial fuel-air mixture is shown as a function of equivalence ratio for compression ratios of 12 and 36.[8] The loss of availability increases as the equivalence ratio decreases below 1.0.[4] The combustion loss is a stronger function of the rise in temperature and pressure which occurs than of the change in the specific heat ratio that occurs.

© McGraw-Hill Education. All rights reserved. Any use is subject to the Terms of Use, Privacy Notice and copyright information.

Figure 5.16 Temperature and entropy of combustion products after constant-volume combustion following isentropic compression from ambient conditions through specified compression ratio as a function of compression ratio and equivalence ratio. (From Flynn et al.[8])

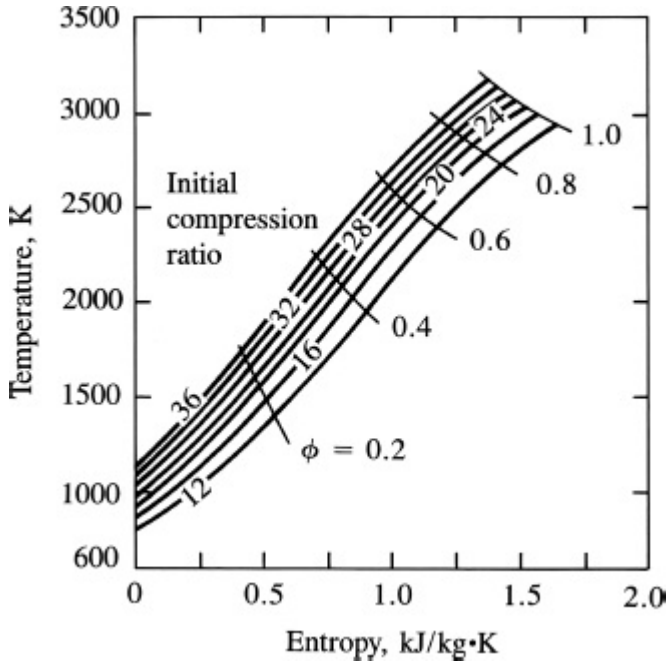
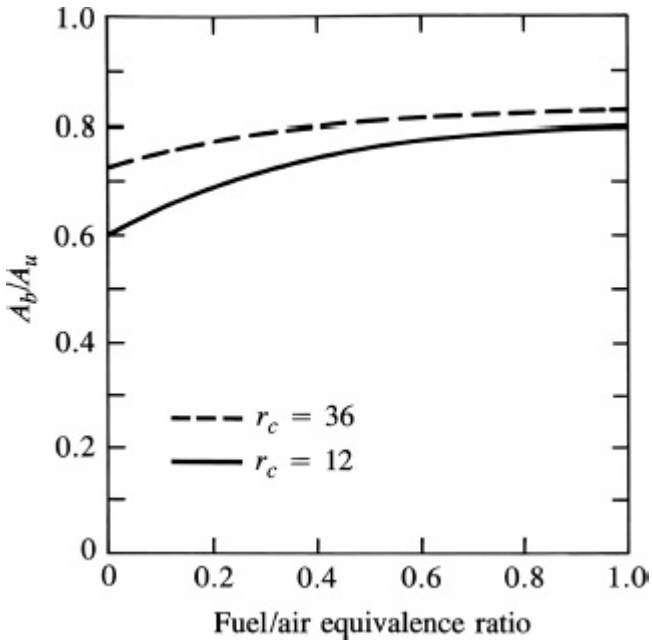


Figure 5.17 Availability of combustion products after constant-volume combustion relative to availability before combustion following isentropic compression from ambient through specified compression ratio as a function of equivalence ratio. (From Flynn et al.[8])



Why then does engine efficiency increase with a decreasing equivalence ratio as shown in Fig. 5.9? The reason is that the expansion stroke work transfer, as a fraction of the fuel availability, increases as the equivalence ratio decreases; hence, the availability lost in the exhaust process, again expressed as a fraction of the fuel availability, decreases. This increase in the expansion stroke work as a fraction of the fuel availability, as the equivalence ratio decreases, more than offsets the increase in the availability lost during combustion; so the availability conversion efficiency (or the fuel conversion efficiency which closely approximates it) increases.

© McGraw-Hill Education. All rights reserved. Any use is subject to the Terms of Use, Privacy Notice and copyright information.

[1] The issue of chemical equilibrium with the atmosphere must also be considered. Attainment of chemical equilibrium with the environment requires the capacity to extract work from the partial pressure differences between the various species in the working fluid and the partial pressures of those same species in the environment. This would require such devices as ideal semipermeable membranes and efficient low input pressure, high-pressure ratio, expansion devices (which are not generally available for mobile power plant systems). Inclusion of these additional steps to achieve full equilibrium beyond equality of temperature and pressure is inappropriate.[8]

[2] Δg_{298} is the Gibbs free energy change for the combustion reaction, per unit mass of fuel.

[3] Δh_{298} is the enthalpy change for the combustion reaction, again per unit mass of fuel.

[4] This is consistent with the ideal gas standard cycle result [Eq. (5.70)]. As ϕ decreases, so does $Q^*/(c_v T_1)$. The factor which multiplies the natural logarithm (which increases) has a greater impact than the logarithmic term (which decreases).

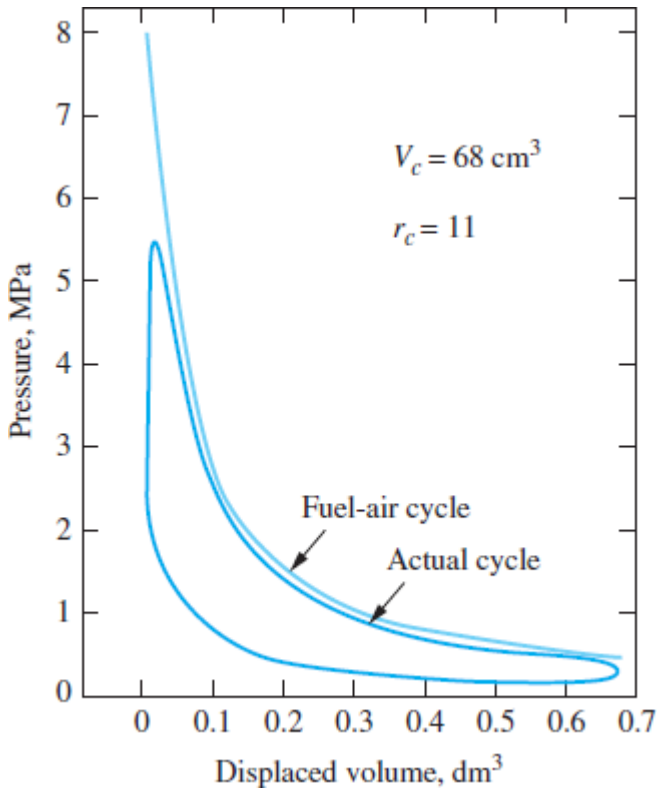
© McGraw-Hill Education. All rights reserved. Any use is subject to the Terms of Use, Privacy Notice and copyright information.

5.8. COMPARISON WITH REAL ENGINE CYCLES

To put these ideal models of engine processes in perspective, this chapter will conclude with a brief discussion of the additional effects which are important in real engine processes.

A comparison of a real engine *p-V* diagram over the compression and expansion strokes with an equivalent fuel-air cycle analysis is shown in Fig. 5.18.[4] The real engine and the fuel-air cycle have the same geometric compression ratio, fuel chemical composition and equivalence ratio, residual fraction, and mixture density before compression. Midway through the compression stroke, the pressure in the fuel-air cycle has been made equal to the real cycle pressure.[1] The compression stroke pressures for the two cycles essentially coincide. Modest differences in pressure during intake and the early part of the compression process result from the pressure drop across the intake valve during the intake process and the closing of the intake valve 40 to 60° after BC in the real engine. The expansion stroke pressures for the engine fall below the fuel-air cycle pressures for the following reasons: (1) heat transfer from the burned gases to the walls; (2) finite time required to burn the charge; (3) exhaust blowdown loss due to opening the exhaust valve before BC; (4) gas flow into crevice regions and leakage past the piston rings; (5) incomplete combustion of the charge.

Figure 5.18 Pressure-volume diagram for actual spark-ignition engine compared with that for equivalent fuel-air cycle. r_c = 11. (From Edson and Taylor.[4])



These differences, in decreasing order of importance, are described below. Together, they contribute to the enclosed area on the *p-V* diagram for a properly adjusted engine with optimum timing being about 85% of the enclosed area of an equivalent fuel-air cycle *p-V* diagram. The indicated fuel conversion or availability conversion efficiency of the actual engine is therefore about 0.85 times the efficiency calculated for the fuel-air cycle. Use is often made of this ratio to estimate the performance of actual engines from fuel-air cycle results.[2] To estimate the imep of actual engines from the fuel-air cycle imep/p_1 data in Fig. 5.10, an additional adjustment is required for the mass of mixture in the cylinder. The indicated efficiency is the ratio of work transferred to the piston to the in-cylinder fuel chemical energy. If the actual engine in-cylinder mass is different from the in-

© McGraw-Hill Education. All rights reserved. Any use is subject to the Terms of Use, Privacy Notice and copyright information.

cylinder mass in the equivalent fuel-air cycle, the work produced will be different by about the same percentage, so mass discrepancies cancel out. However, imep—the normalized work per cycle—is a performance parameter which does depend on the amount of fuel chemical energy in the cylinder. Mixture temperature and pressure, and cylinder volume, at time of intake valve closing affect the mass trapped inside the cylinder. So differences between values in the actual engine and the equivalent fuel-air cycle will affect the actual engine imep, and adjustments should be made. Typically imep (actual engine) is about 0.85 to 1.0 times the imep of the equivalent fuel-air cycle. The lower end of the range corresponds to part load (lower imep) levels; the higher end of the range corresponds to higher loads.

1. *Heat transfer*. Heat transfer from the unburned mixture to the cylinder walls has a negligible effect on the *p-V* line for the compression process. Heat transfer from the burned gases is much more important (see Chap. 12). Due to heat transfer during combustion, the pressure at the end of combustion in the real cycle will be lower. During expansion, heat transfer will cause the gas pressure in the real cycle to fall below an isentropic expansion line as the volume increases. A decrease in efficiency results from this heat loss.

2. *Finite combustion time*. In an SI engine with spark-timing adjusted for optimum efficiency, combustion typically starts 10 to 40 crank angle degrees before TC, is half complete at about 8° after TC, and is essentially complete 30 to 40° after TC. Peak pressure occurs at about 13 to 15° after TC (see Fig. 1.9). In a diesel engine, the burning process starts shortly before TC. The pressure rises rapidly to a peak some 5 to 10° after TC since the initial rate of burning is fast. However, the final stages of burning are much slower, and combustion continues until 40 to 50° after TC (see Fig. 1.24). Thus, the peak pressure in the engine is substantially below the fuel-air cycle peak pressure value because combustion continues until well after TC when the cylinder volume is much greater than the clearance volume. After peak pressure, expansion stroke pressures in the engine are higher than fuel-air cycle values in the absence of other loss mechanisms because less work has been extracted from the cylinder gases. A comparison of the constant-volume and limited-pressure cycles in Fig. 5.6 demonstrates this point.

   For spark or fuel-injection timing which is retarded from the optimum for maximum efficiency, the peak pressure in the real cycle will be lower, and expansion stroke pressures after the peak pressure will be higher than in the optimum timing cycle.

3. *Exhaust blowdown loss*. In the real engine operating cycle, the exhaust valve is opened some 50° before BC to reduce the pressure during the first part of the exhaust stroke in four-stroke engines, and to allow time for scavenging in two-stroke engines. The gas pressure at the end of the expansion stroke is therefore reduced below the isentropic line. A decrease in expansion-stroke work transfer results.

4. *Crevice effects and leakage*. As the cylinder pressure increases, gas flows into crevices such as the regions between the piston, piston rings, and cylinder wall. These crevice regions can comprise a percent or so of the clearance volume. This flow reduces the mass in the volume above the piston crown, and this flow is cooled by heat transfer to the crevice walls. In premixed charge engines, some of this crevice gas is unburned and some of it will not burn. Though much of this gas returns to the cylinder later in the expansion, a fraction, from behind and between the piston rings, flows into the crankcase. However, leakage in a well-designed and maintained engine is small (usually less than one percent of the charge). All these effects reduce the cylinder pressure during the latter stages of compression, during combustion, and during expansion below the value that would result if crevice and leakage effects were absent.

5. *Incomplete combustion*. Combustion of the cylinder charge is incomplete; the exhaust gases contain combustible species. For example, in spark-ignition engines the hydrocarbon emissions from a warmed-up engine (which come largely from the crevice regions) are about 2% of the fuel mass under normal operating conditions; carbon monoxide and hydrogen in the exhaust contain an additional 2 to 3% or more of the fuel energy, even with excess air present (see Sec. 4.9). Hence, the chemical energy of the fuel which is released in the actual engine is about 5% less than the chemical energy of the fuel inducted, that is, the combustion efficiency (see Sec. 3.5.5) is about 95%. The fuel-air cycle pressures after combustion will be higher than engine pressures because complete combustion is assumed. In diesel engines, the combustion inefficiency is usually less, about 1 to 2%, so this effect is smaller.

© McGraw-Hill Education. All rights reserved. Any use is subject to the Terms of Use, Privacy Notice and copyright information.

5.8.1. Summary

The effect of all these loss mechanisms on engine efficiency is best defined by an availability balance for the real engine cycle. A limited number of such calculations have been published (e.g., Refs. 8, 10, and 11). Table 5.4 shows the magnitude of the loss in availability (as a fraction of the initial availability) that occurs due to real cycle effects in a typical naturally-aspirated diesel engine.[10] The combustion and exhaust losses are present in the ideal cycle models also (they are smaller, however[9]). The loss in availability due to heat losses, flow or aerodynamic losses, and mechanical friction are real engine effects.

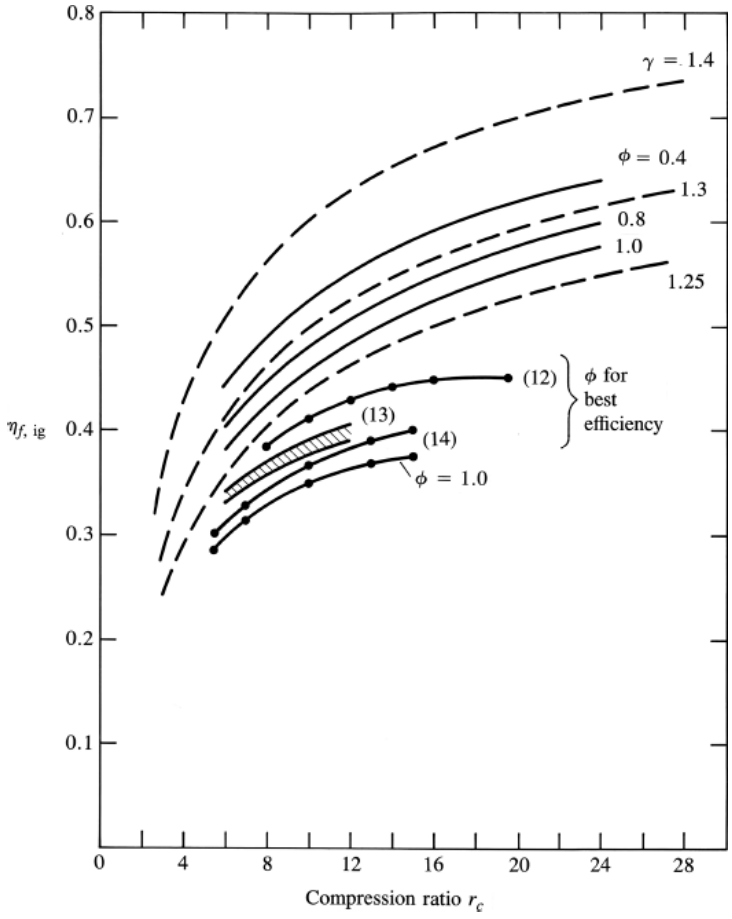
Table 5.4 Availability losses in naturally-aspirated diesel

Loss mechanism	Loss, fraction of fuel availability
Combustion	0.225
Exhaust	0.144
Heat transfer	0.135
Aerodynamic	0.047
Mechanical friction	0.048
Total losses	0.599
Availability conversion efficiency (brake)	0.401
Source: Traupel.[10]	

Figure 5.19 shows standard and fuel-air cycle efficiencies as a function of the compression ratio compared with engine indicated efficiency data. The top three sets of engine data are for the best efficiency air/fuel ratio. Differences in the data are in part due to different fuels [(12) isooctane; (13) gasoline; (14) propane] which affect efficiency slightly through their different composition and heating values (see Table D.4). They also result from different combustion chamber shapes which affect the combustion rate and heat transfer. The trends in the data with increasing compression ratio and the $\phi = 0.8$ fuel-air cycle curve (which corresponds approximately to the actual air/fuel ratios used) are similar. The factor of 0.8 relating these older engine and fuel-air cycle efficiencies holds approximately. At compression ratios above about 15, however, the data show that the indicated efficiency of actual engines becomes essentially constant. Increasing crevice and heat losses offset the calculated ideal cycle efficiency increase as the compression ratio is raised above this value. The standard ideal gas cycle analysis results, with an appropriate choice for the value of γ (1.25 to 1.3), correspond closely to the fuel-air cycle analysis results.

© McGraw-Hill Education. All rights reserved. Any use is subject to the Terms of Use, Privacy Notice and copyright information.

Figure 5.19 Indicated fuel conversion efficiency as a function of compression ratio for ideal gas constant-volume cycle (dashed lines, γ = 1.25, 1.3, 1.4) and fuel-air cycle (solid lines, ϕ = 0.4, 0.8, 0.1). Also shown are available engine data for equivalence ratios given: best efficiency ϕ;[12–14] ϕ = 1.[14]



The ideal cycle provides a convenient but crude approximation to the real engine operating cycle. It is useful for illustrating the thermodynamic principles of engine operation. It can also provide approximate estimates of trends as major engine parameters change. The weakest link in these ideal cycles is the modeling of the combustion processes in SI and CI engines. None of the models examined in this chapter are sufficiently close to reality to provide accurate predictions of engine performance. More sophisticated models of the spark-ignition and diesel engine operating cycles have been developed and are discussed in Chap. 14.

[1] Note that in the fuel-air cycle with idealized valve timing, the compression process starts immediately after BC. In most engines, charge compression starts later, close to the time that the intake valve closes some 30 to 60° after BC. This matching process is approximate.

[2] As actual engines continue to improve, this ratio increases. Historically, a value of about 0.8 has been used to relate the indicated performance of actual engines to equivalent fuel-air cycle predictions.[1] The indicated efficiency of modern engines has steadily increased over the past few decades: the indicated efficiency of a spark-ignition or diesel engine is now about 0.85 times the equivalent fuel-air cycle efficiency for the same values of r_c, ϕ, and initial conditions.

© McGraw-Hill Education. All rights reserved. Any use is subject to the Terms of Use, Privacy Notice and copyright information.

5.9. PROBLEMS

5.1. Many diesel engines can be approximated by a limited-pressure cycle. In a limited-pressure cycle, a fraction of the fuel is burnt at constant volume and the remaining fuel is burnt at constant pressure. Use this cycle approximation with $\gamma = c_p/c_v = 1.3$ to analyze the following problem:

Inlet conditions:	p_1 = 1.0 bar, T_1 = 289 K
Compression ratio:	15:1
Heat added during combustion:	43,000 kJ/kg of fuel
Overall fuel/air ratio:	0.045 kg fuel/kg air

a. Half of the fuel is burnt at constant volume, then half at constant pressure. Draw a p-V diagram and compute the fuel conversion efficiency of the cycle.

b. Compare the efficiency and peak pressure of the cycle with the efficiency and peak pressure that would be obtained if all of the fuel were burnt at constant pressure or at constant volume.

5.2. It is desired to increase the output of a spark-ignition engine by either (1) raising the compression ratio from 8 to 10 or (2) increasing the intake pressure from 1.0 bar to 1.5 bar. Using the constant-volume cycle as a model for engine operation, which procedure will give:

a. The highest cycle pressure?

b. The highest efficiency?

c. The highest mep?

Assume $\gamma = 1.3$ and $(m_f Q_{HV})/(mc_v T_1) = 9.3(r_c = 1)/r_c$.

5.3.

a. Use the ideal gas cycle with constant-volume combustion to describe the operation of an SI engine with a compression ratio of 9. Find the pressure and temperature at points 2, 3, 4, and 5 on Fig. 5.2*a*. Assume a pressure of 100 kPa and a temperature of 320 K at point 1. Assume $m_f/m = 0.06$, $c_v = 946$ J/kg · K, $\gamma = 1.3$. Q_{LHV} for gasoline is 44 MJ/kg.

b. Find the indicated fuel conversion efficiency and imep for this engine under these operating conditions.

5.4. A spark-ignition engine is throttled when operating at part load (the inlet pressure is reduced) while the fuel/air ratio is held essentially constant. Part-load operation of the engine is modeled by the cycle shown in Fig. 5.2*d*; the inlet air is at pressure p_1, the exhaust pressure is atmospheric p_a, and the ambient temperature is T_a. Derive an expression for the *decrease* in net indicated fuel conversion efficiency due to throttling from the ideal constant-volume cycle efficiency, and show that it is proportional to $(p_a/p_1 - 1)$. Assume mass fuel ≪ mass air.

5.5. Use a limited-pressure cycle analysis to obtain a plot of indicated fuel conversion efficiency versus p_3/p_1 for a compression ratio of 15 with light diesel oil as fuel. Assume $m_f/m = 0.04$, $T_1 = 45°C$. Use $\gamma = 1.3$ and $c_v = 946$ J/kg · K.

5.6. Explain why constant-volume combustion gives a higher indicated fuel conversion efficiency than constant-pressure combustion for the same compression ratio.

© McGraw-Hill Education. All rights reserved. Any use is subject to the Terms of Use, Privacy Notice and copyright information.

5.7. Two engines are running at a bmep of 250 kPa. One is an SI engine with the throttle partially closed to maintain the correct load. The second engine is a naturally-aspirated CI engine which requires no throttle. Mechanical friction mep for both engines is 100 kPa. If the intake manifold pressures for the SI and CI engines are 25 kPa and 100 kPa, respectively, and both exhaust manifold pressures are 105 kPa, use an ideal cycle model to estimate and compare the *gross* and *net* imep of the two engines. You may neglect the pressure drop across the valves during the intake and exhaust processes.

5.8.

a. Plot net imep versus p_i for 20 kPa < p_i < 100 kPa for a constant-volume cycle using the following conditions: m_f/m = 0.06, T_1 = 40°C, c_v = 946 J/kg · K, γ = 1.3, r_c = 9.5, Q_{LHV} = 44 MJ/kg fuel. Assume p_e = 100 kPa.

b. What additional information is necessary to draw a similar plot for the engine's indicated torque, and indicated power?

5.9.

a. Draw a diagram similar to those in Fig. 5.2 for a supercharged cycle with constant-pressure combustion.

b. Use the ideal gas cycle with constant-pressure combustion to model an engine with a compression ratio of 14 through such a supercharged cycle. Find the pressure and temperature at points corresponding to 2, 3, 4, and 5 in Fig. 5.2. Assume a pressure of 200 kPa and temperature of 325 K at point 1, and a pressure of 100 kPa at points 5 and 6. m_f/m = 0.03 and the fuel is a light diesel oil.

c. Calculate the gross and net indicated fuel conversion efficiency and imep for this engine under these operating conditions.

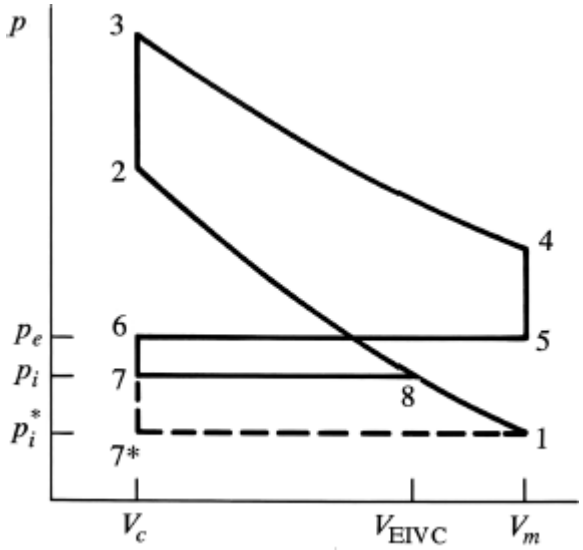
5.10. One method proposed for reducing the pumping work in throttled spark-ignition engines is *early intake valve closing* (EIVC). The ideal cycle *p-V* diagram shown illustrates the concept. The EIVC cycle is 1-2-3-4-5-6-7-8-1 (the conventional throttled cycle is 1-2-3-4-5-6-7*-1). With EIVC, the inlet manifold is held at a pressure p_i (which is higher than the normal engine intake pressure, p_i^*), and the inlet valve is closed *during* the inlet stroke at 8. The trapped fresh charge and residual is then *expanded* to the normal cycle (lower) intake pressure, p_i^*. You can assume that both cycles have the same mass of gas in the cylinder, temperature, and pressure at state 1 of the cycle.

a. On a sketch of the intake and exhaust process *p-V* diagram, shade in the area that corresponds to the difference between the pumping work of the EIVC cycle and that of the normal cycle.

b. What value of p_i and V_{EIVC} will give the maximum reduction in pumping work for the EIVC cycle?

c. Derive an expression for this maximum difference in pumping work between the normal cycle and the EIVC cycle in terms of p_e, p_i^*, V_c, and V_m. You can make the appropriate ideal cycle assumptions.

© McGraw-Hill Education. All rights reserved. Any use is subject to the Terms of Use, Privacy Notice and copyright information.



5.11.

a. Calculate the following parameters for a constant-volume fuel-air cycle (Fig. 5.2*a*):

b. The pressures and temperatures at states 1, 2, 3, 4, 5, and 6

c. The indicated fuel conversion efficiency

d. The imep

e. The residual gas fraction

f. The volumetric efficiency

Inlet pressure = 1 atm, exhaust pressure = 1 atm, inlet temperature = 300 K, compression ratio = 8:1, equivalence ratio = ϕ = 1.

Calculate the above parameters (points a-e) using the SI unit's charts. Use 44.4 MJ/kg for heating value of the fuel. *Hint:* Start the calculations using the residual mass fraction 0.03 and the residual gas temperature 1370 K.

5.12. Calculate the following parameters for a constant-pressure fuel-air cycle (Fig. 5.2*b*):

a. The pressures and temperatures at states 1, 2, 3, 4, 5, and 6

b. The indicated fuel conversion efficiency

c. The imep

d. The residual fraction

e. The volumetric efficiency

Intake pressure = 1 bar, exhaust pressure = 1 bar, intake temperature = 300 K, compression ratio = 18:1, equivalence ratio = ϕ = 0.6.

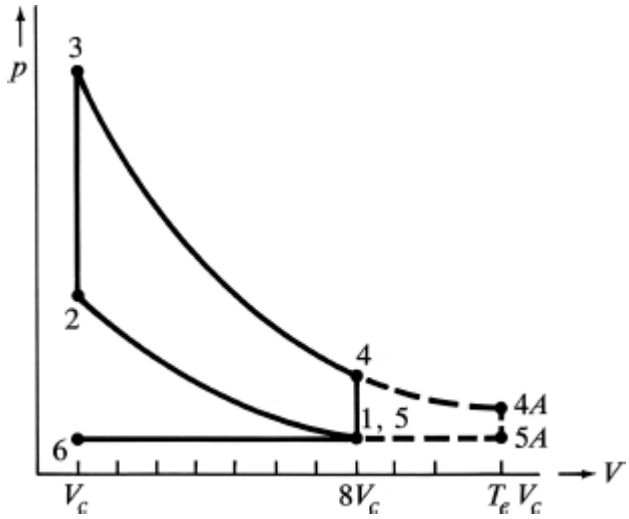
Calculate the above parameters (points a-e) using the SI unit's charts. Use 44.4 MJ/kg for heating value of the fuel. *Hint*: Start the calculations using the residual mass fraction 0.03 and the residual gas temperature 900 K.

5.13. The cycle 1-2-3-4-5-6-1 is a conventional constant-volume fuel-air cycle with a compression ratio of 8. The fuel is isooctane, C_8H_{18}, with a lower heating value of 44.4 MJ/kg. The gas state at 1 is T_1 = 300 K, p_1 = 1 atm with an equivalence ratio of 1.0 and zero residual fraction. The specific volume at state 1 is 0.9 m^3/kg air in the mixture. The temperature at the end of compression at state 2 is 600 K.

© McGraw-Hill Education. All rights reserved. Any use is subject to the Terms of Use, Privacy Notice and copyright information.

a. Find the indicated fuel conversion efficiency and mean effective pressure of this fuel-air cycle model of a spark-ignition engine.

b. The efficiency of the cycle can be increased by increasing the expansion ratio r_e while maintaining the same compression ratio r_c (cycle 1-2-3-4*A*-5*A*-6-1). (This can be done with valve timing.) If the expansion ratio r_e is 12, while the compression ratio and other details of the cycle remain the same as in (*a*), what is the indicated efficiency and mean effective pressure (based on the new, larger, displaced volume) of this new engine cycle?



5.14. We would like to examine the effects of using reformulated gasoline in an SI engine. Reformulated gasoline (for lower emissions) must contain 2% by weight of oxygen. One approach is to blend ethanol (C_2H_6O) with the gasoline (approximate as C_7H_{13}) in the appropriate ratio to provide this 2% oxygen. The heating value of gasoline is 44 MJ/kg; the heating value of ethanol is 26.9 MJ/kg. The density of the two fuels is essentially the same, 0.76 Mg/M^3.

a. Calculate the required mass fraction of ethanol in the ethanol-gasoline mixture.

b. The stoichiometric air/fuel for ethanol and gasoline are 9.0 and 14.6, respectively. Determine the stoichiometric A/F ratio for the mixture.

c. The fuel injection system injects a given volume of fuel based on the measured mass flow rate of air. So in a spark-ignition engine designed for stoichiometric operation with gasoline, the engine will run lean with the ethanol-gasoline mixture. At what lean relative air/fuel ratio will it operate?

d. If the fuel-air cycle results in Fig. 5.9 apply for both fuels, what is the ratio of brake specific fuel consumption of the ethanol-gasoline fuel to that of the gasoline fuel? For a given driving pattern what will be the ratio of miles per gallon for the two fuels?

5.15. In spark-ignition engines, exhaust gas is recycled to the intake at part load to reduce the peak burned gas temperatures and lower emissions of nitrogen oxides.

a. Calculate the reduction in burned gas temperature that occurs when, due to exhaust gas recycle, the burned gas fraction in the unburned gas mixture (x_b) inside the cylinder is increased from 10% (the normal residual fraction) to 30%. Assume combustion occurs at top-center, at constant volume, and is adiabatic. Conditions at the end of compression for both cases are: T = 700 K, p = 1000 kPa, v = 0.2 m^3/kg air in the original mixture; the equivalence ratio is 1.0. The fuel can be modeled as isooctane.

b. The compression ratio is 8. The compression stroke work is 300 kJ/kg air in the original mixture. Find the indicated work per cycle for the compression and expansion strokes, per kilogram of air in the original mixture, for these two cases.

© McGraw-Hill Education. All rights reserved. Any use is subject to the Terms of Use, Privacy Notice and copyright information.

c. Briefly explain how you would increase the work per cycle with 30% burned gas fraction in the unburned mixture to the value obtained with 10% burned gas fraction, with fixed engine geometry. (A qualitative answer, only, is required here.)

5.16. The following cycle has been proposed for improving the operation of a four-stroke cycle engine. Its aim is to expand the post-combustion cylinder gases to a lower pressure and temperature by extending the expansion stroke, and hence extract more work per cycle.

The cycle consists of: (1) an intake stroke; (2) a compression stroke, where the inlet valve remains open (and the cylinder pressure is constant) for the first portion of the stroke; (3) a combustion process, which occurs rapidly close to top-center; (4) an expansion stroke, where the exhaust valve remains closed until the end of the stroke; (5) an exhaust stroke, where the cylinder pressure blows down to the exhaust pressure rapidly and most of the remaining combustion products are expelled as the piston moves from the BC to the TC position. Thus, for this engine concept, the compression ratio r_c (ratio of cylinder volume at inlet valve closing to clearance volume) is less than the expansion ratio r_e (ratio of cylinder volume at exhaust valve opening to clearance volume).

a. Sketch a *p-V* diagram for the cylinder gases for this cycle operating unthrottled.

b. Using the charts in SI units developed for fuel-air cycle calculations, carry out an analysis of an appropriate ideal model for this cycle where the compression ratio r_c is 8 and the expansion ratio r_e is (1) 8; (2) 16.

   Assume the following: pressure in the cylinder at inlet valve close 1 bar; mixture temperature at inlet valve close 300 K; mixture equivalence ratio = 1.0; fuel: isooctane C_8H_{18}; fuel lower heating value = 44.4 MJ/kg; residual gas mass fraction at inlet valve close 0.05; stoichiometric fuel/air ratio = 0.066.

   Calculate the indicated work per cycle per kg of air in the original mixture (the standard chart units) and the indicated mean effective pressure for these two expansion ratios. Base the mean effective pressure on the volume displaced by the piston during the *expansion* stroke. Tabulate your answers. (*Note:* You are given the initial conditions for the cycle calculation; changing the value of r_e requires only modest changes in the cycle calculation.)

c. Comment briefly on the effect of increasing the ratio r_e/r_c above 1.0 with this concept on engine efficiency and specific power (power per unit engine weight). Additional calculations are not required.

5.17. The earliest successful reciprocating internal combustion engine was an engine developed by Lenoir in the 1860s. The operating cycle of this engine consisted of two strokes (i.e., one crankshaft revolution). During the first half of the first stroke, as the piston moves away from its top-center position, fuel-air mixture is drawn into the cylinder through the inlet valve. When half the total cylinder volume is filled with fresh mixture, the inlet valve is closed. The mixture is then ignited and burns rapidly. During the second half of the first stroke, power is delivered from the high-pressure burned gases to the piston. With the piston in its bottom-center position, the exhaust valve is opened. The second stroke, the exhaust stroke, completes the cycle as the piston returns to top-center.

a. Sketch a cylinder pressure versus cylinder volume diagram for this engine.

b. Using the charts in SI units developed for fuel-air cycle calculations, carry out a cycle analysis and determine the indicated fuel conversion efficiency and mean effective pressure for the Lenoir engine.

   Assume the following: intake pressure = 1 bar; intake mixture temperature = 300 K;

   mixture equivalence ratio = 1.0; fuel: isooctane C_8H_{18}, lower heating value = 44.4 MJ/kg. The clearance volume can be neglected.

c. Compare these values with typical values for the constant-volume fuel-air cycle. Explain (with thermodynamic arguments) why the two cycles have such different indicated mean effective pressures and efficiencies.

d. Explain briefly why the real Lenoir engine would have a lower efficiency than the value you calculated in (*b*) (the actual *brake* fuel conversion efficiency of the engine was about 5%).

© McGraw-Hill Education. All rights reserved. Any use is subject to the Terms of Use, Privacy Notice and copyright information.

5.18. Estimate from fuel-air cycle results the indicated fuel conversion efficiency, the indicated mean effective pressure, and the maximum indicated power (in kilowatts) at wide-open throttle of these two four-stroke cycle spark-ignition engines:

1. A six-cylinder engine with a 9.2-cm bore, 9-cm stroke, compression ratio of 7, operated at an equivalence ratio of 0.8
2. A six-cylinder engine with an 8.3-cm bore, 8-cm stroke, compression ratio of 10, operated at an equivalence ratio of 1.1

Assume that actual indicated engine efficiency is 0.85 times the appropriate fuel-air cycle efficiency. The inlet manifold pressure is close to 1 atmosphere. The maximum permitted value of the mean piston speed is 15 m/s. Briefly summarize the reasons why:

a. The efficiency of these two engines is approximately the same despite their different compression ratios.

b. The maximum power of the smaller displacement engine is approximately the same as that of the larger displacement engine.

5.19. In this problem we would like to compare the CO_2-producing potential of natural gas, methanol, and gasoline in vehicles with spark-ignition engines. Assume all three engine/fuel combinations are operating at stoichiometric and that the knock-limited compression ratios for the fuels are:

Fuel	Knock-limited compression ratio
Natural gas	12.0
Methanol	10.5
Gasoline	9.0

a. Calculate the mass of CO_2 produced per unit of each fuel's chemical energy released (i.e., heating value) in gCO_2/MJ.

b. Estimate the best *brake* fuel conversion efficiency of the three engine/fuel combinations at the given operating conditions, and hence their relative CO_2 emissions per unit engine power output. (Normalize by the gasoline value to simplify the comparison.) You will need to make appropriate assumptions in developing these estimates. Assume the air-fuel cycle results in Figs. 5.9 and 5.10 in the text are valid for these three different fuels. At its best efficiency, the gasoline engine has a mechanical efficiency of 0.85.

c. Will these engine/fuel combinations produce the same output? Estimate the maximum bmep for these three engine/fuel combinations, allowing (approximately) for differences, if any, in volumetric efficiency, mechanical efficiency, fuel conversion efficiency, etc. (Look at Fig. 6.3 in the text first.) Assume that the mechanical efficiency at maximum torque can be approximated by the expression
$\eta_m = 1 - r_c/50.$

5.20. The constant-volume combustion fuel-air cycle model can be used to estimate the effect of changes in internal combustion engine design and operating variables on engine efficiency. The following table gives the major differences between a diesel and a spark-ignition engine both operating at half maximum power.

© McGraw-Hill Education. All rights reserved. Any use is subject to the Terms of Use, Privacy Notice and copyright information.

	Diesel engine	Spark-ignition engine
Compression ratio	16:1	9:1
Fuel/air equivalence ratio	0.4	1.0
Inlet manifold pressure	1 bar	0.55 bar

a. Use the graphs of fuel-air cycle results (Figs. 5.9 and 5.10) to estimate the ratio of the diesel engine *brake* fuel conversion efficiency to the spark-ignition engine *brake* fuel conversion efficiency.

b. Estimate what percentage of the higher diesel brake fuel conversion efficiency comes from:

   1. The higher diesel compression ratio
   2. The leaner diesel equivalence ratio
   3. The lack of intake throttling in the diesel compared with the spark-ignition engine

   The values of fuel conversion efficiency and mean effective pressure given in the graphs are *gross* indicated values (i.e., values obtained from $\int pdV$ over the compression and expansion strokes only).

   You may assume, if necessary, that for the real engines, the gross indicated efficiency and gross indicated mean effective pressure are 0.85 times the fuel-air cycle values. Also, the mechanical rubbing friction for each engine is 30% of the *net* indicated power or mep.

© McGraw-Hill Education. All rights reserved. Any use is subject to the Terms of Use, Privacy Notice and copyright information.

5.10. REFERENCES

1. Taylor, C. F.: *The Internal Combustion Engine in Theory and Practice*, vol. 1: *Thermodynamics, Fluid Flow, Performance*, 2d ed., Chaps. 2 and 4, MIT Press, Cambridge, MA, 1966.
2. Lancaster, D. R., Krieger, R. B., and Lienesch, J. H.: "Measurement and Analysis of Engine Pressure Data," SAE paper 750026, *SAE Trans.*, vol. 84, 1975.
3. Edson, M. H.: "The Influence of Compression Ratio and Dissociation on Ideal Otto Cycle Engine Thermal Efficiency,"*Digital Calculations of Engine Cycles, SAE Prog. in Technology*, vol. 7, pp. 49–64, 1964.
4. Edson, M. H., and Taylor, C. F.: "The Limits of Engine Performance--Comparison of Actual and Theoretical Cycles,"*Digital Calculations of Engine Cycles, SAE Prog. in Technology*, vol. 7, pp. 65–81, 1964.
5. Keenan, J. H.: *Thermodynamics*, John Wiley, New York, 1941; MIT Press, Cambridge, MA, 1970.
6. Haywood, R. W.: "A Critical Review of the Theorems of Thermodynamic Availability, with Concise Formulations; Part 1. Availability," *J. Mech. Engng Sci.*, vol. 16, no. 3, pp. 160–173, 1974.
7. Haywood, R. W.: "A Critical Review of the Theorems of Thermodynamic Availability, with Concise Formulations; Part 2. Irreversibility," *J. Mech. Engng Sci.*, vol. 16, no. 4, pp. 258–267, 1974.
8. Flynn, R. F., Hoag, K. L., Kamel, M. M., and Primus, R. J.: "A New Perspective on Diesel Engine Evaluation Based on Second Law Analysis," SAE paper 840032, *SAE Trans.*, vol. 93, 1984.
9. Clarke, J. M.: "The Thermodynamic Cycle Requirements for Very High Rational Efficiencies," paper C53/76 in*Proceedings of 6*th *Thermodynamics and Fluid Mechanics Convention*, 1976, Institution of Mechanical Engineers Publications, London, 1977.
10. Traupel, W.: "Reciprocating Engine and Turbine in Internal Combustion Engineering," in*Proc. CIMAC Int. Congr. on Combustion Engines*, Zurich, pp. 39–54, 1957.
11. Clarke, J. M.: "Letter: Heavy Duty Diesel Fuel Economy,"*Mech. Engng*, pp. 105–106, March 1983.
12. Caris, D. F., and Nelson, E. E.: "A New Look at High Compression Engines,"*SAE Trans.*, vol. 67, pp. 112–124, 1959.
13. Kerley, R. V., and Thurston, K. W.: "The Indicated Performance of Otto-Cycle Engines,"*SAE Trans.*, vol. 70, pp. 5–37, 1962.
14. Bolt, J. A., and Holkeboer, D. H.: "Lean Fuel-Air Mixtures for High-Compression Spark-Ignition Engines,"*SAE Trans.*, vol. 70, p. 195, 1962.

© McGraw-Hill Education. All rights reserved. Any use is subject to the Terms of Use, Privacy Notice and copyright information.

6.0. CHAPTER PRELIMINARIES

INTAKE AND EXHAUST PROCESSES IN THE FOUR-STROKE CYCLE

VOLUMETRIC EFFICIENCY

FLOW THROUGH VALVES AND PORTS

RESIDUAL GAS FRACTION

EXHAUST GAS FLOW RATE AND TEMPERATURE VARIATION

SCAVENGING IN TWO-STROKE CYCLE ENGINES

FLOW THROUGH TWO-STROKE ENGINE PORTS

SUPERCHARGING AND TURBOCHARGING

PROBLEMS

REFERENCES

This chapter deals with the fundamentals of the gas exchange process—intake and exhaust in four-stroke cycle engines and scavenging in two-stroke cycle engines. The purpose of the exhaust and intake processes, or of the scavenging process, is to remove the burned gases at the end of the power stroke and admit the fresh charge for the next cycle. Equation (2.45) shows that the brake power of an internal combustion engine at a given speed is proportional to the mass flow rate of air into the cylinders. Inducting the maximum amount of air into the engine at wide-open throttle (full load) and retaining that mass within each cylinder maximizes engine power and is thus a primary goal of the gas exchange process. Engine gas exchange processes are characterized by overall parameters such as volumetric efficiency (for four-stroke cycles), and scavenging efficiency and trapping efficiency (for two-stroke cycles). These overall parameters depend on the design of engine subsystems such as manifolds, valves, and ports, and the rest of the exhaust and intake systems, as well as engine operating conditions. Thus, the flow through individual components in the engine intake and exhaust system has been extensively studied. Supercharging and turbocharging are used to increase air flow through engines, and hence power density, by increasing the density of the air entering each cylinder. Obviously, whether the engine is naturally aspirated (draws air directly from the atmosphere), or is supercharged or turbocharged, significantly affects the gas exchange processes. The above topics are the subject of this chapter.

The amount of air inducted into each cylinder limits the amount of fuel that can be burned. Thus the ability of the total engine system to flow as much air as possible into each cylinder—its breathing capacity at a given speed—is a very important design objective. The degree to which the burned gases from the previous cycle are expelled from the cylinder also affects the airflow into the cylinder. The exhaust process is therefore important, too. In a spark-ignition engine, the torque produced at any given speed is regulated by controlling the air flow rate into the engine. A valve—usually a throttle plate—partly closes off the intake to limit air flow. This causes the pressure, and hence air density, in the intake manifold to decrease thereby reducing the torque and power. The maximum airflow at any given speed occurs at wide-open throttle or full load.

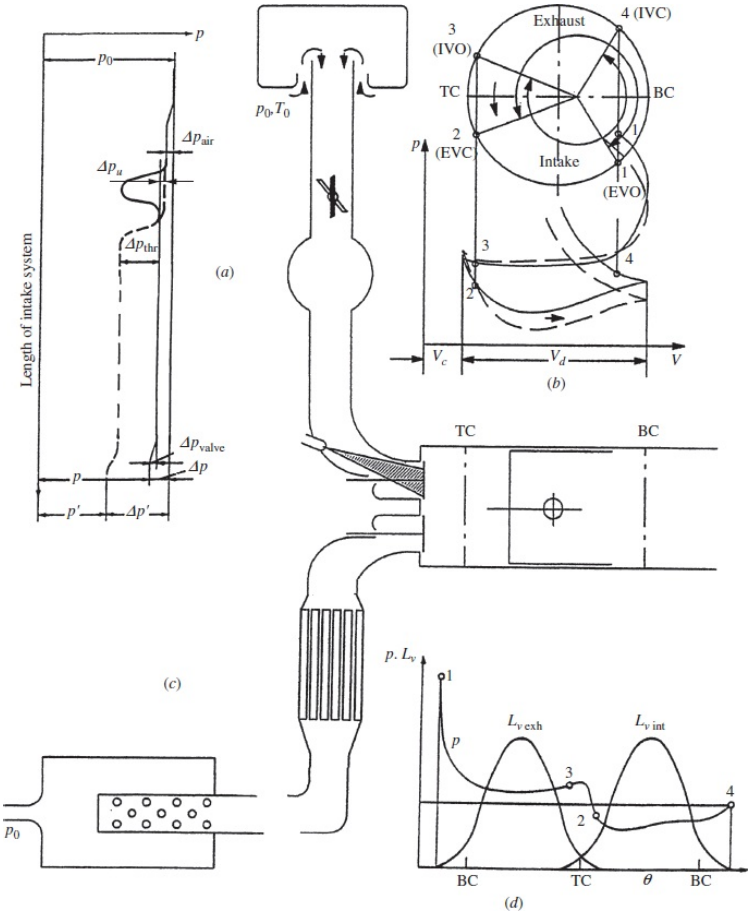
For spark-ignition engines, the fresh charge comprises fuel, air, and (if used for emission control) recycled exhaust, so mixture preparation is also an important goal of the intake process. Mixture preparation includes both achieving the appropriate mixture composition and achieving equal distribution of air, fuel, and recycled exhaust amongst the different cylinders. In diesels, only air (or air plus recycled exhaust) is inducted. Mixture preparation and manifold flow phenomena are discussed in Chap. 7. A third goal of the gas exchange processes is to set up the flow field within the engine cylinders that will give a fast-enough combustion process for satisfactory engine operation. In-cylinder flows are the subject of Chap. 8.

© McGraw-Hill Education. All rights reserved. Any use is subject to the Terms of Use, Privacy Notice and copyright information.

6.1. INTAKE AND EXHAUST PROCESSES IN THE FOUR-STROKE CYCLE

In a four-stroke spark-ignition engine, the intake system typically consists of an air filter, an air duct, a throttle, an intake manifold, and individual cylinder fuel injectors in each intake port or cylinder head. During the induction process, pressure losses occur as the mixture passes through or by each of these components. There is a significant pressure drop across the intake port and valve. The exhaust system typically consists of an exhaust manifold, exhaust pipe, one or more catalytic converters for emission control, and one or more mufflers (or silencers). Figure 6.1 illustrates the intake and exhaust gas flow processes in a conventional spark-ignition engine where the valve opening and closing crank angles are fixed at well-established values. Many modern engines now include variable camshaft phasing, so the valve opening and closing timings can be varied. Other means of varying the valve timing and lift are also used. The flows to each cylinder are pulsating. However, many aspects of these flows can be analyzed on a quasi-steady basis, and the pressures indicated in the intake system in Fig. 6.1*a* represent time-averaged values for a multicylinder engine.

Figure 6.1 Intake and exhaust processes for four-stroke cycle spark-ignition engine: (a) intake system; (b) valve timing and pressure-volume diagrams; (c) exhaust system; (d) cylinder pressure p and valve lift L_v versus crank angle θ. Solid lines are for wide-open throttle, dashed lines are for part throttle; p_0, T_0 are atmospheric conditions; Δp_{air} = pressure losses in air cleaner; Δp_u = intake losses upstream of throttle; Δp_{thr} = losses across throttle; Δp_{valve} = losses across the intake valve.[1]



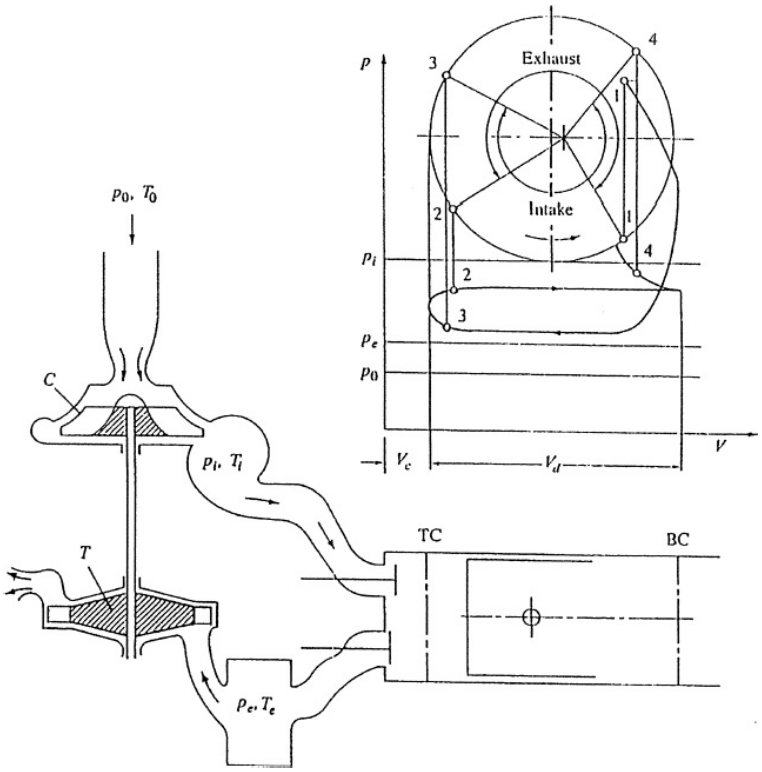
The drop in pressure along the intake system depends on engine speed, the flow resistance of the elements in the system, the cross-sectional area through which the fresh charge moves, and the charge density. Figure 6.1*d* shows the intake and exhaust

© McGraw-Hill Education. All rights reserved. Any use is subject to the Terms of Use, Privacy Notice and copyright information.

valve lifts versus crank angle. The usual practice is to extend the valve open phases beyond the intake and exhaust strokes to improve emptying and charging of the cylinders and make the best use of the inertia of the gases in the intake and exhaust systems. The exhaust process usually begins 40 to 60° before BC (point 1, EVO, Fig. 6.1*b*). Until about BC the burned cylinder gases are discharged due to the pressure difference between the cylinder and the exhaust system. After BC, the cylinder is scavenged by the piston as it moves toward TC. The terms *blowdown* and *displacement* are used to denote these two phases of the exhaust process. Typically, the exhaust valve closes about 15° after TC (point 2, Fig. 6.1*b*), and the intake valve opens 10 to 15° before TC (point 3, Fig. 6.1*b*). Both valves are open during an *overlap period*, and when $p_i/p_e < 1$, backflow of exhausted gas into the cylinder and of cylinder gases into the intake will usually occur. The advantage of valve overlap occurs at high engine speeds when the longer valve open periods improve volumetric efficiency. As the piston moves past TC and the cylinder pressure falls below the intake pressure, gas flows from the intake into the cylinder. The intake valve remains open until 50 to 60° after BC (point 4, Fig. 6.1*b*) so that fresh charge may continue to flow into the cylinder after BC at higher engine speeds.

In a diesel engine intake system, the port fuel injection system and the throttle plate are absent. Diesel engines are more frequently turbocharged. A set of diagrams illustrating the intake and exhaust processes for a turbocharged four-stroke diesel is shown in Fig. 6.2. When the exhaust valve opens (point 1), the burned cylinder gases are fed to a turbine (T), which drives a compressor (C) which compresses the air prior to entry to the cylinder. Charge air cooling is usually employed; a heat exchanger, called an intercooler (ICHE) is placed between the compressor exit and the intake plenum or manifolds to reduce the compressed air temperature and increase its density.

Figure 6.2 Intake and exhaust process for turbocharged four-stroke cycle engine. The turbocharger compressor C raises air pressure and temperature from ambient p_0, T_0 to p_i, T_i. Cylinder pressure during intake is less than p_i. During exhaust, the cylinder gases flow through the exhaust manifold to the turbocharger turbine T. Manifold pressure p_e may vary during the exhaust process and lies between cylinder pressure and ambient.[1]



Due to the time-varying valve open area and cylinder volume, gas inertia effects, and wave propagation in the intake and exhaust systems, the pressures in the intake, the cylinder, and the exhaust during these gas exchange processes vary in complicated ways. Analysis of these processes is complex (see Secs. 7.6.2 and 14.3 for a review of available methods). In

© McGraw-Hill Education. All rights reserved. Any use is subject to the Terms of Use, Privacy Notice and copyright information.

practice, these processes are often treated empirically using overall parameters such as volumetric efficiency to define intake and exhaust system performance.

Figure 6.3 shows an example of an intake manifold system for a V-6 gasoline SI engine. Air ducts lead through two throttles, one on each side of the engine, mechanically connected together, to two plenums from each of which three runners lead to the intake ports. Each plenum has larger cross-sectional flow area than the manifolds so that the different length flow paths through the plenum to the intake ports have little effect on the individual manifold runner airflows. With this intake manifold, a valve connects the two runners closest to the throttle. The valve is closed at low and high speeds so the two plenums are isolated from each other; this valve is opened at mid-speeds so the two intake manifold branches are connected. Changing the intake manifold geometry as engine speed varies can take advantage of different resonant behaviors.

Figure 6.3 Example of a port-fuel-injected gasoline SI engine intake system and cylinder head design: 3.5-liter V-6 engine.[2]

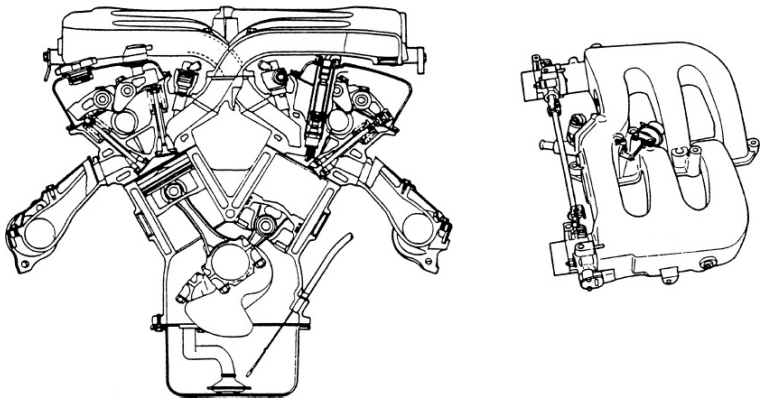
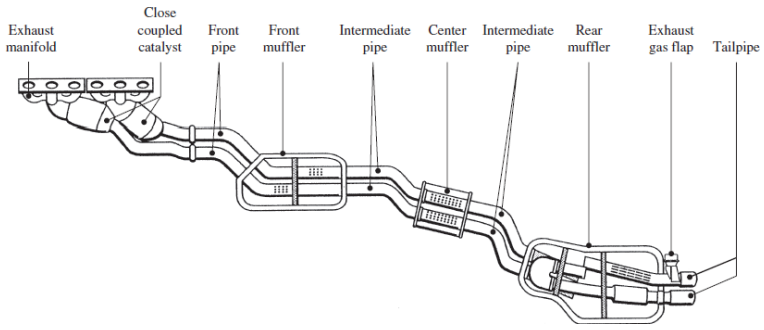


Figure 6.4 shows the components and their layout in the exhaust system of a multicylinder automobile gasoline engine. It consists of an exhaust manifold, a catalytic converter close coupled to the engine for rapid light off which removes the pollutants NO_x, CO, and HC, one or more mufflers to absorb the noise produced by the pulsating exhaust flow, and connecting pipework. For V-6 and V-8 engines, two parallel exhaust systems are often employed. In a spark-ignition engine the exhaust gases are extremely hot so the exhaust system components are made of high-temperature alloy steels.

Figure 6.4 Gasoline 6-cylinder SI engine exhaust system, with close-coupled catalytic converters and three mufflers.[3] *(Courtesy Robert Bosch GmbH and SAE.)*



In diesel engines, the exhaust gas is cooler than in a gasoline engine since the diesel always operates well lean of stoichiometric and the engine extracts more of the high temperature burned gas energy as work. The gasoline engine catalyst is replaced by a particulate trap and a diesel NO_x catalyst (see Chap. 11). Diesel engines are normally turbocharged, and the turbine is close coupled to the exhaust manifold to maximize its effectiveness. In turbocharged gasoline SI engines the turbocharger is also close coupled, and due

© McGraw-Hill Education. All rights reserved. Any use is subject to the Terms of Use, Privacy Notice and copyright information.

to the higher exhaust gas temperature, a turbine bypass valve or wastegate is incorporated to bypass some of the exhaust gas flow to avoid over-boosting the engine.

© McGraw-Hill Education. All rights reserved. Any use is subject to the Terms of Use, Privacy Notice and copyright information.

6.2. VOLUMETRIC EFFICIENCY

Volumetric efficiency is used as an overall measure of the effectiveness of a naturally-aspirated four-stroke cycle engine, and its intake and exhaust systems, as an air pumping device. It is defined [see Sec. 2.10, Eq. (2.33)] as

$$\eta_v = \frac{2\dot{m}_a}{\rho_{a,0} V_d N}$$

The air density
$\rho_{a,0}$ is usually evaluated at atmospheric conditions;
η_v is then the overall volumetric efficiency. It can be evaluated at inlet manifold conditions,
$\rho_{a,i}$;
η_v then measures the pumping performance of the cylinder, intake port, and valve alone. This discussion will cover unthrottled (or wide-open-throttle) engine operation only. It is the air flow under these conditions that constrains maximum engine power. Lesser airflows in SI engines are obtained by restricting the intake system flow area with the throttle valve.

We now examine the several phenomena or factors that have a significant effect on volumetric efficiency: that is, an engine's airflow capability. These factors are:

1. *Quasi-static effects*. Fuel composition, fuel/air ratio, fuel vaporization, intake air temperature, ratio of exhaust to intake manifold pressures, compression ratio, all affect the amount of air inducted.
2. *Intake and exhaust system flow friction.* Due to flow friction, pressure drops occur in the intake and in the exhaust systems.
3. *Port and valve flow friction.* The intake valve and port are the largest flow resistance in the intake system. There is a significant pressure drop across the port and valve due to flow friction.
4. *Intake system heat transfer*. Heat transfer to the mixture in the intake manifold and port decreases the air density.
5. *Valve timing effects*. At low engine speed, a significant amount of mixture which entered the cylinder during the intake stroke is pushed back into the intake by the moving piston during the compression stroke prior to inlet valve closing. At high engine speed, the high momentum of the air in the intake manifold toward the cylinder set-up during the intake stroke forces additional air into the cylinder while the intake valve remains open after BC.
6. *Airflow choking at intake valve and port.* At very high piston speeds, the velocity at the point where the flow area in the intake port and valve is a minimum can become sonic. This phenomenon, called choking, limits the airflow rate into the cylinder.
7. *In-cylinder heat transfer*. The incoming mixture is cooler than the combustion chamber walls. Heat transfer to the fresh charge within the cylinder decreases its density.
8. *Intake (and exhaust) tuning.* By suitable design of intake and exhaust systems, advantage can be taken of wave phenomena resulting from the pulsating flows to increase the pressure in the intake port at the end of the intake process, and lower the pressure in the exhaust port, at specific engine speeds.
9. *Turbocharging or supercharging*. By compressing the intake air before it enters the cylinder in a compressor or blower, the air density is increased and the mass of air entering each cylinder is thus increased.

In addition to the variables listed in (1) above, these factors are influenced by the design, layout, and detailed geometry of the intake and exhaust system components, as well as details of the intake and exhaust ports and valves in the cylinder head and how these valves are controlled by the cam mechanism during the engine cycle. Except for the quasi-static effects (item 1

© McGraw-Hill Education. All rights reserved. Any use is subject to the Terms of Use, Privacy Notice and copyright information.

above), the magnitude of these various factors or phenomena vary significantly with intake mixture velocity in the intake system, manifold, port, and intake valve. Local velocities for quasi-steady flow are equal to the volume flow rate divided by the local cross-sectional area. Since the intake system, port and valve dimensions typically scale with the cylinder bore, air velocities in the intake will scale with piston speed, since it is piston motion that pulls the air into each cylinder in turn. Hence, volumetric efficiency will depend strongly on piston speed. Therefore, volumetric efficiencies for different engines should be compared at constant mean piston speed rather than engine speed.

We will now discuss the phenomena or factors that have a significant impact on airflow and volumetric efficiency, and especially their dependence on speed.

6.2.1. Quasi-Static Effects

6.2.1.1. Volumetric Efficiency of an Ideal Cycle

For the ideal cycles of Fig. 5.2*d* and *e*, an expression for volumetric efficiency can be derived which is a function of the following variables: intake mixture pressure
p_i, temperature
T_i, and fuel/air ratio
(F/A); compression ratio
r_c; exhaust pressure
p_e; and molecular weight *M* and *γ* for the cycle working fluid. The overall volumetric efficiency is

$$\eta_v = \frac{m_a}{\rho_{a,0} V_d} = \frac{m(1-x_r)}{\rho_{a,0}[1+(F/A)]} \frac{r_c}{(r_c-1)V_1}$$

(6.1)

where *m* is the mass in the cylinder at point 1 in the cycle. Since

$$p_i V_1 = m\frac{\widetilde{R}}{M} T_1 \quad \text{and} \quad p_{a,0} = \rho_{a,0}\frac{\widetilde{R}}{M_a} T_{a,0}$$

and Eq. (5.38) relates
T_1 to
T_i, the above expression for
η_v can be written

$$\eta_v = \left(\frac{M}{M_a}\right)\left(\frac{p_i}{p_{a,0}}\right)\left(\frac{T_{a,0}}{T_i}\right)\frac{1}{[1+(F/A)]}\left\{\frac{r_c}{r_c-1} - \frac{1}{\gamma(r_c-1)}\left[\left(\frac{p_e}{p_i}\right)+(\gamma-1)\right]\right\}$$

(6.2)

For
$p_e/p_i = 1$, the term in { } is unity. We see from Eq. (6.2) that there are static effects from variations in
p_i, p_e, T_i, fuel characteristics

© McGraw-Hill Education. All rights reserved. Any use is subject to the Terms of Use, Privacy Notice and copyright information.

F/A and
r_c. There are also dynamic effects from variations in engine speed.

6.2.1.2. Effect of Fuel Composition, Phase, and Fuel/Air Ratio

In a spark-ignition engine, the presence of gaseous fuel (and water vapor) in the intake system reduces the air partial pressure below the mixture pressure. For mixtures of air, water vapor, and gaseous or evaporated fuel we can write the intake manifold pressure as the sum of each component's partial pressure:

$$p_i = p_{a,i} + p_{f,i} + p_{w,i}$$

which, with the ideal gas law, gives

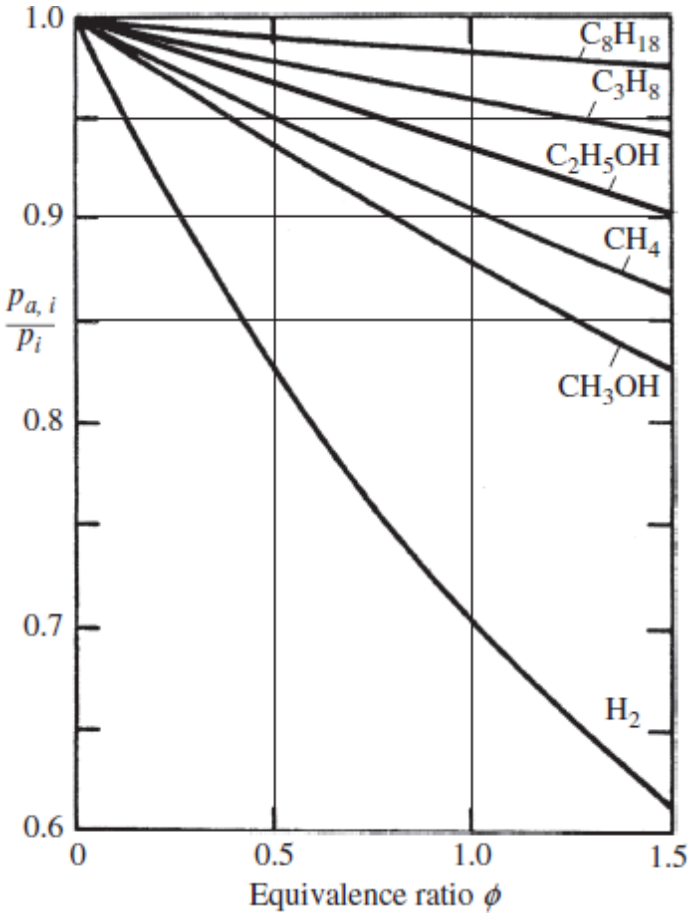
$$\frac{p_{a,i}}{p_i} = \left[1 + \left(\frac{\dot{m}_j}{\dot{m}_a}\right)\left(\frac{M_a}{M_f}\right) + \left(\frac{\dot{m}_w}{\dot{m}_a}\right)\left(\frac{M_a}{M_w}\right)\right]^{-1}$$

(6.3)

The water vapor correction is usually small (≤0.03). This ratio,
$p_{a,i}/p_i$, for several common fuels as a function of
$(\dot{m}_f/\dot{m}_a)$ is shown in Fig. 6.5. Note that
$(\dot{m}_f/\dot{m}_a)$ only equals the engine's operating fuel/air ratio if the fuel is fully vaporized.

© McGraw-Hill Education. All rights reserved. Any use is subject to the Terms of Use, Privacy Notice and copyright information.

Figure 6.5 Effect of fuel (vapor) on inlet air partial pressure. Ratio of air inlet pressure $p_{a,i}$ to mixture inlet pressure p_i versus fuel/air equivalence ratio ϕ for isooctane vapor, propane, ethanol vapor, methane, methanol vapor, and hydrogen.



For conventional liquid fuels such as gasoline, which have higher molecular weights, the effect of fuel vapor, and therefore fuel/air ratio, is relatively small. For gaseous fuels and for ethanol and methanol vapor, the volumetric efficiency is significantly reduced by the fuel vapor in the intake mixture.

6.2.1.3. Fraction Fuel Vaporized and Heat of Vaporization

For a constant-pressure flow with liquid fuel evaporation and with heat transfer, the steady-flow energy equation is

$$\left[\dot{m}_a h_a + (x_{f,e})\dot{m}_f h_{f,L} + x_{f,e}\dot{m}_f h_{f,V}\right]_A = \dot{Q} + (\dot{m}_a h_a + \dot{m}_a h_a + \dot{m}_f h_{f,L})_B$$

(6.4)

where
$x_{f,e}$ is the mass fraction of fuel evaporated and the subscripts denote: *a*, air properties; *f*, fuel properties; *L*, liquid; *V*, vapor; *B*, before evaporation; *A*, after evaporation. Approximating the change in enthalpy per unit mass of each component of the mixture by
$c_p \Delta T$, and with
$h_{f,V} - h_{f,L} = h_{f,LV}$ (the enthalpy of vaporization), Eq. (6.4) becomes

© McGraw-Hill Education. All rights reserved. Any use is subject to the Terms of Use, Privacy Notice and copyright information.

$$T_A - T_B = \frac{(\dot{Q}/\dot{m}_a) - x_{f,e}(F/A)h_{f,LV}}{c_{p,a} + (F/A)c_{f,L}}$$

(6.5)

Since
$c_{f,L} \approx 2c_{p,a}$ the last term in the denominator can often be neglected.

With liquid-fueled port-injected SI engines, much of the injected fuel impinges on the intake valve and port walls. With gasoline, the thermal energy required to vaporize this fuel mostly comes from these walls rather than from the airflow. Thus, only a fraction of the full potential evaporative cooling of the air is realized. As the fuel drop size in the injected spray decreases, the fraction of the fuel evaporated via heat transfer with the airflow increases. With direct injection of a volatile liquid fuel into the cylinder, most of the fuel drops are suspended in the air (and residual gas) charge and undergo an adiabatic evaporation process. If no heat transfer to this mixture occurs, the mixture temperature decreases in proportion to the amount of liquid fuel vaporized. For complete evaporation of isooctane, with ϕ = 1.0,
$T_A - T_B = -20$ deg. C. For ethanol and methanol under the same conditions,
$T_A - T_B$ would be −73 and −122 deg. C, respectively. In practice some air heating occurs: also, with port injection, the fuel is not necessarily fully evaporated prior to entry to the cylinder.

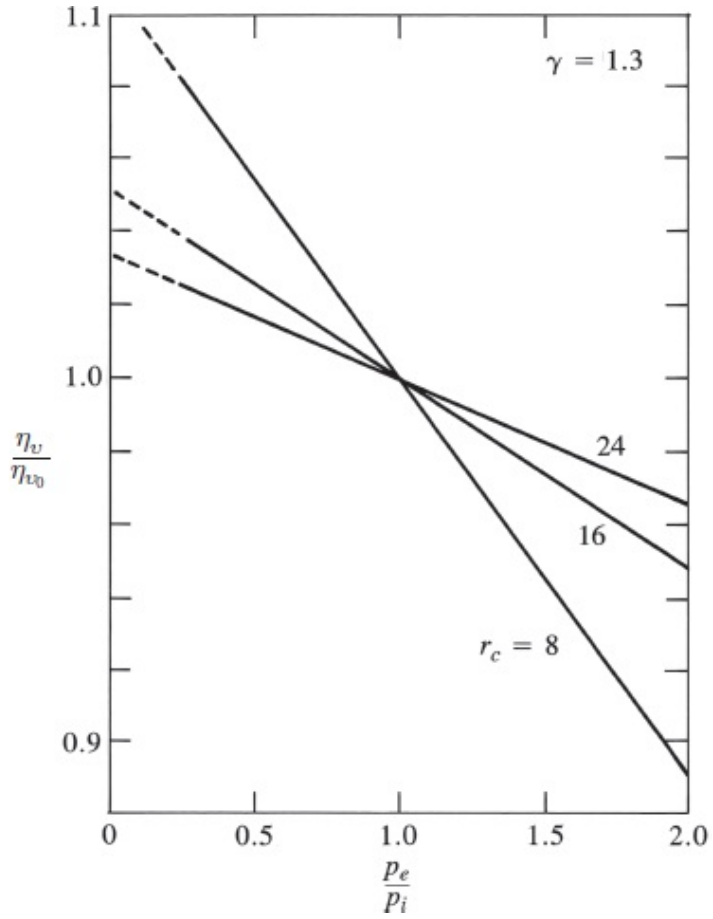
The ideal cycle equation for volumetric efficiency [Eq. (6.2)] shows that the effect of gas temperature variations, measured at entry to the cylinder, is through the factor
$(T_{a,0}/T_i)$. This temperature scaling is appropriate at lower engine speeds. However, engine test data indicate that a square root dependence of volumetric efficiency on temperature ratio is closer to real engine behavior at high engine speeds. The square root dependence on temperature is a standard assumption made in correcting engine maximum power test data (see Sec. 2.12).

6.2.1.4. Effect of Intake and Exhaust Pressure Ratio and Compression Ratio

As the pressure ratio (p_e/p_i) and the compression ratio are varied, the fraction of the cylinder volume occupied by the residual gas *at the intake pressure* varies. As this volume increases, volumetric efficiency decreases. These effects on ideal-cycle volumetric efficiency are given by the { } term in Eq. (6.2). For γ = 1.3 these effects are shown in Fig. 6.6. A more detailed discussion of residual gas behavior is given in Sec. 6.4.

© McGraw-Hill Education. All rights reserved. Any use is subject to the Terms of Use, Privacy Notice and copyright information.

Figure 6.6 Effect of exhaust to inlet pressure ratio on ideal-cycle volumetric efficiency.



6.2.2. Intake and Exhaust Flow Resistances

When gas flows unsteadily through a system of pipes, chambers, ports, and valves, friction, pressure, and inertial forces are present. The relative importance of these forces depends on gas velocity and the size and shape of these passages and their junctions. Both quasi-steady and dynamic effects are usually significant. While the effects of changes in engine speed, and intake and exhaust manifold, port and valve design are interrelated, several separate phenomena which affect volumetric efficiency can be identified.

6.2.2.1. Intake Systems

During the intake stroke, due to flow-induced friction in each part of the intake system, the pressure in the cylinder p_c is less than the intake pressure[1] p_i by an amount dependent on the square of the flow velocity. This total pressure drop is the sum of the pressure loss in each component of the intake system: air filter, ducting, throttle, manifold, intake port, and intake valve. In a boosted engine, the compressor raises the air pressure above atmospheric; each loss is then a few percent, with the cylinder head's ports and valves contributing the largest drop. As a result, the pressure in the cylinder during the period in the intake process when the piston is moving at high speed, can be 10 to 20% lower than p_i. For each component in the intake (and in the exhaust) system, Bernoulli's equation gives

$$\Delta p_j = \xi_j \rho v_j^2$$

© McGraw-Hill Education. All rights reserved. Any use is subject to the Terms of Use, Privacy Notice and copyright information.

where
ξ_j is the flow's resistance coefficient for that component which depends on its geometric details and
v_j is the local velocity. Assuming the flow is quasi-steady, since the piston motion pulls the intake flow
v_j is related to the piston speed
S_p by

$$v_j A_j = S_p A_p$$

where
A_j and
A_p are the component minimum flow area and the piston area, respectively. Hence, the total quasi-steady average pressure loss due to friction is

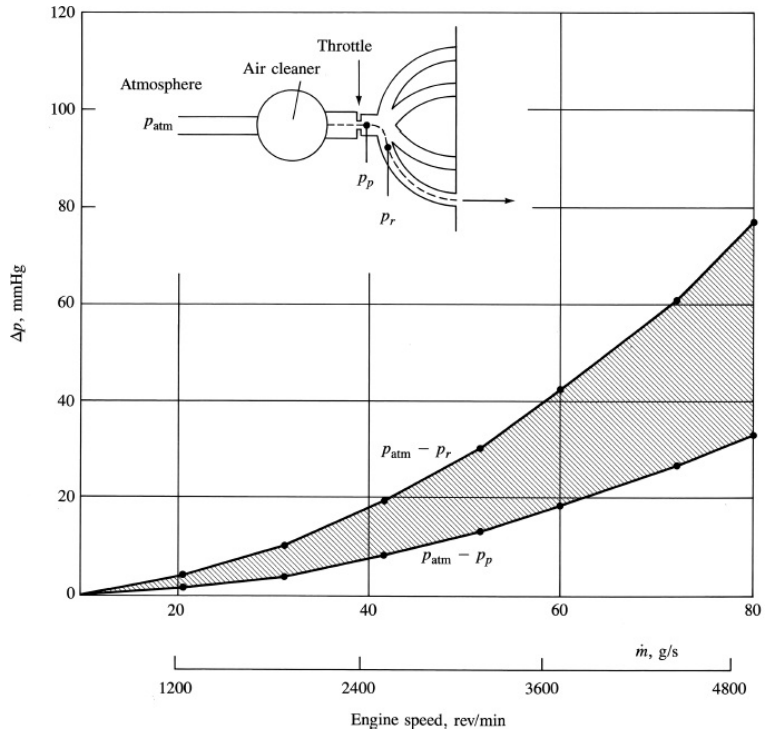
$$p_{atm}(\text{or } p_i) - p_c = \Sigma \Delta p_j = \Sigma \xi j \rho v_j^2 = \rho \overline{S}_p^2 \Sigma \xi_j \left(\frac{A_p}{A_j} \right)^2$$

(6.6)

where, for the average
Δp, we have used the mean piston speed
$\overline{S}_p$ in place of
S_p. Equation (6.6) indicates the importance of large component flow areas for reducing frictional losses, and the dependence of these losses on engine speed. Figure 6.7 shows an example of the pressure losses due to friction across the air cleaner, throttle, and manifold plenum of a standard four-cylinder automobile engine intake system. These steady-flow tests, conducted over the full engine speed range,[4] show that the pressure loss depends on speed squared.

© McGraw-Hill Education. All rights reserved. Any use is subject to the Terms of Use, Privacy Notice and copyright information.

Figure 6.7 Pressure losses in the intake system of a four-stroke cycle spark-ignition engine determined under steady-flow conditions.[4] Stroke = 89 mm, bore = 84 mm.



6.2.2.2. Intake Ports and Valves

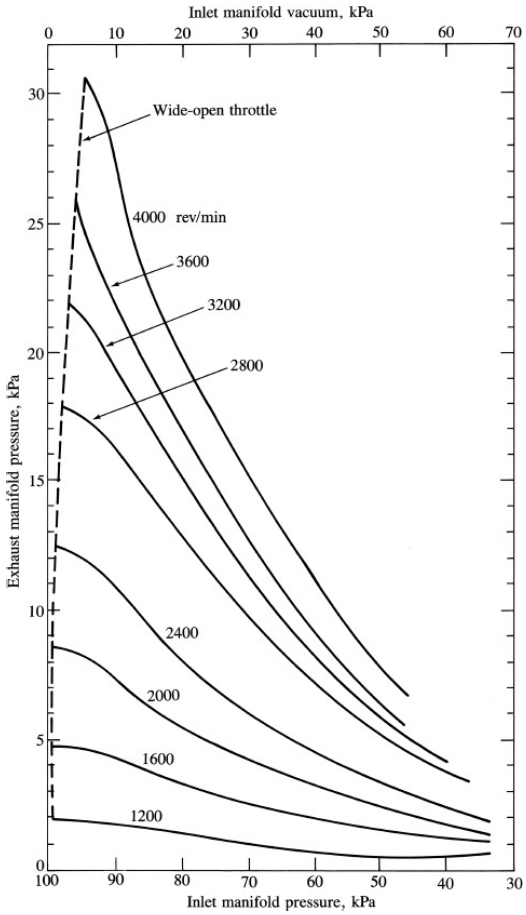
The engine intake ports and valves constitute a comparable flow resistance to that of the intake system. The relative size of the valve heads and seats, and thus their open area, are constrained by the size of the cylinder liner. The open areas they define restrict the airflow. They thus add to the set of flow resistances which are summed in Eq. (6.6), thus causing an additional pressure loss (and density reduction) that increases with the square of engine speed. Note that as the valves lift, the minimum intake flow area in the cylinder head transitions (at about half the maximum valve lift) from being between the valve seat and valve head at low lifts, to the port area close to the valve seat at high lifts; see Sec. 6.3.1.

6.2.2.3. Exhaust System, Ports, and Valves

Equivalent flow-dependent pressure losses in the exhaust system result in the exhaust ports and manifold having average pressure levels that are higher than atmospheric. Figure 6.8 shows the time-averaged exhaust manifold gauge pressure (i.e., relative to atmospheric) as a function of intake manifold pressure (which varies with engine load) and with speed, for a four-cylinder naturally-aspirated automobile SI engine. At high loads (high absolute intake manifold pressures) the gauge pressure in the exhaust manifold increases faster than the square of engine speed. This is because the exhaust gas density decreases with increasing engine speed,[2] as the exhaust system version of Eq. (6.6) would indicate. In turbocharged engines, the exhaust manifold pressure at higher loads and speeds is higher because there is now a significant pressure drop across the turbine—see Fig. 6.2. That pressure drop depends on exhaust gas temperature, engine mass flow rate, and operating boost level, and whether or not the wastegate is partly open (see Sec. 6.8.5). At low engine speeds and loads, the turbocharger has little impact on engine operation so this turbine pressure drop is small.

© McGraw-Hill Education. All rights reserved. Any use is subject to the Terms of Use, Privacy Notice and copyright information.

Figure 6.8 *Exhaust manifold pressure as a function of load (defined by inlet manifold vacuum) and speed, four-stroke cycle, four-cylinder SI engine.*[5]



The flow resistances of the exhaust valves and ports are less significant than on the intake side. This is because a substantial fraction of the in-cylinder burned gas is exhausted between exhaust valve opening (EVO) and about BC in a *blowdown* process, which is driven by the pressure difference between the cylinder and the exhaust system. Then, since the exhaust gas is hot, its density (at atmospheric pressure) is lower than that of the intake air by a factor of 3 to 4. So the pressure drop given by the exhaust system version of Eq. (6.6), due to the exhaust valves and ports during most of the exhaust stroke (BC to TC, when the piston *displaces* the remaining burned gases from the cylinder) is significantly smaller than the cylinder-head flow-resistance pressure drop during intake.

6.2.3. Intake and In-Cylinder Heat Transfer

6.2.3.1. Intake Heat Transfer

As air flows through each intake port (with its walls close to the coolant temperature, ~90°C) and past the hot intake valve surface (at ~150°C) some heating of the intake air occurs. This causes a 2 to 3% loss in volumetric efficiency. This intake heating decreases modestly with increasing speed since while the heat transfer rate for a turbulent flow in a duct increases with speed to the 0.8 power,[3] the time available per cycle for heat transfer varies as the reciprocal of speed. Thus as speed increases, the time available goes down faster than the heat transfer rate increases. The impact of intake heat transfer on volumetric efficiency depends on the intake air temperature.

© McGraw-Hill Education. All rights reserved. Any use is subject to the Terms of Use, Privacy Notice and copyright information.

6.2.3.2. In-Cylinder Heat Transfer

As air flows into the cylinder, it mixes with the hot burned residual gases left in the cylinder from the previous cycle. This process raises the temperature of the air (already mixed with fuel in port-fuel-injected SI engines) and residual-gas mixture. Also, the temperatures of the piston, valves, and cylinder head are higher than this mixture temperature, so heat transfer *to* the in-cylinder unburned mixture occurs, further raising its temperature. When combined, these two processes result in a density decrease (and volumetric efficiency decrease) of some 1 to 2%, since the cylinder has a given displaced volume.

6.2.4. Intake Valve Timing Effects

6.2.4.1. Ram Effect at High Speed

The mass of air inducted into the cylinder each cycle, and hence the volumetric efficiency, is determined by the total pressure level in the intake port during the latter portion of the intake process. This total pressure is the sum of the static pressure and the dynamic kinetic energy pressure component. At higher engine speeds, the inertia of the gas in the intake system as the intake valve is closing increases the pressure in the port and continues the cylinder charging process as the piston slows down as it approaches BC and starts the compression stroke. This effect becomes progressively greater as engine speed increases. The intake valve in fixed-valve-timing engines is closed some 50 to 60° after BC, in part to take advantage of this so-called ram phenomenon. This effect increases the high-speed engine airflow by some 10%. With variable intake valve timing, these airflow benefits can be increased.

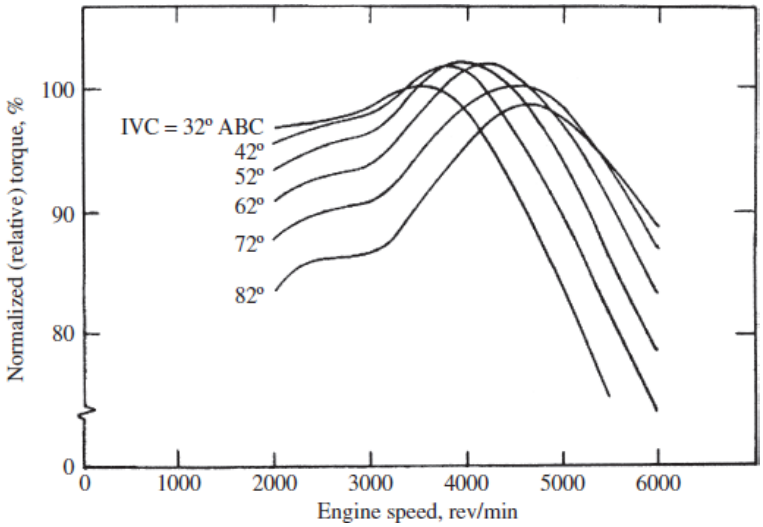
6.2.4.2. Reverse Flow into the Intake at Low Speed

Because the intake valve closes after the start of the compression stroke, a reverse flow of already-inducted fresh charge from the cylinder back into the intake can occur as the cylinder pressure rises due to piston motion toward TC. This reverse flow is largest at the lowest engine speeds. It is an inevitable low-speed consequence of the intake valve closing (IVC) time chosen to take advantage of the ram effect at high speeds. With fixed-valve-timing engines it results in a substantial loss of air from the cylinder (~15% at 1500 rev/min); with earlier IVC at these conditions, the loss is significantly reduced.

The effects of varying the IVC angle on relative full-load engine torque are shown in Fig. 6.9.[6] Torque is proportional to airflow, and thus volumetric efficiency, except that at the highest engine speeds the negative impact of increasing engine friction plays an increasing role. Note that the typical IVC angle of 50 to 55° ABC is an excellent compromise.

© McGraw-Hill Education. All rights reserved. Any use is subject to the Terms of Use, Privacy Notice and copyright information.

Figure 6.9 Effect of IVC angle on gasoline SI engine torque (normalized) versus engine speed. Typical fixed IVC angle is between 50 and 55° ABC.[6]



6.2.5. Airflow Choking at Intake Valve

As the intake valve opens, its minimum flow area—an annular ring between the valve head and valve seat—increases from zero up to about half the maximum valve lift when the intake port area (at the valve seat) becomes the flow restricting area (see Sec. 6.3.1). The air flow in this minimum flow area in the intake valve and port system is pulled into the cylinder by the downward piston motion. Its scaling with piston speed follows this relationship:

$$U_{a,\mathrm{IV}} A_{\min,\mathrm{IV}} \approx S_p A_p$$

At high engine speeds ($\overline{S}_p \sim 20\ \mathrm{m/s}$; see Sec. 2.2), during the first portion of the intake stroke, the valve open area is much less than the piston area so the air velocities in this minimum valve open area become large. Typical numbers (for a 4-valve per cylinder automobile SI engine) would be:

> Engine details:
>
> Bore = stroke = 85 mm; IV diameter (two intake valves) = 36 mm, maximum valve lift = 10 mm, $\overline{S}_p \approx 20\ \mathrm{m/s}$. This gives an airflow velocity past the valve seat of 300 m/s at a valve lift of 2 to 3 mm (attained at about 45° after IVO) at an engine speed of 7000 rev/min.

The speed of sound in air at standard atmospheric conditions is close to 330 m/s. Thus the airflow at valve lifts up to this few mm value, is choked—the velocity is higher than the local sound speed. When a flow is choked, decreasing the pressure downstream of the flow restriction (e.g., by further increasing the piston speed) has no effect on the mass flow rate: only increases in *upstream* pressure can increase the flow rate—see App. C, Sec. C.2. While initially the flow is choked for only a short portion of the intake process, as engine speed is increased the duration of the choked flow period increases. Following the onset of this phenomenon, as engine speed increases at wide-open-throttle and higher speeds, the airflow rate decreases increasingly rapidly because the flow frictional losses in the intake system, port, and valve rise as the square of speed. This onset of airflow choking effectively defines (along with the rapidly rising engine friction) the upper speed limit of the engine since engine brake power now starts to decline.

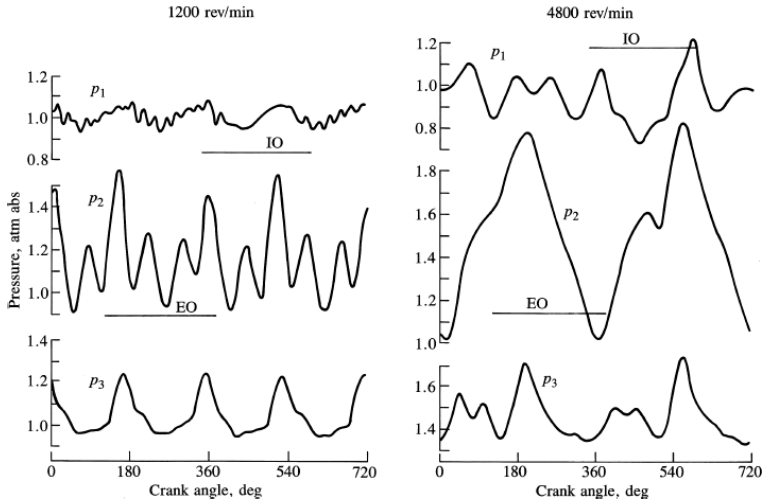
6.2.6. Intake and Exhaust Tuning

© McGraw-Hill Education. All rights reserved. Any use is subject to the Terms of Use, Privacy Notice and copyright information.

6.2.6. Intake and Exhaust Tuning

Figure 6.10 shows the pressure variations with time in the intake and exhaust systems of a four-cylinder automobile spark-ignition engine at wide-open throttle at low and high speed. The complexity of the gas exchange phenomena is apparent. The amplitude of the pressure fluctuations increases substantially with increasing engine speed. The primary frequency in both the intake and exhaust corresponds to the frequency of individual cylinder intake and exhaust processes. Higher harmonics in both the intake and exhaust are apparent also. This pulsating flow into and out of each cylinder during the intake and exhaust processes sets up pressure waves in the intake and exhaust systems. These pressure waves propagate at the local sound speed relative to the moving air or exhaust gas. The pressure waves interact with the pipe junctions and ends in the ducting, plenums, manifolds, and ports. These interactions cause pressure waves to be reflected back toward the engine cylinder. These pressure waves may aid or inhibit the gas exchange processes. When they aid the process by increasing the pressure in the intake ports toward the end of the intake process, or by reducing the pressure in the exhaust ports toward the end of the exhaust process, the intake and exhaust systems are said to be *tuned*.[7]

Figure 6.10 Instantaneous pressures in the intake and exhaust manifolds of a four-stroke cycle four-cylinder spark-ignition engine, at wide-open throttle. Locations: p_1, intake manifold runner 150 mm from cylinder 1; p_2, exhaust manifold runner 200 mm from cylinder 1; p_3, exhaust manifold runner 700 mm from cylinder 1. IO and EO, intake and exhaust valve open periods for that cylinder, respectively. Stroke 89 mm, bore 84 mm.[4]



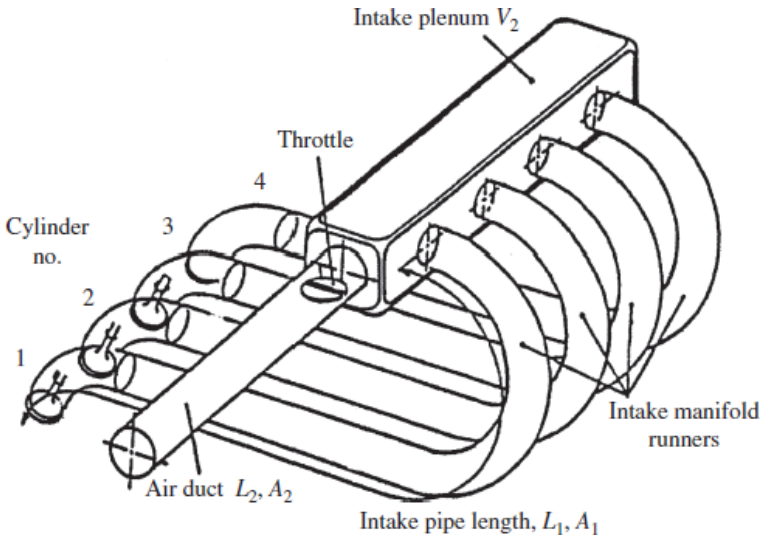
6.2.6.1. Intake System Tuning

As the time-varying intake flow into the cylinder gets started, an expansion wave is propagated back through the intake manifold. As this expansion wave goes through the open end of the manifold into the plenum it causes a positive pressure wave to be propagated back toward the cylinder. If the timing of these waves is appropriately phased, this positive pressure wave will cause the pressure in the intake port to increase above its nominal value toward the end of the intake process. This will increase the inducted air mass.

Figure 6.11 shows a schematic of the intake system, ports, and valves of a four-cylinder automobile spark-ignition engine. It shows the intake air duct leading air past the throttle valve into an enlarged volume of plenum, which then feeds air through the manifold runners and ports and valves in the cylinder head, into the engine's cylinders. Note the relatively long length of the flow path from the plenum to the valves. Such an intake system configuration can be *tuned* in two basic ways: one, based on the length of the flow path—plenum to intake valve—can provide additional airflow at high engine speeds; the other based on air duct and plenum geometry can enhance the airflow at mid-speeds by causing the plenum pressure to oscillate as a Helmoltz resonator.

© McGraw-Hill Education. All rights reserved. Any use is subject to the Terms of Use, Privacy Notice and copyright information.

Figure 6.11 Schematic of tuned intake system for a four-cylinder automobile gasoline SI engine: air duct, throttle, plenum, and manifold runners are indicated.[6]



When the intake valve opens (just before TC) and the piston starts accelerating down the cylinder drawing air into the cylinder, the pressure in the intake port falls and a rarefaction (expansion) wave propagates back toward the plenum at the speed of sound. As this expansion wave propagates into the (larger volume) plenum, a compression wave (which increases the pressure) moves back into the manifold toward the intake valve. If this "high" pressure wave reaches the intake port during the latter part of the intake stroke, then additional air will be "pushed" into the cylinder.

An example of the relevant numbers:

> With L_1 (see Fig. 6.11), the length from the plenum to intake valve seat, equal to 50 cm with the sound speed in air 343 m/s, the pressure wave travel time—intake valve to plenum and back—is 3 ms. This corresponds to the latter 90 degrees of the intake process at about 4500 rev/min, the speed at which the high-speed tuning peak usually occurs.

As engine speed moves away from the tuning peak, the benefits fall off because the match between the pressure wave phenomenon and the phasing of the engine intake flow process becomes increasingly less well matched. Note that to shift these airflow benefits to lower engine speeds would require much longer flow paths from plenum to intake valve (longer manifold runners). This would increase the impact of the manifold runner flow resistance, which is significant at high engine speed; it would also increase the bulk volume of the engine since (as Fig. 6.11 indicates) the runners are already long and the intake system is bulky.

The second tuning mode uses the plenum as a resonator. The flow in the intake air pipe leading to the throttle is the sum of the individual cylinder intake flows. In a four-cylinder four-stroke cycle engine, the beginnings of each cylinder's 720-degree four-stroke cycle are spaced 180 degrees crank angle (CA) apart. Thus, in a four-cylinder engine, there are four flow pulses in this intake pipe every two crank revolutions. This pulsating flow into the intake manifold plenum forces the plenum pressure to oscillate (as a Helmholtz oscillator) at a frequency given by:

$$f_H = \frac{a}{2\pi}\sqrt{\frac{A_2}{L_2 V_2}}$$

(6.7)

where *a* is the speed of sound in the intake air (~340 m/s), and

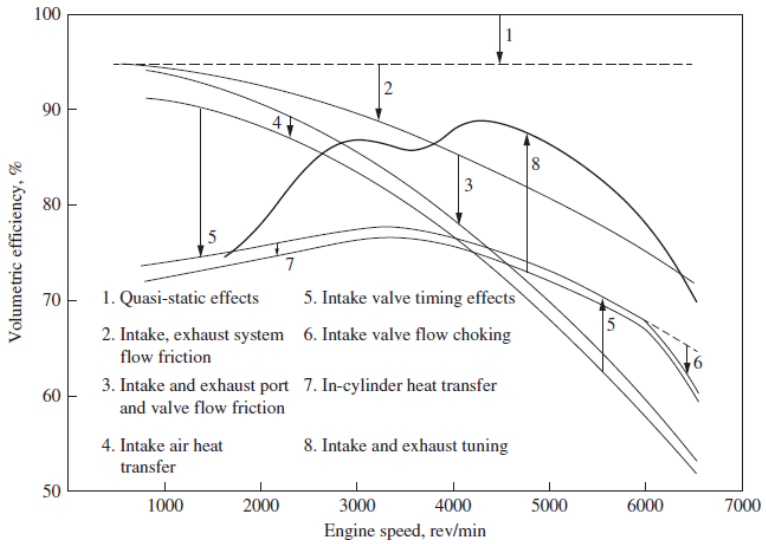
© McGraw-Hill Education. All rights reserved. Any use is subject to the Terms of Use, Privacy Notice and copyright information.

$A_2, L_2,$ and V_2 are defined in Fig. 6.11. If the plenum pressure is higher at about mid-intake-stroke for each cylinder when the airflow "pull" of each piston is at its maximum, extra air will be "pushed" into each cylinder. Approximate numbers are:

> For a typical automobile four-cylinder gasoline engine,
> $A_2 \approx 20\,\text{cm}^2$, $L_2 \approx 40\,\text{cm}$, $V_2 \approx 1500\,\text{cm}^3$, Eq. (6.7) gives a Helmholtz resonance frequency of about 100 Hz. This frequency corresponds to high-pressure peaks (twice per revolution for a four-cylinder engine) at an engine speed close to 3500 rev/min: the "in-phase" engine speed for this second tuning mode.

The additional airflow that employing these two tuning modes provide are shown in Fig. 6.12, which adds together all the airflow phenomena or factors discussed in this section (Sec. 6.2) that impact volumetric efficiency. This figure will be discussed fully in Sec. 6.2.7 which follows. Intake manifold tuning provides an additional 10 to 15 percentage points at around 4500 rev/min. Helmholtz resonance in the intake plenum adds an additional 10 or so percentage points between about 2500 and 3500 rev/min.

Figure 6.12 Effect on SI engine volumetric efficiency of the different phenomena which affect the airflow rate as a function of engine speed. Bold line is final η_v versus speed curve.[8]



Methods which predict the unsteady flows in the intake and exhaust systems of internal combustion engines with good accuracy have been developed. These methods are complicated, however, so more detailed discussion is deferred to Chap. 14.

6.2.6.2. Exhaust System Tuning

The exhaust flow pulses from each individual cylinder are apparent from the low-speed exhaust system pressure traces shown in Fig. 6.10 (also apparent at high speed, but more complex). The total exhaust system—exhaust valves to the atmosphere—has many components (see Fig. 6.4). Some of these components (e.g., mufflers) have additional volume and can act as plenums; these mufflers and the catalyst will provide some damping to flow and pressure oscillations. None-the-less these flow and pressure oscillations will generate wave phenomena which can be used to advantage. If, through suitable layout and geometry, these exhaust pressure wave phenomena result in a *lower* pressure in the exhaust ports during the latter portion of the exhaust stroke, then additional burned gases will be sucked out of the cylinder and the amount of burned gas residual left in the cylinder for the next cycle will be reduced. This increases volumetric efficiency because the (hot) residual gases both occupy volume and, through mixing, heat up the incoming air.

© McGraw-Hill Education. All rights reserved. Any use is subject to the Terms of Use, Privacy Notice and copyright information.

6.2.7. Combined Effects: Naturally-Aspirated Engines

We now combine the effects these several phenomena or factors (discussed in Secs. 6.2.1 through 6.2.6) have on volumetric efficiency, as a function of engine speed.[4] The result shown in Fig. 6.12 is typical of the wide-open-throttle volumetric efficiency versus speed behavior of a modern automobile gasoline engine. The figure shows that the volumetric efficiency of a (fixed-valve-timing, naturally-aspirated engine) steadily increases from about 80% at low speeds to its highest value (95% or more) at about three quarters of the engine's maximum speed, and then declines by about 10% at the speed where airflow choking occurs and the maximum brake power of the engine is reached.

The different phenomena affect volumetric efficiency in the following ways. Quasi-static, non-speed-dependent-effects (such as fuel vapor pressure) drop η_v below 100% (curve 1). Frictional flow losses in the intake and exhaust systems (curve 2), and in the ports and valves in the cylinder head (curve 3), both increase as the square of engine speed. Charge heating in the intake manifold and cylinder head drops the curve modestly to 4. Valve timing effects, the induction ram benefit at higher engine speeds due to the IVC occurring well after BC, and its companion loss of air at lower engine speeds, change curve 4 to curve 5. At the highest engine speeds, the flow into the cylinder during at least part of the intake process becomes chocked. Once this occurs, further increases in speed do not increase the airflow rate (curve 5 to 6) so η_v decreases more steeply. In-cylinder heat transfer heats the intake charge initially, reducing its density and thus the engine's volumetric efficiency, curve 7. Finally, intake system tuning increases the airflow at high speeds by matching the phasing of pressure-wave phenomena generated by the unsteady intake flow in the manifold runners with that of the individual cylinder intake processes; and at mid-speed by creating a Helmholtz resonance in the intake manifold plenum (again appropriately phased to the flows into each cylinder in turn), curve 8. Substantial tuning-generated increases in volumetric efficiency result, as shown.

The factors that have the greatest impacts on this full-load volumetric efficiency versus speed curve are total intake system flow friction, intake-valve closing angle, and intake tuning. In this graph engine speed in rev/min is used: the relevant "speed" is really mean piston speed since piston motion largely drives the intake flow.

6.2.8. Effects of Turbocharging

Turbocharging and supercharging increases the airflow into an engine of a given displaced volume, substantially: see Sec. 6.8. By increasing the air's density at entry to the engine's cylinders, the inducted air mass can be increased by a factor on the order of two or more. All the phenomena described in this section, and combined together in the previous section, are still relevant and important. But this substantial *boosting*—raising the air's density by raising its pressure significantly[5]—has a major impact. Note that volumetric efficiency is not as useful an indicator of the total intake system's airflow capabilities: it can be used with $\rho_{a,i}$ in Eq. (6.1) instead of $\rho_{a,0}$ where $\rho_{a,i}$, the air density at the compressor exit (or intercooler exit if utilized), is used to define the performance of that portion of the intake between the compressor or intercooler and the cylinder. A normalized airflow rate parameter—the *specific air consumption*—may be used to quantify the airflow into an engine in a normalized manner (air mass flow rate is divided by the engine's power, analogously to specific fuel consumption, Sec. 2.8), where

$$\mathrm{sac} = \dot{m}_a / P \tag{6.8}$$

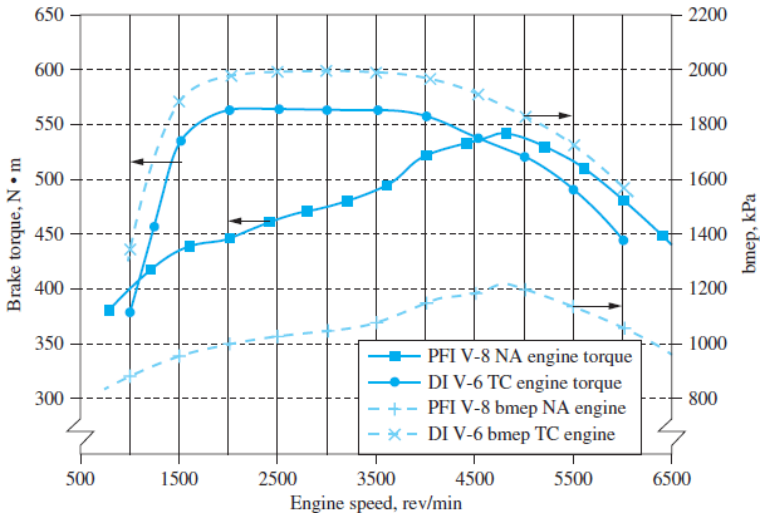
© McGraw-Hill Education. All rights reserved. Any use is subject to the Terms of Use, Privacy Notice and copyright information.

which has both brake and indicated values and units of kg of air/kW·h. Effectively, turbocharging substantially changes the baseline level in the combined, naturally-aspirated, volumetric efficiency versus speed plot (Fig. 6.12).

The air exiting the compressor in a turbocharging gasoline engine is at about 100°C (and may be higher if boost pressures above about 2 bar absolute are used). Cooling the intake air in a heat exchanger (intercooler) prior to entry to the engine's cylinders increases its density which increases the mass of air inducted. This both reduces the peak unburned mixture temperatures which reduces the engine's propensity to knock as well as reduces the peak burned gas temperatures which reduces the NO_x emissions. An intercooler, located between the compressor and the throttle, is normally air-cooled since ambient air is available for cooling at temperatures below that of the engine coolant. Coolant-cooled intercoolers are more compact but require a low temperature coolant supply to be effective. These may be used more often, as turbocharged engine outputs for a given displacement increase, as boost levels increase.

Figure 6.13 shows the wide-open-throttle torque and bmep versus speed curves for both a 3.6-liter V-6 turbocharged direct-injection gasoline SI engine and a 5.7-liter V-8 naturally-aspirated port-fuel-injected gasoline engine. The maximum torque and power of the two engines are closely comparable. The maximum bmep values and shapes of the bmep versus speed curves differ significantly. The airflow rates at entry to the cylinders are proportional to bmep from Eq. (2.48). For the naturally-aspirated engine, the bmep versus speed curve in Fig. 6.13 and the typical volumetric efficiency curve (Fig. 6.12) have closely comparable shapes.[6] The boosted engine's air mass per cylinder per cycle increases sharply from 1000 to about 1700 rev/min, and then remains roughly constant through the mid-speed range before falling off as the highest speeds are approached. This full load torque curve shape is attractive for automobile applications. The turbocharged gasoline engine behavior shown in Fig. 6.13 is the result of choosing a "smaller" turbocharger (relative to the size of the engine) to achieve rapidly rising torque at low engine speeds: a larger size turbocharger would give a rising air mass per cycle, and bmep (and torque) curves through the mid-speed range.

Figure 6.13 Brake torque and bmep as a function of engine speed at wide-open throttle for two gasoline SI engines: a 5.7-liter V-8 two valves per cylinder naturally-aspirated engine, and a 3.6-liter V-6 turbocharged direct-injection engine.



The maximum boost level—intake manifold pressure—for the turbocharged engines shown was about 1.8 bar (absolute) which gives bmep levels of about 2000 kPa. Turbocharged engine boost levels are rising, with bmep values of around 2500 kPa in production and with levels approaching 3000 kPa anticipated.

© McGraw-Hill Education. All rights reserved. Any use is subject to the Terms of Use, Privacy Notice and copyright information.

[1] In a naturally-aspirated engine at wide-open throttle, p_i would be close to atmospheric pressure; in a boosted engine, p_i would be the air pressure at compressor exit.

[2] At higher engine speeds, there is less time per cycle for heat losses to occur. This is only partly offset by the higher heat transfer rates due to higher velocities. Thus the average exhaust gas temperature increases as engine speed increases, and the exhaust gas density decreases.

[3] See Chap. 12.

[4] This was done with physically based models for each of the factors, appropriately integrated together. [8]

[5] The intake air's temperature (in kelvins, also used in the ideal gas law to calculate density) is not substantially changed, especially with intercooling.

[6] Note that engine friction as speed approaches its highest values has a modest distorting effect on the bmep airflow scaling.

© McGraw-Hill Education. All rights reserved. Any use is subject to the Terms of Use, Privacy Notice and copyright information.

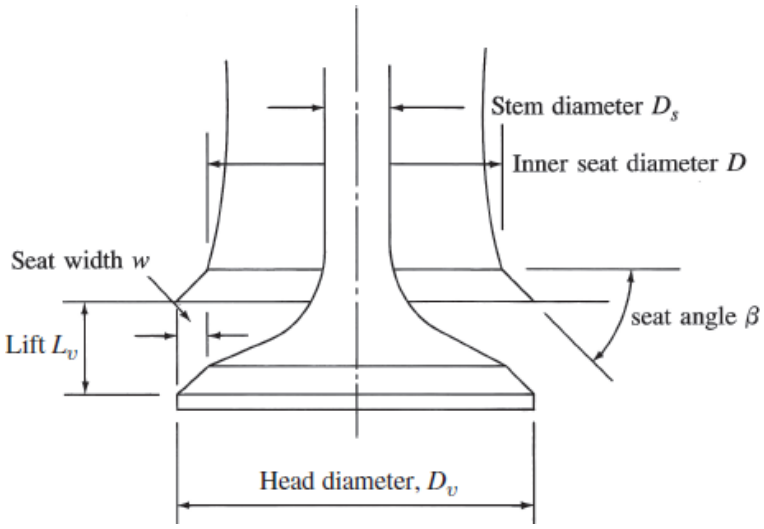
6.3. FLOW THROUGH VALVES AND PORTS

The valves, or valves and ports together, are usually the most important flow restriction in the intake and the exhaust system of four-stroke cycle engines. The characteristics of flows through engine poppet valves will now be reviewed, in the context of both fixed-valve opening and closing timings and of variable valve timing (VVT) and lift.

6.3.1. Valve and Port Geometry and Operation

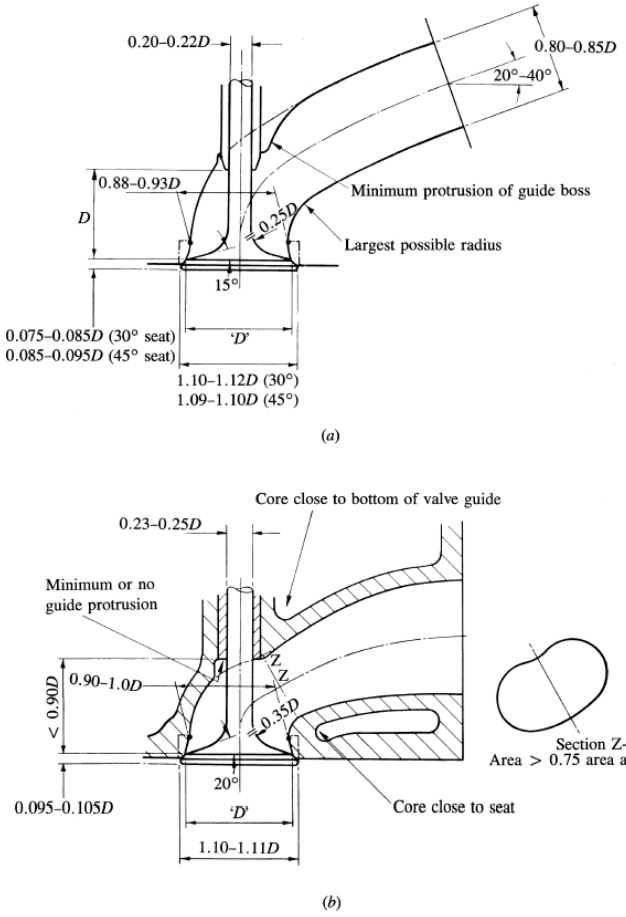
Figure 6.14 shows the main geometric parameters of a poppet valve head and seat. Figure 6.15 shows the proportions of typical intake and exhaust valves and ports, relative to the valve seat inner diameter *D*. The intake port is generally circular, or nearly so, and the cross-sectional area is no larger than is required to achieve the desired power output. For the exhaust port, the importance of good valve seat and guide cooling, with the shortest length of exposed valve stem, leads to a different design. Although a circular cross section is still desirable, a rectangular or oval shape is often essential around the guide boss area.

Figure 6.14 Parameters defining poppet valve geometry.



© McGraw-Hill Education. All rights reserved. Any use is subject to the Terms of Use, Privacy Notice and copyright information.

Figure 6.15 *Shape, proportions, and critical design areas of typical inlet (top) and exhaust (bottom) valves and ports.*[9]



Two, three, four, and even five valves per cylinder engines are in use, in the appropriately shaped cylinder head (of these valves, one, two, or three are intake valves, respectively). With multiple intake and exhaust valves, the individual valves become smaller while the total valve and port flow area per cylinder increases as the total number of valves increases. Historically, two valves per cylinder designs dominated. Now more than two-thirds of automobile engines have four valves per cylinder. Three valves per cylinder have airflow characteristics close to those of 4-valve engines because the intake valve and port flow areas are comparable and the impact of the smaller single exhaust valve and port area is modest. Variable valve timing and control mechanisms are steadily displacing fixed-valve-timing mechanisms and now dominate because the performance benefits of this flexibility in valve operation (largely through airflow increases) are significant. Variable valve control mechanisms and their operating characteristics are discussed more fully in Sec. 6.3.3.

Typical valve head sizes for different shaped combustion chambers in terms of cylinder bore B are given in Table 6.1.[9] Each of these chamber shapes (see Secs. 10.2 and 15.4 for a discussion of spark-ignition and diesel combustion chamber design) imposes different constraints on valve size. Larger valve sizes (or four valves compared with two) allow higher maximum airflows for a given cylinder displacement.

© McGraw-Hill Education. All rights reserved. Any use is subject to the Terms of Use, Privacy Notice and copyright information.

Table 6.1 Valve head diameter in terms of cylinder bore B[9]

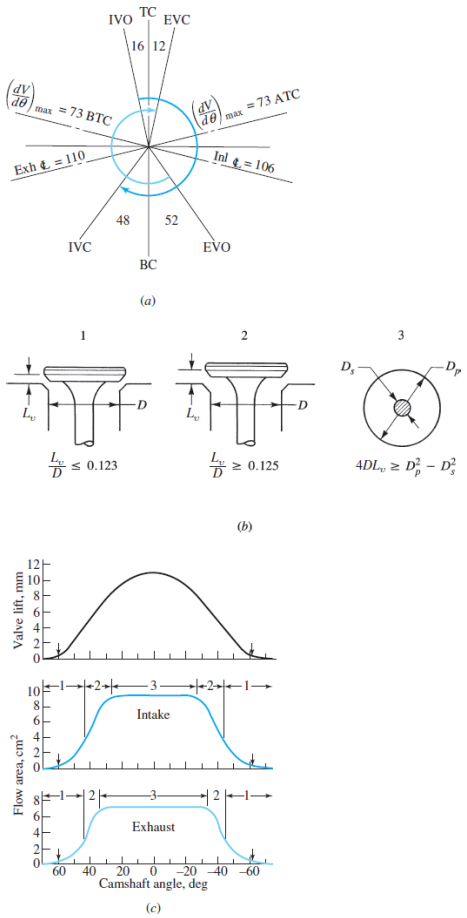
Combustion chamber shape*	Inlet	Exhaust	Approximate mean piston speed, max power, m/s †
Two-valve wedge or bathtub	0.43–0.46B	0.35–0.37B	15–16
Two-valve hemispherical	0.48–0.5B	0.41–0.43B	17
Three-valve open	0.38–0.4B	0.41–0.43B	19
Four-valve pent-roof	0.38–0.41B	0.31–0.35B	20
* See Fig. 15.26.			
† For fixed-valve-timing; values about 5% higher for variable valve timing.			

Typical valve timing, valve-lift profiles, and valve open areas for a four-stroke cycle fixed-valve-timing spark-ignition engine are shown in Fig. 6.16. There is no universally accepted criterion for defining valve timing points. Some are based upon a specific lift criterion. For example, the Society of Automotive Engineers (SAE) defines valve timing events based on reference valve-lift points:[10]

1. Hydraulic lifters: Opening and closing positions are the 0.15-mm (0.006-in.) valve-lift points.
2. Mechanical lifters: Valve opening and closing positions are the points of 0.15-mm (0.006-in.) lift plus the specified lash.

Figure 6.16 (a) Typical valve timing diagram for high-speed 2.2-dm^3 four-cylinder fixed-valve-timing spark-ignition engine; (b) schematic showing three stages of valve lift; (c) valve-lift curve and corresponding minimum intake and exhaust valve open areas as a function of camshaft angle. Intake and exhaust valve diameters are 3.6 and 3.1 cm, respectively.[11]

© McGraw-Hill Education. All rights reserved. Any use is subject to the Terms of Use, Privacy Notice and copyright information.



Alternatively, valve timing events can be defined based on angular criteria along the lift curve.[11] What is important is when significant gas flow through the valve open area either starts or ceases.

The instantaneous valve flow area depends on valve lift and the geometric details of the valve head, seat, and stem. There are three separate stages to the flow area development as valve lift increases, as shown in Fig. 6.16*b*.[12] For low valve lifts, the minimum flow area corresponds to a frustum of a right circular cone where the conical face between the valve and the seat, which is perpendicular to the seat, defines the flow area. For this stage:

$$\frac{w}{\sin\beta\cos\beta} > L_v > 0$$

and the minimum area is

$$A_{\min} = \pi L_v \cos\beta \; D_v - 2w + \frac{L_v}{2}\sin 2\beta$$

(6.9)

where β is the valve seat angle (usually 45° though other angles are used),
L_v is the valve lift,
D_v is the valve head diameter (the outer diameter of the seat), and w is the seat width (difference between the inner and outer seat radii).

For the second stage, the minimum area is still the slant surface of a frustum of a right circular cone, but this surface is no longer perpendicular to the valve seat. The base angle of the cone increases from (90 − β)° toward that of a cylinder, 90°. For

© McGraw-Hill Education. All rights reserved. Any use is subject to the Terms of Use, Privacy Notice and copyright information.

this stage:

$$\left[\left(\frac{D_p^2 - D_s^2}{4D_m}\right) - w^2\right]^{1/2} + w\tan\beta \geq L_v \frac{w}{\sin\beta\cos\beta}$$

and

$$A_{\min} = \pi D_m \left[(L_v - w\tan\beta)^2 + w^2\right]^{1/2}$$

(6.10)

where
D_p is the port diameter,
D_s is the valve stem diameter, and
D_m is the mean seat diameter
$(D_v - w)$.

Finally, when the valve lift is sufficiently large, the minimum flow area is no longer between the valve head and seat; it is the port flow area minus the sectional area of the valve stem. Thus, for

$$L_v > \left[\left(\frac{D_p^2 - D_s^2}{4D_m}\right)^2 - w^2\right]^{1/2} + w\tan\beta$$

then

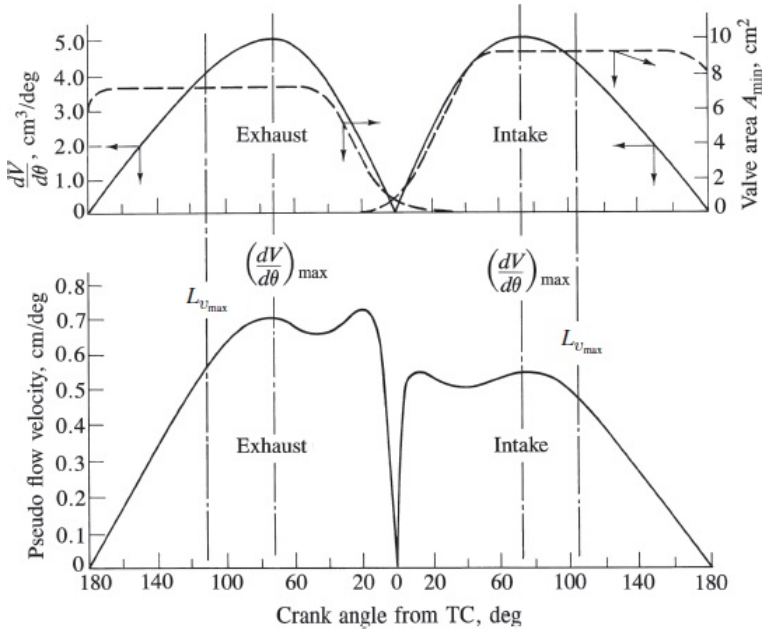
$$A_{\min} = \frac{\pi}{4}(D_p^2 - D_s^2)$$

(6.11)

Intake and exhaust valve open areas corresponding to a typical valve-lift profile are plotted versus camshaft angle in Fig. 6.17c. These three different flow regimes are indicated. The maximum valve lift is normally about 12% of the cylinder bore.

© McGraw-Hill Education. All rights reserved. Any use is subject to the Terms of Use, Privacy Notice and copyright information.

Figure 6.17 Rate of change of cylinder volume dV/dθ, valve minimum flow area A_{min}, and pseudo flow velocity as functions of crank angle for exhaust and intake valves of Fig. 6.16.[11]



Inlet valve opening (IVO) typically occurs 10 to 25° BTC. Engine performance is relatively insensitive to this timing point. It should occur sufficiently before TC so that cylinder pressure does not drop early in the intake stroke. Intake valve closing usually falls in the range 30 to 70° after BC. Later closing provides more time for cylinder filling under conditions where cylinder pressure is below the intake manifold pressure at BC (at higher speeds). IVC is one of the principal factors that determine high-speed volumetric efficiency. It also affects low-speed volumetric efficiency due to backflow into the intake (see Sec. 6.2.4).

Variable valve control allows IVC to be optimized in both these speed ranges. EVO occurs 50 to 60° before BC, well before the end of the expansion stroke, so that the blowdown process can assist in expelling the exhaust gases at higher speeds. The goal here is to reduce the cylinder pressure to close to the exhaust manifold pressure as soon as possible after BC over the full engine speed range. Note that the timing of EVO affects the cycle efficiency since it determines the effective burned gas expansion ratio. Exhaust valve closing (EVC) ends the exhaust process and determines the duration of the valve overlap period. EVC typically falls in the range 8 to 20° after TC. At idle and light load, in spark-ignition engines (which are throttled), it therefore regulates the quantity of exhaust gases that flow back into the combustion chamber through the exhaust valve under the influence of intake manifold vacuum. At high engine speeds and loads, it regulates how much of the cylinder burned gases are exhausted. EVC timing should occur sufficiently far after TC that the cylinder pressure does not rise near the end of the exhaust stroke. Late EVC favors high power at the expense of low-speed torque and idle combustion quality. Note from the timing diagram (Fig. 6.17*a*) that the points of maximum valve lift and of maximum piston velocity (Fig. 2.2) do not coincide.

The effect of valve geometry and timing on air flow can be illustrated conceptually by dividing the rate of change of cylinder volume by the instantaneous minimum valve flow area to obtain a *pseudo flow velocity* for each valve:[11]

$$v_{ps} = \frac{1}{A_{min} d\theta} = \frac{\pi \beta^2}{4 A_{min}} \frac{ds}{d\theta} \tag{6.12}$$

© McGraw-Hill Education. All rights reserved. Any use is subject to the Terms of Use, Privacy Notice and copyright information.

where *V* is the cylinder volume [Eq. (2.4)], *B* is the cylinder bore, *s* is the distance between the wrist pin and crank axis [see Fig. 2.1 and Eq. (2.5)], and
$A_{\min}$ is the valve area given by Eqs. (6.9), (6.10), or (6.11). Instantaneous pseudo-flow-velocity profiles for the exhaust and intake strokes of a four-stroke four-cylinder engine are shown in Fig. 6.17. Note the appearance of two peaks in the pseudo flow velocity for both the exhaust and intake strokes. The broad peaks occurring at maximum piston velocity reflect the fact that valve flow area is constant at this point. The peaks close to TC result from the exhaust valve closing and intake valve opening profiles. The peak at the end of the exhaust stroke is important since it indicates a significant pressure drop across the valve at this point, which will result in higher trapped residual mass. The magnitude of this exhaust stroke pseudo-velocity peak depends strongly on the timing of EVC. The pseudo-velocity peak at the start of the intake stroke is much less important. That the pseudo velocities early in the exhaust stroke and late in the intake stroke are low indicates that phenomena other than quasi-steady flow govern the flow rate. These are the periods when exhaust blowdown, and ram and tuning effects in the intake, are most important.

6.3.2. Flow Rates and Discharge Coefficients

The mass flow rate through a poppet valve is usually described by the equation for compressible flow through a flow restriction [Eq. (C.8) or (C.9) in App. C]. This equation is derived from one-dimensional isentropic flow analysis, and real gas flow effects are included by means of an experimentally determined discharge coefficient
C_D. The airflow rate is related to the upstream stagnation pressure
p_0 and stagnation temperature
T_0, static pressure just downstream of the flow restriction (assumed equal to the pressure at the restriction,
p_T), and a reference area
A_R characteristic of the valve design:

$$\dot{m} = \frac{C_D A_R p_0}{R T_0^{1/2}} \left(\frac{p_T}{p_0}\right)^{1/\gamma} \left\{ \frac{2\gamma}{\gamma - 1} \left[1 - \left(\frac{p_T}{p_0}\right)^{(\gamma - 1/\gamma)} \right] \right\}^{1/2}$$

(6.13)

When the flow is choked, that is,
$p_T/p_0 \leq [2/(\gamma+1)]^{\gamma/(\gamma-1)}$ the appropriate equation is

$$\dot{m} = \frac{C_D A_R p_0}{(R T_0)^{1/2}} \gamma^{1/2} \left(\frac{2}{\gamma + 1}\right)^{(\gamma+1)/2(\gamma-1)}$$

(6.14)

For flow into the cylinder through an intake valve,
p_0 is the intake system pressure
p_i, and
p_T is the cylinder pressure. For flow out of the cylinder through an exhaust valve,
p_0 is the cylinder pressure and
p_T is the exhaust system pressure.

The value of

© McGraw-Hill Education. All rights reserved. Any use is subject to the Terms of Use, Privacy Notice and copyright information.

C_D and the choice of reference area are linked together: their product,
C_D
A_R, is the effective flow area of the valve assembly, A_E. Several different reference areas have been used. These include the valve head area
$\pi D_v^2/4$,[13] the port area at the valve seat
$\pi D_p^2/4$,[14] the geometric minimum flow area [Eqs. (6.9), (6.10), and (6.11)], and the curtain area
$\pi D_v L_v$[15] where
L_v is the valve lift. The choice is arbitrary, though some of these choices allow easier interpretation than others. As has been shown above, the geometric minimum flow area is a complex function of valve and valve seat dimensions. The most convenient reference area in practice is the so-called valve curtain area:

$$A_C = \pi D_v L_v$$

(6.15)

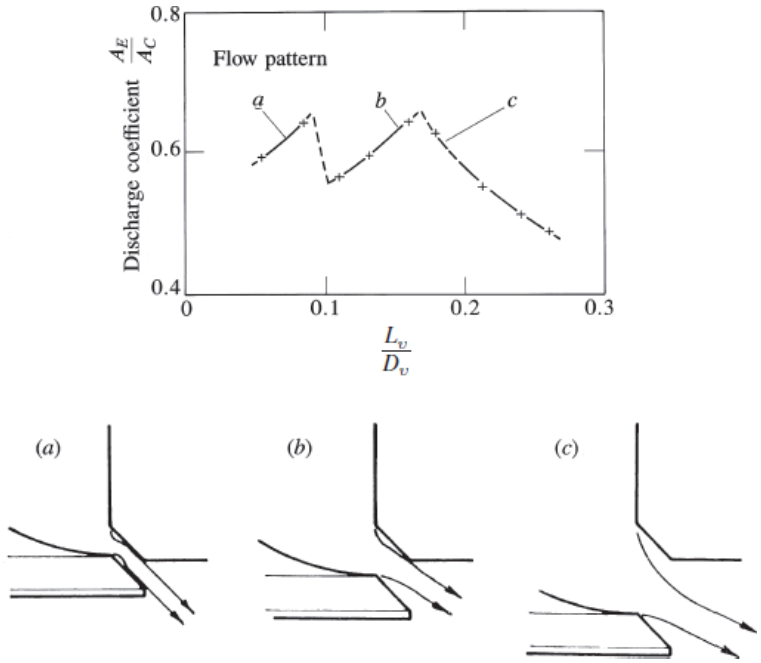
since it varies linearly with valve lift and is simple to determine.

6.3.2.1. Intake Valves

Figure 6.18 shows the results of steady-flow tests on a typical inlet valve configuration with a sharp-cornered valve seat.[15] The discharge coefficient based on valve curtain area is a discontinuous function of the valve-lift/diameter ratio. The three segments shown correspond to different flow regimes as indicated. At low lifts, the flow remains attached to the valve head and seat, giving high values for the discharge coefficient. At intermediate lifts, the flow separates from the valve head at the inner edge of the valve seat as shown. An abrupt decrease in discharge coefficient occurs at this point. The discharge coefficient then increases with increasing lift since the size of the separated region remains approximately constant while the minimum flow area is increasing. At high lifts, the flow separates from the inner edge of the valve seat as well.[12] Typical maximum values of
L_v/D_v are 0.25.

© McGraw-Hill Education. All rights reserved. Any use is subject to the Terms of Use, Privacy Notice and copyright information.

Figure 6.18 Discharge coefficient of typical intake poppet valve (effective flow area/valve curtain area) as a function of valve lift. Different segments correspond to the flow regimes indicated.[15]



An important question is whether these steady-flow data are representative of the dynamic flow behavior of the valve in an operating engine. There is some evidence that the "change points" between different flow regimes shown in Fig. 6.18 occur at slightly different valve lifts under dynamic operation than under steady-flow operation. Also, as shown in Fig. 6.10, the pressure upstream of the valve varies significantly during the intake process. However, it has been shown that over the normal engine speed range, steady-flow discharge-coefficient results can be used to predict dynamic performance with reasonable precision.[12, 16]

In addition to valve lift, the performance of the intake valve assembly is influenced by the following factors: valve seat width, valve seat angle, rounding of the seat corners, port design, and cylinder head shape. In many engine designs the port and valve assembly are used to generate a rotational motion (*swirl*) inside the engine about the cylinder axis during the induction process: for example, the cylinder head can be shaped to restrict the flow through one side of the valve open area and thereby generate swirl. Swirl production is discussed later, in Sec. 8.3. Swirl generation significantly reduces the valve (and port) flow coefficient. The intake ports can also be shaped to guide the airflow preferentially through the upper portion of the intake valve open area (between the valve and the center of the cylinder head), and across the cylinder. This generates a *tumbling* flow—a rotating motion in the plane including the cylinder axis—as the piston travels down the intake stroke. Swirl and tumble are discussed later, in Sec. 8.3.

Changes in seat width affect the L_v/D_v at which the shifts in flow regimes illustrated in Fig. 6.18 occur. C_D increases as seat width decreases. The seat angle β affects the discharge coefficient in the low-lift regime in Fig. 6.18. Rounding the upstream corner of the valve seat reduces the tendency of the flow to break away thus increasing C_D at higher lifts. At low valve lifts, when the flow remains attached, increasing the Reynolds number decreases the discharge coefficient. Once the flow breaks away from the wall, there is no Reynolds number dependence of C_D.[15]

For well-designed ports (e.g., Fig. 6.15) the discharge coefficient of the port and valve assembly need be no lower than that of the isolated valve (except when the port is used to generate swirl or tumble). However, if the cross-sectional area of the port is not sufficient or the radius of the surface at the inside of the bend is too small, a significant reduction in C_D for the assembly can result.[15]

© McGraw-Hill Education. All rights reserved. Any use is subject to the Terms of Use, Privacy Notice and copyright information.

At high engine speeds, unless the intake valve is of sufficient size, the inlet flow during part of the induction process can become choked (i.e., reach sonic velocity at the minimum valve flow area; see Sec. 6.2.5). Choking substantially reduces volumetric efficiency. Various definitions of inlet Mach number have been used to identify the onset of choking. Taylor and coworkers[13] correlated volumetric efficiencies measured on a range of engine and intake valve designs with an *inlet Mach index Z* formed from an average gas velocity through the intake valve:

$$Z = \frac{A_p \overline{S}_p}{C_i A_i a}$$

(6.16)

where A_i is the nominal inlet valve area $\left(\pi D_v^2/4\right)$, C_i is a mean valve discharge coefficient based on the area A_i, and a is the sound speed. From the method used to determine C_i, it is apparent that $C_i A_i$ is the average effective open area of the valve (it is the average value of $C_D \pi D_v L_v$): Z corresponds closely, therefore, to the mean Mach number in the intake valve throat. Taylor's correlations show that η_v decreases rapidly for $Z \geq 0.5$.

An alternative equivalent approach to this problem has been developed, based on the average flow velocity through the valve during the period the valve is open.[17] A *mean inlet Mach number* was defined:

$$\overline{M}_i = \frac{v_i}{a}$$

(6.17)

where
v_i is the mean intake flow velocity during the valve open period.
$\overline{M}_i$ is related to Z via

$$\overline{M}_i = \frac{Z\left(\eta_v/100\right)180}{\theta_{\mathrm{IVC}} - \theta_{\mathrm{IVO}}}$$

(6.18)

This mean intake Mach number correlates volumetric efficiency characteristics better than the Mach index. For a series of small modern four-cylinder engines, when M_i approaches 0.5 the volumetric efficiency decreases significantly more rapidly. This is due to the flow becoming choked during part of the intake process. This relationship can be used to size the intake valve/port combination for the optimum volumetric efficiency at maximum engine speed.

6.3.2.2. Exhaust Valves

In studies of the flow from the cylinder through an exhaust poppet valve, different flow regimes at low and high lift occur, as shown in Fig. 6.19. Values of C_D based on the valve curtain area, for several different exhaust valve and port combinations, are given in Fig. 6.20. A sharp-cornered isolated poppet valve (i.e., straight pipe downstream, no port) gives the best performance.

© McGraw-Hill Education. All rights reserved. Any use is subject to the Terms of Use, Privacy Notice and copyright information.

Figure 6.19 *Flow pattern through exhaust valve at low and high lift.*[15]

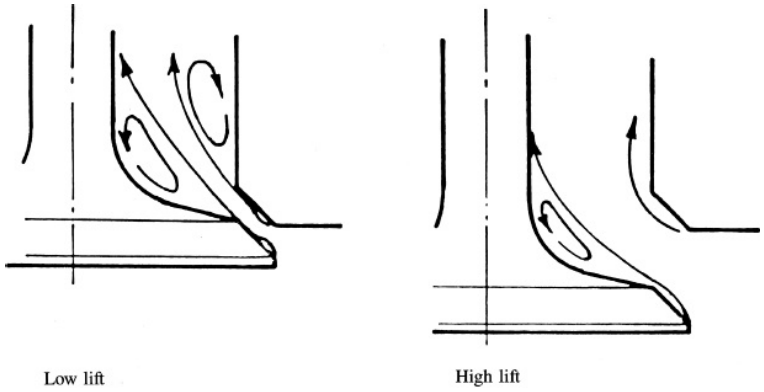
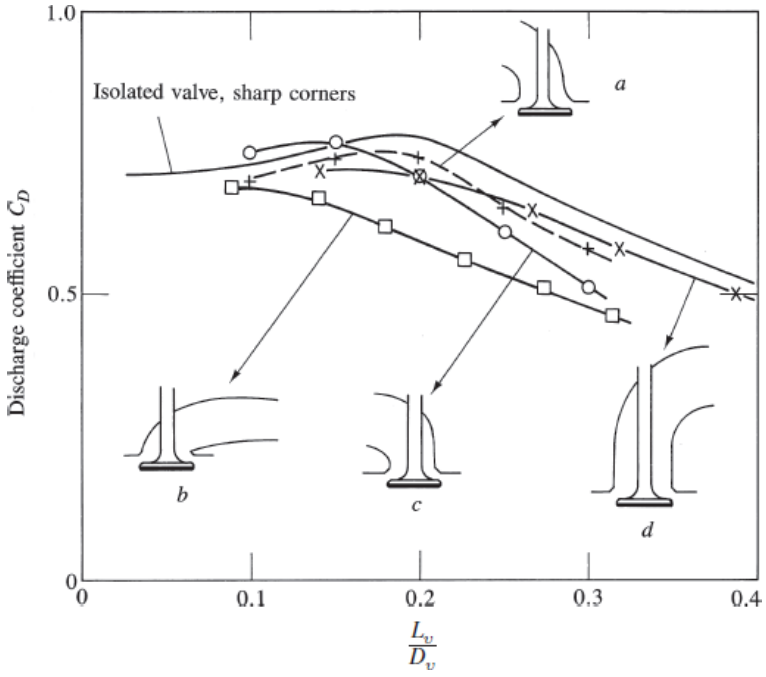


Figure 6.20 *Discharge coefficient as function of valve lift for several exhaust valve and port designs:*[15]*a,*[18]*b,*[17]*c,*[18]*d.*[19]



At high lifts, $L_v/D_v \geq 0.2$ the breakaway of the flow reduces the discharge coefficient. (At $L_v/D_v = 0.25$ the effective area is about 90% of the minimum geometric area. For $L_v/D_v < 0.2$ it is about 95%.[15]) The port design significantly affects C_D at higher valve lifts, as indicated by the data from the four port designs in Fig. 6.20. Good designs can approach the performance of isolated valves, however. Exhaust valves operate over a wide range of pressure ratios (1 to 5). For pressure ratios greater than about 2 the flow will be choked, but the effect of pressure ratio on discharge coefficient is small and confined to higher lifts (e.g., ±5% at $L_v/D_v = 0.3$).[14]

6.3.3. Variable Valve Timing and Control

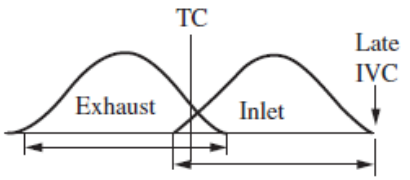
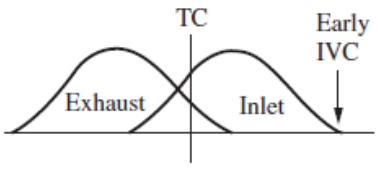
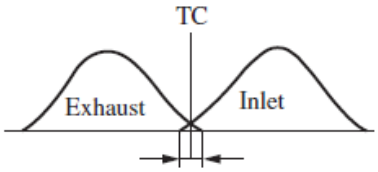
6.3.3.1. Benefits

© McGraw-Hill Education. All rights reserved. Any use is subject to the Terms of Use, Privacy Notice and copyright information.

Increasingly, variable control of valve operation as a function of engine load and speed is being used instead of fixedvalve timing and operation, which used to be the standard approach. The simplest approach—rotation of the camshafts relative to the crankshaft—varies the phasing of the intake and exhaust camshafts via a cam phaser, to improve the engine's airflow capability at high speed (thus allowing the maximum speed to be increased), and increase the torque at low speed. More sophisticated (variable valve control—VVC) valve-actuation mechanisms are also used which can vary valve timing, open duration, and lift. While greater benefits result from controlling the intake valves, there are additional benefits from varying the exhaust valve behavior: increasing the effective expansion ratio of the burned gases before EVO (Miller and Atkinson cycles; see Sec. 5.6); controlling the in-cylinder residual burned gas fraction to improve idle and light-load combustion stability and reduce
NO_x and HC emissions. Variable valve control also has the potential for reducing the engine's pumping work at lighter loads: see Sec. 13.7. As already mentioned in Sec. 6.2, and shown in Fig. 6.21, later IVC (and higher valve lift) increase the air charging of the cylinder at high speed and allow the piston speed to be increased before airflow choking limits are reached (see Sec. 6.2.5). Early IVC at low speed decreases the backflow of air (plus residual) into the intake during the early part of the compression stroke. The engine full load torque benefits are apparent in Fig. 6.9. Note that airflow gains at high speed (and increasing maximum engine speed) increase the maximum brake power of the engine. At fixed engine-in-vehicle performance, a downsized engine can then be used, which at part-load is less throttled, has lower friction, and thus has a higher brake fuel-conversion efficiency.

Figure 6.21 Desired exhaust and intake valve timings as a function of the three listed performance objectives.

Valve Timing Characteristics for Performance Objectives

Engine performance objectives	Required valve timing characteristics
Greater maximum power	 Long valve open duration (intake and exhaust)
Greater low-speed torque	
Better idle combustion stability	 Small valve overlap

6.3.3.2. Mechanical Approaches

Over the years, many valve control mechanisms have been developed, and a number of these are now used in production

© McGraw-Hill Education. All rights reserved. Any use is subject to the Terms of Use, Privacy Notice and copyright information.

automobile and truck engines. One simple approach in multi-cylinder gasoline engines is cylinder cut out at lighter engine loads. The valves (intake and exhaust) are deactivated in some of the engine's cylinders (e.g., 4-cylinders out of 8; 2-cylinders out of 4). The displaced volume of the firing cylinders is reduced: thus at the same output torque each of these (reduced number of cylinders) is operating more highly loaded with a higher intake manifold pressure and reduced pumping work. While the mechanical friction of the non-firing cylinders is still present, a net average-driving fuel-consumption benefit of some 5% results from deactivating half the engine's cylinders.[20]

Figure 6.22 provides a description and assessment of the various mechanistic approaches to variable valve control that are used in practice. These different approaches are illustrated by the changes in intake valve lift profile each mechanism employs. The figure also provides a rating on an excellent to poor scale of their normalized power, torque, fuel consumption, and emissions characteristics, and number of parts (or their complexity).

Figure 6.22 Schematic of intake valve timing and lift profiles for five different valve control approaches/mechanisms, and their rankings on power, torque, fuel consumption, emissions, number of parts.[21]

Assessment of Variable Intake Valve Control

Type	Description	Power	Torque	Fuel consumption	Emissions	Number of parts
Varying cam phasing (continuous)		○	◎	○	◎	◎
Switching between different cam profiles		◎	○	△	△	△
3-D cam profiles (and lateral shift)		◎	◎	○	○	×
Fully variable lift and timing (with camshaft)		○	◎	◎	○	×
Electromagnetic valve drive		○	◎	◎	◎	×

◎ Excellent ○ Good △ Medium × Poor

6.3.3.3. Cam Phasing

Continuously adjusting the phasing of the intake cam and the exhaust cam relative to the crankshaft is the commonest approach. An intake valve closing adjustment range of about 40 degrees (± 20 degrees about 50°ABC) would be typical. A similar range is used for exhaust valve phasing. It is low cost and relatively effective at increasing low-speed torque (10%), high-speed torque (5%), and maximum engine speed (up to 5%), relative to fixed-valve-timing levels. At idle, the camshafts are set for later intake and exhaust valve opening and closing, respectively, to reduce the valve overlap period, and thus the exhaust backflow and in-cylinder residual, to produce more stable idle combustion, allow lower idle speeds, and reduced idle fuel consumption. At high loads and low-to-mid speeds, the intake cam is rotated to close the intake valve earlier to reduce the amount of inducted air pushed back from the cylinder into the intake during the first part of the compression stroke. At mid speeds, normal IVC angles are used: at high speeds, the cam is rotated to retard IVC to take advantage of the extra air inducted due to intake manifold ram charging (see Sec. 6.2.4).

© McGraw-Hill Education. All rights reserved. Any use is subject to the Terms of Use, Privacy Notice and copyright information.

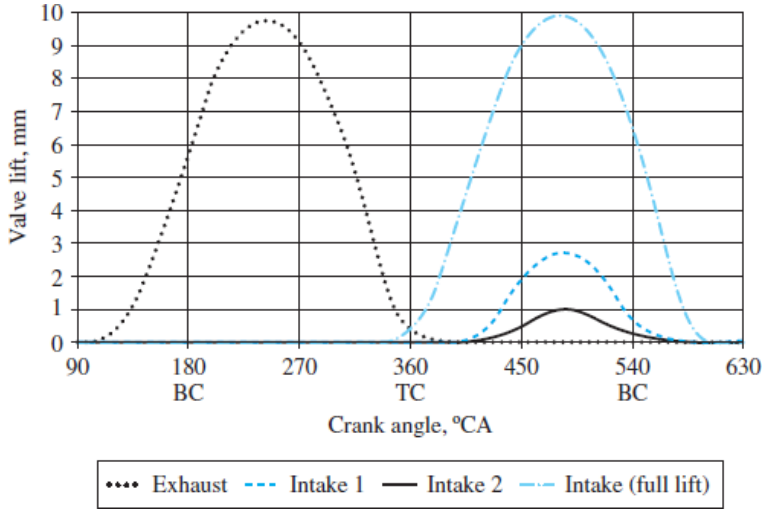
6.3.3.4. Cam Switching

With cam profile switching, the intake valve motion is driven by two (or even three) cams: a lower-lift shorter-duration intake cam profile is used at lower speeds; at higher speed, a higher-lift longer-duration cam profile is used. This can be achieved, for example, with an additional rocker arm that rides freely on the high-speed cam at low speeds when the low-speed cam is controlling, which is then connected/pinned to the low-speed rocker arm (and thus overrides it) at high speeds since the high-speed cam is larger (has higher lift and longer open duration). Cam shifting can provide a larger increase in maximum power (as a result of the larger high-speed intake-valve cam profile), and can also more readily give low valve overlap at low speed and thus good torque along with excellent idle combustion quality.

6.3.3.5. Fully Variable Valve Control

A valve control system that permits variations in lift, open duration, and timing is termed*fully variable*. One approach is to use cams with curved three-dimensional profiles and lateral shift capability which provide substantial degrees of freedom. This type of camshaft control enables fully variable adjustment of intake valve lift, opening angle, and open duration. An alternative is the valvetronic system[22] where an electric motor rotates an eccentric shaft that varies the interaction between the intake cams and the cam roller followers that actuate the valves. Low intake valve lifts are used to throttle the airflow, and the conventional throttle valve can be removed. Such approaches, in addition to improving full load airflow, can be used to increase the in-cylinder flow velocities and turbulence levels and thus enhance the combustion rate and stability. Figure 6.23 illustrates various intake valve lift profiles, where valve lift is varied to both control (throttle) the airflow into the cylinder and generate in-cylinder flows that enhance combustion and improve emissions control (e.g., with different lift profiles for the two intake valves).

Figure 6.23 Exhaust and intake valve lift profiles for the BMW Valvetronic variable valve control mechanism. Changes in intake valve lift and duration variations are used to throttle the airflow as engine load is reduced.[22]



The final valve control mechanism shown in Fig. 6.22 is electrical rather than mechanical valve actuation, where valves are operated electromagnetically with solenoids or by electro-hydraulic actuators. Such systems, without camshafts, can provide fully flexible valve control and thus have significant potential for improving torque, fuel consumption, and emissions. The challenges to deploying this type of technology are the substantial forces required (which increase with the square of engine speed), noise, drive energy requirements to overcome valvetrain friction, packaging, and cost.

6.3.3.6. Pumping Work Reduction

© McGraw-Hill Education. All rights reserved. Any use is subject to the Terms of Use, Privacy Notice and copyright information.

In spark-ignition engines at part-load, the intake airflow is throttled to below atmospheric pressure. Thus, during the exhaust and intake strokes of the standard four-stroke cycle, work is transferred *to* the piston. In naturally-aspirated engines this *pumping work* is counted as a part of engine friction (seeSecs. 2.5 and 13.7). Variable valve control can reduce this pumping work loss, which in the ideal four-stroke-cycle model (Sec. 5.2) is given by $(p_e - p_i)V_d$. At a given (light-load) torque, the mass of (stoichiometric) fuel-air mixture burned in the cylinder is proportional to that torque. The mass trapped in the cylinder is given by the ideal gas law, applied at the intake-valve-closing (IVC) location:

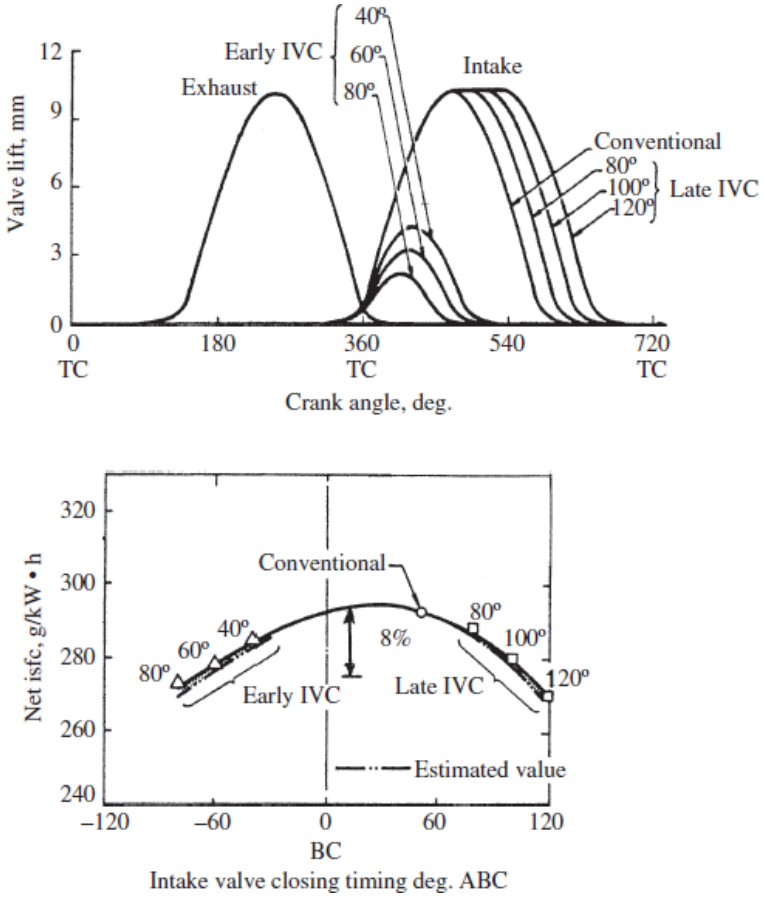
$$p_{\text{cyl}} V_{\text{IVC}} = m_{\text{cyl}} R T_{\text{cyl}}$$

(6.19)

About the same mass of fuel and air is required to produce this torque as the IVC angle changes (the change in gross-indicated fuel-conversion efficiency is modest). Also, T_{cyl} changes little. Thus as V_{IVC} becomes smaller, p_{cyl} during the intake process must be increased, and the pumping work is therefore reduced. Figure 6.24 shows the fuel consumption gains that result as the cylinder volume at IVC is reduced either by *later* IVC during the compression stroke, or much *earlier* IVC during the intake stroke. A benefit in *net-indicated* specific fuel consumption of about 8% relative to typical fixed IVC operation results. Because variable valve control can change the cylinder pressure-volume relationship during the compression and expansion strokes, defining pumping work for these modified cycles requires a more sophisticated approach. See Sec. 13.7 where this topic is discussed in more detail.

© McGraw-Hill Education. All rights reserved. Any use is subject to the Terms of Use, Privacy Notice and copyright information.

Figure 6.24 Illustration of how variations of intake valve timing and lift (with both early and late IVC) improve net isfc by reducing the engine's pumping friction work.[23] Engine conditions: 1400 rev/min, torque 29 N·m, A/F 14.5, MBT timing, no EGR.



© McGraw-Hill Education. All rights reserved. Any use is subject to the Terms of Use, Privacy Notice and copyright information.

6.4. RESIDUAL GAS FRACTION

The residual gas fraction in the cylinder during compression is determined by the details of the exhaust and intake processes. Its magnitude affects volumetric efficiency and engine performance directly, and efficiency and emissions through its effect on working-fluid thermodynamic properties and on combustion. The residual gas fraction is primarily a function of intake and exhaust pressures, engine speed, compression ratio, valve timing, and exhaust system dynamics.

The residual gas mass fraction x_r (or burned gas fraction in the in-cylinder unburned mixture when EGR is used) is usually determined by measuring the CO_2 concentration in a sample of gas extracted from the cylinder during the compression stroke. Then

$$x_r = (\tilde{x}_{CO_2})_c / (\tilde{x}_{CO_2})_e$$

(6.17)

where the subscripts *c* and *e* denote compression and exhaust and $\tilde{x}_{CO_2}$ are mole fractions in the wet gas. Usually CO_2 volume or mole fractions are measured in dry gas streams (see Sec. 4.9). A correction factor *K*,

$$K = \frac{(\tilde{x}_i)_{wet}}{(\tilde{x}_i)_{dry}} = \frac{1}{1 + 0.5\left[y\left(\tilde{x}^*_{CO_2} + \tilde{x}^*_{CO}\right) - 0.74\tilde{x}^*_{CO}\right]}$$

(6.18)

where *y* is the molar hydrogen/carbon ratio of the fuel, and $\tilde{x}^*_{CO_2}$, $\tilde{x}^*_{CO}$ are dry mole fractions, can be used to convert the dry mole fraction measurements to wet mole fractions.

The residual gas mass in the cylinder is the result of two (additive) processes: (1) the gas trapped in the cylinder just before IVO when the valve overlap flow commences, m_{cyl}; (2) the backflow of burned gas from the exhaust port into the cylinder during the valve overlap period (from IVO to EVC), m_{exh}; see Figs. 6.1 and 6.16. Thus, m_r is

$$m_r = m_{cyl,IVO} + \int_{\theta_{IVO}}^{\theta_{EVC}} \dot{m}_{exh} dt$$

(6.19)

All the burned gas that flows from the cylinder into the intake port during the pressure equalization process (cylinder pressure drops to the intake manifold pressure as this backflow occurs) is assumed to flow back into the cylinder during the subsequent intake process.[24] The residual mass fraction x_r, as determined from ideal gas cycle analysis and the in-cylinder mass at intake valve opening (at TC), is given by Eq. (5.35). Its temperature is given by Eq. (5.36).

The residual gas fraction component due the valve overlap backflow is given by:

© McGraw-Hill Education. All rights reserved. Any use is subject to the Terms of Use, Privacy Notice and copyright information.

$$x_{r,\text{backflow}} = \int \frac{\dot{m}_{\text{exh}}}{\rho_a V_d \left[(r_c + 1) / r_c \right]} \frac{1}{6N} dt$$

(6.20)

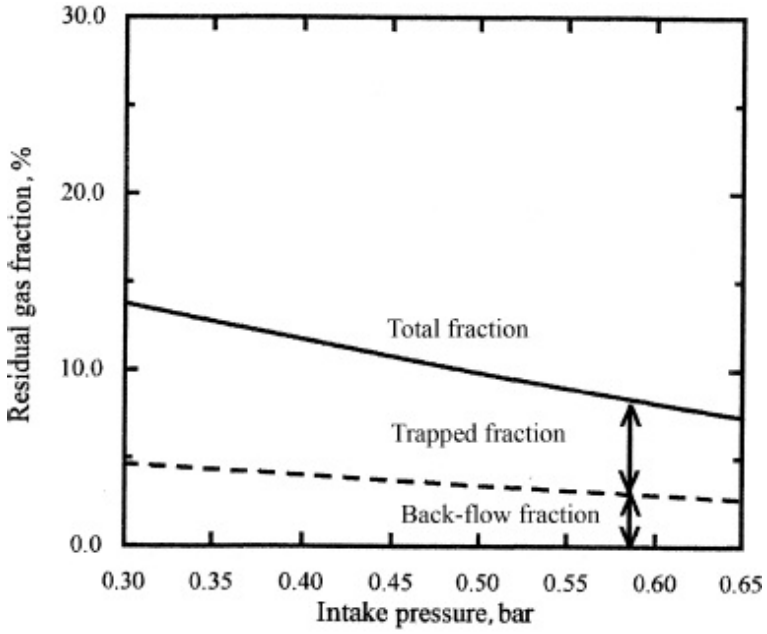
and the total residual gas fraction trapped in the cylinder (after IV closing) is

$$x_r = x_{r,\text{IVO}} + x_{r,\text{backflow}}$$

(6.21)

Several models of the combination of these two processes have been developed and correlated against measured data. Figure 6.25 shows the backflow residual fraction, trapped fraction, and total residual as a function of intake manifold pressure (absolute). An intake pressure of about 0.45 bar is typical of a part-load operating condition for a light-duty vehicle with a naturally-aspirated spark-ignition engine. For a turbocharged SI engine, in a similar vehicle, the engine's intake manifold pressure would be about twice that, and the residual fraction significantly lower.

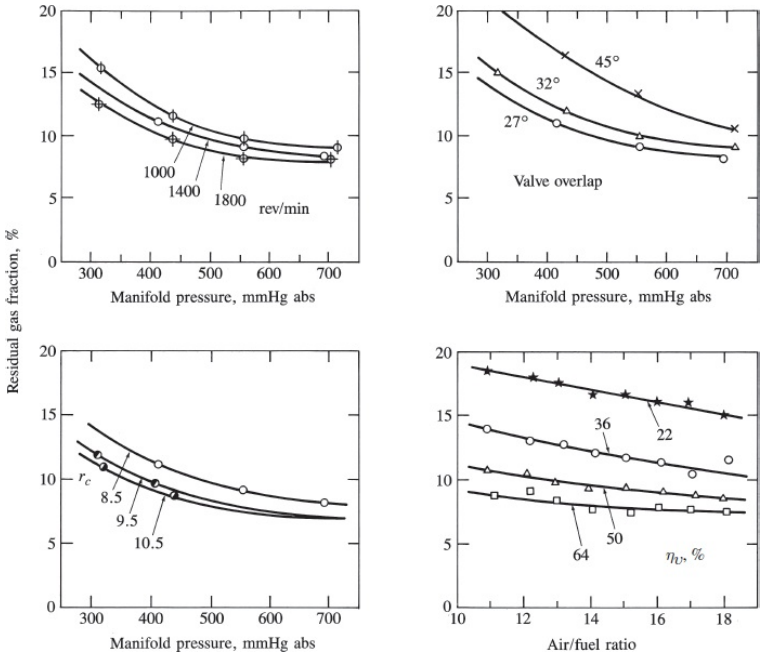
Figure 6.25 Residual gas fraction as a function of intake pressure (bar, absolute) for a naturally-aspirated gasoline engine showing the backflow fraction, the trapped fraction, and the total residual fraction.[24]



Residual gas measurements in a spark-ignition engine are given in Fig. 6.26, which shows the effect of changes in speed, valve overlap, compression ratio, and air/fuel ratio for a range of inlet manifold pressures for a 2-liter, 88.5-mm bore, four-cylinder engine.[25] The effect of variations in spark timing was negligible. Inlet pressure, speed, and valve overlap are the most important variables, though the exhaust pressure also affects the residual fraction. Normal settings for IVO (about 15° before TC) and EVC (about 12° after TC) provide sufficient overlap for good scavenging, but avoid excessive backflow from the exhaust port into the cylinder.

© McGraw-Hill Education. All rights reserved. Any use is subject to the Terms of Use, Privacy Notice and copyright information.

Figure 6.26 Residual gas fraction for a 2-liter four-cylinder spark-ignition engine as a function of intake manifold pressure for a range of speeds, compression ratios, and valve overlaps: also as a function of air/fuel ratios for a range of volumetric efficiencies. Operating conditions, unless noted: speed = 1400 rev/min, A/F = 14.5, spark timing set to give 0.95 maximum torque, compression ratio = 8.5.[25]



Residual gas fractions in diesel engines are substantially lower than in SI engines because inlet and exhaust pressures are comparable in magnitude and the compression ratio is almost twice as large. Also, as consequence of the diesel's lean operation, a substantial fraction of the residual gas is air.

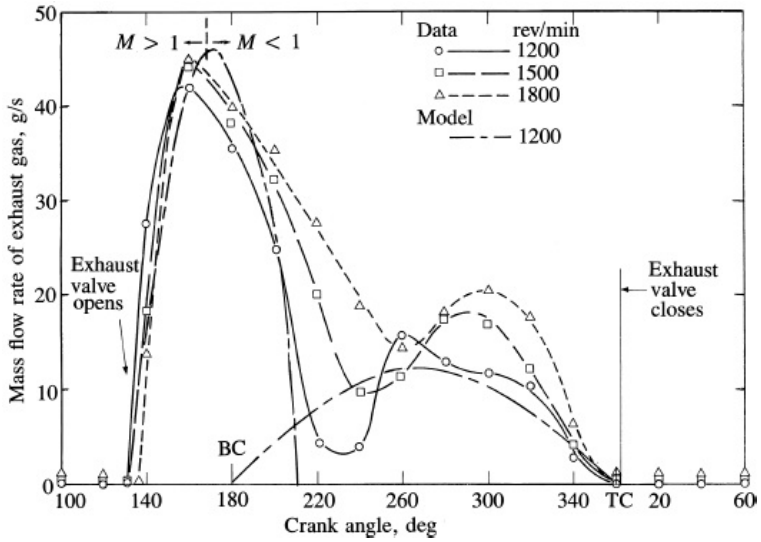
© McGraw-Hill Education. All rights reserved. Any use is subject to the Terms of Use, Privacy Notice and copyright information.

6.5. EXHAUST GAS FLOW RATE AND TEMPERATURE VARIATION

The exhaust gas mass flow rate and the properties of the exhaust gas vary significantly during the exhaust process. The origin of this variation for an ideal exhaust process is evident from Fig. 5.3. The thermodynamic state (pressure, temperature, etc.) of the gas in the cylinder varies continuously during the exhaust blowdown phase, until the in-cylinder pressure closely approaches the exhaust manifold pressure. In the real exhaust process, the exhaust valve restricts the flow out of the cylinder, the valve lift varies with time, and the cylinder volume changes during the blowdown process, but the principles remain the same.

Measurements have been made of the variation in mass flow rate through the exhaust valve and the gas temperature at the exhaust port exit during the exhaust process of a spark-ignition engine.[26] Figure 6.27 shows examples of the instantaneous mass flow rate data at three different engine speeds, at wide-open throttle. The *blowdown* and *displacement* phases of the exhaust process are evident. Simple quasi-steady models of these phases give good agreement with the data at lower engine speeds. The blowdown model shown applies orifice flow equations to the flow across the opening exhaust valve using the measured cylinder pressure and estimated gas temperature for upstream stagnation conditions. Equation (C.9) is used when the pressure ratio across the valve exceeds the critical value. Equation (C.8) is used when the pressure ratio is less than the critical value. The displacement model assumes the gas in the cylinder is incompressible as the piston moves through the exhaust stroke. As engine speed increases, the crank angle duration of the blowdown phase lengthens. There is evidence of dynamic effects occurring at the transition between the two phases. The peak mass flow rate during blowdown does not vary substantially with speed since the flow is choked. The mass flow rate at the time of maximum piston speed during the displacement phase scales approximately with piston speed. As the inlet manifold pressure is reduced below the wide-open-throttle value, the proportion of the charge which exits the cylinder during the blowdown phase decreases but the mass flow rate during the displacement phase remains essentially constant (at a given engine speed). As speed increases, the displacement-phase exhaust flow rate increases in proportion to the piston speed, since the piston motion drives this phase of the exhaust process.

Figure 6.27 Instantaneous mass flow rate of exhaust gas through the valve versus crank angle: equivalence ratio = 1.2, wide-open throttle, compression ratio = 7. Dash-dot line is one-dimensional compressible flow model for blowdown and incompressible displacement model for the exhaust stroke.[26]

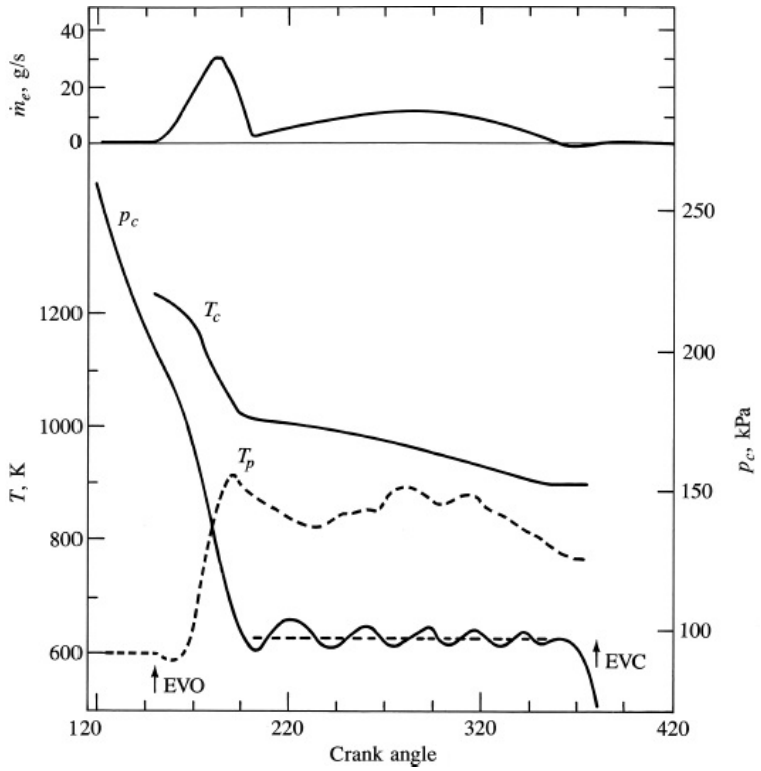


© McGraw-Hill Education. All rights reserved. Any use is subject to the Terms of Use, Privacy Notice and copyright information.

The exhaust gas temperature varies substantially through the exhaust process: it decreases due to gas expansion and to heat loss as the gas flows past the exhaust valve and through the exhaust system.

Figure 6.28 shows the measured cylinder pressure, calculated cylinder gas temperature and exhaust mass flow rate, and measured gas temperature at the exhaust port exit for a single-cylinder spark-ignition engine at mid-load and low speed.[27] The average cylinder-gas temperature falls rapidly during blowdown, and continues to fall during the exhaust stroke due to heat transfer to the cylinder walls. The gas temperature at the port exit at the start of the exhaust flow pulse is a mixture of hotter gas which has just left the cylinder and cooler gas which left the cylinder at the end of the previous exhaust process and has been stationary in the exhaust port while the valve has been closed. The port exit temperature has a maximum about where the transition from blowdown flow to displacement flow occurs, as the gas comes momentarily to rest and loses a fraction of its thermal energy to the exhaust port walls.

Figure 6.28 Measured cylinder pressure p_c, calculated cylinder-gas temperature T_c, exhaust mass flow rate $\dot{m}_e$, and measured gas temperature at exhaust port exit T_p, for single-cylinder spark-ignition engine. Speed = 1000 rev/min, imep = 414 kPa, equivalence ratio = 1.2, spark timing = 10° BTCq, r_c = 7.2.[27]



Variations in engine load and speed impact exhaust gas temperatures. Increasing load increases the mass and temperature in the blowdown pulse. Increasing speed raises the gas temperature throughout the exhaust process. These effects are the result of variations in the relative importance of heat transfer in the cylinder during the expansion stroke, and heat transfer to the exhaust valve and port as gas is exhausted. The time available for heat transfer, which depends on engine speed and exhaust gas flow rate, is the most critical factor. The exhaust temperature variation with equivalence ratio follows from the variation in expansion stroke temperatures, with maximum values at ϕ = 1.0 and lower values for leaner and richer mixtures. Diesel engine exhaust temperatures are significantly lower than spark-ignition engine exhaust temperatures because of their lean overall equivalence ratio (which increases from very low at idle to about 0.7 at high loads) and their higher expansion ratio during the power stroke.

The average exhaust gas temperature is an important quantity for determining the performance of turbochargers, catalytic converters, and particulate traps. The time-averaged exhaust temperature does not correspond to the average energy of the

© McGraw-Hill Education. All rights reserved. Any use is subject to the Terms of Use, Privacy Notice and copyright information.

exhaust gas because the flow rate varies substantially. An enthalpy-averaged temperature

$$\overline{T}_h = \left(\int_{\text{EVO}}^{\text{EVC}} \dot{m} c_p T_g d\theta \right) / \left(\int_{\text{EVO}}^{\text{EVC}} \dot{m} c_p d\theta \right)$$

(6.22)

is the best indicator of exhaust thermal energy. Exhaust gas temperatures are usually measured with a thermocouple. Thermocouple-averaged temperatures are close to time-averaged temperatures. Mass-averaged exhaust temperatures (which are close to $\overline{T}_h$ if c_p variations are small) for a spark-ignition engine at the exhaust port exit are about 100 K higher than time-averaged thermocouple determined temperatures. Mass-average temperatures in the cylinder during the exhaust process are about 200 to 300 K higher than mass-averaged port temperatures.[28]

Exhaust gas temperatures increase with increasing engine speed, load, and spark retard. Relative air/fuel ratio (or equivalence ratio) is especially important, and thus exhaust gas temperatures in gasoline SI engines are higher than exhaust gas temperatures in diesel engines (which vary significantly with load since load and equivalence ratio scale with each other). Gasoline engines with stoichiometric operation have exhaust gas temperatures of about 650°C (925 K). When operated lean, exhaust gas temperatures decrease (e.g., at λ = 1.4, by about 50 deg. C). On the rich side of stoichiometric, exhaust gas temperatures rise slightly, peak at about λ = 0.95 and then decrease. In diesels, where load is controlled by varying the fuel/air equivalence ratio, at light load exhaust gas temperatures are low (200 to 300°C), and at high load (ϕ = 0.7) are about 450°C. Small high-speed DI diesels have somewhat lower exhaust gas temperatures than do heavy-duty truck DI engines.[29] Note exhaust gas temperature values are usually time-average measurements made close to the exhaust port exit.

© McGraw-Hill Education. All rights reserved. Any use is subject to the Terms of Use, Privacy Notice and copyright information.

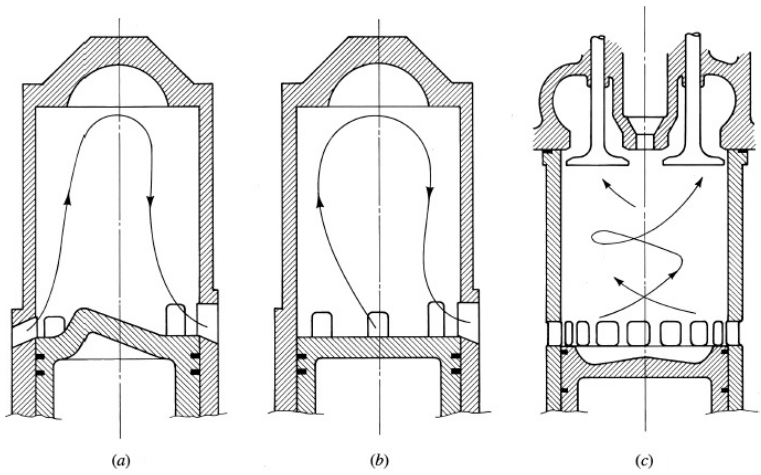
6.6. SCAVENGING IN TWO-STROKE CYCLE ENGINES

6.6.1. Two-Stroke Engine Configurations

In two-stroke cycle engines, every outward (or downward) stroke of the piston is a power stroke. To achieve this behavior, the burned gases have to be replaced by fresh charge while the piston moves through its bottom center (BC) position. The period during which the products of combustion are exhausted from the cylinder and the fresh charge enters, the gas exchange period or scavenging process, begins at the time that the exhaust port is first exposed (see Fig. 1.3) or the exhaust valve opens (Fig. 1.36). It is completed at the time when both the exhaust ports (or valves) and scavenge (or transfer) ports are closed. It is useful and convenient to divide the total gas exchange process into two periods: the *exhaust blowdown period*, from exhaust opening to scavenge port opening; and the *scavenging period*, which is the remainder. The fresh charge must be supplied to the engine cylinder at a high-enough pressure to displace the in-cylinder burned gases from the previous cycle. Raising the pressure of the intake mixture is done with a pump or blower or compressor. Air capacity is just as important as in the four-stroke cycle. However, in the two-stroke cycle scavenging process, a fraction of the air is inevitably lost—it passes straight through the cylinder. Thus a greater air mass flow rate must be achieved to obtain the same output power. This loss of air during scavenging makes tracking the gas exchange process more complicated.

The different categories of two-stroke cycle scavenging flows and the port (and valve) arrangements that produce them are illustrated in Figs. 6.29 and 6.30. Scavenging arrangements are broadly classified into: (*a*) *cross-scavenged*, (*b*) *loop-scavenged*, and (*c*) *uniflow-scavenged configurations*. The location and orientation of the scavenging ports control the scavenging process, and the most common arrangements are indicated. Cross- and loop-scavenging systems use exhaust and ports in the cylinder wall, uncovered by the piston as it approaches BC. The uniflow system may use transfer ports with exhaust valves in the cylinder head, or transfer and exhaust ports with opposed pistons. Despite the different flow patterns obtained with each cylinder geometry, the general operating principles are similar. Air in a diesel, or fuel-air mixture in a spark-ignition engine, must be supplied to the transfer ports at a pressure higher than the exhaust system pressure.

Figure 6.29 (a) Cross-scavenged, (b) loop-scavenged, and (c) uniflow-scavenged two-stroke cycle flow configurations.



© McGraw-Hill Education. All rights reserved. Any use is subject to the Terms of Use, Privacy Notice and copyright information.

Figure 6.30 Common porting arrangements that go with (a) cross-scavenged, (b) loop-scavenged, and (c) uniflow-scavenged configurations.

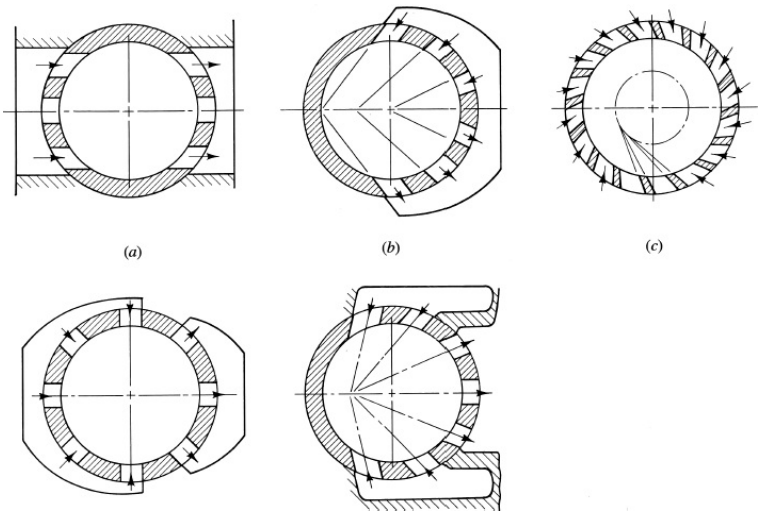
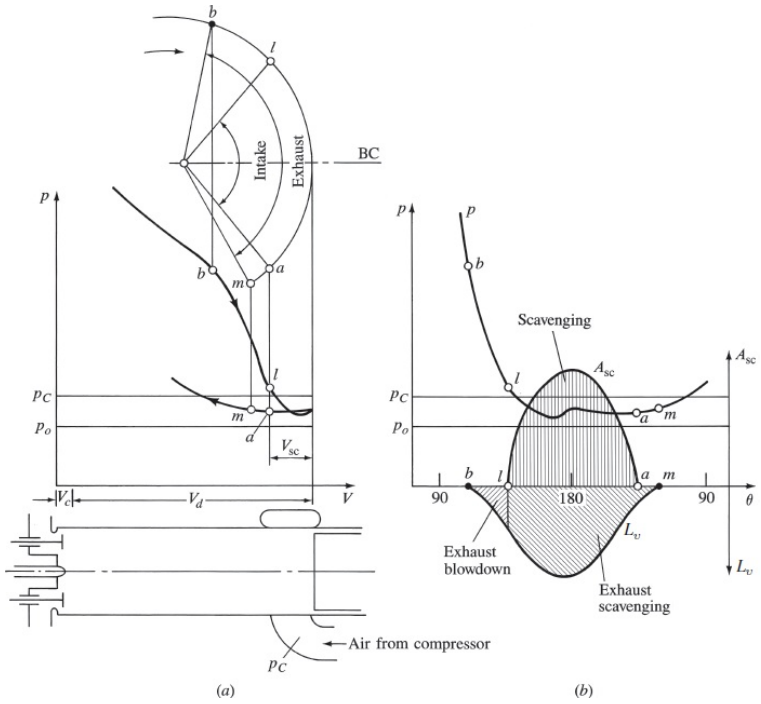


Figure 6.31 illustrates the principles of the scavenging process for a uniflow engine design. Between 100 and 110° after TC, the exhaust valve opens and a blowdown discharge process commences. Initially, the pressure ratio across the exhaust valve exceeds the critical value (see App. C) and the flow at the valve will be sonic: as the cylinder pressure decreases, the pressure ratio drops below the critical value. Following this blowdown (or free exhaust) period, the scavenging ports open between 60 and 40° before BC when the cylinder pressure slightly exceeds the scavenging pump pressure. Because the burned gas flow is toward the exhaust valves, which now have a large open area, the exhaust flow continues and no backflow occurs. When the cylinder pressure falls below the transfer system supply pressure, air enters the cylinder and the scavenging process starts. This fresh charge flow continues as long as the transfer ports are open and the total supply pressure exceeds the pressure in the cylinder. As the cylinder pressure rises above the exhaust pressure, the fresh charge flowing into the cylinder displaces the burned gases; however, some of the fresh charge mixes with the burned gases and is expelled with them. The exhaust valves usually close after the inlet ports close. Since the flow in the cylinder is toward the exhaust valve, additional scavenging is obtained. Proper flow patterns for the fresh charge are extremely important for good scavenging and charging of the cylinder.

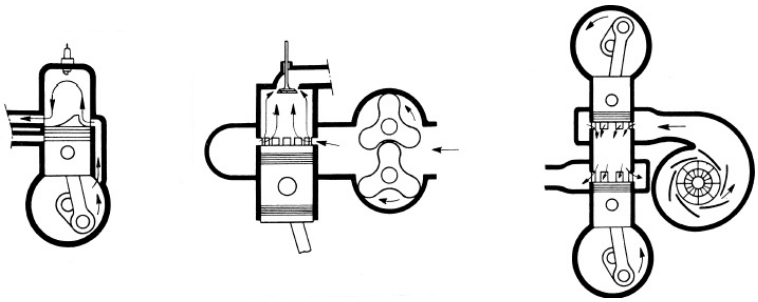
© McGraw-Hill Education. All rights reserved. Any use is subject to the Terms of Use, Privacy Notice and copyright information.

Figure 6.31 Gas exchange process in two-stroke cycle uniflow-scavenged diesel engine: (a) valve and port timing and pressure-volume diagram; (b) pressure, scavenging port open area A_{sc}, and exhaust valve lift L_v as functions of crank angle.[1]



Common methods for supercharging or pressurizing the fresh charge are shown in Fig. 6.32. In large two-stroke cycle engines, more complex combinations of these approaches are often used, as shown in Fig. 1.24. Substantial additional detail on two-stroke cycle engines and their scavenging characteristics can be found in texts by Blair[30] and Heywood and Sher.[31]

Figure 6.32 Common methods of pressurizing the fresh charge in two-stroke cycle engines: left, crankcase compression; center, roots blower; right, centrifugal compressor.[13]



6.6.2. Scavenging Parameters and Models

The following parameters are used to quantify the scavenging process:

The *delivery ratio* Λ:

$$\Lambda = \frac{\text{mass of delivered air (or mixture) per cycle}}{\text{reference mass}}$$

© McGraw-Hill Education. All rights reserved. Any use is subject to the Terms of Use, Privacy Notice and copyright information.

(6.23)

compares the actual scavenging air mass (or mixture mass) to that required in an ideal charging process.[1] The reference mass is defined as displaced volume × ambient air (or mixture) density. Ambient air (or mixture) density is determined at atmospheric conditions or at intake conditions. This definition is useful for experimental purposes. For analytical work, it is often convenient to use the trapped cylinder mass
m_{tr} as the reference mass.

The *trapping efficiency*
η_{tr}:

$$\eta_{\mathrm{tr}} = \frac{\text{mass of delivered air (or mixture) retained}}{\text{mass of delivered air (or mixture)}}$$

(6.24)

indicates what fraction of the air (or mixture) supplied to the cylinder is retained in the cylinder.

The *scavenging efficiency*
η_{sc}:

$$\eta_{\mathrm{sc}} = \frac{\text{mass of delieverd air (or mixture) retained}}{\text{mass of trapped cylinder charge}}$$

(6.25)

indicates to what extent the residual gases in the cylinder have been replaced with fresh air.

The *purity* of the charge, β:

$$\beta = \frac{\text{mass of air trapped cylinder charge}}{\text{mass of trapped cyclinder charge}}$$

(6.26)

indicates the degree of dilution, with burned gases, of the unburned mixture in the cylinder.

The *charging efficiency* n_{ch}:

$$\eta_{\mathrm{ch}} = \frac{\text{mass of delivered air (or mixture) retained}}{\text{displaced volume} \times \text{ambient density}}$$

(6.27)

indicates how effectively the cylinder volume has been filled with fresh air (or mixture). Charging efficiency, trapping efficiency, and delivery ratio are related by

$$\eta_{\mathrm{ch}} = \Lambda \eta_{\mathrm{tr}}$$

© McGraw-Hill Education. All rights reserved. Any use is subject to the Terms of Use, Privacy Notice and copyright information.

(6.28)

When the reference mass in the definition of delivery ratio is the trapped cylinder mass m_{tr} (or closely approximated by it) then

$$\eta_{\mathrm{sc}} = \Lambda \eta_{\mathrm{tr}}$$

(6.29)

In real scavenging processes as the fresh charge pushes the burned gas out of the cylinder, mixing occurs between the fresh charge and the burned gases and some of the fresh charge may is exhausted. Two limiting ideal models of this process are: (1) perfect displacement and (2) complete mixing. Perfect displacement or scavenging would occur if the burned gases were pushed out by the fresh gases without any mixing. Complete mixing occurs if entering fresh mixture mixes instantaneously and uniformly with the cylinder contents.[2]

For *perfect displacement* (with m_{tr} as the reference mass in the delivery ratio),

$$\begin{aligned} \eta_{\mathrm{sc}} &= \Lambda \quad \text{and} \quad \eta_{\mathrm{tr}} = 1 \quad \text{for } \Lambda \leq 1 \\ \eta_{\mathrm{sc}} &= 1 \quad \text{and} \quad \eta_{\mathrm{tr}} = \Lambda^{-1} \quad \text{for } \Lambda > 1 \end{aligned}$$

(6.30)

For the *complete mixing* limit, consider the scavenging process as a quasi-steady flow process. Between time *t* and *t* + *dt*, a mass element dm_{ad} of air is delivered to the cylinder and is uniformly mixed throughout the cylinder volume. An equal amount of fluid, with the same proportions of air and burned gas as the cylinder contents at time *t*, leaves the cylinder during this time interval. Thus the mass of air delivered between *t* and *t* + *dt* which is retained, dm_{ar}, is given by

$$dm_{\mathrm{ar}} = dm_{\mathrm{ad}} \left(1 - \frac{m_{\mathrm{ar}}}{m_{\mathrm{tr}}}\right)$$

Assuming m_{tr} is constant, this integrates over the duration of the scavenging process to give

$$\frac{m_{\mathrm{ar}}}{m_{\mathrm{tr}}} = 1 - \exp\left(\frac{m_{\mathrm{ad}}}{m_{\mathrm{tr}}}\right)$$

(6.31)

Thus, for *complete mixing*, with the above definitions,

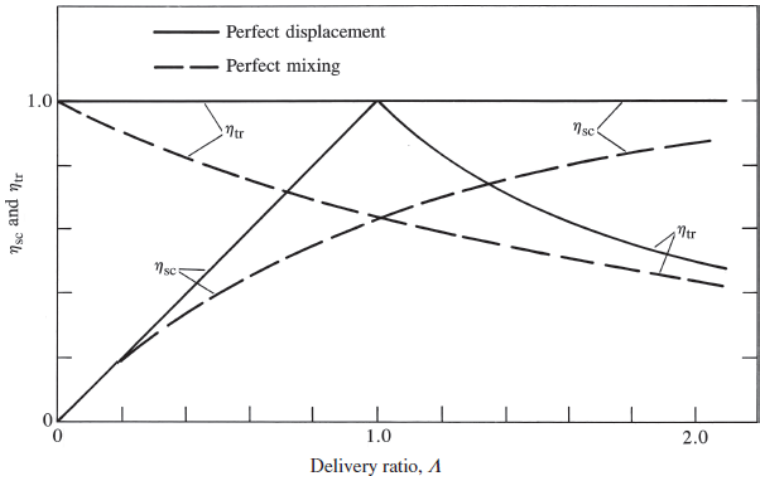
$$\begin{aligned} \eta_{\mathrm{sc}} &= 1 - e^{-\Lambda} \\ \eta_{\mathrm{tr}} &= \frac{1}{\Lambda}(1 - e^{-\Lambda}) \end{aligned}$$

© McGraw-Hill Education. All rights reserved. Any use is subject to the Terms of Use, Privacy Notice and copyright information.

(6.32)

Figure 6.33 shows
η_{sc} and
η_{tr} for the perfect displacement and complete mixing assumptions as a function of Λ, the delivery ratio.

Figure 6.33 Scavenging efficiency η_{sc} and trapping efficiency η_{tr} versus delivery ratio Λ for (isothermal) perfect displacement and complete mixing models.



An additional possibility is the direct flow of fresh mixture through the cylinder into the exhaust without entraining burned gases. This is called *short-circuiting*; it is obviously undesirable since some fresh air or mixture is wasted. There is no simple model for this process. When short-circuiting occurs, lower scavenging efficiencies result even though the volume occupied by the short-circuiting flow through the cylinder does displace an equal volume of the burned gases. Another phenomenon which reduces scavenging efficiency is the formation of *pockets* or *dead zones* in the cylinder volume where burned gases can become trapped and escape displacement or entrainment by the fresh scavenging flow. These unscavenged zones are most likely to occur in regions of the cylinder that remain secluded from the main fresh mixture flow path.

6.6.3. Actual Scavenging Processes

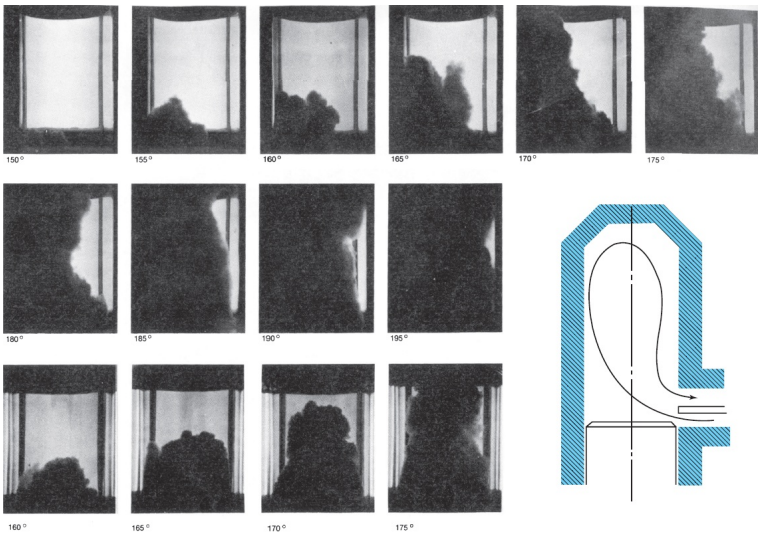
Several methods have been developed for determining what occurs in actual cylinder scavenging processes. Accurate measurement of scavenging efficiency is difficult due to the problem of measuring the trapped air mass. Estimation of η_{sc} from indicated mean effective pressure, and from gas sampling, are the most reliable methods.[13] Flow visualization experiments in liquid analogs of the cylinder and flow velocity mapping techniques have proved useful in providing a qualitative picture of the scavenging flow field and identifying problems such as short-circuiting and dead volumes.

Flow visualization studies indicate the key features of the scavenging process. Figure 6.34 shows a sequence of frames from a movie of one liquid scavenging another in a model of a large two-stroke cycle loop-scavenged diesel. The physical variables were scaled to maintain the same values of the appropriate dimensionless numbers for the liquid analog flow and the real engine flow. The density of the liquid representing air (which is dark) was twice the density of the liquid representing burned gas (which is clear). Early in the scavenging process, the fresh air jets penetrate into the burned gas and displace it first toward the cylinder head and then toward the exhaust ports (the schematic gives the location of the ports). During this initial phase, the outflowing gas contains no air; pure displacement of the burned gas from the cylinder is being achieved. Then short-circuiting losses start to occur, due to the damming-up or buildup of fresh air on the cylinder wall opposite the exhaust ports. The short-circuiting fluid flows directly between the scavenge ports and the exhaust ports above them. Since this damming-up of the inflowing fresh air back toward the exhaust ports continues, short-circuiting losses will also continue.

© McGraw-Hill Education. All rights reserved. Any use is subject to the Terms of Use, Privacy Notice and copyright information.

While the scavenging front remains distinct as it traverses the cylinder, its turbulent character indicates that mixing between burned gas and air across the front is taking place. For both these reasons (short-circuiting and short-range mixing), the outflowing gas, once the displacement phase is over, contains an increasing amount of fresh air.

Figure 6.34 Photos of one fluid scavenging another in liquid analog experiments in model loop-scavenged engine cylinder. Top two rows: view perpendicular to scavenging loop. Bottom row: orthogonal views. Dark denser fluid displacing light less-dense fluid.[32]



Outflowing fluid composition measurements from this model study of a Sulzer two-stroke loop-scavenged diesel engine confirm this sequence of events. At 24 crank angle degrees after the onset of scavenging, fresh air due to short-circuiting was detected in the exhaust. At the time the displacement front reached the exhaust port (65° after the onset of scavenging), loss of fresh air due to scavenging amounted to 13% of the scavenge airflow. The actual plot of degree of purity (or η_{sc}) versus delivery ratio (Λ) closely followed the perfect displacement line for $\Lambda < 0.4$. For $\Lambda > 0.4$, the shape of the actual curve was similar in shape to the complete mixing curve.

Engine tests confirm these results from model studies. Initially, the exhausted gas contains no fresh air or mixture; only burned gas is being displaced from the cylinder. However, within the cylinder both displacement *and* mixing at the interface between burned gas and fresh gas are occurring. The departure from perfect scavenging behavior is evident when fresh mixture first appears in the exhaust. For loop-scavenged engines this is typically when $\Lambda \approx 0.4$. For uniflow scavenging this perfect scavenging phase lasts somewhat longer; for cross-scavenging it is over sooner (because the short-circuiting path is shorter).

A three-zone model developed by Benson,[33] based on observations and measurements such as those described above, provides a useful framework for the two-stroke loop- and cross-scavenging processes: see Fig. 6.35. He suggested that the gas exchange process takes place in three places. In phase I, the fresh charge jets enter the cylinder and displace some of burnt in-cylinder gases. Mixing occurs at the boundaries of the jets. In phase II, some of the fresh charge entering the cylinder passes straight through and exits. In this phase only fresh charge is passing through the exhaust ports; mixing, however, continues to take place at the boundaries of the (fresh charge) jets. In phase III, a mixture of fresh charge and burnt gases leaves the cylinder; the composition of this mixture changes with time. In summary, three processes occur: (1) Fresh air displaces burned gases from the cylinder (desirable), at lower values of the delivery ratio, Λ; then (2) some of the fresh air (mixture) flows straight through the cylinder—short-circuiting occurs (undesirable); and throughout (3), short-range mixing occurs between the fresh air and burned gases: later in the scavenging process these mixed gases exit the cylinder (undesirable). Benson suggested these phase durations:

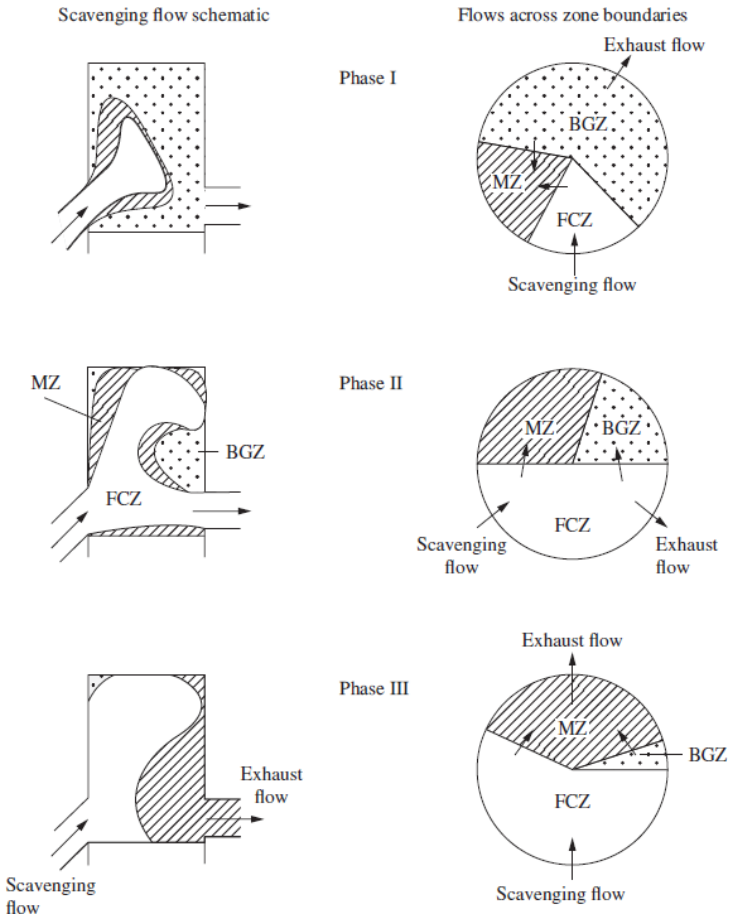
Phase I: $95° < \theta < 155°$ ATC

© McGraw-Hill Education. All rights reserved. Any use is subject to the Terms of Use, Privacy Notice and copyright information.

Phase II: $155° < \theta < 200°$ ATC

Phase III: $200° < \theta < 265°$ ATC

Figure 6.35 Three-zone two-stroke cycle engine scavenging model, showing early (I), mid (II), and later (III) phases of the process. BGZ, burned gas zone; FCZ, fresh charge zone; MZ, mixing zone.[33]



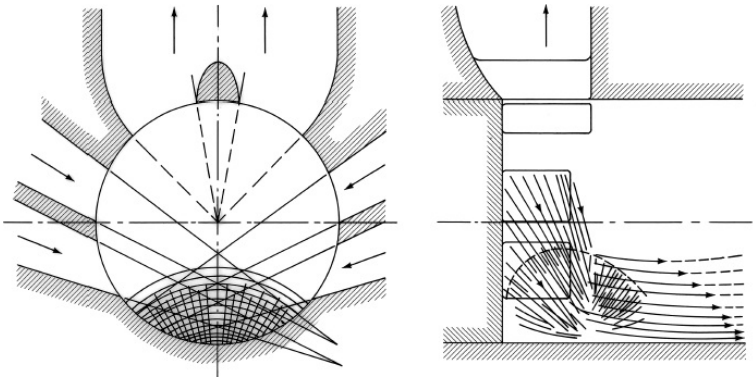
The value of this model is the conceptual framework it proposes: that the scavenging process proceeds in sequential phases where different flow behavior occurs.

The mixing that occurs is short-range mixing, not mixing throughout the cylinder volume. The jets of scavenging mixture, on entering the cylinder, mix readily with gases in the immediate neighborhood of the jet efflux. More efficient scavenging—that is, less mixing—is obtained by reducing the size of the inlet ports while increasing their number. It is important that the jets from the inlet ports slow down significantly once they enter the cylinder. Otherwise the scavenging front will reach the exhaust ports or valves too quickly. The jets are frequently directed to impinge on each other or against the cylinder wall. Swirl in uniflow-scavenged systems may be used to obtain an equivalent result.

The desirable loop-scavenging flow is illustrated in Fig. 6.36. The scavenging jets enter symmetrically with sufficient velocity to fill up about half the cylinder cross-section, and thereafter flow at lower velocity along the cylinder wall toward the cylinder head. By proper direction of the scavenging jets, it is possible to achieve almost no outflow in the direction of the exhaust from the cross-hatched stagnation zone on the opposite cylinder wall. In fact, measurement of the velocity profile in this region is a good indicator of the effectiveness of the scavenging flow. If the flow along the cylinder wall toward the head is stable, that is, if its maximum velocity occurs near the wall and the velocity is near zero on the plane perpendicular to the axis of symmetry of the ports (which passes through the cylinder axis), the scavenging flow will follow the desired path. If there are "tongues" of scavenging flow toward the exhaust port, either in the center of the cylinder or along the walls, then significant short-circuiting will occur.

© McGraw-Hill Education. All rights reserved. Any use is subject to the Terms of Use, Privacy Notice and copyright information.

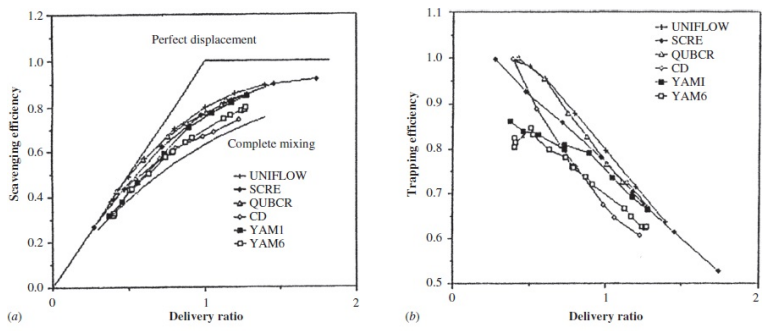
Figure 6.36 Desirable airflow in loop-scavenged engine: air from the entering jets impinges on far cylinder wall and flows toward the cylinder head.[34]



In uniflow-scavenged configurations, the inlet ports are evenly spaced around the full circumference of the cylinder and are usually directed so that the scavenging jets create a swirling flow within the cylinder (see Fig. 6.30). Results of measurements of scavenging front location in rig flow tests of a uniflow-scavenged two-stroke diesel cylinder (with an exhaust valve), as the inlet port angle was varied to give a wide range of swirl, showed that inlet jets directed tangentially to a circle of half the cylinder radius gave the most stable scavenging front profile over a wide range of conditions.

Though the scavenging processes in spark-ignition and diesel two-stroke engines are similar, these two types of engine operate with quite different delivery ratios. In mixture-scavenged spark-ignition engines, any significant expulsion of fresh fluid with the burned gas results in a significant loss of fuel and causes high hydrocarbon emissions as well as loss of the energy expended in pumping the flow which passes straight through the cylinder. In diesels the scavenging medium is air, so only the pumping work is lost. One consequence of this is that two-stroke spark-ignition engines are usually crankcase pumped. This approach provides the maximum pressure and thus also the maximum velocity in the scavenging medium at the start of the scavenging process just after the cylinder pressure has blown down; as the crankcase pressure falls during the scavenging process, the motion of the scavenging front within the cylinder also slows down. Figure 6.37 shows the trapping and scavenging efficiencies as a function of delivery ratio, of several different designs of crankcase-scavenged spark-ignition engines. These quantities depend significantly on intake and exhaust port design and open period, and the exhaust system configuration. For two-stroke cycle spark-ignition engines, which use crankcase pumping, delivery ratios range from about 0.5 to close to 1.0.

Figure 6.37 (a) Trapping efficiency η_{tr} and (b) scavenging efficiency η_{sc}, of several experimental scavenging system designs of two-stroke cycle spark-ignition engines, as a function of delivery ratio; these two parameters characterize scavenging effectiveness. Perfect displacement and perfect mixing model scavenging efficiencies are also shown.[30]

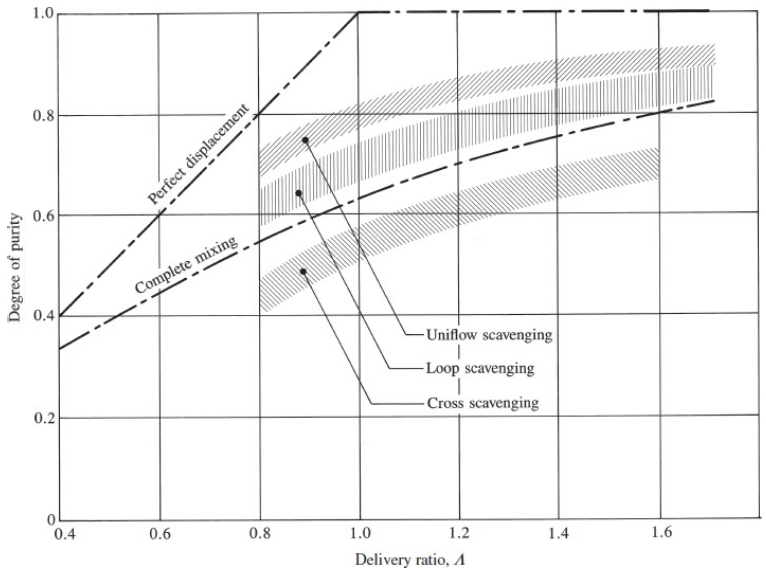


Name	Type	Comments
UNIFLOW	Ported uniflow	Very good scavenging
SCRE	3 port loop	Good scavenging
YAM1	5 port loop	Quite good scavenging
YAM6	5 port loop	Bad loop scavenging
CD	Classic cross	Normal cross type
QUBCR	QUB cross	QUB radial ports

© McGraw-Hill Education. All rights reserved. Any use is subject to the Terms of Use, Privacy Notice and copyright information.

Figure 6.38 shows scavenging data typical of large two-stroke diesels. The purity (mass of air in trapped cylinder charge/mass of trapped cylinder charge) is shown as a function of the delivery ratio. The different scavenging configurations have different degrees of effectiveness, with uniflow scavenging being the most efficient. These diesel engines normally operate with delivery ratios in the range 1.2 to 1.4. Their large size (and slower engine speeds) results in more effective scavenging than in smaller engine loop, and especially cross-scavenged designs.

Figure 6.38 Purity as a function of delivery ratio Λ for different types of large marine two-stroke diesel engines.[35]



[1] If scavenging is done with fuel-air mixture, as in most two-stroke spark-ignition engines, then mixture mass is used instead of air mass.

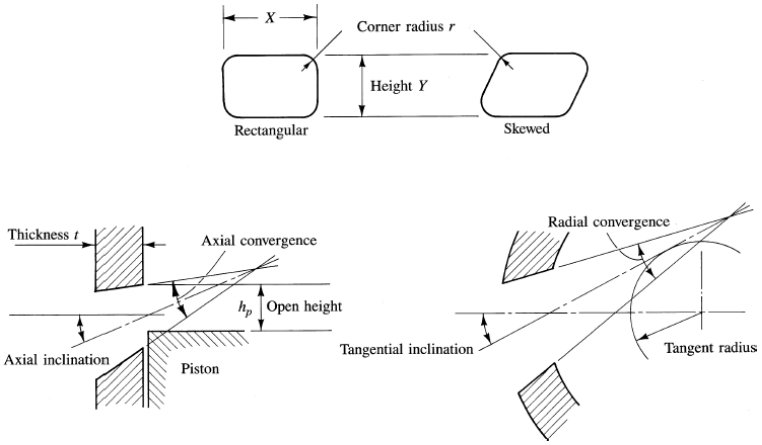
[2] The simplest versions of these ideal models assume the processes are isothermal. More complex versions of these models are available (Heywood and Sher[31]).

© McGraw-Hill Education. All rights reserved. Any use is subject to the Terms of Use, Privacy Notice and copyright information.

6.7. FLOW THROUGH TWO-STROKE ENGINE PORTS

The importance of the scavenging and exhaust ports to the proper functioning of the two-stroke cycle scavenging process is clear from the above discussion. The crank angle at which the ports open; the size, number, geometry, and location of the ports around the cylinder circumference; and the direction and velocity of the jets issuing from the ports into the cylinder, all affect the scavenging flow. A summary of the information available on flow through piston-controlled ports can be found in Annand and Roe.[15] Both the flow resistance of the intake (or transfer) and exhaust port configurations, as well as the details of the flow pattern produced by the port system inside the cylinder during scavenging, are important. Figure 6.39 defines the essential geometrical characteristics of such ports. Rectangular ports make best use of the cylinder wall area and give precise timing control. Ports can be tapered, and may have axial and tangential inclination as shown.

Figure 6.39 Parameters which define the geometry of scavenging or transfer ports.[15]



6.7.1.1. Scavenging Ports

Figure 6.40 illustrates the flow patterns expected downstream of piston-controlled inlet ports. For small openings, the flow remains attached to the port walls. For fully-open ports with sharp corners the flow detaches at the upstream corners. Both a rounded entry and converging taper to the port help prevent flow detachment within the port. Discharge coefficients for ports have been measured as a function of the open fraction of the port, the pressure ratio across the port, and port geometry and inclination (see Ref. 12 for a detailed summary). The most appropriate reference area for evaluating the discharge coefficient is the open area of the port (see Fig. 6.39). When the open height h_p is less than ($Y - r$) but greater than r, this is

$$A_R = Xh_p - 0.43r^2$$

(6.33)

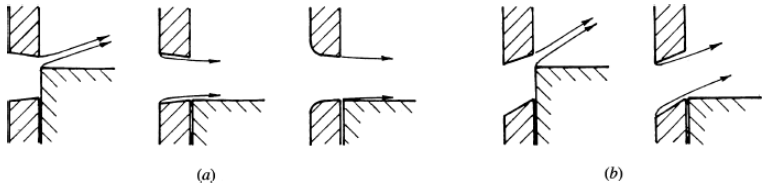
where Y is the port height, X the port width, and r the corner radius. For $h_p = Y$, the reference area is

$$A_R = XY - 0.86r^2$$

(6.34)

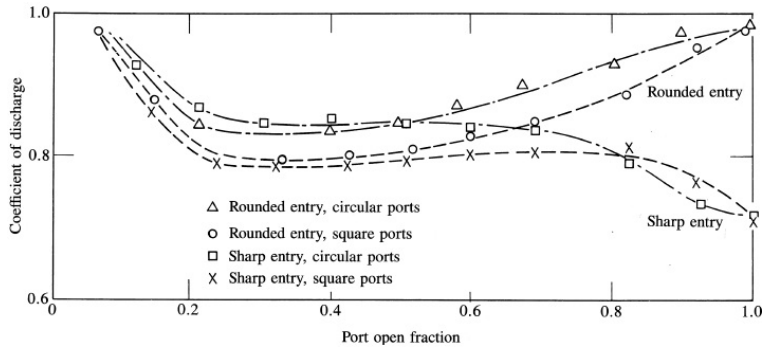
© McGraw-Hill Education. All rights reserved. Any use is subject to the Terms of Use, Privacy Notice and copyright information.

Figure 6.40 Flow pattern through piston-controlled scavenging ports. (a) Port axis perpendicular to wall; small opening and large opening with sharp and rounded entry. (b) Port axis inclined.[15]



The effect of variations in geometry and operating conditions on the discharge coefficient C_D can usually be interpreted by reference to the flow patterns illustrated in Fig. 6.40. The effects of inlet port open fraction and port geometry on C_D are shown in Fig. 6.41: geometry effects are most significant at small and large open fractions. C_D varies with pressure ratio, increasing as the pressure ratio increases. Empirical relations that predict this variation with pressure ratio have been developed.[36]

Figure 6.41 Steady-state discharge coefficients as a function of port open fraction (uncovered height/port height) for different scavenge port designs. Pressure ratio across port = 2.35.[18]



Tangentially inclined scavenge ports are used when an in-cylinder swirling motion is desired to improve scavenging or when jet focusing or impingement within the cylinder off the cylinder axis is required (see Sec. 6.6.3). The discharge coefficient decreases as the jet tangential inclination increases. The jet angle and the port angle can deviate significantly from each other depending on the details of the port design and the open fraction.

6.7.1.2. Exhaust Ports

In piston-controlled exhaust ports, the angle of the jet from a thin-walled exhaust port increases as indicated in Fig. 6.42. With thick ports, the walls are usually tapered to allow the outward flow to diffuse. The pressure ratio across the exhaust ports varies substantially during the exhaust process. The pressure ratio has a significant effect on the exhaust port discharge coefficient, as shown in Fig. 6.43. The changes in exit jet angle and separation point explain the effects of increasing open fraction and pressure ratio. The discharge coefficient also increases modestly with increasing gas temperature.

© McGraw-Hill Education. All rights reserved. Any use is subject to the Terms of Use, Privacy Notice and copyright information.

Figure 6.42 *Angle of jet exiting the exhaust port as a function of open port height.*[34]

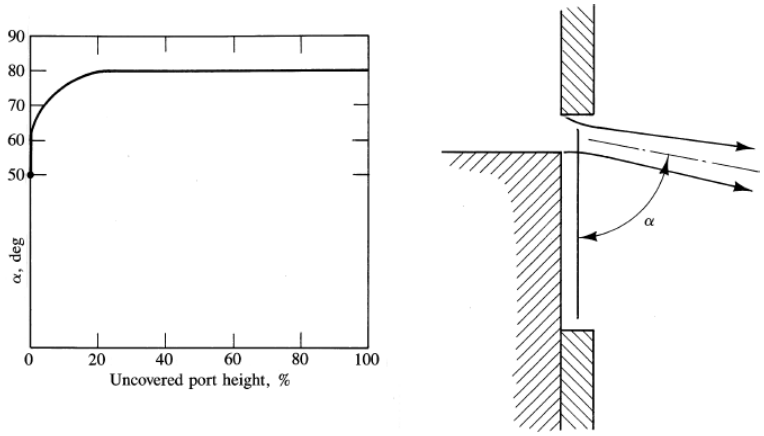
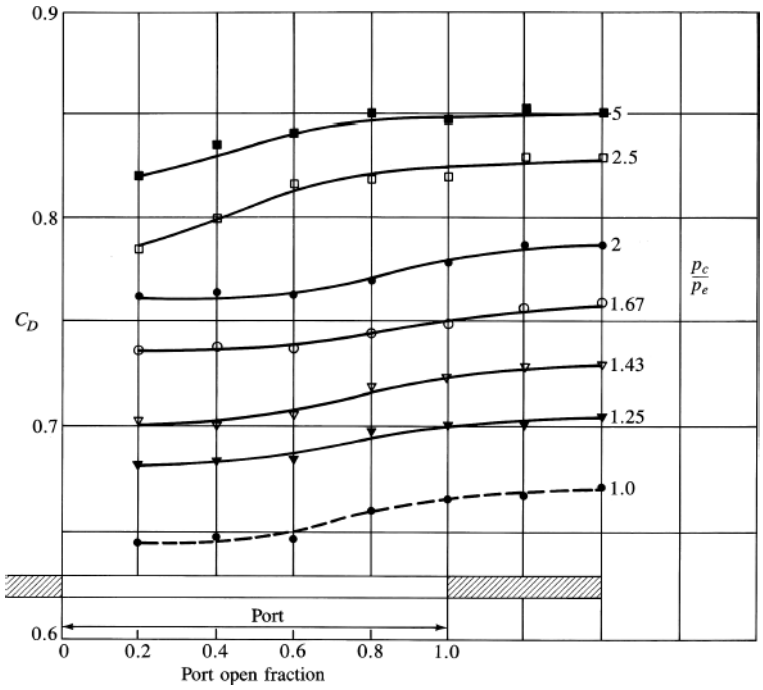


Figure 6.43 *Discharge coefficient of a single rectangular exhaust port (7.6-mm wide × 12.7-mm high) in the wall of a 51-mm bore cylinder as a function of open fraction and pressure ratio. Steady-flow rig tests at 21°C. p_c = cylinder pressure, p_e = exhaust system pressure.*[36, 37]



6.7.1.3. Piston Deflectors

With simple cross-scavenged two-stroke (gasoline) engines, a deflector on the piston crown is often used to force the scavenging flow toward the cylinder head and away from the exhaust port. Figure 1.3 shows a typical deflector shape. This type of piston, with cross-scavenging, has good scavenging characteristics at low power when the engine is throttled, and at low engine speed. At higher throttle openings the scavenging efficiency is not especially good. Also, the impact of the deflector on combustion chamber shape, and the engine's knock and surface ignition limits is detrimental. Usually cross-scavenged engines use a lower compression ratio than loop-scavenged engines. However, the cross-scavenged port design simplifies the block casting and machining significantly, providing manufacturing and packaging advantages. Also, narrow ports can be used, which permits the piston rings to operate without pinning, which evens out and reduces ring wear.

Figure 6.44 shows the major geometric features of a piston deflector. Blair[30] recommends the following geometric

© McGraw-Hill Education. All rights reserved. Any use is subject to the Terms of Use, Privacy Notice and copyright information.

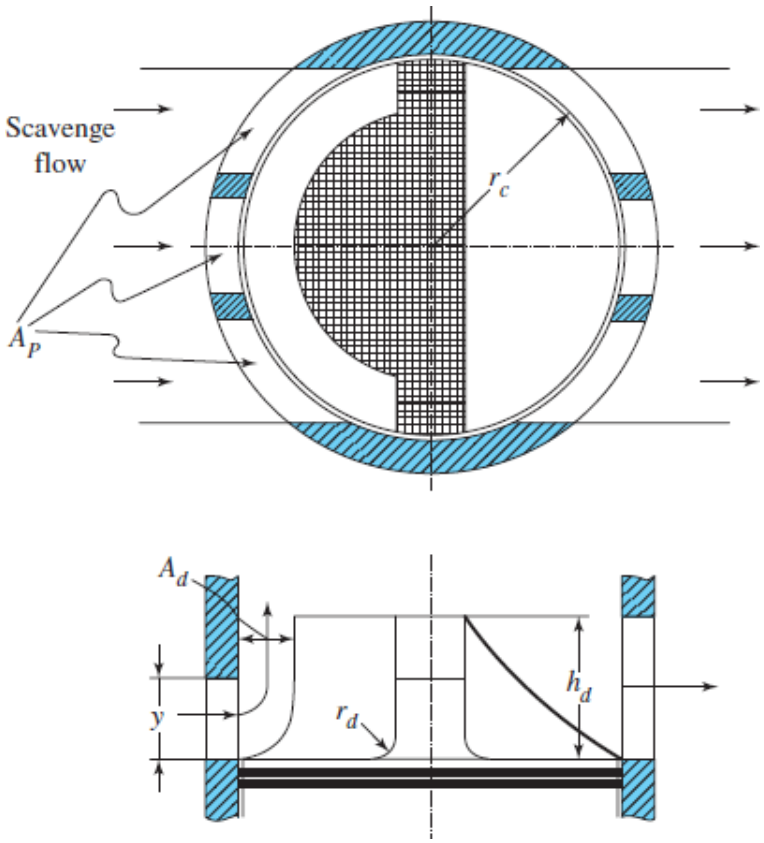
proportions. The deflector open or flow area A_d, the area between the liner and vertical deflector surface, should be slightly larger than the total scavenging port open area [given by $n_p A_p$, where A_p (=A_R) is given by Eq. (6.34)]. Thus the entering flow will be turned smoothly through 90° and flow axially up the cylinder. A deflection ratio R_d can be defined:

$$R_d = A_d/(n_p A_p)$$

(6.35)

where A_d is defined in Fig. 6.44. R_d should be between 1.1 and 1.2. The deflector height is the other critical parameter. It should be higher than the port by about 50%, but no higher than necessary. The deflector wall is placed about midway between the exhaust and scavenge ports. Its sides are usually sloped at 45°, or curved, so it will fit the combustion chamber at TC with adequate clearance. The radius of the deflector as it joins the piston is usually about one-third of the height. Increasing the deflection ration, R_d in Eq. (6.35), steadily decreases the trapping efficiency as the delivery ratio increases. Smaller deflector flow areas (R_d = 1.1 – 1.2) deflect the flow better, reduce short-circuiting, and hence improve charge trapping.

Figure 6.44 Geometry of scavenge flow and exhaust flow ports, and piston deflector.[30, 31]



© McGraw-Hill Education. All rights reserved. Any use is subject to the Terms of Use, Privacy Notice and copyright information.

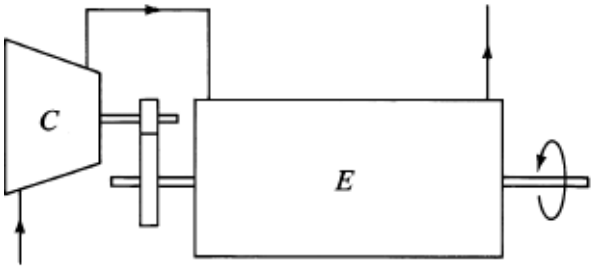
6.8. SUPERCHARGING AND TURBOCHARGING

6.8.1. Methods of Power Boosting

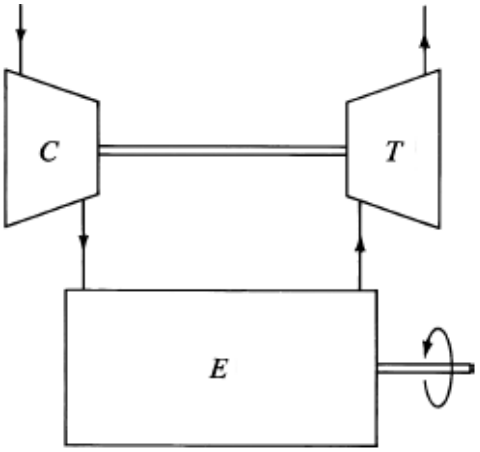
The maximum power a given engine can deliver is limited by the amount of fuel that can be burned efficiently inside the engine cylinder. This is limited by the amount of air that is inducted into each cylinder each cycle. If this air is compressed to a higher density than ambient, prior to entry into the cylinder, the maximum power an engine of fixed dimensions can deliver will be increased. This is the primary purpose of supercharging; Eqs. (**2.39 (/mhe-lookup/atom-id/eb1dc6c1855fa93d#ch02eq39)**) to (**2.41 (/mhe-lookup/atom-id/eb1dc6c1855fa93d#ch02eq41)**) show how power, torque, and mean effective pressure are proportional to inlet air density. The term *supercharging* refers to increasing the air (or mixture) density by increasing its pressure prior to entering the engine cylinder. Three basic methods are used to accomplish this. The first is *mechanical supercharging* where a separate pump or blower or compressor, usually driven by power taken from the engine, provides the compressed air. The second method is *turbocharging*, where a turbocharger—a compressor and turbine on a single shaft—is used to boost the inlet air (or mixture) density. Energy available in the engine's exhaust stream is used to drive the turbocharger turbine which drives the turbocharger compressor which raises the inlet fluid density prior to entry to each engine cylinder. The third method—*pressure wave supercharging*—uses wave action in the intake and exhaust systems to compress the intake mixture. The use of intake and exhaust manifold tuning to increase volumetric efficiency (see **Sec. 6.2.2 (/mhe-lookup/atom-id/a98a8da1fe93ac07#c9781260116106ch06lev2sec02)**) is one example of this method of increasing air density. An example of a pressure wave supercharging device is the Comprex, which uses the pressure available in the exhaust gas stream to compress the inlet mixture stream by direct contact between the two fluids in narrow flow channels (see **Sec. 6.8.5**). **Figure 6.45** shows typical arrangements of the different supercharging and turbocharging systems. The most common arrangements use a mechanical supercharger (**Fig. 6.45*a***) or turbocharger (**Fig. 6.45*b***). Combinations of an engine-driven compressor and a turbocharger (**Fig. 6.45*c***) are also used (e.g., in large marine engines; **Fig. 1.36 (/mhe-lookup/atom-**

id/6593730f409895b1#ch01fig36)). Two-stage turbocharging (**Fig. 6.45*d***) is one viable approach for providing very high boost pressures (4 to 7 bar) to obtain even higher engine brake mean effective pressures. Turbocompounding, which uses a second turbine in the exhaust directly geared to the engine drive shaft to extract additional exhaust energy, **Fig. 6.45**, is an alternative method of increasing engine power and efficiency. Charge cooling with a heat exchanger (often called an aftercooler or intercooler), after compression, prior to gas entry to the cylinder, is commonly used to decrease the temperature of the air and thus further increase the air or mixture density, as shown in **Fig. 6.45*f***.

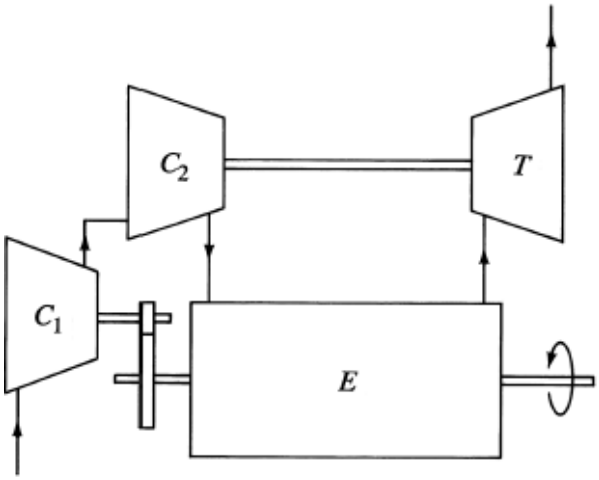
Figure 6.45 Supercharging and turbocharging configurations: (a) mechanical supercharger; (b) turbocharger; (c) engine-driven compressor, and turbocharger; (d) two-stage turbocharging; (e) turbocharging with turbocompounding; (f) turbocharger with intercooler. C compressor, E engine, I inter-cooler, T turbine.



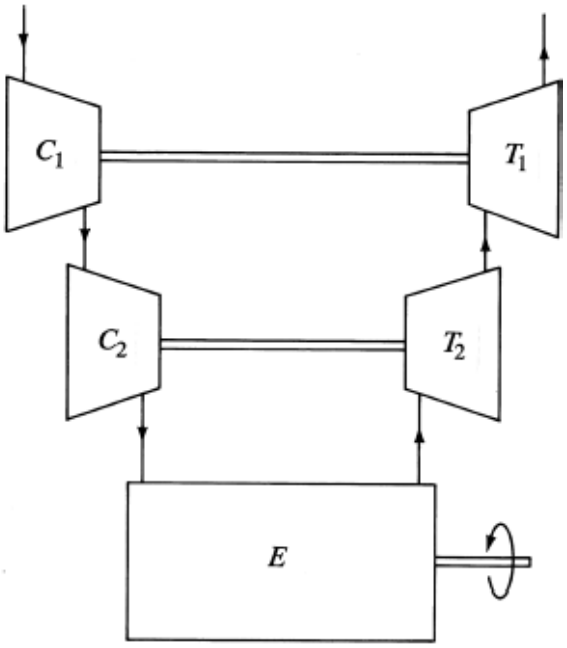
(a)



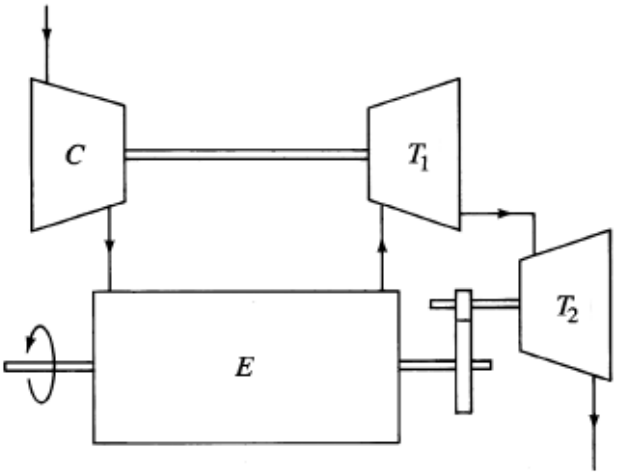
(b)

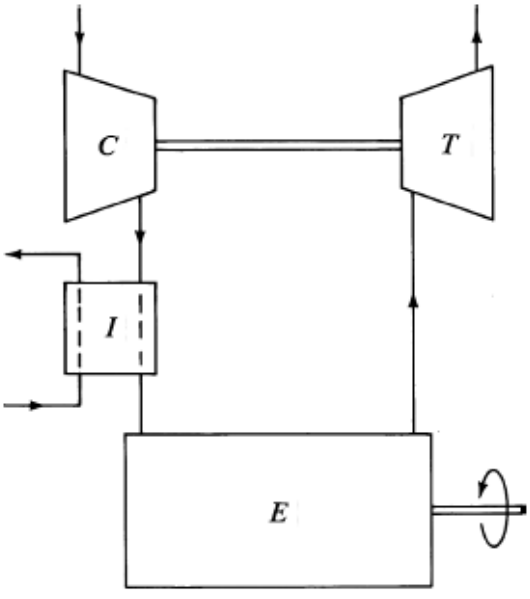


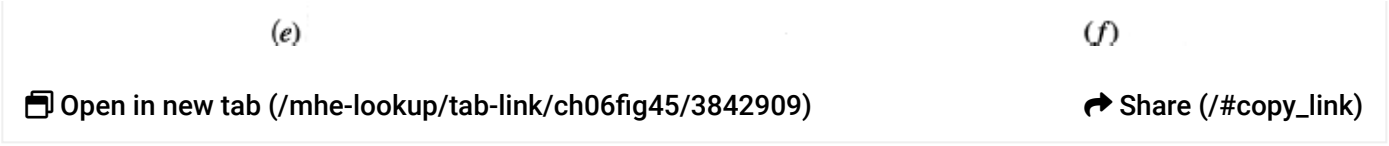
(c)



(d)







Open in new tab (/mhe-lookup/tab-link/ch06fig45/3842909) Share (/#copy_link)

Supercharging is used in four-stroke cycle engines to boost the power per unit displaced volume. Some form of supercharging is necessary in two-stroke cycle engines to raise the fresh air (or mixture) pressure above the exhaust pressure so that the cylinders can be scavenged effectively. With additional boost in two-stroke cycle engines, the power density is also raised. This section reviews the operating characteristics of the blowers, compressors, turbines, and wave-compression devices used to increase inlet air or mixture density or convert exhaust-gas availability to work. The operating characteristics of supercharged and turbocharged engine systems are discussed in **Chap. 15 (/mhe-lookup/atom-id/d329c3e7fe379ad6)**.

Diesel engines, especially in automotive applications, are usually turbocharged. Diesels always operate fuel lean: thus, they do not fully use the air's oxygen in the cylinder for combustion. So forcing additional (i.e., compressed) air into the engine's cylinders and burning more fuel, thus increasing the engine's torque per unit volume, are especially attractive. High-performance gasoline-fueled spark-ignition engines have a history of being boosted with a mechanically driven supercharger to increase the power output of a given base engine. Turbocharged gasoline engines are replacing naturally-aspirated gasoline engines in the automotive sector to enable engine downsizing and down-speeding, and realize a significant fuel consumption benefit. The limiting abnormal combustion phenomenon of *knock* becomes more of a constraint, however, though the fuel-evaporation charge-cooling effect of the direct-injection fuel spray somewhat offsets that problem.

6.8.2. Basic Relationships

Expressions for the work required to drive a blower or compressor and the work produced by a turbine are obtained from the first and second laws of thermodynamics. The first law, in the form of the steady-flow energy equation, applied to a control volume around the turbomachinery component is

$$\dot{Q} - \dot{W} = \dot{m}\left[\left(h + \frac{C^2}{2} + gz\right)_{\text{out}} - \left(h + \frac{C_2}{2} + gz\right)_{\text{in}}\right]$$

(6.36)

where $\dot{Q}$ is the heat-transfer rate into the control volume, $\dot{W}$ is the shaft work-transfer rate out of the control volume, $\dot{m}$ is the mass flow rate, *h* is the fluid specific enthalpy, $C^2/2$ is the specific kinetic energy, and *gz* is the specific potential energy (which is not important and can be omitted).

A *stagnation* or *total enthalpy*, h_0, can be defined as

$$h_0 = h + \frac{C^2}{2}$$

(6.37)

For an ideal gas, with constant specific heats, a *stagnation* or *total temperature* follows from Eq. (**6.33 (/mhe-lookup/atom-id/55cbe86ee41f5200#ch06eq33)**):

$$T_0 = T + \frac{C^2}{2c_p}$$

(6.38)

A *stagnation* or *total pressure* is also defined: It is the pressure attained if the gas is isentropically brought to rest:

$$p_0 = p\left(\frac{T_0}{T}\right)^{\gamma/(\gamma-1)}$$

(6.39)

$\dot{Q}$ in Eq. (**6.36**) for pumps, blowers, compressors, and turbines is usually small enough to be neglected. Equation (**6.36**) then gives the work-transfer rate as

$$\dot{W} = \dot{m}(h_{0,\,\mathrm{out}} - h_{0,\,\mathrm{in}})$$

(6.40)

A component efficiency is used to relate the actual work-transfer rate to the work-transfer rate required (or produced) by an equivalent reversible adiabatic device operating between the same pressures. The second law is then used to determine this reversible adiabatic work-transfer rate, which is that occurring in an isentropic process.

For a compressor, the *compressor isentropic efficiency* η_C is

$$\eta_C = \frac{\text{reversible power requirerment}}{\text{actual power requirement}}$$

(6.41)

Figure 6.46 shows the end states of the gas passing through a compressor on an *h*-*s* diagram. Both static (p_1, p_2) and stagnation (p_{01}, p_{02}) constant-pressure lines are shown. The total-to-total isentropic efficiency is, from Eq. (**6.41**),

$$\eta_{\mathrm{CTT}} = \frac{h_{02s} - h_{01}}{h_{02} - h_{01}}$$

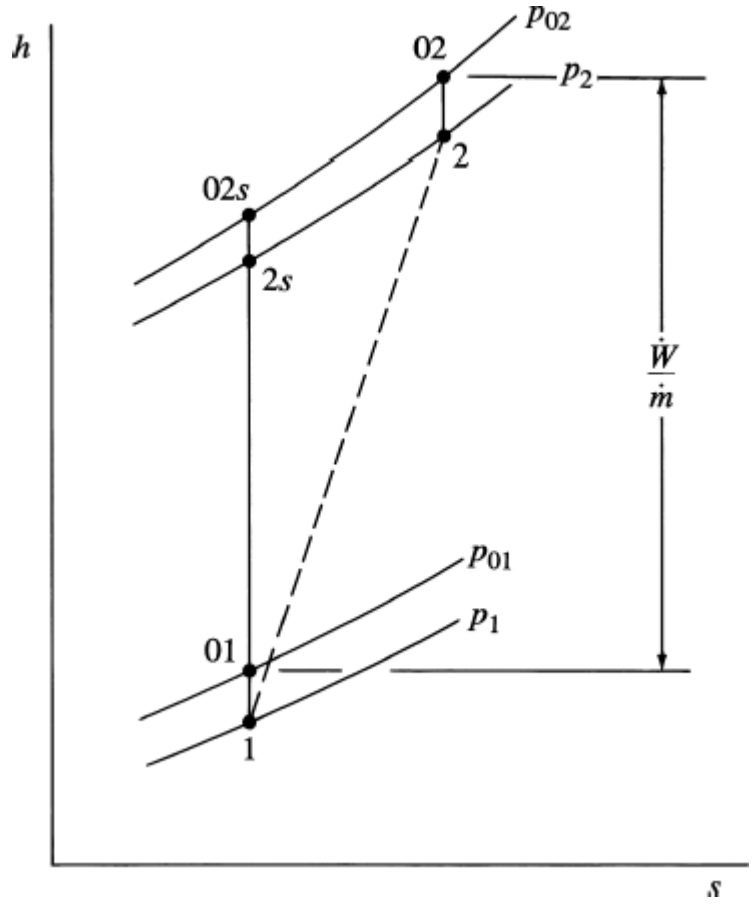
(6.42)

which, since c_p is essentially constant for air, or fuel-air mixture, becomes

$$\eta_{\mathrm{CTT}} = \frac{T_{02s} - T_{01}}{T_{02} - T_{01}}$$

(6.43)

Figure 6.46 Enthalpy-entropy diagram for compressor. Inlet state 01, exit state 2; equivalent isentropic compressor exit state 2s.



Open in new tab (/mhe-lookup/tab-link/ch06fig46/3842909) Share (/#copy_link)

Since the process 01 to 02*s* is isentropic,

$$T_{02s} = T_{01}\left(\frac{p_{02}}{p_{02}}\right)^{(\gamma-1)/\gamma}$$

Equation (**6.43**) becomes

$$\eta_{\mathrm{CTT}} = \frac{(p_{02}/p_{01})^{(\gamma-1)/\gamma} - 1}{(T_{02}/T_{01}) - 1}$$

(6.44)

In deriving Eq. (**6.44**) it has been tacitly assumed that the kinetic-energy pressure head (p_{02} – p_2) can be recovered. In internal combustion engine applications the compressor feeds the engine via a large manifold, and much of this kinetic energy will be dissipated. The blower or compressor

should be designed for effective recovery of this kinetic energy before the exit duct. Since the kinetic energy of the gas leaving the compressor is not usually recovered, a more realistic definition of efficiency is based on exit static conditions:[38 (/mhe-lookup/atom-id/a977319a43adac2e#ch06ref38)]

$$\eta_{\mathrm{CTS}} = \frac{T_{2s} - T_{01}}{T_{02} - T_{01}} = \frac{(p_2/p_{01})^{(\gamma-1)/\gamma} - 1}{(T_{02}/T_{01}) - 1}$$

(6.45)

This is termed the total-to-static efficiency. The basis on which the efficiency is calculated should always be clearly stated.

The work-transfer rate or power required to drive the compressor is obtained by combining Eq. (**6.40**), the ideal gas model, and Eq. (**6.44**):

$$-\dot{W}_C = \dot{m}_i c_{p,i}(T_{02} - T_{01}) = \frac{\dot{m}_i c_{p,i} T_{01}}{\eta_{\mathrm{CTT}}} \left[\left(\frac{p_{02}}{p_{01}} \right)^{(\gamma-1)/\gamma} - 1 \right]$$

(6.46)

where the subscript *i* denotes inlet mixture properties. If η_{CTS} is used to define the compressor performance, then p_2 replaces p_{02} in Eq. (**6.46**). Equation (**6.46**) gives the thermodynamic power requirement. There will also be mechanical losses in the blower or compressor. Thus the power required to drive the device, $-\dot{W}_{C,D}$ will be

$$-\dot{W}_{C,D} = -\frac{\dot{W}_C}{\eta_m}$$

(6.47)

where η_m is the blower or compressor mechanical efficiency.

Figure 6.47 shows the gas states at inlet and exit to a *turbine* on an *h-s* diagram. State 03 is the inlet stagnation state; 4 and 04 are the exit static and stagnation states, respectively. States 4*s* and 04*s* define the static and stagnation exit states of the equivalent reversible adiabatic turbine. The *turbine isentropic efficiency* is defined as

$$\eta_T = \frac{\text{actual power output}}{\text{reversible power output}}$$

(6.48)

Thus, the total-to-total turbine efficiency is

$$\eta_{\mathrm{TTT}} = \frac{h_{03} - h_{04}}{h_{03} - h_{04s}}$$

(6.49)

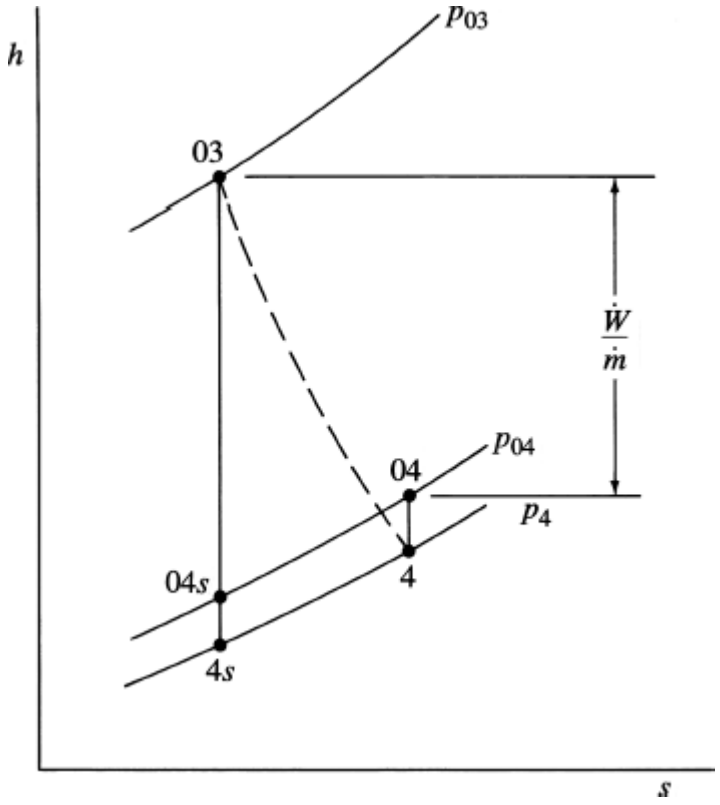
If the exhaust gas is modeled as an ideal gas with constant specific heats, then Eq. (**6.49**) can be written

$$\eta_{\mathrm{TTT}} = \frac{T_{03} - T_{04}}{T_{03} - T_{04s}} = \frac{1 - (T_{04}/T_{03})}{1 - (p_{04}/p_{03})^{(\gamma-1)/\gamma}}$$

(6.50)

Note that for exhaust gas over the temperature range of interest, c_p may vary significantly with temperature (see **Figs. 4.10 (/mhe-lookup/atom-id/0f8397b0ba4caa06#ch04fig10)** and **4.17 (/mhe-lookup/atom-id/e05a5523ebbb8455#ch04fig17)**).

Figure 6.47 Enthalpy-entropy diagram for a turbine. Inlet state 03, exit state 4; equivalent isentropic turbine exit state 4s.



Open in new tab (/mhe-lookup/tab-link/ch06fig47/3842909) Share (/#copy_link)

Since the kinetic energy at the exit of a turbocharger turbine is usually wasted, a total-to-static turbine isentropic efficiency, where the reversible adiabatic power output is that obtained between inlet stagnation conditions and the exit static pressure, is more realistic:[38 (/mhe-lookup/atom-id/a977319a43adac2e#ch06ref38)]

$$\eta_{\mathrm{TTS}} = \frac{h_{03} - h_{04}}{h_{03} - h_{4s}} = \frac{T_{03} - T_{04}}{T_{03} - T_{4s}} = \frac{1 - (T_{04}/T_{03})}{1 - (p_4/p_{03})^{(\gamma-1)/\gamma}}$$

(6.51)

The power delivered by the turbine is given by [Eqs. (**6.40**) and (**6.50**)]:

$$\dot{W}_T = \dot{m}_e(h_{03} - h_{04}) = \dot{m}_e c_{p,e}(T_{03} - T_{04}) = \dot{m}_e c_{p,e}\eta_{\mathrm{TTT}} T_{03}\left[1 - \left(\frac{p_{04}}{p_{03}}\right)^{(\gamma_e-1)/\gamma_e}\right]$$

(6.52)

where the subscript *e* denotes exhaust gas properties. If the total-to-static turbine efficiency (η_{TTS}) is used in the relation for $\dot{W}_T$, then p_4 replaces p_{04} in Eq. (**6.52**). With a turbocharger, the turbine is mechanically linked to the compressor. Hence, at constant turbocharger speed,

$$\dot{W}_C = \eta_m \dot{W}_T$$

(6.53)

where η_m is the mechanical efficiency of the turbocharger. The mechanical losses are mainly bearing friction losses. The mechanical efficiency is usually combined with the turbine efficiency since these losses are difficult to separate out.

It is advantageous if the operating characteristics of blowers, compressors, and turbines can be expressed in a manner that allows easy comparison between different designs and sizes of devices. This can be done by describing the performance characteristics in terms of dimensionless numbers.[38 (/mhe-lookup/atom-id/a977319a43adac2e#ch06ref38)] The most important dependent variables are: mass flow rate $\dot{m}$, component isentropic efficiency η, and temperature difference across the device ΔT_0. Each of these is a function of the independent variables: $p_{0,\text{in}}, p_{0,\text{out}}\ (\text{or}\ p_{\text{out}}), T_{0,\text{in}}$, *N* (speed), *D* (characteristic dimension), *R* (gas constant), $\gamma\ (c_p/c_v)$, and μ(viscosity); i.e.,

$$\dot{m}, \eta, \Delta T_0 = f\left(p_{0,\text{in}}, p_{0,\text{out}}, T_{0,\text{in}}, N, D, R, \gamma, \mu\right)$$

(6.54)

By dimensional analysis, these eight independent variables can be reduced to four dimensionless groups:

$$\dot{m}\frac{\sqrt{RT_{0,\text{in}}}}{p_{0,\text{in}}D^2}, \eta, \frac{\Delta T_0}{T_{0,\text{in}}} = f\left(\frac{ND}{\sqrt{RT_{0,\text{in}}}}, \frac{p_{0,\text{out}}}{p_{0,\text{in}}}, \frac{\dot{m}}{\mu D}, \gamma\right)$$

(6.55)

The Reynolds number, $\dot{m}/(\mu D)$, has little effect on performance and *γ* is fixed by the gas. Therefore, these variables can be omitted and Eq. (**6.51**) becomes

$$\dot{m}\frac{\sqrt{RT_{0,\text{in}}}}{p_{0,\text{in}}D^2}, \eta, \frac{\Delta T_0}{T_{0,\text{in}}} = f\left(\frac{ND}{\sqrt{RT_{0,\text{in}}}}, \frac{p_{0,\text{out}}}{p_{0,\text{in}}}\right)$$

(6.56)

For a particular device, the dimensions are fixed and the value of *R* is fixed. So it has become the convention to plot

$$\dot{m}\frac{\sqrt{T_{0,\text{in}}}}{p_{0,\text{in}}}, \eta, \frac{\Delta T_0}{T_{0,\text{in}}} = f\left(\frac{N}{\sqrt{T_{0,\text{in}}}}, \frac{p_{0,\text{out}}}{p_{0,\text{in}}}\right)$$

(6.57)

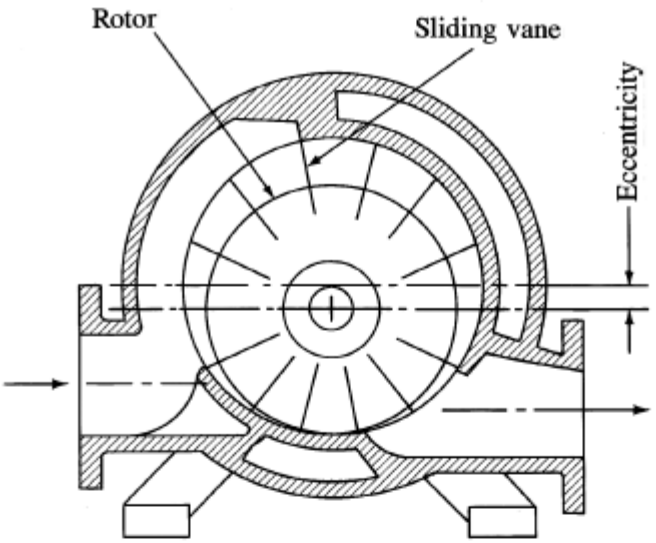
$\dot{m}\sqrt{T_{0,\text{in}}}/p_{0,\text{in}}$ is referred to as the corrected mass flow; $N/\sqrt{T_{0,\text{in}}}$ is referred to as the corrected speed. The disadvantage of this convention of removing *D* and *R* is that the groups of variables are no longer dimensionless, and performance plots or maps relate to a specific machine.

Compressor characteristics are usually plotted in terms of the pressure ratio (p_{02}/p_{01}) or (p_2/p_{01}) against the corrected mass flow $\left(\dot{m}\sqrt{T_{01}}/p_{01}\right)$ along lines of constant corrected speed $\left(N/\sqrt{T_{01}}\right)$. Contours of constant efficiency are superposed. Similar plots are used for turbines: (p_{03}/p_4) against $\dot{m}\sqrt{T_{03}}/p_{03}$ along lines of constant $N/\sqrt{T_{03}}$. Since these occupy a narrow region of the turbine performance map, other plots are often used (see **Sec. 6.8.4**).

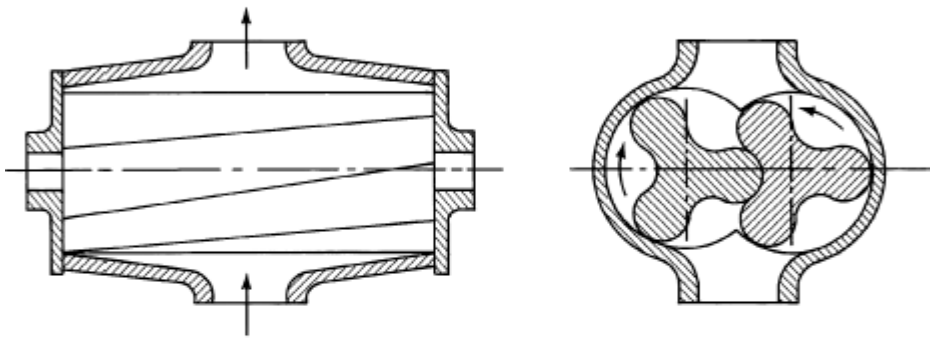
6.8.3. Compressors

Practical mechanical supercharging devices can be classified into: (1) sliding vane compressors; (2) rotary compressors; and (3) centrifugal compressors. The first two types are positive displacement compressors; the last type is an aerodynamic compressor. Four different examples of positive displacement compressors are illustrated in **Fig. 6.48**.

Figure 6.48 Positive displacement compressors: (a) sliding vane compressor; (b) roots blower; (c) Lysholm compressor; (d) screw compressor.[39 (/mhe-lookup/atom-id/a977319a43adac2e#ch06ref39)]

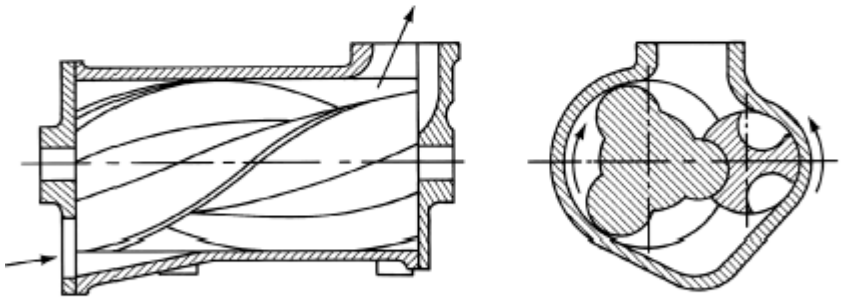


(*a*)



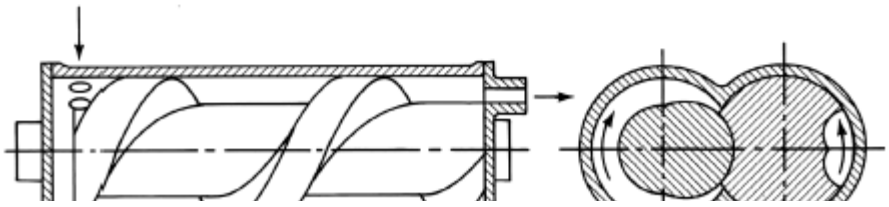
Roots blower

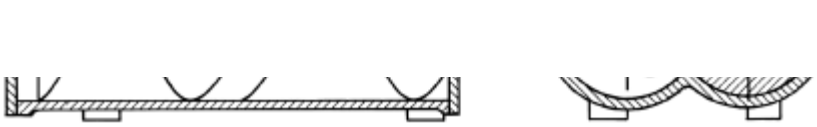
(*b*)



Lysholm compressor

(*c*)





Screw compressor

(*d*)

Open in new tab (/mhe-lookup/tab-link/ch06fig48/3842909) Share (/#copy_link)

In the *sliding vane compressor* (**Fig. 6.48*a***), deep slots are cut into the rotor to accommodate thin vanes which are free to move radially. The rotor is mounted eccentrically in the housing. As the rotor rotates, the centrifugal forces acting on the vanes force them outward against the housing, thereby dividing the crescent-shaped space into several compartments. Ambient air is drawn through the intake port into each compartment as its volume increases to a maximum. The trapped air is then compressed as the compartment volume decreases, and discharged through the outlet port. The flow capacity of the sliding vane compressor depends on the maximum induction volume which is determined by the housing cylinder bore, rotor diameter and length, eccentricity, number of vanes, and dimensions of the inlet and outlet ports. The actual flow rate and pressure rise at constant speed will be reduced by leakage. Also, heat transfer from the moving vanes and rotor and stator surfaces will reduce compression efficiency unless cooling is used to remove the thermal energy generated by friction between the vanes, and the rotor and stator. The volumetric efficiency can vary between 0.6 and 0.9 depending on the size of the machine, the quality of the design, and the method of lubrication and cooling employed. The mass flow rate at constant speed depends on the pressure ratio only through its (weak) effect on volumetric efficiency. The isentropic efficiency is relatively low.

A more commonly used positive displacement supercharger is the *Roots blower* (**Fig. 6.48*b***). The two rotors are connected by gears. The working principles are as follows. Air trapped in the recesses between the rotor lobes and the housing is carried toward the delivery port without significant change in volume. As these recesses open to the delivery line, since the suction side is closed, the trapped air is rapidly compressed by the backflow from the higher-pressure delivery line. This intermittent delivery produces nonuniform torque on the rotor and pressure pulses in the delivery line. Roots blowers are most suitable for small pressure ratios (about 1.2); for example, in two-stroke cycle engines. The volumetric efficiency depends on the running clearances, rotor length, rotational speed, and pressure ratio. In the three-lobe machines shown (two lobes are sometimes used) the volume of each recess V_R is

$$V_R = 0.564R^2l$$

where R is the rotor radius and l the blower length. The mass flow parameter is

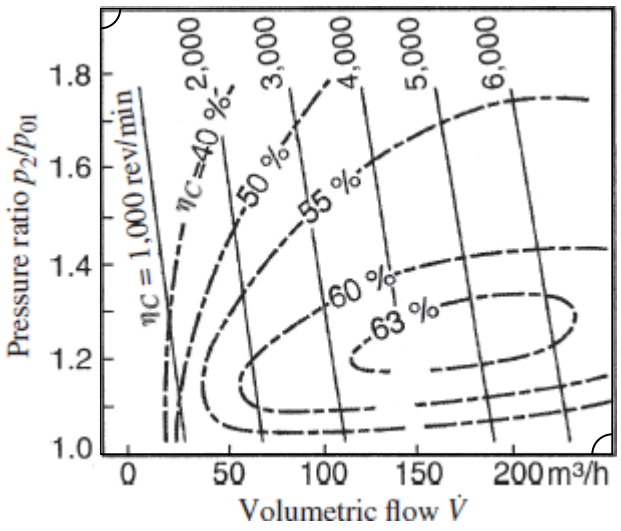
$$\frac{\dot{m}\sqrt{T_0/T_{\text{std}}}}{p_0/p_{\text{std}}} = \text{constant} \times \rho_i \eta_v N R^2 l$$

(6.58)

A performance map of a Roots blower is shown in **Fig. 6.49**. At constant speed, the flow rate depends on increasing pressure ratio only through the resulting decrease in volumetric efficiency [Eq. (**6.56**)].[39 (/mhe-lookup/atom-id/a977319a43adac2e#ch06ref39)] One advantage of the Roots blower is that its performance range is not limited by surge and choking as is the centrifugal compressor (see below). Its disadvantages are its high noise level, poorer efficiency, and large size.[40 (/mhe-lookup/atom-id/a977319a43adac2e#ch06ref40)]

Figure 6.49 Performance map at standard inlet conditions for Roots blower: p_1, total pressure before compressor; p_2, total pressure after compressor; η_C, supercharger speed, rev/min; η_C, isentropic efficiency, $\dot{V}$ airflow rate, m^3/h.[3] (Courtesy Robert Bosch GmbH and SAE.)

Interactive Graph



Click on the graph to launch interactivity.

Reset

Open in new tab (/mhe-lookup/tab-link/ch06fig49/3842909) Share (/#copy_link)

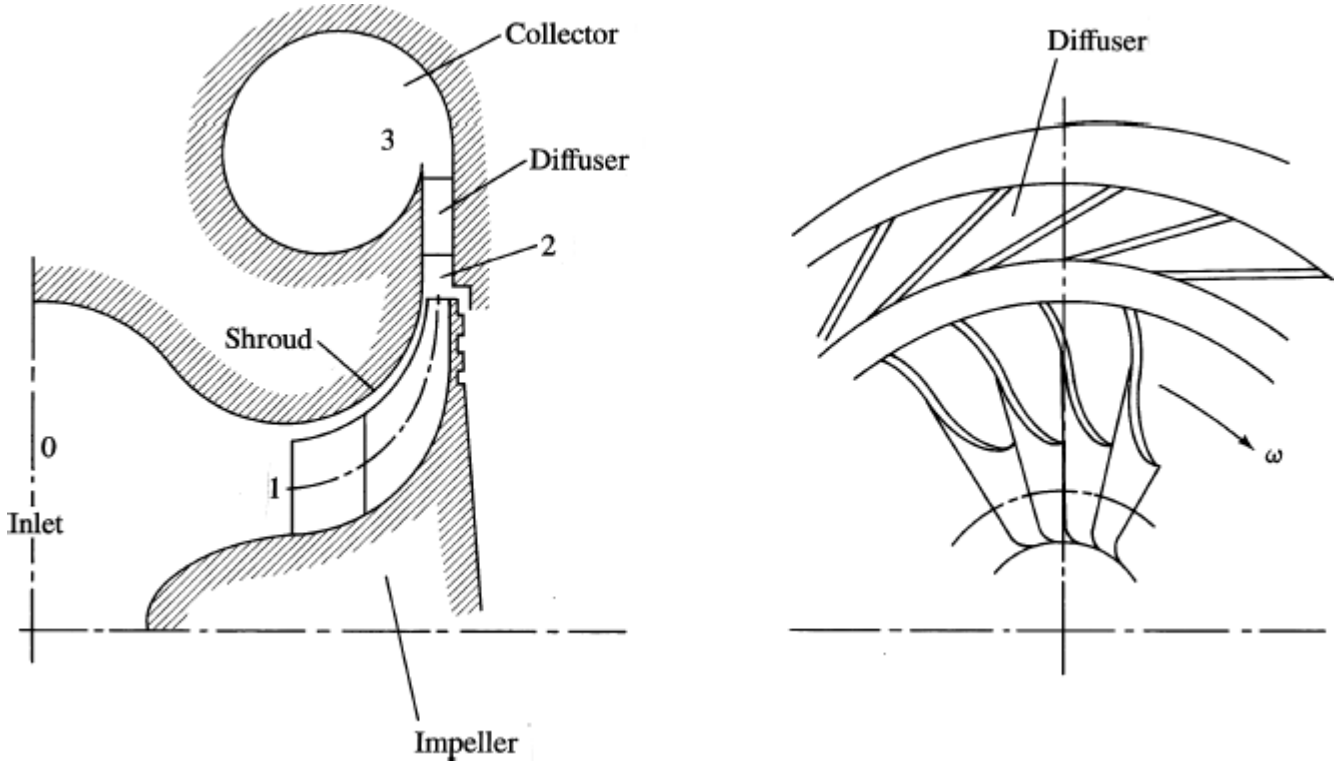
Screw compressors (**Fig. 6.48c** and ***d***) must be precision machined to achieve close tolerances between rotating and stationary elements for satisfactory operation. They run at speeds between 3000 and 30,000 rev/min. It is usually necessary to cool the rotors internally. High values of volu-

metric and isentropic efficiency are claimed.[39 (/mhe-lookup/atom-id/a977319a43adac2e#ch06ref39)]

The other compressors used with engines are aerodynamic devices. A *centrifugal compressor* is primarily used to boost inlet air or mixture density coupled with an exhaust-driven turbine in a turbocharger. It is a single-stage radial flow device, well suited to the high mass flow rates at the relatively low pressure ratios (up to about 3.5) required by the engine. To operate efficiently it must rotate at high angular speed. It is therefore much better suited to direct coupling with the exhaust-driven turbine of the turbocharger than to mechanical coupling through a gearbox to the engine for mechanical supercharging. It is widely used to boost diesel and gasoline engine outputs.

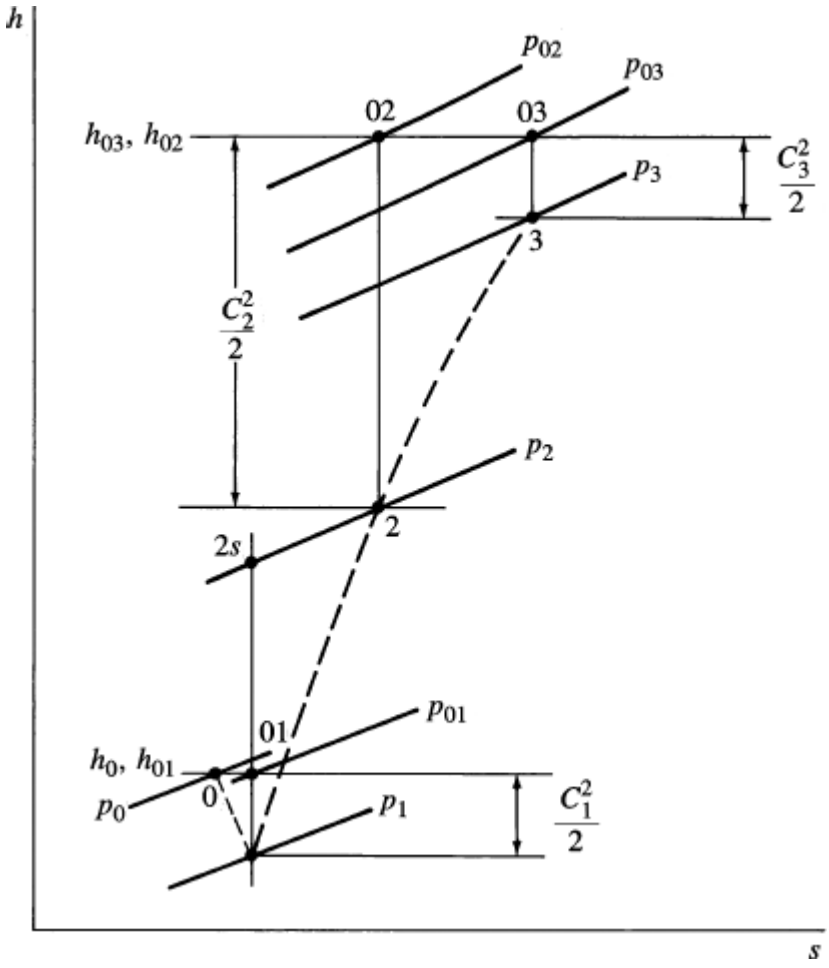
The centrifugal compressor consists of a stationary inlet casing, a rotating bladed impellor, a stationary diffuser (with or without vanes), and a collector or volute to bring the compressed air leaving the diffuser to the engine intake system (see **Fig. 6.50**). **Figure 6.51** indicates, on an *h-s* diagram, how each component contributes to the overall pressure rise across the compressor. Air at stagnation state 0 is accelerated in the inlet to pressure p_{I} and velocity C_1. The enthalpy change, 01 to 1, is $C_1^2/2$. Compression in the impeller flow passages increases the pressure to p_2 and velocity to C_2, corresponding to a stagnation state 02 if all the exit kinetic energy were recovered. The isentropic equivalent compression process has an exit static state 2*s*. The diffuser, 2 to 3, converts as much as practical of the air kinetic energy at exit to the impeller $(C_2^2/2)$ to a pressure rise ($p_3 - p_2$) by slowing down the gas in carefully shaped expanding passages. The final state, in the collector, has static pressure p_3, low kinetic energy $C_3^2/2$, and a stagnation pressure p_{03} which is less than p_{02} since the diffusion process is incomplete as well as irreversible.

Figure 6.50 Schematic of centrifugal compressor.[38 (/mhe-lookup/atom-id/a977319a43adac2e#ch06ref38)]



Open in new tab (/mhe-lookup/tab-link/ch06fig50/3842909) Share (/#copy_link)

Figure 6.51 Enthalpy-entropy diagram for flow through centrifugal compressor.



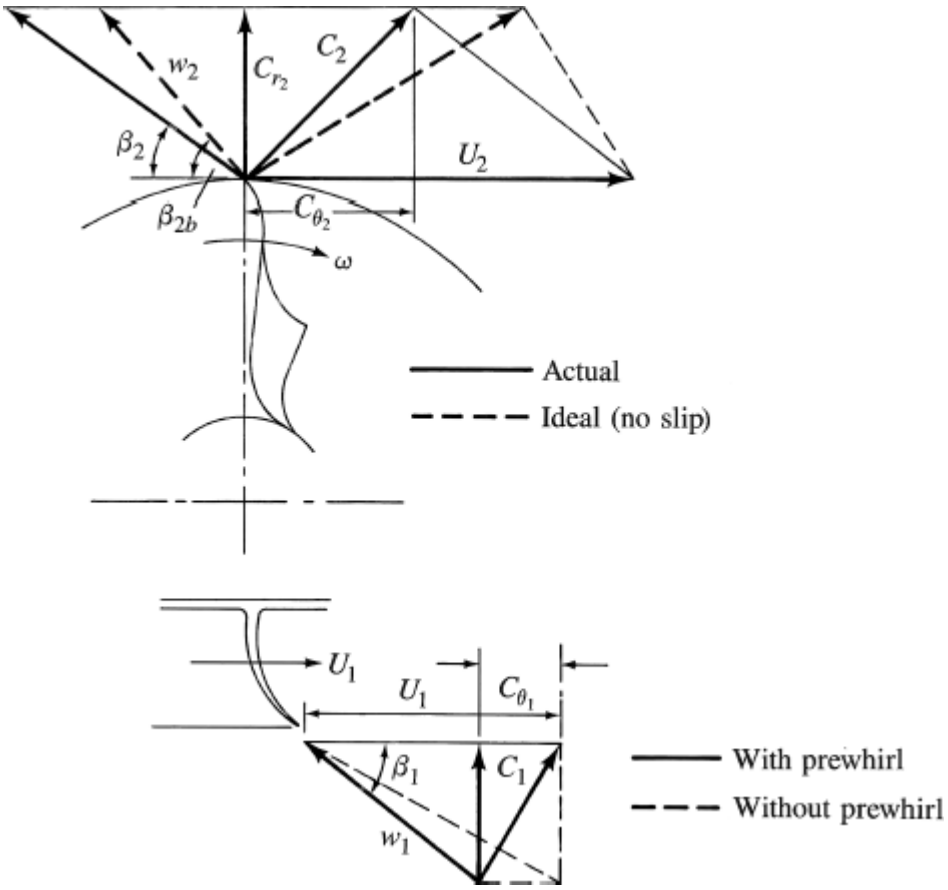
Open in new tab (/mhe-lookup/tab-link/ch06fig51/3842909) Share (/#copy_link)

The work transfer to the gas occurs in the impeller. It can be related to the change in gas angular momentum via the velocity components at the impeller entry and exit, which are shown in **Fig. 6.52**. Here C_1 and C_2 are the absolute gas velocities, U_1 and U_2 are the tangential blade velocities, and w_1 and w_2 are the gas velocities relative to the impeller, all at inlet (1) and exit (2), respectively. The torque T exerted on the gas by the impeller equals the rate of change of angular momentum:

$$T = \dot{m}\left(r_2 C_{\theta 2} - r_1 C_{\theta 1}\right)$$

(6.59)

Figure 6.52 Velocity diagrams at inlet (1) and exit (2) to centrifugal compressor rotor or impeller.[38 (/mhe-lookup/atom-id/a977319a43adac2e#ch06ref38)]



Open in new tab (/mhe-lookup/tab-link/ch06fig52/3842909) Share (/#copy_link)

The rate of work transfer to the gas is given by

$$-\dot{W}_C = T\omega = \dot{m}\omega\left(r_2 C_{\theta 2} - r_1 C_{\theta 1}\right) = \dot{m}\left(U_2 C_{\theta 2} - U_1 C_{\theta 1}\right)$$

(6.60)

This is often called the Euler equation. Normally in compressors the inlet flow is axial so $C_{\theta 1} = 0$. Thus Eq. (**6.60**) can be written:

$$\frac{\dot{W}_C}{\dot{m}} = U_2 C_{\theta 2} = U_2\left(1 - \frac{C_{r2}}{U_2}\cot\beta_2\right)$$

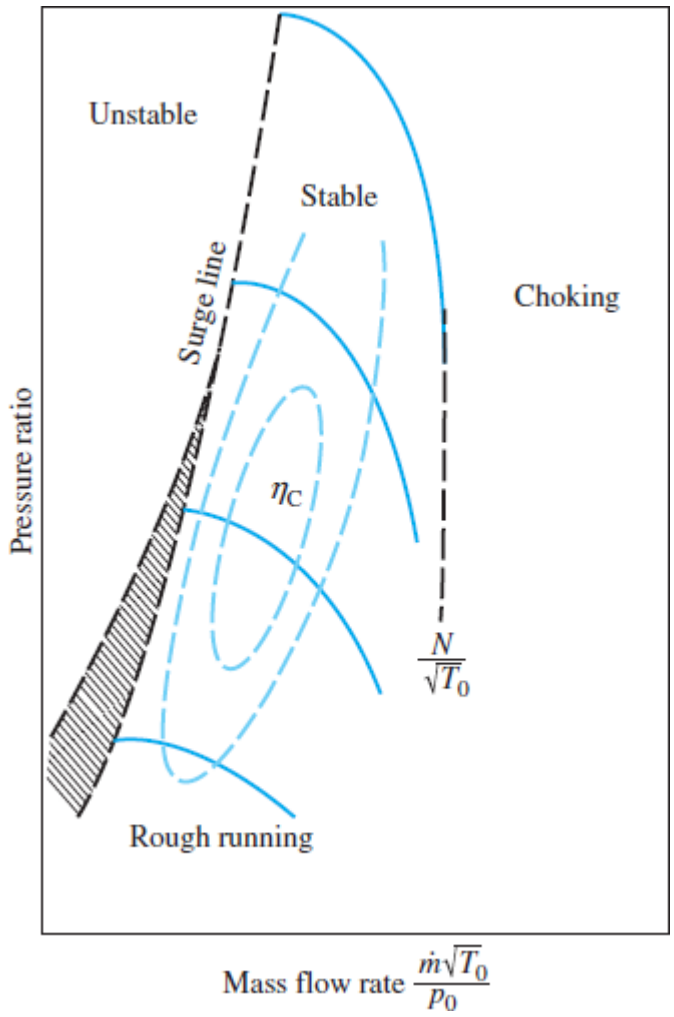
(6.61)

where β_2 is the backsweep angle. In the ideal case with no slip, β_2 is the blade angle, β_{2b}. In practice, there is slip and β_2 is less than β_{2b}. Many compressors have radial vanes (i.e., $\beta_{2b} = 90°$). A recent trend is backswept vanes ($\beta_{2b} < 90°$) which give higher efficiency. Since work transfer to

the gas occurs only in the impeller, the work-transfer rate given by Eq. (**6.61**) equals the change in stagnation enthalpy ($h_{03} - h_{01}$) in **Fig. 6.51** [see Eq. (**6.40**)].

The operating characteristics of a centrifugal compressor are usually described by a *performance map*. This shows lines of constant compressor efficiency , and constant corrected speed $N/\sqrt{T_{0,\text{in}}}$ on a plot of pressure ratio $p_{0,\text{out}}/p_{0,\text{in}}$ against corrected mass flow $\dot{m}\sqrt{T_{0,\text{in}}}/p_{0,\text{in}}$ [see Eq. (**6.57**)]. **Figure 6.53** indicates the form of such a map. The stable operating range in the center of the map is separated from an unstable region on the left by the *surge line*. When the mass flow is reduced at constant pressure ratio, local flow reversal eventually occurs in the boundary layer. Further reductions in mass flow cause the flow to reverse completely, causing a drop in pressure. This relieves the adverse pressure gradient. The flow reestablishes itself, builds up again, and the process repeats. Compressors should not be operated in this unstable regime. The stable operating regime is limited on the right by choking. The velocities increase as $\dot{m}$ increases, and eventually the flow becomes sonic in the limiting area of the machine. Extra mass flow through the compressor can only be obtained by higher speed. When the diffuser is choked, compressor speed may rise substantially with only a limited increase in the mass flow rate.[38] (/mhe-lookup/atom-id/a977319a43adac2e#ch06ref38)

Figure 6.53 Schematic of compressor operating map showing stable operating range.[38] *(/mhe-lookup/atom-id/a977319a43adac2e#ch06ref38)*



Open in new tab (/mhe-lookup/tab-link/ch06fig53/3842909) Share (/#copy_link)

Figure 6.54 shows an actual turbocharger compressor performance map. In practice, the map variables corrected speed and mass flow rate are usually defined as

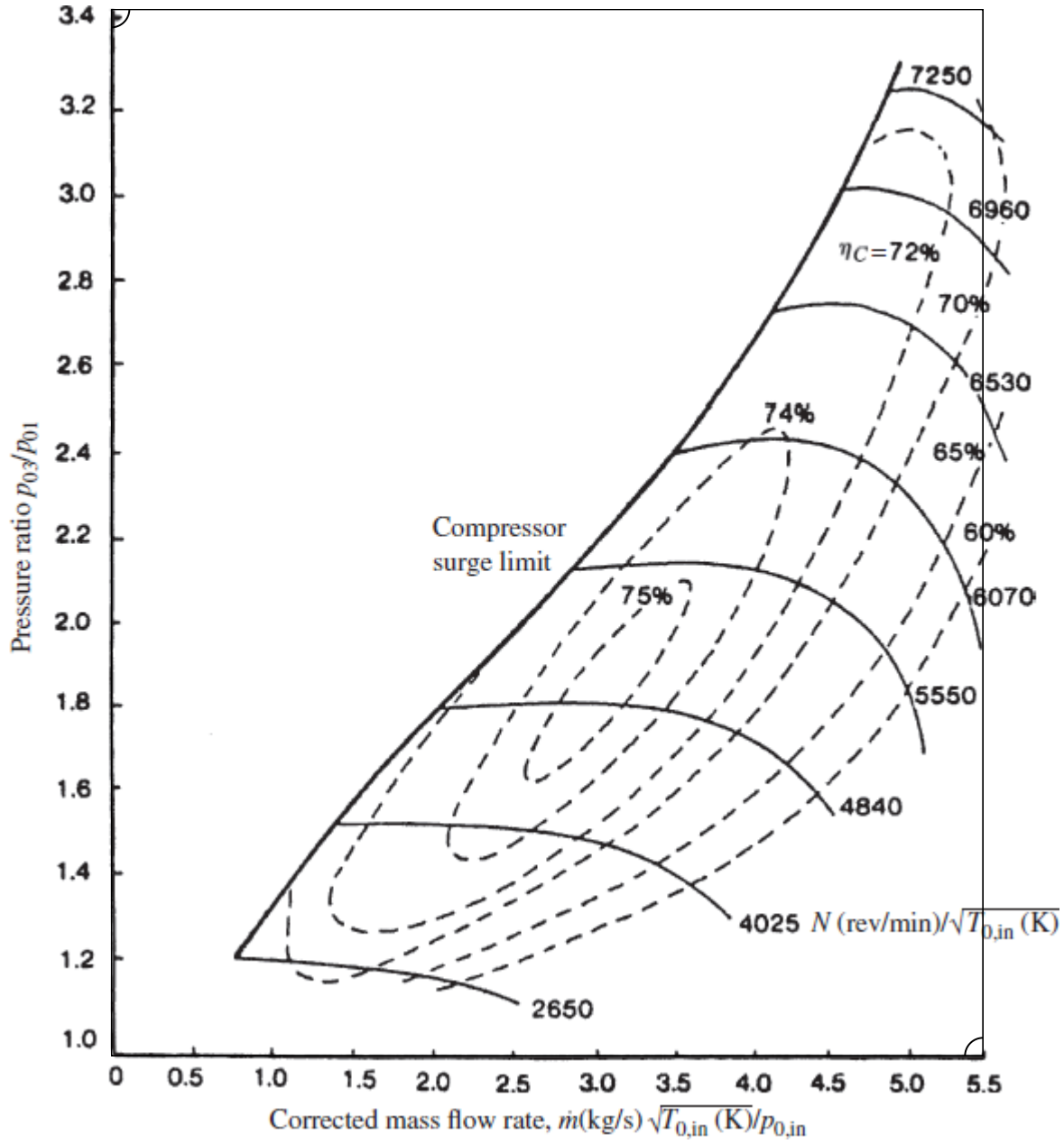
$$N_{\text{cor}} = N\left(\frac{T_{\text{ref}}}{T_{0,\text{in}}}\right)^{1/2} \qquad \dot{m}_{\text{cor}} = \dot{m}\left(\frac{T_{0,\text{in}}}{T_{\text{ref}}}\right)^{1/2}\left(\frac{p_{\text{ref}}}{p_{0,\text{in}}}\right)$$

(6.62)

where T_{ref} and p_{ref} are standard atmospheric temperature and pressure, respectively. Though the details of different compressor maps vary, their general characteristics are similar. The high efficiency region runs parallel to the surge line (and close to it for vaneless diffusers). A wide *flow range* for the compressor (see **Fig. 6.46**) is important in turbochargers used for transportation applications.

Figure 6.54 Centrifugal compressor operating map. Lines of constant corrected speed and compressor efficiency are plotted on a graph of pressure ratio against corrected mass flow.[41] *(/mhe-lookup/atom-id/a977319a43adac2e#ch06ref41)* *T_{01} = inlet temperature (K), p_{01} = inlet pressure (bar), p_{03} = exit pressure (bar), N = speed (rev/min), m = mass flow rate (kg/s). Figure 6.51 defines the end states.*

Interactive Graph



Click on the graph to launch interactivity or enter values below.

Corrected mass flow rate, m(kg/s) $\sqrt{T_{0,\,in}}$ (K)/$p_{0,\,in}$

Pressure ratio P_{03}/P_{01}

Apply Reset

Open in new tab (/mhe-lookup/tab-link/ch06fig54/3842909) Share (/#copy_link)

6.8.4. Turbines

The turbocharger turbine is driven by the energy available in the engine exhaust. The ideal energy available is the blowdown work transfer produced by reversibly expanding the gas in the cylinder at exhaust valve opening to atmospheric pressure, and (for the four-stroke cycle engine) the work done by the piston displacing the gases remaining in the cylinder after blowdown.

The reciprocating internal combustion engine is inherently an unsteady pulsating flow device. Turbines can be designed to accept such an unsteady flow, but they operate more efficiently under steady-flow conditions. In practice, two approaches for recovering a fraction of the available exhaust energy are commonly used: constant-pressure turbocharging and pulse turbocharging. In *constant-pressure turbocharging*, an exhaust manifold of sufficiently large volume to damp out the mass flow and pressure pulses is used so that the flow to the turbine is essentially steady. The disadvantage of this approach is that it does not make full use of the high kinetic energy of the gases leaving the exhaust port; the losses inherent in the mixing of this high-velocity gas with a large volume of low-velocity gas cannot be recovered. With *pulse turbocharging*, short small-cross-section pipes connect each exhaust port to the turbine so that much of the kinetic energy associated with the exhaust blowdown can be utilized. By suitably grouping the different cylinder exhaust ports so that the exhaust pulses are sequential and have minimum overlap, the flow unsteadiness can be held to an acceptable level. The turbine must be specifically designed for this pulsating flow to achieve adequate efficiencies. The combination of increased energy available at the turbine, with reasonable turbine efficiencies, results in the pulse system being more commonly used in engines with mostly transient operation since it provides faster turbocharger response (primarily automotive engines). Constant-pressure turbocharging is used in larger, highly charged, slow-speed diesel engines in stationary use where loads are largely steady.[42] (/mhe-lookup/atom-id/a977319a43adac2e#ch06ref42)

Two types of turbines are used in turbochargers: radial and axial flow turbines. The radial flow turbine is similar in appearance to the centrifugal compressor: however, the flow is radially inward not outward. Radial flow turbines are normally used in automotive or truck applications. Larger engines—locomotive, stationary, or marine—may use axial flow turbines.

A drawing of a radial flow turbine is shown in **Fig. 6.55**. It consists of an inlet casing or scroll, a set of inlet nozzles (often omitted with small turbines), and the turbine rotor or wheel. The function of each component is evident from the *h*-*s* diagram and velocity triangles in **Fig. 6.56**. The nozzles (01-2) accelerate the flow, with modest loss in stagnation pressure. The drop in stagnation enthalpy, and hence the work transfer, occurs solely in the rotor passages, 2-3: hence, the rotor is designed for minimum kinetic energy $C_3^2/2$ at exit. The velocity triangles at inlet and exit relate the work transfer to the change in angular momentum via the Euler equation:

$$\dot{W}_T = T\omega = \dot{m}\omega(r_2 C_{\theta 2} - r_3 C_{\theta 3}) = \dot{m}(U_2 C_{\theta 2} - U_3 C_{\theta 3})$$

(6.63)

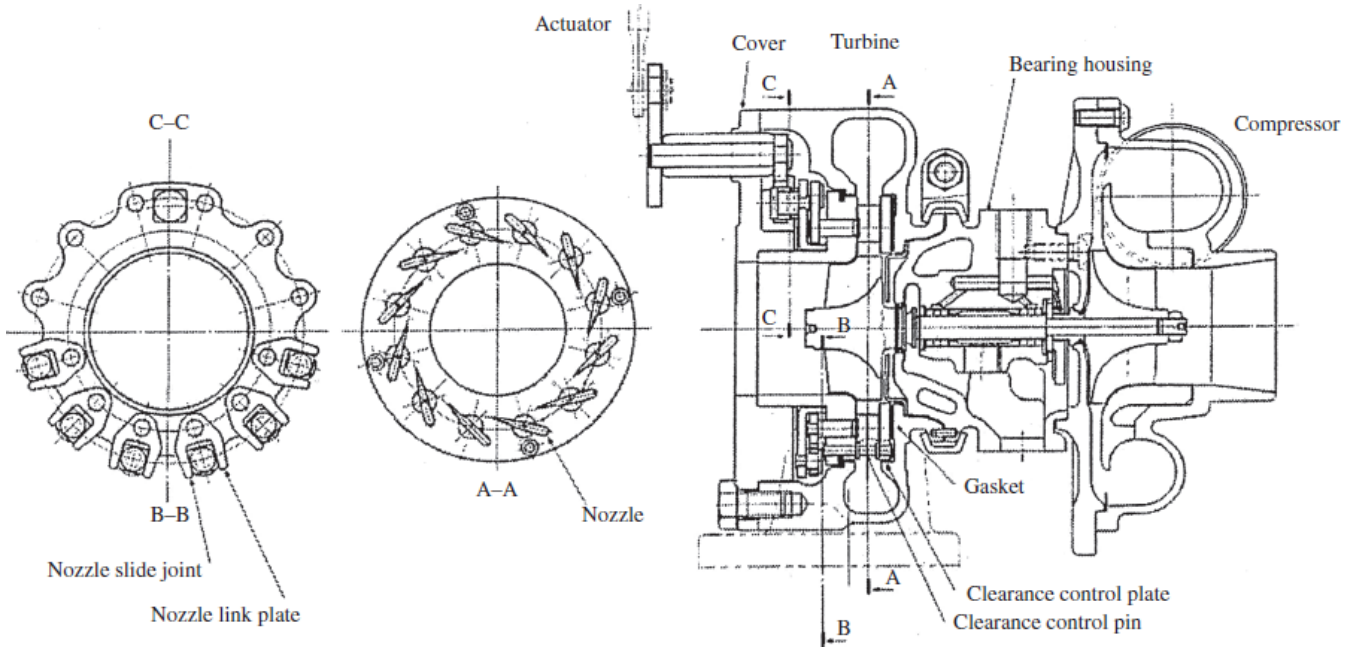
where *T* is the torque and *ω* the rotor angular speed. Variable geometry nozzles can better direct the flow entering the rotor to be tangential to the vanes. For maximum work transfer the exit velocity should be axial. The work-transfer rate relates to the change in stagnation enthalpy via

$$\dot{W}_T = \dot{m}(h_{02} - h_{03}) = \dot{m}(h_{01} - h_{03})$$

(6.64)

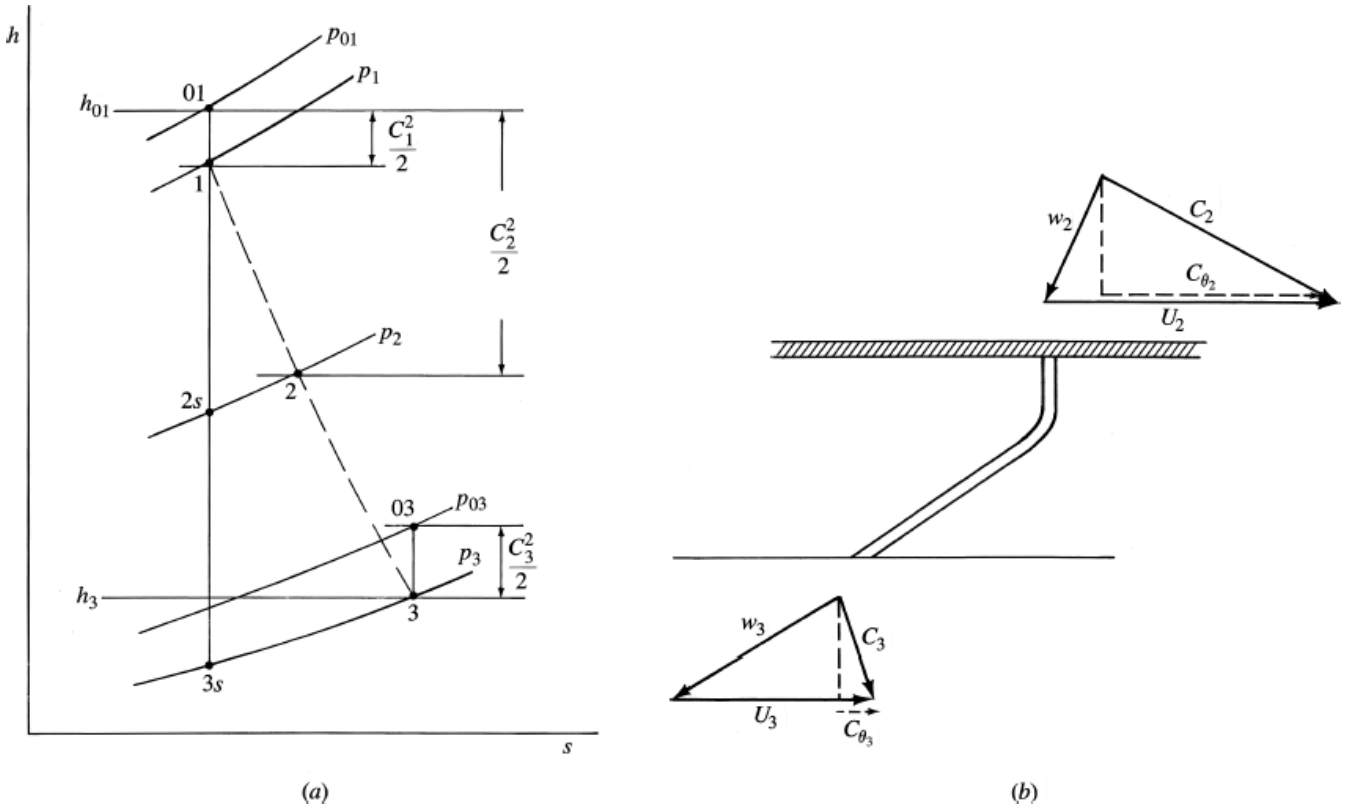
The turbine isentropic efficiency is given by Eqs. (**6.44**) to (**6.47**).

Figure 6.55 Cross-section and layout drawings of a radial flow turbine for a passenger car diesel engine with variable geometry nozzle inlet vanes.[43 (/mhe-lookup/atom-id/a977319a43adac2e#ch06ref43)]



Open in new tab (/mhe-lookup/tab-link/ch06fig55/3842909) Share (/#copy_link)

Figure 6.56 (a) Enthalpy-entropy diagram for radial turbine; (b) velocity diagrams at turbine rotor inlet (2) and exit (3).

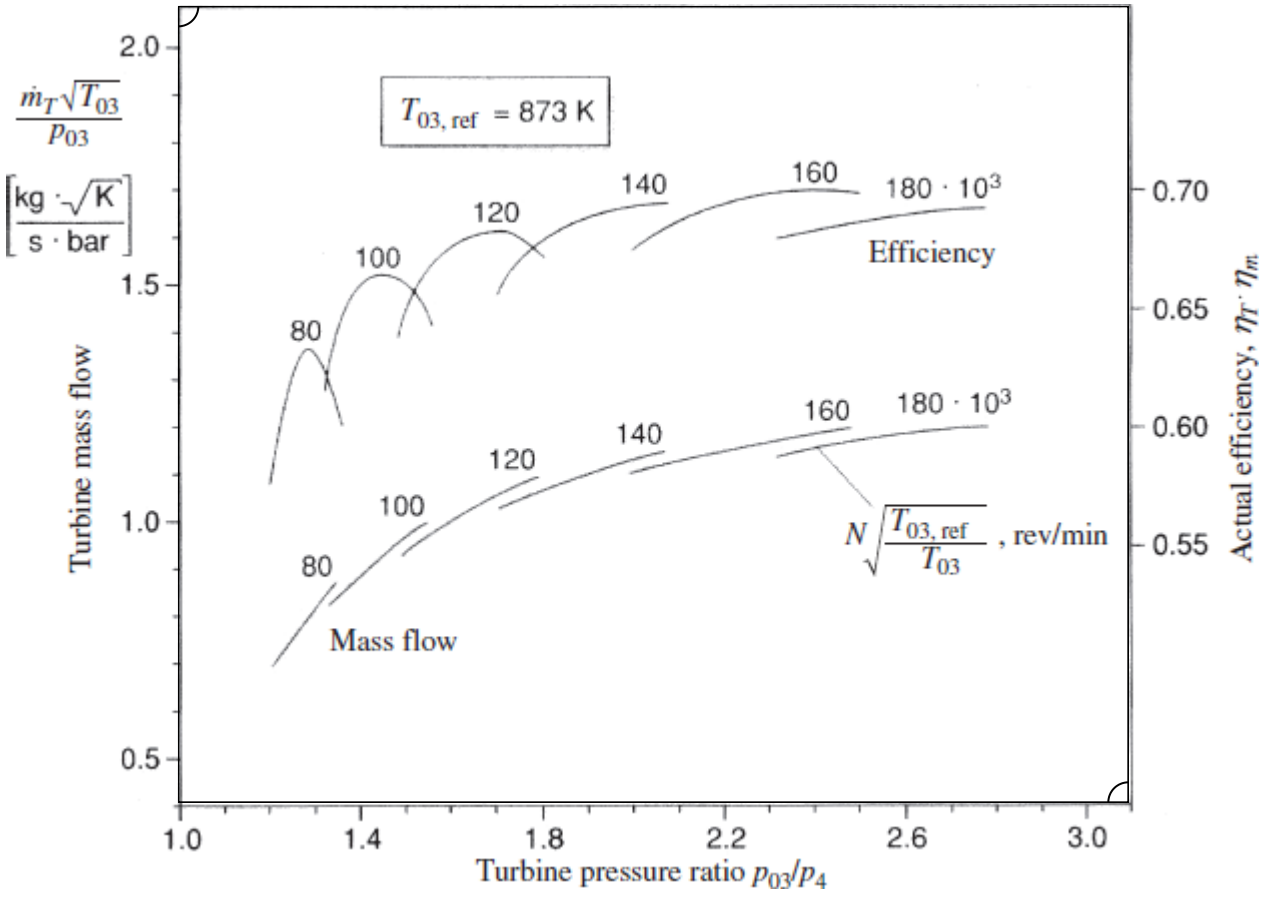


Open in new tab (/mhe-lookup/tab-link/ch06fig56/3842909) Share (/#copy_link)

Many different types of plots have been used to define radial flow turbine characteristics. **Figure 6.57** shows lines of constant corrected speed and efficiency on a plot of corrected mass flow rate versus pressure ratio, with the actual turbine efficiency. As flow rate increases at a given speed, it approaches a limit corresponding to the flow becoming choked in the nozzle blades or the rotor. For turbines, efficiency is often presented separately because the turbine operating regime is narrow.

Figure 6.57 Radial turbine performance map showing lines of constant corrected speed on plots of corrected mass flow rate and actual efficiency versus turbine pressure ratio. T_{01} = turbine inlet temperature (K), p_{01} = turbine inlet pressure (bar), p_3 = turbine exit pressure (bar), $\dot{m}$ = mass flow rate (kg/s), N = speed (rev/min). See Figs. 6.49 and 6.50 for nomenclature. (Source: BorgWarner Turbo Systems.[41 (/mhe-lookup/atom-id/a977319a43adac2e#ch06ref41)])

Interactive Graph



Click on the graph to launch interactivity or enter values below.

Turbine pressure ratio p_{03}/p_4

⊖ [ ] ⊕

Turbine pressure, flow

Apply Reset

Open in new tab (/mhe-lookup/tab-link/ch06fig57/3842909) Share (/#copy_link)

A schematic of a turbocharger axial-flow turbine is shown in **Fig. 6.58**. Usually a single stage is sufficient to expand the exhaust gas efficiently through the pressure ratios associated with engine turbocharging. This turbine consists of an annular flow passage, a single row of nozzles or stator blades, and a rotating blade ring. The changes in gas state across each component are similar to those of the radial turbine shown in the *h*-*s* diagram of **Fig. 6.56*a***. The velocity triangles at entry and exit to the rotor, shown in **Fig. 6.59**, relate the work transfer from the gas to the rotor to the change in angular momentum:

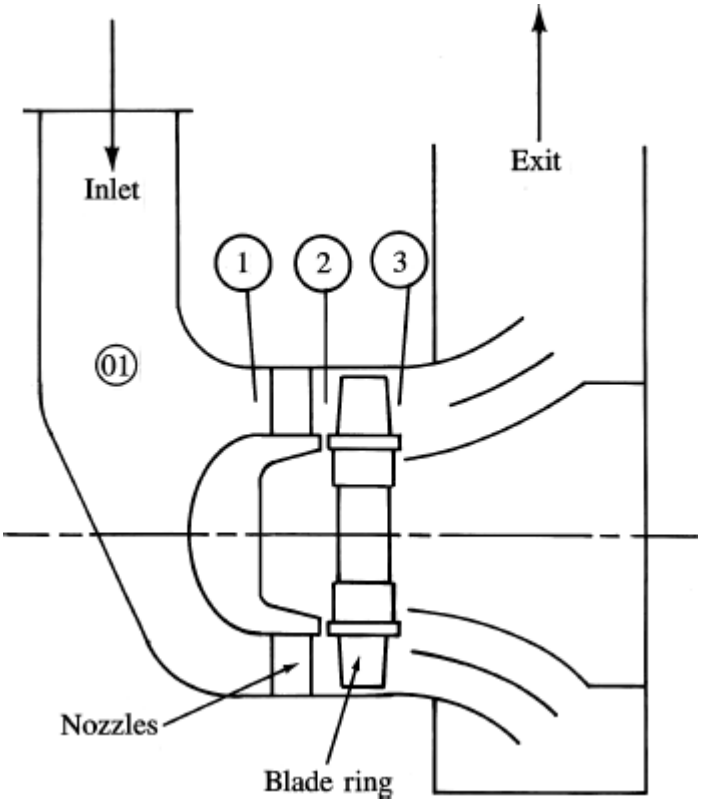
$$\dot{W}_T = \omega T = \dot{m}\omega(r_2 C_{\theta 2} + r_3 C_{\theta 3})$$

Since the mid-radius r_2 usually equals the mid-radius r_3,

$$\begin{aligned} \dot{W}_T &= \dot{m}U(C_{\theta 2} + C_{\theta 3}) = \dot{m}U(C_2 \sin\alpha_2 + C_3 \sin\alpha_3) \\ &= \dot{m}U(C_{z2} \tan\beta_2 + C_{z3} \tan\beta_3) \end{aligned}$$

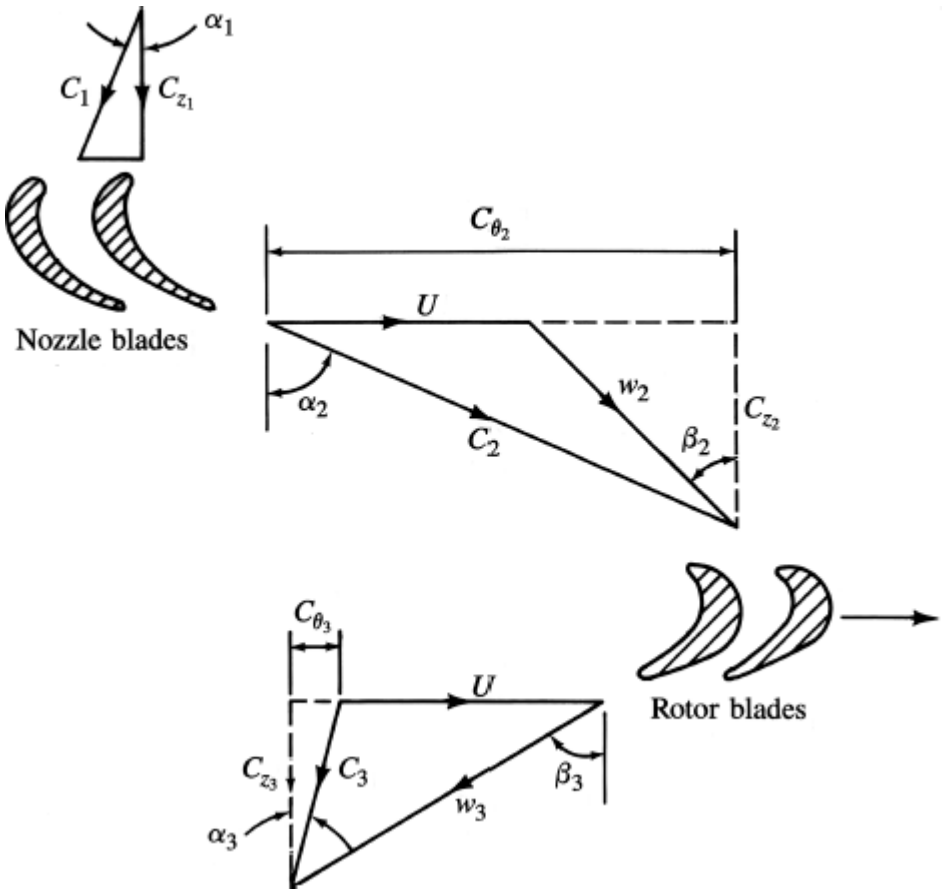
(6.65)

Figure 6.58 Schematic of single-stage axial flow turbine.



Open in new tab (/mhe-lookup/tab-link/ch06fig58/3842909) Share (/#copy_link)

Figure 6.59 Velocity diagrams at entry (2) and exit (3) to axial-flow turbine blade ring.[38 (/mhe-lookup/atom-id/a977319a43adac2e#ch06ref38)]



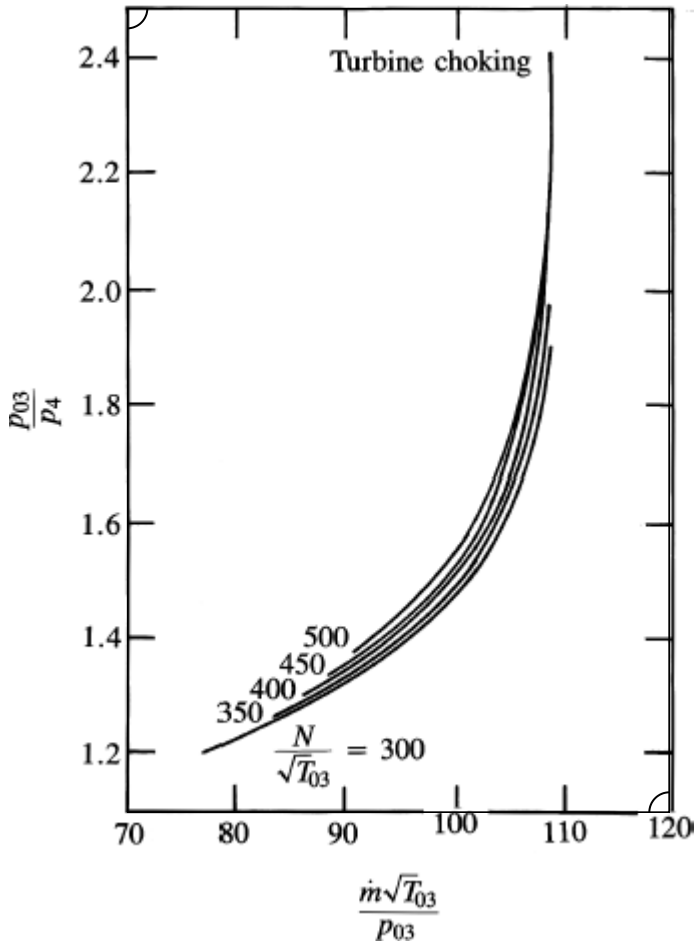
Open in new tab (/mhe-lookup/tab-link/ch06fig59/3842909) Share (/#copy_link)

Equation (**6.64**) relates the work-transfer rate to the stagnation enthalpy change as in the radial turbine.

Figure 6.60 shows axial turbine performance characteristics on the standard dimensionless plot of pressure ratio versus corrected mass flow rate. Here the constant speed lines converge to a single choked flow limit as the mass flow is increased. In the radial turbine, the variation in centrifugal effects with speed cause a noticeable spread in the constant speed lines (**Fig. 6.57**).

Figure 6.60 Axial flow turbine performance map: pressure ratio is plotted against corrected mass flow rate. T_{03} = turbine inlet temperature (K), p_{03} = turbine inlet pressure (bar), p_4 = turbine exit pressure (bar), $\dot{m}$ = mass flow rate (kg/s), N = speed (rev/min).[38 (/mhe-lookup/atom-id/a977319a43adac2e#ch06ref38)]

Interactive Graph



Click on the graph to launch interactivity or enter values below.

$\dot{m}\sqrt{T_{03}}/p_{03}$

p_{03}/p_4

Apply Reset

Open in new tab (/mhe-lookup/tab-link/ch06fig60/3842909) Share (/#copy_link)

An alternative performance plot for turbines is efficiency versus *blade speed ratio*. This ratio is the blade speed U (at its mean height for an axial flow turbine or the wheel tip speed for a radial flow turbine), divided by the velocity equivalent of the isentropic enthalpy drop across the turbine stage, C_s: that is,

$$\text{Blade speed ratio} = \frac{U}{C_s}$$

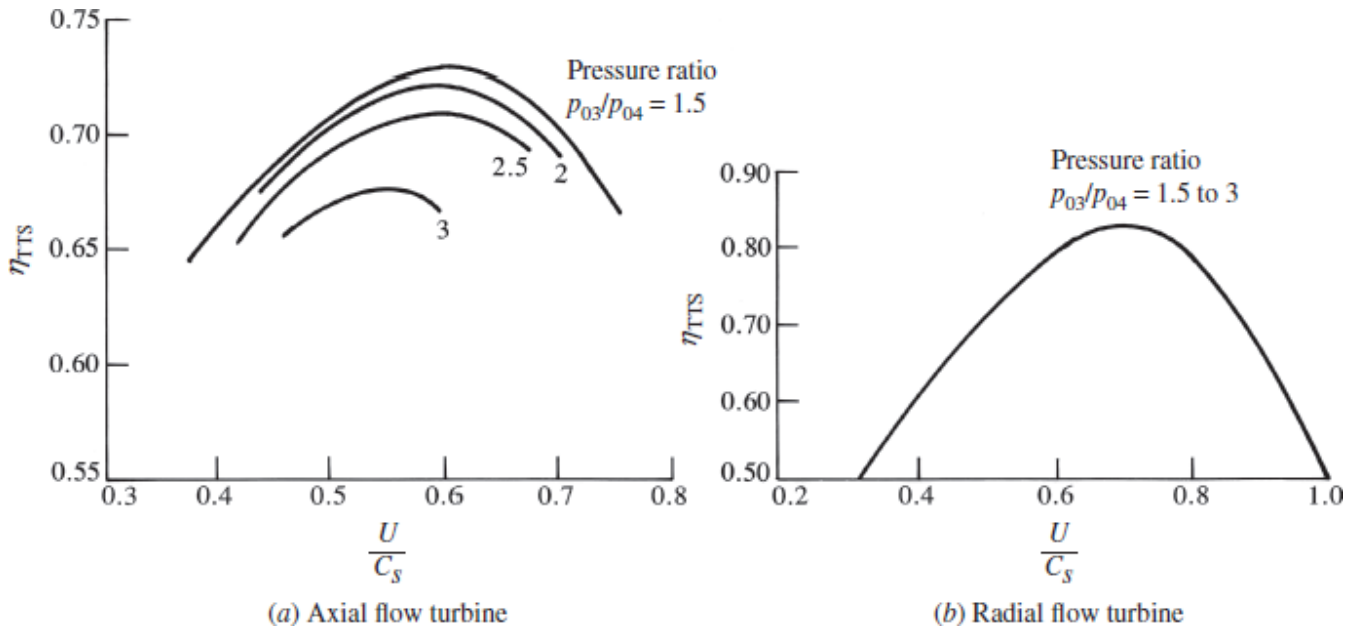
where

$$C_s = [2(h_{03} - h_{4s})]^{1/2}$$

(6.66)

This method of displaying performance is useful for matching compressor and turbine wheel size for operation of the turbine at optimum efficiency. **Figure 6.61** shows such plots for an axial and radial flow turbine. The peak efficiency can occur for U/C_s between 0.5 and 0.8, depending on turbine design and application.[38 (/mhe-lookup/atom-id/a977319a43adac2e#ch06ref38)]

Figure 6.61 Plot of turbine total-to-static efficiency versus blade speed ratio U/C_s for (a) axial-flow and (b) radial-flow turbines.[38 (/mhe-lookup/atom-id/a977319a43adac2e#ch06ref38)]

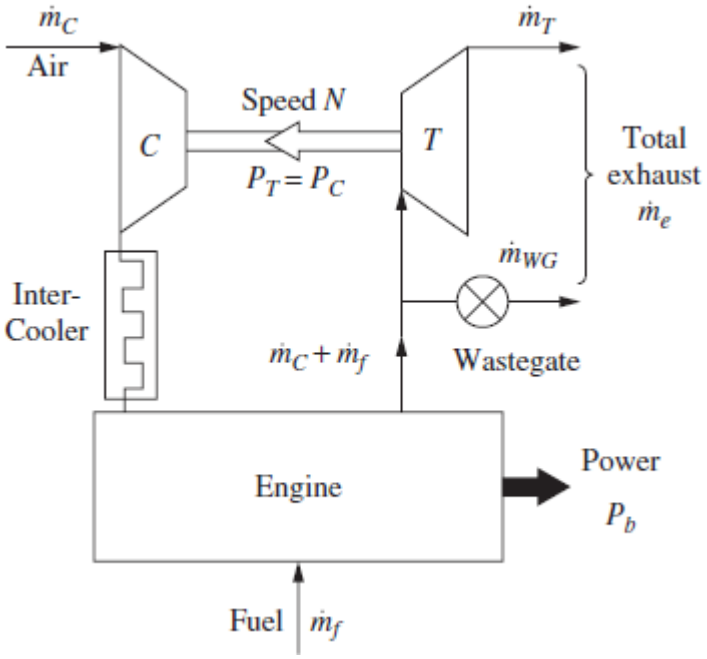


Open in new tab (/mhe-lookup/tab-link/ch06fig61/3842909) Share (/#copy_link)

6.8.5. Compressor, Engine, Turbine Matching

The mass flows through the compressor, engine, turbine, and wastegate in a turbocharged engine must be consistent. The turbine inlet temperature depends on how the engine is operating: fuel and air flow rates, engine speed and power, are key variables. The turbine supplies the power that drives the compressor, and turbine and compressor operate at the same speed. The sum of the turbine mass flow rate plus that through the wastegate equals the engine exhaust flow. Further, the relative geometric sizing of the turbocharger and the engine affect their joint performance (especially as a function of engine speed). **Figure 6.62** illustrates the connections between these components, and the matching logic.

Figure 6.62 Schematic illustrating compressor, engine, turbine, matching.



Open in new tab (/mhe-lookup/tab-link/ch06fig62/3842909) Share (/#copy_link)

Note that for the turbocharger to be providing significant boost, the engine must be operating at mid to higher load. Under lightly loaded conditions, especially at lower engine speeds, there is in-sufficient engine exhaust flow to generate enough turbine power to provide significant air compression. Under these conditions, the turbocharger effectively "idles." Accordingly, a *boost threshold* is defined: It is the engine speed (rev/min), at wide- open throttle, at which turbocharger air compression starts to occur.

For a given turbocharger, the compressor and turbine characteristics are linked with the engine as indicated in **Fig. 6.62**. Since the compressor and turbine are on a common shaft with speed *N*, their respective corrected speeds $\left(N/\sqrt{T_{01}} \text{ and } N/\sqrt{T_{03}}\right)$ are linked by:

$$\frac{N}{\sqrt{T_{01}}} = \frac{N}{\sqrt{T_{03}}} \left(\frac{T_{03}}{T_{01}} \right)^{1/2}$$

(6.67)

For $\dot{m}_C = \dot{m}_T = \dot{m}$ their corrected mass flow rates are linked by:

$$\frac{\dot{m}\sqrt{T_{01}}}{p_{01}} = \frac{\dot{m}\sqrt{T_{03}}}{p_{03}} \left(\frac{p_{03}}{p_{01}} \right) \left(\frac{T_{01}}{T_{03}} \right)^{1/2}$$

(6.68)

When $\dot{m}_C \left[1 + (F/A) \right] = \dot{m}_T$, the equation is easily modified.

Since the compressor and turbine powers are equal in magnitude, when $\dot{m}_C$ equals $\dot{m}_T$,

$$h_{02} - h_{01} = \eta_m (h_{03} - h_{04})$$

(6.69)

or, with an ideal gas model,

$$c_{p,C}(T_{02} - T_{01}) = \eta_m c_{p,T}(T_{03} - T_{04})$$

(6.70)

Equation (**6.70**), with Eqs. (**6.44**) and (**6.50**), gives

$$\left(\frac{p_{02}}{p_{01}} \right)^{(\gamma_C - 1)/\gamma_C} - 1 = \eta_C \eta_T \eta_m \frac{c_{p,T}}{c_{p,C}} \left[1 - \left(\frac{p_4}{p_{04}} \right)^{(\gamma_T - 1)/\gamma_T} \right] \frac{T_{03}}{T_{01}}$$

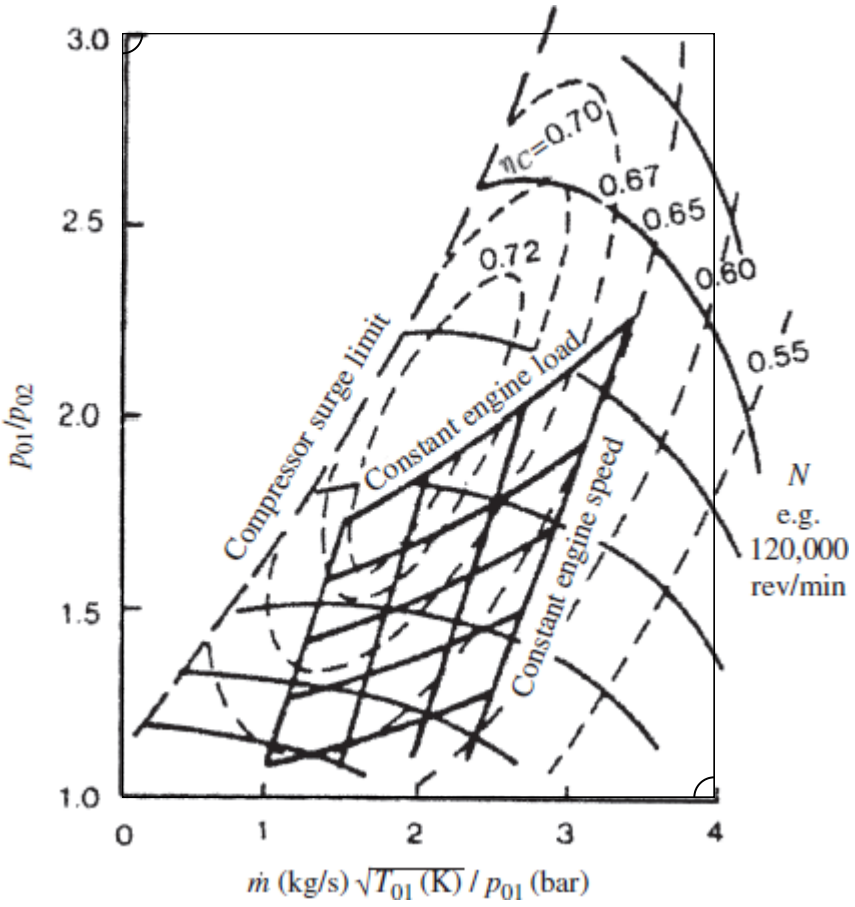
(6.71)

Assuming that the turbine exit pressure p_4 equals atmospheric pressure p_{01}, the equilibrium or steady-state running lines for constant values of T_{03}/T_{01} can be determined.

Figure 6.63 shows an example of such a set of matched turbocharger characteristics, plotted on a turbocharger compressor map for a radial turbine with characteristics similar to **Fig. 6.57**.

Figure 6.63 Illustration of steady-state turbocharger operating characteristics: compressor operating map (such as that in Fig. 6.54), with the airflow requirements of a four-stroke truck diesel engine superposed.[41 (/mhe-lookup/atom-id/a977319a43adac2e#ch06ref41)] *Mass flows through the compressor, engine, and turbine have to be consistent. See Fig. 6.62.*

Interactive Graph



Click on the graph to launch interactivity or enter values below.

$\dot{m}$ (kg/s) $\sqrt{T_{01}}$(K)/p_{01} (bar)

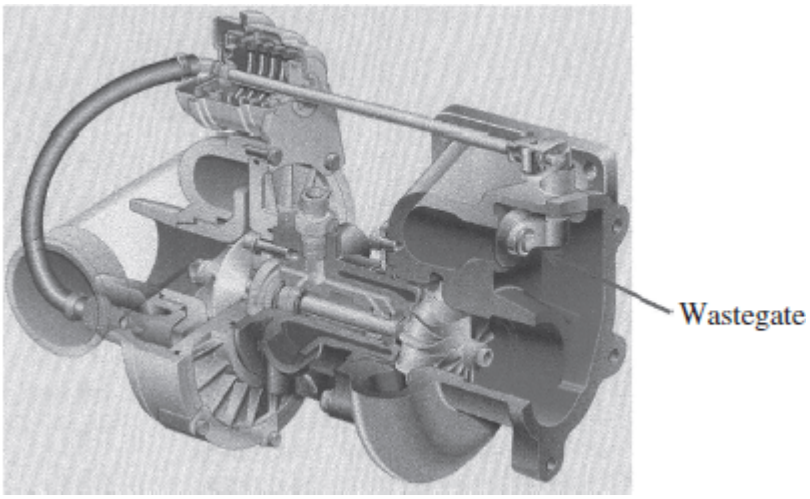
p_{01}/p_{02}

Apply Reset

Open in new tab (/mhe-lookup/tab-link/ch06fig63/3842909) Share (/#copy_link)

The problem of overspeeding the turbocharger and generating high boost levels, and very high cylinder pressures often requires that some of the exhaust be bypassed around the turbine. A bypass valve or *wastegate* (as shown in **Fig. 6.64**) is usually built into the turbocharger casing. It consists of a spring-loaded valve acting in response to the intake manifold pressure acting on a controlling diaphragm. When the wastegate is open, only a portion of the exhaust gases will flow through the turbine and generate power; the remainder passes directly into the exhaust system downstream of the turbine.

Figure 6.64 Cutaway drawing of turbocharger with a wastegate. (Courtesy: BorgWarner Turbo Systems.)



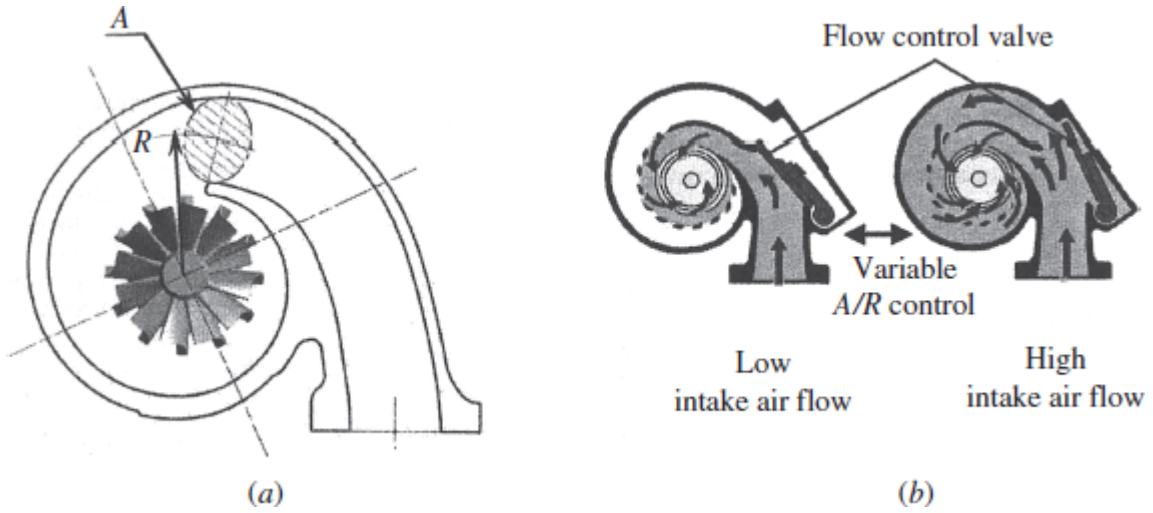
Open in new tab (/mhe-lookup/tab-link/ch06fig64/3842909) Share (/#copy_link)

The relative sizing of the turbocharger and the engine significantly influences their combined behavior. A relatively smaller turbocharger provides higher compressor boost levels in the lower engine speed range, and less boost at higher engine speeds. A larger turbocharger has the inverse behavior: lower boost at lower speeds and higher boost at higher speeds. Higher boost at lower speeds is effective at offsetting "turbo lag": a phenomenon in automotive applications where, following a rapid opening of the throttle valve, the rotational inertia of the turbocharger delays its speeding up which delays the production of the desired increase in boost pressure (and thus airflow and torque).

In the commonly used turbocharger radial turbine, the *A/R* ratio is used as a measure of the above turbocharger characteristics (see **Fig. 6.65*a***). *A* is the cross-sectional area of the turbine housing throat, and *R* is the distance between the center of the throat and the turbocharger shaft axis. There is interest for gasoline engine applications in using a variable flow turbocharger which uses a control valve located in the turbine intake port (see **Fig. 6.65*b***) to reduce the turbine intake cross-sectional area at low speeds and flows and to increase that flow area at high speeds. The turbine has two scrolls, inner and outer circumferences, separated by a fixed vane. With low intake

airflow, the outer scroll is closed off and higher torque at low engine speed is achieved. With high intake airflow, both scrolls are open achieving high torque at high speed.[43 (/mhe-lookup/atom-id/a977319a43adac2e#ch06ref43)]

Figure 6.65 (a) Definition of A/R for a conventional turbine and (b) schematic of flow control valve.[43 (/mhe-lookup/atom-id/a977319a43adac2e#ch06ref43)]



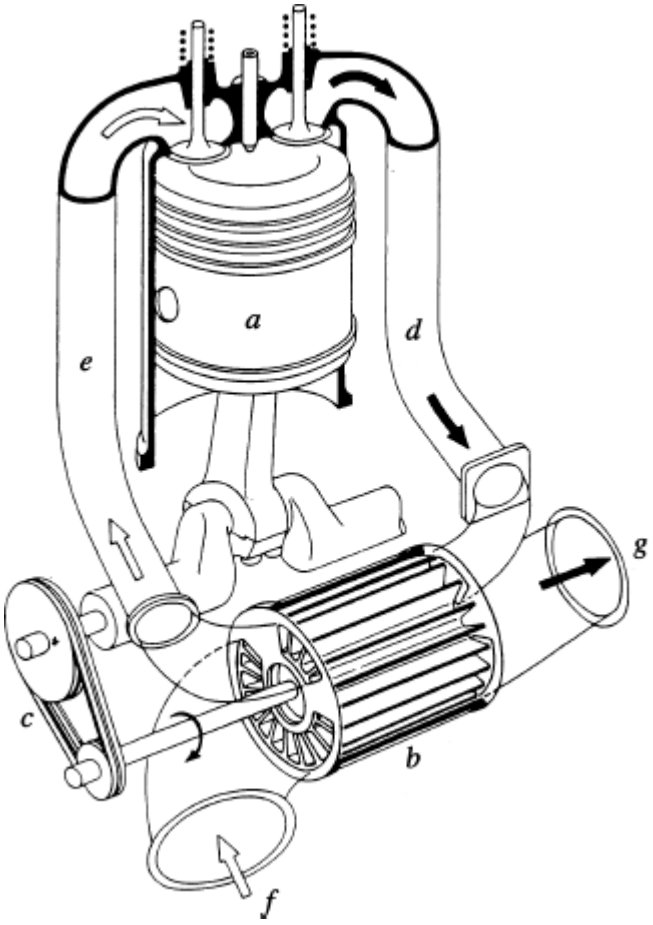
Open in new tab (/mhe-lookup/tab-link/ch06fig65/3842909) Share (/#copy_link)

6.8.6. Wave-Compression Devices

Pressure wave superchargers make use of the fact that if two fluids having different pressures are brought into direct contact in long narrow channels, equalization of pressure occurs faster than mixing. One such device, the Comprex, has been developed for internal combustion engine supercharging which operates using this principle.[44 (/mhe-lookup/atom-id/a977319a43adac2e#ch06ref44)] It is shown schematically in **Fig. 6.66**. The working channels of the Comprex are arranged on a rotor or cell wheel (*b*) which is rotated between two castings by a belt driven from the crankshaft (*c*). There is no contact between the rotor and the casing, but the gaps are kept small to minimize leakage. The belt drive merely overcomes friction and maintains the rotor at a speed proportional to engine speed (usually four or five times faster): It provides no compression work. One casing (the air casing) contains the passage which brings low-pressure air (*f*) to one set of ports and high-pressure air (*e*) from another set of ports in the rotor-side inner casing. The other casing (the gas casing) connects the high-pressure engine exhaust gas (*d*) to one set of ports at the other end of the rotor, and connects a second set of ports to the exhaust system (*g*). Fluid can flow into and out of the rotor channels through these ports. The exhaust gas inlet port is made small enough to cause a significant pressure rise in the exhaust manifold (e.g., 2 atm) when the engine is operated at its rated power. The pressure wave process does not depend on the pressure and

flow fluctuations within the manifold caused by individual cylinder exhaust events: its operation can be explained assuming constant pressure at each set of ports. As the rotor makes one revolution, the ends of each channel are alternatively closed, or are open to a flow passage. By appropriate arrangement of these passages and selection of the geometry and location of the ports, an efficient energy transfer between the engine exhaust gases and the fresh charge can be realized.[44 (/mhe-lookup/atom-id/a977319a43adac2e#ch06ref44)]

Figure 6.66 Schematic of Comprex supercharger.[44 (/mhe-lookup/atom-id/a977319a43adac2e#ch06ref44)] ***a engine, b cell wheel or rotor, c belt drive, d high-pressure exhaust gas (G-HP), e high-pressure air (A-HP), f low-pressure air (A-LP), g low-pressure exhaust gas (G-LP).***

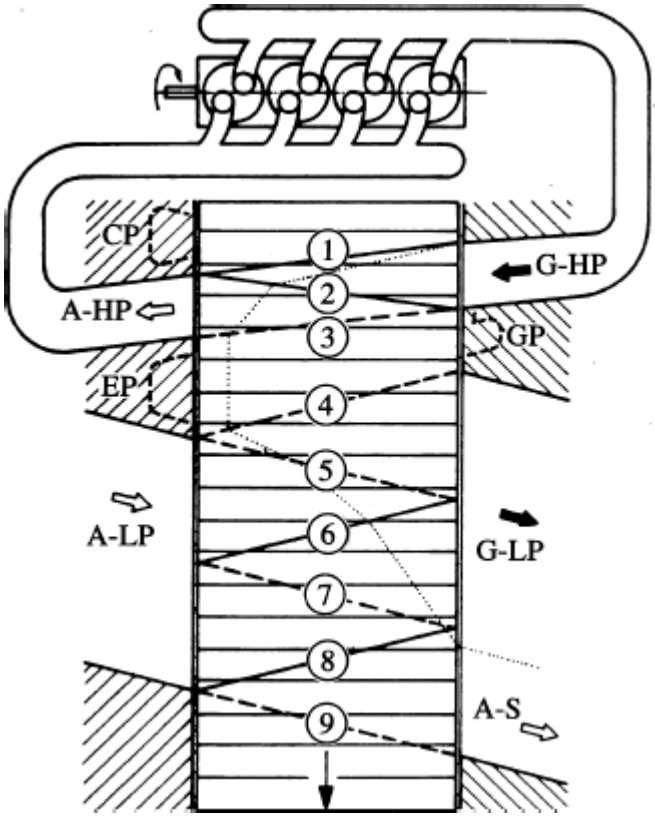


Open in new tab (/mhe-lookup/tab-link/ch06fig66/3842909) Share (/#copy_link)

The wave-compression process in the Comprex can be explained in more detail with the aid of **Fig. 6.67** where the rotational motion of the channels has been unrolled. Consider the channel starting at the top; it is closed at both ends and contains air at atmospheric pressure. As it opens at the upper edge of the high-pressure gas (G-HP) duct, a compression or shock wave (1) propagates from the right end of the channel toward the left, compressing the air through which it passes. The compressed air behind the wave occupies less space so the high-pressure exhaust gas moves into the channel as indicated by the dotted line. This line is the boundary between the

two fluids. As this wave (1) reaches the left end, the channel is opened and compressed air flows into the engine inlet duct (A-HP). The inlet duct is shaped to provide the same mass flow at lower velocity: This deceleration of the air produces a second compression wave (2) which propagates back into the channel. As a result the compressed air leaving the cell on the left has a higher pressure than the driving gas on the right. As this wave (2) arrives at the right-hand side, the high-pressure gas (G-HP) channel closes. An expansion wave (3) then propagates back to the left, separating the now motionless and partly expanded fluid on the right from still-moving fluid on the left. When this wave (3) reaches the left-hand end, A-HP is closed and all the gases in the channel are at rest. Note that the first gas particles (dotted line) have not quite reached the air end of the channel: A cushion of air remains to prevent breakthrough.

Figure 6.67 Unrolled view of the Comprex pressure-wave process.[44 (/mhe-lookup/atom-id/a977319a43adac2e#ch06ref44)] ***A air, G exhaust gas, S scavenging, HP high pressure, LP low pressure; CP, EP, GP are pockets.***



Open in new tab (/mhe-lookup/tab-link/ch06fig67/3842909) Share (/#copy_link)

The cell's contents are still at a higher pressure than the low pressure in the exhaust gas duct. When the right-hand end of the cell reaches this duct, the cell's contents expand into the exhaust. This motion is transferred through the channel by an expansion wave (4) which propagates to the left at sonic speed. When this wave reaches the left-hand end, the cell opens to the low-pressure air duct (A-LP) and fresh air is drawn into the cell. The flow to the right continues, but with de-

creasing speed due to wave action (5, 6, 7, 8) and pressure losses at each end of the cell. When the dotted line—the interface between air and the exhaust gas—reaches the right end of the cell, all the driving gas has left. The cell is then purged by the scavenging airflow (A-S) and filled with fresh air at atmospheric pressure. At wave (9), the cell is closed at both ends, restoring it to its initial state.[45 (/mhe-lookup/atom-id/a977319a43adac2e#ch06ref45)]

The speed of these pressure waves is the local sound speed and is a function of local gas temperature only. Thus, the above process will only work properly for a given exhaust gas temperature at a particular cell speed. The operating range is extended by the use of "pockets" as shown in **Fig. 6.67**. The pockets prevent the reflection of sound waves from a closed channel end which would cause a substantial change in flow velocity in the channel. These pockets, marked CP and EP on the air side and GP on the exhaust gas side, allow flow from one channel to adjacent channels via the pocket if the wave action requires it. Thus the device can be tuned for full-load medium-speed operation and still give acceptable performance at other loads and speeds because the pockets allow the particle paths to change without major losses.[44 (/mhe-lookup/atom-id/a977319a43adac2e#ch06ref44)]

The values of compressor efficiency [defined by Eq. (**6.41**)] are comparable to those of mechanical and aerodynamic compressors over a wide range of engine speeds.[44 (/mhe-lookup/atom-id/a977319a43adac2e#ch06ref44)]

6.9. PROBLEMS

6.1. For four-stroke cycle engines, the inlet and exhaust valve opening and closing crank angles are typically: IVO 15° BTC; IVC 50° ABC; EVO 55° BBC; EVC 10° ATC. Explain why these valve timings improve engine breathing relative to valve opening and closing at the beginnings and ends of the intake and exhaust strokes. Discuss the additional design issues that are important.

6.2. For four-stroke engines, the inlet and exhaust valve opening and closing crank angles are typically:

IVO: 15° BTC

IVC: 50° ABC

EVO: 55° BBC

EVC: 10° ATC

a. Explain why these valve timings improve engine breathing relative to valve opening and closing at the beginnings and ends of the intake and exhaust strokes.

b. Mention and explain at least one modification you would make to the above valve timings if the engine you are designing is:

- intended for a race car
- turbocharged
- operating at low speeds

c. With fully variable valve timing to improve the wide-open-throttle (WOT) performance of this spark-ignition engine, explain how you would change these "fixed-valve-timing" opening and closing angles.

6.3. A conventional spark-ignition engine operating with gasoline will not run smoothly (due to incomplete combustion) with an equivalence ratio leaner than about $\phi = 0.8$. It is desirable to extend the smooth operating limit of the engine to leaner equivalence ratios so that at part-throttle operation (with intake pressure less than 1 atmosphere) the pumping work is reduced. Leaner than normal operation can be achieved by adding hydrogen gas (H_2) to the mixture in the intake system. The addition of H_2 makes the fuel-air mixture easier to burn.

a. The fuel composition with "mixed" fuel operation is $H_2 + C_8H_{18}$—one mole of hydrogen to every mole of gasoline, which is assumed the same as isooctane. What is the stoichiometric air/fuel ratio for the "mixed" fuel?

b. The lower heating value of H_2 is 120 MJ/kg and for isooctane is 44.4 MJ/kg. What is the heating value per kilogram of fuel mixture?

c. Engine operation with isooctane and the mixed ($H_2 + C_8H_{18}$) fuel is compared in a particular engine at a part-load condition (brake mean effective pressure of 275 kPa and 1400 rev/min). You are given the following information about the engine's operation:

© McGraw-Hill Education. All rights reserved. Any use is subject to the Terms of Use, Privacy Notice and copyright information.

Fuel	C_8H_{18}	$H_2 + C_8H_{18}$
Equivalence ratio	0.8	0.5
Gross indicated fuel conversion efficiency	0.35	0.4
Mechanical + accessory friction mep	138 kPa	138 kPa
Inlet manifold pressure	46 kPa	?
Pumping mep	55 kPa	?

Estimate approximately the inlet manifold pressure and the pumping mean effective pressure with ($H_2 + C_8H_{18}$) fuel. Explain your method and assumptions clearly. Note that mechanical efficiency η_m is defined as

$$\eta_m = \frac{\text{bmep}}{\text{imep}_g} = \frac{\text{bmep}}{\text{bmep} + \text{mfmep} + \text{pmep}}$$

6.4. With variable-valve-timing spark-ignition engines, by closing the intake valve much later than a standard fixed-valve-timing engine, the pumping work can be reduced.

a. The average brake mean effective pressure (bmep) required to drive a car is 250 kPa. The intake manifold pressure with a standard fixed intake-valve-timing engine (closing 50° ABC) is 50 kPa and the exhaust manifold pressure is 105 kPa. The mechanical plus accessory friction mep is 90 kPa. What indicated (gross) mep must the engine produce? The intake valve closing angle is now retarded so that the intake manifold pressure is 90 kPa. What imep (gross) will now be required? Other parameters remain the same.

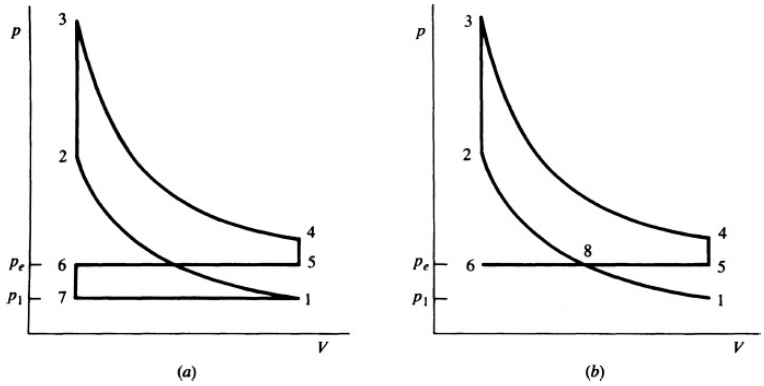
b. Sketch a carefully drawn and proportioned cylinder pressure versus cylinder volume graph showing the *real engine* four-stroke cycles for the fixed and variable intake valve closings, with other details as in (*a*). Clearly identify the two intake and the exhaust manifold pressures, the intake valve closing locations, and ensure that areas on the *p-V* diagram that correspond to any of these various mean effective pressures are in the appropriate proportions. Think carefully about the details of what is happening!

c. Estimate the ratio of the cylinder volume at which the late intake-valve-timing engine should end the intake process, to the cylinder volume at which the standard intake-valve-timing engine ends the intake process, to give the same bmep (250 kPa) as the standard valve-timing engine. Give an approximate estimate of the late closing angle (you do not need to solve the volume versus crank angle equation to get this crank angle: You can use a simpler approximate approach). Both engines operate at stoichiometric. They have the same indicated fuel conversion efficiency.

6.5. Sketch (*a*) shows an ideal cycle *p-V* diagram for a conventional throttled spark-ignition engine, 1-2-3-4-5-6-7-1. The gas properties c_v, c_p, γ, R throughout the cycle are constant. The mass of gas in the cylinder is m. The exhaust pressure is p_e.

Sketch (*b*) shows an ideal cycle *p-V* diagram 1-2-3-4-5-6-8-1 for a spark-ignition engine with different intake valve timing. The intake manifold is unthrottled; it has essentially the same pressure as the exhaust. To reduce the mass inducted at part load, the inlet valve is closed *partway through the intake stroke* at point 8. The gas in the cylinder at intake valve closing at 8 is then expanded isentropically to 1 with the intake valve closed. The pressure p_1 at the start of compression is the same for both cycles.

© McGraw-Hill Education. All rights reserved. Any use is subject to the Terms of Use, Privacy Notice and copyright information.



a. Indicate on *p-V* diagrams the area that corresponds to the pumping work per cycle for cycles (*a*) and (*b*). Which area is greater?

b. Derive expressions for the pumping work per cycle W_p in terms of m, c_v, γ, T_u (p_e/p_1), and the compression ratio r_c for cycles (*a*) and (*b*). Be consistent about the signs of the work transfers to and from the gas.

c. For $\gamma = 1.3$, $r_c = 8$, and $(p_e/p_1) = 2$, find the ratio $W_p(b)/W_p(a)$, assuming the values of T_1 and m are the same in both cases.

6.6. Estimate approximately the pressure drop across the inlet valve about halfway through the intake stroke, and across the exhaust valve halfway through the exhaust stroke, when the piston speed is at its maximum for a typical four-stroke cycle spark-ignition engine with $B = L = 85$ mm at 2500 and 5000 rev/min at WOT. Assume appropriate values for any valve and port geometric details required, and for the gas composition and state.

6.7. Compare the engine residual gas fraction data in Fig. 6.26 with ideal cycle estimates of residual gas fraction as follows. Using Eq. (5.47) plot the fuel-air cycle residual mass fraction x_r against p_i/p_e for $r_c = 8.5$ on the same graph as the engine data in Fig. 6.19 at 1400 rev/min and 27° valve overlap. Assume $T_r = 1400$ K and $(\gamma - 1)/\gamma = 0.24$ in Eq. (5.47). Suggest an explanation for any significant differences.

6.8. One concept that would increase SI engine efficiency is early intake valve closing (EIVC) where the intake valve closes *before* the piston reaches BC on the intake stroke, thus limiting the amount of charge inducted into the cylinder.

a. Explain why EIVC improves engine efficiency at part load. (*Hint*: Consider what must happen to the inlet manifold pressure in order to maintain constant mass in the cylinder as the intake valve is closed sooner.)

b. This part load reduction in charge could be achieved by using late intake valve closing where the intake valve is not closed until the compression stroke has pushed some of the cylinder gases back out into the intake manifold. Based on a comparison of *p-V* diagrams, is this method inferior to EIVC?

6.9. An eight-cylinder turbocharged aftercooled four-stroke cycle diesel engine operates with an inlet pressure of 1.8 atmospheres at its maximum rated power at 2000 rev/min. $B = 128$ mm; $L = 140$ mm; η_v (based on inlet manifold conditions of 1.8 atm and 325 K after the aftercooler) = 0.9. The compressor isentropic efficiency is 0.7.

a. Calculate the power required to drive the turbocharger compressor.

b. If the exhaust gas temperature is 650°C and the turbocharger isentropic efficiency is 0.65, estimate the pressure at turbine inlet. The turbine exhausts to the atmosphere.

6.10. The charging efficiency of two-stroke cycle diesel engines can be estimated from measurement of the concentration of O_2 and CO_2 in the burned gases within the cylinder, or in the exhaust blowdown pulse prior to any mixing with fresh air. The engine bore = 125 mm; stroke = 150 mm; compression ratio = 15. The fuel flow rate at 1800 rev/min is 1.6 g/s per cylinder. The conditions used to evaluate the air density for the reference mass are 300 K and 1 atm. The molar concentrations (dry) of CO_2 and O_2 in the in-cylinder burned gases are 7.2 and 10.4% (see Fig. 4.22). The scavenging

© McGraw-Hill Education. All rights reserved. Any use is subject to the Terms of Use, Privacy Notice and copyright information.

airflow rate is 80 g/s. Evaluate (*a*) the charging efficiency, (*b*) the delivery ratio, and (*c*) the trapping efficiency (assuming the trapped mass equals the reference mass).

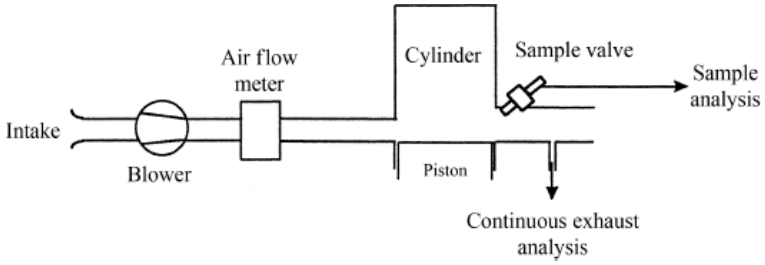
6.11. In order to evaluate the scavenging quality of a two-stroke diesel engine, the composition of in-cylinder gases at the end of combustion has to be determined. For this purpose an electromagnetic gas-sampling valve is being placed next to the exhaust port of a single cylinder test engine. The engine is a two-stroke diesel with direct in-cylinder injection. During the blowdown period (between "exhaust open" and "intake open") the valve samples from the burnt exhaust gases exiting the cylinder into the exhaust system: from an analysis of these samples the equivalence ratio of the in-cylinder gases can be determined. The overall equivalence ratio of the engine (including short-circuiting fresh charge) is determined from a continuous exhaust gas downstream of the exhaust port.

Data:	Bore	B = 240 mm
	Stroke	L = 250 mm
	Connecting rod length	L_C = 530 mm
	Height of intake port	s_{in} = 48.0 mm
	Height of exhaust port	s_{ex} = 80.7 mm
	Min. opening duration of sampling valve	t_{min} = 80.7 mm
	Engine speed	N = 1000 rev/min
	Ambient pressure	p_{amb} = 1 bar
	Pressure difference across blower	Δp = 0.32 bar
	Temperature of scavenge air	T_{sc} = 313 K
	Ambient temperature	T_{amb} = 298 K
	Volumetric flow rate of scavenge air	V_{in} = 0.173 m^3/s
	In-cylinder equivalence ratio	ϕ_{cyl} = 0.588
	Overall equivalence ratio	ϕ_{del} = 0.328

a. Determine the intake and exhaust timing (in degrees crank angle) of the test engine.

b. Up to what engine speed can this sampling valve be used for the analysis described?

c. Determine the delivery ratio, the trapping efficiency, and the charging efficiency of the test engine.



© McGraw-Hill Education. All rights reserved. Any use is subject to the Terms of Use, Privacy Notice and copyright information.

6.10. REFERENCES

1. Khovakh, M.: *Motor Vehicle Engines*, English Translation, Mir Publishers, Moscow, 1976.
2. Witte, T., and Wright, K.: "Chrysler 3.5 Liter V-6 Engine", SAE paper 930875, SAE, 1993.
3. Bosch, R.: *Automotive Handbook*, 8th edition, Robert Bosch GmbH, SAE, 2011.
4. Takizawa, M., Uno, T., Oue, T., and Yura, T.: "A Study of Gas Exchange Process Simulation of an Automotive Multi-Cylinder Internal Combustion Engine," SAE paper 820410, *SAE Trans.*, vol. 91, 1982.
5. Kay, I. W.: "Manifold Fuel Film Effects in an SI Engine," SAE paper 780944, 1978.
6. Amann, C.A.: "The Automotive Engine—A Future Perspective," SAE paper 891666, 1989.
7. Benson, R. S., and Whitehouse, N. D.: *Internal Combustion Engines*, vol. 2, Pergamon Press, Oxford, 1979.
8. Patton, K. J.: "Development and Evaluation of a Performance and Efficiency Model for Spark-Ignition Engines," M.S. Thesis, Mechanical Engineering Dept., MIT, Cambridge, MA, 1989.
9. Barnes-Moss, H. W.: "A Designers Viewpoint," in *Passenger Car Engines, Conference Proceedings*, pp. 133–147, Institution of Mechanical Engineers, London, 1975.
10. SAE Recommended Practice: "Engine Terminology and Nomenclature—General," in *SAE Handbook*, J604d.
11. Asmus, T. W.: "Valve Events and Engine Operation," SAE paper 820749,*SAE Trans.*, vol. 91, 1982.
12. Kastner, L. J., Williams, T. J., and White, J. B.: "Poppet Inlet Valve Characteristics and Their Influence on the Induction Process," *Proc. Instn. Mech. Engrs.*, vol. 178, pt. 1, no. 36, pp. 955–978, 1963–1964.
13. Taylor, C. F.: *The Internal-Combustion Engine in Theory and Practice*, vol. 1, 2nd edition, revised, MIT Press, Cambridge, MA, 1985.
14. Woods, W. A., and Khan, S. R.: "An Experimental Study of Flow through Poppet Valves,"*Proc. Instn. Mech. Engrs.*, vol. 180, pt. 3N, pp. 32–41, 1965–1966.
15. Annand, W. J. D., and Roe, G. E.: *Gas Flow in the Internal Combustion Engine*, Haessner Publishing, Newfoundland, NJ, 1974.
16. Bicen, A. F., and Whitelaw, J. H.: "Steady and Unsteady Air Flow through an Intake Valve of a Reciprocating Engine," in *Flows in Internal Combustion Engines—II*, FED-vol. 20, Winter Annual Meeting, ASME, New York, 1984.
17. Fukutani, I., and Watanabe, E.: "An Analysis of the Volumetric Efficiency Characteristics of 4-Stroke Cycle Engines Using the Mean Inlet Mach Number Mim," SAE paper 790484, *SAE Trans.*, vol. 88, 1979.
18. Wallace, W. B.: "High-Output Medium-Speed Diesel Engine Air and Exhaust System Flow Losses,"*Proc. Instn. Mech. Engrs.*, vol. 182, pt. 3D, pp. 134–144, 1967–1968.
19. Cole, B. N., and Mills, B.: "The Theory of Sudden Enlargements Applied to Poppet Exhaust-Valve, with Special Reference to Exhaust-Pulse Scavenging," *Proc. Instn. Mech. Engrs.*, pt. IB, pp. 364378, 1953.
20. Leone, T. G., and Pozar, M.: "Fuel Economy Benefit of Cylinder Deactivation-Sensitivity to Vehicle Application and Operating Constraints," SAE paper 2001-01-3591, 2001.
21. Moriya, Y., Watanabe, A., Uda, H., Kawamura, H., Yoshioka, M., and Adachi, M.: "A Newly Developed Intelligent Variable Valve Timing System-Continuously Controlled Cam Phasing as Applied to a New 3-Liter Inline 6 Engine," SAE paper 960579, 1996.
22. Lutlermann, C., Schünemann, E., and Klauer, N.: "Enhanced VALVETRONIC Technology for Meeting SULEV Emission

© McGraw-Hill Education. All rights reserved. Any use is subject to the Terms of Use, Privacy Notice and copyright information.

Requirements," SAE Technical Paper 2006-01-0849, SAE, 2006.

23. Nagumo, S., and Hara, S.: "Study of Fuel Economy Improvement through Control of Intake Valve Closing Timing: Cause of Combustion Deterioration and Improvements," *JSAE Review*, vol. 16, pp. 13–19, 1995.
24. Chao, H., Lee, K., Lee, J., Yoo, J., and Min, K.: "Measurements and Modeling of Residual Gas Fraction in SI Engines," SAE paper 2001-01-1910, 2001.
25. Toda, T., Nohira, H., and Kobashi, K.: "Evaluation of Burned Gas Ratio (BGR) as a Predominant Factor to NO_x," SAE paper 760765, *SAE Trans.*, vol. 85, 1976.
26. Tabaczynski, R. J., Heywood, J. B., and Keck, J. C: "Time-Resolved Measurements of Hydrocarbon Mass Flow Rate in the Exhaust of a Spark-Ignition Engine," SAE paper 720112, *SAE Trans.*, vol. 81, 1972.
27. Caton, J. A., and Heywood, J. B.: "An Experimental and Analytical Study of Heat Transfer in an Engine Exhaust Port,"*Int. J. Heat. Mass. Transfer.*, vol. 24, no. 4, pp. 581–595, 1981.
28. Caton, J. A.: "Comparisons of Thermocouple, Time-Averaged and Mass-Averaged Exhaust Gas Temperatures for a Spark-Ignited Engine," SAE paper 820050, 1982.
29. Majewski, W. A., and Khair, M. K.: *Diesel Emissions and Their Control*, SAE International, 2006.
30. Blair, G. P.: *The Basic Design of Two-Stroke Engines*, SAE, Warrendale, PA, 1990.
31. Heywood, J. B., and Sher, E.: *The Two-Stroke Cycle Engine: Its Development, Operation, and Design*, Taylor & Francis, Philadelphia, SAE, Warrendale, PA, 1999.
32. Dedeoglu, N.: "Scavenging Model Solves Problems in Gas Burning Engine," SAE paper 710579,*SAE Trans.*, vol. 80, 1971.
33. Benson, R.S.: "A New Gas Dynamic Model for the Gas Exchange Process in Two-Stroke Loop and Cross Scavenged Engines," *Int. J. Mech. Sci.*, vol. 19, pp. 693–711, 1977.
34. Jante, A.: "Scavenging and Other Problems of Two-Stroke Cycle Spark-Ignition Engines," SAE paper 680468,*SAE Trans.*, vol. 77, 1968.
35. Gyssler, G.: "Problems Associated with Turbocharging Large Two-Stroke Diesel Engines,"*Proc. CIMAC*, paper B.16, 1965.
36. Annand, W. J. D.: "Compressible Flow through Square-Edged Orifices: An Empirical Approximation for Computer Calculations," *J. Mech. Engng Sci.*, vol. 8, p. 448, 1966.
37. Benson, R. S.: "Experiments on a Piston Controlled Port," *The Engineer*, vol. 210, pp. 875–880, 1960.
38. Watson, N., and Janota, M. S.: *Turbocharging the Internal Combustion Engine*, Wiley-Interscience Publications, John Wiley, New York, 1982.
39. Blunder, F. S.: "Supercharging Compressors—Problems and Potential of the Various Alternatives," SAE paper 840243, 1984.
40. Bhinder, F. S.: "Some Fundamental Considerations Concerning the Pressure Charging of Small Diesel Engines," SAE paper 830145, 1983.
41. Haddad, S. D., and Watson, N.: *Principles and Performance in Diesel Engineering*, Ellis Horwood Ltd., 1984.
42. Hiereth, H., and Prenninger, P.: *Charging the Internal Combustion Engine*, Springer-Verlag, Wien, New York, 2003.
43. Kawamoto, A., Takahashi, Y., Koiken, T., and Nakamura, F.: "Variable Geometry System Turbocharger for Passenger Car Diesel Engine," SAE paper 2001-01-0273, 2001.
44. Gyarmathy, G.: "How Does the Comprex Pressure-Wave Supercharger Work?" SAE paper 830234, 1983.
45. Kollbrunner, T. A.: "Comprex Supercharging for Passenger Diesel Car Engines," SAE paper 800884, *SAE Trans.*, vol. 89, 1980.

© McGraw-Hill Education. All rights reserved. Any use is subject to the Terms of Use, Privacy Notice and copyright information.

7.0. CHAPTER PRELIMINARIES

SPARK-IGNITION ENGINE MIXTURE REQUIREMENTS

FUEL METERING OVERVIEW

CENTRAL (THROTTLE-BODY) FUEL INJECTION

PORT (MULTIPOINT) FUEL INJECTION

AIR FLOW PHENOMENA

FUEL FLOW PHENOMENA: PORT FUEL INJECTION

DIRECT FUEL INJECTION

EXHAUST GAS OXYGEN SENSORS

FUEL SUPPLY SYSTEMS

LIQUID PETROLEUM GAS AND NATURAL GAS

PROBLEMS

REFERENCES

© McGraw-Hill Education. All rights reserved. Any use is subject to the Terms of Use, Privacy Notice and copyright information.

7.1. SPARK-IGNITION ENGINE MIXTURE REQUIREMENTS

Spark-ignition engines operate by burning a premixed mixture of fuel vapor and air. The task of the engine induction and fuel systems is to prepare such a mixture inside the cylinder from ambient air, and fuel in the tank, that satisfies the requirements of the engine over its entire operating regime. In principle, the optimum fuel-air mixture ratio for a spark-ignition engine is that which gives the required power output with the lowest fuel consumption, consistent with smooth and reliable operation. In practice, the constraints of emissions control may dictate a different mixture composition from this ideal, and may also require a fraction of the exhaust gases to be recycled (EGR—exhaust gas recirculation) into the intake system. The relative proportions of fuel and air that provide the lowest fuel consumption, smooth reliable operation, and satisfy the emissions requirements, at the required power level, depend on engine speed and load. Mixture requirements and preparation are usually discussed in terms of the air/fuel ratio or fuel/air ratio (see Sec. 2.9) and percent EGR [see Eq. (4.2)]. While the fuel metering system is designed to provide the appropriate fuel flow for the *actual* air flow at each speed and load, the relative proportions of fuel and air can be stated more generally in terms of the relative air/fuel ratio λ, or the fuel/air equivalence ratio ϕ, which are the actual air/fuel ratio, or fuel/air ratio, normalized by dividing by the stoichiometric air/fuel or fuel/air ratio [Eqs. (3.8) and (3.9)]. The combustion characteristics of fuel-air mixtures and the properties of combustion products, which govern engine performance, efficiency, and emissions, correlate best for a wide range of fuels relative to the stoichiometric mixture proportions. Therefore, where appropriate, the relative air/fuel ratio, or the fuel/air equivalence ratio will be used as the defining parameter. A typical value for the stoichiometric air/fuel ratio of gasoline is 14.6.[1] Thus, for gasoline,

$$\lambda \approx \frac{(A/F)}{14.6}; \quad \phi \approx \frac{14.6}{(A/F)}$$

(7.1*a*, *b*)

Note that other fuels such as ethyl alcohol, (often blended with gasoline), liquid petroleum gas (LPG), natural gas (NG), and hydrogen are used in spark-ignition engines. Each of these has a different stoichiometric air/fuel ratio. However, their relative air/fuel ratio (or fuel/air equivalence ratio) is still the appropriate mixture composition correlating parameter.

This chapter is about mixture preparation in spark-ignition engines. There is no equivalent chapter on mixture preparation in diesels; that important topic is discussed in Chap. 10 as part of diesel or compression-ignition engine combustion. The reason for the different treatment of this topic for these two types of engines is that, in spark-ignition engines, the fuel-air mixture preparation and the combustion process are largely separable: the first process is normally completed before the second process occurs. In the diesel engine, the preparation of the combustible fuel-air mixture starts when fuel injection is initiated. Combustion then begins, spontaneously, shortly thereafter: the two processes overlap and are, therefore, intimately linked.

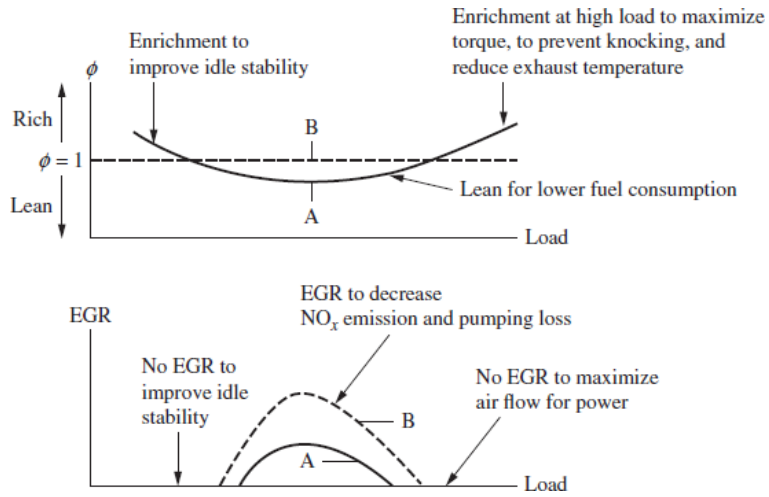
The effects of relative air/fuel ratio or equivalence ratio variations on spark-ignition engine combustion, emissions, and performance are discussed more fully in Chaps. 9, 11, and 15. A brief summary is sufficient here. Mixture requirements are different for full-load (wide-open-throttle, WOT) and for part-load operation. At the former operating condition, full utilization of the *inducted air* to obtain maximum power for a given displaced volume is the critical issue. Where less than the maximum power at a given speed is required, efficient utilization of the *fuel* is the critical issue. At WOT, maximum power for a given volumetric efficiency is obtained with rich-of-stoichiometric mixtures, $\lambda \approx 0.9, \phi \approx 1.1$ (see the discussion of the fuel-air cycle results in Sec. 5.5.3). Mixtures that are richer still are at times used to increase volumetric efficiency by increasing the amount of charge cooling that accompanies fuel vaporization [see Eq. (6.5)], reduces the potential for knock, and holds down exhaust gas temperatures.

© McGraw-Hill Education. All rights reserved. Any use is subject to the Terms of Use, Privacy Notice and copyright information.

At part-load (or part-throttle) operating conditions, there are advantages to diluting the fuel-air mixture, either with excess air or with recycled exhaust gas. This dilution improves the engine's fuel conversion efficiency for three reasons: (1) the expansion stroke work for a given expansion ratio is increased as a result of the change in thermodynamic properties of the burned gases—see Secs. 5.5.3 and 5.7.4; (2) for a given mean effective pressure, the intake pressure increases with increasing dilution, so pumping work decreases—see Fig. 5.10; (3) the heat losses to the walls are reduced because the burned gas temperatures are lower. In the absence of strict engine NO_x emission requirements, excess air is the obvious diluent and at part throttle, engines have historically often operated lean. When tight control of NO_x, HC, and CO emissions is required, operation of the engine with a stoichiometric mixture is advantageous so that a three-way catalyst[2] can be used to clean up the exhaust. The appropriate diluent is then recycled exhaust gases which significantly reduce NO_x emissions from the engine itself. The amount of diluent that the engine will tolerate at any given speed and load depends on the details of the engine's combustion process. Increasing excess air or the amount of recycled exhaust slows down the combustion process and increases its variability from cycle to cycle. A certain minimum combustion repeatability or stability level is required to maintain smooth engine operation. Deterioration in combustion stability therefore limits the amount of dilution an engine can tolerate. As load decreases, less dilution of the *fresh* mixture can be tolerated because the internal dilution of the mixture with residual gas increases (see Sec. 6.4). At idle conditions, the fresh mixture will not usually tolerate any EGR and may need to be stoichiometric or even fuel-rich to obtain adequate combustion stability.

Mixture composition requirements over the engine's load range are illustrated schematically for the two approaches outlined above in Fig. 7.1. If full load torque is to be maximized, and part-load fuel consumption is to be minimized, then ϕ can be varied over the load range as shown. Lower levels of EGR could then be used with a lean NO_x catalyst or trap to realize low NO_x exhaust emissions. If emissions reduction requirements are more demanding and the very efficient three-way catalyst technology is needed, then the engine must be operated with a stoichiometric mixture, and larger percentages of EGR over the low to mid-low range can be tolerated. When EGR is used, the percentage of recycled exhaust increases from zero at light load to a maximum at mid-load, and then decreases to zero as WOT conditions are approached so air is no longer displaced and maximum bmep can be obtained. Combinations of these strategies are possible.

Figure 7.1 Typical mixture requirements for two operating strategies. Top diagram shows the relative air/fuel ratio variation as a function of load. Lower diagram shows recycled exhaust (EGR) schedule. The two strategies are: A, optimized for maximum torque, part-load efficiency, and idle stability; B, optimized for emissions reduction—stoichiometric operation.



In practical spark-ignition engine induction systems, the fuel and air distribution between engine cylinders is not necessarily uniform (and also can vary in each individual cylinder on a cycle-by-cycle basis). The spread in air/fuel ratios between the

© McGraw-Hill Education. All rights reserved. Any use is subject to the Terms of Use, Privacy Notice and copyright information.

leanest and richest cylinders (and in EGR levels), over the engine's load and speed range, is now carefully controlled to optimize emissions control in the engine's catalyst system, and avoid excessive combustion variability in the leanest operating cylinder.

Table 7.1 shows the relative amounts (mass percent) of the components air, fuel, residual burned gas, and EGR in the in-cylinder unburned mixture in a gasoline-fueled spark-ignition engine. These proportions, shown at idle, a typical part-load, and at full load, at low-to-mid engine speed, define the *mixture* we will be discussing in this chapter. The definitions of residual fraction and EGR percentage are given by Eqs. (4.1) and (4.3), respectively. A stoichiometric fuel/air ratio was used for idle and part-load: at WOT a 20% fuel rich mixture was assumed. At the one-quarter load condition 10% EGR was assumed: at mid loads EGR might increase to 15%. The residual (burned gas) fraction is high (some 25%) at idle, and decreases to a low value (about 5%) at WOT for a naturally-aspirated gasoline engine. In a turbocharged spark-ignition engine, the residual gas amounts at part-load and WOT would be about one-third lower because at the same torque levels (with a downsized turbocharged engine) the bmep levels would be higher.

Table 7.1 Percentage by mass of in-cylinder unburned mixture components: air, fuel, residual, EGR*

In-cylinder mixture component	Idle Mass %	Part (one-quarter) load Mass %	Full load (WOT) Mass %
Air	70	76.3	88
Gasoline fuel	5	5.2	7.2
Residual gas†	25	9.2	5.0
EGR	0	9.2	0
Total	100	100	100
*Naturally-aspirated gasoline SI engine.			
†In a turbocharged engine, the residual gas amounts at the part-load and full-load conditions will be about half these values.			

Adjustments to these numbers for different fuels and EGR levels can readily be made using the appropriate equations: Sec. 3.4 and Eqs. (4.1) and (4.3). For example, with ethanol, the stoichiometric fuel/air ratio increases from 0.0655 to 0.111: App. D, Table D.4.

[1] Typical value only. Most gasolines have $(A/F)_s$, in the range of 14.4 to 14.7. $(A/F)_s$ could lie between 14.1 and 15.2.

[2] A three-way catalyst system, when operated with a close-to-stoichiometric mixture, achieves substantial reductions in NO_x, CO, and HC emissions simultaneously; see Sec. 11.6.2.

© McGraw-Hill Education. All rights reserved. Any use is subject to the Terms of Use, Privacy Notice and copyright information.

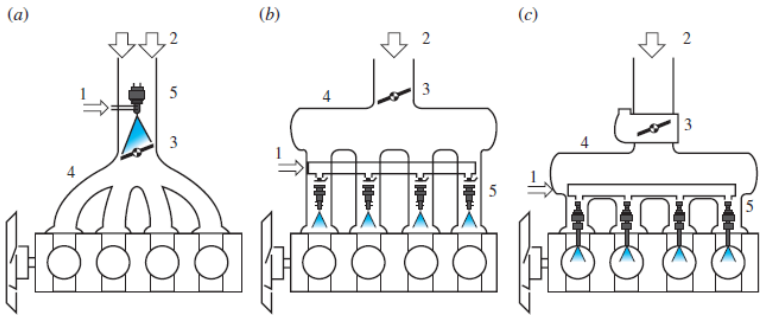
7.2. FUEL METERING OVERVIEW

7.2.1. Mixture Formation Approaches

Historically, carburetors were used to control the fuel flow into spark-ignition engine intake manifolds and distribute the fuel across the air stream. In a carburetor, the airflow through a converging-diverging nozzle sets up a pressure difference between the carburetor inlet and the throat of the nozzle which depends on the airflow rate. This pressure difference is used to meter the appropriate fuel flow for that airflow. The fuel entered the air stream through the carburetor body, was atomized, and then convected by the air stream past the throttle plate and into the intake manifold. While carburetors developed into complex devices, eventually the more precise fuel-metering requirements for attaining low emissions levels forced their replacement by electronically controlled fuel-injection systems where an electromagnetic fuel injector injects fuel intermittently into the intake manifold or ports.[1]

Several different fuel-injection concepts have been developed and used, starting in about 1980. These are illustrated in Fig. 7.2. The first of these, single-point fuel injection (or central, or throttle-body, fuel injection), is shown in Fig. 7.2*a*. The fuel is injected upstream of the throttle body, usually with one injector per engine for in-line engines or one per throttle body with V engines. The injector is pulsed (opened) intermittently, synchronized with the operation of each cylinder (usually with ignition system triggering). This approach is the simplest and cheapest of the three shown. Its major disadvantage is that the point of injection is well away from the engine, which, due to the much more extensive fuel wall wetting that occurs, makes precise control of fuel behavior during engine transients more difficult.

Figure 7.2 Schematics of different fuel-injection system arrangements: (a) single point, (b) multipoint (port), and (c) direct in-cylinder injection (DI). (1) Fuel; (2) Air; (3) Throttle; (4) Intake manifold; (5) Fuel injector.[2] *(Courtesy Robert Bosch GmbH and SAE.)*



Multipoint fuel injection, shown in Fig. 7.2*b*, has been the dominant approach for the past two decades. Here one injector per cylinder is used, positioned close to the intake manifold intake-port interface, to direct an intermittent fuel spray toward the intake valve. Usually each injector delivers one injection pulse per cylinder per cycle, phased sequentially with each cylinder's gas exchange process. The advantage of the multipoint injection approach is its short distance between point of injection and intake valve, and that the fuel spray can be directed largely toward the hot surface of the valve head. This allows for more precise control of the fuel's metering.

The third approach in Fig. 7.2*c* is injection of fuel directly into each cylinder of the engine. Gasoline direct-injection (GDI) is being used in automobile SI engines in significant volumes. With GDI, only air (or air with EGR) is inducted into the cylinder. During intake (and/or the compression process) the fuel is injected using an injector located in the cylinder head into the in-cylinder air (and residual gas), to form a well-mixed fuel vapor, air, residual gas (and EGR, if used) mixture. There are two modes of operation. With fuel injection during the intake stroke, an essentially *homogeneous* fuel-air mixture is produced before combustion is initiated. With fuel injection during compression, a stratified in-cylinder fuel-air mixture can be produced,

© McGraw-Hill Education. All rights reserved. Any use is subject to the Terms of Use, Privacy Notice and copyright information.

with only part of the air being mixed with the fuel vapor. This *stratified* operation (at part-load) is designed to create a close-to-stoichiometric readily combustible fuel-vapor air "mixture cloud" in contact with the spark plug, the excess air surrounds this "cloud" so that the engine operates fuel lean overall which (like the diesel) results in more efficient engine operation. Stratified direct-injection operation at part-load is usually combined with homogeneous DI operation at higher and full-load. The advantages of direct fuel injection are its inherently faster mixture-preparation control during engine transients (because the fuel is injected right into the cylinder where it will be burned), and the part-load engine efficiency benefits from lean operation when stratified. The primary disadvantage is high fuel-injection system cost.

These three approaches to fuel metering with solenoid actuated fuel injectors will be discussed in more detail in the following sections, 7.3 and 7.4.

7.2.2. Relevant Characteristics of Fuels

Fuels requirements for internal combustion engines are especially demanding because the engine combustion process is integrated into the power-generating operating cycle. The fuel's characteristics impact the engine's combustion and emissions formation processes, the onset of any abnormal combustion phenomenon such as knock, and especially mixture preparation—the topic of this chapter. Successful mixture preparation requires much more than achieving fast-enough stable combustion under warmed-up engine conditions over the full engine load and speed map. It requires satisfactory engine starting under cold and hot engine conditions. It requires maintaining good combustion and effective emissions control during all engine transients (e.g., during engine warm-up, and vehicle accelerations and decelerations). It requires minimizing the constraint that knocks onset places on engine torque and efficiency. It must also enable meeting regulatory emissions control constraints.

With conventional spark-ignition engine liquid-fuel metering systems, the fuel enters the air stream as a liquid jet. The jet atomizes into droplets that move through the air and start to vaporize. With manifold or port fuel injection, a major fraction of these droplets deposit on the walls of the intake system components. Vaporization of the liquid fuel on these walls then occurs. The flow of liquid fuel along the walls can also be significant. The transport of fuel as vapor, droplets, and liquid streams or films into the cylinder can all be important.

For direct fuel-injection approaches, these fuel spray phenomena occur inside the engine's cylinders, where the surrounding gas is air mixed with the burned residual gases. This in-cylinder charge is thus warmer than the intake air temperature so fuel vaporization occurs at a faster rate, and the wetting of the combustion chamber walls by the spray droplets is thereby reduced. Note also that evaporation of fuel drops through heat transfer with the in-cylinder charge cools the charge and drops its temperature. Evaporation of liquid fuel off the intake port and valve surfaces mostly cools the walls, and not the airflow. This evaporative cooling of the charge with direct-injection has a significant effect on the subsequent temperatures of the unburned mixture as it is compressed: much more so for the alcohols (e.g., E85) than for gasoline due to their higher heat of vaporization per unit chemical energy than gasoline.

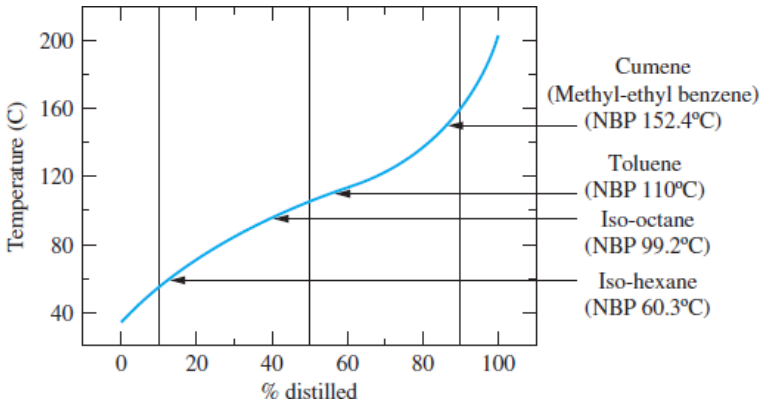
The predominant fuel for spark-ignition engines is gasoline (petrol) refined from petroleum (seeSec. 1.11.1). Another liquid fuel in common use is ethanol (ethyl alcohol), either blended with gasoline (e.g., E10, a 10% blend) or as a stand-alone fuel (usually as E85, 85% ethanol and 15% gasoline, by volume). Other fuels in use are LPG, which is a mixture of propane (C_3H_8) and butane (C_4H_{10}), and natural gas, which is predominantly methane (CH_4). LPG is stored in pressurized tanks as a liquid at ambient temperatures and about 500 kPa (80 psia): it vaporizes in the intake system of spark-ignition engines and enters the cylinder as a gas, mixed with air. Natural gas on vehicles is usually stored as compressed gas in high-pressure tanks at up to 7 Mbar (10,000 psi). It can, with difficulty, be stored cryogenically. Storage of NG on the vehicle is expensive and significantly raises the cost of this fuel option. Natural gas is used in large stationary engines to generate power (e.g., for pumping the gas through pipelines). Other spark-ignition engine fuels are the gasoline-equivalent liquid hydrocarbon blends made from oil sands and heavy oils. Also, two synthetic fuels—hydrogen and methanol could be used in SI engines.

The *volatility* of a liquid fuel—its potential for vaporizing at a given temperature and pressure—is the key mixture preparation

© McGraw-Hill Education. All rights reserved. Any use is subject to the Terms of Use, Privacy Notice and copyright information.

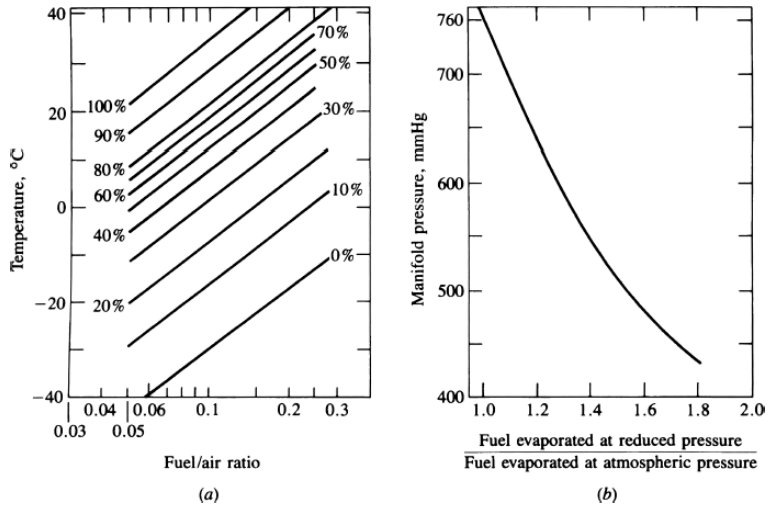
characteristic. Gasoline (petrol), the standard SI engine fuel, is a mixture of a large number of individual hydrocarbons: it thus has a boiling temperature range rather than a single boiling point. Typically, this range is 30 to 200°C. Individual hydrocarbons have the saturation pressure-temperature relationships of a pure substance. The lower the molecular weight, the higher will be the saturated vapor pressure at a given temperature. The boiling point of hydrocarbons depends primarily on their molecular weight: the vapor pressure also depends on molecular structure. The equilibrium state of a hydrocarbon-air mixture depends therefore on the vapor pressure of the hydrocarbon at the given temperature, the relative amounts of the hydrocarbon and air, and the total pressure of the mixture. The equilibrium fraction of fuel evaporated at a given temperature and pressure can be calculated from Bridgeman charts[3] and the distillation characteristics of the fuel (defined by the ASTM distillation curve[4]). The (equilibrium) distillation curve of a standard test gasoline (UTG91) is shown in Fig. 7.3. This U.S. regular (91 RON) gasoline, *at atmospheric pressure*, has a boiling point range of about 30 to 200°C. The boiling points of several gasoline components are shown. Note that these temperatures do not denote the engine air (or wall surface) temperatures required to vaporize the fuel components: the fuel vapor pressure in the engine mixture is well below 1 bar. For a stoichiometric gasoline vapor-air mixture at 1 bar, the fuel vapor partial pressure is about 0.02 bar. Thus the fuel components vaporize at much lower temperatures than the atmospheric pressure distillation curve in Fig. 7.3 indicates. Figure 7.4*a* shows the percentage of a standard gasoline (indolene) evaporated at equilibrium at 1 bar *mixture* pressure as a function of fuel/air ratio: the stoichiometric gasoline fuel/air ratio is 0.0685. Figure 7.4*b* shows the effect of reducing the intake manifold pressure below 1 bar (760 mmHg) on the amount of indolene fuel evaporated. While insufficient time is usually available in the manifold to establish equilibrium, the trends shown are indicative of what happens in practice: lower pressures increase the relative amount of fuel vaporized significantly.

Figure 7.3 Evaporative characteristics of a standard (UTG91) gasoline: equilibrium distillation curve, at atmospheric pressure (ASTM D86).[5] NBP, normal boiling point. T_{10}, T_{50}, T_{90} distillation points are used to calculate the Drivability Index of the fuel; see Eq. (7.2).



© McGraw-Hill Education. All rights reserved. Any use is subject to the Terms of Use, Privacy Notice and copyright information.

Figure 7.4 (a) Percentage of indolene fuel evaporated at equilibrium at 1 atmosphere pressure. (b) Effect of pressure on amount of indolene fuel evaporated.[6]



Under warmed-up engine conditions, the vaporization of gasoline fuel is not a significant issue. Under cold-starting conditions, with stringent hydrocarbon emissions requirements, achieving a rapid engine start-up with stable combustion is more challenging: use of fuel-rich vaporized fuel-air mixtures which burn faster significantly increases engine HC emissions.

Additional tests and parameters are used to define a fuel's volatility: (gasoline, or blends with ethanol).

The *Reid vapor pressure* (RVP) test is used to determine the vapor pressure of gasolines and other refinery products having a vapor pressure below atmospheric. The test apparatus has two chambers. One is filled with a liquid fuel sample at 0 to 4°C (32 to 40°F); the other, four times the size of the liquid-containing volume and fitted with a pressure gauge, filled with atmospheric air, is rapidly connected to the fuel chamber. The assembly is then immersed in an electrically heated water bath at 37.8°C (100°F). After 5 minutes, the assembly is shaken and the pressure gauge is read. The immersion is repeated for another 2 minutes; the assembly is removed, shaken again, and the pressure read again. The procedure is repeated until two successive readings within 0.35 kPa (0.05 psi) are recorded. Typical Reid vapor pressures for gasolines are about 0.5 bar (7 psi).

The RVP of a fuel (with higher RVP corresponding to a more volatile fuel) is a measure of how quickly and smoothly a cold engine will start and warm up. Also, air pollution regulatory agencies use RVP to limit gasoline vapor pressure to control the fuel system evaporative emissions of smog forming hydrocarbons.

A *Drivability Index* (DI) is used (in the United States) to characterize the impact of a gasoline's volatility on SI engine in-vehicle drivability. Such drivability aspects are ease of engine starting, warm-up driving and acceleration transients; and with respect to vehicle driving, smoothness, hesitations, and surges. The DI is defined from the fuel's distillation curve, Fig. 7.3, using the T_{10}, T_{50}, and T_{90} temperatures; the temperature for a specific fuel at which 10, 50, and 90% of the fuel is vaporized, respectively. The formula for DI is:

$$\mathrm{DI} = 1.5\,T_{10} + 3\,T_{50} + T_{90}$$

(7.2)

with the temperatures in °F. T_{10} describes a fuel's ability to vaporize quickly and enable cold starting. T_{90} is a measure of the high boiling point gasoline components which impact fuel economy—the higher molecular weight hydrocarbons have a higher heating value. T_{50} defines the fuel's average behavior. The DI of a typical gasoline is between 1100 and 1175. It varies seasonally to a maximum of some 1250 in areas with hot summers. Blending modest amounts (≤10%) of ethanol with gasoline requires raising DI values to about 1300.

© McGraw-Hill Education. All rights reserved. Any use is subject to the Terms of Use, Privacy Notice and copyright information.

The composition of the fuel-vapor air mixture in spark-ignition engines operating with a homogeneous charge is constrained by several requirements: fast enough combustion (over the full operating map), emissions control constraints, complete air (oxygen) utilization at full load, and high engine efficiency. For homogeneous charge operation, a stoichiometric mixture satisfies these requirements effectively: a choice reinforced by the widely used three-way catalyst technology, which needs a stoichiometric composition exhaust gas stream to achieve its high effectiveness. (Note that even in stratified direct-fuel-injection SI engines, combustion of the fuel-air mixture locally, at close-to-stoichiometric composition, is preferred.)

The stoichiometric mixture air/fuel ratio depends on the molecular composition of the fuel, as discussed in Sec. 3.4. Here we focus on gasolines, ethanol, and blends of ethanol with gasoline, the most commonly used SI engine fuels. For stoichiometric operation, the amount of air required per unit injected fuel is given by the $(A/F)_s$: one can also work with its inverse, $(F/A)_s$. Figure 7.5 shows the stoichiometric (A/F) and (F/A) as a function of the hydrocarbon's molar H:C ratio. The average value for gasoline is close to 14.6, or 0.0685 for $(F/A)_s$. The approximate range in H:C ratio is indicated. These numbers are for hydrocarbons containing carbon and hydrogen only, for both individual compounds and blends or mixtures.

Figure 7.5 Stoichiometric air/fuel ratio for air-hydrocarbon fuel mixtures as a function of the fuel's molar H/C ratio.

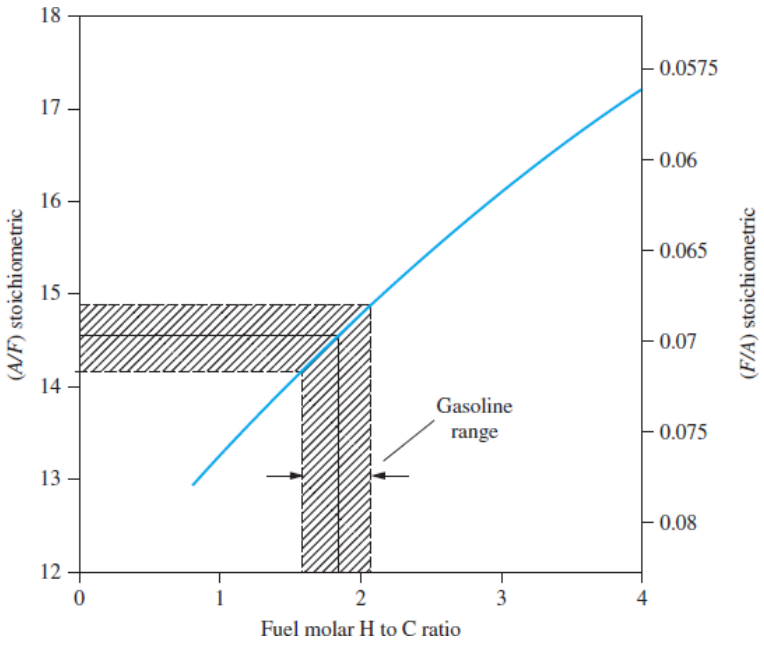
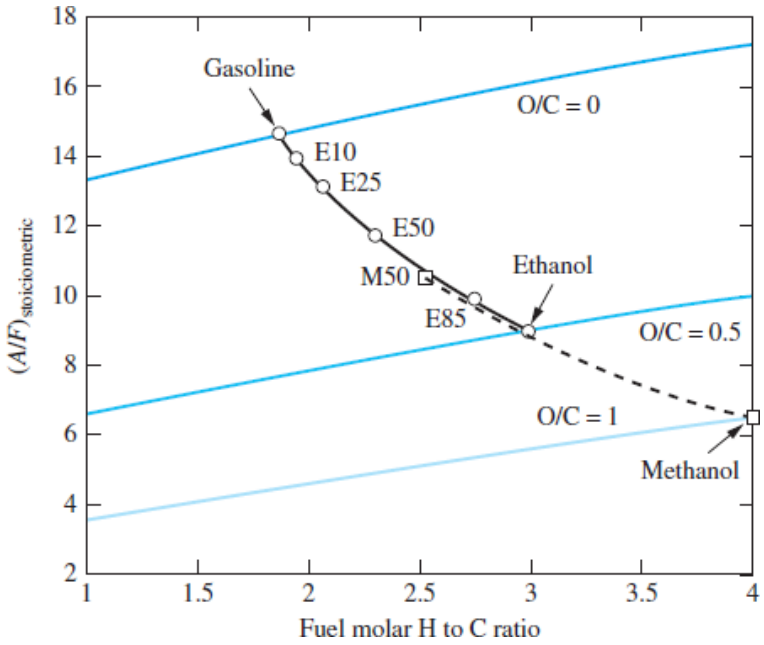


Figure 7.6 shows these stoichiometric ratios for gasoline-ethanol mixtures (also for methanol). Note that the addition of oxygen to the carbon and hydrocarbon combustibles changes the mass of fuel relative to the mass of air in a stoichiometric mixture significantly. The molar proportion of oxygen in methanol is a factor of 2 higher than in ethanol. The curves for methanol blends with gasoline closely parallel those for the ethanol blends, and are displaced downward.

© McGraw-Hill Education. All rights reserved. Any use is subject to the Terms of Use, Privacy Notice and copyright information.

Figure 7.6 Stoichiometric air/fuel ratio of mixtures of air with hydrocarbon-alcohol fuel blends, as a function of fuel's molar H/C ratio and O/C ratio. (E10 means a blend of 10% ethanol with 90% gasoline, by volume.)



Note that for these significant changes in the stoichiometric mass of fuel per unit mass of air, the torque (and bmep) of a given engine at a given intake manifold pressure changes little. This is because an internal combustion engine is a device with given size cylinders, and the chemical energy content of a stoichiometric fuel-air mixture, per unit mass or per unit volume of mixture, is almost independent of the fuel composition: see the lower heating values of such stoichiometric fuel-air mixtures (in MJ/kg) in Table D.4, App. D. When expressed per unit volume of stoichiometric mixture, the hydrogen-air mixture value lines up more closely than the MJ/kg value. The amount of oxygen available in the air for carbon and hydrogen oxidation is the key factor in this common value of mixture chemical energy density.

Natural gas and LPG are also used as spark-ignition engine fuels. They, of course, are gases at ambient pressure and temperature. Their composition varies depending on the source of these fuels and their processing. This variation in molecular (and thus elemental) composition affects the fuel's stoichiometric air-fuel ratio and heating value, modestly. With NG the antiknock octane rating can be affected more significantly. Also, with NG, the presence of small (and varying) percentages of nitrogen and carbon dioxide dilute the fuel's hydrocarbons of which methane CH_4 dominates (see typical NG composition in Table D.4). Note that in close-to-stoichiometric fuel-vapor air mixtures, these smaller fuel molecules CH_4, C_3H_8, also ethanol C_2H_6O, and methanol CH_4O, displace a significant fraction of the air. The partial pressure of air in an atmosphere pressure natural-gas fuel-air mixture is some 10% lower than with gasoline (see Fig. 6.3).

Hydrogen has been explored as an SI engine fuel. Combustion of hydrogen produces no CO_2, a greenhouse gas. However, hydrogen is really an *energy carrier* rather than a fuel since it must be manufactured. The standard production process for hydrogen is steam reforming of NG (where the carbon is fully oxidized to CO_2 and removed, and the water decomposed in the process provides additional hydrogen). Flame propagation in premixed hydrogen-air mixtures is extremely rapid—much faster than in equivalent stoichiometry hydrocarbon-air mixtures. Thus hydrogen-fueled SI engines usually operate with well lean of stoichiometric mixtures, and are boosted to obtain acceptable bmep levels and burn rates.

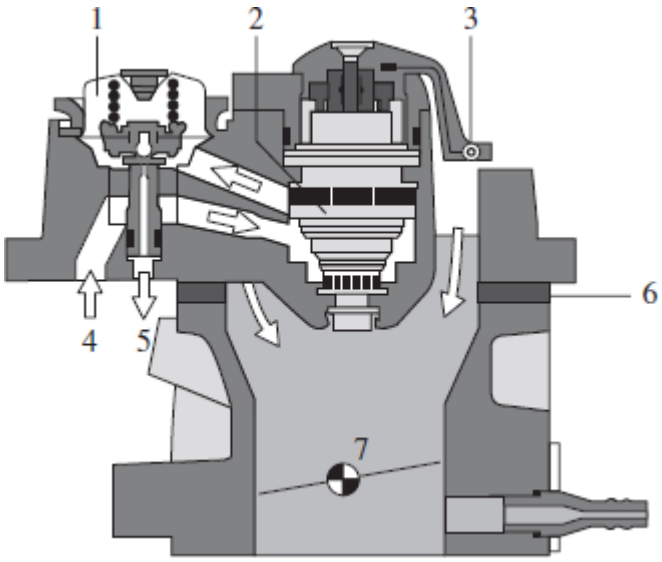
[1] A detailed discussion of carburetor operation can be found in the first edition of this text.[1]

© McGraw-Hill Education. All rights reserved. Any use is subject to the Terms of Use, Privacy Notice and copyright information.

7.3. CENTRAL (THROTTLE-BODY) FUEL INJECTION

Central or throttle-body fuel-injection systems, where one or two electronically controlled injectors meter the fuel into the airflow directly above the throttle body, can be used: see Fig. 7.2. They provide straightforward electronic control of fuel metering at lower cost than multipoint port injection systems. However, the problems associated with slower transport of fuel than the air from upstream of the throttle plate to the cylinder must now be overcome. Figure 7.7 shows a drawing of one such system: the Bosch Mono-Jetronic low-pressure single-point injection system for four-cylinder engines. An injector, placed above the throttle plate, meters the fuel in response to calibrations of airflow, measured or based on intake manifold pressure, air temperature, engine speed, and other signals. The fuel spray directs the fuel toward the crescent shaped opening between the throttle plate and its housing. The airflow provides effective atomization of the liquid fuel, minimizing liquid fuel deposition on the manifold walls. The high air velocity created by the pressure drop across the throttle opening shears and atomizes the liquid sheet on the throttle plate. Vigorous mixing of fuel and air then occurs, especially at part throttle, and provides good mixture uniformity and distribution between cylinders. Injector fuel delivery is synchronized with the ignition pulses. The injection duration is controlled with an exhaust gas oxygen sensor (see Sec. 7.8) to provide a stoichiometric mixture to each cylinder. The injection duration is extended to provide additional fuel during cold starts and engine warm-up, and provide injection enrichment during accelerations. The throttle valve potentiometer recognizes changes in throttle valve position. During accelerations, additional fuel beyond the steady-state requirement is injected to offset delays in fuel reaching each open intake valve to maintain the desired in-cylinder stoichiometry. As WOT is approached, mixture enrichment can be provided to control knock and maximize torque. The injector operates with a fuel supply pressure of about 2 bar (absolute).[2]

Figure 7.7 Schematic of central fuel injection system, upstream of the throttle: (1) Pressure regulator; (2) Injector; (3) Air temperature sensor; (4) Fuel inlet; (5) Fuel return; (6) Insulator plate; (7) Throttle. Bosch Mono-Jetronic unit (Courtesy Robert Bosch GmbH and SAE).[2]



© McGraw-Hill Education. All rights reserved. Any use is subject to the Terms of Use, Privacy Notice and copyright information.

7.4. PORT (MULTIPOINT) FUEL INJECTION

From about 1980, over a decade or so, a steady transition occurred from the use of carburetors to meter the gasoline flow in gasoline spark-ignition engines, to use of port fuel injection where the fuel is injected into the intake port of each engine cylinder. Such systems require one fuel injector per cylinder. While there are both mechanical and electromagnetically controlled injection systems, both are electronically controlled. The advantages of port fuel injection are increased power and torque through improved volumetric efficiency and more uniform fuel distribution, more rapid engine response to changes in throttle position, and more precise control of the in-cylinder air-fuel ratio. Electronically controlled fuel injection allows the amount of fuel injected per cycle for each cylinder to be varied in response to inputs derived from sensors, which define actual engine operating conditions. Two basic approaches have been developed; the major difference between the two is the method used to determine the airflow rate: direct measurement, or estimation based on air density and engine speed.

7.4.1. System Layout, Components, and Function

Figure 7.8 shows a schematic of a port-fuel-injection system where the airflow is measured. The electrically driven fuel pump delivers the fuel through a filter to the fuel line. A pressure regulator maintains the pressure in the line at a fixed value (e.g., 270 kN/m^2, 39 psi, usually relative to manifold pressure to maintain a constant fuel pressure drop across the injectors). Branch lines lead to each injector. Depending on the fuel supply approach (see Sec. 7.9) the excess fuel may be returned to the tank. The inducted air flows through the air filter, past the airflow meter, then the throttle to the intake manifold plenum volume. Separate runners (and branches) lead to each inlet port and engine cylinder. An electromagnetically actuated fuel-injection valve (see Fig. 7.9) is located either in the downstream end of each intake manifold runner or the entrance to the intake port. The major components of the injector are the valve housing, the injector needle and its pintle, the armature to which the needle is connected, the helical spring, and the solenoid coil. When the solenoid is not excited, the solenoid armature is forced, with its seal, against the valve seat by the helical spring and closes the fuel nozzle. When the solenoid coil is excited, the armature is attracted and lifts the needle about 0.15 mm so that fuel can flow through the calibrated annular passage around the valve stem. The front end of the injector needle is shaped as a pintle with a ground top to atomize the injected fuel. The relatively narrow spray cone of the injector minimizes the wetting of the intake port wall with liquid fuel. The mass of fuel injected per injection is controlled by varying the duration of the current pulse that excites the solenoid coil. In a 2-liter four-cylinder engine at typical part-load conditions, it is about 10 mg of fuel; at WOT it is about 40 mg. Typical injection times for automobile applications range from about 1.5 to 10 ms.[2] Many different designs of port fuel injectors are available ranging from single hole to two or more multi-hole nozzles. Spray targeting, an important injection system characteristic, is discussed below. Droplet sizes for port fuel injector sprays (with injection pressures of 3 to 7 bar) are in the 80 to 200 μm diameter range.

© McGraw-Hill Education. All rights reserved. Any use is subject to the Terms of Use, Privacy Notice and copyright information.

Figure 7.8 Multipoint port fuel-injection system: schematic of Bosch L-Jetronic System: (1) Fuel tank; (2) Electric fuel pump; (3) Fuel filter; (4) Electronic control unit; (5) Injector; (6) Fuel pressure regulator; (7) Intake manifold; (8) Electric cold-start valve; (9) Throttle valve switch; (10) Airflow sensor; (11) Exhaust oxygen sensor; (12) Thermal-time switch; (13) Engine-temperature sensor; (14) Ignition distributor; (15) Auxiliary-air valve; (16) Battery; (17) Ignition switch. (Courtesy: Robert Bosch GmbH and SAE.[2])

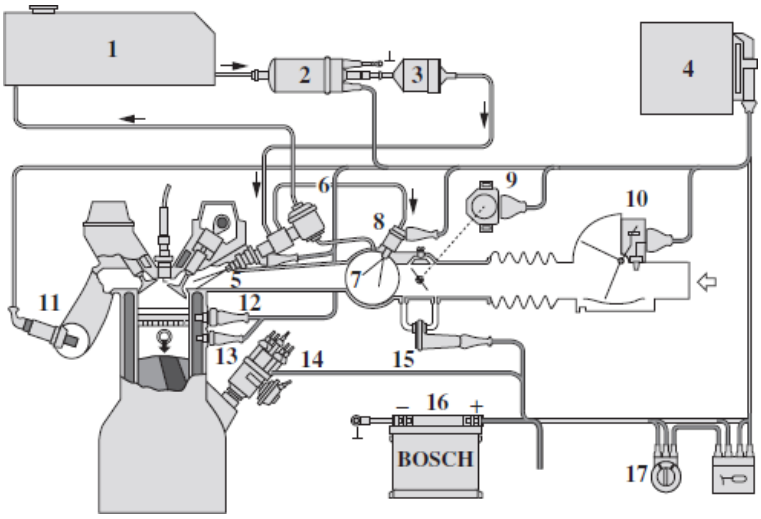
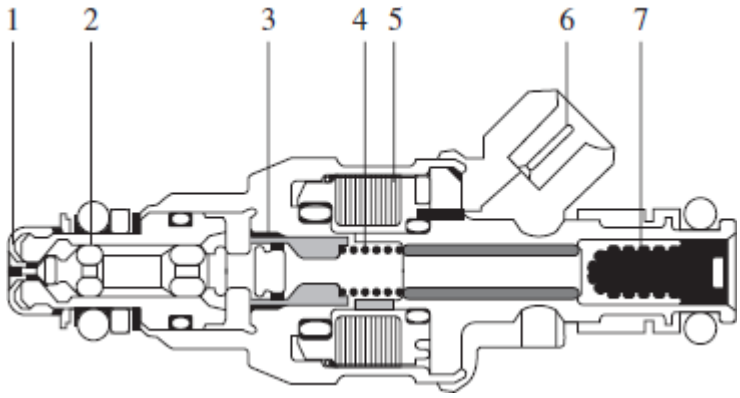


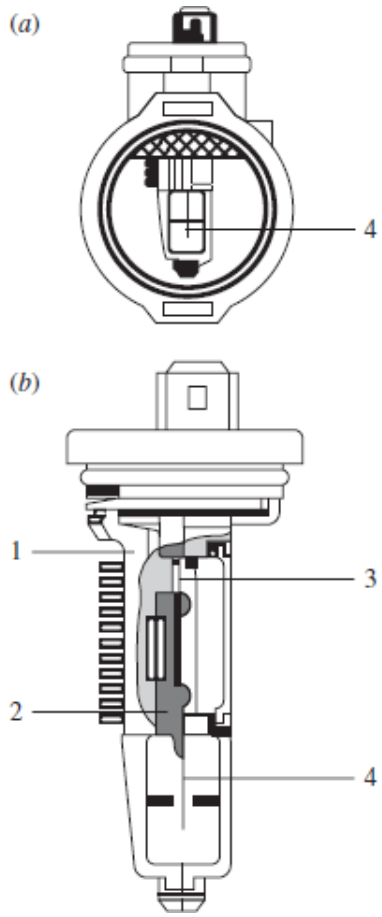
Figure 7.9 Cross-section of port fuel injector: (1) Pintle; (2) Valve needle; (3) Armature; (4) Spring; (5) Solenoid winding; (6) Electrical terminals; (7) Fuel strainer. (Courtesy: Robert Bosch GmbH and SAE.[2])



The multipoint (port) fuel injection system shown in Fig. 7.8 measures the airflow directly. The airflow meter is placed upstream of the throttle, just downstream of the air filter. Several approaches to airflow measurement have been used. One approach is that shown in Fig. 7.8, where the air flow deflects a sensor plate against a constant return force spring.[2] Another is the hot-film air mass flow meter shown in Fig. 7.10. The advantages of direct air-flow measurement are:[2] (1) automatic compensation for tolerances, combustion chamber deposit buildup, wear and changes in valve adjustments; (2) the dependence of volumetric efficiency on speed and exhaust backpressure is automatically accounted for; (3) less acceleration enrichment is required because the air-flow signal precedes the filling of the cylinders; (4) improved idling stability; and (5) lack of sensitivity of the system to EGR since only the fresh air flow is measured.

© McGraw-Hill Education. All rights reserved. Any use is subject to the Terms of Use, Privacy Notice and copyright information.

Figure 7.10 Hot-film air mass-flow meter: (a) Housing; (b) Hot-film sensor within the housing: (1) Heat sink; (2) Spacer; (3) Driver stage; (4) Metallic film sensor element.[2] (Courtesy Robert Bosch GmbH and SAE.)



The mass of air inducted per cycle to each cylinder, m_a, varies as

$$m_a \alpha \frac{\dot{m}_a}{N}$$

(7.3)

Thus the primary signals for the electronic control unit (ECU) are airflow rate and engine speed. The injector pulse width, which at fixed Δp across the injector determines the amount of fuel injected, is inversely proportional to engine speed and directly proportional to air flow. The engine block temperature sensor, starter switch, and throttle valve switch provide input signals for the necessary adjustments for cold-start, warm-up, idling, and WOT enrichment (when used).

For cold-start enrichment, one (or more) cold-start injector valve may be used to inject additional fuel into the intake manifold plenum as shown in Fig. 7.8. Since short opening and closing times are not important, this valve can be designed to provide extremely fine atomization of the fuel to minimize the enrichment required.

An alternative to direct airflow measurement is air mass estimation based on other sensor signals. The appropriate coil excitation pulse duration or width is set by the ECU. In the speed-density system, the primary inputs to the engine's ECU are the outputs from the manifold pressure sensor, the engine speed sensor (usually integral with the distributor), and the temperature sensors installed in the intake manifold to monitor air temperature and engine block to monitor the water-jacket

© McGraw-Hill Education. All rights reserved. Any use is subject to the Terms of Use, Privacy Notice and copyright information.

temperature—the latter being used to indicate fuel-enrichment requirements during cold-start and warm-up. For warm-engine operation, the mass of air per cylinder per cycle m_a is given by

$$m_a = \eta_v(N)\rho_a(T_i, p_i)V_d = \frac{\eta_v V_d p_i}{R_a T_i}$$

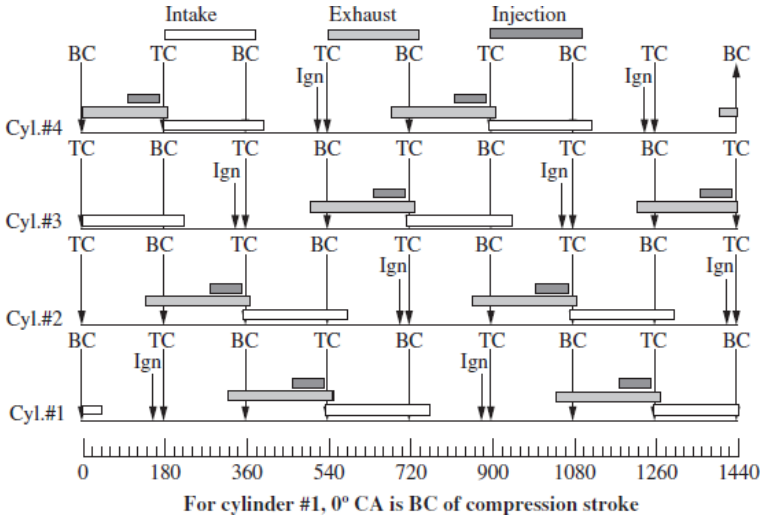
(7.4)

where η_v is the volumetric efficiency, N is engine speed, ρ_a is the inlet air density, and V_d is the displaced volume per cylinder. The ECU then determines the pulse width, which excites the injector solenoids, which provides the desired amount of injected fuel. The pulse width depends primarily on the manifold pressure; it also depends on the variation in volumetric efficiency η_v with speed N and variations in air density due to variations in air temperature. The control unit also initiates mixture enrichment during cold-engine operation and during accelerations that are detected by the throttle sensor.

Port fuel-injection systems offer several options regarding the timing and location of each injection relative to the intake event. The spray is directed toward the back of the intake valves. With electronically controlled injection systems, the fuel is injected intermittently toward the intake valves. The fuel-injection pulse width to provide the appropriate mass of fuel for each cylinder air charge varies from about 1.5 to 10 ms over the engine load and speed range. In crank angle degrees this varies from 10 to 20° at light load and low speed to up to 300° at maximum speed and load. Thus the pulse width varies from being much less than to greater than the duration of the intake stroke. In the early fuel injection systems, all injectors were operated simultaneously. Now, to achieve mixture uniformity sequential injection timing is used, where the phasing of *each* injection pulse relative to its cylinder's intake valve lift profile is the same. Figure 7.11 shows the fuel injection timing for each cylinder of a four-cylinder engine, at mid-load and speed. Fuel injection into the intake port toward the back of the (closed) intake valve ends prior to the start of the intake stroke. This timing, with injection toward a closed intake valve, results in most of the injected fuel impinging on the valve head and stem, and on the port walls close to the valve seat. More of the fuel then vaporizes before entry into the cylinder than would be the case with open (intake) valve injection. Also, injection toward the end of the valve closed period allows engine transients to be followed better: the time lag in the information the ECU uses to calculate the amount of fuel to be injected is then at its minimum. Note, some fuel metering strategies use open valve injection during engine starting as a way to get more of the injected fuel, rapidly, into the cylinder. Engine performance and emissions do change as the timing of the start of injection relative to inlet valve opening is varied. Injection toward an open intake valve usually results in higher HC emissions—more liquid fuel droplets pass directly into the cylinder. Injection with valve lift approaching its maximum, or decreasing, is least desirable because the air flow velocities through the valve open area are becoming lower, and atomization vaporization and mixing are slower (see Sec. 6.3).

© McGraw-Hill Education. All rights reserved. Any use is subject to the Terms of Use, Privacy Notice and copyright information.

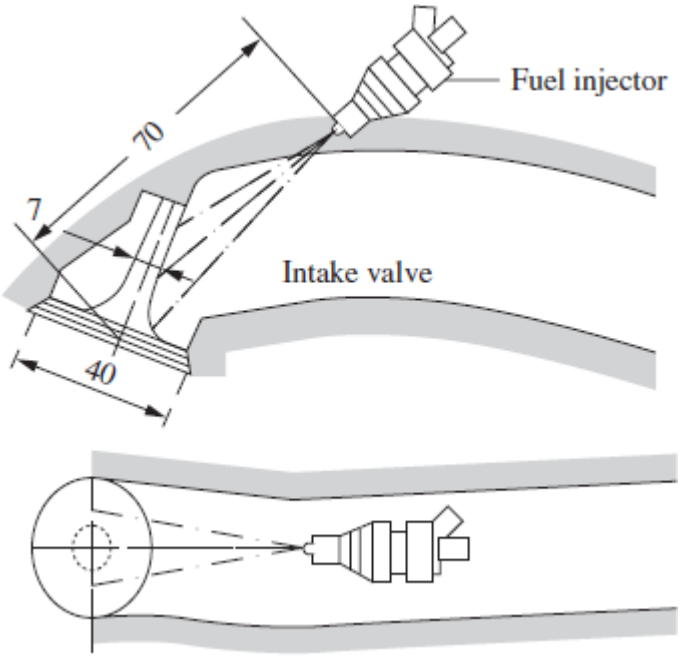
Figure 7.11 Event diagram showing the intake and exhaust processes, and fuel injection pulse, and ignition for the individual cylinders of a four-stroke cycle four-cylinder engine.



7.4.2. Fuel Spray Behavior

The overall objective of the geometric layout of a port-fuel-injection system is to place most of the liquid fuel on the intake valve surface (the hottest surface available) near the valve seat toward the end of the valve closed period. Figure 7.12 shows the preferred geometry with the injector close enough to the intake valve head so that, with realistic spray spreading angles, the amount of port wall wetting is minimized. Since the intake valve head in a warmed-up engine reaches a temperature in the 150 to 200°C range, it is the surface that will most effectively evaporate liquid fuel. In most cylinder head designs, it proves infeasible to locate the injector that close to the valve, and use that straight a port design. Thus significant wetting of the intake port wall occurs. The port walls are at a temperature close to that of the engine coolant.

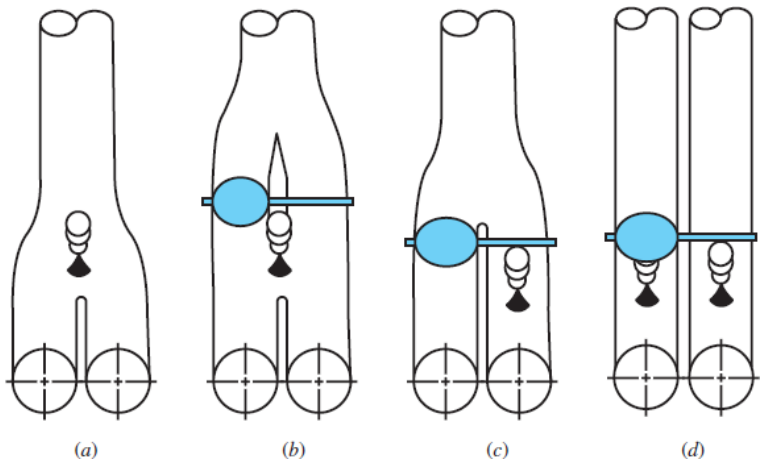
Figure 7.12 Preferred geometric targeting arrangement of fuel injector and intake valve head. Dimensions in mm.



© McGraw-Hill Education. All rights reserved. Any use is subject to the Terms of Use, Privacy Notice and copyright information.

Figure 7.13 illustrates additional spray targeting complexities in injector location and intake port and valve design. Shown are various potential intake manifold, port and valve layouts, of multi-valve cylinder heads for four-valve per cylinder (two intake valves) engines. With the simplest layout (Fig. 7.13*a*), with two intake valves and one fuel injector per cylinder, the spray cannot fully target each intake valve head, and substantial wetting of the wall dividing the two intake ports is inevitable. The other schematics add additional issues. In some cylinder head designs, port throttles are incorporated as shown to close off one of the intake ports at part load to generate a swirling flow within the cylinder (see Sec. 8.3) which speeds up the engine's combustion process which improves the engine's operating smoothness, and its NO_x emissions control potential. The increasing complexity and resulting wall-wetting issues of (*b*) and (*c*) are clear: the cost of these increasingly complex approaches increases (*a*) → (*b*) → (*c*) → (*d*).

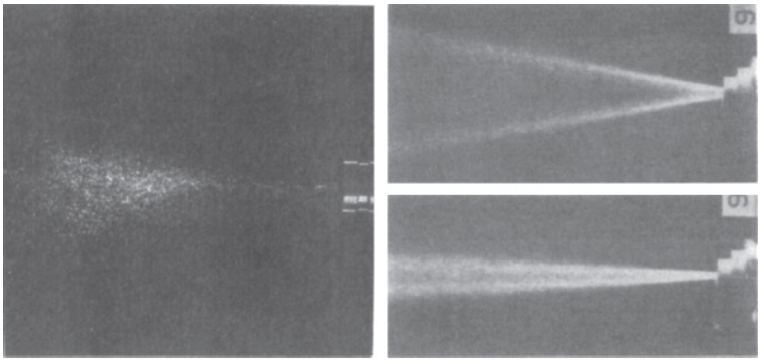
Figure 7.13 Four-valve-per-cylinder engine intake runner, port and port-throttling arrangements, illustrating fuel-injector spray targeting challenges.



Many different designs of fuel injectors for multipoint injection systems intended to improve mixture preparation have been developed and used. Spray geometry and droplet size distribution are key injector parameters. Figure 7.14 shows two examples of photographs of port fuel-injector sprays: (a) a single hole spray with a 30° spreading angle, once the liquid column exiting the injector nozzle breaks up into droplets; and (b) a dual spray injector which would fit with the two intake valve with short separating wall geometry shown in Fig. 7.13*a*. A single hole, two, four, and up to 12-hole nozzle designs, which produce the appropriate number of sprays of different spreading angles—narrower (~10°) and broader (~ 25°)—have been tried. Injection pressures are typically in the range of 3 to 7 bar. The droplet size distribution in injection designs is in the 80 to 200 μm range. For the droplets to follow the air flow around bends, as needs to occur as the intake flow goes past the valve seat and around the valve head into the cylinder, they must have a diameter close to or less than about 20 μm: thus most of the droplets in standard sprays impinge on the port and valve surfaces. To achieve these small average drop sizes in the fuel spray requires different spray generating mechanisms: one example is air-assist atomization where pressurized air flows through the injector and, in the injector nozzle, shatters the fuel into these much smaller drop sizes.

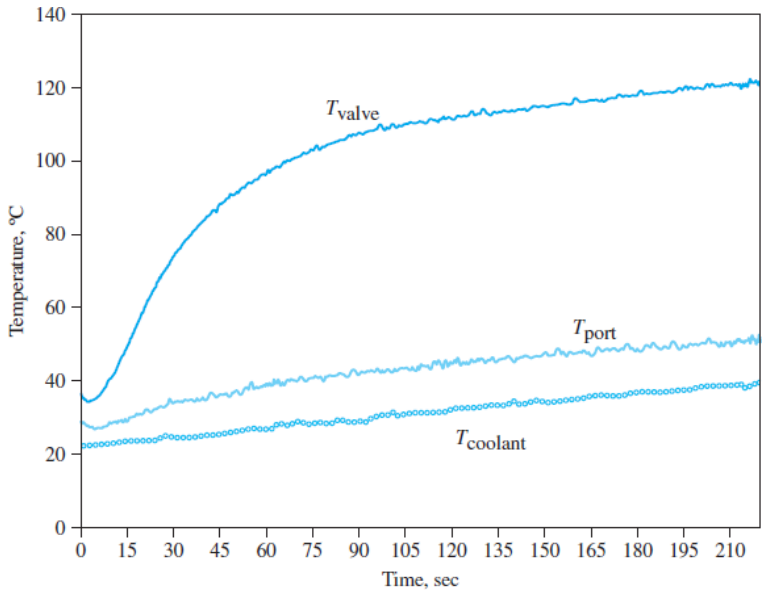
© McGraw-Hill Education. All rights reserved. Any use is subject to the Terms of Use, Privacy Notice and copyright information.

Figure 7.14 (a) Short time-exposure photograph of liquid spray from Bosch-type port fuel-injector like that shown in Fig. 7.9. (Courtesy: Robert Bosch.) (b) Twin sprays from a two-stream port fuel-injector designed for four-valve-per-cylinder engines.[8]



As mentioned several times above, the valve and port surface temperatures have a major impact on the liquid fuel vaporization process from these surfaces. The temperatures of these surfaces start at ambient levels in a cold engine, and steadily rise during warm up. Figure 7.15 shows how the thermal environment in the intake port evolves following start-up at light load and low speed. Once the engine starts firing, heat is transferred from the hot in-cylinder burned gases to the combustion chamber (and exhaust port) surfaces. This thermal energy is then transferred to the coolant. The intake valve-head temperature rises rapidly during the first minute or so of operation: the coolant (and thus intake port wall) temperature rises more slowly. After about 10 minutes of operation, these temperatures stabilize with the coolant at about 90°C, the port slightly higher (due to backflow of hot residual gases into the intake; see below), and the intake valve between about 150 and 200°C. The eventual valve temperature will depend on engine load and speed.

Figure 7.15 Intake port and valve surface, and coolant temperatures, as a function of time following an ambient temperature engine start.[9]



7.4.3. Reverse Flow Impacts

An important phenomenon in mixture preparation with port fuel-injection systems is the reverse blowdown of hot residual burned gases from the cylinder into the intake port at lighter loads and low to moderate speeds. In light-duty vehicle

© McGraw-Hill Education. All rights reserved. Any use is subject to the Terms of Use, Privacy Notice and copyright information.

applications, much engine operation is with intake manifold pressures (in naturally-aspirated gasoline engines) of about 0.5 bar or lower. Under these conditions, the ratio of the intake manifold pressure to the exhaust pressure is less than the critical ratio of about 0.5 (see App. C) so the burned gas velocity in this reverse blowdown process, past the valve seat and head, is close to sonic. Strong jets emanate from this steadily opening annulus between the valve-head and valve-seat, flowing into the intake port. These jets disrupt, blast backward, and atomize the liquid fuel that has accumulated in an annular ring around the intake port side of the intake valve seat. This atomizing backflow vaporizes some of this fuel: it also redistributes liquid fuel over a larger port surface area; see Ref. 10.

The relationship between this backflow, the exhaust, cylinder and intake pressures, and the valve events, under these partly loaded conditions, is as follows. Around TC, from intake valve opening (IVO) to exhaust valve closing (EVC), burned gases flow from the exhaust port into the cylinder because $p_e > p_c$: from IVO to the point where $p_c = p_i$ (the cylinder and intake pressures equalize), burned gas flows from the cylinder back into the intake port. At this point, the flow in the intake reverses direction (backward to forward), pulled by the descending piston during the intake stroke. These burned gases in the intake (which have mixed vigorously with the fresh air there) flow back into the cylinder along with the fresh air.

Also, at lower engine speeds, after BC of the intake stroke, there is a reverse (backward) displacement flow as the piston moves up the compression stroke prior to IVC. This reverse displacement flow pushes air, fuel vapor, and burned residual gases (mixed together) back into the intake. At higher engine speeds, the intake-air-flow's momentum toward the still-open intake valve overcomes this upward piston motion, and this reverse flow does not occur (see Sec. 6.2.4).

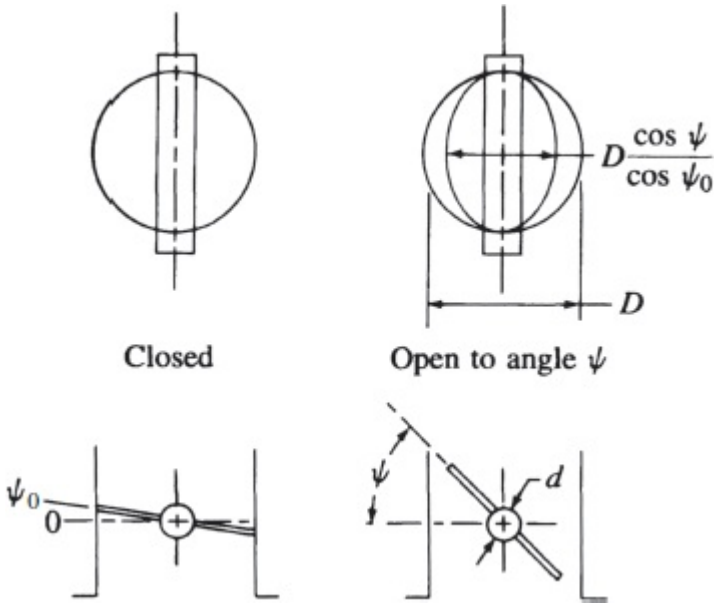
© McGraw-Hill Education. All rights reserved. Any use is subject to the Terms of Use, Privacy Notice and copyright information.

7.5. AIR FLOW PHENOMENA

7.5.1. Flow Past the Throttle Plate

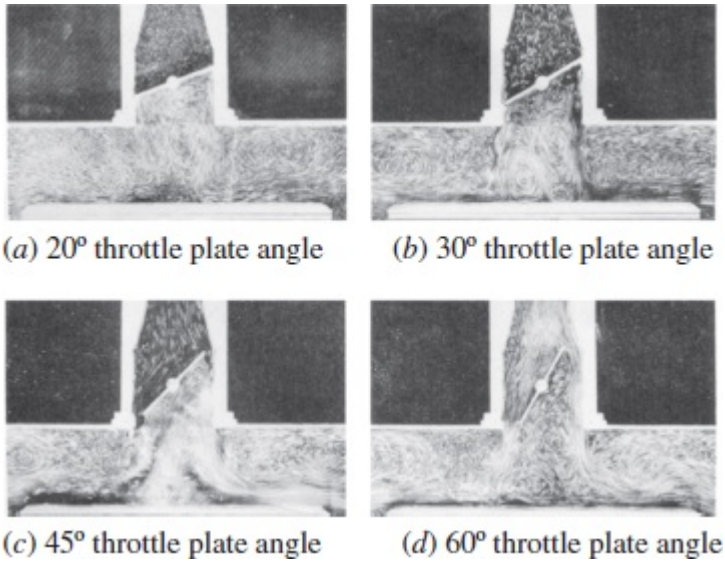
Except at or close to WOT, the throttle assembly provides the minimum flow area in the entire intake system. Under typical road-load conditions with a standard SI engine, more than 90% of the total pressure loss occurs across the throttle plate. The minimum-to-maximum flow area ratio is large—typically of order 100. Throttle plate geometry and parameters are illustrated in Fig. 7.16. A throttle plate of conventional design as shown creates a three-dimensional flow field. At typical part-throttle operating conditions, the throttle plate angle is in the 20 to 45° range and jets issue from the "crescent moon"-shaped open areas on either side of the throttle plate. The jets are primarily two dimensional. Figure 7.17 shows photographs taken of a two-dimensional hydraulic analog of a steady flow past a throttle plate at different throttle open angles. The path lines traced by the particles in the flow indicate the relative magnitude of the flow velocities.[18] The flow accelerates as it divides on either side of the throttle plate. There is a stagnation point on the upstream side of the plate. The wake of the throttle plate contains two vortices, which rotate in opposite directions. The air jets exiting the throttle openings are at or near the sonic velocity. There is little or no mixing between the two jets.

Figure 7.16 Throttle plate geometry.[11]



© McGraw-Hill Education. All rights reserved. Any use is subject to the Terms of Use, Privacy Notice and copyright information.

Figure 7.17 Photographs of flow in two-dimensional hydraulic analog of flow past a throttle plate onto the manifold plenum floor at different throttle plate angles.[6]



In analyzing the flow past the throttle plate, the following factors should be considered:[11, 12]

- The throttle plate shaft is usually of sufficient size to affect the throttle open area.
- To prevent binding in the throttle bore, the throttle plate is usually completely closed at some non-zero angle (10° or so).
- The discharge coefficient of the throttle plate is less than that of a smooth converging-diverging nozzle, and varies with throttle angle, pressure ratio, and throttle plate Reynolds number.
- Due to the manufacturing tolerances involved, there is often some leakage area even when the throttle plate is closed against the throttle bore. This leakage area at small throttle openings is one reason why gasoline engine management systems have a solenoid-controlled throttle by-pass passage to more accurately manage the idle airflow (see Fig. 7.8).
- The measured pressure drop across the throttle depends (±10%) on the circumferential location of the downstream pressure tap.
- The pressure loss across the throttle plate under the actual flow conditions (which are unsteady even when the engine speed and load are constant) may be less than under steady flow conditions.

The throttle plate open area A_{th}, as a function of angle ψ for the geometry in Fig. 7.16, is given by[11]

$$\frac{4A_{\text{th}}}{\pi D^2} = \left(1-\frac{\cos\psi}{\cos\psi_0}\right)+\frac{2}{\pi}\left[\frac{a}{\cos\psi}\left(\cos^2\psi-a^2\cos^2\psi_0\right)^{1/2}+\frac{\cos\psi}{\cos\psi_0}\sin^{-1}\left(\frac{a\cos\psi_0}{\cos\psi}\right)-a\left(1-a^2\right)^{1/2}-\sin^{-1}a\right] \tag{7.5}$$

where $a = d/D$, d is the throttle shaft diameter, D is the throttle bore diameter, and ψ_0 is the throttle plate angle when tightly closed against the throttle bore. When $\psi = \cos^{-1}(a\cos\psi_0)$, the throttle open area reaches its maximum value $(\approx \pi D^2/4 - dD)$. The throttle plate discharge coefficient (which varies with A_{th}), and minimum leakage area, must be determined experimentally.

© McGraw-Hill Education. All rights reserved. Any use is subject to the Terms of Use, Privacy Notice and copyright information.

The mass flow rate through the throttle valve can be calculated from standard orifice equations for compressible fluid flow [see App. C, Eqs. (C.8) and (C.9)]. For pressure ratios across the throttle less than the critical value(p_T/p_0 = 0.528), the mass flow rate is given by

$$\dot{m}_{\text{th}} = \frac{C_D A_{\text{th}} p_0}{\sqrt{RT_0}} \left(\frac{p_T}{p_0}\right)^{1/\gamma} \left\{ \frac{2\gamma}{\gamma - 1} \left[1 - \frac{p_T}{p_0}\right]^{(\gamma-1)/\gamma} \right\}^{1/2}$$

(7.6)

where A_{th} is the throttle plate open area [Eq. (7.5)], p_0 and T_0 are the upstream pressure and temperature, p_T is the pressure downstream of the throttle plate (assumed equal to the pressure at the minimum area: i.e., no pressure recovery occurs), and C_D is the discharge coefficient (determined experimentally). For pressure ratios greater than the critical ratio, when the flow at the throttle plate is choked,

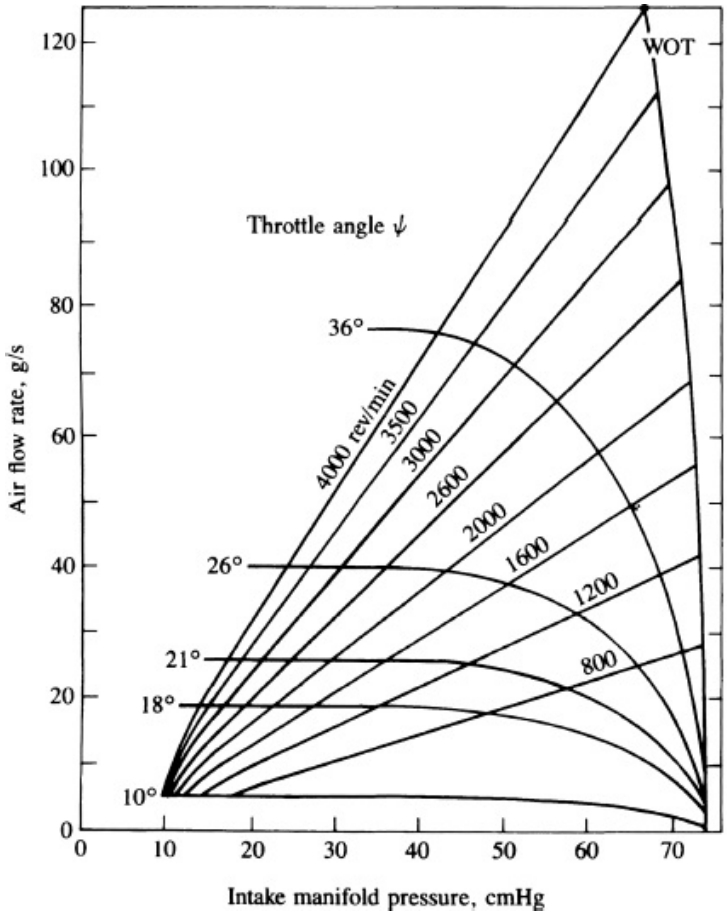
$$m_{\text{th}} = \frac{C_p A_{\text{th}} \rho_0}{\sqrt{RT_0}} \gamma^{1/2} \left(\frac{2\gamma}{\gamma + 1}\right)^{(\gamma+1)/2(\gamma-1)}$$

(7.7)

The relation between airflow rate, throttle angle, intake manifold pressure, and engine speed for a 4.7-dm^3 (288-in^3) displacement eight-cylinder production engine is shown in Fig. 7.18. While the lines are predictions from a quasi-steady computer simulation, the agreement with data is excellent. The figure shows that for an intake manifold pressure below the critical value (0.528 × p_{atm} = 53.5 kN/m^2 = 40.1 cmHg), the air flow rate at a given throttle position is independent of manifold pressure and engine speed because the flow at the throttle plate is choked.

© McGraw-Hill Education. All rights reserved. Any use is subject to the Terms of Use, Privacy Notice and copyright information.

Figure 7.18 Variation in air flow rate past a throttle, with intake manifold pressure, throttle angle, and engine speed. 4.7-liter displacement eight-cylinder engine.[11]



Traditionally, in vehicle engines, the driver controlled the throttle open area to obtain the desired engine torque via the position of the accelerator pedal, which was linked mechanically to the throttle. With electronic throttle control, now widely used, the airflow required to produce the desired torque is calculated based on the position (and thus the open area) of the throttle plate.

7.5.2. Flow in Intake Manifolds

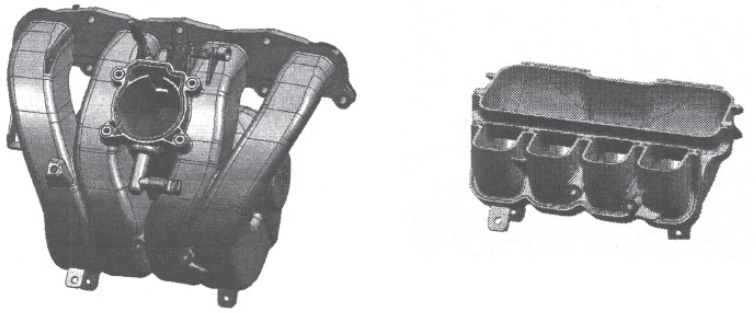
The details of the airflow in intake manifolds are complex. The combination of pulsating flow into each cylinder, different geometry flow paths through the plenum (below the throttle), through each of the manifold runners to each inlet port, and the mixing of EGR with the air just downstream of the throttle plate, under steady-state engine operating conditions are difficult enough areas to untangle. During engine transients, when the throttle position is changed, the fact that the processes which govern the air and the fuel flow to the cylinder are then substantially different introduces additional problems. This section reviews our current understanding of these airflow phenomena.

Intake manifolds consist typically of a plenum, to the inlet of which bolts the throttle body, feeding individual runners which lead to each cylinder. Important design criteria are: low air flow resistance; good distribution of air between cylinders; runner and branch lengths that take advantage of ram and tuning effects (see Secs. 6.2.4. and 6.2.6). Some of the design choices are illustrated in Fig. 7.19, which shows an intake manifold for a modern four-cylinder engine. In this design the four branches that link the plenum beneath the throttle with the intake ports are similar in length and geometry, to provide closely comparable flow paths and tuning benefits. The manifold shown is made of a nylon composite and manufactured by a lost core molding

© McGraw-Hill Education. All rights reserved. Any use is subject to the Terms of Use, Privacy Notice and copyright information.

process. This allowed larger runner width and flow area, and increased runner taper or narrowing, plenum to port, increasing airflow and thus engine power.

Figure 7.19 Intake manifold for a four-cylinder gasoline spark-ignition engine: (a) throttle and manifolds; (b) plenum (bottom half) and manifold entrances.[13]



With port fuel-injection systems, the task of the intake manifold is to control the airflow (and EGR flow at low- to mid-loads). Fuel does not have to be transported from the throttle body through the entire manifold. Thus, larger and longer runners and branches, with larger angle bends, can be used to provide equal runner lengths and take greater advantage of ram and tuning effects. With port fuel injection it is not necessary to heat the manifold.

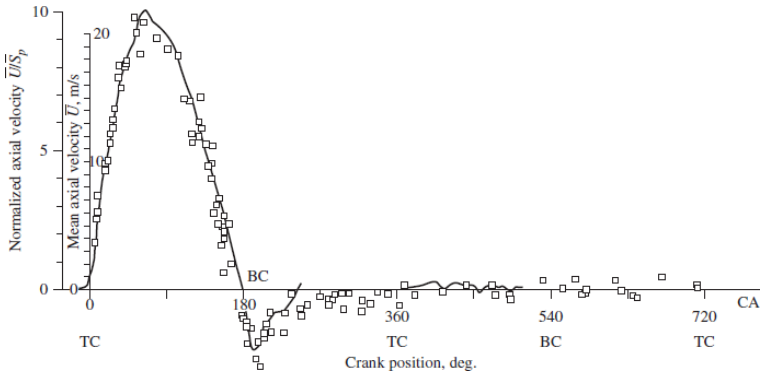
Many different intake manifold arrangements are used in practice. Different cylinder arrangements (e.g., four, V-six, in-line-six, etc.) provide quite different air distribution problems and require different solutions.

The airflow out of the manifold occurs in a series of pulses, one going to each cylinder. Since each pulse is pulled into the cylinder by the descending piston during the intake stroke, the pulse shape follows that of the piston speed versus crank angle curve (Fig. 2.2). Each pulse is approximately sinusoidal in shape. For four- and eight-cylinder engines, these flow pulses sequence such that the outflow is essentially zero between pulses. For six-cylinder arrangements the pulses will overlap. When the engine is throttled (as discussed in Sec. 7.4), backflow from the cylinder into the intake manifold occurs during the early part of the intake process until the cylinder pressure falls below the manifold pressure. Backflow can also occur early in the compression stroke before the inlet valve closes, due to rising cylinder pressure. The flow at the throttle will fluctuate as a consequence of the pulsed flow out of the manifold into the cylinders. At high intake manifold vacuum, the flow will be continuously inward at the throttle and flow pulsations will be small. When the outflow to the cylinder which is undergoing its intake stroke is greater than the flow through the throttle, the cylinder will draw air from the rest of the intake manifold. During the portion of the intake stroke when the flow into the cylinder is lower than the flow through the throttle, air (and EGR) will flow back into the rest of the manifold. At WOT when the flow restriction at the throttle is a minimum, flow pulsations at the throttle location will be much more pronounced.

Detailed measurements of the flow velocities in intake manifolds confirm the above description. At low- to mid-speeds, the airflow within the active manifold runner is approximately one dimensional and quasi-steady, and during the intake stroke follows the piston speed, as indicated in Fig. 7.20. The mean (averaged across the flow area) flow velocity $\overline{U}$ closely follows the instantaneous piston velocity S_p. These two velocities scale together: the maximum intake manifold flow velocity is about 10 times the mean piston speed, or about 6 times the maximum piston speed (these numbers depending on the location in the manifold runner since the cross-sectional area vary). Note that at the low engine speed shown in Fig. 7.20, as the piston moves up the cylinder during the compression stroke, it pushes some of the in-cylinder mixture back into the intake prior to the intake valve closing. As engine speed increases, the momentum of the air in the manifold runner increasingly opposes this backflow: at mid-engine speed this backflow has largely disappeared. At higher engine speeds this momentum (ram) effect continues the positive airflow after BC: see Sec. 6.2.4. Also at higher engine speeds, the higher frictional flow resistance (which depends on $\overline{U}^2$) and pressure-wave-induced flow rate variations distort this quasi-steady behavior to some degree.

© McGraw-Hill Education. All rights reserved. Any use is subject to the Terms of Use, Privacy Notice and copyright information.

Figure 7.20 Mean and instantaneous intake manifold air velocities during the engine's operating cycle in a production diesel engine: speed = 717 rev/min; mean piston speed = 2.2 m/s; stroke = 92 mm.[14]



The airflows to each cylinder of a multi-cylinder engine, even under steady operating conditions, are not identical. This is due to differences in runner layout and length, as well as other geometric details of the flow path to each cylinder. Also, as each cylinder's intake flow commences, air is drawn from the branch or runner leading to the cylinder, the plenum, and the other runners feeding the plenum, as well as past the throttle. This "drawing down" of other parts of the intake manifold depends on the arrangement of the plenum, and runners, and the firing order of the cylinders. Thus the air flow to each individual cylinder is affected by the details of its own branch, how that branch connects to the rest of the intake manifold, and the cylinder firing order.[15] Modern manifold designs keep these differences between the air flows to individual cylinders modest: variations in the average air mass flow rate to each individual cylinder are less than a couple percent.

Typical quantities that characterize manifold air flow are given in Table 7.2 for a four- and an eight-cylinder naturally-aspirated gasoline engine. The volume of air pulled into each cylinder per cycle is about the same as the volume of one direct flow path between the throttle plate and inlet valve. Thus, one intake stroke loads the manifold, and the next one pulls that air into the cylinder.

Table 7.2 Parameters that characterize manifold air flow

Engine geometry	I-4*	V-8†
Typical flow-path distance between throttle bore and intake valve, cm	33	30
Average intake-passage flow area, cm^2	10	16
Volume of one direct flow path from throttle bore to intake valve, cm^3	350	500
Range of speeds, etc.	**Maximum**	**Minimum**
Crankshaft, rev/min	6500–5500	600
Peak air velocity in manifold branch, m/s	180*, 140†	15
Peak Reynolds number in manifold branch	5×10^5	5×10^4
Duration of individual cylinder intake process, ms	35	3–4
*1.8-liter four-cylinder in-line SI engine.[16]		
† 5.6-liter V-8 cylinder SI engine.[17]		

© McGraw-Hill Education. All rights reserved. Any use is subject to the Terms of Use, Privacy Notice and copyright information.

An additional phenomenon becomes important when engine load is changed by opening or closing the throttle: the mass of air in the induction system volume takes a finite time to adjust to the new engine operating conditions. For example, as the throttle is opened the airflow into the manifold increases as the throttle open area increases. However, due to the finite volume of the manifold, the pressure level in the manifold increases more slowly than would be the case if steady-state conditions prevailed at each throttle position. Thus, the pressure difference across the throttle is larger than it would be under steady flow conditions and the throttle airflow overshoots its steady-state value. The airflow into each cylinder depends on the pressure in the manifold, so this lags the throttle airflow. This transient airflow phenomenon affects fuel metering. For throttle-body injection, fuel flow should be related to throttle airflow. For port fuel injection, fuel flow should be related to the airflow into the cylinder. Actual results for the airflow rate and manifold pressure in response to an opening of the throttle (increase in throttle angle) are shown in Fig. 7.21. The overshoot in throttle airflow and lag in manifold pressure as the throttle angle is increased are evident. Opposite effects will occur for a decrease in throttle angle—reduction in airflow through the throttle.

7.5.3. Air Flow Models

Several approaches to modeling the flow in an intake manifold have been proposed. One simple manifold model that describes many of the above phenomena is the *plenum* or *filling and emptying* approach. It is based on the assumption that at any given time, the manifold pressure is uniform. The continuity equation for air flow into and out of the intake manifold is

$$\frac{dm_{a,m}}{dt} = \dot{m}_{a,\mathrm{th}} - \sum \dot{m}_{a,\mathrm{cyl}}$$

(7.8)

where
$m_{a,m}$ is the mass of air in the manifold, and
$\dot{m}_{a,\mathrm{th}}$ and
$\dot{m}_{a,\mathrm{cyl}}$ are the air mass flow rates past the throttle and into each cylinder, respectively. The flow rate past the throttle is given by Eq. (7.6) or (7.7). For manifold pressures sufficiently low to choke the flow past the throttle plate, the flow rate is independent of manifold pressure. The mass flow rate to the engine cylinders can be modeled at several levels of accuracy. The airflow through the valve to each cylinder can be computed from the valve area, discharge coefficient, and pressure difference across the valve; or a sine wave or
$S_p(\theta)$ function can be assumed. In the general case, Eq. (7.8) must be combined with the first law for an open system (see Sec. 14.2.2). For calculating the manifold response to a change in load or throttle setting, simplifying assumptions can be made. A quasi-steady approximation for the air flow into the cylinder

$$\sum \dot{m}_{a,\mathrm{cyl}} = \frac{\eta_v \rho_{a,m} V_d N}{2}$$

is usually adequate, and the air temperature can be assumed constant. Then, using the ideal gas law for the manifold, $p_m V_m = m_{a,m} R_a T_m$, Eq. (7.8) can be written as

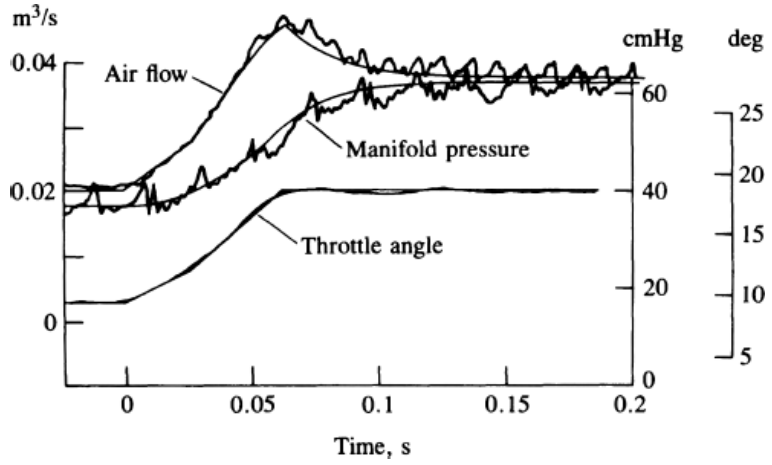
$$\frac{dp_m}{dt} + \frac{\eta_v V_d N}{2V_m} p_m = \dot{m}_{a,\mathrm{th}} \frac{RT_m}{V_m}$$

(7.9)

© McGraw-Hill Education. All rights reserved. Any use is subject to the Terms of Use, Privacy Notice and copyright information.

Both η_v and $\dot{m}_{a,\mathrm{th}}$ have some dependence on p_m [e.g., see Eq. (6.2)]. In the absence of this weak dependence, Eq. (7.9) would be a first-order equation for p_m with a time constant $\tau = 2V_m/(\eta_v V_d N) \approx V_m/\dot{V}_{\mathrm{cyl}}$ which is two to four times the intake stroke duration. The smooth curves in Fig. 7.21 are predictions made with Eq. (7.9) and show good agreement with the data. The plenum model is useful for investigating manifold pressure variations that result from load changes. It provides no information concerning pressure variations associated with momentum and wave effects.

Figure 7.21 Throttle angle, intake manifold pressure, and airflow rate past the throttle versus time for 10° part-load throttle opening. 5-liter V-8 engine.[17]



The dynamics of the flow in multi-cylinder intake (and exhaust) systems can be modeled using one-dimensional unsteady compressible flow equations. Historically, the governing equations were solved using the method of characteristics (see Benson et al.[18]). Finite difference techniques are now used.[19] The assumptions usually made in this unsteady flow analysis are:

- The intake (and exhaust) system can be modeled as a combination of pipes, junctions, and plenums.
- Flow in the pipes is one dimensional and no axial heat conduction occurs.
- States in the engine cylinders and plenums are uniform.
- Boundary conditions are considered quasi steady.
- Coefficients of discharge, heat transfer, pipe friction, and bend losses for steady flow are valid for unsteady flow.
- The gases can be modeled as ideal gases.

This approach to intake and exhaust flow analysis is discussed more fully in Sec. 14.3.4.

© McGraw-Hill Education. All rights reserved. Any use is subject to the Terms of Use, Privacy Notice and copyright information.

7.6. FUEL FLOW PHENOMENA: PORT FUEL INJECTION

7.6.1. Liquid Fuel Behavior

With port-fuel-injection liquid-fuel metering systems, the fuel enters the air stream as a liquid jet, which atomizes into droplets. These drops then move through the air and mostly deposit on the walls of the intake ports and valve heads. Some of the smaller droplets vaporize; vaporization of the now hotter liquid fuel on the walls also occurs. The flow of liquid fuel along the walls is significant: the transport of fuel as vapor, droplets, and liquid streams or films can all be important. The fuel transport processes in the intake port region are obviously extremely complex.

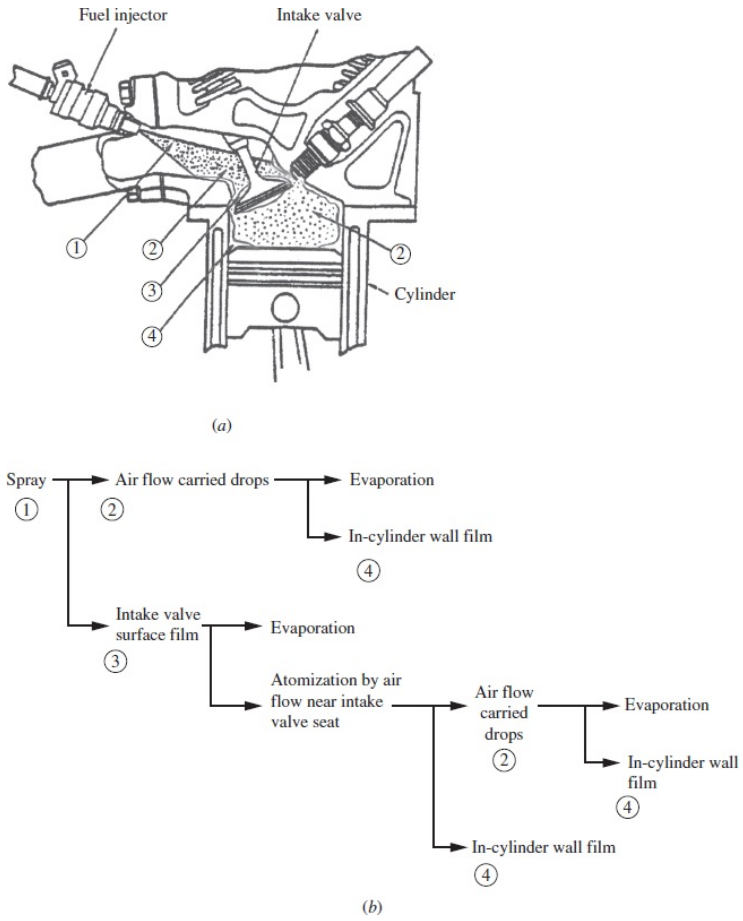
The details of the fuel transport process are different for multipoint port fuel-injection systems than for throttle-body injection systems. For the latter systems, fuel must be transported past the throttle plate and through the complete intake manifold. For the former systems, the liquid fuel is injected into the inlet port, toward the back of the intake valve. For all these practical fuel metering systems, the quality of the mixture entering the engine is imperfect. The fuel, air, recycled exhausts, mixture is not homogeneous; the fuel may not be fully vaporized as it enters the engine. The charge going into each cylinder is not usually uniform in fuel/air ratio throughout its volume, and the distribution of fuel between the different engine cylinders is not exactly equal. During engine transients (e.g., during vehicle accelerations and decelerations) when engine fuel and air requirements and manifold conditions change, it is obvious that the above fuel transport processes will not all vary with time in the same way. Thus, in addition to the transient non-quasi-steady airflow phenomena described in the previous section, there are transient fuel-flow phenomena. These have to be compensated for in the fuel metering strategy.

Gasoline (which may be blended with 5, 10, or more percent ethanol), the standard spark-ignition engine fuel, is a mixture of a large number of individual hydrocarbons: it has a boiling temperature range rather than a single boiling point as discussed in Sec. 7.2.2. That discussion indicates how the equilibrium fraction of fuel evaporated at a given temperature and pressure can be calculated. Figure 7.3 shows the effect of mixture temperature on percent of indolene fuel (a specific gasoline) evaporated. While insufficient time is usually available in the manifold to establish equilibrium, the trends shown are indicative of what happens in practice: lower pressures increase the relative amount of fuel vaporized and fuel heating from warm or hot surfaces is required to vaporize a substantial fraction of the fuel in the engine intake. With port fuel-injection systems the fuel is injected onto the back of the inlet valve (and surrounding port walls), usually while the valve is closed or only partly open. Vaporization of liquid fuel off the valve and walls occurs, enhanced by the backflow of hot residual gases from the cylinder (especially at part-load). Even under fully warmed-up engine conditions, some fuel is carried into the cylinder as liquid.

These fuel pathways into and within the cylinder are illustrated diagrammatically, and in a flow diagram, in Fig. 7.22. During the injection period, liquid fuel drops in the spray impinge on the back of the intake valve head, and on the port walls approaching the valve seat, adding to the liquid films already there. This occurs with both closed-valve injection (the most common approach at part-load and lower speeds), as well as open-valve injection. When the intake valve opens, under throttled conditions (manifold pressure below atmospheric), the blowdown backflow (see Sec. 7.4) can significantly redistribute these liquid films. When, following any backflow, the forward flow of fresh charge commences and the piston accelerates down the cylinder, the high velocity airflow past the valve seat and head strips liquid from these films, and shatters that liquid into small drops which are carried by the airflow into the cylinder. Fuel vaporization from airborne drops and these films adds more fuel vapor to the in-cylinder fuel, air, residual gas, mixture. Inside the cylinder, larger drops can impinge on the combustion chamber walls forming liquid films on the intake valve head, the cylinder head, the liner, even the piston, depending on geometric details and the temperatures of the air-residual gas mixture and these wall surfaces. When the engine is cold—during starting and the first few minute or so of operation, there can be substantial liquid on these walls (both in the intake port and the cylinder). In a warmed-up engine, only a few percent of the injected fuel enters the cylinder as a liquid.

© McGraw-Hill Education. All rights reserved. Any use is subject to the Terms of Use, Privacy Notice and copyright information.

Figure 7.22 (a) Schematic of fuel behavior during port-fuel-injection gasoline-engine intake process. (b) Fuel flow diagram from port fuel injector into and within the cylinder.[20]



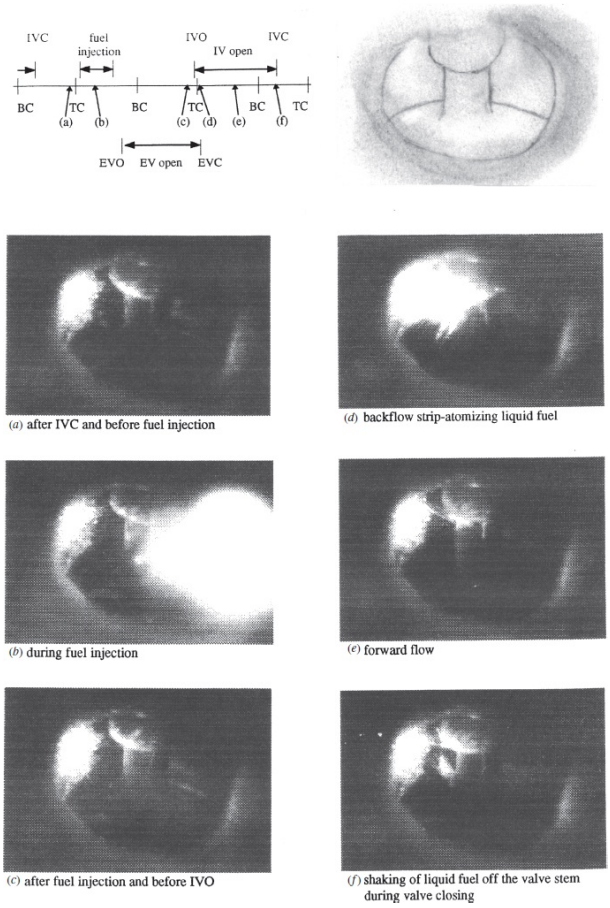
During cold engine starting, substantial additional fuel beyond that required if fully vaporized to produce a stoichiometric in-cylinder mixture, is injected in the first (and sometimes second) injection for each cylinder. This is because, as Fig. 7.4*a* and *b* indicate, at these ambient temperatures, only a moderate fraction of the fuel injected will vaporize. However, with excess (liquid) fuel in the intake port from these first injections, succeeding injections must be reduced below the nominal stoichiometric requirement to (over time) vaporize and burn the initial excess.

Calibrating the engine to manage the fuel metering at these different thermal conditions and through these thermal transients requires time-consuming engine testing. Superimposed on these thermal transients are engine throttle-change transients where the driver accelerates or decelerates the vehicle. These latter transients have characteristic time constants of 0.1 to 1 seconds. Engine start-up transients have similar time constants. Engine warm-up can take several minutes, depending on the initial engine temperature, and the engine load and speed (engine heat transfer from the hot burned gases to the cylinder walls varies significantly with these two parameters). Section 7.6.2 discusses controlling the fuel metering during engine acceleration and deceleration transients in more detail.

Figure 7.23 illustrates several of the above described fuel behaviors with photos extracted from intake port and in-cylinder high-speed videos taken under lightly loaded lower-speed operating conditions in engines with appropriate optical access. The white areas in the photos indicate where light is being reflected from liquid fuel on the walls (around the valve seat, and the valve boss and stem), from drops in the fuel injection spray (Fig. 7.23*b*), and drops produced by the high velocity exhaust backflow (Fig. 7.23*d*). In sequence, once the engine starts firing (one or a few injections), it then takes several injections into each intake port to build-up significant liquid fuel close to the valve seat and on the valve head and stem. Then as liquid accumulates in these regions, a quasi-steady behavior becomes apparent.

© McGraw-Hill Education. All rights reserved. Any use is subject to the Terms of Use, Privacy Notice and copyright information.

Figure 7.23 Images from video visualizing fuel spray and liquid film behavior in one intake port of a four-valve cylinder head gasoline engine: stoichiometric operation at 1200 rev/min, 0.5 bar intake pressure, cylinder head at 25°C. White regions indicate where light is being reflected from liquid fuel (as films or moisture on wetted surfaces), or from droplets in the primary fuel-injected spray, or produced by the exhaust backflow atomizing liquid fuel that has accumulated around the valve seat.[10]



During the hot cylinder gas blowback into the intake port, there is obviously no fuel transport into the cylinder. But once liquid fuel has accumulated near the valve seat, the high velocity reverse flow starting at IVO causes substantial atomization and transport of fuel droplets backward into the intake port. When the forward flow of gases from the intake port past the valve seat commences (about 30° ATC at which time the piston is moving at about two-thirds of its mean piston speed: see Fig. 2.2), that forward flow drags liquid fuel from the films on the port walls toward the valve seat region and atomizes that liquid fuel on the port walls and on the valve head into fine drops that enter the cylinder in a short burst or "puff" some 20 to 30° later. The duration and extent of that burst decreases as the engine starts to warm up and the amount of liquid fuel on the port and valve walls decreases. As the forward airflow continues beyond this point, there is no obvious sign of continuing liquid fuel transport into the cylinder (through vapor fuel flow may continue). Also, under engine conditions where there is still substantial liquid fuel in the port near the valve seat, when the intake valve closes, the liquid fuel between the valve head and seat is squeezed out of the closing gap splattering large drops of fuel into the combustion chamber (where they impinge on the cylinder liner) and also back into the intake port. While the engine is still cold and in-cylinder liquid films persist on the valve head, cylinder head (and maybe other surfaces), the passage of the flame over these films (which are thick enough to "ripple") causes no visible change in their appearance. As the surface temperatures steadily rise, the films become thinner, smaller in area extent, transition in appearance to a "moist surface," and then disappear.[21]

7.6.1.1. Fuel Droplet Behavior

© McGraw-Hill Education. All rights reserved. Any use is subject to the Terms of Use, Privacy Notice and copyright information.

With fuel injection systems, the liquid fuel atomizes as it enters the air stream. The velocity of the liquid jet once it exits the nozzle is high enough to shatter the flowing liquid, and its interaction with the airflow further atomizes the fuel. Typical droplet-size distribution varies over the load and speed range. Droplet diameters in the 25 to 100 μm range are usually assumed to be representative: larger drops are also produced. The liquid fuel drops are accelerated by the surrounding air stream and start to vaporize. Vaporization rates have been calculated using established formulas for heat and mass transfer between a droplet and a surrounding flowing gas stream (see Ref. 22 for a review of methods of calculating droplet vaporization rates). Calculations of fuel vaporization show that the temperature of the liquid fuel droplets decrease rapidly (by up to about 30°C), and the fraction of the fuel vaporized in the intake port is small (in the 2 to 15% range).

Liquid fuel drops, due to their density being many times that of the air, will not exactly follow the air flow. Droplet impaction on the walls may occur as the flow changes direction, when the inertia of the droplets causes them to move across the streamlines. The equation of motion for an individual droplet in a flowing gas stream is

$$\left(\frac{1}{6}\pi D_d^3 \rho_f\right) \mathrm{a} = m_d \mathrm{g} - \frac{1}{2}(\mathrm{v}_d - \mathrm{v}_g)|\mathrm{v}_d - \mathrm{v}_g|\rho_g C_D \frac{\pi D_d^2}{4}$$

(7.10)

where D_d is the droplet diameter, ρ_f and ρ_g are liquid and gas densities, $\mathbf{v}_d$ and $\mathbf{v}_g$ are the droplet and gas velocities, **a** is the droplet acceleration, **g** acceleration due to gravity, and C_D is the droplet drag coefficient. For 6 < Re < 500 the drag coefficient of an evaporating droplet is a strong function of the Reynolds number, Re: for example,

$$C_D = 27\mathrm{Re}^{-0.84}$$

(7.11)

where
$\mathrm{Re} = (\rho_g D_d |\mathrm{v}_d - \mathrm{v}_g| / \mu_g)$

Studies of droplet impaction and evaporation using the above equations and typical manifold conditions and geometries indicate the following. For 90° bends, drops of less than 10 μm diameter are essentially carried by the gas stream (<10% wall impaction); almost all droplets larger than 25 μm impact on the walls. Droplet sizes produced by secondary atomization away from the fuel nozzle exit depend on the local gas velocity: higher local relative velocities between the gas and liquid produce smaller drop sizes. Approximate estimates which combine the two phenomena outlined above show that at low engine air flow rates, almost all of the fuel will impact on the port walls as the flow turns as it approaches the valve head. At high air flows, because the drops are smaller, a substantial fraction of the drops may stay entrained in the air flow. Secondary atomization as the air flows over fuel films at the valve seat is important to the fuel transport process: the high air velocities at the edge of the valve seat and head produce droplets of order or less than 10 μm diameter. However, coalescence and deposition on the walls and subsequent re-entrainment are likely to increase the mean droplet size.

Estimates of droplet evaporation rates in the manifold indicate the following. With a residence time in the manifold of about 10 ms (100 deg. CA at 1800 rev/min), only drops of size less than about 10 μm will evaporate. Thus, only drops small enough to be carried by the air stream are likely to vaporize in the intake: the larger droplets will impact on the walls, anyway.

7.6.1.2. Fuel-Film Behavior

The fuel which impacts on the wall will also vaporize and, depending on where fuel deposition occurs and the local wall geometry, may be dragged by the flowing air along the wall as a liquid film or rivulet. If the vaporization rate off the wall is sufficiently high, then a liquid film will not build up. Any liquid film or pool on the intake port or valve walls is important

© McGraw-Hill Education. All rights reserved. Any use is subject to the Terms of Use, Privacy Notice and copyright information.

because it introduces additional fuel transport processes—deposition, liquid transport, and evaporation—which together have a much longer time constant than the air transport process. Thus changes in the air and the fuel flow rate into each engine cylinder, during a change in engine load, will not occur in phase with each other unless compensation is made for the slower fuel transport. Models for following these transients are discussed next.

7.6.2. Transients: Fuel-Film Models

Several models of the behavior of liquid fuel wall-films have been developed. One approach analyzes the liquid fuel mass on the walls of the intake port and valve as one or more "puddles." Figure 7.24 illustrates the fuel transport processes involved. (The puddles are real: the model is conceptual.) A portion *x* of the injected fuel in the spray enters the puddle; fuel leaves the puddle through vaporization and, as liquid pulled from the puddle by the flowing air. The equation for the rate of change of the puddle fuel mass $m_{f,p}$ is

$$\dot{m}_{f,p} = \dot{m}_{f,\text{in}} - \dot{m}_{f,\text{out}} = x\,\dot{m}_{f,m} - \frac{m_{f,p}}{\tau}$$

(7.12)

where
$\dot{m}_{f,p}$ is the mass of fuel in the puddle,
$\dot{m}_{f,m}$ is the metered fuel flow rate, and *x* is the fraction of the metered flow that enters the puddle. It is assumed that the re-entrainment plus evaporation rate is proportional to the mass of fuel in the puddle divided by the characteristic time τ of the re-entrainment/evaporation process. The puddle behavior predicted by this model in response to a step increase in engine load is shown in Fig. 7.25*a*. The fuel delivery rate to the cylinder,
$\dot{m}_{f,c}$, is given by

$$\dot{m}_{f,c} = (1 - x)\,\dot{m}_{f,m} + \frac{m_f}{\tau}$$

(7.13)

Because only a fraction of the fuel, (1 − *x*), flows directly with the air into the cylinder, when the throttle is opened rapidly a lean air/fuel ratio excursion is predicted. Figure 7.25 shows that this behavior (without any metering compensation) is observed in practice. Estimates of the volume of fuel in the puddle (for a 5-liter V-8 engine) are of order 1000 mm^3, and increase with increasing load and speed. The time constant is of order 1 second for a fully warmed-up engine; it varies with engine operating conditions and is especially sensitive to the puddle, and therefore wall temperature. Such models have been used primarily to develop fuel metering strategies which compensate for the fuel transport lag.[23] Since the valve head and port wall temperatures differ significantly and warm-up at different rates, these puddles or *x* − τ models need additional sophistication and substantial calibration.

© McGraw-Hill Education. All rights reserved. Any use is subject to the Terms of Use, Privacy Notice and copyright information.

Figure 7.24 Schematic of x − τ transient fuel spray and puddle model indicating how a fraction (x) of the injected fuel in the spray $(\dot{m}_f)$ *impacts the port and valve head surfaces forming a "puddle" before entering the cylinder:τ is the average fuel residence time in the puddle.*

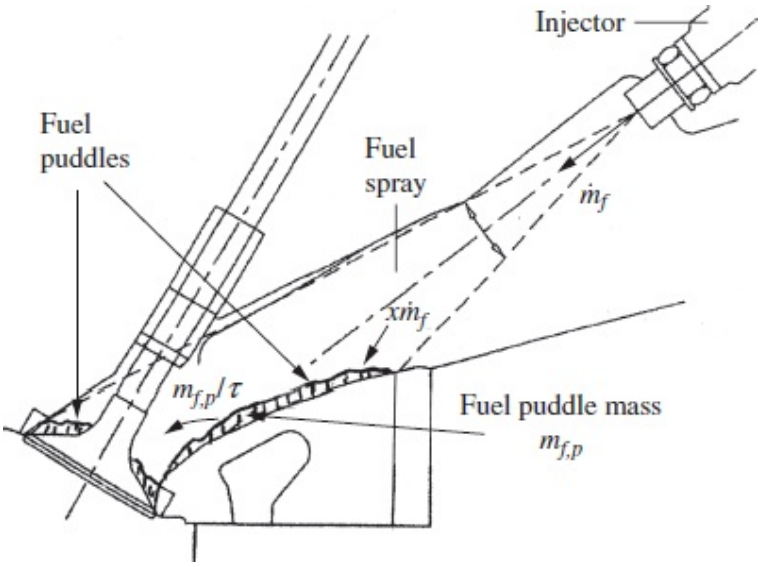
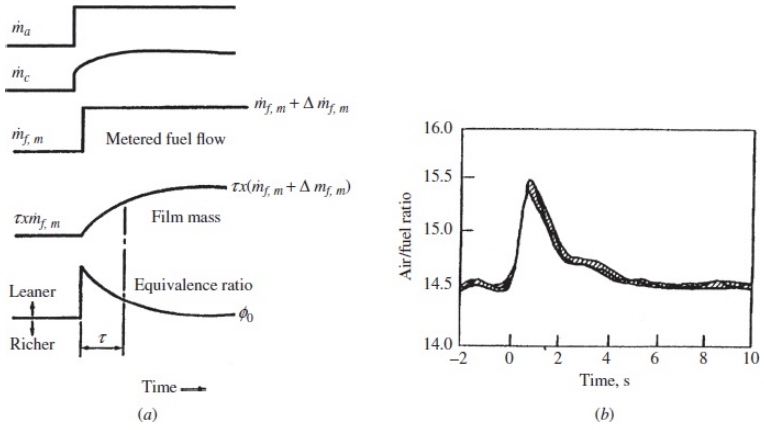


Figure 7.25 (a) Predicted behavior of the fuel film for an uncompensated step change in engine operating conditions. (b) Observed variation in air/fuel ratio for an uncompensated throttle opening at 1600 rev/min which increased manifold pressure from 48 to 61 cmHg.[23]



With these multipoint port fuel-injection systems, the fuel transport processes can be summarized as follows: the air flow to each cylinder depends on throttle open angle, engine speed, geometric details of the intake manifold and port design, and valve timing and lift. Because the manufacture and operation of individual fuel injectors are not identical, there is some variation in fuel mass injected cylinder-to-cylinder and cycle-to-cycle. Since individual cylinder airflows depend on the design of the manifold, whereas the amount of fuel injected does not, uniform air distribution is especially important with these port injection systems. The fuel vaporization and transport processes depend on the duration of injection and the timing of injection pulse(s) relative to the intake valve-lift profile. Much of the injected fuel will impinge on the port walls, valve stem, and the valve head, especially when injection toward a closed intake valve occurs. Backflow into the intake port of hot residual gases at part-load operation will have a significant effect on fuel vaporization. Compensation for fuel lag during transient engine operation is still required; sudden throttle openings are accompanied by a "lean spike" in the mixture delivered to the engine unless fuel compensation—injection of additional fuel—is utilized. Thus wall wetting, evaporation of liquid fuel off the walls, and liquid flow along these walls are all likely to be important components of the mixture preparation process.

© McGraw-Hill Education. All rights reserved. Any use is subject to the Terms of Use, Privacy Notice and copyright information.

With port fuel-injection systems, some liquid fuel does enter the cylinder, and droplets are present in the cylinder during intake and compression. Measurements made of the distribution, size, and number density of these in-cylinder fuel droplets indicate that during intake with open-valve fuel injection, the droplet number density in the clearance volume increased to a maximum at the end of injection (injection lasted from 45 to 153° ATC) and then decreased due to evaporation during compression to a very small value at the time of ignition. Average in-cylinder droplet size during intake was 10 to 20 μm in diameter; it increased during compression as the smaller drops in the distribution evaporated. At the conditions tested, some 10 to 20% of the fuel was in droplet form at the end of injection. At ignition, the surviving droplets contained a negligible fraction of the fuel. During injection, the distribution of droplets across the clearance volume was non-uniform. It became much more uniform with time, after injection ended.[24]

© McGraw-Hill Education. All rights reserved. Any use is subject to the Terms of Use, Privacy Notice and copyright information.

7.7. DIRECT FUEL INJECTION

7.7.1. Overview of Direct-Injection Approaches

Direct-injection of gasoline (or another liquid fuel) into the cylinders of a spark-ignition engine offers several advantages. The two primary operational advantages of DI are first, that the fuel goes directly into the combustion chamber (the cylinder) where it will be burned (see Fig. 7.2); second, the fuel distribution within the cylinder can be controlled and *stratified* by mixing the injected fuel with only part of the in-cylinder air, and confining the fuel-air mixture to a specific region of the combustion chamber. The first of these advantages allows more rapid and precise control of mixture preparation as engine operating requirements change since the fuel transport delay from the intake port into the cylinder with port fuel injection (Sec. 7.6.2) is removed. Better engine-in-vehicle drivability results. The second opportunity allows the engine to operate fuel lean overall, like a diesel—at least at part-load—while maintaining an easily combustible close-to-stoichiometric fuel-vapor air mixture in the proximity of the spark plug.

Secondary benefits follow from these. Fuel vaporization within the air charge in the cylinder cools the charge, allowing higher compression ratios to be used since that cooling delays the onset of knock. It also results in the engine inducting more air thereby increasing WOT torque. Tighter control of mixture preparation, and especially stratified overall-lean operation, improve the engine's specific fuel consumption (as does the higher compression ratio). Thus, direct fuel injection offers increased output, higher fuel conversion efficiency, though at higher fuel-system cost.

Early efforts to develop direct-injection spark-ignition engines go back many decades. The primary objective then was stratified operation, and even a multi-fuel operating capability: see Sec. 1.7.4. With the fuel injection technology then available, and our much more limited understanding of fuel spray behavior, these efforts were not successful. Improvements in fuel injection technology and our knowledge of and capability for analyzing in-cylinder flows, spray behavior, ignition, and combustion, have resulted in production direct-injection gasoline engines being developed and marketed in the late 1990s.[25, 26, 27] These engines operated stratified (lean overall) at low- to mid-loads and transitioned to operation with a homogeneous stoichiometric fuel-vapor air mixture at mid- to higher-loads. Stratified operation requires fuel injection to occur during the latter part of the engine's compression stroke (*late injection*) to restrict the extent of fuel-air mixing that occurs. The homogeneous stoichiometric operating mode requires *early injection*, during the intake stroke, to allow as much time as possible for more complete fuel-air mixing. Direct-injection applications have focused more on homogeneous (stoichiometric) operation with early fuel injection since the very high effectiveness of the three-way catalyst technology[1] makes this an exceptionally low emissions DI engine concept with superior fuel economy. DI engines also offer significant additional benefits when turbocharged. While stratified DI engine concepts do offer enhanced fuel consumption at lighter loads, developing highly effective lean-
NO_x catalysts is challenging: see Sec. 11.6.3. These two DI classifications—homogeneous and stratified—are now widely used. Extensive discussion of GDI spark-ignition engines can be found in Zhao et al.,[28] and Ando and Acroumanis.[29]

7.7.2. DI Mixture Preparation Processes

The fuel-air mixture preparation processes in direct-injection spark-ignition engines connect with the engine's ignition and combustion processes in a much more detailed way than with port fuel injection into the intake. The reasons are obvious: the mixture preparation takes place within the same space (the cylinder) where combustion will occur, and the time available for mixing is shorter. The fuel drops within the injected spray must be dispersed appropriately (throughout the full combustion chamber with homogenous operation—in a specific region of the combustion chamber with stratified operation). The drops must vaporize rapidly and should not impinge significantly on the chamber walls. The in-cylinder flow, which is generated by the details of the flow past the intake valve head and seat, and then the cylinder head and piston crown geometry, must

© McGraw-Hill Education. All rights reserved. Any use is subject to the Terms of Use, Privacy Notice and copyright information.

enhance this droplet distribution and vaporization, and the fuel-vapor, air, residual, and EGR (if used) mixing processes to achieve the desired homogeneous or stratified mixture objective.

The factors involved in these two DI mixture preparation processes—homogeneous and stratified—are the following: the desired mixture composition (its stoichiometry), the fuel injector and injection timing details, the geometry of the combustion system—injector location and orientation, nozzle design, intake generated in-cylinder flow (tumble or swirl), cylinder head and piston crown geometry (e.g., bowl-in-piston shape for stratified operation), spark plug gap location. Several of these vary with engine load and speed; satisfactory mixture preparation must be achieved over the full engine operating range.

Table 7.3 summarizes the commonly made choices for these several mixture preparation factors for the two different DI applications: homogeneous and stratified engine operation. Note that when the stratified mixture approach is used at part-load, this requires homogeneous operation at higher-loads (and speeds). Most of the development and design effort has focused on direct-injection engines with gasoline fuel (which may contain some 10% ethanol): DI ethanol (or E85) fueled engines are also an option. With homogeneous mixture combustion where creation of a relatively uniform fuel-air mixture is the objective, a convenient injector location is below the intake ports. With a wide-angle spray and a tumbling[2] in-cylinder motion, good fuel dispersion, vaporization, and mixing can be achieved. Fuel injection during the mid-portion of the intake stroke provides adequate mixture preparation time and holds liner and piston wetting with liquid fuel to a minimum. With homogeneous-charge engine operation, other engine processes are similar to those with port fuel injection (except for the in-cylinder evaporative cooling of the charge with DI; see below).

Table 7.3 Major mixture preparation features of homogeneous and stratified direct-injection SI engines

Feature	Homogeneous mixture	Stratified mixture
Load/speed range	Full load and speed range	Part-load, low- to mid-speed
Nat. asp./turbo	Both	Both: but only at part-load
Stoichiometry	Stoichiometric *A/F*	Lean overall: locally close-to-stoichiometric
Mixture preparation approach	Early injection: mid-intake stroke Wide spray dispersion: uniform mixture	Late injection: mid to late compression stroke. Confined mixture cloud around spark plug
Fuel injector: Location	Usually below the intake ports	Below intake ports (wide spacing); or close to spark plug (narrow spacing)*
Design	Usually multi-hole nozzle with wide spray angle	Various designs to fit with stratified combustion approach
Fuel supply pressure (MPa)	5–15	5–20
Airflow	Tumble, to improve fuel-air mixing and realize faster combustion	Specific airflow (tumble or swirl) to match with spray and bowl-in-piston geometry
Piston geometry	Close to conventional piston crown design	Specific bowl-in-piston to direct and confine developing fuel spray
Emission control approach	Spark retard (cold start), EGR, three-way catalyst	Spark retard (cold start), lean with EGR, lean-NO_x storage catalyst
*Wide or narrow spacing refers to injector nozzle to spark plug spacing: see text.		

With stratified charge operation, the injector nozzle and spark-plug locations, the fuel injection details, the combustion chamber geometry, and the in-cylinder airflow are all key components of the various combustion approaches used. These are

© McGraw-Hill Education. All rights reserved. Any use is subject to the Terms of Use, Privacy Notice and copyright information.

often grouped into three air and fuel flow mixture preparation categories: wall-guided, air-guided, and spray-guided. In practice, two basic approaches have evolved: (1) where the injector nozzle and spark plug are *widely spaced*; (2) where these two components are *closely spaced*. See Fig. 7.26. These sketches illustrate in (*a*) how, with widely spaced injector nozzle and spark plug, both wall-guiding with a specially shaped piston crown combined with air-guiding (e.g., tumble) are used to create the desired fuel spray behavior—an approximately stoichiometric fuel-vapor/air mixture cloud that arrives at the spark plug by time of ignition. In Fig. 7.26*b*, the spark plug electrodes are placed within the developing fuel spray: it is the spray behavior (guiding) that brings a combustible mixture to the spark plug location at the time of ignition.

Figure 7.26 Two major categories of mixture preparation for ignition and combustion used in direct-injection stratified-charge SI engines: (a) widely spaced injector and spark plug (wall- and air-guided); (b) closely spaced injector and spark plug (spray-guided).[7]

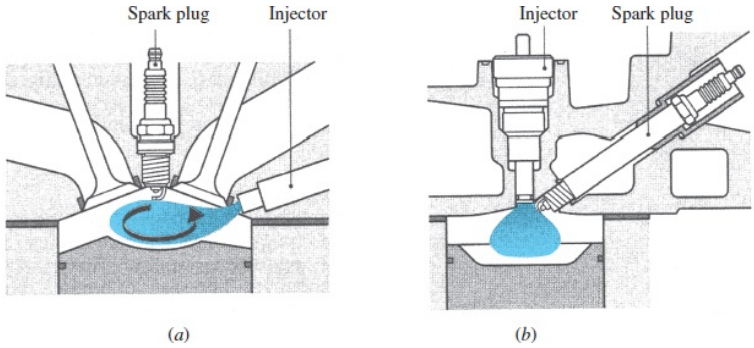
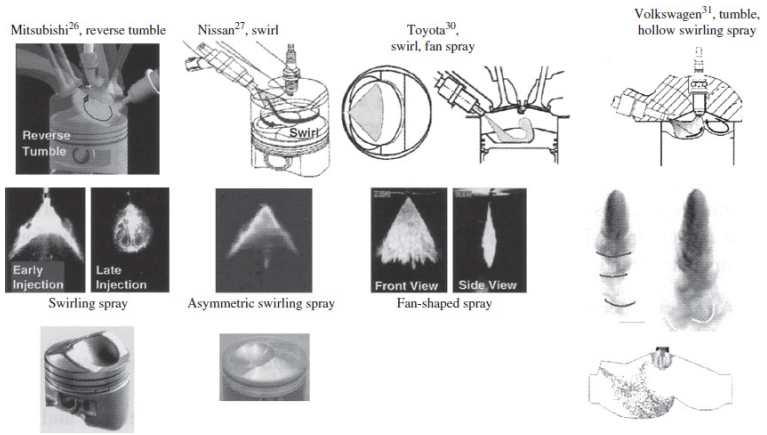


Figure 7.27 shows four different examples of production wall- and air-guided, widely spaced, stratified DI engine concepts. One can see how the piston crown shape, air flow, and fuel spray characteristics all combine to enable a stable (fast and repeatable) spark-ignited combustion process.

Figure 7.27 Examples of stratified air- and wall-guided gasoline direct-injection engines showing their combustion chamber geometries, airflow patterns, and fuel spray coinfigurations.[26, 27, 29, 30, 31]



Note that with lean operation at part-load, the engine intake will be less throttled than with stoichiometric operation, at a given torque. While slightly less fuel is required to produce the torque when lean because the engine is more efficient, significantly more airflow is required. Thus the intake manifold pressure when operating lean at a given torque is higher, and the pumping work (negative at part-load) is reduced. This is one of several factors that make lean engines at part-load more efficient.

An important feature of DI mixture preparation is the charge cooling that occurs due to the in-cylinder evaporation of the fuel droplets as the fuel spray moves through the chamber. By drawing the thermal energy required to vaporize the liquid fuel from the in-cylinder gases, these gases are cooled significantly. If the liquid fuel is at a lower temperature than the in-cylinder charge, then there is a fuel heating process involved, as well, but that produces a relatively small change in charge

© McGraw-Hill Education. All rights reserved. Any use is subject to the Terms of Use, Privacy Notice and copyright information.

temperature. The mixture temperature change produced by the vaporization of liquid fuel drops embedded in an air plus residual gas mass (with both fuel and charge initially at the same temperature) is given by:

$$\Delta T = \frac{m_f}{(m_a + m_f)} \frac{h_{fg}}{c_p}(1 - x_r)$$

(7.14)

where liquid and vapor fuel heating (or cooling)—a less than 10% effect—has been neglected. Values for ΔT for gasoline, ethanol, an ethanol water mixture, and methanol are given in Table 7.4. These charge cooling effects are substantial: approximately 20 deg C for gasoline and 100 deg C or so for the alcohols. Adding 20% water to ethanol, using an expanded version of Eq. (7.14), with h_{fg} for water 2442 kJ/kg, increases the ethanol evaporative cooling impact by about 50%.

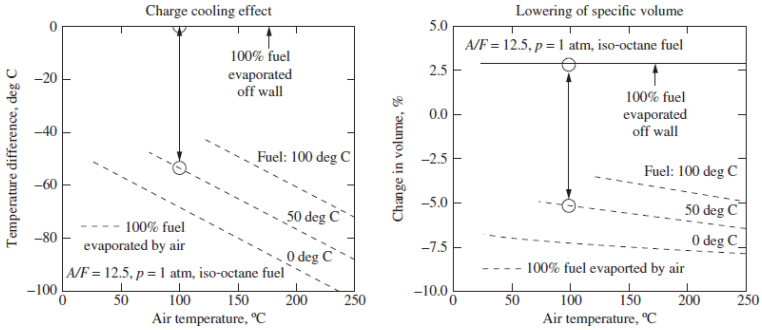
Table 7.4 Evaporative cooling effects of fuel drops in stoichiometric mixtures of liquid SI engine fuels

Fuel	$(A/F)_s$	h_{fg} kJ/kg	$h_{fg}/Q_{HV} \times 10^3$	ΔT cooling deg. C*
Gasoline	14.6	350	8.0	19
Ethanol	9.0	910	30	82
Ethanol/water	20% (H_2O)	2442 (H_2O)	52	123
Methanol	6.47	1100	49	132
*From Eq. (7.14): c_p (mixture) ≈ 1.06 kJ/kg·K, x ≈ 0.05.				

Charge cooling during the intake process affects the amount of air inducted by increasing the density of the in-cylinder charge. Figure 7.28 shows the effect of several variables on the charge cooling temperature difference (at TC, at the end of the compression stroke), and the change in specific volume (inverse of the density) of the in-cylinder mixture at the end of intake. The solid arrow shows the spread from all the fuel vaporizing off the combustion chamber (or intake port and valve walls) at the top, to 100% of the fuel evaporated by heat transfer with the air.[3] Experimentally based efforts to quantify actual charge cooling with various fuels indicate that the fraction of the maximum or ideal ΔT shown in Table 7.4 achieved is above 80% for gasoline DI engine operation (in a turbocharged engine operating at stoichiometric) and 60 to 70% for E85 DI operation.[32] This DI fuel-evaporation charge cooling effect also impacts the onset of knock, and therefore the engine's compression ratio. Lower charge temperatures at the start of compression lead to lower unburned mixture temperatures at spark and at the crank angle of maximum cylinder pressure—the mixture conditions at which combustion onset and knock onset occur, respectively. Thus the onset of knock is delayed, and a higher engine compression ratio and engine turbocharging with higher boost can be used to increase engine output and, with engine downsizing, increase efficiency. Note also that use of alcohol and alcohol/gasoline blends give significant additional knock suppression beyond gasoline alone, an approach that can be realized with two separate tanks on the vehicle, or with the separation of the high octane fuel species (e.g., ethanol) through on-board separation of the fuel into higher and lower octane components.

© McGraw-Hill Education. All rights reserved. Any use is subject to the Terms of Use, Privacy Notice and copyright information.

Figure 7.28 Mixture temperature reduction (at TC of compression), and decrease in the in-cylinder gas-mixture specific volume at the end of the intake process, as a function of initial air and fuel temperature, for 100 and zero percent fuel evaporation off the walls. A/F = 12.5, p = 1 atm, isooctane fuel.[33]



Note that when fuel evaporation within the cylinder occurs during the closed valve portion of the compression stroke, its impact on charge temperature increases. Fuel that then evaporates, e.g. (Δm_f), causes a temperature change proportional to $(\Delta m_{f,v} h_{fg}/c_v)$ rather than $(\Delta m_{f,v} h_{fg}/c_p)$ which quantifies the impact at constant pressure during the intake process. The ratio of c_p/c_v for the air, residual, fuel vapor charge is about 1:35.

7.7.3. DI Engine System and Components

Figure 7.29 shows a schematic of the overall engine management system for a direct-injection turbocharged gasoline engine.[34] Air enters the system via the air flow meter and turbocharger compressor, upper right. Exhaust gases leave the engine, moving right from the center, and exit via the turbine/wastegate combination, oxygen sensors, and catalysts at lower right. The mixture preparation components determine the air mass flow (compressor-intercooler/manifold pressure, electronic throttle, manifold/port swirl control valve, cam phaser for intake valve timing control) and the fuel flow (in-tank fuel pump, fuel rail, high-pressure pump, fuel-injection pressure-regulator, direct fuel injector). The engine's electronic control unit determines the fuel mass required based on the desired torque and the corresponding required air mass (based on the intended stoichiometry of the mixture—stratified or homogeneous). The exhaust gas oxygen sensors monitor the exhaust gas mixture's relative air/fuel ratio (normally stoichiometric or lean if operating stratified). The boost pressure required for the airflow is controlled by the wastegate (through the amount of exhaust gas flow it bypasses around the turbine). The mixture preparation management system in these automotive applications, therefore, sets the fuel and air charge required for the desired engine output, generates the necessary fuel injection pressure, defines the start of injection, meters the required fuel quantity for that accelerator pedal and throttle setting, and introduces that fuel into the cylinder in the appropriate way. This sets up the fuel, air, residual gas (and EGR, not shown in Fig. 7.29) mixture within the cylinder both overall and especially at the spark location to achieve a stable low-emission combustion process.[7]

© McGraw-Hill Education. All rights reserved. Any use is subject to the Terms of Use, Privacy Notice and copyright information.

Figure 7.29 Layout schematic of DI engine management system.[34]

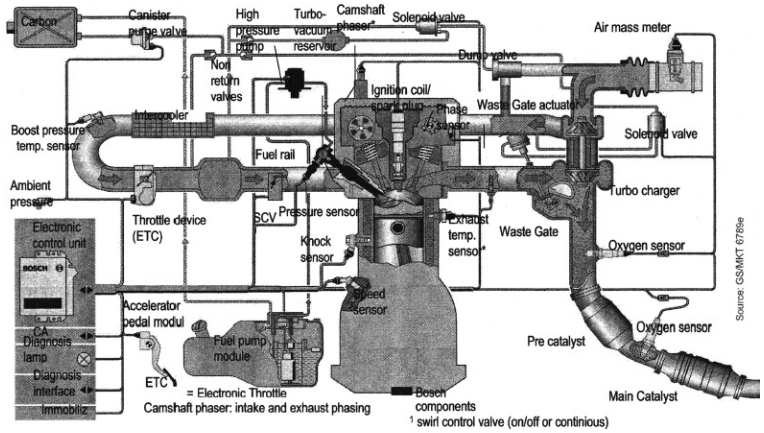
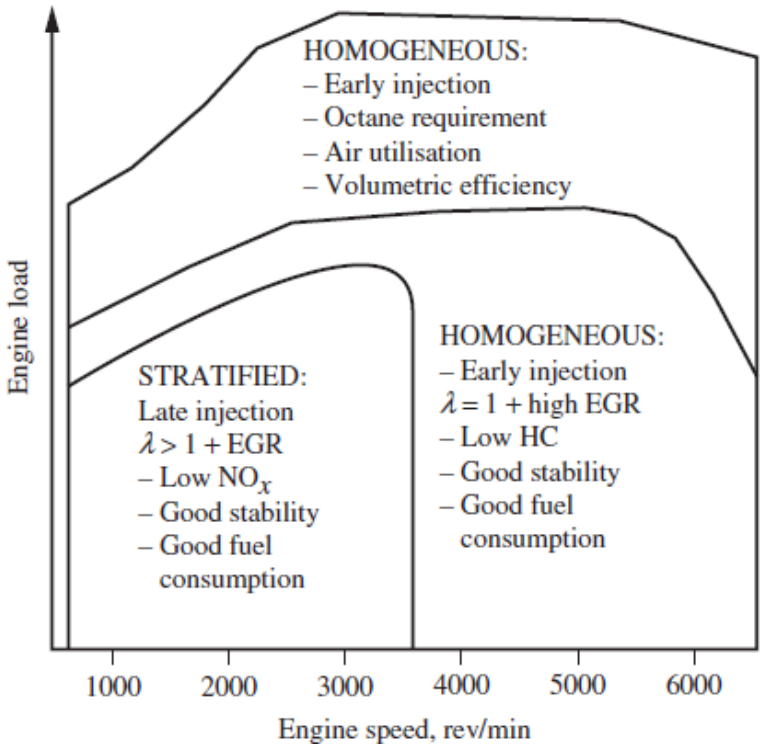


Figure 7.30 shows the normal mixture preparation objectives of this DI management system on an engine load and speed map for stratified DI operation and lean overall, at part-load and low- to mid-speed, and homogeneous mode operation at higher loads. The vertical scale is load or bmep or normalized torque. The relative air/fuel ratio λ is shown in each region. While the exact boundaries between these regions may vary, engine concept to engine concept, this use of stratified and homogeneous operation, the values of λ and EGR in each mode, and the reasons for and impacts of these choices, are typical.

Figure 7.30 Typical stratified GDI engine operating map showing the different operating regimes.[35]



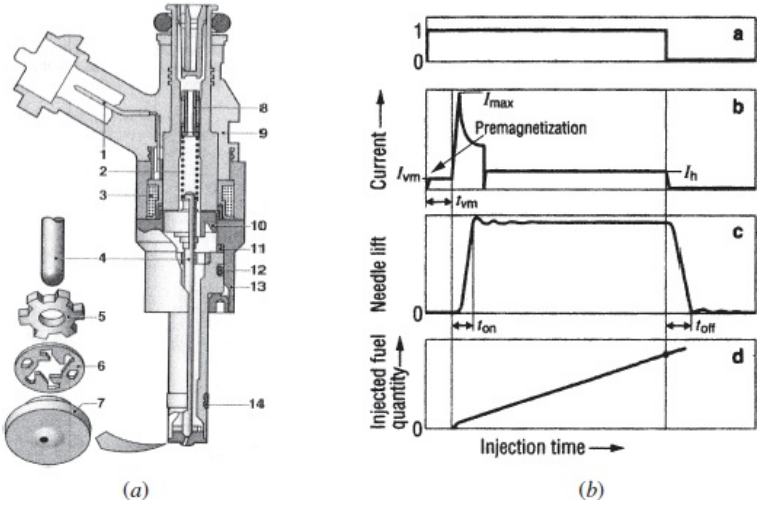
7.7.3.1. Nozzle Designs and Spray Characteristics

Fuel injectors have been specifically developed for the higher pressures required for GDI spark-ignited engines. The injected liquid fuel must be atomized into small droplets and appropriately dispersed throughout the appropriate region of the cylinder or combustion chamber. For homogeneous operation, a uniform distribution within the cylinder is desired: for stratified operation the spray must provide a readily ignitable mixture in the vicinity of the spark plug, and within a restricted volume. A

© McGraw-Hill Education. All rights reserved. Any use is subject to the Terms of Use, Privacy Notice and copyright information.

close-to-stoichiometric mixture region is necessary for stable ignition and combustion. An example of a swirl-type injector, a commonly used high-pressure DI injector, is shown in Fig. 7.31*a* along with the signals that activate the fuel injection, Fig. 7.31*b*. The fuel is forced by the swirl guide to rotate about the needle axis so that it exits the nozzle with a swirling motion. This use of a swirling motion decreases the drop size and helps disperse the spray. Such a swirl-type injector was used in two of the stratified DI engines shown in Fig. 7.27. The quantity of fuel injected depends on the difference between the fuel rail pressure and the in-cylinder gas pressure, and on the needle open time. A short needle opening and closing time is necessary for the desired metering precision. To achieve this, the injector is triggered by a digital signal, which the injector driver stage uses to activate the injector armature and needle, with a high initial current pulse to open the injector rapidly. The modest delays involved, and the needle opening and closing times, are included in the control logic.

Figure 7.31 (a) High-pressure DI fuel injector layout diagram: (1) Electrical connection; (2) Spring; (3) Coil; (4) Nozzle needle; (5) Guide washer; (6) Swirl plate; (7) Seat washer; (8) Adjusting nozzle; (9) Housing; (10) Solenoid armature; (11) Shim; (12) O-ring; (13) Valve housing; (14) Teflon ring. (b) Signal profiles for activating the injector: (a) Triggering signal calculated by ECU; (b) Injector current; (c) Needle lift; (d) Amount of fuel injected.[7] (Courtesy Robert Bosch GmbH and SAE.)



Other types of injector designs are used. Multi-hole nozzles and outward-opening pintle nozzles are two significantly different injector designs and are illustrated in Fig. 7.32. Also shown in that figure are photographs of the fuel sprays each of these injectors—swirl-type, outward opening pintle, and multi-hole nozzles—produce. Swirl-type fuel injectors have been widely used in stratified systems where wall and flow spray guiding are utilized in combination. Variations in injection pressure cause the dispersion angle of the spray to change which can prove useful in transitioning from the narrower spray required for stratified operation to the wider spray required for homogeneous operation. Multi-hole nozzles, and outward-opening pintle nozzles, produce clearly defined spray boundaries (Fig. 7.32) and thus are good candidates for spray-guided stratified DI systems. Figure 7.33 illustrates the injector, fuel spray, and spark plug locations for a multi-spray nozzle, and an outward-opening swirl nozzle for such spray-guided DI mixture preparation and combustion systems. The spark-plug electrodes are located just within the fuel spray boundary where the local relative fuel-vapor air mixture is close to the stoichiometric composition so that ignition and flame development occur rapidly.

© McGraw-Hill Education. All rights reserved. Any use is subject to the Terms of Use, Privacy Notice and copyright information.

Figure 7.32 Three types of high-pressure injector nozzles and the spray patterns they generate: (a) swirl nozzle; (b) outward opening nozzle; (c) multi-hole nozzle.[29]

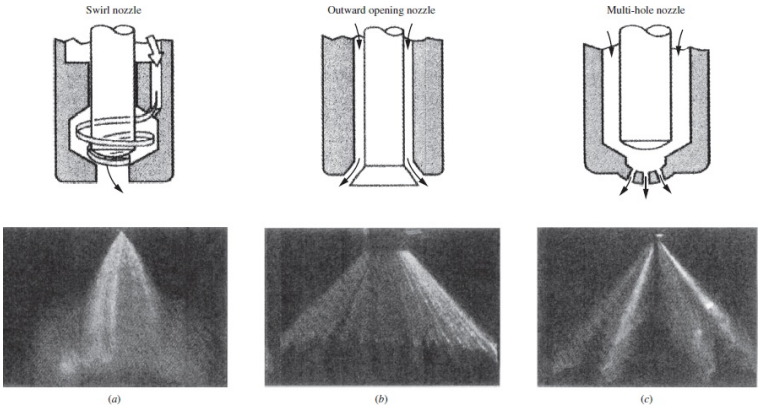
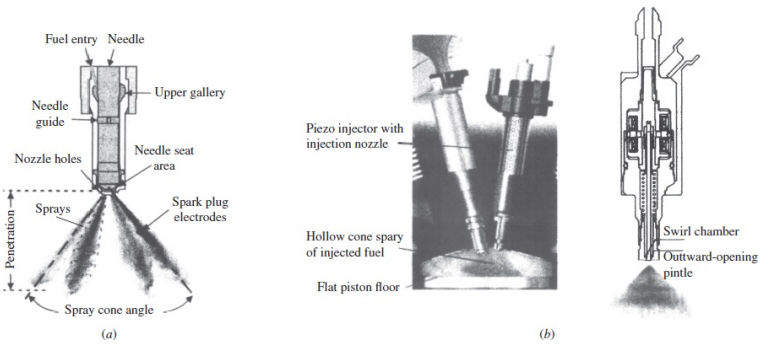


Figure 7.33 (a) Multi-hole injector for spray-guided gasoline direct-injection engine, with its several fuel sprays. (b) Outward-opening pintle injector with swirl chamber nozzle with its wide hollow-cone spray.[29]



[1] Three-way catalyst technology can reduce the three gaseous gasoline engine air pollutants HC, CO, and NO_x to extremely low levels (≈ 98% removal) when the engine is operated stoichiometric.

[2] See Sec. 8.4.

[3] Note that with port fuel injection, if droplets enter the cylinder and evaporate by taking thermal energy from the in-cylinder gases there will be some charge cooling.

© McGraw-Hill Education. All rights reserved. Any use is subject to the Terms of Use, Privacy Notice and copyright information.

7.8. EXHAUST GAS OXYGEN SENSORS

It is possible to reduce engine emissions of the three gaseous pollutants—hydrocarbons, carbon monoxide, and oxides of nitrogen—with a single catalyst in the exhaust system if the engine is operated at close to the stoichiometric air/fuel ratio. Such systems (a three-way catalyst and closed-loop sensor) are described in more detail in Sec. 11.6.3. The engine operating air/fuel ratio is maintained close to stoichiometric through the use of a sensor in the exhaust system, which provides a voltage signal dependent on the oxygen concentration in the exhaust gas stream. This signal is the input to a feedback system, which controls the fuel and air feeds to the engine's cylinders.

The sensor, called an oxygen or lambda sensor—λ being the symbol used for the relative air/fuel ratio, Eq. (3.9)—uses as its basis an electrolytic cell with a solid electrolyte through which at elevated temperatures the current is carried by oxygen ions. The electrolyte is yttria (Y_2O_3) stabilized zirconia (ZrO_2) ceramic which separates two gas-containing regions (the exhaust manifold and the atmosphere), which have different oxygen partial pressures. The cell can be represented as a series of regions, separated by interfaces as follows:

Exhaust	Metal	Ceramic	Ceramic	Air
p'_{O_2}	M_e	ZrO_2, Y_2O_3	M_e	p''_{O_2}

p''_{O_2} is the oxygen partial pressure of the air (≈ 20 kN/m^2) and
p'_{O_2} is the equilibrium oxygen partial pressure in the exhaust gases. At elevated temperatures, an electrochemical reaction takes place at the metal electrodes:

$$O_2 + 4M_e \rightleftharpoons 2O^{2-}$$

and the oxygen ions transport the current across the cell. The open-circuit output voltage of the cell V_0 can be related to the oxygen partial pressures
p'_{O_2} and
p''_{O_2} through the Nernst equation:

$$V_0 = \frac{RT}{4F} \ln \left(\frac{p''_{O_2}}{p'_{O_2}} \right)$$

(7.15)

where F is the Faraday constant. Equilibrium is established on the exhaust gas side electrode by the catalytic activity of the platinum catalyst on the metal electrode. The oxygen partial pressure in equilibrated exhaust gases decreases by many orders of magnitude as the equivalence ratio changes from 0.99 to 1.01, as shown in Fig. 7.34*a*. Thus the sensor output voltage increases rapidly in this transition from a lean to a rich mixture at the stoichiometric point, as shown in Fig. 7.34*b*. Since this transition is not temperature dependent, it is well suited as a sensor signal for a feedback system.

© McGraw-Hill Education. All rights reserved. Any use is subject to the Terms of Use, Privacy Notice and copyright information.

Figure 7.34 Oxygen-sensor electrolytic cell operating characteristics. Variation as a function of relative air/fuel ratio and temperature of: (a) oxygen partial pressure in equilibrated combustion products and (b) sensor output voltage.[36]

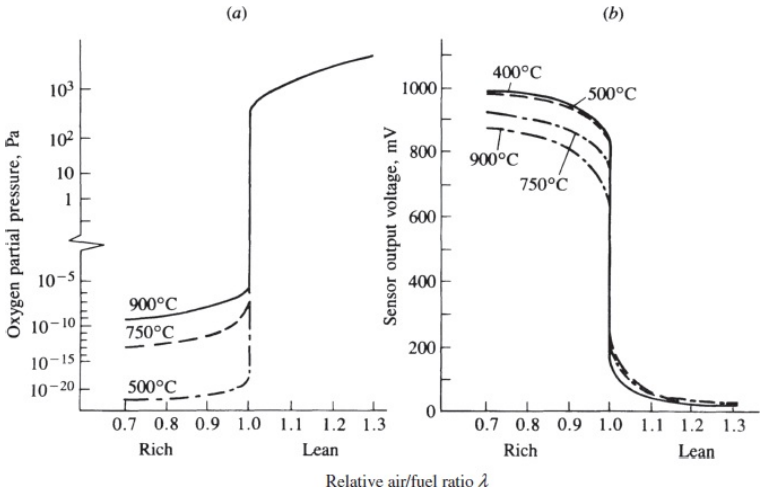
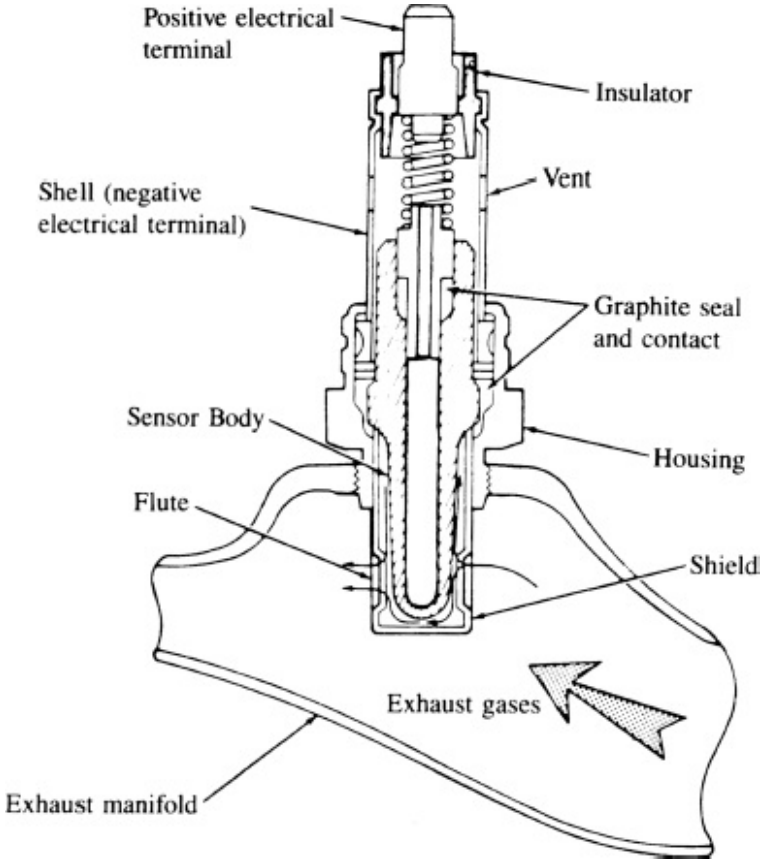


Figure 7.35 shows a cross-section drawing of simple lambda sensor, screwed into the wall of the exhaust manifold. The senor is electrically heated to provide rapid warm-up, following engine start-up. A close to the exhaust port location gives the shortest flow time from the fuel injector location (upstream of the engine) to the sensor—a delay time which is important in the operation of the feedback system. The sensor is made of ZrO_2 ceramic stabilized with Y_2O_3 to give adequate electrical conductivity. The inner and outer electrodes are 10-μm thick porous platinum layers to provide the required catalytic equilibration. The outer electrode which is exposed to the exhaust gases is protected against corrosion and erosion by a 10-μm spinal coat and a slotted shield. Air passes to the inner electrode through holes in the protective sleeve. The protective sleeve and housing are made from heat- and corrosion-resistant steel alloys. Such sensors were first developed for air/fuel ratio control close to the stoichiometric value.

© McGraw-Hill Education. All rights reserved. Any use is subject to the Terms of Use, Privacy Notice and copyright information.

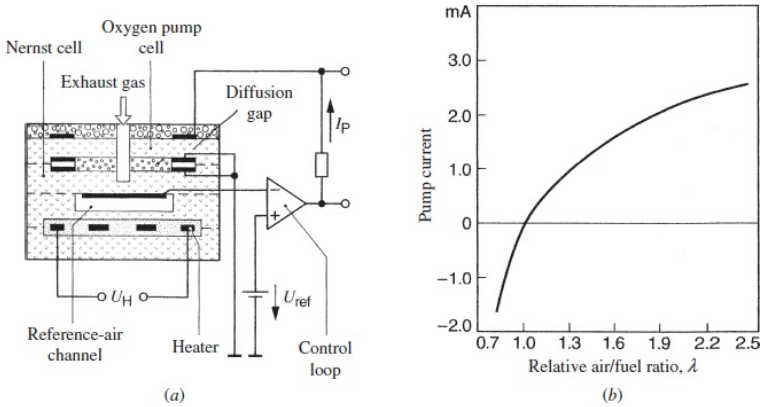
Figure 7.35 Cross-section drawing of exhaust oxygen (lambda) sensor.[37]



Wide-range lambda sensors are used when fuel lean or fuel rich measurement of exhaust gas relative air-fuel ratio is required. Wide-band sensors combine the conventional exhaust gas oxygen sensor described above, with a second such sensor operating as an oxygen pump. Figure 7.36*a* shows a schematic of such a sensor and its electrical circuit. The oxygen pump cell (at the top) is paired with an exhaust gas oxygen concentration (Nernst) cell beneath it, on either side of a diffusion gap to which exhaust gas is supplied. If the exhaust gas in the diffusion gap is not stoichiometric, a current I_p is passed through the oxygen pump cell, driven by an applied voltage difference in the appropriate direction, to either transfer oxygen atoms out of or into the gas in the diffusion gap, depending on whether the gas is lean or rich, to bring it to the stoichiometric composition (as detected by the Nernst cell, relative to its reference-air cell just below it, with its constant 21% oxygen concentration). An electrical heater is mounted underneath these sensing elements to heat and then control the temperature of the sensor. The response (pump current) to restore the exhaust gas relative air/fuel ratio λ to stoichiometric, versus λ, is shown in Fig. 7.36*b*. Such wide-band exhaust gas oxygen sensors are important in any lean stratified DI engine concepts. They can also be used in diesels.

© McGraw-Hill Education. All rights reserved. Any use is subject to the Terms of Use, Privacy Notice and copyright information.

Figure 7.36 (a) Schematic of wide-range exhaust oxygen (lambda) sensor. (b) Sensor signal (pumping current) as a function of lambda.[7]



For closed-loop feedback control at close-to-stoichiometric engine operation, use is made of the sensor's low-voltage output for lean mixtures and high-voltage output for rich mixtures in the following way. A control voltage reference level is chosen at about the mid-point of the steep transition in Fig. 7.37*b*. In the ECU the sensor signal is compared to the reference voltage in the comparator as shown in Fig. 7.37*a*. The comparator output is then integrated in the integral controller whose output varies the fuel quantity linearly in the opposite direction to the sign of the comparator signal. There is a time lag τ_L in the loop composed of the transport time of fuel-air mixture from the point of fuel admission in the intake system to the sensor location in the exhaust, and the sensor and control system time delay. Because of this time lag, the controller continues to influence the fuel flow rate in the same direction, although the stoichiometric reference point has been passed, as shown in Fig. 7.37*b*. Thus, oscillations in the relative air/fuel or fuel/air equivalence ratio delivered to the engine exist even under steady-state conditions of closed-loop control. This behavior of the control system is called the *limit cycle*. The frequency *f* of this limit cycle is given by

$$f_{\mathrm{LC}} = \frac{1}{4\tau_{\mathrm{L}}}$$

(7.16)

and the change in equivalence ratio, peak-to-peak, is

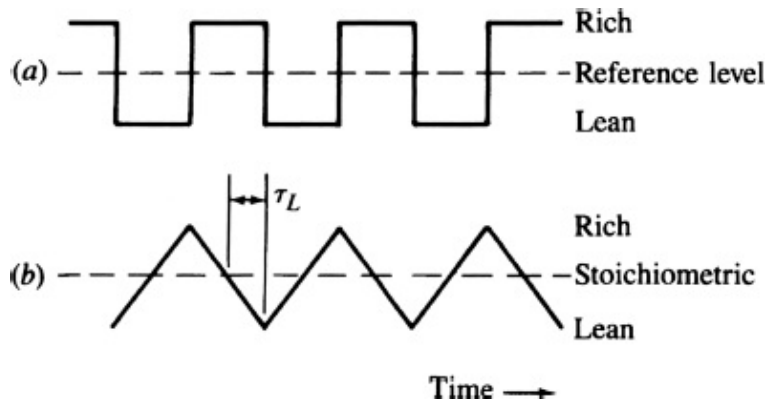
$$\Delta\phi = 2K_{\tau L}$$

(7.17)

where *K* is the integrator gain (in equivalence ratio units per unit time).

© McGraw-Hill Education. All rights reserved. Any use is subject to the Terms of Use, Privacy Notice and copyright information.

Figure 7.37 Operation of electronic control unit for closed-loop feedback: (a) sensor signal compared with reference level; (b) controller output voltage—the integrated comparator output.[38]



Depending on the details of the three-way catalyst used for cleanup of the three pollutants CO, HC, and NO_x in the exhaust, the optimum average equivalence ratio may not be precisely the stoichiometric value. Furthermore, the reference voltage for maximum sensor durability may not correspond exactly to the stoichiometric point or the desired catalyst mean operating point. While a small shift (~ ± 1%) in operating point from the stoichiometric can be obtained by varying the reference voltage level, larger shifts are obtained by modifying the control loop to provide a steady-state bias. One method of providing a bias— asymmetrical gain rate biasing—uses two separate integrator circuits with different gain rates K^+ and K^- to integrate the comparator output, depending on whether the comparator output is positive (rich) or negative (lean). An alternative biasing technique incorporates an additional delay time τ_D so that the controller output continues decreasing (or increasing) even though the sensor signal has switched from the high to the low level (or vice versa). By introducing this additional delay only on the negative slope of the sensor signal, a net lean bias is produced. Introducing the additional delay on the positive slope of the sensor signal produces a net rich bias.[38]

Note that the sensor only operates at elevated temperatures. The sensor heater is used immediately after engine start-up to ensure that the feedback system operates as soon as possible to obtain the appropriate fuel-air mixture for satisfactory engine operation. Two lambda sensors are used in emission control systems with modern three-way catalysts, which contain *oxygen storage capability* through incorporating ceria onto the catalyst washcoat (see Sec. 11.6.3). A sensor upstream of the catalyst provides feedback control for the engine's mixture preparation system. The oscillations deliberately induced in the relative air/fuel ratio around the stoichiometric value (of about ± 0.3% of lambda at close to 1 Hz frequency), in the fuel-air mixture entering the engine, are used to ensure there is always sufficient oxygen stored in the catalyst to offset or absorb any random short-term rich or lean mixture excursions. With its oxygen storage capacity still effective, the three-way catalyst will absorb these fluctuations in λ and the catalyst exit burned gases will have an almost constant stoichiometric air/fuel ratio. The second oxygen sensor is thus positioned downstream of the catalyst to ensure its oxygen storage is functioning effectively since any oscillations are much reduced below the input λ oscillations. This second oxygen sensor is also used to improve the precision of the feedback signal obtained from the first sensor.

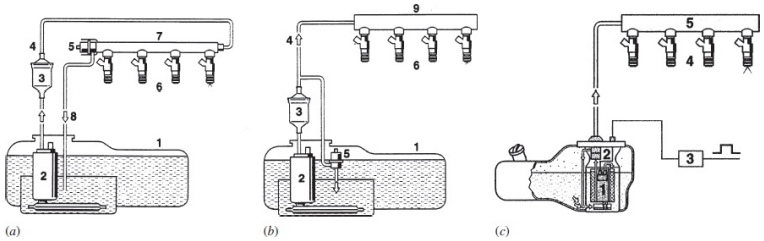
© McGraw-Hill Education. All rights reserved. Any use is subject to the Terms of Use, Privacy Notice and copyright information.

7.9. FUEL SUPPLY SYSTEMS

7.9.1.1. Port Fuel Injection

Fuel supply and delivery with intake-manifold injection have evolved through several stages. These are illustrated in Fig. 7.38. Two critical requirements for fuel supply systems are ensuring that adequate fuel is available to the injectors for any conceivable change in demand, and enabling high injection precision, both cylinder-to-cylinder and cycle-by-cycle. In what has been the standard system, Fig. 7.38*a*, under most operating conditions excess fuel was supplied to the fuel rail which operates at a constant pressure differential above the intake manifold pressure (controlled by the pressure regulator). Thus, adequate fuel was always available. The excess fuel supplied to the fuel rail was returned to the tank via a return line. One consequence of this fuel flow from the tank to the engine and back to the tank was fuel heating: the temperature of the fuel in the tank steadily rose creating problems with excessive hydrocarbon vapor pressures in the fuel supply system. Returnless fuel systems were developed (see Fig. 7.38*b*), where only the fuel required by the injectors was supplied to the fuel rail at the regulated pressure, and there is no return line to the tank from the rail. The additional fuel conveyed by the electric fuel pump returns directly to the tank without flowing to the engine compartment and back. This returnless system reduces the in-tank fuel temperatures by about 10 deg. C thus reducing fuel vaporization by approximately one-third.[7]

Figure 7.38 Fuel supply and delivery systems with manifold (port) fuel injection. (a) System with fuel return to tank. (b) Returnless system: (1) Fuel tank; (2) Electric fuel pump; (3) Fuel filter; (4) High-pressure line; (5) Pressure regulator; (6) Injectors; (7) Fuel rail, with return flow; (8) Return line; (9) Fuel rail, no return flow. (c) Demand-controlled system with no return line: (1) Electric fuel pump (with fuel filter); (2) Pressure relief valve and pressure sensor; (3) Timing module; (4) Injectors; (5) Fuel rail, no return flow.[2] (Courtesy Robert Bosch GmbH and SAE.)



The third intake-manifold injection system shown in Fig. 7.38*c*, the demand-controlled system, further reduces fuel heating and improves the precision of fuel metering. Here, the fuel pump only supplies the quantity of fuel actually required by the engine, and controls the fuel rail pressure by means of a closed control loop in the engine control unit. The fuel quantity the pump delivers is controlled by varying the pump's operating voltage. Adjustments which vary the fuel rail pressure can be used to aid with cold and hot engine starting, and to increase the dynamic range of the injector system by raising the pressure difference across the injector and thereby increasing the fuel flow rate (e.g., when the engine is operating turbocharged). Thus, the pressure difference across the injector is taken into account, along with injector open duration, in determining the quantity of fuel injected. This improves the precision of the fuel metering.

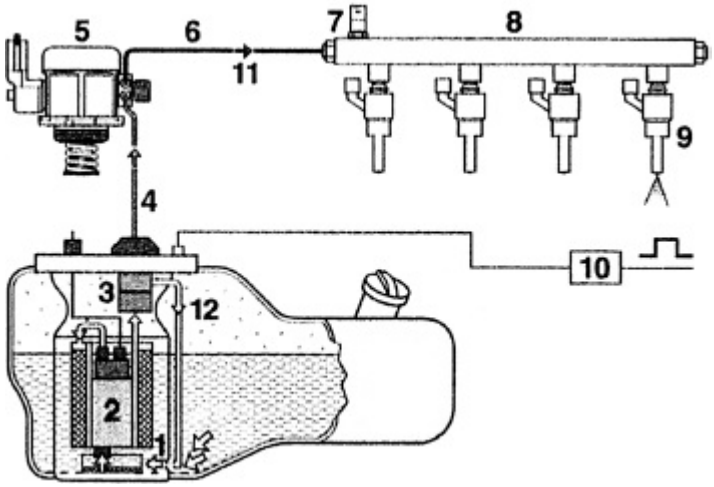
7.9.1.2. Direct Fuel Injection

With direct-injection spark-ignition engines, the liquid fuel (normally gasoline) must be injected at higher pressures since wide spray dispersion, deep spray penetration, and smaller drop sizes are required. Also, when operating stratified with late injection the in-cylinder pressure during injection can be several atmospheres. Note that the time available for injection is less than with port injection systems, so higher fuel flow rates are required.

© McGraw-Hill Education. All rights reserved. Any use is subject to the Terms of Use, Privacy Notice and copyright information.

The fuel system comprises a low-pressure system, which uses the same components and layout as the port-fuel-injection supply system, and a high-pressure system. The key elements of the high-pressure system are a high-pressure pump (5 to 15 MPa), a high-pressure accumulator (fuel rail), a high-fuel-pressure sensor, and a pressure control valve or limiter. Figure 7.39 shows one such system—a demand-controlled fuel supply and delivery system. Here the high-pressure pump only supplies the fuel rail with the amount of fuel the injectors require; there is no excess supply to be returned. A mechanical pressure-relief valve is incorporated in the fuel pump. An alternative is a continuous-supply system where the pump fuel delivery pressure cannot be adjusted. The pressure of the fuel not required for injection, or to maintain rail pressure, is controlled by the pressure-control valve and the excess returned to the low-pressure system. This approach requires additional engine power to compress the excess fuel to the primary pressure, and this additional compression and venting combined with fuel circulating cause a rise in fuel temperature. The demand-control fuel system avoids these drawbacks.[7]

Figure 7.39 Fuel supply and delivery with demand-controlled direct fuel injection system: (1) Suction jet pump; (2) Electric fuel pump with filter; (3) Pressure sensor, and relief valve; (4) Low-pressure line; (5) Demand-controlled high-pressure pump, fuel-supply control valve, pressure-limiting valve; (6) High-pressure line; (7) High-pressure sensor; (8) Fuel rail; (9) High-pressure injectors; (10) Electric pump control; (11) Fuel flow direction.[7] (Courtesy Robert Bosch GmbH and SAE.)



© McGraw-Hill Education. All rights reserved. Any use is subject to the Terms of Use, Privacy Notice and copyright information.

7.10. LIQUID PETROLEUM GAS AND NATURAL GAS

These two fuels are quite widely used in spark-ignition engines. They can be used in vehicles dedicated to each of these fuels: they can be used in dual fuel vehicles where the LPG or NG fuel system is added in parallel to the gasoline fueling system, and the driver can switch from one to the other.

7.10.1.1. Liquid Petroleum Gas

LPG is a mixture of propane and butane. It can be stored in a cylindrical tank in the liquid state under pressure (up to 27 bar). The liquid LPG fill volume is restricted to 80% of the tank volume to allow the liquid gas to expand at higher temperatures. When used in engines, LPG is injected into the intake manifold in similar fashion to multipoint gasoline injection. A common fuel rail and the individual injectors inject the LPG either continuously at variable pressure, or intermittently. The liquid LPG may be vaporized in a pressure regulator prior to injection, or may be injected as a liquid and then vaporizes in the intake manifold. The fuel system uses an exhaust gas oxygen sensor to maintain close-loop stoichiometric mixture control, to enable use of a three-way catalyst. Because its fuel molecules (propane and butane) are smaller than those typical of gasoline (average C_7H_{13}), the LPG fuel vapor displaces more air in the fuel-air mixture (seeFig. 6.3) and, accordingly, the engine's maximum power and torque are reduced by about 5%. Due to its higher H:C ratio, use of LPG produces about 10% less CO_2 emissions than equivalent use of gasoline. Hydrocarbon emissions with LPG are lower than equivalent gasoline-engine HC emissions.

7.10.1.2. Natural Gas

Natural gas is used as a spark-ignition engine fuel, both in vehicles as an alternative to gasoline, and in buses and larger engines for power generation as an alternative to diesel. Its main component is methane, CH_4, whose concentration can vary from about 80 to close to 100%. It is usually stored on the vehicle as compressed gas in high pressure (up to 700 bar) in cylindrical reinforced tanks. While it can be stored cryogenically, that has not yet proved practical. As compressed gas, its stored energy density in an appropriate fuel tank is about four times lower than that of liquid hydrocarbons. Natural gas engine-fuel-systems operate similarly to those used in multipoint-injected gasoline engines. The NG is usually injected into the intake manifold. A low-pressure common rail supplies the injector valves that inject intermittently. Due to its displacement of air in the fuel-air mixture, NG-powered engines have about 10 to 15% lower output than when operated (naturally-aspirated) with gasoline. However, it has a high antiknock octane rating, which as a stand-alone fuel would allow significantly higher engine compression ratios (about 13:1). Variations in NG composition (methane is the high antiknock component) in practice reduce this benefit. Compared to gasoline engines, natural gas engines have lower CO_2 emissions by 20 to 30% due to its lower C:H ratio than gasoline (by about a factor of 2). Its air pollutant emissions can be made very low. Methane, a major component of the hydrocarbon emissions, is not photochemically active in the atmospheric smog chemistry though it is one of the significant greenhouse gases.

© McGraw-Hill Education. All rights reserved. Any use is subject to the Terms of Use, Privacy Notice and copyright information.

7.11. PROBLEMS

7.1. The relative air/fuel ratio and the EGR rate in a conventional spark-ignition engine varies from no load (idle) to full load, at a fixed engine speed, as shown in Fig. 7.1. (By load is meant the percentage of the maximum brake torque at that speed.) Using formats similar to those shown, draw *carefully proportioned qualitative* graphs of the following parameters versus load (0 to 100%):

Combustion efficiency, η_c

Gross indicated fuel conversion efficiency, $\eta_{f,ig}$

Gross indicated mean effective pressure, imep_g

Brake mean effective pressure, bmep

Mechanical efficiency, η_m

Indicate clearly where the maximum occurs if there is one, and where the value is zero or unity or some other obvious value, if appropriate. Provide a *brief justification* for the shape of the curves you draw.

7.2. The four-cylinder spark-ignition engine shown in the figure uses an oxygen sensor in the exhaust system to determine whether the exhaust gas composition is lean or rich of the stoichiometric point, and a port fuel injection system with feedback to maintain engine operation close to stoichiometric. However, since there is a time delay between a change in the fuel/air ratio at the injector location and the detection of that change by the sensor (corresponding to the flow time between the injector and the sensor), the control system shown results in oscillations in fuel/air ratio about the stoichiometric point.

a. Estimate the average flow time between the injector and the sensor at an engine speed of 2000 rev/min.

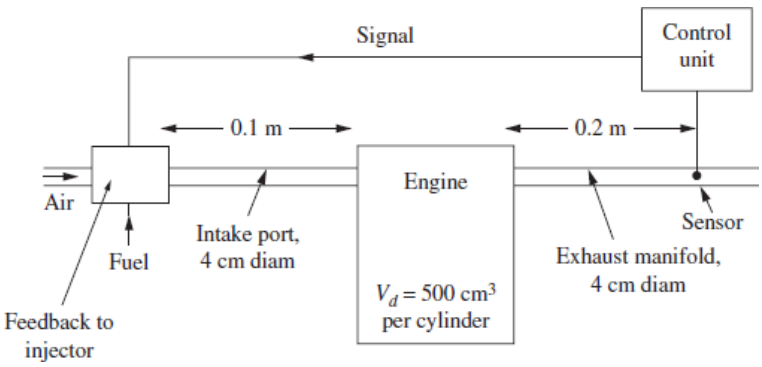
b. The sensor and control unit provide a voltage V of $+V_s$ volts when the fuel/air equivalence ratio ϕ is less than one and a voltage of $-V_s$ volts when ϕ is greater than one. The feedback injection system provides a fuel/air ratio (F/A) given by

$$\left(\frac{F}{A}\right) = \left(\frac{F}{A}\right)_{t=0} (1 + CVt)$$

where t is the time (in seconds) after the voltage signal last changed sign, $(F/A)_{t=0}$ is the fuel/air ratio at the injector at $t = 0$, and C is a constant. Develop carefully proportioned quantitative sketches of the variation in the fuel/air ratio at the injector and at the exhaust sensor, with time, showing the phase relation between the two curves. Explain briefly how you developed these graphs.

c. Find the value of the constant C, in volts $^{-1}$ seconds^{-1} (the feedback system gain), such that (F/A) variations about the stoichiometric value do not exceed ± 10% for V_s = 1 V.

© McGraw-Hill Education. All rights reserved. Any use is subject to the Terms of Use, Privacy Notice and copyright information.



7.3. In many spark-ignition engines, liquid gasoline is added to the inlet air upstream of the engine. With port fuel-injection the gasoline is injected into the intake port using an electronically controlled fuel injector. The intake port and valve are warmed by the coolant to ensure that under steady-state conditions the fuel is essentially vaporized before the mixture enters the cylinder.

a. At normal wide-open-throttle operating conditions, in a four-stroke cycle 1.6 dm^3 displacement four-cylinder engine, at 2500 rev/min, the temperature of the entering air is 40°C. The heart of vaporization of the fuel is 350 kJ/kg and the rate of heat transfer to the intake mixture if 1.4 kW. Estimate the temperature of the inlet mixture as it passes through the inlet valve, assuming that the fuel is fully vaporized. The volumetric efficiency is 0.85. The air density is 1.06 kg/m^3 and c_p for air is 1 kJ/kg·K. You may neglect the effects of the heat capacity of the liquid and vapor fuel.

b. With port electronic fuel-injection systems, the fuel is only 90% vaporized prior to entering the cylinder. Estimate the mixture temperature as it passes through the inlet valve with the PFI system, assuming that the air temperature leaving the intake manifold is still 40°C and that the fuel that is vaporized draws the heat required from the intake port walls.

c. With direct injection of gasoline into the cylinder during the intake stoke, all the thermal energy required to vaporize the fuel is drawn from the in-cylinder air plus residual gas. If the residual fraction at these conditions is 5% and the entering air temperature is 40°C, estimate the in-cylinder charge temperature after all the directly injected gasoline has vaporized at the end of the intake process. You will need to estimate the residual gas temperature.

d. Briefly explain the implications of the above three fuel injection approaches on the engine's torque at these conditions.

7.4. With multipoint port fuel injection, the fuel flow rate is controlled by the injection pulse duration. If each injector operates continuously at the maximum rated power point (wide-open throttle, *A/F* = 12, 5500 rev/min) of an automobile spark-ignition engine, estimate approximately the injection pulse duration (in crank angle degrees) for the same engine at idle. Idle conditions are: 700 rev/min, 0.3 atm inlet manifold pressure, stoichiometric mixture.

7.5. The fuel-air cycle results indicate that the maximum imep is obtained with gasoline-air mixtures at equivalence ratios of about 1.0. In practice, the maximum wide-open-throttle power of a spark-ignition engine at a given speed is obtained with an air/fuel ratio of about 12. The vaporization of the additional gasoline lowers the temperature of the inlet air and the richer mixture has a lower ratio of specific heats γ_u during compression. Estimate approximately the change in mixture temperature due to vaporization of the additional fuel used to decrease *A/F* from 14.6 (an equivalence ratio of 1.0) to 12.2 in the intake system, and the combined effect of vaporization and lower γ_u on the unburned mixture temperature at WOT when the cylinder pressure is at its peak of 40 atm. (The principal effect of the richer mixture is its impact on knock.)

7.6.

a. Plot dimensionless throttle plate open area $4A_{\text{th}}/(\pi D^2)$ as a function of throttle plate angle Ψ. Assume Ψ_0 = 10°, *D* (throttle bore diameter) = 57 mm, *d* (throttle shaft diameter) = 10.4 mm. What is the *throttle plate* area?

b. Estimate the average velocity of the air flowing through the throttle plate open area for Ψ = 26° at 3000 rev/min and Ψ = 36° at 2000 rev/min. Use the relationship between Ψ, engine speed, and inlet manifold pressure given in Fig. 7.22. Assume a discharge coefficient C_D = 0.8.

© McGraw-Hill Education. All rights reserved. Any use is subject to the Terms of Use, Privacy Notice and copyright information.

c. For the throttle of part (*a*), estimate and plot the total force on the throttle plate and shaft, and the force parallel and perpendicular to the throttle bore axis (i.e., in the mean flow direction and normal to that direction) as a function of throttle angle at 2000 rev/min. Again use Fig. 7.22 for the relationship between Ψ and inlet manifold pressure.

7.7. For the engine and intake manifold shown in Fig. 7.19, estimate the ratio of the intake manifold runner cross-sectional area to $\pi B^2/4$ (B is the cylinder bore); the ratio of the length of the flow path from the intake manifold entrance to the inlet valve seat, to the bore; the ratio of the volume of each inlet port to each cylinder's displaced volume; and the ratio of the volume of each intake manifold runner to each cylinder's displaced volume. The cylinder bore is 89 mm.

© McGraw-Hill Education. All rights reserved. Any use is subject to the Terms of Use, Privacy Notice and copyright information.

7.12. REFERENCES

1. Heywood, J. B.: *Internal Combustion Engine Fundamentals*, McGraw-Hill, New York, 1988.
2. Bosch, R.: *Automotive Handbook*, 6th edition, Robert Bosch GmbH, SAE, Warrendale, PA, 2004.
3. Bridgeman, O. C: "Equilibrium Volatility of Motor Fuels from the Standpoint of Their Use in Internal Combustion Engines," National Bureau of Standards research paper 694, 1934.
4. ASTM Standard Method: "Distillation of Petroleum Products," ANSI/ASTM D86 (IP 123/68).
5. Cheng, W. K.: MIT IC Engine Summer Course Notes, 2006.
6. Liimatta, D. R., Hurt, R. F., Deller, R. W., and Hull, W. L.: "Effects of Mixture Distribution on Exhaust Emissions as Indicated by Engine Data and the Hydraulic Analogy," SAE paper 710618, *SAE Trans.*, vol. 80, 1971.
7. Bosch, R.: *Automotive Handbook*, 8th edition, Robert Bosch GmbH, SAE, Warrendale, PA, 2011.
8. Okamoto, Y., Arai, N., Nakagawa, K., Klosuge, T., and Atago, T.: "Atomization Characteristics of Two-Stream Injector for 4-Valve Engines," SAE paper 920705, 1992.
9. Cowart, J., and Cheng, W.K., "Intake Valve Thermal Behavior During Steady-State and Transient Engine Operation," SAE paper 1999-01-3643, *SAE Trans.*, vol. 108, 1999.
10. Shin, Y., Min, K., and Cheng, W.K.: "Visualization of Mixture Preparation in a Port Fuel Injection Engine During Engine Warm-up," SAE paper 952481, 1995.
11. Harrington, D. L., and Bolt, J. A.: "Analysis and Digital Simulation of Carburetor Metering," SAE paper 700082,*SAE Trans.*, vol. 79, 1970.
12. Woods, W. A., and Goh, G. K.: "Compressible Flow through a Butterfly Throttle Valve in a Pipe," in*Proceedings of Institution of Mechanical Engineers*, vol. 193, no. 10, pp. 237–244, 1979.
13. Dugdale, P., Rademacher, R., Price, B., Subhedar, J., and Duguay, R.: "Ecotec 2.4 ℓ VVT: A Variant of GM's Global 4-Cylinder Engine," SAE paper 2005-01-1941, 2005.
14. Arcoumanis, C., Whitelaw, J. H., and Flamang, Jr., P.: "Flow in the Inlet Manifold of a Production Diesel Engine,"*Proc. Instn. Mech. Engrs.*, vol. 203, pp. 39–49, 1989.
15. Chapman, M.: "Two Dimensional Numerical Simulation of Inlet Manifold Flow in a Four Cylinder Internal Combustion Engine," SAE paper 790244, 1979.
16. Walker, J. W.: "The GM 1.8 Liter L-4 Gasoline Engine Designed by Chevrolet," SAE paper 820111,*SAE Trans.*, vol. 91, 1982.
17. Aquino, C. F.: "Transient *A/F* Control Characteristics of the 5 Liter Central Fuel Injection Engine," SAE paper 810494,*SAE Trans.*, vol. 90, 1981.
18. Benson, R. S., Baruah, P. C., and Sierens, I. R.: "Steady and Non-steady Flow in a Simple-Carburetor," in*Proceedings of Institution of Mechanical Engineers*, vol. 188, no. 53/74, pp. 537–548, 1974.
19. Chapman, M., Novak, J. M., and Stein, R. A.: "Numerical Modeling of Inlet and Exhaust Flows in Multi-cylinder Internal Combustion Engines," in *Flows in Internal Combustion Engines*, ASME Winter Annual Meeting, Nov. 14–19, 1982, ASME, New York.
20. Zhao, F-Q., Lai, M-C., and Harrington, D.L.: "The Spray Characteristics of Automotive Port Fuel Injection—A Critical Review," SAE paper 950506, 1995.

© McGraw-Hill Education. All rights reserved. Any use is subject to the Terms of Use, Privacy Notice and copyright information.

21. Shin, Y., Cheng, W. K., and Heywood, J. B.: "Liquid Gasoline Behavior in the Engine Cylinder of a SI Engine," SAE paper 941872, *SAE Trans.*, vol. 103, Sec. 4, 1994.

22. Sirignano, W. A.: "Fuel Droplet Vaporization and Spray Combustion Theory," *Prog. Energy and Combust. Sci.*, vol. 9, pp. 291–322, 1983.

23. Hires, S. D., and Overington, M. T.: "Transient Mixture Strength Excursions—An Investigation of Their Causes and the Development of a Constant Mixture Strength Fueling Strategy," SAE paper 810495, *SAE Trans.*, vol. 90, 1981.

24. Peters, B. D.: "Laser-Video Imaging and Measurement of Fuel Droplets in a Spark-Ignition Engine," in *Proceedings of Conference on Combustion in Engineering*, Oxford, Apr. 11–14, 1983, Institution of Mechanical Engineers, London, 1983.

25. Haroda, J., Tomita, T., Mizuno, H., Mashiki, Z., and Ito, Y.: "Development of Direct Injection Gasoline Engine," SAE paper 970540, 1997.

26. Iwamoto, Y., Noma, K., Nakayama, O., Yamauchi, T., and Ando, H.: "Development of Gasoline Direct Injection Engine," SAE paper 970541, *SAE Trans.*, 1997.

27. Tagaki, Y., Itoh, T., Muranaka, S., et al.: "Simultaneous Attainment of Low Fuel Consumption, High Output Power and Low Exhaust Emissions in Direct Injection SI Engines," SAE paper 980149, 1998.

28. Zhao, F., Harrington, D. L., and Lai, M-C.: *Automotive Gasoline Direct-Injection Engines*, SAE, Inc., 2002.

29. Ando, H., and Acroumanis, C.: "Flow Mixture Preparation and Combustion in Four-Stroke Direct-Injection Gasoline Engines," in *Flow and Combustion in Reciprocating Engines*, Chapter 3. Arcoumanis and T. Kamimoto (eds), Springer-Verlag, Berlin, pp. 137–171, 2009.

30. Kanda, M., Baika, T., Kato, S., Iwamuro, M., Koike, M., and Sito, A.: "Application of New Combustion Concept to Direct Injection Gasoline Engine," SAE paper 2000-01-0531, 2000.

31. Hentschel, W., Block, B., Hovestadt, T., et al.: "Optical Diagnostics and CFD-Simulations to Support the Combustion Process Development of the Volkswagen FSI Direct-Injection Gasoline Engine," SAE paper 2001-01-3648, 2001.

32. Kasseris, E., and Heywood, J. B.: "Charge Cooling Effects on Knock Limits in SI DI Engines Using Gasoline/Ethanol Blends: Part 1—Quantifying Charge Cooling," SAE paper 2012-01-1275, 2012.

33. Anderson, W., Yang, J., Brehob, D. D., Vallance, J. K., and Whitaker, R. M., "Understanding the Thermodynamics of Direct-Injection Spark Ignition (DISI) Combustion Systems: An Analytical and Experimental Investigation," SAE paper 962018, 1996.

34. Woldring, D., Landenfeld, T., and Christie, M. J., "DI Boost: Application of a High Performance Gasoline Direct Injection Concept," SAE paper 2007-01-1410, 2007.

35. Lake, T. H., Stokes, J., Whitaker, P. A., and Crump, J. V.: "Comparison of Direct Injection Gasoline Combustion Systems," SAE paper 980154, 1998.

36. Hamann, E., Manger, H., and Steinke, L.: "Lambda-Sensor with Y_2O_3-Stabilized ZrO_2-Ceramic for Application in Automotive Emission Control Systems," SAE paper 770401, *SAE Trans.*, vol. 86, 1977.

37. Seiter, R. E., and Clark, R. J.: "Ford Three-Way Catalyst and Feedback Fuel Control System," SAE paper 780203, *SAE Trans.*, vol. 87, 1978.

38. Gorille, I., Rittmannsberger, N., and Werner, P.: "Bosch Electronic Fuel Injection with Closed Loop Control," SAE paper 750368, *SAE Trans.*, vol. 84, 1975.

© McGraw-Hill Education. All rights reserved. Any use is subject to the Terms of Use, Privacy Notice and copyright information.

8.0. CHAPTER PRELIMINARIES

INTAKE-GENERATED FLOWS

MEAN VELOCITY AND TURBULENCE CHARACTERISTICS

SWIRL

TUMBLE

PISTON-GENERATED FLOWS: SQUISH

SWIRL, TUMBLE, SQUISH FLOW INTERACTIONS

PRECHAMBER ENGINE FLOWS

CREVICE FLOWS AND BLOWBY

FLOWS GENERATED BY PISTON CYLINDER-WALL INTERACTION

PROBLEMS

REFERENCES

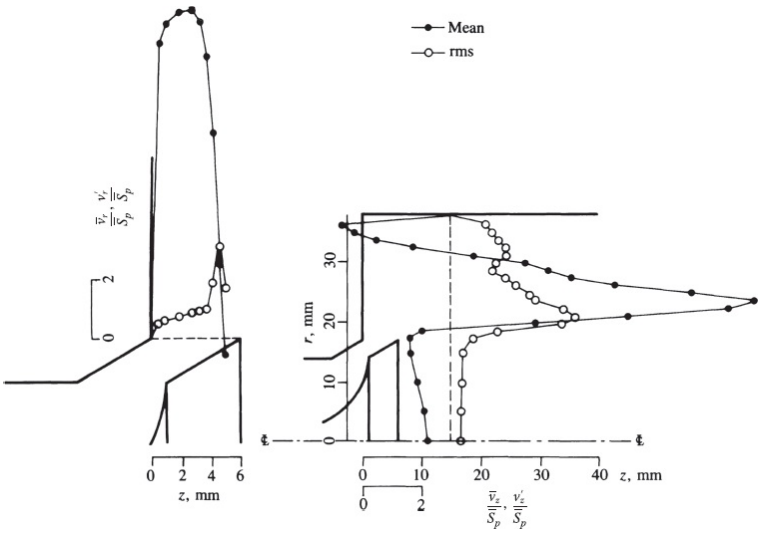
Gas motion within the engine cylinder is one of the major factors that controls the combustion process in spark-ignition (SI) engines, and the fuel-air mixing and combustion processes in diesel engines. It also has a significant impact on engine heat transfer. Both the bulk gas motion and the turbulence characteristics of the flow are important. The initial in-cylinder flow pattern is set up by the intake process. It may then be substantially modified during compression. This chapter reviews the important features of gas motion within the cylinder set up by flows into and out of the cylinder through valves or ports, and by the motion of the piston.

© McGraw-Hill Education. All rights reserved. Any use is subject to the Terms of Use, Privacy Notice and copyright information.

8.1. INTAKE-GENERATED FLOWS

The engine intake process governs many important aspects of the flow within the cylinder. In four-stroke cycle engines, the downward motion of the piston pulls air into the cylinder. The intake flow velocities scale with piston speed. For much of the intake stroke, the annular gap between the intake valve head and valve seat is the minimum area for the flow (see Sec. 6.3) so gas velocities through this gap are the highest velocities set up during the intake process. The gas issues from the valve opening into the cylinder as an annular conical jet and the radial and axial velocities in the jet are about 10 times the mean piston speed. Figure 8.1 shows the radial and axial velocity components close to the valve exit, measured during the intake process, in a motored model engine with transparent walls and single valve located on the cylinder axis, using laser doppler anemometry (see next section).[1] The jet separates from the valve seat and head, producing shear layers with large velocity gradients which generate turbulence. This separation of the jet sets up recirculation regions beneath the valve head and in the corner between the cylinder wall and cylinder head.

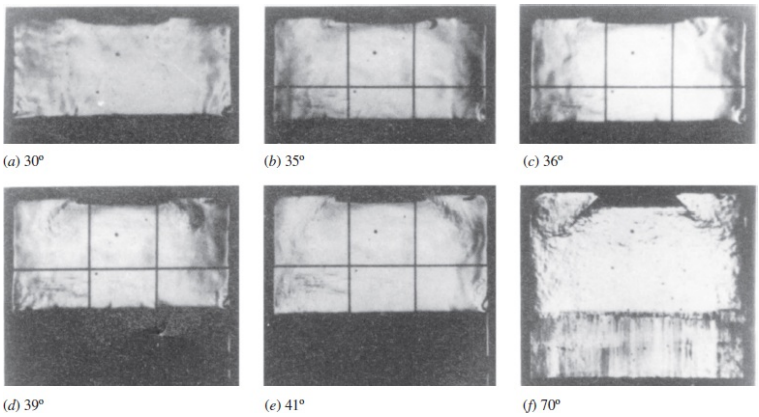
Figure 8.1 Radial mean velocity
v_r and root mean square (rms) velocity fluctuations
v'_r at the valve exit plane, and axial mean velocity
v_z and rms velocity fluctuation
v'_z $15\ \mathrm{mm}$ below the cylinder head, at 36° ATC in model engine operated at 200 rev/min. Valve lift = 6 mm. Velocities normalized by mean piston speed.[1]



The motion of the intake jet into the cylinder is shown in the schlieren photographs in Fig. 8.2 taken in a firing transparent engine. This engine had a square cross-section cylinder made up of two quartz walls and two steel walls, to permit easy optical access. The schlieren technique makes regions with density gradients in the flow show up as lighter or darker regions on the film.[2] The engine was throttled to one-half an atmosphere intake pressure, so the jet starts after the intake stroke has commenced, at 35° after top center (ATC), following the backflow of residual into the intake manifold. The front of the intake jet can be seen propagating from the valve toward the cylinder wall at several times the mean piston speed. Once the jet reaches the wall ($\theta > 41°$ ATC), the wall deflects the major portion of the jet downward toward the piston; however, a substantial fraction flows upward toward the cylinder head. The highly turbulent nature of this intake jet is evident.

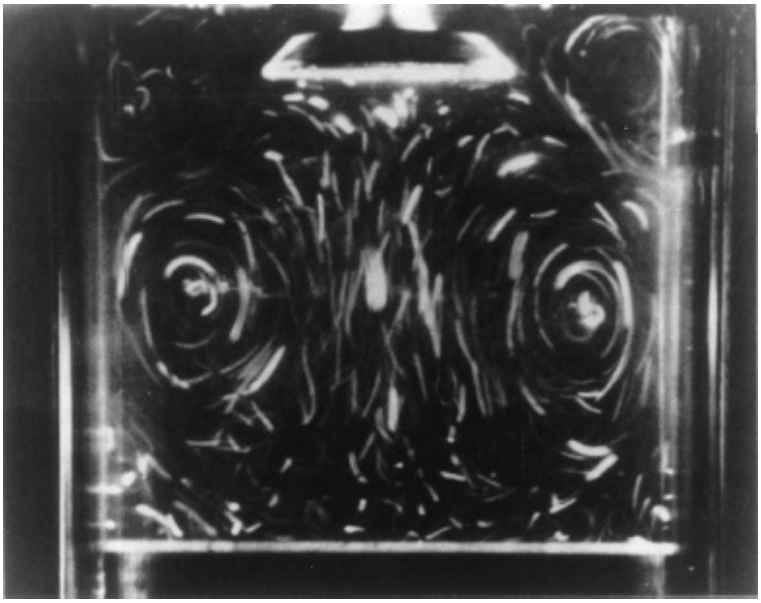
© McGraw-Hill Education. All rights reserved. Any use is subject to the Terms of Use, Privacy Notice and copyright information.

Figure 8.2 Sequence of schlieren photographs of intake jet as it develops during the intake stroke. Numbers are crank-angle degrees after TC.[2]



The interaction of jet with the wall produces large-scale rotating flow patterns within the cylinder volume. These are easiest to visualize where the engine geometry has been simplified so the flow into the cylinder is axisymmetric. The photograph in Fig. 8.3 of a water analog of an engine intake flow was taken in a transparent model of an engine cylinder and piston. The valve is located in the center of the cylinder head, and the flow into the valve is along the cylinder axis. The experimental parameters have been scaled so that the appropriate dimensionless numbers which govern the flow, the Reynolds and Strouhal numbers, were maintained at typical engine values. The photograph shows the major features of the intake-generated flow in a thin illuminated plane through the cylinder axis. The streaks are records of the paths of tracer particles in the flow during the period the camera shutter is open. The bulk of the cylinder as the piston moves down is filled with a large ring vortex, whose center moves downward and remains about halfway between the piston and the head. The upper corner of the cylinder contains a smaller vortex, rotating in the opposite direction. These vortices persist until about the end of the intake stroke, when they became unstable and break up.[3]

Figure 8.3 Large-scale rotating flow pattern setup within the cylinder by the intake jet. Photograph of streak lines in water flow into model engine cylinder with axisymmetric valve.[3]

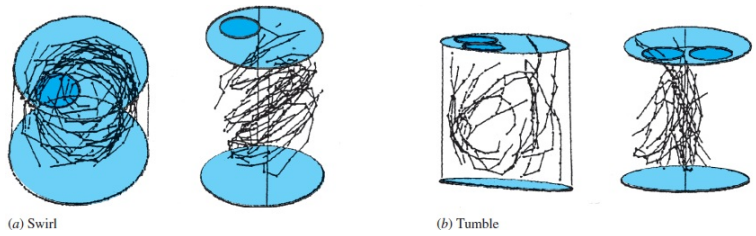


With intake valve location and port geometry more typical of normal engine practice, and with two intake valves per cylinder, the intake-generated flow is more complex. However, the presence of these large-scale rotating flow patterns, produced by the airflow into the cylinder, can still be discerned. Such flows are inherent to the poppet valve geometry in the cylinder head:

© McGraw-Hill Education. All rights reserved. Any use is subject to the Terms of Use, Privacy Notice and copyright information.

they bring into the cylinder significant fluid kinetic energy and create shear, both of which can generate turbulence. The intake valve(s) and port geometries can be designed to augment these jet-created flows by generating large-scale in-cylinder rotating flows. Two of these, swirl and tumble, are illustrated in Fig. 8.4 by the flow streak lines highlighted by flow tracers in water analog studies of real cylinder airflows. Swirl, Fig. 8.4*a*, organized fluid rotation about the cylinder axis, is usually generated by bringing the air into the cylinder with net angular momentum about the cylinder axis. It is used in smaller higher speed diesel engines to promote more rapid fuel-air mixing, and also in spark-ignition engines to increase the engine's combustion rate. Tumble, Fig. 8.4*b*, is the name given to flow rotation about an axis orthogonal to the cylinder axis. It is generated by using closer to horizontal intake ports which direct the intake airflow across the cylinder head and down the far side of the liner as illustrated. Tumble is used to increase the kinetic energy stored in the in-cylinder charge during intake: the upward motion of the piston during compression breaks up this tumbling flow which generates additional turbulence, and as a result speeds up the spark-ignition engine combustion process. Tumble and swirl can occur together, or separately. These flows are discussed in more detail in Secs. 8.3 and 8.4.

Figure 8.4 In-cylinder flow streaklines from tracers in water analog studies of (a) swirl and (b) tumble in-cylinder flows. With one intake port off axis (a), air enters the cylinder with net angular momentum about the cylinder axis, and a swirling in-cylinder flow is set up. With two intake ports which direct the air across the cylinder head and down the liner (b), a tumbling flow rotating about an axis orthogonal to the cylinder axis is created.[4,5]



(*a*) Swirl (*b*) Tumble

In summary, the jet-like character of the four-stroke cycle intake flow, interacting with the cylinder walls and moving piston, creates large-scale rotating flow patterns within the cylinder. Additionally, large-scale flows such as swirl and tumble can be deliberately set up through use of specific port (and valve) geometries. The details of these flows are strongly dependent on the inlet port, valve, and cylinder head geometry. These flow structures are thought to become unstable, either late in the intake or during the compression process, and break down into more turbulent motions (less so in the case of swirl). Such rotating flows are usually sensitive to variations in the flow: thus their breakup is likely to vary, cycle-by-cycle.

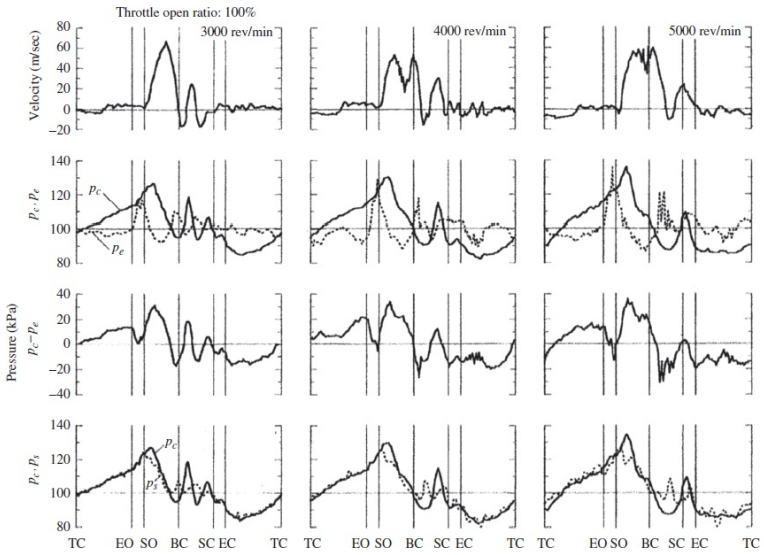
In two-stroke engines, the flow of air into the cylinder differs markedly from the flow generated by the four-stroke cycle engine intake process. This flow occurs while the piston is close to bottom center (BC). It is the key part of the cylinder scavenging process and overlaps the burned gas exhaust process. The entering airflow is driven through the transfer ports near the bottom of the cylinder liner which open as the piston uncovers them, by a pressure difference between the supplied air (which has been compressed prior to being fed to the transfer passages) and the cylinder. The airflow into the cylinder is not pulled by the downward motion of the piston, as occurs in the four-stroke cycle during its intake stroke. The air velocities generated in the air flowing into the two-stroke engine cylinder do not therefore scale with engine speed, except in two-stroke engines where air compression is achieved through use of a compressor or blower mechanically coupled to and driven by the engine's crankshaft.[6]

Figure 8.5 shows how the air velocity at the transfer or scavenge port varies during the scavenging process in a crankcase-compression loop-scavenged Schnürle-type single-cylinder 98 cm^3 displacement two-stroke cycle SI engine. The exhaust and scavenge port opening and closing angles are indicated. Also shown are the crankcase pressure p_c, the exhaust-port pressure p_e, their difference, and the scavenge-port pressure p_s, at wide-open-throttle conditions. The maximum air velocities at each of the three engine speeds shown are comparable in magnitude, though at the higher speeds the crank-angle extent of the blowdown process from the crankcase into the cylinder is longer. Pressure and flow oscillations due to compression and expansion waves are evident. It is the pressure difference, $p_c - p_e$, that largely drives the air into the cylinder in this type of

© McGraw-Hill Education. All rights reserved. Any use is subject to the Terms of Use, Privacy Notice and copyright information.

two-stroke engine. At higher engine speeds there is less time available for the scavenging process; thus the pressure blowdown and duration of the airflow pulse occur over a longer crank-angle interval.

Figure 8.5 The effect of engine speed on the fresh-charge velocity at the scavenge port, and the pressure variation in the crankcase (p_c), the exhaust port (p_e), and scavenge port (p_s) at wide-open-throttle conditions. Engine details: two-stroke crankcase-compression loop-scavenged SI engine of Schnürle type, 98 cm^2 cylinder displaced volume, bore 5 cm, stroke 5 cm, compression ratio 6.59; EO 83° BBC; EC 82° ABC; SO 57° BBC; SC 60° ABC.[7]



At loads less than wide-open throttle in two-stroke SI engines, the amount of air entering the cylinder each cycle is reduced by throttling the airflow into the crankcase. At lower engine speeds, closing the throttle to 20% of its wide-open area does not significantly affect the mean entering air velocity. At high engine speed, the maximum velocity decreases by about 50% when the throttle is closed to 20% of its wide-open-throttle (WOT) flow area. Backflow from the cylinder into the transfer ports occurs at low engine speed during a large part of the gas exchange period, but only to a limited extent at high engine speed. At low speed, the time available for the crankcase to be filled is long enough at these throttle positions (some 20% of the fully open area) for the total cylinder trapped mass to be unaffected. The throttle open area must be further reduced to affect the trapped fuel-air mass. At high speed, the velocity of the incoming charge through the intake system is high, and so is the pressure drop across the throttle. Consequently, at higher speeds, the throttle position affects the crankcase pressure and thus the mass of air trapped within the cylinder.[6]

These two-stroke transfer or scavenging port jet flows are usually symmetric as they enter the cylinder, and have velocities in the 50–100 m/s range and modest root-mean-square velocities (or turbulence intensities—see Sec. 8.2) or order 10% of the mean velocities. However, the interaction of these jets with each other and the combustion chamber walls produces an in-cylinder flow with strong asymmetry and high rms velocities of 30 to 40% of the mean values. As the strong inflow diminishes and the crankcase and cylinder pressure equilibrate, the scavenging-loop rotating (vortex) flow becomes evident (see Fig. 6.34), though the flow details are complex. As the rising piston compresses this scavenging-loop flow, it first speeds up and then breaks down into turbulence shortly before TC (similarly to the tumbling flow often produced in four-stroke cycle SI engines). In the crankcases-scavenged two-stroke engines described here, the gas exchange process is driven primarily by the blowdown of compressed air from the crankcase into the cylinder when the piston uncovers the transfer ports. Unlike four-stroke cycle engines where piston motion during the intake stroke pulls the air into the cylinder, and thus the velocity of the air entering the cylinder scales with piston speed, these two-stroke entering airflow velocities do not scale in any simple way with piston or engine speed. However, the charge motion produced by the piston during compression does scale with piston speed, so the mean piston speed
$\overline{S}_p\,(=2NS)$ is still useful as a normalizing velocity, provided we recognize that the normalized velocities will vary with engine speed and load (delivery ratio) as discussed above. At a typical part-load low-speed two-stroke SI engine operating

© McGraw-Hill Education. All rights reserved. Any use is subject to the Terms of Use, Privacy Notice and copyright information.

condition (1600 rev/min, delivery ratio = 0.5), the largest velocities in the entering air jets are in the range of about $40 - 50\overline{S}_p$ and the largest rms velocities are about $8–10\overline{S}_p$ and are found near the cylinder center. These values are large relative to four-stroke cycle intake-generated flow velocities and rms velocities, which typically are in the ranges of $3–10\overline{S}_p$ and $1–2\overline{S}_p$ respectively. In four-stroke engines with simple open chambers, the rms velocities (or turbulence intensities—see Sec. 8.2) at TC of the compression stroke are about $0.5\overline{S}_p$. When intake-generated tumble is used to enhance four-stroke cycle SI engine combustion rates, the turbulence intensity (the major flow component driving the engine's flame propagation) rises to about $(0.8–1)\overline{S}_p$ at TC piston position. Such values are only slightly less than the rms velocities or turbulence intensities of about $(1–1.2)\overline{S}_p$ measured at TC in small two-stroke cycle SI engines.[8]

© McGraw-Hill Education. All rights reserved. Any use is subject to the Terms of Use, Privacy Notice and copyright information.

8.2. MEAN VELOCITY AND TURBULENCE CHARACTERISTICS

8.2.1. Definitions of Relevant Parameters

The charge motions into and within the engine cylinder are turbulent. In turbulent flows, the rates of transfer and mixing are several times greater than the rates due to molecular diffusion. This "turbulent diffusion" results from the local fluctuations in the flow field. It leads to increased rates of momentum, heat, and mass transfer, and is essential to the satisfactory operation of spark-ignition and diesel engines. Turbulent flows are always dissipative. Viscous shear stresses perform deformation work on the fluid, which increases its internal energy at the expense of its turbulent kinetic energy. Energy is required to generate turbulence: if no energy is supplied, turbulence decays. A common source of energy for turbulent velocity fluctuations is shear in the mean flow. Turbulence is rotational and is characterized by high fluctuating vorticity: these vorticity fluctuations can only persist if the velocity fluctuations are three dimensional.[9]

The character of a turbulent flow depends on its environment. In the engine cylinder, the flow involves a combination of turbulent shear layers, recirculating regions, and boundary layers. The flow is unsteady and may exhibit substantial cycle-to-cycle fluctuations. Both large-scale and small-scale turbulent motions are important factors governing the overall behavior of the flow.

An important characteristic of a turbulent flow is its irregularity or randomness. Statistical methods are therefore used to define such a flow field. The quantities normally used are: the mean velocity, the fluctuating velocity about the mean, and several length and time scales. In a steady turbulent flow situation, the instantaneous local fluid velocity *U* (in a specific direction) is written:

$$U(t) = \overline{U} + u(t)$$

(8.1)

where
$\overline{U}$, the mean velocity, is the time average of *U(t)*:

$$\overline{U} = \lim_{\tau \to \infty} \frac{1}{\tau} \int_{t_0}^{t_0+\tau} U(t)dt$$

(8.2)

The fluctuating velocity component *u* is characterized by its root mean square value, the turbulence intensity, u':

$$u' = \lim_{\tau \to \infty} \left(\frac{1}{\tau} \int_{t_0}^{t_0+\tau} u^2 dt \right)^{1/2}$$

(8.3a)

Alternatively,

© McGraw-Hill Education. All rights reserved. Any use is subject to the Terms of Use, Privacy Notice and copyright information.

$$u' = \lim_{\tau \to \infty} \left(\frac{1}{\tau} \int_{t_0}^{t_0+\tau} \left(U^2 - \overline{U}^2 \right) dt \right)^{1/2}$$

(8.3b)

since the time average of
$(u\overline{U})$ is zero.

In engines, the application of these turbulence concepts is complicated by the fact that the flow pattern within the cylinder changes during the engine cycle. Also, while the overall features of the flow in each cylinder repeat each cycle, the details do not because the mean flow can vary significantly from one cycle to the next. There are both cycle-to-cycle variations in the mean or bulk flow at any point in the cycle, as well as turbulent fluctuations about that specific cycle's mean flow.

One approach used in quasi-periodic flows, such as that which occurs in the engine cylinder, is *ensemble-averaging* or *phase-averaging*. Usually, velocity measurements are made over many engine cycles, and over a range of crank angles. The instantaneous velocity at a specific crank-angle position θ in a particular cycle i can be written as

$$U(\theta, i) = \overline{U}(\theta, i) + u(\theta, i)$$

(8.4)

The ensemble- or phase-averaged velocity,
$\overline{U}(\theta)$, is defined as the average of values at a specific phase or crank angle in the basic cycle. Figure 8.6 shows this approach applied schematically to the velocity variation during a two-stroke engine cycle, with small and large cycle-to-cycle variations. The ensemble-averaged velocity is the average over a large number of measurements taken at the same crank angle (two such points are indicated by dots):

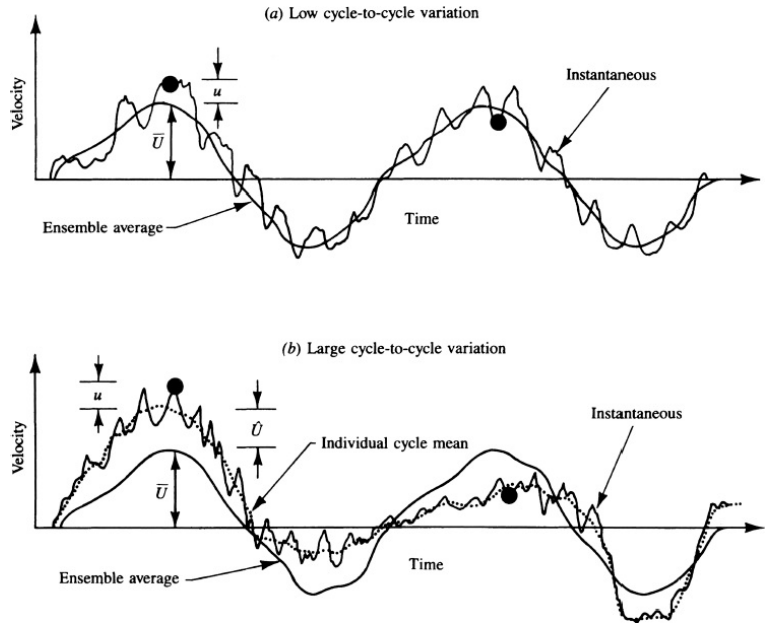
$$\overline{U}_{\mathrm{EA}}(\theta) = \frac{1}{N_c} \sum_{i=1}^{N_c} U(\theta, i)$$

(8.5)

where N_c is the number of cycles for which data are available. By repeating this process at many crank-angle locations, the ensemble-averaged velocity profile over the complete cycle is obtained.

© McGraw-Hill Education. All rights reserved. Any use is subject to the Terms of Use, Privacy Notice and copyright information.

Figure 8.6 Schematic of velocity variation with crank angle at a fixed location in the cylinder during two consecutive engine cycles. Dots indicate measurements of instantaneous velocity at two specific crank angles. The ensemble- or phase-averaged velocity is obtained by averaging over a large number of such measurements shown as solid smooth line. Top graph (a): low cycle-to-cycle flow variations. Here the individual-cycle mean velocity and ensemble-averaged velocity are closely comparable. Bottom graph (b): large cycle-to-cycle variations. Here the individual-cycle mean velocity (dotted line) is different from the ensemble-averaged mean by $\hat{U}$. The turbulent fluctuation u is then defined in relation to the individual-cycle mean.[10]



The ensemble-averaged mean velocity at a given location is only a function of crank angle since the cyclic variation has been averaged out. The difference between the mean velocity in a particular cycle and the ensemble-averaged mean velocity over many cycles is defined as the cycle-by-cycle variation in mean velocity, $\hat{U}$:

$$\hat{U}(\theta,i) = \overline{U}(\theta,t) - \overline{U}_{\mathrm{EA}}(\theta)$$

(8.6)

Thus the instantaneous velocity, given by Eq. (8.4), can be split into three components:

$$U(\theta,i) = \overline{U}_{\mathrm{EA}}(\theta) + \hat{U}(\theta,i) + u(\theta,t)$$

(8.7)

Figure 8.6 illustrates this breakdown of the instantaneous velocity into an ensemble-averaged component, an individual-cycle mean velocity, and a component which randomly fluctuates in time at a particular point in space in a single cycle. This last component is the conventional definition of the turbulent velocity fluctuations. Whether this differs significantly from the fluctuations about the ensemble-averaged velocity depends on whether the cycle-to-cycle fluctuations are small or large. The figure indicates these two extremes.[1]

© McGraw-Hill Education. All rights reserved. Any use is subject to the Terms of Use, Privacy Notice and copyright information.

In turbulent flows, a number of length scales exist that characterize different aspects of the flow behavior. The largest eddies in the flow are limited in size by the system boundaries. The smallest scales of the turbulent motion are limited by molecular diffusion. The important length scales are illustrated by the schematic of the jet issuing into the cylinder from the intake valve in Fig. 8.7. The eddies responsible for most of the turbulence production during intake are the large eddies in the conical inlet jet flow between the valve head and seat. These are roughly equal in size to the local jet thickness. This scale is called the *integral length scale,* l_I: it is a measure of the largest scale structures in the turbulent flow. Velocity measurements made at two points separated by a distance x significantly less than l_I will correlate with each other; with $x \gg l_I$, no correlation will exist. The integral length scale is defined, therefore, as the integral of the autocorrelation coefficient of the fluctuating velocity at two adjacent points in the flow with respect to the variable distance between the points, as shown in Fig. 8.8: that is,

$$l_I = \int_0^\infty R_x dx$$

(8.8a)

where

$$R_x = \frac{1}{N_m - 1} \sum_{i=1}^{N_m} \frac{u(x_0)\, u(x_0 + x)}{u'(x_0)\, u(x_0 + x)}$$

(8.8b)

This technique for determining the integral scale requires simultaneous measurements at two points. Due to the difficulty of applying this technique in engines, most efforts to determine length scales have first employed correlations to determine the *integral time scale,* τ_I. The integral time scale of the turbulence is defined as a correlation between two velocities at a fixed point in space, but separated in time:

$$\tau_I = \int_0^\infty R_t dt$$

(8.9a)

where

$$R_t = \frac{1}{N_m - 1} \sum_{i=1}^{N_m} \frac{u(t_0)\, u(t_0 + t)}{u'(t_0)\, u'(t_0 + t)}$$

(8.9b)

and N_m is the number of measurements. Under conditions where the turbulence pattern is convected past the observation point without significant distortion and the turbulence is relatively weak, the integral length and time scales are related by

$$l_I = \overline{U}\, \tau_I$$

(8.10)

© McGraw-Hill Education. All rights reserved. Any use is subject to the Terms of Use, Privacy Notice and copyright information.

In flows where the large-scale structures are convected, τ_I is a measure of the time it takes a large eddy to pass between two points. In flows without mean motion, the integral time scale is an indication of the lifetime of an eddy.[10,11]

Figure 8.7 Schematic of jet created by the flow through the intake valve indicating its turbulent structure.[9,10]

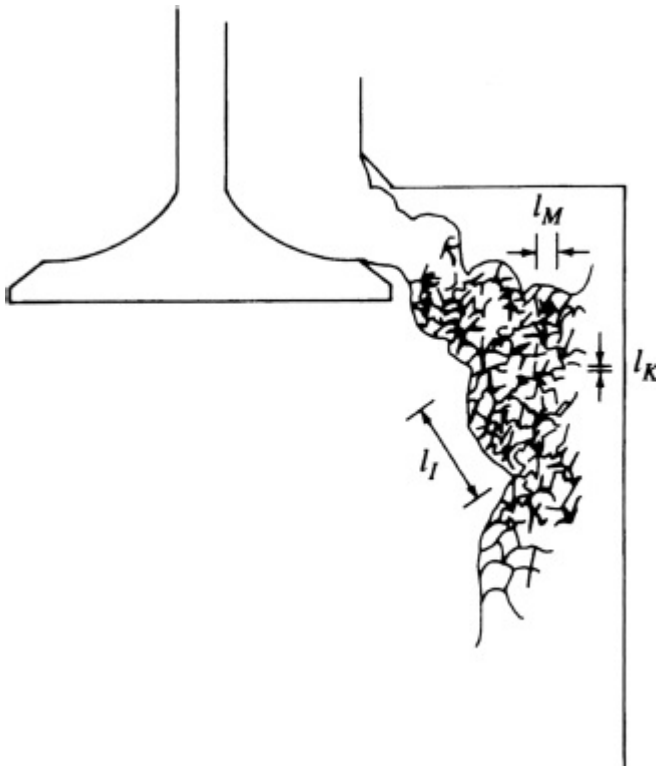
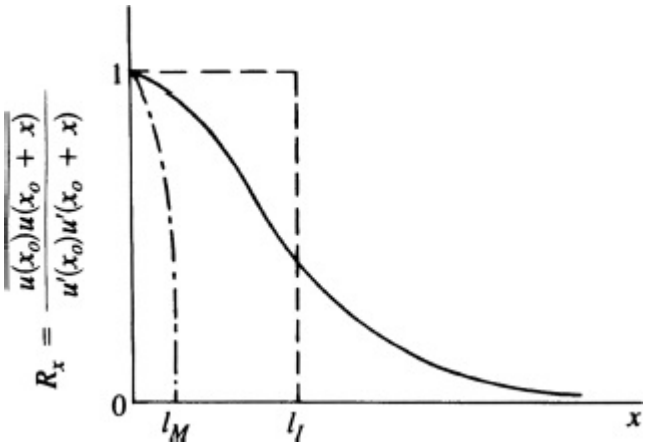


Figure 8.8 Spatial velocity autocorrelation R_x as a function of x, defining the integral length scale l_I and the micro length scale l_M.



Superposed on this large-scale flow is a range of eddies of smaller and smaller size, fed by the continual breakdown of larger eddies. Since the smaller eddies respond more rapidly to changes in local flow pattern, their characteristics are more likely to be isotropic (have no preferred direction) than are the large eddies, and have a structure like that of other turbulent flows. The dissipation of turbulence energy takes place in the smallest structures. At this smallest scale of the turbulent motion, called the *Kolmogorov scale,* the kinetic energy in these smallest flow structures is dissipated via molecular viscosity into thermal energy. If ε is the energy dissipation rate per unit mass and v the kinematic viscosity, Kolmogorov length and time scales are defined by:

© McGraw-Hill Education. All rights reserved. Any use is subject to the Terms of Use, Privacy Notice and copyright information.

$$l_K = \left(\frac{\nu^3}{\varepsilon}\right)^{1/4} \quad \tau_K = \left(\frac{\nu}{\varepsilon}\right)^{1/2}$$

(8.11)

The Kolmogorov length scale characterizes the size of the smallest eddies in the flow. The Kolmogorov time scale characterizes the momentum diffusion rate at this smallest structure level.

A third scale is useful in characterizing a turbulent flow. It is called the *microscale* (or *Taylor microscale*). The micro length scale l_M is defined by relating the fluctuating strain rate of the turbulent flow field to the turbulence intensity:

$$\frac{\partial u}{\partial x} \approx \frac{u'}{l_M}$$

(8.12)

It can be determined from the curvature of the spatial correlation curve at the origin, as shown in Fig. 8.8.[9,10] More commonly, the micro time scale τ_M is determined from the temporal auto correlation function of Eq. (8.9):

$$\tau_M^2 = -\frac{2}{\left(\partial^2 R_t / \partial t^2\right)_{t_0}}$$

For turbulence which is homogeneous (has no spatial gradients) and is isotropic (has no preferred direction), the microscales l_M and τ_M are related by

$$l_M = \overline{U}\,\tau_M$$

(8.13)

These different scales are related as follows. The turbulent kinetic energy per unit mass in the large-scale eddies is proportional to
u'^2. Large eddies lose a substantial fraction of this energy in one "turnover" time l_I/u'. In an equilibrium situation the rate of energy supply equals the rate of dissipation:

$$\varepsilon \approx \frac{u'^3}{l_I}$$

Thus,

$$\frac{l_K}{l_I} \approx \left(\frac{u' l_I}{\nu}\right)^{-3/4} = \mathrm{Re}_T^{-3/4}$$

(8.14)

where Re_T is the turbulent Reynolds number, $u' l_I/\nu$.

Within the restrictions of homogeneous and isotropic turbulence, an energy budget can be used to relate l_I and l_M:[9]

© McGraw-Hill Education. All rights reserved. Any use is subject to the Terms of Use, Privacy Notice and copyright information.

$$\varepsilon = \frac{Au'^3}{l_I} = \frac{15\nu u'^2}{l_M^2}$$

where *A* is a constant of order 1. Thus,

$$\frac{l_M}{l_I} = \left(\frac{15}{A}\right)^{1/2} \mathrm{Re}_T^{-1/2}$$

(8.15)

These restrictions are not usually satisfied within the engine cylinder during intake. They are approximately satisfied at the end of compression.

8.2.2. Application to Engine Velocity Data

As explained above, it is necessary to analyze velocity data on an individual cycle basis as well as using ensemble-averaging techniques. The basic definitions for obtaining velocities which characterize the flow will now be developed. The ensemble-averaged velocity
$\overline{U}_{\mathrm{EA}}$ has already been defined by Eq. (8.5). The ensemble-averaged fluctuation intensity
$u'_{F,\mathrm{EA}}$ is given by

$$u'_{F,\mathrm{EA}}(\theta) = \left\{\frac{1}{N_c}\sum_{i=1}^{N_c}[u(\theta,i)]^2\right\}^{1/2} = \left\{\frac{1}{N_c}\sum_{i=1}^{N_c}[U(\theta,i)^2 - \overline{U}_{\mathrm{EA}}(\theta)^2]\right\}^{1/2}$$

(8.16)

It includes all fluctuations about the ensemble-averaged mean velocity.

Flow fields in fired engines are readily measured using two-dimensional particle-image velocimetry (PIV). Use of Eqs. (8.5) and (8.16) requires values for *U* and *u* at each specific crank angle under consideration. While some measurement techniques can provide this, a commonly used point velocity measurement method (laser Doppler velocimetry) provides an intermittent signal. With laser doppler velocimetry (LDV), interference fringes are produced within the small volume created by the intersection of two laser beams within the flow field. When a small particle passes through this volume, it scatters light at a frequency proportional to the particle velocity. By seeding the flow with particles small enough to be carried without slip by the flow and collecting this scattered light, the flow velocity can be determined. A signal is only produced when a particle moves through the measurement volume; thus one collects data as velocity crank-angle pairs. It is necessary, therefore, to perform the ensemble-averaging over a finite crank-angle window Δ*θ* around the specific crank angle of interest,
$\bar{\theta}$. The ensemble-averaged velocity equation becomes

$$\overline{U}_{\mathrm{EA}}(\theta) = \frac{1}{N_t}\sum_{i=1}^{N_c}\sum_{j=1}^{N_i} U_{i,j}\left(\bar{\theta} \pm \frac{\Delta\theta}{2}\right)$$

(8.17)

© McGraw-Hill Education. All rights reserved. Any use is subject to the Terms of Use, Privacy Notice and copyright information.

where N_i is the number of velocity measurements recorded in the window during the ith cycle, N_c is the number of cycles, and N_t is the total number of measurements. The corresponding equation for the ensemble-averaged root-mean-square velocity fluctuation is

$$u'_{F,\mathrm{EA}}(\theta) = \left\{ \frac{1}{N_t} \sum_{i=1}^{N_c} \sum_{j=1}^{N_i} \left[u_{i,j} \left(\theta \pm \frac{\Delta\theta}{2} \right) \right]^2 \right\}^{1/2}$$

(8.18)

where

$$u_{i,j} = U_{i,j} - \overline{U}_{\mathrm{EA}}$$

(8.19)

As has already been explained, this definition of fluctuation intensity [the ensemble-averaged rms velocity fluctuation, Eq. (8.18)] includes cyclic variations in the mean flow as well as the turbulent fluctuations about each cycle's mean flow. It is necessary to determine the mean and fluctuating velocities on an individual-cycle basis to characterize the in-cylinder flow field more completely. The critical part of this process is defining the mean velocity at a specific crank angle (or within a small window centered about that crank angle) in each cycle. In this individual-cycle velocity analysis, the individual-cycle time-averaged or mean velocity
$u_{i,j} = U_{i,j} - \overline{U}_{\mathrm{EA}}$ is first determined.[12] The ensemble average of this mean velocity

$$\overline{U}_{\mathrm{EA}}(\theta) = \frac{1}{N_c} \sum_{i=1}^{N_c} \overline{U} \left(\theta \pm \frac{\Delta\theta}{2}, i \right)$$

(8.20)

is identical to the ensemble-averaged value given by Eq. (8.17). The root mean square fluctuation in individual-cycle mean velocity can then be determined from

$$U_{\mathrm{RMS}}(\theta) = \left\{ \frac{1}{N_c} \sum_{i=1}^{N_c} \left[\overline{U} \left(\theta \pm \frac{\Delta\theta}{2}, i \right) - \overline{U}_{\mathrm{EA}}(\theta) \right]^2 \right\}^{1/2}$$

(8.21)

This indicates the magnitude of the cyclic fluctuations in the mean motion. The instantaneous velocity fluctuation from the mean velocity, within a specified window
$\Delta\theta$ at a particular crank angle
θ, is obtained from Eq. (8.4). This instantaneous velocity fluctuation is ensemble-averaged, because it varies substantially cycle-by-cycle and because the amount of data is usually insufficient to give reliable individual-cycle results:

© McGraw-Hill Education. All rights reserved. Any use is subject to the Terms of Use, Privacy Notice and copyright information.

$$u'_{T,\mathrm{EA}}(\theta) = \left\{ \frac{1}{N_c} \sum_{i=1}^{N_c} \left[U\left(\bar{\theta} \pm \frac{\Delta\theta}{2}, i\right) - \overline{U}\left(\bar{\theta} \pm \frac{\Delta\theta}{2}, i\right) \right]^2 \right\}^{1/2}$$

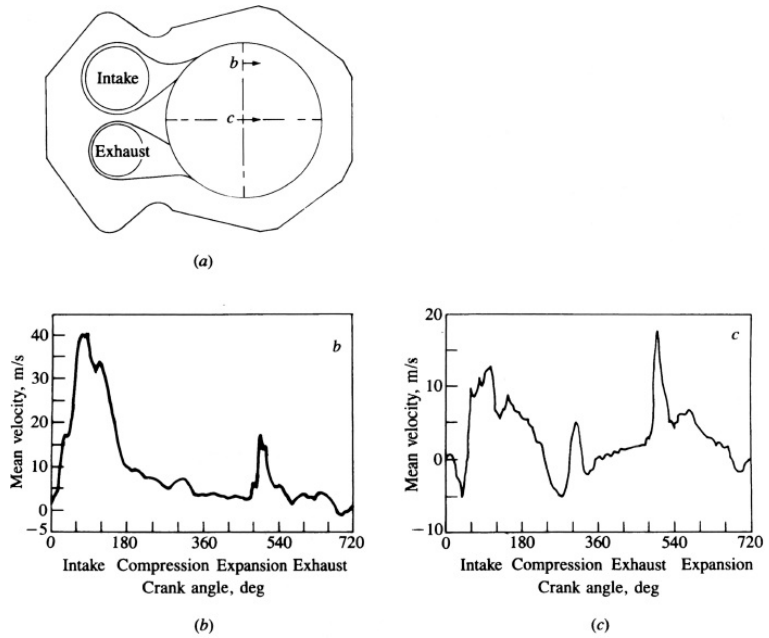
(8.22)

This quantity is the ensemble-averaged turbulence intensity.

Results obtained with this approach will now be reviewed to illustrate the major features of the in-cylinder gas motion. While some of these results were obtained in special engines where the geometry and flow have been modified to make the experiments and their interpretation easier, they illustrate key features of the in-cylinder flow. Note, the flow within the cylinder is three dimensional in nature. It takes measurements at many points within the flow field, coupled with flow visualization, to characterize the flow.

Figure 8.9 shows ensemble-averaged velocities throughout the engine cycle at two measurement locations in a special L-head engine designed to generate a swirling flow within the cylinder. The engine was motored at 300 rev/min, giving a mean piston speed of 0.76 m/s. Figure 8.9*b* shows the mean velocity within the intake-generated swirling flow, within the clearance volume, in the swirl direction. High velocities are generated during the intake process, rising to a maximum and then decreasing in response to the piston motion (see Fig. 2.2). During the compression stroke, the velocity continues to decrease but at a much slower rate. This is a motored engine cycle. A comparison of intake and compression velocities with an equivalent firing cycle showed close agreement.[13] The late expansion and exhaust stroke velocities are not typical of firing engine behavior, however, and the increase in velocity when the exhaust valve opens is due to the flow of gas *into* the cylinder because in this motored cycle, due primarily to heat losses, the cylinder pressure is then below 1 atm. Figure 8.9*c* shows the mean velocity in the clearance volume in the same direction but on the cylinder axis. At this location, positive and negative flow velocities were measured. Since this location is out of the direct path of the intake-generated flow, velocities during the intake stroke are much lower. The non-homogeneous character of this particular ensemble-mean flow is evident.

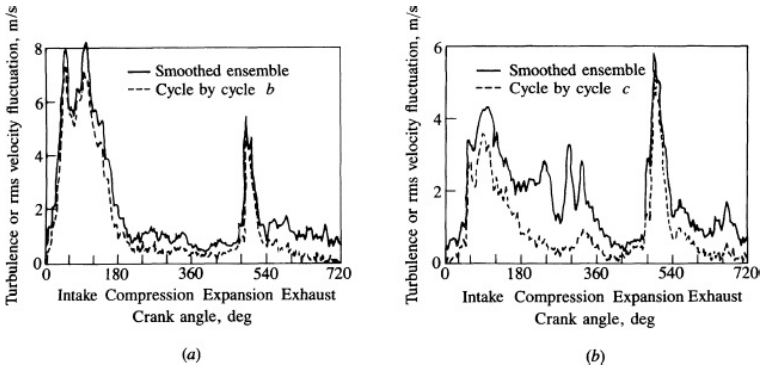
Figure 8.9 Ensemble-averaged velocities throughout the engine cycle in motored four-stroke L-head engine: 300 rev/min, mean piston speed 0.76 m/s. (a) Engine schematic showing measurement locations and velocity directions; (b) velocity at b in the intake flow path; (c) velocity at c on cylinder axis.[14]



© McGraw-Hill Education. All rights reserved. Any use is subject to the Terms of Use, Privacy Notice and copyright information.

Figure 8.10 shows the ensemble-averaged rms velocity fluctuation (which includes contributions from cycle-by-cycle variations in the mean flow and turbulence) and the ensemble-averaged individual-cycle turbulence intensity at these same two locations and directions. The difference between the two curves in each graph is an indication of the cycle-by-cycle variation in the mean flow [see Eq. (8.7)]. During the intake process, within the directed intake flow pattern, the cycle-by-cycle variation in the mean flow is small in comparison to the high turbulence levels created by the strong intake flow. Outside this directed flow region, again during intake, this cycle-by-cycle contribution is more significant relative to the turbulence. During compression, the cycle-by-cycle mean flow variation is comparable in magnitude to the ensemble-averaged turbulence intensity. It is therefore highly significant.

Figure 8.10 Ensemble-averaged rms velocity fluctuation and ensemble-averaged individual-cycle turbulence intensity as a function of crank angle: (a) at location b in Fig. 8.9a; (b) at location c in Fig. 8.9a.[14]



The above examples of intake-flow-generated in-cylinder motion set the stage for the subsequent flow development. Mean flow structures such as the vortex structures formed by the flow through an intake valve have usually decayed by BC. The only mean flow structures surviving into the compression stroke are swirl and tumble. The bulk of the turbulent kinetic energy observed during intake is generated, in-cylinder, by the air flowing through the valve head and seat flow restriction into the cylinder. Intake port-generated turbulence convected into the cylinder is a minor contribution. Peak turbulence levels occur around mid-intake stroke when piston speed is a maximum and decay rapidly thereafter. As the compression stroke proceeds, the spatial distribution of turbulence becomes reasonably homogeneous (uniform) and isotropic (independent of direction).

It is the character of the turbulence at the end of the compression process that is most important: that is what controls the fuel-air mixing and burning rates. These specific results support the broader conclusion that the intake flow plays the dominant role in the generation of the in-cylinder mean flow and turbulence fields during the intake stroke. However, in the absence of swirl or tumble, this intake-generated flow structure has almost disappeared by the time the compression process commences. The turbulence levels follow this mean-flow trend, and also decay significantly by intake valve closing.

When a swirling flow is generated during intake, an almost solid-body rotating flow about the cylinder axis develops which remains stable for much longer than the intake-jet generated rotating flows illustrated in Fig. 8.3. With simple open combustion chambers, the turbulence still appears to become almost homogeneous at the end of compression. With swirl and bowl-in-piston geometry chambers, however, the flow is more complex (see Sec. 8.3). When a tumbling flow is generated during intake, it persists (and lengthens, axially) as the piston travels down the cylinder. Then, during compression, it is steadily "squashed" until mid-to-late compression stroke when it becomes unstable and breaks up. The kinetic energy stored in this tumbling motion as it breaks up is transferred to the ensuing turbulence that breakup generates.

During compression, many features of these flows affect the levels of turbulence within the cylinder. Quantifying the development of this turbulence through modeling the evolution of the turbulent kinetic energy k is an important component of quantifying the engines fuel-air mixing and combustion processes. The conservation equation for the turbulent kinetic energy is:

© McGraw-Hill Education. All rights reserved. Any use is subject to the Terms of Use, Privacy Notice and copyright information.

$$\frac{\overline{D}k}{\overline{D}t} = P - \varepsilon - (\nabla \bullet \mathrm{T})$$

(8.23)

where P is the rate of production, ε the viscous dissipation rate, and the vector **T** is the transport of turbulent kinetic energy. (Turbulence modeling of engine flows is discussed fully in Sec. 14.5.2.) There are three orthogonal components of k: for example,
$k_i = (u_i u_i/2)$. The turbulent transport term is not a dominant source of turbulent kinetic energy![2] Production results from the turbulent stresses in the flow which have the form:

$$P = -\left(u_i u_j\right) S_{ij}$$

(8.24)

where (S_{ij}) is the mean rate of strain tensor, the terms of which depend on the gradients in the components of the turbulent fluctuating velocities. Thus one can see that the specific in-cylinder motions—swirl, tumble, and also *squish* (that results from the displacement of mixture toward the center of the cylinder as the piston approaches TC: see Sec. 8.5)—and their interactions (see Sec. 8.6), can lead to significant turbulence production. Of course the viscous dissipation of turbulent kinetic energy (ε) continues throughout this evolution of the in-cylinder motions.[16]

The flow through the intake valve is responsible for many features of the four-stroke cycle in-cylinder motion. The flow velocity through the valve is proportional to the piston speed [see Eq. (6.10) for pseudo valve-flow velocity definition, and Eq. (2.10)]. It would be expected therefore that in-cylinder flow velocities at different engine speeds would scale with mean piston speed [Eq. (2.11)]. Figure 8.11 shows ensemble-averaged mean and rms velocity fluctuations, normalized by the mean piston speed through the cycle at three different engine speeds. The measurement location is in the path of the intake generated swirling flow (point *b* in Fig. 8.9*a*). All the curves have approximately the same shape and magnitude, indicating the appropriateness of this velocity scaling.[3] Other results support this conclusion, though in the absence of an ordered mean motion such as swirl or tumble when the ensemble-averaged mean velocities at the end of compression are low, this scaling for the mean velocity does not always hold.[15,16]

Figure 8.11 Ensemble-averaged mean and rms velocity fluctuations, normalized by mean piston speed, throughout the engine cycle for three engine speeds. Location b engine layout in Fig. 8.9a.[14]

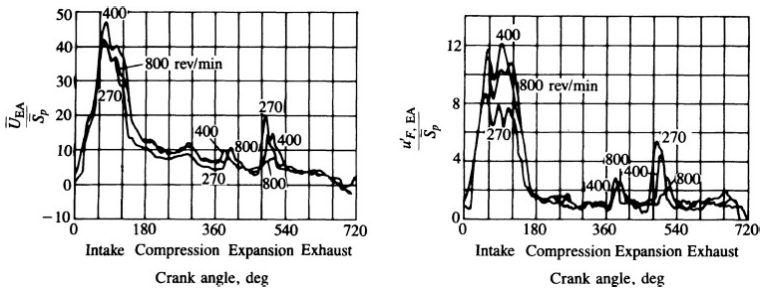
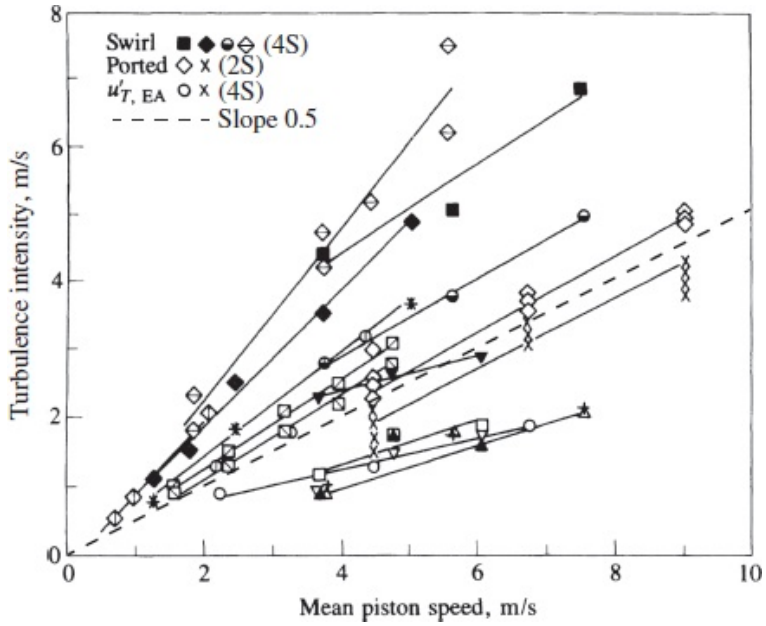


Figure 8.12 shows a compilation of ensemble-averaged rms fluctuation velocity or ensemble-averaged individual-cycle turbulence intensity results at TC at the end of compression, from 13 different flow configurations and combustion chamber geometries. Two of these sets of results are from two-stroke cycle ported configurations. The measured fluctuating velocities or turbulence intensities at TC are plotted against mean piston speed. The linear relationship holds well. There is a substantial variation in the proportionality constant, in part, because in most of these studies (identified in the figure) the ensemble-averaged rms fluctuation velocity was the quantity measured. Since this includes the cycle-by-cycle fluctuation in the mean velocity, it is larger than the average turbulence intensity

© McGraw-Hill Education. All rights reserved. Any use is subject to the Terms of Use, Privacy Notice and copyright information.

$u'_{T,\mathrm{EA}}$

Figure 8.12 Individual-cycle turbulence intensity $u'_{T,\mathrm{EA}}\,(\mathrm{o},\times)$ *and ensemble-averaged rms fluctuation velocity (remaining symbols) at TC at the end of compression, for a number of different flow configurations and chamber geometries as a function of mean piston speed. Two data sets are for two-stroke ported engines: four data sets with intake generated swirl.*[17] *(* $u' = 0.5\overline{S}_p$ *line also shown.)*



A consensus has emerged from these studies that the turbulence intensity at around top-center of the compression process, as combustion commences, has a value equal to between half the mean piston speed and the mean piston speed, that is,

$$u'_{T,\mathrm{EA}}(\mathrm{TC}) \approx (0.5\,\mathrm{to}\,1.0)\overline{S}_p \tag{8.25}$$

Open combustion chamber shapes of four-stroke-cycle engines without significant swirl or tumble are at the lower end of this range. Small high-speed direct-injection diesel engine chambers with deep, re-entrant-shaped bowl-in-piston geometries, with high swirl, have the highest values of $u'/\overline{S}_p$. Addition of swirl, or tumble in pent-roof gasoline engine combustion chamber designs have intermediate values of $u'/\overline{S}_p$. The flow and turbulence levels in the various types of combustion chamber geometries used in gasoline SI engines, and in diesel engines, are explored in more detail in Sec. 8.6. The ensemble-averaged cyclic variation in individual-cycle mean velocity at the end of compression also scales with mean piston speed. This quantity is normally lower in magnitude than the turbulence intensity, especially when there is a strong directed mean flow.[16]

Turbulence length and time scales in automobile engine flows have been characterized. They are important in determining fuel, air, residual gas mixing rates and, especially at TC of compression, in quantifying the scale of flame sheet wrinkling of the turbulent SI engine flame. During the intake process, the integral length scale is of the order of the intake jet diameter, which is comparable to the valve lift (≤10 mm in automobile-size engines). During compression the flow pattern relaxes to the shape of the combustion chamber. The integral length scale which defines the largest coherent structures (or eddies) in the turbulent flow can be determined using spatial correlation functions from instantaneous fluctuating velocity component measurements at multiple points in the flow via Eq. (8.8)—see Fig. 8.8. More commonly they are determined from single-point

© McGraw-Hill Education. All rights reserved. Any use is subject to the Terms of Use, Privacy Notice and copyright information.

experimental data using Taylor's hypothesis via Eq. (8.10). Taylor's hypothesis is valid when the characteristic time scale (or lifetime) of a turbulent eddy is much larger than the time required for that eddy to be convected through the measurement location by the mean flow: that is, when $u' \ll \overline{U}$. This condition is usually satisfied in engines with significant swirl, tumble, or squish-generated flows: little variation in integral length scales occurs as engine speed changes. Also, comparisons of the above two approaches for determining l_I give comparable results. These findings indicate that at around TC of compression, the in-cylinder flow turbulence is close to isotropic: that is, the fluctuating velocity components have no preferred direction. In such flows, applying Eq. (8.8) results in two integral length scales: $l_{I,\text{long}}$ and $l_{I,\text{lat}}$ which correspond to fluctuating velocity components parallel to the separating length vector (**x**), and lateral to the separating vector, respectively.[4]

Generally, lateral integral length scales, $l_{I,\text{lat}}$ determined near TC of compression, are in the range of 1 to 3 mm while longitudinal scales range from about 2 to 8 mm,[16] thus indicating that turbulence isotropy often exists. Temporarily, integral length scales exhibit a broad minimum around TC, and the value is relatively insensitive to engine speed. Strong velocity gradients in the in-cylinder flow can lead to significant spatial variations in length scales throughout the combustion chamber. While integral scales are comparable to the largest scales characterizing in-cylinder flow, and the physical flow boundaries which the combustion chamber shape imposes limit the integral scale, there is no fundamental reason beyond the above started constraints why the integral scale should be proportional to geometric features such as the clearance height as is sometimes claimed.

The integral time scale at the end of compression decreases with increasing engine speed. It is of order 1 ms at engine speeds of about 1000 rev/min. The integral length scale at the end of compression, as explained above, is a few mm, varies little with engine speed, and decreases as the piston approaches TC. The micro time scale at the end of compression is of order 0.1 ms at 1000 rev/min, and decreases as engine speed increases (again in automobile-size engine cylinders). Micro length scales are of order 1 mm at the end of compression and vary little with engine speed. Kolmogorov length scales at the end of compression are of order 10^{-2} mm.[11, 18, 19]

[1] There is considerable debate as to whether the fluctuating components of the velocity $U(\theta,i)$ defined by Eq. (8.7), cycle-by-cycle fluctuations in the mean velocity and fluctuations in time about the individual cycle mean, are physically distinct phenomena. The high-frequency fluctuations in velocity about the individual cycle mean are usually defined as "turbulence." The low-frequency fluctuations are generally attributed to the variations in the mean flow between individual cycles, a phenomenon that is well established.

[2] $\overline{D}/\overline{D}t$ is the substantive or convective derivative operator $\partial/\partial t + \nabla\bullet$, following a fluid element along its streamline.

[3] Note that because of the valve and combustion chamber of this particular engine, the ratio of $\overline{U}$ to $\overline{S}_p$ is higher than is typical of normal engine geometries.

[4] Note that the turbulence is approximately isotropic since the fluctuating velocities can be thought of as having three orthogonal components (one longitudinal and two lateral), with $l_{I,\text{long}}$ often about $2l_{I,\text{lat}}$.

© McGraw-Hill Education. All rights reserved. Any use is subject to the Terms of Use, Privacy Notice and copyright information.

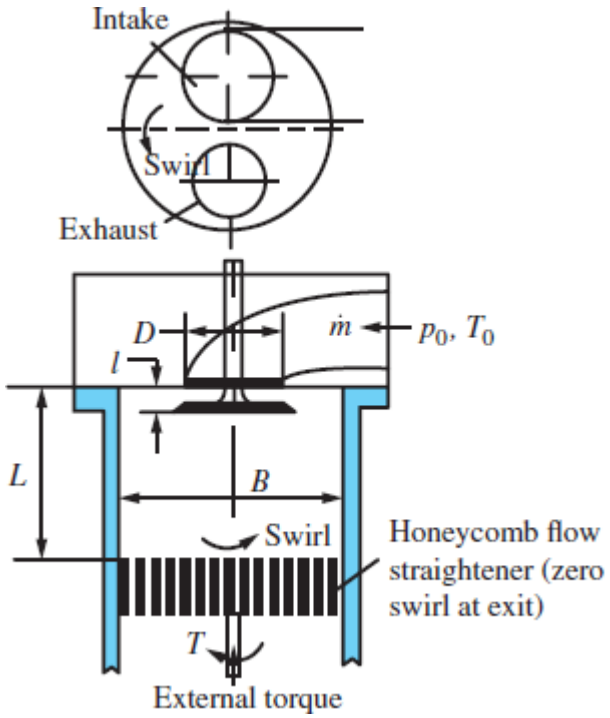
8.3. SWIRL

Swirl is defined as organized rotation of the charge about the cylinder axis. Swirl is created by bringing the intake flow into the cylinder with an initial angular momentum. While some decay in swirl due to friction occurs during the engine cycle, intake-generated swirl usually persists through the compression, combustion, and expansion processes. In engine designs with bowl-in-piston combustion chambers, the rotational motion setup during intake is substantially amplified during compression. Swirl is used in diesels and some stratified-charge engine concepts to promote more rapid mixing between the inducted air charge and the injected fuel. Swirl is also used to speed up the combustion process in spark-ignition engines. In two-stroke engines, it is used to improve scavenging. In some designs of prechamber engines, organized rotation about the prechamber axis is also characterized as swirl. In prechamber engines where swirl within the precombustion chamber is important, the flow into the prechamber during the compression process creates the rotating flow. Prechamber flows are discussed in Sec. 8.7.

8.3.1. Swirl Measurement

The nature of the swirling flow in an actual operating engine is difficult to determine. Accordingly, steady flow tests are often used to characterize the swirl. Air is blown steadily through the inlet port and valve assembly in the cylinder head into an appropriately located equivalent of the cylinder. A common technique for characterizing the swirl within the cylinder has been to use a light paddle wheel, pivoted on the cylinder centerline (with low friction bearings), mounted between 1 and 1.5 bore diameters down the cylinder. The paddle wheel diameter is close to the cylinder bore. The rotation rate of the paddle wheel is used as a measure of the air swirl. However, this rotation rate depends on the location of the wheel and its design, as well as the details of the swirling flow. A more precise technique is the impulse swirl meter shown in Fig. 8.13. A honeycomb flow straightener replaces the paddle wheel: it measures the total torque exerted by the swirling flow. This torque equals the flux of angular momentum through the plane coinciding with the flow-straightener upstream face.

Figure 8.13 Schematic of steady-flow angular-momentum flux swirl meter.[20]



© McGraw-Hill Education. All rights reserved. Any use is subject to the Terms of Use, Privacy Notice and copyright information.

For each of these approaches, a *swirl coefficient* is defined which essentially compares the flow's angular momentum with its axial momentum. For the paddle wheel, the swirl coefficient C_s is defined by

$$C_s = \omega_p B / v_0$$

(8.26)

where ω_0 is the paddle wheel angular velocity (= $2\pi N_p$, where N_p is the rotational speed) and the bore B has been used as the characteristic dimension. The characteristic velocity, v_0, is derived from the pressure drop across the valve using an incompressible flow equation:

$$v_0 = \left[\frac{2\left(p_0 - p_c\right)}{\rho} \right]^{1/2}$$

(8.27)

or a compressible flow equation:

$$v_0 = \left\{ \frac{2\gamma}{(\gamma - 1)} \frac{p_0}{\rho_0} \left[1 - \left(\frac{p_c}{p_0} \right)^{(\gamma-1)/\gamma} \right] \right\}^{1/2}$$

(8.28)

where the subscripts 0 and c refer to upstream stagnation and cylinder values, respectively. The difference between Eqs. (8.27) and (8.28) is usually small. With the impulse torque meter, characteristic velocity and length scales must also be introduced. Several swirl parameters have been defined. The simplest is

$$C_s = \frac{8T}{\dot{m} v_0 B}$$

(8.29)

where T is the torque and
$\dot{m}$ the air mass flow rate. The velocity, v_0, defined by Eq. (8.27) or Eq. (8.28), and the bore have again been used to obtain a dimensionless coefficient. Note that for solid-body rotation of the fluid within the cylinder at the paddle wheel speed ω_p, Eqs. (8.26) and (8.29) give identical swirl coefficients. In practice, because the swirling flow is not solid-body rotation and because the paddle wheel usually lags the flow due to slip, the impulse torque meter gives higher swirl coefficients.[21] When swirl measurements are made in an operating engine, a *swirl ratio* is normally used to define the swirl. It is defined as the angular velocity of a solid-body rotating flow ω_s that has equal angular momentum to the actual flow, divided by the crankshaft angular rotational speed:

$$R_s = \frac{\omega_s}{2\pi N}$$

(8.30)

Typically, values for swirl ratio are in the range of 1 to 4. During the induction stroke in an engine, the flow and the valve open

© McGraw-Hill Education. All rights reserved. Any use is subject to the Terms of Use, Privacy Notice and copyright information.

area, and consequently the angular momentum flux into the cylinder, vary with crank angle. Whereas in the above described rig tests, the flow and valve open area are fixed, and the angular momentum passes down the cylinder continuously, in the engine intake process the momentum produced under corresponding conditions of flow and valve lift remains in the cylinder. Steady-state impulse torque-meter flow-rig data can be used to estimate engine swirl in the following manner.[21] Assuming that the port and valve retain the same characteristics under the transient conditions of the engine as on the steady-flow rig, the equivalent solid-body angular velocity ω_s at the end of the intake process is given by

$$\omega_s = \frac{8}{B^2}\left[\int_{\theta_1}^{\theta_2} T d\theta\right] / \left[\int_{\theta_1}^{\theta_2} \dot{m}\, d\theta\right]$$

where θ_1 and θ_2 are crank angles at the start and end of the intake process and the torque T and mass flow rate $\dot{m}$ are evaluated at the valve lift corresponding to the local crank angle. Using Eq. (8.29) for T, Eq. (6.11) for $\dot{m}$, assuming v_0 and ρ are constant throughout the intake process, and introducing volumetric efficiency η_v based on intake manifold conditions via Eq. (2.27), it can be shown that

$$R_s = \frac{\omega_s}{2\pi N} = \pi \eta_v B L \left[\int_{\theta_1}^{\theta_2} (A_v C_D)\, C_s d\theta\right] / \left[\int_{\theta_1}^{\theta_2} (A_v C_D)\, d\theta\right]^2$$

(8.31)

where $A_V C_D$ is the effective valve open area at each crank angle. Note that crank angle in Eq. (8.31) should be in radians. Except for its (weak) dependence on η_v, Eq. (8.31) gives R_s independent of operating conditions directly from rig test results and engine geometry.

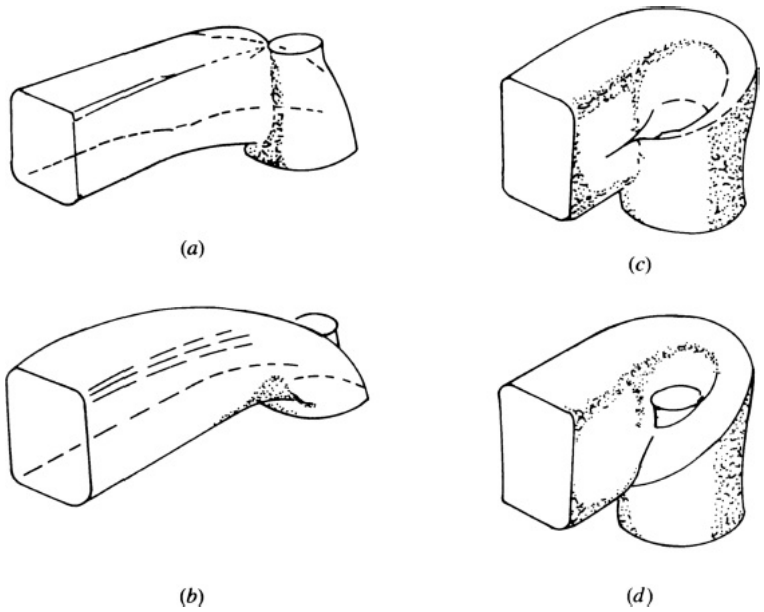
The relationship between steady-flow rig tests (which are used because of their simplicity) and actual engine swirl patterns is complex. Steady-flow tests adequately define the swirl generating characteristics of the intake port and valve (at fixed valve lift) and are used extensively for this purpose. However, the swirling flow set up in the cylinder during intake can change significantly during compression.

8.3.2. Swirl Generation during Induction

Two general approaches are used to create swirl during the induction process. In one, the flow is discharged into the cylinder tangentially, where it is deflected sideways and downward in a swirling motion. In the other, the swirl is largely generated within the inlet port: the flow is forced to rotate about the valve axis *before* it enters the cylinder. The former type of motion is achieved by forcing the flow distribution around the circumference of the inlet valve to be nonuniform so that the intake flow has substantial net angular momentum about the cylinder axis. The directed port and deflector wall port in Fig. 8.14 are two common ways of achieving this result. The directed port brings the flow toward the valve opening in the desired tangential direction. Its passage is straight, which due to other cylinder head requirements restricts the flow area and results in a relatively low discharge coefficient. The deflector wall port uses the port's inner side wall to force the flow preferentially through the outer periphery of the valve opening, in a tangential direction. Since only one wall is used to obtain a directional effect, the port areas are less restrictive.

© McGraw-Hill Education. All rights reserved. Any use is subject to the Terms of Use, Privacy Notice and copyright information.

Figure 8.14 Different types of swirl-generating inlet ports: (a) deflector wall; (b) directed; (c) shallow ramp helical; (d) steep ramp helical.[22]

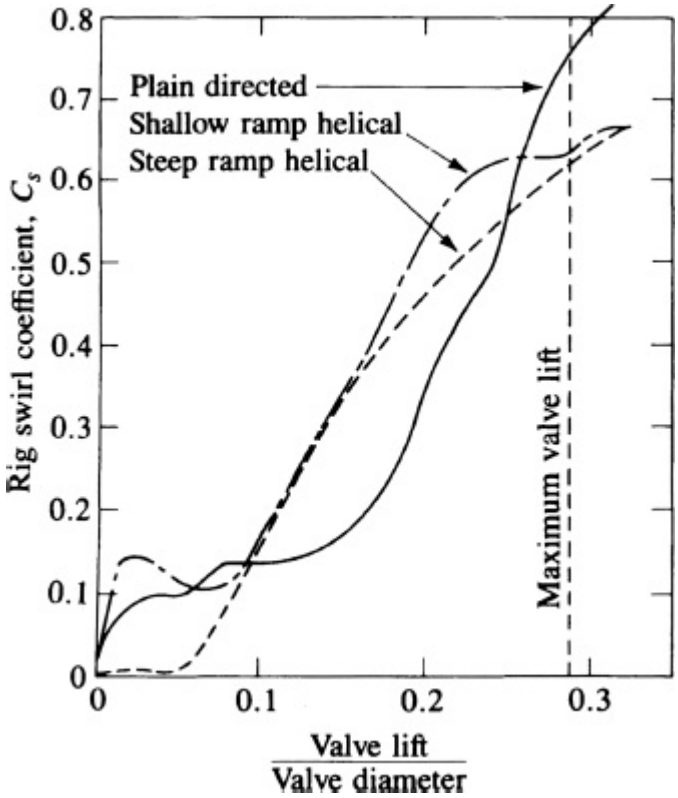


The second broad approach is to generate swirl within the port about the valve axis, prior to the flow entering the cylinder. Two examples of such *helical ports* are shown in Fig. 8.14. With helical ports, a higher flow discharge coefficient (lower flow resistance) at equivalent levels of swirl is usually obtained, since the whole periphery of the valve open area can be more fully utilized. A higher volumetric efficiency—important at high loads—results. Also, helical ports are less sensitive to position displacements such as can occur in casting, since the swirl generated depends mainly on the port geometry above the valve and not the position of the port relative to the cylinder axis.

Figure 8.15 compares steady-state swirl-rig measurements of examples of the ports inFig. 8.14. The rig swirl number increases with increasing valve lift, reflecting the increasing impact of the port shape and decreasing impact of the flow restriction between the valve head and seat. Helical ports normally impart more angular momentum at medium lifts than do directed ports.[21,23] The swirl ratios for these ports calculated from this rig data using Eqs. (8.27) and (8.29) are: 2.5 for the directed port, 2.9 for the shallow ramp helical, and 2.6 for the steep ramp helical. Vane swirl-meter swirl ratios were about 30% less. These impulse-swirl-meter-derived engine swirl ratios are within about 20% of the solid-body rotation rate which has equal angular momentum to that of the cylinder charge determined from tangential velocity measurements made within the cylinder of an operating engine with the same port, at the end of the induction process.[23]

© McGraw-Hill Education. All rights reserved. Any use is subject to the Terms of Use, Privacy Notice and copyright information.

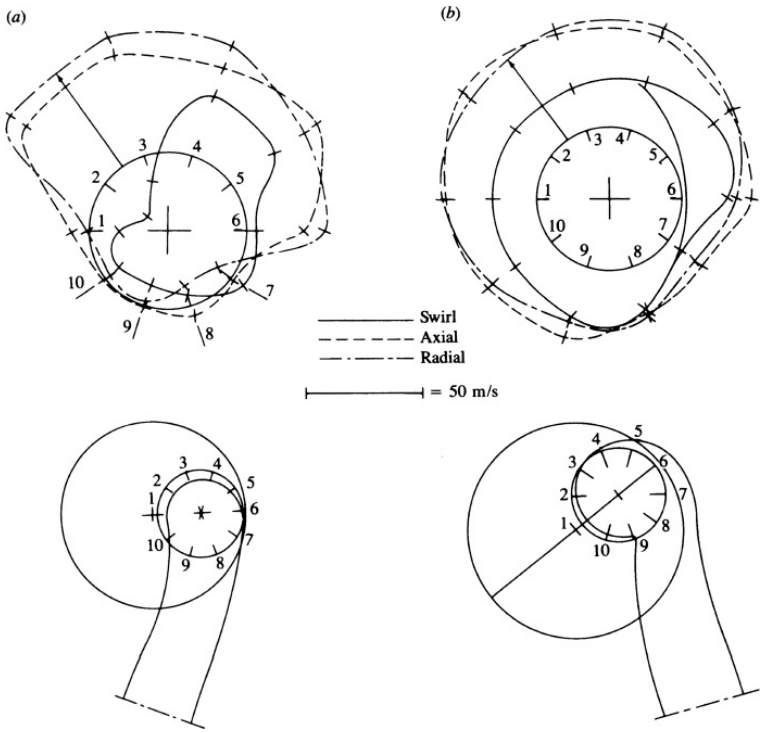
Figure 8.15 Steady-state torque meter swirl measurements of directed, shallow ramp, and steep ramp helical ports as a function of inlet valve lift/diameter ratio.[21]



Directed and deflector wall ports, and masked valve or head designs produce a tangential flow into the cylinder by increasing the flow resistance through that part of the valve open area where flow is not desired. A highly non-uniform flow through the valve periphery results, and the flow into the cylinder has a substantial v_θ velocity component in the same direction about the cylinder axis. In contrast, helical ports produce the swirl in the port upstream of the valve, and the velocity components v_r, and v_z through the valve opening, and v_θ *about the valve axis* are approximately uniform around the valve open area. Figure 8.16 shows velocity data measured at the valve exit plane in steady-flow rig tests with examples of these two types of port. The valve and cylinder wall locations are shown. In Fig. 8.16*a*, the deflector wall of the tangentially oriented port effectively prevents any significant flow around half the valve periphery. In contrast, in Fig. 8.16*b* with the helical port, the air flows into the cylinder around the full valve open area. The radial and axial velocities are essentially uniform around the valve periphery. The swirl velocity about the valve axis (anticlockwise when viewed from above) for this helical port is relatively uniform and is about half the magnitude of the radial and axial velocities through the valve open area.

© McGraw-Hill Education. All rights reserved. Any use is subject to the Terms of Use, Privacy Notice and copyright information.

Figure 8.16 Swirl, axial, and radial velocities measured 2 mm from cylinder head around the valve circumference for (a) tangential deflector-wall port and (b) helical port; magnitude of velocity is given by the distance along a radial line (from valve axis), from valve outline to the respective curve scaled by the reference length (examples of radial velocity indicated by two arrows); valve lift = 12.8 mm.[24, 25]



The swirling airflow within the cylinder of an operating engine is not uniform. The velocities generated between the valve head and seat at each point in the induction process depend on the valve open area and piston velocity. The velocities are highest during the first half of the intake process as indicated by the pseudo valve-flow velocity curve in Fig. 6.17. Thus, the swirl velocities generated during this portion of the induction stroke are higher than the swirl generated during the latter half of the stroke: there is swirl stratification. Also, the flow pattern close to the cylinder head during induction is comparatively disorganized, and not usually close to a solid-body rotation. It consists of a system of vortices, created by the high-velocity tangential or spiraling intake jet. Further down the cylinder, the flow pattern is closer to solid-body rotation with the swirl velocity increasing with increasing radius.[21, 22] This more ordered flow directly above the piston produces higher swirl velocities in that region of the cylinder. As the piston velocity decreases during intake, the swirl pattern redistributes, with swirl speeds close to the piston decreasing and swirl speeds in the center of the cylinder increasing.[25] Note that the axis of rotation of the swirling in-cylinder gases may rotate about the cylinder and not exactly coincide with the cylinder axis. This discussion indicates that there is a close to linear scaling of swirl with engine speed, though at higher speeds, flow fiction somewhat reduces this scaling.

8.3.3. Swirl Modification within the Cylinder

The angular momentum of the air, which enters the cylinder at each crank angle during induction, decays throughout the rest of the intake process and during the compression process due to friction at the walls and turbulent dissipation within the fluid. Typically one-quarter to one-third of the initial moment of momentum about the cylinder axis will be lost by top-center at the end of compression. However, swirl velocities in the charge can be substantially increased during compression by suitable design of the combustion chamber. In many designs of direct-injection diesel combustion systems, air swirl is used to obtain much more rapid mixing between the fuel injected into the cylinder and the air than would occur in the absence of swirl. The

© McGraw-Hill Education. All rights reserved. Any use is subject to the Terms of Use, Privacy Notice and copyright information.

tangential velocity of the swirling airflow set up inside the cylinder during induction is substantially increased by forcing most of the air into a compact bowl-in-piston combustion chamber, usually centered on the cylinder axis, as the piston approaches its top-center position. Neglecting the effects of friction, angular momentum is conserved: so as the moment of inertia of the air is decreased, its angular velocity must increase.

However, the total angular momentum of the charge within the cylinder decays due to friction at the chamber walls. Thus the angular momentum of the cylinder charge Γ_c changes with time according to the moment of momentum conservation equation:

$$\frac{d\Gamma_c}{dt} = J_i - T_f$$

(8.32)

where J_i is the flux of angular momentum into the cylinder and T_f is the torque due to wall friction. At each point in the intake process J_i is given by

$$J_i = \int_{A_v} \rho r \mathrm{v} \bullet \mathrm{dA_v}$$

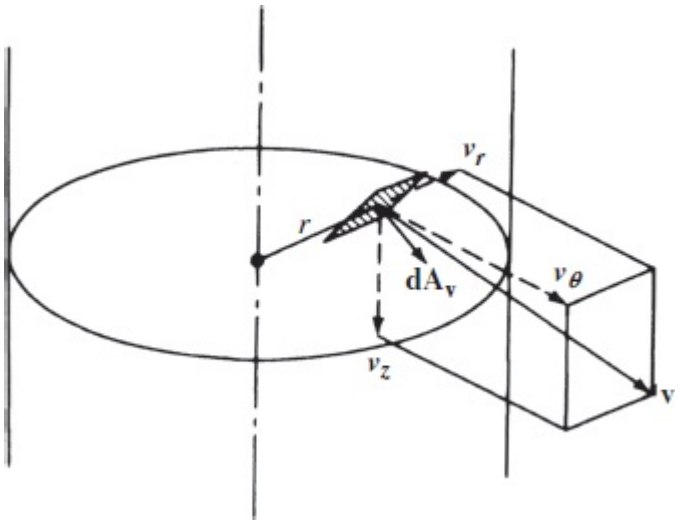
(8.33)

where $\mathbf{dA_v}$ is a vector element of the valve open area, as defined in Fig. 8.17. While the angular momentum entering the cylinder during the intake process is

$$\gamma_{c,i} = \int_{t_{\mathrm{ivo}}}^{t_{\mathrm{ive}}} \rho r v_\theta \mathrm{v} \bullet \mathrm{dA_v} dt$$

the actual angular momentum within the cylinder at the end of induction will be less, due to wall friction during the intake process. Friction continues through the compression process so the total charge angular momentum at the end of compression is further reduced.

Figure 8.17 Definition of symbols in equation for angular momentum flux into the cylinder [Eq. (8.33)].



© McGraw-Hill Education. All rights reserved. Any use is subject to the Terms of Use, Privacy Notice and copyright information.

There is friction on the cylinder liner, cylinder head, and piston crown (including any bowl or cut outs within the crown). This friction can be estimated using friction formulas developed for flow over a flat plate, with suitable definitions of characteristic length and velocity scales. Friction on the cylinder liner can be estimated from the wall shear stress:

$$\tau = \frac{1}{2}\rho\left(\frac{\omega_s B}{2}\right)^2 C_F$$

(8.34)

where ω_s is the equivalent solid-body swirl. The friction factor C_F is given by the flat plate formula:

$$C_F = 0.037\lambda(\mathrm{Re}_B)^{-0.2}$$

(8.35)

where λ is an empirical constant introduced to allow for differences between the flat plate and cylinder wall($\lambda \approx 1.5$)[23] and Re_B is the equivalent of the flat plate Reynolds number [$\mathrm{Re}_B = \rho(Bw_s/2)(\pi B/m)$]. Friction on the cylindrical walls of a piston cup or bowl can be obtained from the above expressions with D_B, the bowl diameter, replacing the bore.

Friction on the cylinder head, piston crown, and piston bowl floor can be estimated from expressions similar to Eqs. (8.34) and (8.35). However, since the tangential velocity v_θ at the wall varies with radius, the shear stress should be evaluated at each radius and integrated over the surface: for example,[26]

$$\tau(r) = C_1\frac{1}{2}\rho[v_\theta(r)]^2\mathrm{Re}^{-0.2}$$

(8.36)

with

$$\mathrm{Re} = \rho v_\theta(r) r/\mu$$

where C_1 is an empirical constant (≈ 0.055). An alternative approximate approach is to evaluate these components of the wall shear stress at the mean radius.

Next, consider the effects on swirl of radially inward displacement of the air charge during compression. The most common example of this phenomenon occurs with the bowl-in-piston combustion chamber design of medium- and high-speed direct-injection diesels (see Sec. 10.2). However, in spark-ignition engines where swirl can be used to increase the burning rate, the shape of the combustion chamber close to top-center can also force radially inward motion of the charge. For a given swirling in-cylinder flow at the end of induction, and neglecting the effects of friction, as the moment of inertia of the air about the cylinder axis is decreased the air's angular velocity must increase to conserve angular momentum. For example, for solid-body rotation of the cylinder air charge of mass m_c, the initial angular momentum $\Gamma_{c,i}$ and solid-body rotation $\omega_{s,i}$ are related at bottom-center by

$$\Gamma_{c,i} = I_c\omega_{s,i}$$

where I_c is the moment of inertia of the charge about the cylinder axis. For a disc-shaped combustion chamber, $I_c = m_cB^2/8$ and is constant. For a bowl-in-piston combustion chamber,

© McGraw-Hill Education. All rights reserved. Any use is subject to the Terms of Use, Privacy Notice and copyright information.

$$I_c = \frac{m_c B^2}{8} \frac{\left[(z/h_B) + (D_B/B)^4\right]}{\left[(z/h_B) + (D_B/B)^2\right]}$$

(8.37)

where D_B and h_B are the diameter and depth of the bowl, respectively, and z is the distance of the piston crown from the cylinder head. At TC crank position, $z \approx 0$ and $I_c \approx m_c D_B^2/8$. At the end of induction, $I_c \approx m_c B^2/8$. Thus, in the absence of friction, ω_s would increase by $(B/D_B)^2$, usually a factor of about 4.

In an operating engine with this bowl-in-piston chamber design, the observed increase in swirl in the bowl is less; it is usually a factor of 2 to 3.[21,23] This is because of wall friction, dissipation in the fluid due to turbulence and velocity gradients, and the fact that a fraction of the fluid remains in the clearance region above the piston crown. The loss in angular momentum due to these effects will vary with geometric details, initial swirl flow pattern, and engine speed.

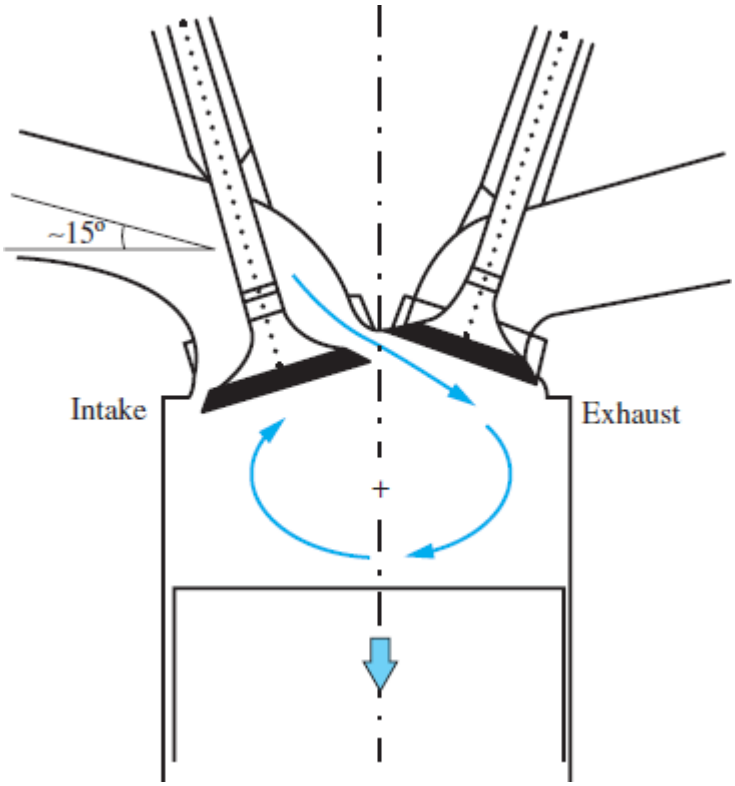
Swirl velocity distributions in the cylinder at the end of induction show the tangential velocity increasing with radius, except close to the cylinder wall where friction causes the velocity to decrease. While the velocity distribution is not that of a solid-body rotation, depending on port design and operating conditions, it is often close to solid-body rotation.[21,23] Departures from the solid-body velocity distribution are greater at higher engine speeds, suggesting that the flow pattern in the cylinder at this point in the cycle is still developing with time.[21,27] In the absence of radially inward gas displacement during compression, the flow pattern continues to develop toward a solid-body distribution throughout the compression stroke.[23] Swirl ratios of 3 to 5 at top-center can be achieved with the ports shown in Fig. 8.13, with flat-topped pistons (i.e., in the absence of any swirl amplification during compression).

© McGraw-Hill Education. All rights reserved. Any use is subject to the Terms of Use, Privacy Notice and copyright information.

8.4. TUMBLE

An in-cylinder *tumble flow* is used in spark-ignition engines to speed up the combustion process. As Fig. 8.4 indicates, tumble is charge rotation about an axis orthogonal to the cylinder axis. It is set up, usually in pent-roof combustion chambers with four valves (two intake valves) with inclined valve stems (see Fig. 8.18), by positioning the intake ports to bring the entering airflow into the cylinder through the upper portion of the open area between the valve head and valve seat. This imparts a transverse (across the cylinder) motion to the entering air. The descending piston then pulls that flow down the liner on the side opposite to the intake valves; it then moves back across the piston crown and upward along the liner to complete this flow rotation. Because the intake-valve open area is not used uniformly, these transverse flow velocities past the valve for a given piston speed are higher, thus additional kinetic energy is stored in this in-cylinder tumbling flow. Note also that, as a result of the uneven use of the valve (and port) open area, the flow resistance of the intake valve and port system is higher so the engine's maximum volumetric efficiency is lowered. During compression, this tumble flow is "squashed" by the upward-moving piston, becomes unstable as a consequence, and breaks up into smaller-scale vortices generating turbulent kinetic energy which, following the spark discharge, increases the engine's mixture burning rate. In spark-ignition engines, tumble is commonly used to achieve faster burn rates (important at part-load to achieve good EGR tolerance and improve part-load efficiency); the modest loss in engine breathing capacity at higher loads and speeds is accepted as a necessary consequence.

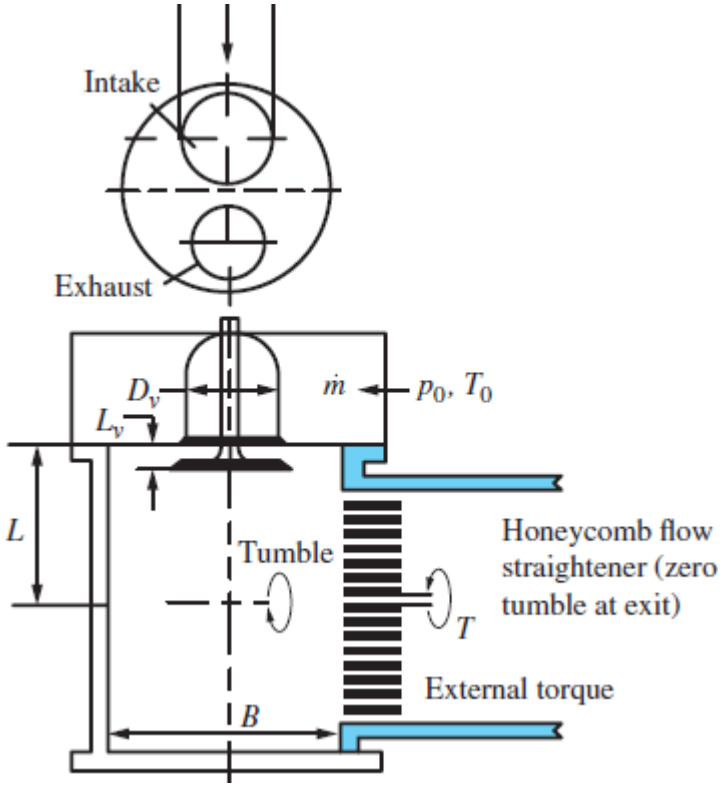
Figure 8.18 Schematic showing how the intake ports and valves (in a four-valve-per-cylinder engine), and piston motion down the cylinder, generate tumble. Key feature is low-angle intake ports that direct the flow primarily through the upper portion of the open valve gap across the cylinder head.



Measuring and characterizing tumble are done analogously to swirl. Figure 8.19 illustrates how the tumble flow angular momentum can be measured in a steady flow rig (analogous to the swirl meter rig shown in Fig. 8.15). The measured torque T, is proportional to the mass flow rate into the cylinder through the intake ports, the in-cylinder flow's (average) angular velocity, and the mean radius of rotation about the tumble flow axis (about $B/4$).[20]

© McGraw-Hill Education. All rights reserved. Any use is subject to the Terms of Use, Privacy Notice and copyright information.

Figure 8.19 Schematic of steady-flow angular-momentum-flux tumble meter.[20]



Tumble flows are characterized by their angular momentum. Figure 8.18 shows what is often called *normal tumble* where flow rotation is about an axis (shown in the figure) that is parallel to the ridge of the pent roof cylinder head. *Reverse tumble*, where the flow would rotate in the opposite direction to that in Fig. 8.18 (counter-clockwise), is generated with the intake ports directed vertically downward toward the intake valve, rather than almost horizontal (as in Fig. 8.18). Reverse tumble is used in certain designs of stratified-charge direct-injection gasoline engines to control the motion of the evolving fuel-air mixture "cloud" the evaporating fuel spray creates (see Sec. 7.7.2). When tumble is created in the presence of swirl, the air charge rotation about the cylinder axis can result in a tumbling flow component in the plane at 90° to the rotation plane shown in Fig. 8.18. This *cross tumble* flow, orthogonal to the normal tumble flow, should be combined with the normal tumble angular momentum to quantify the total in-cylinder tumble flow angular momentum.

These various tumbling flows are characterized by a *tumble ratio*, analogous to the swirl ratio defined by Eq. (8.30). The tumble ratio is defined as

$$R_t = \frac{\omega_t}{2\pi N}$$

(8.38)

where ω_t is the total angular momentum of the charge divided by the moment of inertia of the in-cylinder fluid: i.e., the equivalent solid-body angular speed divided by the angular rotation rate of the crankshaft.[28] Thus:

$$R_t = \frac{\int_{\theta_1}^{\theta_2} \rho(\mathrm{r} \times \mathrm{v}) \bullet \mathrm{i} d\theta}{2\pi N \int_{\theta_1}^{\theta_2} \rho(\mathrm{r} \bullet \mathrm{r}) d\theta} v$$

© McGraw-Hill Education. All rights reserved. Any use is subject to the Terms of Use, Privacy Notice and copyright information.

(8.39)

When both normal- and cross-tumble are significant, the overall tumble ratio,$R_{t,o}$, is given by:

$$R_{t,o} = \left(R_{t,n}^2 + R_{t,c}^2 \right)^{1/2}$$

(8.40)

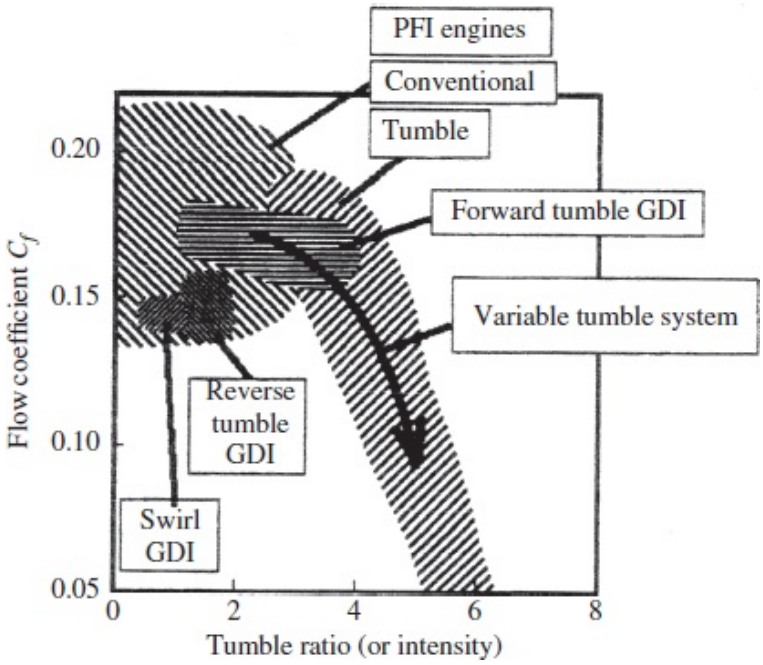
For a given geometry cylinder-head design, the tumble ratio increases as the intake valve lift and the piston speed increase during the first half or so of the intake stroke. With four-valve cylinder heads, with intake ports of the geometry shown in Fig. 8.18, tumble ratios of 1 to 2 or so are realized. With additional flow-directing restrictions in the intake ports (e.g., throttles or baffles) higher tumble ratios of up to about 4 can be obtained. Then, during compression the tumbling flow is squashed by the piston moving up the cylinder. As the clearance height becomes small, this squashed tumble flow breaks up into smaller-scale rotating eddies that decay into turbulence.

Intake port baffles (which close off specific portions of the port flow area) can be used to enhance the tumble (and swirl) levels generated with the cylinder during the intake process. These close off that portion of the intake port cross section leading to the part of the annular valve-head valve-seat open area where flow is *not* desired. For tumble, with angled valve stems, increasing the flow through the upper portion of the intake valve opening creates a stronger tumbling flow: with swirl, the airflow is directed through the valve open area closest to the cylinder liner wall.[29]

Creating more vigorous in-cylinder flows such as swirl and tumble involve higher pressure losses and flow restrictions across the intake port, and the valve and seat opening, and thus lower maximum engine airflows. The challenge is to achieve the desired faster combustion rates that these higher in-cylinder kinetic energy flows produce while minimizing the loss in airflow at the higher engine speeds and loads, where the combustion process is usually "fast enough." Thus many cylinder-head intake-port and piston-crown geometries have been explored to improve the combustion benefits and reduce the flow losses. These include fixed geometry designs, as well as use of throttles or plates in the intake ports to achieve benefits at part-load and lower speed, and avoid the penalties elsewhere. With port fuel injected engine system, the usual application is for homogeneous gasoline-air mixture SI engine concepts. With direct-injection fuel systems, both homogeneous mixture gasoline-direct-injection (GDI) engine concepts, and stratified engine concepts (at part load) are important application areas. The flow characteristics of several different tumble motion approaches (at full load) are shown in Fig. 8.20.[30] The port-fuel-injected (PFI) engine characteristics indicate the flow losses incurred in the absence of efforts to increase the in-cylinder motion to enhance the combustion rate. Some of these engines as a result of their cylinder-head design do create a modest tumbling flow during the intake process. Forward tumble is generated as indicated in Fig. 8.18 (shown in the clockwise direction). Reverse tumble rotates anti-clockwise, and uses vertically downward directed intake ports to achieve such a flow. As the in-cylinder tumble flow is intensified (with, for example, rotatable plates in the intake ports to block off the lower portion of the intake port—at lighter loads), the intake port and valve flow resistance at high loads and speeds) increases substantially. That, however, is not so important, as this partial port blocking to achieve high in-cylinder tumble would neither be needed nor utilized at these higher-load operating conditions.

© McGraw-Hill Education. All rights reserved. Any use is subject to the Terms of Use, Privacy Notice and copyright information.

Figure 8.20 Comparison of flow characteristics—flow coefficient (resistance) based on the pressure loss across the intake ports and valves, and tumble intensity (or ratio); see Eqs. (8.38) and (8.39)—of different tumble and swirl generating concepts. GDI, gasoline-direct-injection SI engines; PFI, port-fuel-injection SI engines. [30]



In gasoline SI engines operating with a homogeneous (usually stoichiometric) mixture, moderate tumble is usually preferred over swirl as the way to increase the burning rate so that it is fast enough to provide low combustion variability (good enough combustion stability) at low- to mid-loads and speeds.

© McGraw-Hill Education. All rights reserved. Any use is subject to the Terms of Use, Privacy Notice and copyright information.

8.5. PISTON-GENERATED FLOWS: SQUISH

The movement of the piston up and down the cylinder obviously produces charge motion. In its simplest form, with a flat piston crown and cylinder head, the fluid moves axially as charge compression occurs, with the gas in contact with the piston moving at the piston speed (see Fig. 2.2). When the valves are closed, the gas in contact with the cylinder head is at rest. In between the piston crown and cylinder head, the axial or *z*-component of the gas velocity will be the piston speed scaled linearly by the ratio of the axial distance of the in-cylinder location from the mean cylinder head location relative to the axial distance of the piston crown:

$$v_z(z) = \frac{z}{c_c + c} \cdot S_p$$

(8.41)

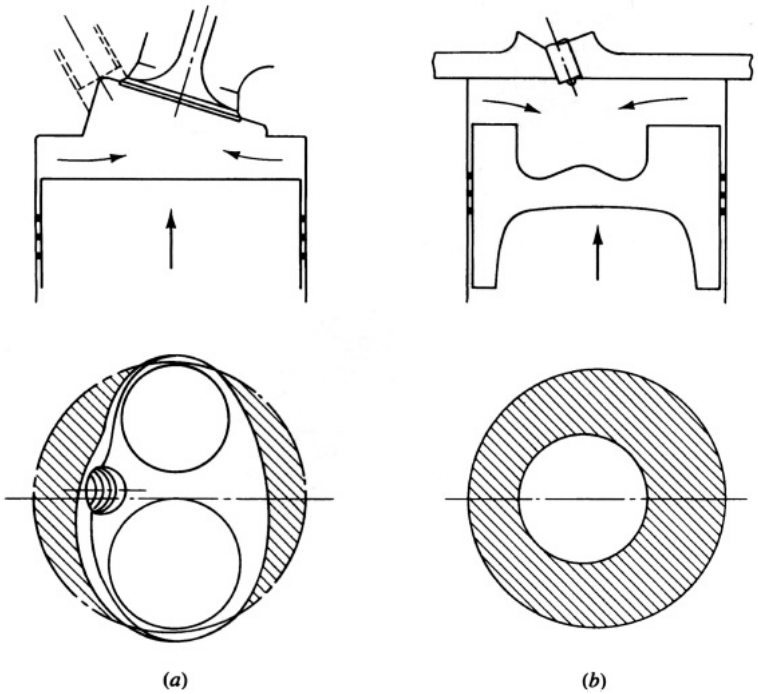
c is the piston displacement from its TC position and c_c is the average height of the clearance volume [see Fig. 2.1 and Eq. (2.6)], and the *z*-coordinate is zero at the TC piston-crown location. (Note: $z = -c_c$ at the average cylinder-head location.)

8.5.1.1. Squish

When the cylinder head or piston crown surfaces are not flat but are shaped (e.g., pent-roof cylinder heads in spark-ignition engines, and bowl-in-piston combustion chambers in diesels) this piston-generated axial velocity during compression and expansion produces transverse or radial flows due to differences in the axial distance between the cylinder head and piston crown surfaces across the cylinder cross section. *Squish* is the name given to the radial or transverse gas motion that occurs toward the end of the compression stroke (and early part of the expansion stroke) when a portion of the piston face and cylinder head approach (or separate from) each other closely. Figure 8.21 shows how gas is thereby displaced into the more open region of the combustion chamber at the end of compression. Figure 8.21*a* shows a wedge-shaped SI engine combustion chamber and Fig. 8.21*b* shows a bowl-in-piston diesel combustion chamber. The amount of squish is often defined by the *percentage squish area:* that is, the percentage of the cylinder cross-sectional area, $\pi B^2/4$, where the cylinder head and piston (the shaded areas in Fig. 8.21) approach each other closely. Squish-generated gas motion results from using a compact combustion chamber geometry.

© McGraw-Hill Education. All rights reserved. Any use is subject to the Terms of Use, Privacy Notice and copyright information.

Figure 8.21 *Schematics of how piston motion generates squish: (a) wedge-shaped SI engine combustion chamber; (b) bowl-in-piston direct-injection diesel combustion chamber.*



A theoretical squish velocity can be calculated from the instantaneous displacement of gas across the inner edge of the squish region (across the dashed lines in the drawings in Fig. 8.22*a* and *b*), required to satisfy mass conservation. Ignoring the effects of gas dynamics (nonuniform pressure), friction, leakage past the piston rings, and heat transfer, expressions for the squish velocity are:

1. *Bowl-in-piston chamber* (Fig. 8.22*a*):

$$\frac{v_{\mathrm{sq}}}{S_p} = \frac{D_B}{4Z}\left[\left(\frac{B}{D_B}\right)^2 - 1\right]\frac{V_B}{A_c Z + V_B}$$

(8.42)

where V_B is the volume of the piston bowl, A_c is the cross-sectional area of the cylinder ($\pi B^2/4$), S_p is the instantaneous piston speed [Eq. (2.12) or (2.13)], and Z is the distance between the top of the piston crown and the cylinder head surface above the squish area ($Z = c + c_c$; $c = l + a - s$; see Fig. 2.1).

2. *Simple wedge chamber* (Fig. 8.22*b*):[31]

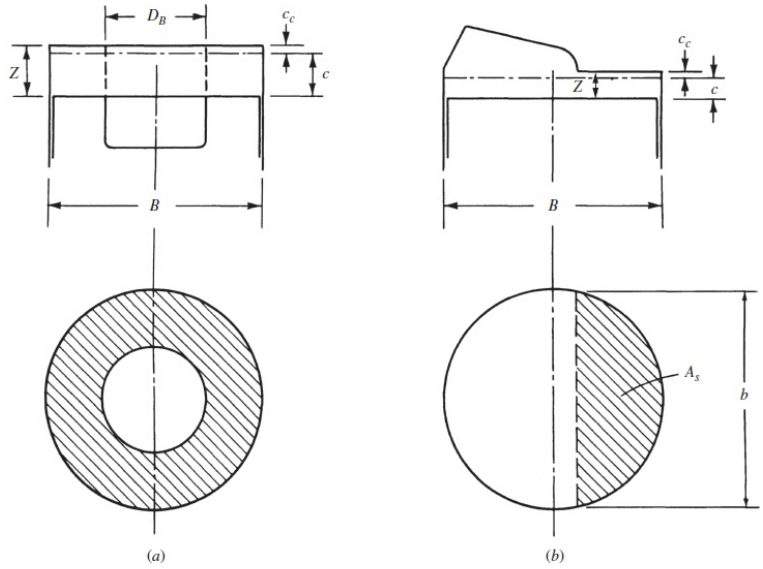
$$\frac{v_{\mathrm{sq}}}{S_p} = \frac{A_s}{b\,(c + c_c)}\left(1 - \frac{c + c_c}{C + c}\right)$$

(8.43)

where A_s is the squish area, b is the width of the squish region, and C is $c/(r_c - 1)$ evaluated at the end of induction.

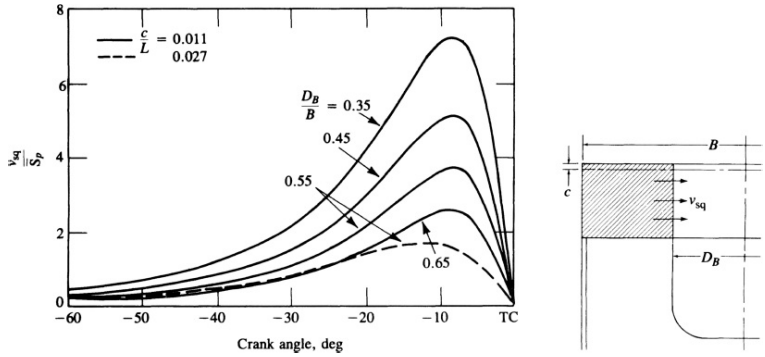
© McGraw-Hill Education. All rights reserved. Any use is subject to the Terms of Use, Privacy Notice and copyright information.

Figure 8.22 (a) Schematic of axisymmetric bowl-in-piston chamber for Eq. (8.42). (b) Schematic of wedge chamber with transverse squish for Eq. (8.43). Dash-dot line is piston top-center position.



This theoretical squish velocity for a bowl-in-piston engine normalized by the mean piston speed $\overline{S}_p$ is shown in Fig. 8.23 for different ratios of D_B/B and clearance heights c_c. The maximum squish velocity occurs at about 10° before TC. After TC, v_{sq} is negative; a reverse squish motion occurs as gas flows out of the bowl into the clearance height region. Under motored conditions this is equal to the forward motion.

Figure 8.23 Theoretical squish velocity divided by mean piston speed for bowl-in-piston chambers for different D_B/B and c_c/L (clearance height/stroke). B/L = 0.914, V_B/V_d = 0.056, connecting rod length/crank radius = 3.76.[32]



These models omit the effects of gas inertia, friction, gas leakage past the piston rings, heat transfer, and combustion. Gas inertia and friction effects have been shown to be small. The effects of gas leakage past the piston rings and of heat transfer are more significant. The squish velocity decrement Δv_L due to leakage is proportional to the mean piston speed and a dimensionless leakage number:

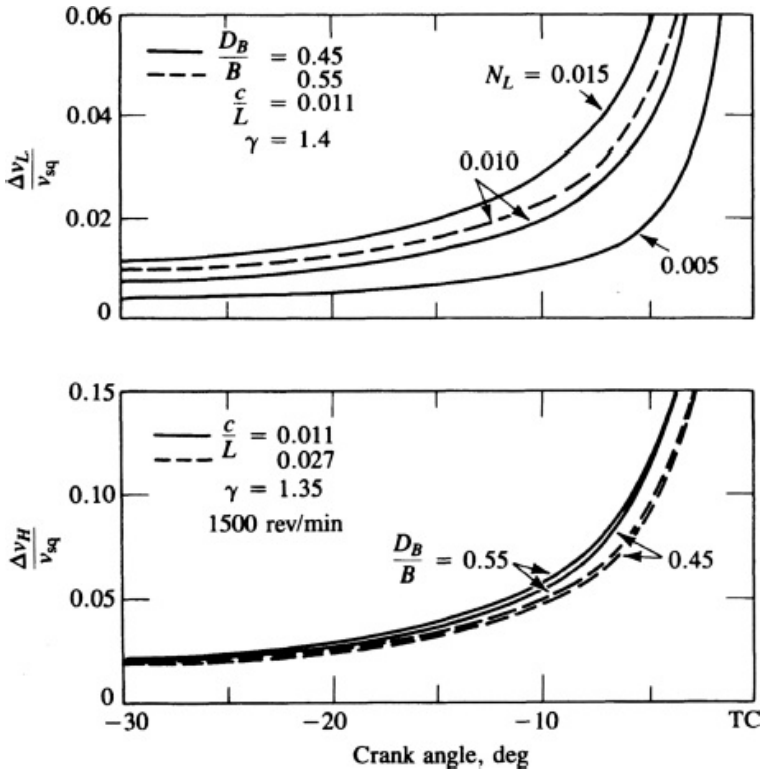
$$N_L = A_{\mathrm{E,L}} \frac{\sqrt{\gamma R T_{\mathrm{IVC}}}}{N V_d}$$

(8.44)

© McGraw-Hill Education. All rights reserved. Any use is subject to the Terms of Use, Privacy Notice and copyright information.

where $A_{E,L}$ is the effective leakage area and T_{IVC} is the temperature of the cylinder gases at inlet valve closing. Leakage was modeled as a choked flow through the effective leakage area. Values of $\Delta v_L v_{sq}$ are shown in Fig. 8.24. The effect of leakage on v_{sq} is small for normal gas leakage rates. A decrement on squish velocity due to heat transfer, Δv_H has also been derived, using standard engine heat-transfer correlations (see Sec. 12.4). Values of $\Delta v_H v_{sq}$ are also shown in Fig. 8.24, also. Again the effects are small in the region of maximum squish, though they become more important as the squish velocity decreases from its maximum value as the piston approaches TC. Combustion has limited impact on the squish flow at the end of compression because little of the in-cylinder charge has burned before TC. It has a much more significant effect on the "reverse squish" flow after TC, as the piston moves down the cylinder, because increasingly more of the charge has burned, and burning (usually in the more open part of the chamber) results in substantial gas expansion (by a factor of 4) which further drives flow out of the opening chamber.

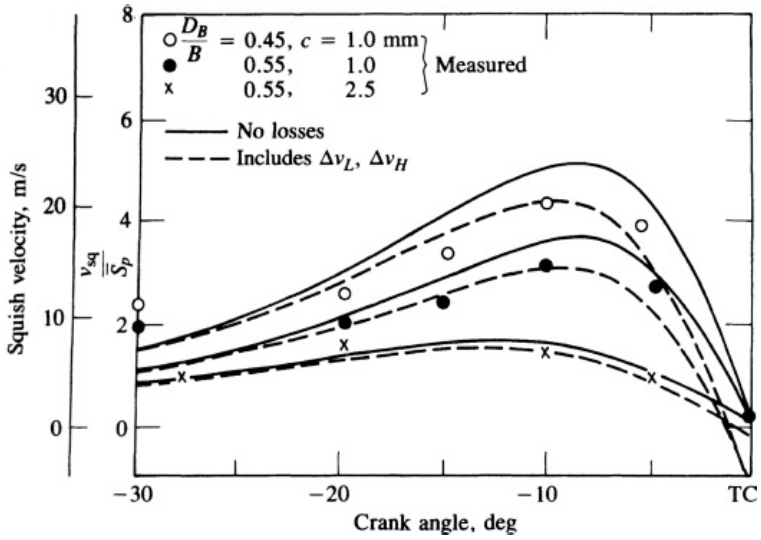
Figure 8.24 Values of squish velocity decrement due to leakage Δv_L and heat transfer Δv_H normalized by the ideal squish velocity, as a function of crank angle.[32]



Velocity measurements in engines provide good support for the above model. The ideal theory adequately predicts the dependence on engine speed. With appropriate corrections for leakage and heat-transfer effects, the above theory predicts the effects of the bowl diameter/bore ratio and clearance height on squish velocity (see Fig. 8.25). The change in direction of the radial motion as the piston moves through TC has been demonstrated under motored engine conditions. Under firing conditions, the combustion-generated gas expansion in the open portion of the combustion chamber substantially increases the magnitude of the reverse squish motion after TC.

© McGraw-Hill Education. All rights reserved. Any use is subject to the Terms of Use, Privacy Notice and copyright information.

Figure 8.25 *Comparison of measured squish velocities in bowl-in-piston combustion chambers, with different bowl diameter/bore ratios and clearance heights, to calculated ideal squish velocity (solid lines) and calculations corrected for leakage and heat transfer (dashed lines). Bore = 85 mm, stroke = 93 mm, 1500 rev/min.*[32]



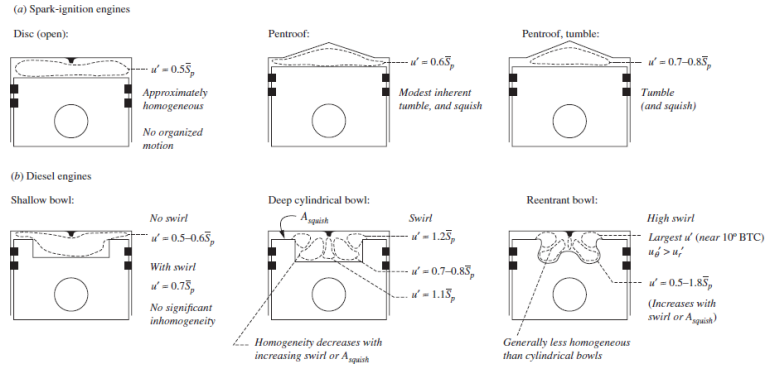
© McGraw-Hill Education. All rights reserved. Any use is subject to the Terms of Use, Privacy Notice and copyright information.

8.6. SWIRL, TUMBLE, SQUISH FLOW INTERACTIONS

The three basic in-cylinder flow patterns, discussed in Secs. 8.3, 8.4, and 8.5, interact. For example, in spark-ignition engines, with pent-roof cylinder heads, the primary in-cylinder motion generated to increase the turbulence intensity and thus the burn rate during combustion is tumble. Often the tumble is accompanied by some swirl. Also, in diesels with deep bowl-in-piston combustion systems, the intake-generated swirl is significantly amplified by the radially-inward squish motion as the piston approaches TC, and the within-the-bowl turbulence intensity is increased by the strong swirl-squish interaction.

An important in-cylinder flow characteristic is the turbulence intensity u', or turbulent kinetic energy k [see Eq. (8.23)] around TC, since this impacts the fuel-air mixture burning rate as well as the fuel-air mixing rate in diesels. Figure 8.26 provides a summary of the TC end-of-compression turbulence intensity u' (expressed as a fraction of the mean piston speed, $\overline{S}_p$) for different SI engine combustion chamber shapes and flow configurations, and for a range of bowl-in-piston designs for diesels (shallow bowl with no or modest swirl for larger low-speed diesels; deeper bowl with swirl for medium-duty diesels; reentrant deep bowl with high swirl for smaller, high-speed, diesels). Each chamber shape matches with an engine size and speed range, an appropriate swirl or tumble level, and impact of the squish flow on the swirl. Note that smaller size cylinders can operate at higher engine speeds before intake flow choking occurs (see Sec. 6.2.5). Thus, at their maximum speed there is less time available for fuel-air mixing and for combustion than in larger engines. So mixing and burning rates must be increased as cylinder bore and stroke are decreased.

Figure 8.26 Schematics of near-TC turbulence structures and levels for a range of combustion chamber designs: (a) For spark-ignition engines (disc or open, and pent root chambers with increasing levels of tumble or swirling motions). (b) For diesel engines, with different depth and shape of bowl-in-piston chambers (shallow—larger engines, deep—medium-size engines, deep and reentrant—for small high-speed engines).[16]



With combustion chambers such as the bowl-in-piston, the tangential velocity distribution with radius will change during compression. Even if the solid-body rotation assumption is a reasonable approximation at the end of induction, the profile will distort as gas moves into the piston bowl. Neglecting the effects of friction, the angular momentum of each fluid element will remain constant as it moves radially inward. Thus the increase in tangential velocity of each fluid element as it moves radially inward is proportional to the change in the reciprocal of its radius. Measurements of the swirl velocity distribution within the cylinder of bowl-in-piston engine designs support this description. The rate of displacement of gas into the bowl depends on the bowl volume V_B, cylinder volume V, and piston speed S_p, at that particular piston position:

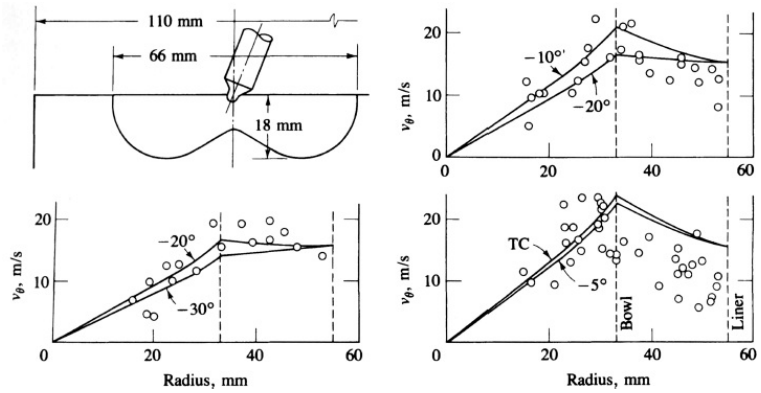
$$\frac{dm_B}{dt} = \frac{m_c}{L}\left(\frac{V_B}{V}\right)\left(\frac{V_d}{V}\right)S_p$$

© McGraw-Hill Education. All rights reserved. Any use is subject to the Terms of Use, Privacy Notice and copyright information.

The gas velocity into the bowl will therefore increase rapidly toward the end of the compression stroke and reach a maximum just before TC (see Sec. 8.5 where this radial "squish motion" is discussed more fully). Thus, there is a rapid increase in v_θ in the bowl as the crank angle approaches TC. The lower layers of the bowl rotate slower than the upper layers because that gas entered the bowl earlier in the compression process.[21, 23]

Velocity measurements illustrating the development of this radial distribution in tangential velocity are shown in Fig. 8.27. These measurements were made by analyzing the motion of burning carbon particles in the cylinder of an operating diesel engine from movies of the combustion process. The figure shows the engine geometry and the data compared with a model based on gas displacement and conservation of angular momentum in each element of the charge as it is displaced inward. Different swirl velocity profiles exist within and outside the bowl as the piston approaches TC. Swirl velocities within the bowl increase as TC is approached, roughly as predicted by the ideal model. Outside the bowl, the swirl velocity decreases with increasing radius due to the combined effects of friction and inward gas displacement as the clearance height decreases.

Figure 8.27 Velocity measurements as a function of radius across the combustion chamber of a firing, bowl-in-piston, direct-injection diesel engine. Schematic shows the chamber geometry. Solid lines are calculations based on the assumption of constant angular momentum for fluid elements as they move radially inward.[33]



Swirl ratios in bowl-in-piston engine designs of up to about 15 can be achieved with $D_B \approx 0.5B$, at top-center. Amplification factors relative to flat-topped piston swirl are typically about 2.5 to 3, some 30% lower than the ideal factor of $(B/D_B)^2$ given by Eq. (8.37) as $z \to 0$. This difference is due to the mass remaining within the clearance height which does not enter the bowl, and the effects of wall friction (enhanced by the higher gas velocities in the bowl). Sometimes the bowl axis is offset from the cylinder axis and some additional loss in swirl amplification results.[23]

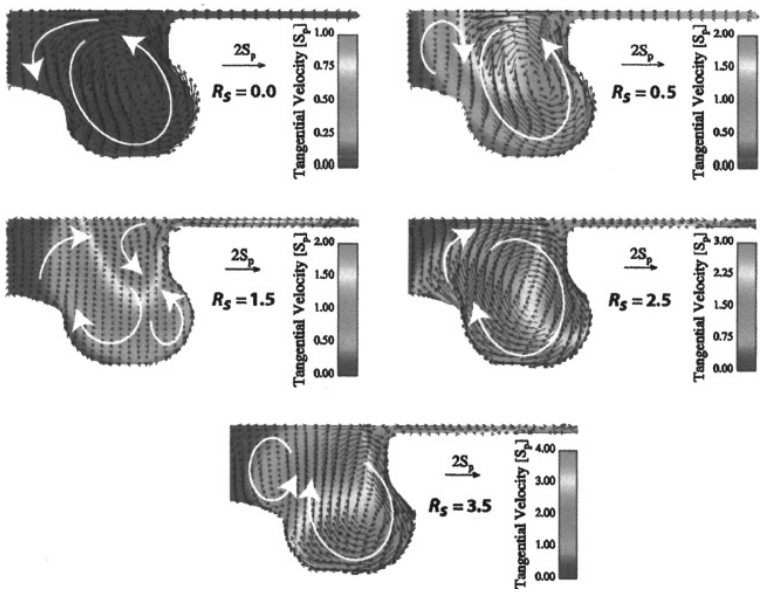
The turbulence intensity with swirl was higher than without swirl (with the same chamber geometry). Integral scales of the turbulence were smaller with swirl than without. Cyclic fluctuations in the mean velocity are, apparently, reduced by swirl. There is evidence that swirl makes the turbulence intensity more homogeneous.[27]

These flow interactions become especially important when strong in-cylinder charge motion is essential—as in smaller-size high-speed direct-injection diesels—which use high swirl and deep, high-squish-area bowl-in-piston combustion systems to achieve rapid mixing and combustion. Computational fluid dynamic (CFD—see Sec. 14.5) calculations are an essential tool for mapping out the close-to-TC end-of-compression flow field resulting from both the increase in azimuthal (tangential) velocity as the swirling charge is moved radially inward into the bowl by the strong inward squish flow generated by the piston's motion as it approaches top-center. Some general observations of this high-speed diesel example are the following. The mean flow velocities essentially scale with mean piston speed, and with swirl ratio. The flow structures within the piston bowl change as the piston moves upward, and consist of both a swirling flow (with v_θ increasing as more mass flows into the bowl) and one or more annular vortices. These are illustrated in Fig. 8.28, which shows how the spatial distribution of the high-swirl regions of the flow penetrate deeper into the bowl as the swirl ratio increases. This study also showed that the turbulent velocity fluctuations (which are not uniform) exhibit a near-linear scaling with engine speed. The turbulence intensity is about

© McGraw-Hill Education. All rights reserved. Any use is subject to the Terms of Use, Privacy Notice and copyright information.

one-third of the average tangential component of velocity (the largest). Because the large-scale turbulent eddies have a time scale comparable to the mean flow deformation time, and (like the mean flow structures) these large-scale motions are constrained by the near-TC combustion chamber geometry, this near-linear scaling with engine speed is inherent. The effect of increasing flow Reynolds number is primarily to change the smaller scales of the flow and not the larger-scale structures. Since the large-scale motions are the major contributor to the turbulent fluctuations, a near-linear scaling of these velocity fluctuations would be expected.[16, 34]

Figure 8.28 Illustration of squish-swirl interaction with reentrant bowl-in-piston high-speed diesel engine combustion system: CFD modeling results. Contours of different tangential (swirl) velocities (scaled with mean piston speed $\overline{S}_p$*) in the r-z plane, as swirl is increased from zero to a swirl ratio of 3.5. White arrows illustrate the structure of the large-scale motions.*[34]



The four-valve pent-roof gasoline SI engine provides another example of how these different types of in-cylinder flows are used. The cylinder head cross section shown in Fig. 8.18 indicates the basic geometry. The 20° inclination of the intake ports directs the intake flow across the cylinder head and down the liner as the piston moves down, creating a tumbling flow. Depending on intake port and cylinder head geometric details, some swirl may be generated, as well. Then, for several reasons (e.g., to create a more open chamber above much of the piston), the pent-roof chamber usually has squish regions on either side similar to the shaded areas in Fig. 8.21*a*. As the piston moves up during the compression stroke, the tumbling vortex (which is not a natural fit inside the circular cross-section cylinder, as is a swirling flow about the cylinder axis) breaks up into several smaller vortices as its aspect ratio (width to height ratio) increases and transitions into more irregular "turbulence" before TC. Any swirl present would persist for longer. Then, on the crank-angle scale indicated in Fig. 8.23, the inward squish flow analogous to that indicated for the two-valve open-chamber geometry of Fig. 8.21*a* generates jet-driven shear flows and turbulence within the combustion chamber close to TC.

The effects of tumble and swirl, augmented as discussed above by the squish flow, on SI engine breathing and combustion characteristics are indicated in Fig. 8.29. The data are for four-valve per-cylinder gasoline SI engines which generate various levels of tumble: one of these has divided intake ports, and a port throttle plate in one of the two intake ports was used to generate swirl. At high airflows (at higher engine speeds and loads) with this approach, when the port throttle is opened and both ports and intake valves flow air comparably, tumble is generated. At lighter loads, the port throttle is closed, only the other intake port and valve flow air, and high levels of swirl are generated. The flow coefficient, C_f, indicates the resistance to airflow of the tumble- or swirl-generating intake ports and valves, in the cylinder head.[1]

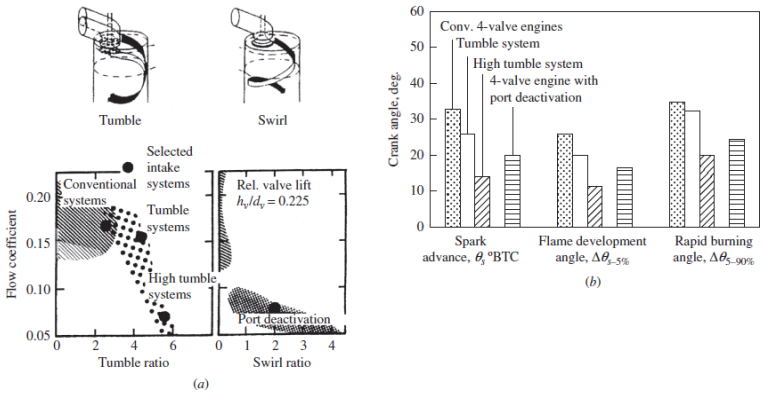
© McGraw-Hill Education. All rights reserved. Any use is subject to the Terms of Use, Privacy Notice and copyright information.

$$C_f = \Delta p / \left(\frac{1}{2} \rho v_a^2 \right)$$

(8.45)

where Δp is the pressure drop across the intake port and valve, and v_a is the airflow velocity. The flow coefficients as a function of the tumble and swirl ratios for a range of cylinder head designs for multivalve engines are shown in Fig. 8.29*a*. Increasing the charge velocities (and thus the stored kinetic energy) in these intake-generated rotating in-cylinder flows requires greater restricting of the intake flow past the valve, and thus the cylinder head has a lower flow coefficient.

Figure 8.29 (a) Influence of various cylinder head designs on the resistance to airflow into the cylinder (quantified by the flow coefficient) versus tumble and swirl ratios: data points are specific examples. (b) Influence of these various charge motion types and levels on flame development and rapid burn durations. Engine at 3 bar bmep, 2000 rev/min, stoichiometric operation, and maximum-brake-torque (MBT) spark-timing.[35]



The impacts of tumble and swirl on these spark-ignition engine's combustion characteristics are shown in Fig. 8.29*b*. Increasing the tumble ratio speeds up the burning process: both the flame development angle ($\Delta\theta_{spark-5\%}$) and the burn duration ($\Delta\theta_{5-90\%}$) decrease (see Sec. 9.3.1). The port-deactivation-generated swirl is intermediate in its impacts, between medium and high tumble cases. This is in line with the broader assessment that moderate tumble is usually the appropriate choice to achieve stable SI engine combustion: it provides a fast-enough burn rate (see Sec. 9.4.1), while maintaining a relatively high flow coefficient at high speeds and loads.

Other important in-cylinder flow interactions are those between in-cylinder fuel sprays (which have significant momentum) and the charge motions within the combustion chamber at around TC in both direct-injection gasoline engines and diesel engines. These are discussed in Secs. 7.7 and 10.4 respectively. Also, in stratified DI gasoline engines of the wall-guided and flow-guided category (see Sec. 7.7.2), the DI fuel spray interacts with the flow pattern within the combustion chamber (often in a complex shape "bowl in piston"). Usually, this flow is set up by generating a swirling or tumbling flow during intake, by modifying that flow during compression through wall guiding as gas displacement into the bowl (resulting from the upward piston motion) occurs, and finally by incorporating the transverse squish-type flow as the TC piston location is approached.

[1] C_f is determined in steady airflow measurements through the cylinder head from the pressure drop across the cylinder head, and the air mass flow rate.

© McGraw-Hill Education. All rights reserved. Any use is subject to the Terms of Use, Privacy Notice and copyright information.

8.7. PRECHAMBER ENGINE FLOWS

Historically, small high-speed diesel engines used an auxiliary combustion chamber, or pre-chamber, to achieve fast fuel-air mixing rates. In this type of diesel, the prechamber is connected to the main combustion chamber above the piston via a nozzle, passageway, or one or more orifices. Flow of air through this restriction into the prechamber during the compression process sets up high velocities in the prechamber at the time the fuel-injection process commences. This results in the required high fuel-air mixing rates. Figure 10.2*b* shows examples of these prechamber or indirect-injection diesels. The two most common designs of auxiliary chamber are: the swirl chamber, where the flow through the passageway enters the chamber tangentially producing rapid rotation within the chamber, and the prechamber with one or more connecting orifices designed to produce a highly turbulent flow but no ordered motion within the chamber. Auxiliary chambers are sometimes used in spark-ignition engines. The torch-ignition three-valve stratified-charge engine (Fig. 1.21) is one such concept. Fuel is injected into the prechamber to create a rich mixture in the vicinity of the spark plug to promote rapid flame development. An alternative concept uses the prechamber around the spark plug to generate turbulence to enhance the early stages of combustion, but has no mixture enrichment.

The most critical phase of flow into the prechamber occurs toward the end of compression. While this flow is driven by a pressure difference between the main chamber above the piston and the auxiliary chamber, this pressure difference is small and the mass flow rate and velocity at the nozzle, orifice, or passageway can be estimated using a simple gas displacement model. Assuming that the gas density throughout the cylinder is uniform (a reasonable assumption toward the end of compression—the most critical period), the mass in the prechamber m_p is given by $m_c(V_p/V)$, where m_c is the cylinder mass, V the cylinder volume, and V_p the prechamber volume. The mass flow rate through the throat of the restriction is, therefore,

$$\dot{m} = \frac{dm_p}{dt} = -\frac{m_c V_p}{V^2}\frac{dV}{dt}$$

(8.46)

During compression, using the relations $dV/dt = -(\pi B^2/4)S_p$ where S_p is the instantaneous piston speed, $V_d = \pi B^2 L/4$, and $\overline{S}_p = 2NL$, Eq. (8.46) can be written as

$$\frac{\dot{m}}{m_c N} = 2(r_c - 1)\left(\frac{V_p}{V_c}\right)\left(\frac{S_p}{\overline{S}_p}\right)\left(\frac{V_c}{V}\right)$$

(8.47)

where V_c is the clearance volume,
$S_p/\overline{S}_p$ is given by Eq. (2.11), and V/V_c is given by Eq. (2.6). The gas velocity at the throat v_T can be obtained from
$\dot{m}$ via the relation
$\rho v_T A_T = \dot{m}$, the density $\rho = m_c/V$, and Eq. (8.47) becomes:

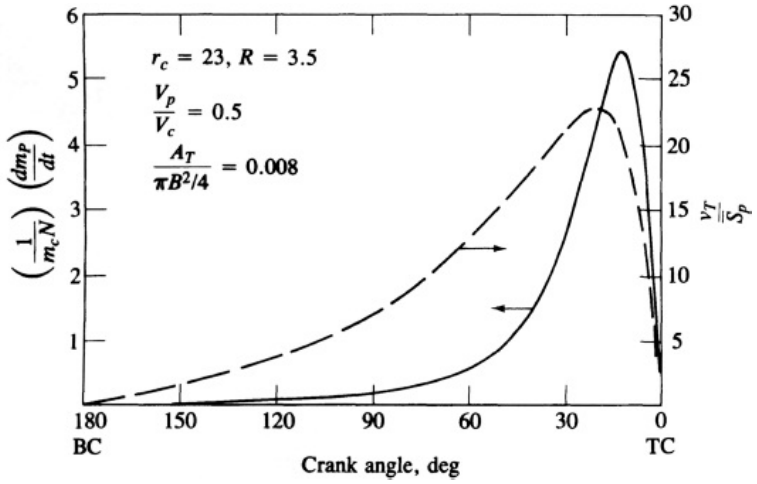
$$\frac{v_T}{\overline{S}_p} = \left(\frac{V_p}{V_c}\right)\left(\frac{\pi B^2/4}{A_T}\right)\left(\frac{S_p}{\overline{S}_p}\right)\left(\frac{V_c}{V}\right)$$

(8.48)

© McGraw-Hill Education. All rights reserved. Any use is subject to the Terms of Use, Privacy Notice and copyright information.

where A_T is the effective cross-sectional area of the throat. The variations of $\dot{m}/(m_c N)$ and $v_T/\overline{S}_p$ with crank angle during the compression process for values of r_c, V_p/V_c, and $A_T/(\pi B^2/4)$ typical of a swirl prechamber diesel are shown in Fig. 8.30. The velocity reaches its peak value about 20° before TC: very high gas velocities, an order of magnitude or more larger than the mean piston speed, can be achieved depending on the relative effective throat area. Note that as the piston approaches TC, first the nozzle velocity and then the mass flow rate decrease to zero. After TC, in the absence of combustion, an equivalent flow in the reverse direction out of prechamber would occur. Combustion in the prechamber diesel usually starts just before TC, and the pressure in the prechamber then rises significantly above the main chamber pressure. The outflow from the prechamber is then governed by the development of the combustion process, and the above simple gas displacement model no longer describes the flow.

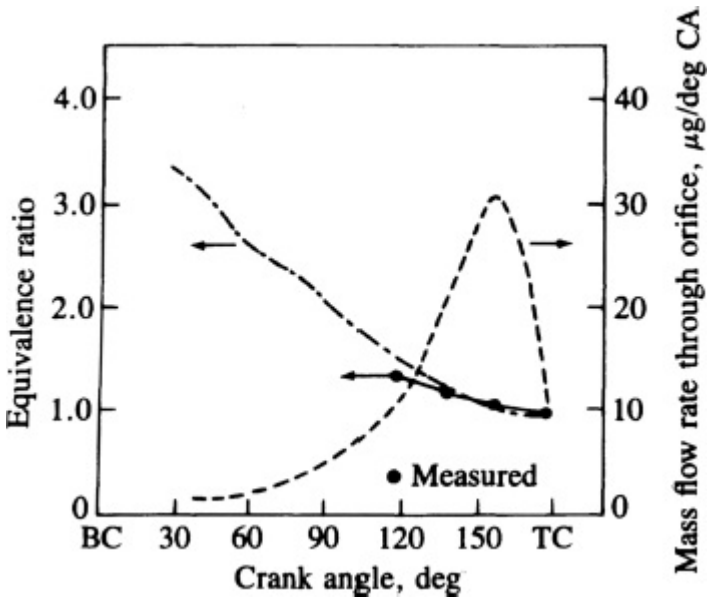
Figure 8.30 Velocity and mass flow rate at the prechamber nozzle throat, during compression, for a typical small swirl-prechamber automotive diesel.



In prechamber stratified-charge spark-ignition engines, the flow of gas into the prechamber during compression is critical to the creation of an appropriate mixture in the prechamber at the crank angle when the mixture is ignited. In the concept shown in Fig. 1.21, a very rich fuel-air mixture is fed directly to the prechamber during intake via the prechamber intake valve, while a lean mixture is fed to the main chamber via the main intake valve. During compression, the flow into the prechamber reduces the prechamber equivalence ratio to a close-to-stoichiometric value at the time of ignition. Figure 8.31 shows a gas displacement calculation of this process and relevant data; the prechamber equivalence ratio, initially greater than 3, is leaned out to unity as mass flows through the orifice into the prechamber (whose volume is 8.75% of the clearance volume). Estimates of the final equivalence ratio, based on gas displacement, for this prechamber concept are available.[36]

© McGraw-Hill Education. All rights reserved. Any use is subject to the Terms of Use, Privacy Notice and copyright information.

Figure 8.31 *Effect of gas flow into the prechamber during compression on the prechamber equivalence ratio in a three-valve prechamber stratified-charge engine. Calculations based on gas displacement model.*[37]



The velocity field set up inside the prechamber during compression is strongly dependent on the details of the nozzle and prechamber geometry. Velocities vary linearly with mean piston speed. In swirl prechambers, the nozzle flow sets up a rotating flow within the chamber. The velocities within the prechamber increase with increasing crank angle as the compression process proceeds, and reach a maximum about 20° before TC. Then, as the piston approaches TC and the flow through the passageway decreases to zero, the vortex in the swirl chamber expands to fill the entire chamber and mean velocities decay. Very high swirl rates can be achieved just before TC: local swirl ratios of up to 60 at intermediate radii and up to 20 at the outer radius have been measured. These high swirl rates produce large centrifugal accelerations.

© McGraw-Hill Education. All rights reserved. Any use is subject to the Terms of Use, Privacy Notice and copyright information.

8.8. CREVICE FLOWS AND BLOWBY

The engine combustion chamber is connected to several small volumes usually called *crevices* because of their narrow entrances. Gas flows into and out of these volumes during the engine operating cycle as the cylinder pressure and volume change.

The largest crevices are the volumes between the piston, piston rings, and cylinder wall. Some gas flows out of these regions, through the ring gaps and into the crankcase; it is called *blowby.* Other crevice volumes in production engines are the threads around the spark plug, the space between the plug center-electrode-insulator and casing, crevices between the intake and exhaust valve heads and seats in the cylinder head, and the head gasket cutout. Table 8.1 shows the size and relative importance of these crevice regions in one cylinder of a production-design spark-ignition engine determined from measurements of cold-engine components. Total crevice volume is a few percent of the clearance volume, and the piston and ring crevices are the dominant contributors. When the engine is warmed up, dimensions and crevice volumes will change some.

Table 8.1 Engine crevice data*[38]

	cm^3	%
Displaced volume per cylinder	465	
Clearance volume per cylinder	45	100
Compression ratio	11.2	
Piston crevice	0.782	1.74
Spark plug crevice	0.187	0.42
Valve seat crevice	0.032	0.07
Head gasket crevice	0.037	0.08
Total crevice volume	1.038	2.31
*Per cylinder; determined for cold engine.		

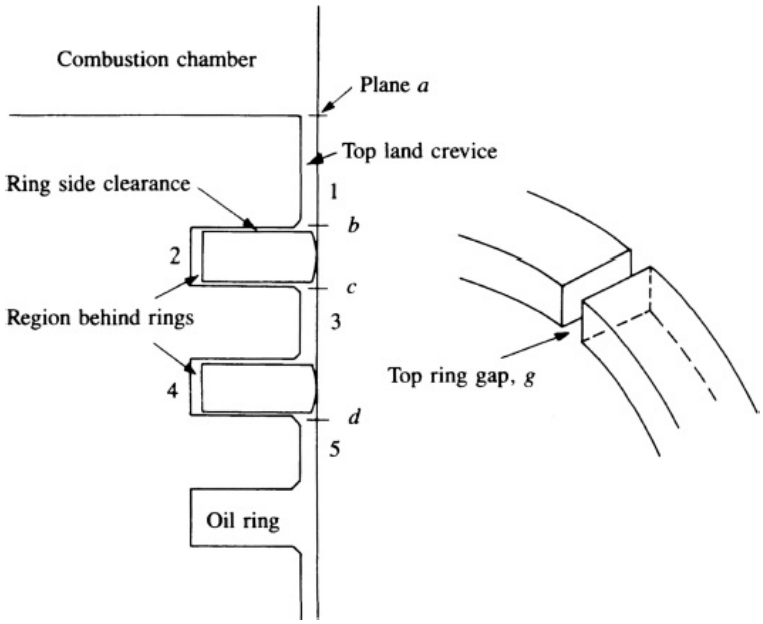
The important crevice processes occurring during the engine cycle are the following. As the cylinder pressure rises and cylinder volume decreases during compression, unburned mixture or air is forced into each crevice region. Since these volumes are thin they have a large surface/volume ratio; the gas flowing into the crevice cools by heat transfer to close to the wall temperature. During combustion while the pressure continues to rise, unburned mixture or air, depending on engine type, continues to flow into these crevice volumes. After flame arrival at the crevice entrance, burned gases will flow into each crevice until the cylinder pressure starts to decrease. Once the cylinder pressure starts to fall, gas flows back from each crevice into the cylinder.

The volumes between the piston, piston rings, and cylinder wall are shown schematically in Fig. 8.32. These crevices consist of a series of volumes (numbered 1 to 5) connected by flow restrictions such as the ring side clearance and ring gap. The geometry changes as each ring moves up and down in its ring groove, sealing either at the top or bottom ring surface. The gas flow, pressure distribution, and ring motion are therefore coupled. Figure 8.33 illustrates this behavior: pressure distributions, ring motion, and mass flow of gas into and out of the regions defined by planes *a*, *b, c, d,* and through the ring gap *g* are plotted

© McGraw-Hill Education. All rights reserved. Any use is subject to the Terms of Use, Privacy Notice and copyright information.

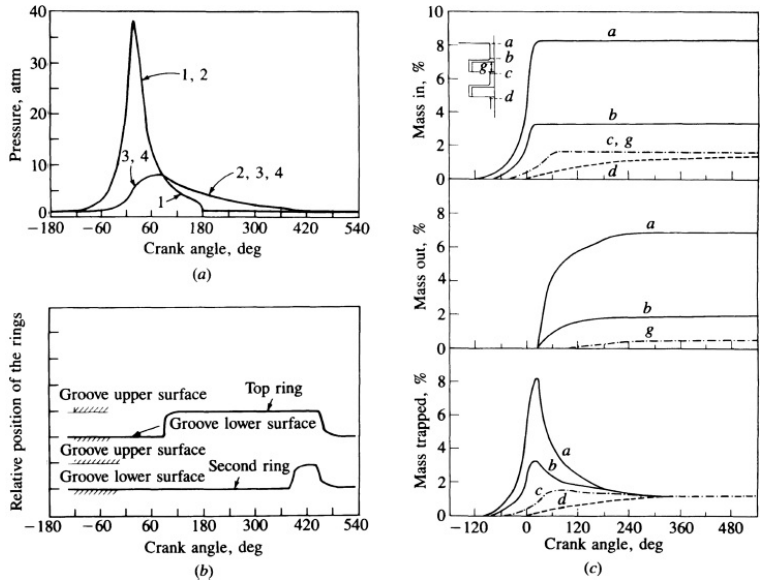
versus crank angle through compression and expansion. These results come from an analysis of these regions as volumes connected by passageways, with a prescribed cylinder-pressure versus crank-angle profile coupled with a dynamic model for ring motion, and assuming that the gas temperature equals the wall temperature.[39] During compression and combustion, the rings are forced to the groove lower surfaces and mass flows *into* all the volumes in this total crevice region. The pressure above and behind the first ring is essentially the same as the cylinder pressure; there is a substantial pressure drop across each ring, however. Once the cylinder pressure starts to decrease (around 15° ATC) gas flows out of regions 1 and 2 in Fig. 8.32 into the cylinder, but continues to flow *into* regions 3, 4, and 5 until the pressure in the cylinder falls below the pressure beneath the top ring. The top ring then shifts to seal with the upper grove surface and gas flows out of regions 2, 3, and 4 (which now have the same pressure), both into the cylinder and as blowby into the crackcase. Some 5 to 10% of the total cylinder charge is trapped in these regions at the time of peak cylinder pressure. Most of this gas returns to the cylinder; about 1% goes to the crankcase as blowby. The gas flow back into the cylinder continues throughout the expansion process. In spark-ignition engines this phenomenon is a major contributor to unburned hydrocarbon emissions (see Sec. 11.4.3). It results in a loss in torque and efficiency since any fuel that does not burn during the normal combustion process does not contribute. In diesel engines, air in these crevices during combustion is not available for combustion which additionally limits the amount of fuel that can be burned without producing soot emissions.

Figure 8.32 Schematic of piston and ring assembly in automotive spark-ignition engine.



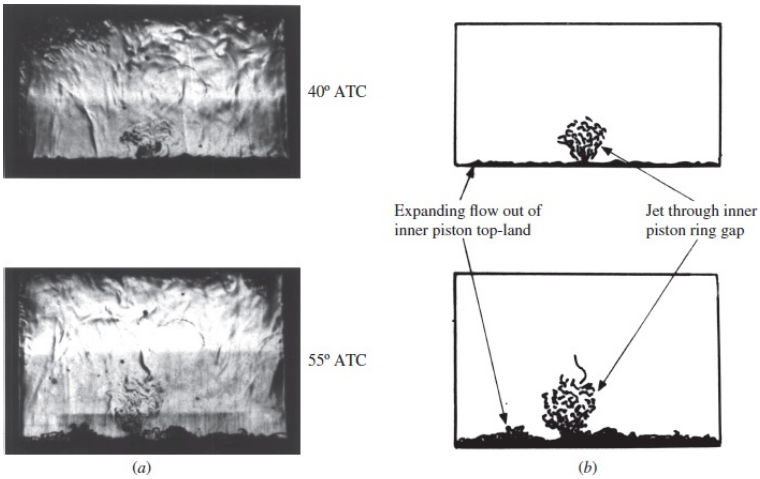
© McGraw-Hill Education. All rights reserved. Any use is subject to the Terms of Use, Privacy Notice and copyright information.

Figure 8.33 (a) Pressures in the combustion chamber (1), in region behind top ring (2), in region between rings (3), and behind second ring (4); (b) relative position of top and second rings; (c) percentage of total cylinder mass that flows into and out of the different crevice regions across planes a, b, c, and d and through the ring gap g in Fig. 8.32, and the percentage of mass trapped beneath these planes, as a function of crank angle. Automotive spark-ignition engine at wide-open throttle and 2000 rev/min.[39]



There is substantial experimental evidence to support the above description of flow in the piston ring crevice region. In a special square-cross-section flow visualization engine, both the low-velocity gas expansion out of the volume above the first ring after the time of peak pressure, and the jet-like flows through the top ring gap later in the expansion process when the pressure difference across the ring changes sign have been observed. Figure 8.34 shows these flows with explanatory schematics.

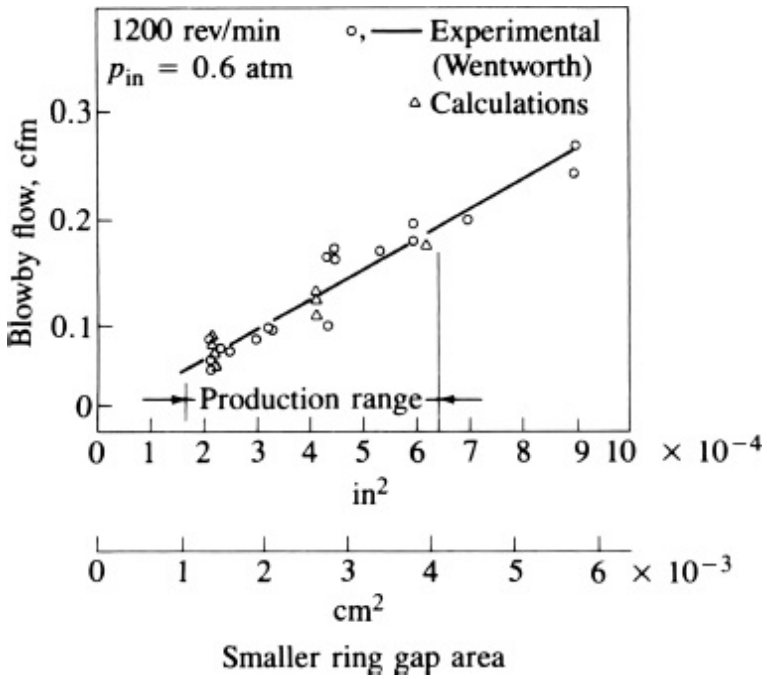
Figure 8.34 Schlieren photographs of the flow out of the piston-cylinder wall crevices during the expansion stroke. A production piston was inserted into the square cross-section piston of a special visualization engine. Gas flows, at low velocity, out of the top land-crevice entrance all around the production piston circumference once the cylinder pressure starts decreasing early in the expansion stroke. Gas flows out of the ring gap as a jet once the pressure above the ring falls below the pressure beneath the ring.[39]



© McGraw-Hill Education. All rights reserved. Any use is subject to the Terms of Use, Privacy Notice and copyright information.

Blowby is defined as the gas that flows from the combustion chamber past the piston rings and into the crankcase. It flows through any leakage paths in the piston-bore-ring assembly driven by the high combustion-chamber pressure. If there is good contact between the compression rings and the bore, and the rings and the bottom of the grooves, then the only leakage path of consequence is the ring gap. Blowby of gases from the cylinder to the crankcase removes gas from these crevice regions and thereby prevents some of the crevice gases from returning to the cylinder. Crankcase blowby gases used to be vented directly to the atmosphere and constituted a significant source of HC emissions. The crankcase is now vented to the engine intake system and the blowby gases are recycled. Blowby at a given speed and load is controlled primarily by the greatest flow resistance in the flow path between the cylinder and the crankcase. This is the smallest of the first and second ring-gap areas. Figure 8.35 shows how measured blowby flow rates increase linearly with the smallest gap area.[40]

Figure 8.35 Measured blowby for one cylinder of an automobile spark-ignition engine as a function of the smallest ring gap area, compared with blowby calculations based on flow model described in text.[39, 40] Blowby of 0.1 cfm (some 0.05 liter/s) for this engine at these conditions is about 2% of the engine airflow.



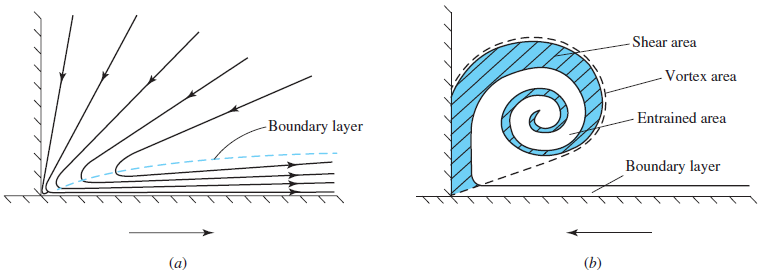
Calculations of blowby based on the model described earlier are in good agreement with this data.[39] Extrapolation back to the zero gap area gives nearly zero blowby. Note, however, that if the bore finish is rough or if, through bore distortion, the rings do not contact the bore all around, or if the first or second rings lift off the bottom of their groove, this linear relationship may no longer hold. Blowby in production gasoline spark-ignition engines is typically about 1% of the engine airflow.

© McGraw-Hill Education. All rights reserved. Any use is subject to the Terms of Use, Privacy Notice and copyright information.

8.9. FLOWS GENERATED BY PISTON CYLINDER-WALL INTERACTION

Because a boundary layer exists on the cylinder wall, the motion of the piston generates unusual flow patterns in the corner formed by the cylinder wall and the piston face. When the piston is moving away from top-center a sink-type flow occurs. When the piston moves toward top-center a vortex flow is generated. Figure 8.36 shows schematics of these flows (in a coordinate frame with the piston at rest). The vortex flow has been studied because of its effect on gas motion at the time of ignition and because it is thought to be a mechanism for removing hydrocarbons off the cylinder wall during the exhaust stroke (see Sec. 11.4.3).

Figure 8.36 Schematics of the flow pattern set up in the piston face-cylinder wall corner, in piston-stationary coordinates, due to the boundary layer on the cylinder wall. Piston crown on left; cylinder wall at bottom. (a) Sink flow set up during intake and expansion; (b) vortex flow set up up during compression and exhaust.[41] Arrows show cylinder wall velocity relative to piston.



This vortex flow has been studied in cylinders with water as the fluid over the range of Reynolds numbers typical of engine operation.[41,42] Laminar, transition, and turbulent flow regimes have been identified. It has been shown that a quasi-steady flow assumption is valid and that

$$\frac{A_v}{L^2} = f\left(\frac{v_w L}{v}\right)$$

where A_v is the vortex area (area inside the dashed line in Fig. 8.35), L is the stroke, v_w is the wall velocity in piston stationary coordinates ($v_w = S_p$ in the engine), v is the kinematic viscosity, and ($v_w L/v$) is a Reynolds number.

For the laminar flow regime, a good assumption is that A_v is proportional to the shear area in the vortex (shown cross-hatched in Fig. 8.36), which equals the boundary-layer area; this can be estimated from boundary-layer theory. In the turbulent flow regime an entrainment theory was used which assumed that the rate of change of vortex area was proportional to the product of the exposed perimeter of the vortex and the velocity difference between the vortex and the stationary fluid ($\approx v_w$). The relevant relationships are:

For

$$(v_w L/v) \leq 2 \times 10^4$$

$$\frac{A_v}{L^2} = \left(\frac{v_w L}{v}\right)^{-1/2}$$

© McGraw-Hill Education. All rights reserved. Any use is subject to the Terms of Use, Privacy Notice and copyright information.

(8.49a)

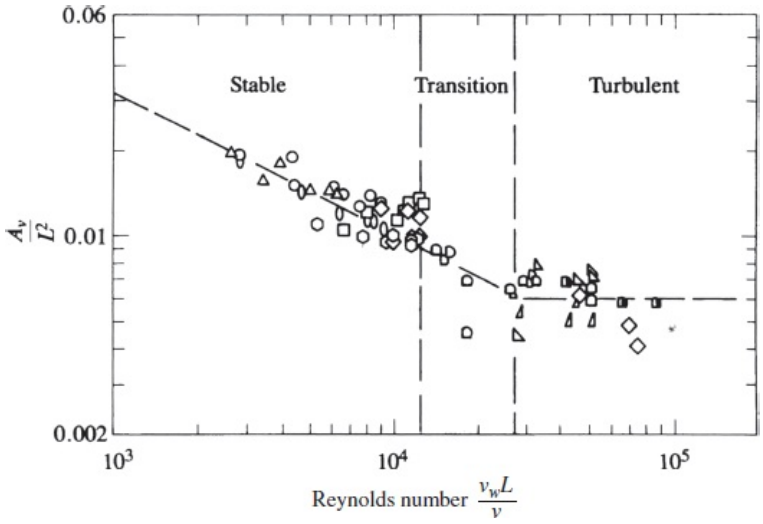
For
$(v_w L/v) \geq 2 \times 10^4$

$$\frac{A_v}{L^2} = 0.006$$

(8.49b)

Figure 8.37 shows these two theories correlated against hydraulic analog data.

Figure 8.37 Ratio of area of vortex in piston face-cylinder wall corner to square of stroke, as a function of Reynolds number based on piston velocity, for piston moving toward the cylinder head.[41]

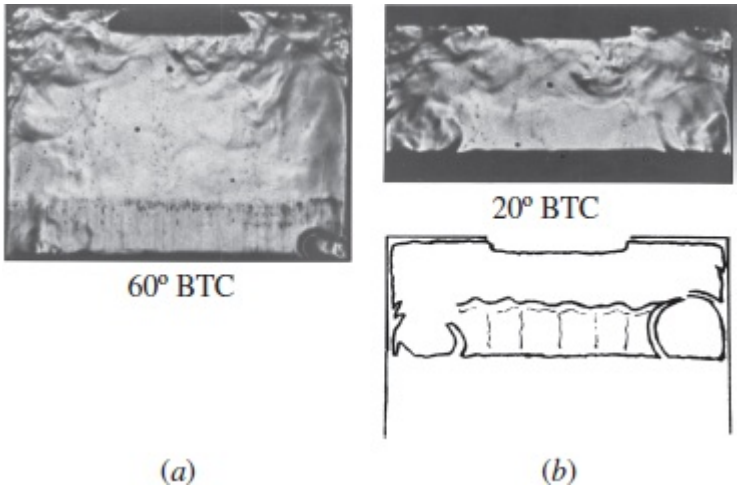


These theories are for constant values of kinematic viscosity, *v*. During compression, *v* decreases substantially as the gas temperature and pressure increase (*v* decreases by a factor of 4 for a compression ratio of 8). This will decrease the size of the vortex until the turbulent regime is reached. During the exhaust stroke following blowdown, *v* will remain approximately constant as the pressure and temperature do not change significantly. Typical parameter values at 1500 rev/min are: $\overline{S}_p = 5\ \mathrm{m/s}$, *L* = 0.1 m; average values of*v* are 1.2 × 10^{-5} and 1.4 × 10^{-4} m^2/s for compression and exhaust stroke, respectively. Hence, a Reynolds number for the compression stroke is 4 × 10^4, A_v/L^2 ≈ 0.006, and the vortex diameter d_v ≈ 0.09*L*. For the exhaust stroke, the Reynolds number is 4 × 10^3, A_v/L^2 ≈ 0.015, and d_v ≈ 0.14*L*. Thus the vortex dimensions at the end of the upward stroke of the piston are comparable to the engine clearance height.

This vortex flow has been observed in an operating engine.Figure 8.38 shows schlieren photographs taken during the exhaust stroke in a special square-cross-section flow visualization spark-ignition engine. The accompanying schematic identifies the vortex structure which is visible in the photo because the cool boundary-layer gas is being scraped off the cylinder wall by the upward-moving piston and "rolled up." The vortex diameter as the piston approaches TC is about 20% of the bore, larger than the engine's clearance height.

© McGraw-Hill Education. All rights reserved. Any use is subject to the Terms of Use, Privacy Notice and copyright information.

Figure 8.38 *Schlieren photographs of in-cylinder flow during later stages of exhaust stroke. (a) Growing vortex in the piston face–cylinder wall corner and turbulent flow toward the exhaust valve are apparent at 60° before top center (BTC); (b) At 20° BTC, the vortex has grown to a diameter of about 0.2B. Sketch illustrates the flow structure.*[39]



© McGraw-Hill Education. All rights reserved. Any use is subject to the Terms of Use, Privacy Notice and copyright information.

8.10. PROBLEMS

8.1.

a. Estimate the ratio of the maximum gas velocity in the center of the hollow cone inlet jet to the mean piston speed from the data in Fig. 8.1.

b. Compare this ratio with the ratio of inlet valve pseudo flow velocity determined from Fig. 6.15 to the mean piston speed at the same crank angle. The engine is that of Fig. 1.4.

c. Are the engine velocity data in (*a*) consistent with the velocity calculated from the simple piston displacement model of (*b*)? Explain.

8.2. Given the relationship between turbulence intensity and mean piston speed [Eq. (8.23)] and that the turbulence integral scale is ≈ 0.2 × clearance height, use Eqs. (8.14) and (8.15) to estimate the following quantities for a spark-ignition engine with bore = stroke = 86 mm, r_c = 9, at 1000 and 5000 rev/min and wide-open throttle:

a. Mean and maximum piston speed, maximum gas velocity through the inlet valve (seeProb. 8.1)

b. Turbulence intensity, integral length scale, micro length scale, and Kolmogorov length scale, all at TC

8.3. The swirl ratio at the end of induction at 2000 rev/min in a direct-injection diesel engine of bore = stroke = 100 mm is 4.0. What is the average tangential velocity (evaluated at the inlet valve-axis radial location) required to give this swirl ratio? What is the ratio of this velocity to the mean piston speed and to the mean flow velocity through the inlet valve estimated from the average valve open area and open time?

8.4.

a. Derive a relationship for the depth (or height) h_B of a disc-shaped bowl-in-piston direct-injection diesel engine combustion chamber in terms of compression ratio r_c, bore B, stroke L, bowl diameter D_B, and top-center cylinder-head to piston-crown clearance c. For $B = L = 100$ mm, $r_c = 16$, $D_B = 0.5B$, $c = 1$ mm, find the fraction of the air charge within the bowl at TC.

b. If the swirl ratio at the end of induction at 2500 rev/min is 3, find the swirl ratio and average angular velocity in the bowl-in-piston chamber of dimensions given above. Assume the swirling flow is always a solid-body rotation. Compare the tangential velocity at the bowl edge with the mean piston speed. Neglect any friction effects.

c. What would the swirl ratio be if the top-center clearance height was zero?

8.5. Using Eq. (8.43) and Fig. 8.22*b* plot the squish velocity divided by the mean piston speed at 10° BTC (the approximate location of the maximum) as a function of squish area expressed as a percentage of the cylinder cross section, $A_s/(\pi B^2/4) \times 100$, from 50 to 0%. $r_c = 10$, $c_c/B = 0.01$, $B/L = 1$, $R = l/a = 3.5$.

8.6. The total crevice volume in an automobile spark-ignition engine is about 2% of the clearance volume. If the gas in these crevice regions is close to the wall temperature (450 K) and at the cylinder pressure, estimate the fraction of the cylinder mass within these crevice regions at these crank angles: inlet valve closing (50° ABC), spark discharge (30° BTC), maximum cylinder pressure (15° ATC), exhaust valve opening (60° BBC), TC of the exhaust stroke. Use the information in Fig. 1.9 for your input data, and assume the inlet pressure is 0.67 bar.

8.7. The piston crevice between the piston top land and cylinder wall, above the first ring, is the major source of engine-out hydrocarbon emissions. Unburned mixture in the cylinder is forced into this crevice as the cylinder pressure increases and flows out of this crevice as the cylinder pressure decreases.

© McGraw-Hill Education. All rights reserved. Any use is subject to the Terms of Use, Privacy Notice and copyright information.

Calculate the mass fraction of the cylinder gas, which is in the crevice between the piston and cylinder wall and above the first piston ring, at the time of peak pressure when the engine is cold (at ambient temperature) and fully warmed up. Assume that gas trapped in this crevice is all unburned mixture (the maximum amount).

Engine geometry and operating conditions:

Bore = 86 mm, stroke = 86 mm

Piston diameter above top ring = 85.3 mm

Distance from piston crown top to top ring = 8 mm

Volumetric efficiency = 0.85

Ambient temperature = 300 K

Piston temperature (cold) = 300 K

Piston temperature at warmed-up conditions = 460 K

Cylinder wall temperature at fully warmed-up condition = 360 K

Coefficient of linear expansion of piston = 2.41×10^{-5} m/K

Coefficient of linear expansion of cylinder wall = 1.29×10^{-5} m/K

ϕ = 1.0, residual fraction = 0.08, fuel = isooctane

Max. cylinder pressure = 3.5 MPa

The gas temperature in the crevice can be assumed to be the average between piston and cylinder wall temperature.

© McGraw-Hill Education. All rights reserved. Any use is subject to the Terms of Use, Privacy Notice and copyright information.

8.11. REFERENCES

1. Bicen, A. F., Vafidis, C., and Whitelaw, J. H.: "Steady and Unsteady Airflow through the Intake Valve of a Reciprocating Engine," *ASME Trans., J. Fluids Engng.,* vol. 107, pp. 413–420, 1985.
2. Namazian, M., Hansen, S. P., Lyford-Pike, E. J., Sanchez-Barsse, J., Heywood, J. B., and Rife, J.: "Schlieren Visualization of the Flow and Density Fields in the Cylinder of a Spark-Ignition Engine," SAE paper 800044, *SAE Trans.*, vol. 89, 1980.
3. Ekchian, A., and Hoult, D. P.: "Flow Visualization Study of the Intake Process of an Internal Combustion Engine," SAE paper 790095, *SAE Trans.*, vol. 88, 1979.
4. Kent, J., Mikulec, A., Rimai, L., et al.: "Observations on the Effects of Intake-Generated Swirl and Tumble on Combustion Duration," SAE paper 892096, 1989.
5. Khalghi, B.: "Intake-Generated Swirl and Tumble Motions in a 4-Valve Engine with Various Intake Configurations—Flow Visualization and Particle Tracking Velocimetry," SAE paper 900059, 1990.
6. Heywood, J. B., and Sher, E.: *The Two-Stroke Cycle Engine: Its Development, Operation, and Design*, SAE, Warrendale, PA, Taylor and Francis, Philadelphia, 1999.
7. Ikeda, Y., Hikosaka, M., Nakajima, T., and Ohhira, T.: "Scavenging Flow Measurements in a Fired Two-Stroke Engine by Fiber LDV," SAE paper 910670, *SAE Trans.*, vol. 100, 1991.
8. Fansler, T. D., and Drake, M. C.: "Flow, Mixture Preparation and Combustion in Direct-Injection Two-Stroke Gasoline Engines," in *Flow and Combustion in Reciprocating Engines,* C. Arcoumanis and T. Kamimoto (eds), Ch. 2, pp. 67–136, Springer-Verlag, Berlin, 2009.
9. Tennekes, H., and Lumley, J. L.: *A First Course in Turbulence,* MIT Press, Cambridge, MA, 1972.
10. Reynolds, W. C.: "Modeling of Fluid Motions in Engines—An Introductory Overview," in *Combustion Modelling in Reciprocating Engines*, J. N. Mattavi and C. A. Amann (eds), pp. 69–124, Plenum Press, New York, 1980.
11. Tabaczynski, R. J.: "Turbulence and Turbulent Combustion in Spark-Ignition Engines," *Prog. Energy Combust. Sci.,* vol. 2, pp. 143–165, 1976.
12. Liou, T.-M., and Santavicca, D. A.: "Cycle Resolved LDV Measurements in a Motored IC Engine," *ASME Trans., J. Fluids Engng*, vol. 107, pp. 232–240, 1985.
13. Rask, R. B.: "Laser Doppler Anemometer Measurements in an Internal Combustion Engine," SAE paper 790094, *SAE Trans.*, vol. 88, 1979.
14. Rask, R. B.: "Comparison of Window, Smoothed-Ensemble, and Cycle-by-Cycle Data Reduction Techniques for Laser Doppler Anemometer Measurements of In-Cylinder Velocity," in *Fluid Mechanics of Combustion Systems,* T. Morel, R. P. Lohmann, and J. M. Rackley (eds), pp. 11–20, ASME, New York, 1981.
15. Arcoumanis, C., and Whitelaw, J. H.: "Fluid Mechanics of Internal Combustion Engines: A Review," *Proc. Instn Mech. Engrs.,* vol. 201, pp. 57–74, 1987.
16. Miles, P. C., "Turbulent Flow Structures in Direct-Injection, Swirl-Supported Diesel Engines," in *Flow and Combustion in Reciprocating Engines,* C. Arcoumanis and T. Kamimoto (eds), Ch. 4, pp. 173–256, Springer-Verlag, Berlin, 2009.
17. Liou, T.-M., Hall, M., Santavicca, D. A., and Bracco, F. V.: "Laser Dopper Velocimetry Measurements in Valved and Ported Engines," SAE paper 840375, *SAE Trans.,* vol. 93, 1984.
18. Fraser, R. A., Felton, P. G., and Bracco, F. V.: "Preliminary Turbulence Length Scale Measurements in a Motored IC Engine," SAE paper 860021, 1986.

© McGraw-Hill Education. All rights reserved. Any use is subject to the Terms of Use, Privacy Notice and copyright information.

19. Ikegami, M., Shioji, M., and Nishimoto, K.: "Turbulence Intensity and Spatial Integral Scale during Compression and Expansion Strokes in a Four-cycle Reciprocating Engine," SAE paper 870372, 1987.

20. Dai, W., Newman, C. E., and Davis, G. C.: "Predictions of In-Cylinder Tumble Flow and Combustion in SI Engines with a Quasi-Dimensional Model," SAE paper 961962, 1996.

21. Monaghan, M. L., and Pettifer, H. F.: "Air Motion and Its Effects on Diesel Performance and Emissions," SAE paper 810255, in *Diesel Combustion and Emissions,* pt. 2, SP-484,*SAE Trans.*, vol. 90, 1981.

22. Tindal, M. J., Williams, T. J., and Aldoory, M.: "The Effect of Inlet Port Design on Cylinder Gas Motion in Direct Injection Diesel Engines," in *Flows in Internal Combustion Engines,* pp. 101–111, ASME, New York, 1982.

23. Brandl, F., Reverencic, I., Cartellieri, W., and Dent, J. C.: "Turbulent Air Flow in the Combustion Bowl of a D.I. Diesel Engine and Its Effect on Engine Performance," SAE paper 790040, *SAE Trans.*, vol. 88, 1979.

24. Brandstätter, W., Johns, R. J. R., and Wigley, G.: "Calculation of Flow Produced by a Tangential Inlet Port," in *International Symposium on Flows in Internal Combustion Engines—III,* FED, vol. 28, pp. 135–148, ASME, New York, 1985.

25. Brandstätter, W., Johns, R. J. R., and Wigley, G.: "The Effect of Inlet Port Geometry on In-Cylinder Flow Structure," SAE paper 850499, 1985.

26. Borgnakke, C., Davis, G. C., and Tabaczynski, R. J.: "Predictions of In-Cylinder Swirl Velocity and Turbulence Intensity for an Open Chamber Cup in Piston Engine," SAE paper 810224, *SAE Trans.*, vol. 90, 1981.

27. Arcoumanis, C., Bicen, A. F., and Whitelaw, J. H.: "Squish and Swirl-Squish Interaction in Motored Model Engines,"*Trans. ASME, J. Fluids Engng,* vol. 105, pp. 105–112, 1983.

28. Trigui, N., Kent, J. C., Guezennec, Y., and Choi, W.-C.: "Characterization of Intake Generated Fluid Flow Fields in IC Engines Using 3-D Particle Tracking Velocimetry," SAE paper 940279, 1994.

29. Floch, A., VanFrank, J., and Ahmed, A.: "Comparison of the Effects of Intake-Generated Swirl and Tumble on Turbulence Characteristics in a 4-Valve Engine," SAE paper 952457, 1995.

30. Baumagarten, H., Bozelie, P., Geiger, J., and Wolters, P.: "Vehicle Application of a 4-Cylinder Tumble DISI Engine," SAE paper 2001-01-0735, 2001.

31. Lichty, L. C.: *Combustion Engine Processes,* McGraw-Hill, New York, 1967.

32. Shimamoto, Y., and Akiyama, K.: "A Study of Squish in Open Combustion Chambers of a Diesel Engine,"*Bull. JSME,* vol. 13, no. 63, pp. 1096–1103, 1970.

33. Ikegami, M., Mitsuda, T., Kawatchi, K., and Fujikawa, T.: "Air Motion and Combustion in Direct Injection Diesel Engines," JARI technical memorandum no. 2, pp. 231–245, 1971.

34. Miles, P. C., RempelEwert, B. H., and Reitz, R. D.: "Squish-Swirl and Injection-Swirl Interaction in Direct-Injection Diesel Engines," in *6th International Conference on Engines for Automobile ICE2003*, Sept. 14–18, Capri/Naples, Italy, 2003.

35. Endres, H., Neuber, H., and Wurms, R.: "Influence of Swirl and Tumble on Economy and Emissions of Multi-Valve SI Engine," SAE paper 920516, 1992.

36. Hires, S. D., Ekchian, A., Heywood, J. B., Tabaczynski, R. J., and Wall, J. C.: "Performance and NO_x Emissions Modelling of a Jet Ignition Prechamber Stratified Charge Engine," SAE paper 760161, *SAE Trans.*, vol. 85, 1976.

37. Asanuma, T., Babu, M. K. G., and Yagi, S.: "Simulation of Thermodynamic Cycle of Three-Valve Stratified Charge Engine," SAE paper 780319, *SAE Trans.*, vol. 87, 1978.

38. Smith, P., Cheng, W. K., and Heywood, J. B.: "Crevice Volume Effect on Spark-Ignition Engine Efficiency," SAE paper 2014-01-2602, 2014.

© McGraw-Hill Education. All rights reserved. Any use is subject to the Terms of Use, Privacy Notice and copyright information.

39. Namazian, M., and Heywood, J. B.: "Flow in the Piston-Cylinder-Ring Crevices of a Spark-Ignition Engine: Effect on Hydrocarbon Emissions, Efficiency and Power," SAE paper 820088, *SAE Trans.*, vol. 91, 1982.

40. Wentworth, J. T.: "Piston and Ring Variables Affect Exhaust Hydrocarbon Emissions," SAE paper 680109,*SAE Trans.*, vol. 77, 1968.

41. Tabaczynski, R. J., Hoult, D. P., and Keck, J. C.: "High Reynolds Number Flow in a Moving Corner,"*J. Fluid Mech.,* vol. 42, pp. 249–255, 1970.

42. Daneshyar, H. F., Fuller, D. E., and Deckker, B. E. L.: "Vortex Motion Induced by the Piston of an Internal Combustion Engine," *Int. J. Mech. Sci.,* vol. 15, pp. 381–390, 1973.

© McGraw-Hill Education. All rights reserved. Any use is subject to the Terms of Use, Privacy Notice and copyright information.

9.0. CHAPTER PRELIMINARIES

ESSENTIAL FEATURES OF PROCESS

THERMODYNAMICS OF SI ENGINE COMBUSTION

FLAME STRUCTURE AND SPEED

CYCLIC VARIATIONS IN COMBUSTION, PARTIAL BURNING, AND MISFIRE

SPARK IGNITION

ABNORMAL COMBUSTION: SPONTANEOUS IGNITION AND KNOCK

PROBLEMS

REFERENCES

© McGraw-Hill Education. All rights reserved. Any use is subject to the Terms of Use, Privacy Notice and copyright information.

9.1. ESSENTIAL FEATURES OF PROCESS

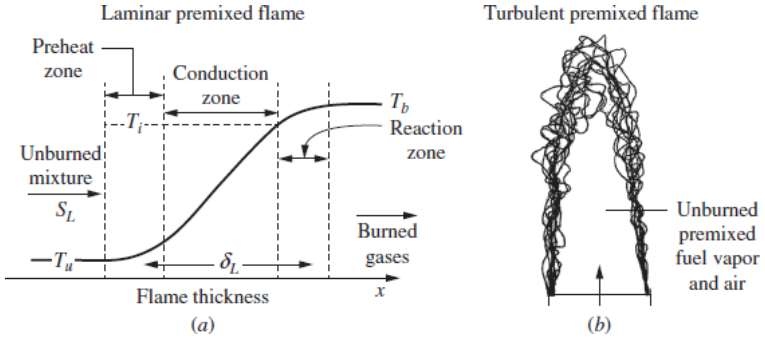
The combustion process is an especially important part of the internal combustion engine's operating cycle. Combustion must release the chemical energy of the fuel—the primary source of energy for the engine—in a relatively short time period between the compression and expansion processes, thereby producing the high-pressure high-temperature burned gases that then expand within the cylinder transferring work to the piston. A robust combustion process is important for smooth and reliable engine operation. The combustion process must be fast, that is, it must occupy a small fraction of the total cycle time, so that the engine's energy conversion process is efficient, and highly repeatable so that variations from one cycle to the next are small enough to be barely noticeable.

Combustion is also important for its impact on several other engine characteristics or requirements. The processes by which the engine's emissions form within the cylinder are closely linked with the details of the combustion process. The antiknock and volatility requirements of fuels for spark-ignition (SI) engines and the ignition quality of diesel fuels are dictated by each engine's combustion process. Even the gas exchange process of the engine, and hence its power, are affected by what the designer must do to achieve good combustion.

9.1.1. Combustion Fundamentals

Combustion in engines takes place in a *flame*. A flame is the (confined) region within which the fuel oxidizing reactions and chemical energy release occur. Engine flames are normally thin: the actual reaction region is a fraction of a millimeter thick. In the spark-ignition engine, the fuel-vapor air charge is well mixed so the flame is a *premixed flame*. The speed at which such a premixed flame propagates into the unburned gas ahead of it is called the *flame speed* or burning velocity. In a laminar or well-ordered flow, this velocity S_L is a characteristic property of the unburned mixture ahead of the flame: it depends on the composition of the mixture, the properties of the fuel, and the mixture temperature and pressure. The values of S_L are usually less than about 1 m/s. Figure 9.1 shows the structure of a laminar premixed flame. In flame-stationary coordinates, the unburned mixture—fuel vapor and air—enters the flame from the left at temperature T_u. (In unburned-mixture stationary coordinates, the flame moves toward the left into that mixture.) The unburned mixture temperature starts to rise in the preheat zone, and steadily increases due to the thermal energy conducted through the gas moving through the conduction zone, that thermal energy coming from the reaction zone where the fuel oxidation chemical reactions occur (after the unburned mixture reaches its ignition temperature T_i). It is in this reaction zone that the bulk of the chemical energy release occurs: the thermal energy produced is conducted into the unburned mixture moving through the conduction zone as described above, and convected out of the flame in the (hot) burned gases (at temperature, T_b).

Figure 9.1 Structure of a premixed flame: (a) temperature profile within the different regions of a laminar premixed flame; (b) several realizations of a turbulent premixed flame attached to a tube supplying premixed fuel vapor and air.

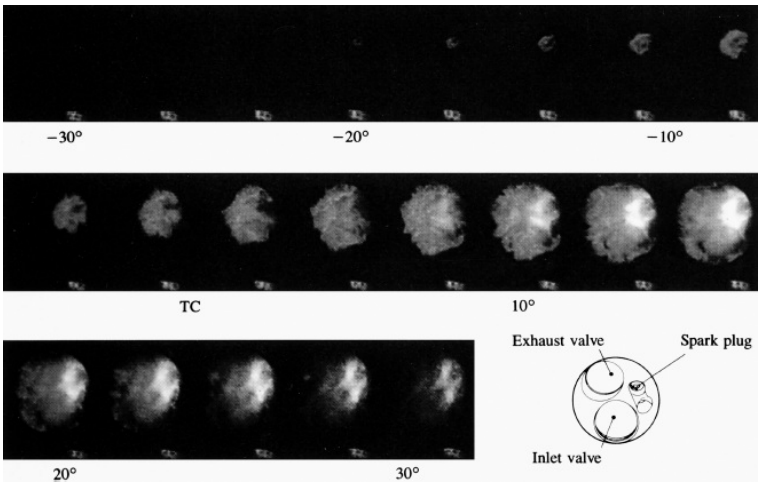


© McGraw-Hill Education. All rights reserved. Any use is subject to the Terms of Use, Privacy Notice and copyright information.

This conduction of thermal energy that steadily raises the unburned mixture temperature, along with the diffusion of reactive species within the flame, is what causes the flame to propagate. The flame speed thus scales with the temperature gradient in this conduction zone, $(T_b - T_u)/\delta_f$. A premixed flame with a stoichiometric or slightly fuel-rich mixture (which produces the highest T_b for a given T_u) has the highest laminar flame speed. Lean mixtures, and mixtures diluted with burned residual gas and exhaust-gas recirculation (EGR), decrease T_b and lengthen δ_f, so their flame speeds are lower (see Sec. 9.3.3 where the dependence of S_L on mixture composition, temperature, and pressure, is described).

In spark-ignition engines, the fuel and air are mixed together either in the intake system or in the cylinder where mixing with residual gas takes place, and are then compressed. Combustion is initiated toward the end of the compression stroke at the spark plug by an electrical discharge. Following inflammation, a *turbulent flame* develops, propagates through this essentially premixed fuel vapor, air, burned gas mixture until it reaches the combustion chamber walls, and then extinguishes. Photographs of this process taken in operating engines illustrate its essential features. Figure 9.2 shows a sequence of frames from a high-speed movie of the combustion process in a special single-cylinder engine with a glass piston crown.[1] The spark discharge is at 30° before top center (BTC). The flame first becomes visible in the photos at about 20° BTC. The flame, approximately circular in outline in this view through the piston, propagates outward from the spark plug location. The blue light from the flame is emitted most strongly from the flame front. The irregular shape of the turbulent flame front is apparent. At TC the flame diameter is about two-thirds of the cylinder bore. The flame reaches the cylinder wall farthest from the spark plug about 15° ATC, but combustion continues around parts of the chamber periphery for another 10 degrees. At about 10° ATC, additional radiation—initially white, turning to pinky-orange—centered at the spark plug location is evident. This afterglow comes from the gases behind the flame which burned earlier in the combustion process as they are compressed to the highest temperatures attained within the cylinder (at about 15° ATC), while the rest of the charge burns.[2,3]

Figure 9.2 Sequence of images of flame and burned-gas radiation from high-speed movie of spark-ignition engine combustion process, taken through glass piston crown. Ignition timing 30° BTC, light load, 1430 rev/min, (A/F) = 19.[1]



Premixed SI engine flames become turbulent as they develop from the spark discharge, and their propagation rate is then defined by their *turbulent flame speed*. Figure 9.1*b* shows several realizations of a turbulent premixed flame, attached to a tube through which premixed fuel vapor and air enter the unburned-mixture region inside the conical flame. Each line is a short-time-exposure realization of the irregular randomly moving thin flame sheet above the burner tube. The burned gases emerge, moving upward and outward from the flame contour. These flame profiles indicate that this turbulent flame is a *wrinkled laminar flame*.

The turbulent flow inside the engine cylinder during combustion both convects and distorts or wrinkles the thin reaction sheet flame through its combination of bulk or mean flow pattern and local turbulence or random velocity fluctuations. The higher the local turbulence, the faster the flame propagates and becomes wrinkled. If engine flames were not turbulent, with a turbulent flame speed several times the laminar flame speed, engines could not operate satisfactorily because combustion,

© McGraw-Hill Education. All rights reserved. Any use is subject to the Terms of Use, Privacy Notice and copyright information.